

MARCH 1957

AIChE JOURNAL

Published by the American Institute of Chemical Engineers

UNIVERSITY
OF MICHIGAN

MAR 9 1959

CONTENTS

ENGINEERING
LIBRARY

Agitation of Non-Newtonian Fluids

Material Transport in Turbulent Gas Streams: Radial Diffusion in a Circular Conduit

Study of Bubbling Performance in Relation to Distillation and Absorption

Calculated Performance of a Dissolved—gas-drive Reservoir by a Phase-behavior Method

Vapor-liquid Equilibria for Hydrogen-light-hydrocarbon Systems at Low Temperatures

Mass Transfer at Low Pressures

Mass and Heat Transfer to Single Spheres and Cylinders at Low Reynolds Numbers

Heat Transfer in the Critical Region

Liquid-liquid Extraction in a Pulsed Perforated-plate Column

Mechanics of Vertical-moving Fluidized Systems

Effect of Concentration Level on Mass Transfer Rates

Vapor-liquid Equilibria of Nitrogen-argon-oxygen Mixtures

Axial Mixing of Binary Gas Mixtures Flowing in a Random Bed of Spheres

Heat Transfer to Non-Newtonian Fluids

Spray-extraction-tower Studies

Viscosity of Suspensions of Spherical and Other Isodimensional Particles in Liquids

An Empirical Correlation for Velocity Distribution of Turbulent Fluid Flow

Studies of Thermal Conductivity of Liquids: Part III

Mass and Heat Transfer from Drops in Liquid-liquid Extraction

Void Fractions in Two-phase Steam-water Flow

A. B. Metzner and R. E. Otto

Scott Lynn, W. H. Corcoran,
and B. H. Sage

Ju Chin Chu, John Forgrieve,
Robert Grosso, S. M. Shah, and
Donald F. Othmer

F. H. Brinkman and
C. F. Weinaug

Alvin L. Benham and
Donald L. Katz

Thomas K. Sherwood and
Norman E. Cooke

S. K. Friedlander

R. P. Bringer and J. M. Smith

W. H. Li and W. M. Newton

Leon Lapidus and J. C. Elgin

L. E. Westkaemper and
Robert R. White

R. E. Latimer

K. W. McHenry, Jr., and
R. H. Wilhelm

A. B. Metzner, R. D. Vaughn,
and G. L. Houghton

A. I. Johnson, G. W. Minard,
Chen-Jung Huang, J. H.
Hansuld, V. M. McNamara

Andrew Pusheng Ting and
Ralph H. Luebbers

B. F. Ruth and H. H. Yang

Byron C. Sakiadis and
Jesse Coates

A. E. Handlos and T. Baron

H. S. Isbin, Neil C. Sher, and
K. C. Eddy

Practical, Efficient, and Economical

ENGIN. LIB.

TP

1

A42

SOLVENT EXTRACTION

with

YORK-SCHEIBEL LIQUID-LIQUID EXTRACTORS

The YORK-SCHEIBEL patented multi-stage extraction column:

- Is ideal for the common multi-stage, countercurrent extractions in which the feed material is contacted with a single solvent.
- Is effective and efficient for fractional liquid extraction in which the feed material is contacted with two selective and immiscible solvents flowing countercurrent through the column.
- May be designed for liquid streams carrying solids in suspension.

The columns employ agitators in each stage to insure complete liquid-liquid contacting. The phase separating sections between the mixing zones consist of wire mesh packing, a new arrangement of baffles, or both baffles and packing.

High stage efficiencies are obtained even with difficult-to-separate materials. Here are a few of the extractions for which York-Scheibel columns have no equal:

- close boiling mixtures
- non-volatile mixtures
- structural isomers
- materials from dilute solutions
- azeotropic mixtures
- impurities and color bodies
- heat sensitive materials

Check these outstanding features:

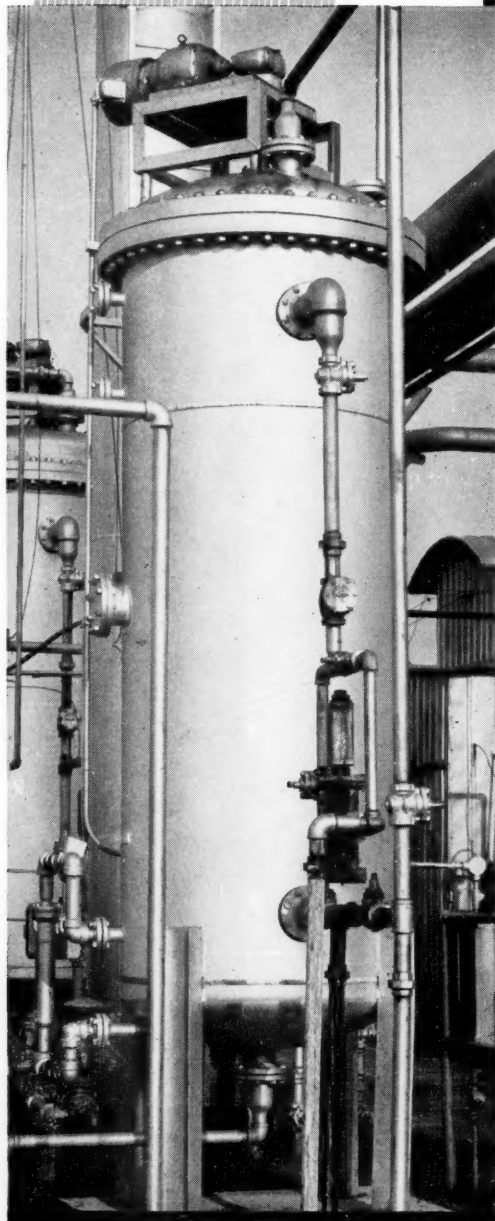
- ✓ Single, compact column
- ✓ High efficiency
- ✓ High throughput capacity
- ✓ Low cost per stage
- ✓ Efficient laboratory, pilot plant and large scale performance
- ✓ Low stage height

SEND INFORMATION on your requirements and let York engineers recommend the best design for your conditions.

YORK

YORK PROCESS EQUIPMENT CORP
4 Central Avenue, West Orange, N.J.

Send for latest literature giving complete details



A.I.Ch.E. JOURNAL

MARCH 1957 · VOL. 3, NO. 1

PUBLISHER

F. J. Van Antwerpen

EDITOR

Harding Bliss

ADVERTISING MANAGER

L. T. Dupree

ADVISORY BOARD

C. M. Cooper, O. E. Dwyer, W. C. Edmister, E. R. Gilliland,
A. N. Hixson, W. R. Marshall, Jr., R. H. Newton, R. L. Pigford,
J. M. Smith, Theodore Vermeulen, R. R. White, R. H. Wilhelm

The A.I.Ch.E. Journal, an official publication of the American Institute of Chemical Engineers, is devoted in the main to theoretical developments and research in chemical engineering and allied branches of engineering and science. Manuscripts should be submitted to the New York office.

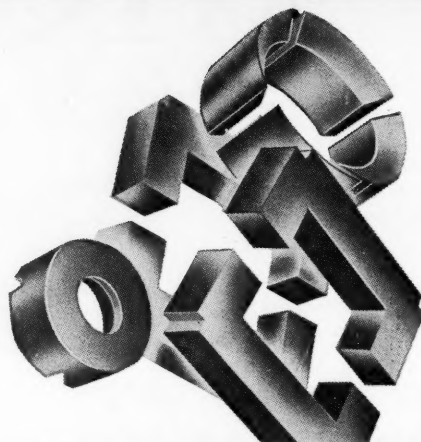
Engineering in History	1
Agitation of Non-Newtonian Fluids	A. B. Metzner and R. E. Otto 3
Material Transport in Turbulent Gas Streams: Radial Diffusion in a Circular Conduit	Scott Lynn, W. H. Corcoran, and B. H. Sage 11
Study of Bubbling Performance in Relation to Distillation and Absorption	Ju Chin Chu, John Forgrieve, Robert Grosso, S. M. Shah, and Donald F. Othmer 16
Calculated Performance of a Dissolved—gas-drive Reservoir by a Phase-behavior Method	F. H. Brinkman and C. F. Weinaug 29
Vapor-liquid Equilibria for Hydrogen-light-hydrocarbon Systems at Low Temperatures	Alvin L. Benham and Donald L. Katz 33
Mass Transfer at Low Pressures	Thomas K. Sherwood and Norman E. Cooke 37
Mass and Heat Transfer to Single Spheres and Cylinders at Low Reynolds Numbers	S. K. Friedlander 43
Heat Transfer in the Critical Region	R. P. Bringer and J. M. Smith 49
Liquid-liquid Extraction in a Pulsed Perforated-plate Column	W. H. Li and W. M. Newton 56
Mechanics of Vertical-moving Fluidized Systems	Leon Lapidus and J. C. Elgin 63
Effect of Concentration Level on Mass Transfer Rates	L. E. Westkaemper and Robert R. White 69
Vapor-liquid Equilibria of Nitrogen-argon-oxygen Mixtures	R. E. Latimer 75
Axial Mixing of Binary Gas Mixtures Flowing in a Random Bed of Spheres	K. W. McHenry, Jr., and R. H. Wilhelm 83
Heat Transfer to Non-Newtonian Fluids	A. B. Metzner, R. D. Vaughn, and G. L. Houghton 92
Spray-extraction-tower Studies	A. I. Johnson, G. W. Minard, Chen-Jung Huang, J. H. Hansuld, and V. M. McNamara 101
Viscosity of Suspensions of Spherical and Other Isodimensional Particles in Liquids	Andrew Pusheng Ting and Ralph H. Luebbers 111
An Empirical Correlation for Velocity Distribution of Turbulent Fluid Flow	B. F. Ruth and H. H. Yang 117
Studies of Thermal Conductivity of Liquids: Part III	Byron C. Sakiadis and Jesse Coates 121
Mass and Heat Transfer from Drops in Liquid-liquid Extraction	A. E. Handlos and T. Baron 127
Void Fractions in Two-phase Steam-water Flow	H. S. Isbin, Neil C. Sher, and K. C. Eddy 136
Communications to the Editor	143
Books	9M

Publication Office, Richmond, Virginia. Published quarterly in March, June, September, and December by the American Institute of Chemical Engineers, 25 West 45 Street, New York 36 New York. Manuscripts and other communications should be sent to the New York office. Correspondence with the editor may be addressed to him at Yale University, 225 Prospect Street, New Haven 11, Connecticut. Statements and opinions in the *A.I.Ch.E. Journal* are those of the contributors, and the American Institute of Chemical Engineers assumes no responsibility for them. Subscriptions: one year, member \$4.50, nonmember \$9.00; two years, member \$7.50, nonmember \$16.00; additional yearly postage, Canada 50 cents, Pan American Union \$1.50, other foreign \$2.00 (foreign subscriptions payable in advance). Single copies: \$3.00. Second-class mail privileges authorized at Richmond, Virginia. Copyright 1957 by the American Institute of Chemical Engineers. National headquarters of A.I.Ch.E. is concerned about nondelivery of copies of the *A.I.Ch.E. Journal* and urgently requests subscribers to give prompt notification of any change of address. Sixty days must be allowed for changes to be made in the records.

SPRAY DRYER PIONEER

Stackpole Carbon uses Bowen Spray Dryer to produce Metallic Oxide Powders to meet high electrical specifications.

Stackpole Carbon Produces First Spray Dried Ferrites



"Ceramag[®]" cores made from the spray dried ferrites have lower eddy current losses, less corona effect, high permeability and ability to withstand elevated ambient temperatures, thus they insure superior performance in the electrical and electronic fields where they are used in pulse generation, magnetic amplifying, television and similar applications.

Because of its spherical shape, free-flowing characteristics and high density the spray dried metallic oxide ferrites can be molded into small and intricate shapes. Ceramag[®] material of Stackpole Carbon has thus been an important factor in meeting the growing demand for miniaturized components.

Bowen Engineering is proud to have had the opportunity to cooperate in this project.

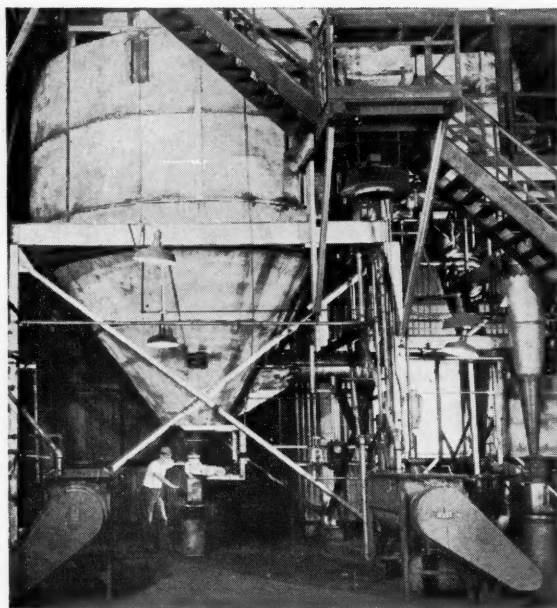


GET BULLETIN 41

We'll be glad to send it to you
now without obligation.

BOWEN ENGINEERING, INC.
NORTH BRANCH 12, NEW JERSEY

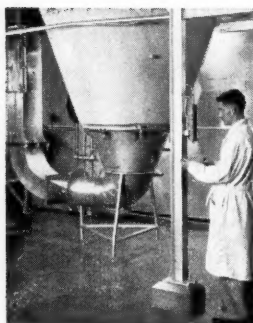
BOWEN SPRAY DRYERS
Always Offer You More!



Bowen Spray Dryer used for the production of metallic oxide ferrites

BOWEN TEST LABORATORY—

If you have some ideas where spray drying might present a profitable solution, Bowen Engineers will be glad to show you at the Bowen Laboratory what Spray Drying can produce for you. Equipment available will handle small batch lots of a gallon or two, a few drums or a car load for sampling or manufacturing development. Bulletin "The Bowen Laboratory for the Evaluation of Spray Drying" more fully describes these research facilities.



Ceramag—Registered trade mark of Stackpole Carbon Company

Recognized Leader in Spray Dryer Engineering Since 1926

Engineering in History

The excellent book *Engineering in History* by Kirby, Withington, Darling, and Kilgour¹ has recently been named as one of a small number of best books published in 1956. We agree emphatically with this selection and heartily recommend this fine book to all who are proud of the achievements of the engineering profession.

The title is accurate, in that it distinguishes the book from a mere history of engineering. The authors have preferred the broader view of history as a whole and the part engineering has played in it. Indeed, a large portion of our knowledge of ancient history is due to the permanence of some of the structures on which records are preserved and from which certain intellectual attainments of the ancients may be surmised.

The book is an excellent source of information, and repeated reference to it will be fruitful. For aid in digesting the news of the day, such as that of the Suez Canal, we found a good deal of supplementary material. The size of this canal has had much to do with the sizes of ships designed for the Oriental routes, and this, in turn, has generated an almost total dependence on the canal. In lighter reading about the times of Richard III a mention of London Bridge led us again to *Engineering in History*. It was astonishing to learn that London Bridge was almost 300 years old at the time of the last Plantagenet and that it stood for over 300 years after his sad reign.

In the course of the development of history, as outlined by these writers, one may see the evolution of the civil engineer from the earliest artisan to the designer of the modern suspension bridge or skyscraper. Mechanical engineering, perhaps beginning with Archimedes, has since led through the Industrial Revolution to the modern jet engine. Electrical engineering, a relatively recent arrival, is credited with its wonderful contributions in power, transportation, and communications. Metallurgy has played a basic part in all, and much of what the others have accomplished can be traced to the improvements in the basic metals with which they work. It is

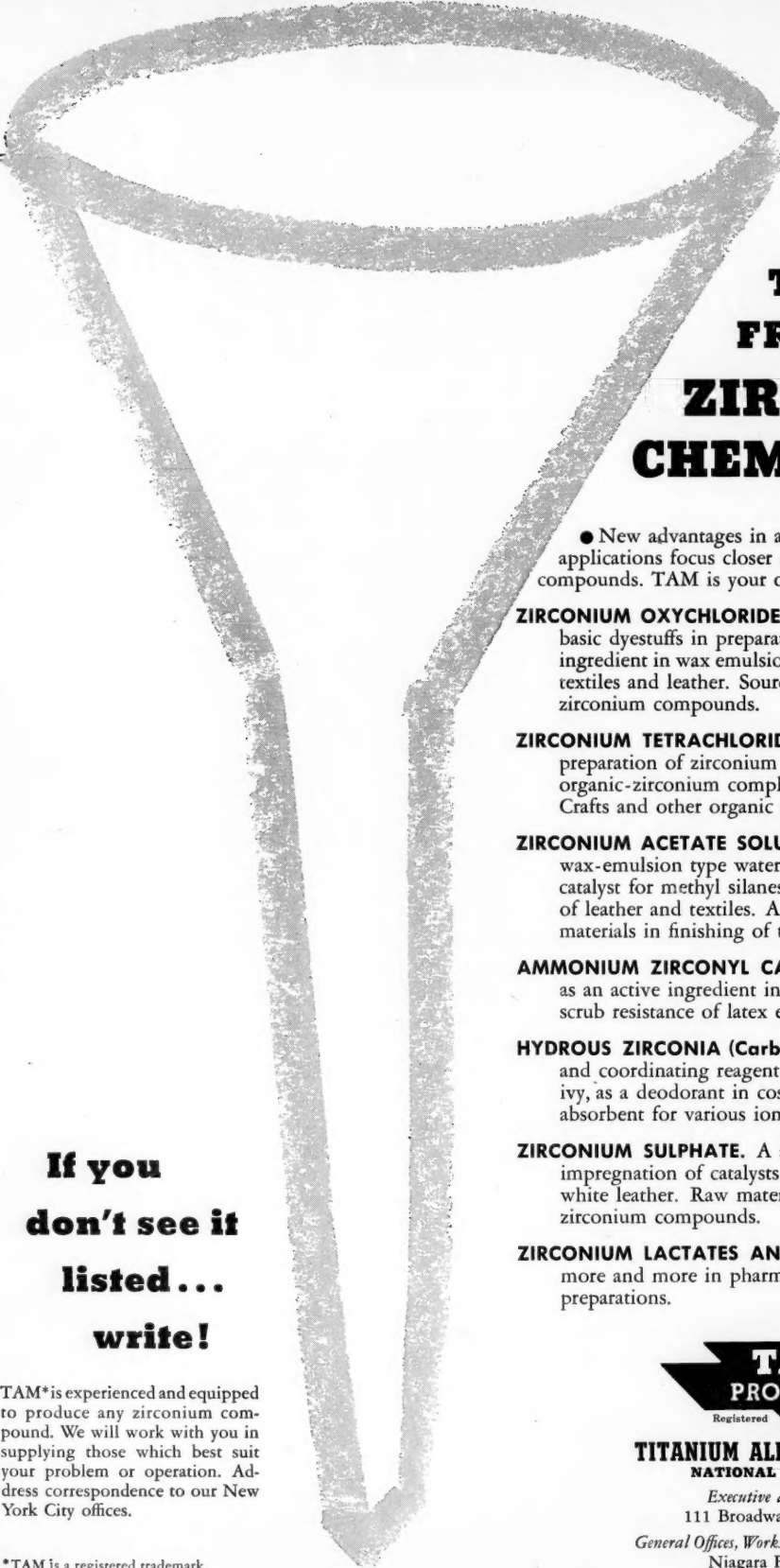
regrettable that chemical engineering is only briefly mentioned; yet it is understandable, for this branch of the profession is so new that its achievements must wait for another chronicle.

There is a great value to this book which is not immediately apparent and which comes to the reader only after contemplation. This feature of it deserves a much wider audience than the engineering profession alone; the book should be read with particular attention by the academic historians and by the general public as well. For here is a history book in which war is scarcely mentioned. (Indeed, the word does not occur in the index.) Here is a history book which does not trace the rise and fall of empires and emperors. Caesar and Napoleon have no place here. Man's error-filled history of myths, persecutions, and inquisitions is not to be found here. This is an account of constructive man, man the builder. It is a much more admirable account than the recital of political machinations and authoritarian arrogance which constitutes a large part of the usual history.

Buildings, whether used for housing the individual or his priests or his government or the remains of his rulers, have a proud history of their own. They may have been put to corrupt uses, but the evolution of man's ingenuity and inventiveness which they represent cannot be overemphasized. Roads, although they may have carried aggressive armies, were built to open up new regions and to promote intercourse among peoples. Bridges have the same fine purposes and our world has grown because of them. Aqueducts and canals made possible the settlement of people in regions otherwise barren or inaccessible and led to the growth of cities and the establishment of trade. The distinguishing feature of all these structures is not the king or emperor under whom they were built. It is not the arrogant disregard for human life with which some of them were built. The distinguishing features are the patient study of physical principles, the careful experimental confirmation of these wherever possible, the ingenuity with which these principles were combined, and the responsibility with which the plans were executed—the fundamentals from which modern engineering evolved.

H.B.

¹ Kirby, R. S., S. Withington, A. B. Darling, and F. G. Kilgour, *Engineering in History*, McGraw-Hill Book Company, Inc., New York (1956).



Take a FRESH LOOK at ZIRCONIUM CHEMICALS

● New advantages in a growing list of commercial applications focus closer attention upon soluble zirconium compounds. TAM is your one source for all.

ZIRCONIUM OXYCHLORIDE. A precipitant for acid and basic dyestuffs in preparation of lakes and toners. Active ingredient in wax emulsion type water repellents for textiles and leather. Source material for other zirconium compounds.

ZIRCONIUM TETRACHLORIDE. Raw material for preparation of zirconium metal, zirconium alloys, and organic-zirconium complexes. Catalyst for Friedel-Crafts and other organic syntheses.

ZIRCONIUM ACETATE SOLUTION. Active ingredient in better wax-emulsion type water repellents for textiles. A catalyst for methyl silanes in silicone repellent treatments of leather and textiles. A precipitant for many proteinic materials in finishing of textiles, leather, etc.

AMMONIUM ZIRCONYL CARBONATE SOLUTION. Used as an active ingredient in basic water repellents. Improves scrub resistance of latex emulsion paints.

HYDROUS ZIRCONIA (Carbonated). A strong chelating and coordinating reagent. Useful in treatment of poison ivy, as a deodorant in cosmetic creams, and as an absorbent for various ions.

ZIRCONIUM SULPHATE. A source for zirconia for the impregnation of catalysts. As a tanning agent... processing white leather. Raw material for preparation of organic-zirconium compounds.

ZIRCONIUM LACTATES AND GLYCOLATES. Being used more and more in pharmaceuticals and personal deodorant preparations.

**If you
don't see it
listed...
write!**

TAM* is experienced and equipped to produce any zirconium compound. We will work with you in supplying those which best suit your problem or operation. Address correspondence to our New York City offices.

*TAM is a registered trademark.



**TITANIUM ALLOY MFG. DIVISION
NATIONAL LEAD COMPANY**

Executive and Sales Offices:
111 Broadway, New York City

General Offices, Works and Research Laboratories:
Niagara Falls, New York

Agitation of Non-Newtonian Fluids

A. B. METZNER and R. E. OTTO

University of Delaware, Newark, Delaware

Since the shear rate of a non-Newtonian fluid is of importance in fixing the rheological or viscometric behavior of such a material, the present study has been concerned with the development of a general relationship between impeller speed and the shear rate of the fluid. The resulting relationship was then used to interpret and correlate power-consumption data on three non-Newtonian fluids by use of a generalized form of the conventional power-number-Reynolds-number plot for Newtonians.

Flat-bladed turbines from 2 to 8 in. in diameter were used exclusively. Tank diameters ranged from 6 to 22 in. and power inputs from 0.5 to 176 hp./1,000 gal. The study encompassed a 130-fold range of Reynolds numbers in the laminar and transition regions. The results to date indicate that power requirements for the rapid mixing of non-Newtonian fluids are much greater than for comparable Newtonian materials.

The literature in the field of agitation and mixing of fluids may be divided into two general categories. First and most extensive are the numerous papers dealing with the dependence of power consumption upon geometric, kinematic, and fluid-property parameters. The broad fundamental and applications studies of Mack, Miller, Oldshue, Rushton, and various coworkers (5, 8, 15, 21, 22, for example) are representative of work of this nature. Studies of rates and quality of mixing, and of the effect of agitator geometric variables on these factors comprise the second group. The com-

plexity of this problem has resulted in little quantitative progress in this field except in the mixing of particulate solids, and the literature, therefore, presents primarily qualitative guides as opposed to the quantitative generalizations available for prediction of power requirements. The most recent review by Rushton (20) discusses progress in this field.

A major limitation of the prior art is that it deals almost exclusively with Newtonian fluids. The comparative simplicity of Newtonian systems has made them the logical first choice for explora-

tory work, but because of the importance of non-Newtonian materials a study of these systems is long overdue. The purposes of the present investigation therefore were as follows: (1) establishment of the quantitative relationships between power consumption and the geometric, kinematic, and fluid property parameters for non-Newtonian fluids; (2) qualitative study of rates and quality of mixing in non-Newtonian systems to shed some preliminary light on these factors; and attaining (3) a quantitative method of approach in classification of non-Newtonian fluids and ascertaining its relation to mixing.

REVIEW OF PRIOR ART

In the study of the agitation or mixing of fluids, the system which has received the most attention consists of a single impeller centered in a cylindrical tank, as shown in Figure 1. The results of Newtonian power-consumption studies are presented in terms of dimensionless groups involving power ($P_g/D^3N^3\rho$) and a mixing Reynolds number ($D^2N\rho/\mu$) or modifications of these. Below a Reynolds number of 300 the Froude number (DN^2/g), which measures the variation in flow due to changes in the free surface, was not important (22). The effects of geometrical parameters other than the impeller diameter [such as (C/D) , (T/D) , and (B/D)] were not important within the wide ranges specified by previous workers. The entire power-number-Reynolds-number curve (Figure 2) has been divided into three sections which are directly analogous to the familiar three regions of flow in a circular pipe, i.e., the turbulent region in which the power number (or friction factor) is not greatly affected by Reynolds number, the laminar region where power number and friction factor are inversely proportional to Reynolds number, and the intermediate or transition region. However, unlike the case of flow in a round tube, the transition from laminar to turbulent flow does not occur over the narrow range of Reynolds numbers between 2,000 and 4,000 (6) but extends over the large range from 10 to 1,000, as shown in Figure 2.

To date only three papers have been concerned with the agitation-power requirements of non-Newtonian fluids. Brown and Petsiavas (2) presented a power-number plot for a Bingham-plastic type* of non-Newtonian that makes use of the Bingham-plastic Reynolds and Hedstrom numbers (4, 13) to correlate the data. Their viscometric data, taken with a Brookfield viscometer, indicated that their fluids deviated appreciably from Bingham-plastic behavior, but for those few fluids which closely approach the ideal Bingham plastic this method of attack can be reworked into

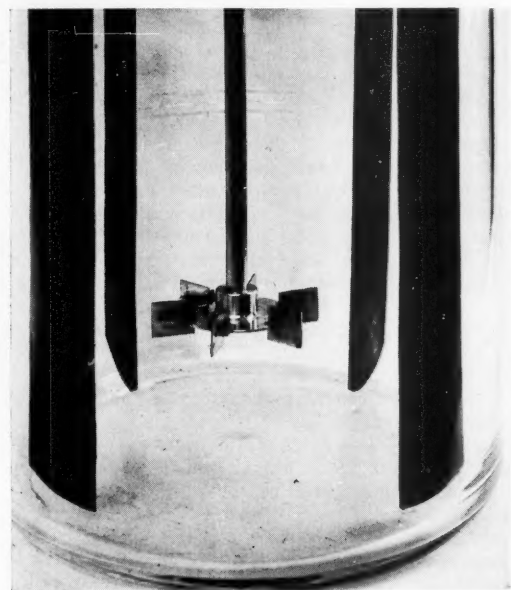


Fig. 1. Mixing system.

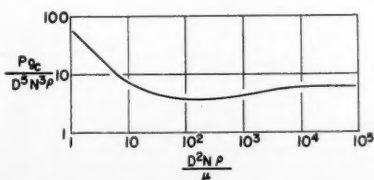


Fig. 2. Power-number-Reynolds-number curve for Newtonian fluids in a baffled tank (22).

*Appendix A presents and discusses the classical types of non-Newtonian behavior.

a rigorous and convenient design method. Magnusson (9) reported a procedure for calculating the apparent viscosity of non-Newtonian fluids in agitated tanks by comparison with the power number curve for a Newtonian fluid but presented no method whereby such results might be used for equipment design. Schultz-Grunow (23) studied power requirements for the agitation of slightly non-Newtonian fluids in the laminar region and developed a correlation by means of dimensional analysis. Since fluid density was not included in the analysis, this correlation cannot be used outside the laminar region and may not accurately predict the end of the laminar-flow region. These are rather serious limitations in view of the fact that little actual mixing of non-Newtonian fluids appears to occur within the laminar region.

Summarizing, it may be concluded that the prior art presents indications of several different approaches to the problem of non-Newtonian power consumption in agitated vessels. However, no useful equipment-design methods have been developed and no over-all physical understanding of the problem has as yet been presented.

DESCRIPTION AND CLASSIFICATION OF NON-NEWTONIAN FLUIDS

In view of the previously reported (12, 13) limitations of the common rheological classifications of non-Newtonian behavior, the method of approach suggested in this work is to define the extent of non-Newtonian behavior by the property n , as given by the power-law equation:

$$\tau = K \left(\frac{du}{dr} \right)^n \quad (1)$$

Newtonian fluids are defined as those materials which in laminar flow exhibit a linear relationship between the imposed shear stress and the resulting shear rate; i.e., n has a constant value of unity and K is equal to μ/g_c where μ is termed the viscosity of the Newtonian fluid. Since the property n is a measure of the type of fluid behavior, it has been termed the *flow-behavior index* of a fluid (13). Similarly, K may be considered to be a *fluid-consistency index*.

Non-Newtonian fluids are those materials for which the flow-behavior index is not equal to unity although it is frequently a constant, or nearly so, over wide ranges of shear rates. The fact that it is not a true constant—over all conceivable ranges of shear rate—is frequently irrelevant in view of the fact that one needs a rheological equation which correctly portrays only the fluid behavior over the particular range of shear rates which happen to be of interest in a given engineering problem. The rigor and utility with which a similar method of approach has been applied to the analogous problem of flow in pipes (12) suggest its utility in the field of agitation. As a matter of fact, for flow in pipes the

property analogous to n in Equation (1) does not need to be a constant in order for the analysis to be rigorous, but may be allowed to vary with the shear rate of the fluid. The problem of agitation of fluids in vessels has been too complex to enable a similar theoretical analysis to date, and one cannot yet say whether or not the exponent n must be a constant to make the approach a rigorous one. From an engineering viewpoint it is important to note that no fluids have yet been found for which n changes rapidly enough with shear rate to permit an experimental analysis of this problem or to reveal any discrepancies of data attributable to this factor. Severs (25) has suggested that studies using dilatant fluids, for which n sometimes does change rapidly with shear rate, would be illuminating.

In view of the mathematical simplicity of Equation (1) it is remarkable that it correlates rheological data as well as it does. For example, the data of reference 3 are correlated at least as perfectly by Equation (1) as by the much more complex Eyring-Powell equation used by Stevens et al. This statement of fact may be readily verified by simply plotting both the rheological data and the Eyring-Powell equation for each fluid (as given by reference 3) on logarithmic coordinates and comparing the fit obtained with that obtainable by the simple straight line which depicts Equation (1) on such coordinates. The rheological data of the fluids used in the present work (Figure 5) do not fall on a perfect straight line over the entire range of shear rates for which data are available, but for all fluids except the 1.0% CMC the deviation from such a straight line is less than the scattering of the data points. Even for this CMC gel the data which are within the range of average shear rates used in the agitation studies fall on a perfect straight line.

DEVELOPMENT OF THE CORRELATION

The flow of a fluid about a mixing impeller is complex, but the controlling factors of the drag on an impeller blade may be examined by comparison with simpler flow situations. Figure 3 shows the laminar flow of a fluid around a sphere. There is no separation of the flow and viscous dissipation of energy is the controlling factor. The total force on the sphere is due to two effects: (1) the shearing forces on the surface of the object (of magnitudes indicated approximately by arrows tangent to the surface on Figure 3) and (2) the differences in pressure between the front and the rear of the sphere. These pressure differences in turn are due to the viscous dissipation of energy in the fluid stream and are indicated by the arrows perpendicular to the surface of sphere.

For a Newtonian fluid two thirds of the drag is due to shear-stress forces on the surface (17), the remainder being due to differences in pressure caused by the flow of material in the region of the surface. For a flat plate of zero thickness normal to the flow of fluid (Figure 4), which may be assumed similar to a flat-bladed turbine or paddle rotating in a fluid, all the drag is due to differences in pressure caused by the flow of the fluid in the region of the object, as there is no area along which the shear stress at the surface can exert a component causing a net drag in the direction of the motion of the fluid.* One may conclude from this analogy that the study of such an object moving through the fluid must include the study of the fluid in the general region of the object, since this determines the viscous-energy dissipation and hence the drag or power requirement.

In non-Newtonian technology, study of the flow in this over-all region must obviously include a consideration of the shearing rates or shearing stresses. This is a necessary consequence of the fact that the response (viscosity) of these fluids to an imposed stress is not a constant but depends on the magnitude of either the shearing rate or shearing stress. Another way of arriving at the same conclusion is to note that no simple equation for the relationship between shear stress and shear rate [such as Equation (1)] has been found which will correlate such data over all conceivable ranges of these variables. Therefore, it is necessary to know at least approximately the ranges into which the shear rates about an impeller may fall and the variables which determine or control these shear rates. Figure 5 shows the shear-stress-shear-rate relationships for the materials used. Evaluation of the ratio of shear stress to shear rate (apparent viscosity) at a given point showed for the 1.25% Carbopol solution a variation in apparent viscosity from 134,000 centipoises at a shear rate of 1.5 sec.⁻¹ to 1,100 centipoises at 1,000 sec.⁻¹. With such a large variation in apparent viscosity one could not make a one-point measurement of the apparent viscosity indiscriminately and expect to obtain a correlation when the range of shear rates in the viscometer was different from that of the shear rates in the system being studied.

The mathematical description of a non-Newtonian material may be accomplished by the use of an equation [such as Equation (1)] relating the shear stress to shear rate or, equally well, by the

*This analogy of flow over a flat plate as compared with flow past a mixing impeller is not completely exact as the postulated types of flow do not include the radial components of velocity which are parallel to the surface of the flat plate or impeller. Such radial flow is necessary to produce mixing. This does not invalidate the argument, however, because the drag due to radial flow does not produce any forces perpendicular to the surface of the impeller and therefore does not directly affect the torque felt by the shaft and hence the power consumption of the system.

ratio of its shear stress to shear rate as a function of, say, shear rate. If one chooses the latter, one has a simple comparison with a Newtonian fluid because in the limiting case, a Newtonian, the ratio of shear stress to shear rate is not a function of shear rate. Of course, the choice is arbitrary. The latter was chosen in this case to simplify the visualization of the behavior of the non-Newtonian fluid.

In order to pinpoint the shear-rate range in a mixing system, one may devise a means of measuring the apparent viscosity of the system and then determine its relation to the other variables of the system. To define apparent viscosity one may consider two identical sets of mixing equipment, one of which contains a Newtonian fluid and the other a non-Newtonian. If these fluids are agitated in the laminar region, with the same impeller speed used in each, and one varies the viscosity of the Newtonian by diluting it or thickening it so that the power measured at each impeller is the same, then, because all variables are identical, one may say that the average viscosities are the same in both pieces of equipment. Upon measuring the viscosity of the Newtonian fluid one knows the apparent viscosity of the non-Newtonian existing under the given experimental conditions.

The preceding experiment defines the apparent viscosity in the system. It is necessary to determine its dependence on the variables of the system. In this paper it is assumed that the fluid motion in the general region of the impeller can always be characterized by an average shear rate which is linearly related to the rotational speed of the impeller, viz:

$$\left(\frac{du}{dr}\right)_{\text{average}} = kN \quad (2)$$

If this line of reasoning is followed, the only necessary fluid properties are the apparent viscosity and density, although the latter would not be expected to be a significant variable in the laminar region. Until means are developed both for measuring and averaging shear rates the evaluation of k in Equation (2) must be done indirectly.

In Figure 6 the power number for a 2.5% CMC solution is plotted as a function of impeller speed in the system previously described. Since the comparable Newtonian data for this system are known (22), the viscosity which a Newtonian fluid would have under identical conditions of speed and power consumption in the same equipment can be obtained merely by referring to the Newtonian power-number curve. According to the preceding arguments, this must be identical to the apparent viscosity of the non-Newtonian. When the apparent viscosity is thus obtained, reference may be made to the visco-

metric curve for the fluid (such as Figure 5) to obtain the corresponding average shear rate in the system. The best value for the proportionality constant k in Equation (2), obtained in this manner, was 13. Consideration was given to all fluids and T/D ratios studied in the laminar region. It may be noted that only data in the laminar region are useful for this purpose as power data outside the laminar region are insensitive to viscosity.

RESULTS

The non-Newtonian materials tested were two colloidal suspensions, CMC or sodium carboxymethylcellulose (Hercules Powder Company) and Carbopol 934 (Goodrich Chemical Company) and a suspension of Attasol clay (Attapulugus Mineral and Chemical Company). As shown in Figure 5, two concentrations of CMC and of Carbopol and one of Attasol were used. On a logarithmic diagram such as Figure 5 the linear shear-stress-shear-rate relationship of Newtonian fluids appears as a straight 45-deg. line ($n = 1.00$). The deviation from Newtonian behavior, therefore, is indicated by the divergence of the slope from the value of unity. Attasol was accordingly the most non-Newtonian ($n = 0.24$) of the fluids tested. Because all these materials were of the pseudoplastic type the slopes of the curves were all less than unity. The Attasol-clay suspensions of the concentration studied are frequently termed *Bingham plastic* by the engineering literature and the

other materials are commonly, and correctly, termed *pseudoplastic*.

The apparent viscosity of a given material at a particular shear rate was determined by dividing the shear stress by the particular shear rate. An important point to note here is that the shear rates in Figure 5 were not calculated by presuming a shear-stress-shear-rate relationship, nor were they calculated by assuming that the shear rates were those which a Newtonian fluid would exhibit in the same viscometer. Both these erroneous attacks, common in the literature, are not necessary at the present state of the art. (Cf. Appendix C.) The variation of the viscometric data with temperature was shown to be negligible for the small variations in room temperature encountered and were not always recorded.

Figure 7 shows the power correlation for all the materials tested. Of over 130 data points taken, all but ten lie within 15% of the curve drawn through the data. The ranges of data were as follow:

Impeller diameters	2 to 8 in.
Tank diameters	6 to 22 in.
T/D	1.3 to 3.7 (laminar region) 2.0 to 5.5 (transition region)
Power input	0.5 to 176 hp./1,000 gal.
Speed	95 to 1,190 rev./min.
Apparent viscosity	7 to 180 poises
Reynolds number	2.0 to 270

Both baffled ($B = 0.1T$) and unbaffled systems were studied. The equipment used is described in Appendix B; the

TABLE 4. MIXING-RATE DATA

Run	Fluid	Minimum h.p./1,000 gal.*	Minimum N_{Re} *	T/D
Movement at wall of tank				
2	2.0% CMC	40.2	87.4	2.95
14	Attasol	21.6	122.	2.95
3A	1.0% CMC	8.66	94.0	2.95
12	Carbopol	50.0	49.0	1.97
†	Carbopol	74.0	42.5	2.00
15	Attasol	16.8	75.8	1.97
17	Attasol	5.09	32.4	1.48
13	Carbopol	27.7	9.8	1.33
Movement of fluid surface				
3A	1.0% CMC	53.1	268.	2.95
8	1.0% CMC	17.3	81.7	3.00
15	Attasol	35.8	113.	1.97
5	1.0% CMC	23.0	94.0	2.00
17	Attasol	35.0	98.0	1.48
	Median of all:	25-35	50-100	

*Minimum values at which fluid movement could first be observed visually.

†Run taken in conjunction with run 10. See footnote ** in Table 3 [footnote on page 6].

detailed dimensions of the equipment and the experimental data are tabulated in Tables 1 to 4.*

DISCUSSION OF RESULTS

Laminar Region

With the exception of 1.0% CMC and the Attasol suspension, Table 3 and Figure 7 show that all fluids were studied in the laminar region in at least one run. The agreement between the data and the conventional Newtonian correlating curve is good.

Transition Region

In general, the gradual development of turbulence and departure from laminar behavior may be stated to be due to the formation of eddies. Consideration of the flow properties of the pseudoplastic

ventional form, and since Newtonian systems leave the laminar region at a power number of 7.1 no conceivable change in Reynolds number could shift the curve to coincide with the usual Newtonian behavior, shown as a dashed line in Figure 7. Furthermore, the data indicate that baffling had no effect on power consumption under the conditions evaluated; hence this extension of the laminar region was found to be common to baffled as well as to unbaffled systems. The more gradual transition from laminar to turbulent flow for pseudoplastic fluids has also been shown to occur in flow through pipes (12), and Brown and Petsiavas (2) noted the same behavior in independent mixing studies.

Validity of Assumptions

The correlation of Figure 7 confirms the basic assumption made [Equation (2)] regarding the relationship between shear rate and impeller speed, at least over the range of variables investigated and in both the laminar and transition regions. The conclusion that the average shear rate, hence apparent viscosity, of the non-Newtonian fluid depends only on the rotational speed of the impeller may not, at first glance, appear to be obvious. However, supporting evidence may also be obtained from Equation (10) for the shear rate at the bob of a viscometer in an infinite fluid. In this case the rate of shear also depends only on the rotational speed, and not on dimensions of the bob. In the laminar region the analogy between a viscometer bob and the impeller of a mixer is rather close, since as a matter of fact, many commercial viscometers employ bobs which are geometrically similar to mixing impellers. In both the laminar and transition regions investigated in this work the impellers generally behaved as though in an infinite fluid since changing the distance between the tip of the impeller and the wall of the tank (i.e., changing the T/D ratio) had no effect on power consumption. As will be discussed later, this is in agreement with extensive work on Newtonian fluids. However, as the T/D ratio decreases toward unity, i.e., as the diameter of the impeller approaches that of the tank, a point must eventually be reached where the shear rate, hence power consumption, is at least partly dependent on either the T/D ratio (clearance between impeller and tank wall) or the peripheral speed of the impeller or both. It appears plausible that at T/D ratios close to unity the shear rate at the impeller may take a mathematical form similar to that for a bob-and-cup viscometer, Equation (6).

Reconciliation of data in previous papers on non-Newtonian fluid agitation might appear desirable to extend the results of this work; however, sufficiently detailed tabulations of experimental data were not available from one source (2)

and the other two papers (9, 23) either did not measure the rheological properties of the fluid or worked with only slightly non-Newtonian systems. One may, however, cite the work of Magnusson (9) to extend the generality of the unique relationship between average shear rate and rotational speed of the impeller, as follows.

Equation (2) implies that scale-up of a model should be carried out at constant speed for a given non-Newtonian fluid, so that the flow properties of the fluid may be identical in the prototype and the model. Figure 7 proves this for the flat-bladed turbines of the present work, and Magnusson's data confirm this for two S-shaped paddles with diameters of 2.8 and 6.2 in. It may be concluded that since the same type of relationship between shear rate and impeller speed

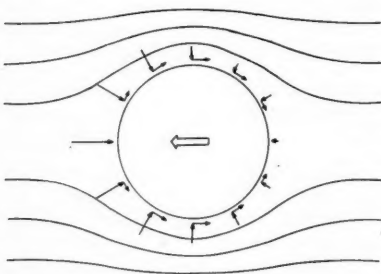


Fig. 3. Flow of a Newtonian fluid about a sphere.

fluids used in this work shows that their apparent viscosity must increase with increasing distance from the impeller, in view of the lower velocities, hence shear rates, of the fluids as they leave the vicinity of the impeller. A small volume of fluid leaving the high-shear-rate region near the impeller therefore encounters progressively more viscous material. This, in turn, would cause a depressive effect on the propagation of eddies. The last factor would tend to decrease the rapidity with which the power-number-Reynolds-number curve begins to diverge from the 45-deg. line of the laminar region as the fluid becomes more non-Newtonian in the direction of greater pseudoplasticity (n approaching zero). The net result of this behavior should be an extension of the laminar region to Reynolds numbers above 10 or to power numbers below 7.1, the point at which Newtonian fluids enter the transition region. Figure 7 shows that such a retardation was indeed observed. It must be emphasized that this extension of the laminar region is not due to the particular form of the Reynolds number chosen in this work. The power number is used in its con-

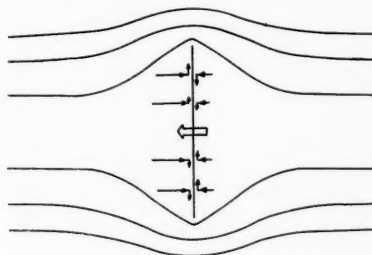


Fig. 4. Flow of a Newtonian fluid about a flat plate.

holds for two greatly different types of impellers, as well as for various different fluids, it appears to be of general utility. No data are available, however, to confirm the constancy of k at a value of 13.0 for systems other than those discussed here. In particular, k might be expected to vary with the flow-behavior index n of the fluid, which was not varied widely in the present studies. [Cf. Equation (10).] It should be noted in passing that scale-up procedures cannot be carried out in the usual sense of the term, however, because the Reynolds numbers will not be identical in the prototype and model when N , ρ , and μ_s are all held constant.

Ranges of Variables

The power range encompassed in this study was higher than the range which is used industrially for Newtonian fluids (16), because pseudoplastic non-Newtonian fluids are inherently more difficult to agitate. Since the exact power requirements for different levels of mixing rate are not yet known for these materials, the power input was varied over an extremely wide range to ensure applicability of the results to industrial conditions.

While the range of Reynolds numbers covered was only 130-fold, it is the range in which viscous, highly non-Newtonian fluids are most likely to be agitated. With less viscous non-Newtonians the range

* Tabular material has been deposited as document 5119 with the American Documentation Institute, Photoduplication Service, Library of Congress, Washington 25, D. C., and may be obtained for \$1.25 for photoprints or 35-mm. microfilm.

may be extended to higher Reynolds numbers, but usually the same highly non-Newtonian character is not observed in such less viscous systems.

Effect of Geometric Variables

The position of the impeller did not critically affect power consumption when vortices were not formed. Vortices could be formed, however, if the impeller were placed closer to the surface than specified in Appendix B.

No consistent effects due to baffling or T/D ratios greater than 2 were found, which is in agreement with the work of Rushton et al. (22). Hirsekorn and Miller (5) report that in the laminar region T/D can be made much smaller than the value of 2 reported by Rushton. Runs 13 and 17, with T/D ratios of 1.33 and 1.45 respectively, indicate that these

must be a function of $(D^2 N^{2-n} \rho) / g_c K$ and n . The function of n cannot be evaluated for mixing work at present but the assumption that it is the same as in the pipe-flow case, i.e. power number is a function of $[(D^2 N^{2-n} \rho) / g_c K] [8(n/6n + 2)^n]$ or $(D^2 N^{2-n} \rho) / \gamma$, yields a Reynolds number which is numerically proportional to the $(D^2 N \rho) / \mu_a$ reported here. Further, more extensive data are needed to determine whether use of the generalized Reynolds number in mixing work is of widespread generality or merely a coincidence in the case of the present data.

Quality of Mixing

The type of flow or the quality of mixing is, of course, the end result of the choice of a given agitator. However, as mentioned before, the logical procedure for studying agitation is first to determine

Although decreasing the T/D ratio to nearly unity would almost certainly reduce the Reynolds numbers, and hence the power required for complete movement of the fluid, it appears questionable whether this power reduction would be great enough to bring the power consumption at a given mixing rate down to the level of Newtonian fluids. Most of the data of Table 4 do, however, show an appreciable decrease in power required to mix a given fluid completely (as defined by movement at the tank wall) as T/D is decreased. Such complete fluid turnover does not, on the other hand, imply higher shear rates, as these are probably affected adversely by use of larger impellers (lower T/D ratios) and lower rotational speeds, as shown by Equation (2). Thus it is more difficult to obtain simultaneously both high rates

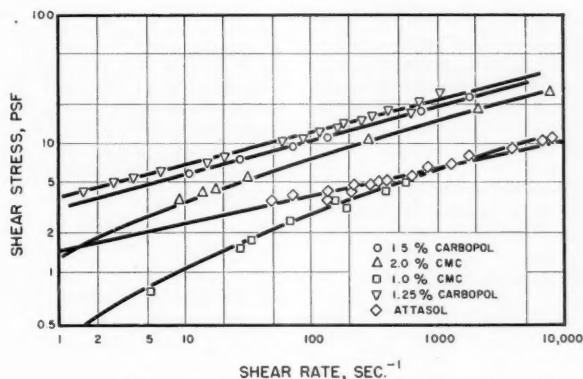


Fig. 5. Flow curves of fluids used.

conclusions are valid also for non-Newtonian materials in both the laminar and transition regions. However, the number of data points available is too small to support such a conclusion firmly.

Similarity to Pipe Flow

An interesting similarity appears to exist between the means of correlating pipe-flow data and mixing-power-consumption data which suggests an alternate means of correlation for the latter. For a non-Newtonian fluid which obeys Equation (1) it may be readily shown that the friction factor for pipe flow is a function of $(D^2 V^{2-n}) / g_c K \cdot 8(n/6n + 2)^n$, which is a special form of the generalized number $(D^2 V^{2-n} \rho) / \gamma$ proposed for pipe-flow work (12). One will notice that these groups both degenerate to the usual Reynolds number for Newtonian fluids ($K = \mu / g_c$ and $n = 1.00$). Application of dimensional analysis to the mixing problem (with the only important length dimension assumed to be the impeller diameter) shows that the power number

the amount of power dissipation and then to turn to the more complex problem of mixing patterns and rates. The measures of the rates of mixing studied to date (Table 4) are, therefore, qualitative. Nevertheless, several important conclusions may be drawn at this time concerning the comparative rates of mixing of Newtonian and non-Newtonian fluids at a given power input per unit volume of fluid.

Hirsekorn and Miller (5) found that particles could be suspended in viscous Newtonian fluids during agitation within the laminar region (N_{Re} below 10). The maximum power input required to suspend the particles was 6.0 hp./1,000 gal. of fluid. While the data of Table 4 are very irregular in the sense that Reynolds numbers and power requirements for movement of all the fluid vary widely, in only one case out of thirteen was reasonably complete fluid movement attained in the laminar region and, again in only one case, was any fluid movement at the tank wall noticeable at power inputs as low as 6.0 hp./1,000 gal.

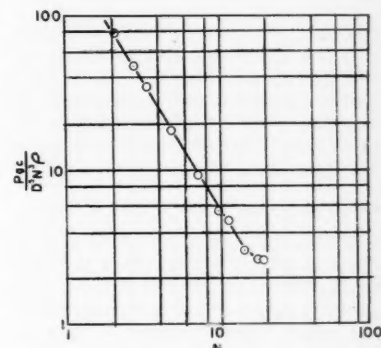


Fig. 6. Power number vs. impeller speed for 2.5% CMC.

of fluid turnover and high shear rates in these non-Newtonian systems without high power requirements.

Until really definitive data become available, adoption of the median values of power input and Reynolds numbers given in Table 4 is suggested as the criterion below which mixing will frequently be ineffective in these non-Newtonian systems. Some confirmation of these high power-input levels may be obtained from industrial practice: in one installation the mixing of non-Newtonian fluids is in the range of 5 to 50 hp./1,000 gal. in full-scale equipment, while pilot plant work (indicative of future operations) ranges from 50 to 160 hp./1,000 gal. This industrial experience also indicates that to date no enormously improved agitator or system designs which might be particularly suitable for the non-Newtonian fluids described here have been developed. Fundamentally, this problem arises because the apparent viscosity of a pseudoplastic fluid increases with distance from the impeller; hence the fluid tends to "set up," or

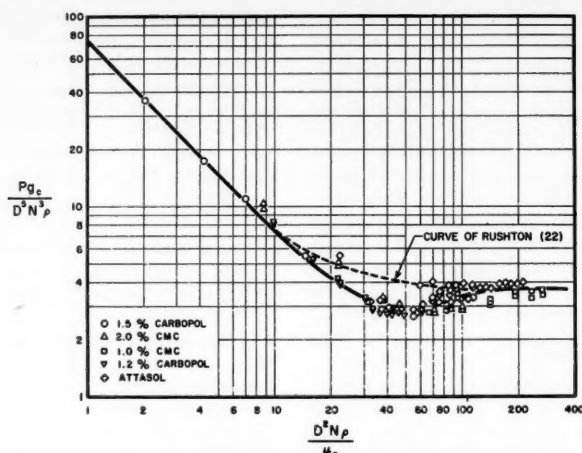


Fig. 7. Power-number-Reynolds-number curve for non-Newtonian fluids; all points in the crowded regions not shown.

remain motionless, under conditions where a Newtonian fluid is mixed relatively completely. Therefore the problem is somewhat alleviated by use of multiple impellers inside a single tank and by use of very low T/D ratios in the industrial examples cited.

Design Procedure

Within the laminar region ($N_{Re} < 20$ when n ranges between about 0.25 and 0.45, and $N_{Re} < 10$ when $n = 1.00$) conditions are sufficiently well defined for the mixing equation, which is somewhat analogous to Poiseuille's law for friction in a round tube, to be written as suggested by Rushton and Oldshue (21). This equation is the same for Newtonian and non-Newtonian fluids:

$$N_p = 71/N_{Re} \quad (3)$$

Substitution of the definitions of the Reynolds numbers used in this work gives

$$P = \frac{71\mu_a}{g_c} D^3 N^2 \quad (4)$$

It has been suggested that these equations are particularly useful for design purposes. The constant given was developed for Mixco turbines with six flat blades and is dependent on the particular type of impeller used. As would be expected from the analogous problem of flow in tubes (12), highly non-Newtonian fluids with a flow-behavior index n near zero show a smaller change of power with impeller speed than do Newtonian fluids ($n = 1.00$), since μ_a decreases as N increases.

Under any flow conditions the recommended procedure for estimating power consumption once the type, size, and speed of the impeller have all been fixed may be reviewed as follows:

1. Knowing N , one may evaluate kN [Equation (2)] to determine the average shear rate in the system.

2. From viscometric data (shear stress vs. shear rate) for the fluid in question, μ_a is calculated at the above-average shear rate.

3. The Reynolds number ($D^2 N \rho / \mu_a$) is then calculated and the corresponding power number read from Figure 7.

As the procedure is empirical, extrapolation of the variables beyond the ranges covered cannot be recommended.

CONCLUSIONS AND SUMMARY

1. The assumption that average fluid shear rates are related only to impeller speed has led to an understanding and correlation of the power requirements for agitation of non-Newtonian fluids. The quantitative relationships, which are applicable to both Newtonian and non-Newtonian fluids over the ranges of variables investigated, represent a simple generalization of the well-known results from Newtonian systems.

2. The laminar region may extend to higher Reynolds numbers in pseudoplastic fluids than in Newtonian systems.

3. Preliminary qualitative observations indicate that more power is required for the rapid mixing of highly non-Newtonian systems than for Newtonian fluids.

RECOMMENDATIONS FOR FURTHER WORK

1. Although data were taken on 8-in. impellers, the limitations of the present equipment did not allow high rotational speeds for these larger systems. Therefore, in order to approach plant-scale conditions more closely one must extend the data to larger and more powerful mixing systems.

2. In some commercial installations the T/D ratio may be smaller than the values studied in the present work. Limited data indicate that the power consumption may not be significantly affected by such changes, but this influence of small values of T/D should be investigated further for both Newtonian and non-Newtonian fluids.

3. The quality of mixing of Newtonian

as well as non-Newtonian fluids requires quantitative study.

4. Extension of the present work to a greater variety of non-Newtonian fluids, including dilatant materials, should be of considerable interest to prove conclusively whether or not the value of k [Equation (2)] depends on the flow behavior index of the fluid and whether the generalized Reynolds number is truly applicable to correlation of power-consumption data for all fluids.

ACKNOWLEDGMENT

The authors would like to thank J. Y. Oldshue and the Mixing Equipment Company for their assistance in designing equipment and J. H. Rushton and J. Y. Oldshue for reviewing the manuscript. The Attapulgis Clay and Mineral Company and Continental Diamond Fibre Company are to be thanked for donating test materials and equipment, respectively. This work was sponsored by the Office of Ordnance Research, U. S. Army.

NOTATION

NOTE:—Since the final correlation is based on dimensionless groups, any consistent set of units may be used. The units given in the following table refer to those used by the authors in the data tables unless specific units are given.

B	= width of baffles, ft.
C	= height of impeller off bottom of tank, ft.
D	= impeller diameter or bob diameter, ft.
g	= gravitational acceleration, ft./sec. ²
g_c	= conversion factor, (lb. mass)(ft.)/(lb. force)(sec. ²)
h	= height of viscometer bob, ft.
K	= fluid property in Equation (1), (lb. force)(sec. ^{n} /sq. ft.)
k	= proportionality constant, dimensionless
L	= length of pipe or capillary, ft.
N	= rotational speed, rev./sec.
N_p	= power number, dimensionless, $Pg_c / D^5 N^3 \rho$
N_{Re}	= Reynolds number, dimensionless, taken as $(D^2 N \rho) / \mu_a$
n	= flow-behavior index, dimensionless

$$n' = \frac{d \ln (\Delta p D / 4L)}{d \ln (8Q / \pi D^3)}$$

$$n'' = \frac{d \ln (2t / \pi D_i^2 h)}{d \ln (4\pi N / 1 - 1/s^2)}$$

P	= power, (ft.)(lb. force)/sec.
p	= pressure, lb. force/sq. ft.
Q	= flow rate, cu. ft./sec.
r	= radius, ft.
S	= scale reading, lb. force
s	= D_o / D_i
T	= tank diameter, ft.
t	= torque, ft.(lb. force)
u	= point velocity, ft./sec.
V	= volumetric average velocity, ft./sec.

- γ = generalized viscosity coefficient,
 $\gamma = (g_c K) / 8 \cdot (6n + 2/n)^n$, lb. mass/(ft.) (sec.^{2-n})
 Δ = difference of
 μ_a = apparent viscosity, lb. mass/(ft.)
 (sec.)
 ρ = density, lb. mass/cu. ft.
 τ = shear stress, lb. force/sq. ft.

Subscripts

- i = bob wall
 0 = cup wall

LITERATURE CITED

- Alves, G. E., D. F. Boucher, and R. L. Pigford, *Chem. Eng. Progr.*, **48**, 385 (1952).
- Brown, G. A., and D. N. Petsiavas, paper presented at New York A.I.Ch.E. Meeting (December, 1954).
- Christiansen, E. B., N. W. Ryan, and W. E. Stevens, *A.I.Ch.E. Journal*, **1**, 544 (1955).
- Hedstrom, B. O. A., *Ind. Eng. Chem.*, **44**, 651 (1952).
- Hirsehorn, F. S., and S. A. Miller, *Chem. Eng. Progr.*, **49**, 459 (1953).
- Hunsaker, J. C., and B. G. Rightmire, "Engineering Applications of Fluid Mechanics," McGraw-Hill Book Company, Inc., New York (1947).
- Krieger, I. M., and S. H. Maron, *J. Appl. Phys.*, **25**, 72 (1954).
- Mack, D. E., and V. W. Uhl, *Chem. Eng.*, **54**, 119 (1947).
- Magnusson, Karl, *Iva. (Sweden)*, **23**, 86 (1952).
- Matthews, T. A., II, private communication (April 29, 1954).
- Metzner, A. B., *Chem. Eng. Progr.*, **50**, 27 (1954).
- , and J. C. Reed, *A.I.Ch.E. Journal*, **1**, 434 (1955).
- Metzner, A. B., in "Advances in Chemical Engineering," Vol. I, Academic Press, Inc., New York (1956).
- Mooney, Melvin, *J. Rheol.*, **2**, 210 (1931).
- O'Connell, F. P., and D. E. Mack, *Chem. Eng. Progr.*, **46**, 358 (1950).
- Oldshue, J. Y., private communication (1954).
- Otto, R. E., Ph.D. thesis, Univ. Delaware, Newark (1957).
- Reed, J. C., M.Ch.E. thesis, Univ. Delaware, Newark (1954).
- Reiner, M., "Deformation and Flow," H. K. Lewis and Company, London (1949).
- Rushton, J. H., *Ind. Eng. Chem.*, **47**, 582 (1955).
- , and J. Y. Oldshue, *Chem. Eng. Progr.*, **49**, 161 and 267 (1953).
- Rushton, J. H., E. W. Costich, and H. J. Everett, *Chem. Eng. Progr.*, **46**, 395 and 467 (1950).
- Schultz-Grunow, F., *Chem. Ing. Tech.*, **26**, 18 (1954).
- Severs, E. T., and J. M. Austin, *Ind. Eng. Chem.*, **46**, 2369 (1954).
- , private communication (1956).

APPENDIX

A. Definitions of Non-Newtonian Behavior

Figure 8 illustrates on arithmetic coordinates the classical definitions used by

rheologists. These definitions are based on the relationship between the shearing stress imposed on a fluid, τ , and the resulting shear rate, du/dr , as measured in various kinds of viscometers. Newtonian fluids show the familiar straight-line relationship, the slope of the line being defined as the viscosity of the fluid. A Bingham-plastic fluid is defined as one which also shows a linear relationship between shear stress and shear rate, but the relationship does not pass through the origin. Pseudoplastic and dilatant fluids do not show a linear relationship. Figure 9 shows the equivalent logarithmic plot.

For the Newtonian fluid the ratio of shear stress divided by shear rate is a constant and defined as the viscosity of the fluid. For the non-Newtonian, the equivalent, or "apparent," viscosity is not a constant. Instead the ratio of shear stress divided by shear rate changes with shear rate. For Bingham-plastic and pseudoplastic materials this ratio decreases with increasing values of shear rate; for dilatant materials it increases.

There are two other kinds of non-Newtonian behavior, termed *thixotropy* and *rheopexy*. The apparent viscosities of thixotropic and rheopexic fluids depend on the time of shear as well as on rate of shear. These two kinds of behavior have been too complex to study and, since they are of less frequent industrial importance, will not be discussed here. Industrially, pseudoplastic behavior is probably more important than the other types of non-Newtonian behavior combined.

All the foregoing definitions are restricted to materials which do not exhibit elastic recovery or "viscoelasticity." That is to say, once they have been sheared there is no tendency for the fluid to return to its original shape or configuration. The necessity of this assumption may prove to be a more serious limitation of the present work than the assumed absence of thixotropy and rheopexy but cannot be dealt with until the engineering problems of design for pseudoplastic, Bingham-plastic, and dilatant behavior have been well-developed.

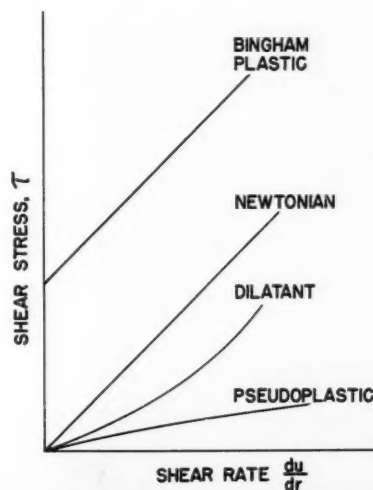


Fig. 8. Fluid characteristics (arithmetic scale).

These classifications are discussed in more detail elsewhere (1, 4, 11, 13, 19, for example). Many engineering publications have been concerned with fluids which were believed to be of the Bingham-plastic type. At the beginning of the present experimental program extensive determinations of the shear-stress-shear-rate relationships of fluids which have been claimed to be Bingham plastics led to the conclusion that true Bingham plastics probably exist only very rarely, if at all. Except for a few specially prepared materials this type of behavior broke down over shear-rate ranges greater than about 1:100.

B. Experimental Apparatus and Procedure

The mixing equipment used in this work is shown in Figures 10 and 11. It consisted of a $\frac{1}{4}$ -hp. variable-speed motor, four Mixco Standard flat-bladed turbines (Mixing Equipment Co.), and four cylindrical tanks. To measure torque accurately, the motor was mounted on a large ball-bearing ring fixed in a cast-aluminum plate; the motor rotated freely with very little friction. The reaction torque developed by the motor in driving the turbine was taken from the motor by a torque ring attached to the motor head and transferred by a small, essentially frictionless pulley to a dynamometer scale. The turbine shaft was fitted inside a special hollow shaft provided on the motor by the manufacturer (Mixco) so that the shaft height was variable. Turbine speeds were measured by an electric tachometer geared to the motor shaft.

Four cylindrical flat-bottomed tanks 6, 8.2, 11.6, and 22 in. in diameter were used in this work. The smallest was a beaker, the next two were Pyrex tanks, and the final one was a 55-gal. drum. All tanks except the smallest one were fitted with four removable baffles with a width of one tenth of the tank diameter.

The impellers which were used had diameters of 2, 4, 6, and 8 in. The ratios of the width and length of the impeller blades relative to their diameter were 1:5 and 1:4 respectively. With the smallest flat-bladed turbine the torque readings were too low

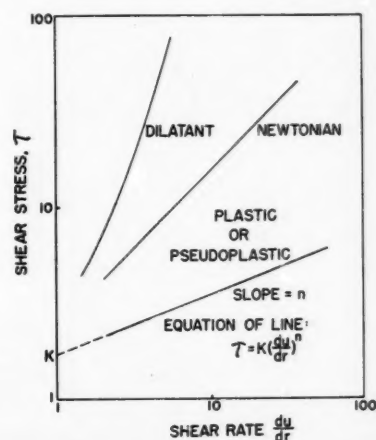


Fig. 9. Fluid characteristics (logarithmic scale).

for the dynamometer scale; hence a torque table was improvised from a dead-weight tester connected through a system of pulleys to a smaller spring scale.

In order not to vary a large number of geometric variables at once, the fluid level in the tanks was maintained at one

tank diameter. The impeller was placed at one impeller diameter off the bottom of the tank unless this placement brought the impeller within one impeller diameter of the fluid surface. In this case the impeller was centered halfway between the liquid surface and the tank bottom.

Rheological properties were measured both on a Stormer rotational viscometer and with a capillary-tube viscometer (Figure 11). The capillary-tube viscometer was an instrument used for the extrusion of plastics (24).

The fluid to be tested was placed in a stainless steel pressure chamber and extruded under pressure from a capillary tube mounted in the bottom of the chamber. The flow rate of the fluid was measured by use of a stop watch and a weighing balance. The extrusion pressure was supplied by a nitrogen cylinder and was measured on laboratory test gauges. During the experimental runs the pressure chamber was surrounded by water to control the temperature.

The Stormer viscometer was modified in that a smooth-walled cylinder was used for the cup. End effects on the bob were corrected by calculation of the equivalent bob height from data taken with National Bureau of Standards calibrated oils. This equivalent bob height was about 25% greater than the actual height. The fact that the data (Figure 5 and Table 2) from both instruments coincide within experimental error supports the adequacy of this procedure for accounting for end effects in the rotational viscometer as well as for the absence of any similar problems with the capillary-tube viscometer.

Detailed equipment dimensions are given in Table 1.

C. Viscometry

General equations (which do not require the presumption of a shear-stress-shear-rate relationship) have been reported in the literature; these were used exclusively to interpret the viscometric measurements.

For the rotational viscometer, Krieger and Maron (7) have succeeded in writing an infinite series which converges rapidly for cup-to-bob diameter ratios of less than 1.2:1. Their equations are

Shear stress at the bob:

$$\tau_i = \frac{2}{\pi} \frac{t}{D_i^2 h} \quad (5)$$

Shear rate at the bob:

$$-\frac{du}{dr} = \frac{4\pi N}{1 - 1/s^2} \left[1 + k_1 \left(\frac{1}{n'} - 1 \right) + k_2 \left(\frac{1}{n'} - 1 \right)^2 \right] \quad (6)$$

n'' is evaluated at the shear stress calculated by means of Equation (5). The instrument constants k_1 and k_2 are

$$k_1 = \frac{s^2 - 1}{2s^2} \left(1 + \frac{2}{3} \ln s \right);$$

$$k_2 = \frac{s^2 - 1}{6s^2} \ln s \quad (7)$$

In any one run n'' is the slope of a logarithmic plot of the torque plotted against rotational speed, as all other factors in n'' are constant.

Rabinowitsch's solution of the motion of fluids flowing through a pipe or capillary tube gives upon rearrangement (18)

$$\tau = \frac{\Delta p D}{4L} \quad (8)$$

$$-\frac{du}{dr} = \frac{32Q}{\pi D^3} \left[\frac{3n' + 1}{4n'} \right] \quad (9)$$

Again n' must be evaluated at the corresponding shear stress given in Equation (8). For a given capillary tube n' is found from a logarithmic plot of pressure drop vs. flow rate.

Another general equation given by Krieger and Maron (7) is of use in viscometric equipment approximating a long cylinder rotating in an infinite fluid:

$$\frac{du}{dr} = \frac{4\pi N}{n''} \quad (10)$$

Brookfield viscometers (Brookfield Engineering Laboratories) may fall into this category, depending on the shapes of the bobs used. The shear stress is given by Equation (5). One cannot use the Brookfield conversion factors to determine the apparent viscosity directly because the formulas supplied with the instrument are for Newtonian fluids ($n'' = 1.00$). However, since a Brookfield has several speeds n'' can be obtained from a logarithmic plot of scale reading vs. rotational speed, and the shear rates calculated by means of Equation (10).

For a power-function non-Newtonian [Equation (1)]:

$$n = n' = n'' \quad (11)$$

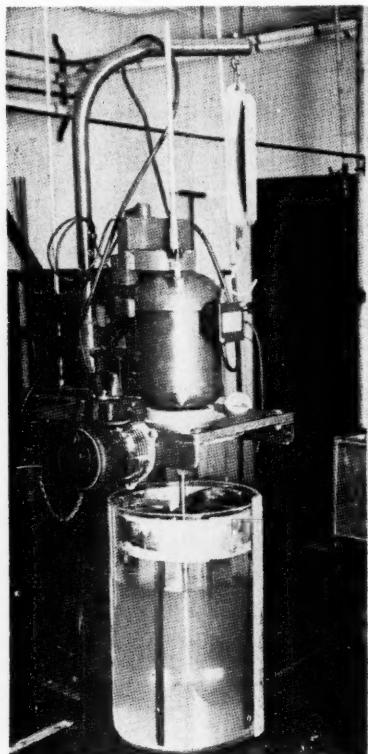


Fig. 10. Mixing equipment.

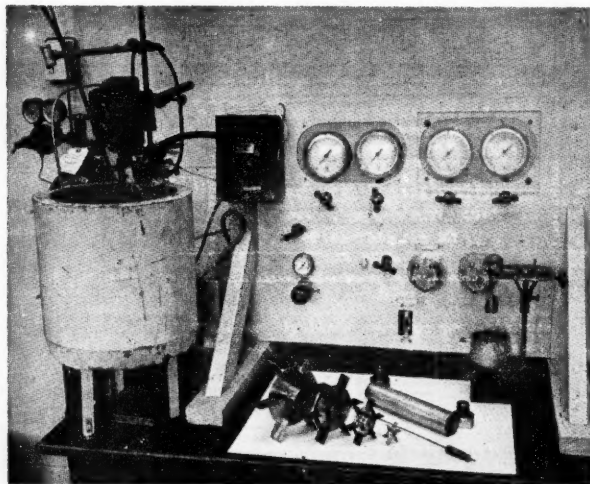


Fig. 11. Impellers and viscometric equipment.

Material Transport in Turbulent Gas Streams: Radial Diffusion in a Circular Conduit

SCOTT LYNN, W. H. CORCORAN, and B. H. SAGE

California Institute of Technology, Pasadena, California

Experimental studies of the mixing of coaxial streams of a natural gas and air at atmospheric pressure were made at Reynolds numbers of 44,000 and 79,000 under conditions where the turbulent-velocity profile of nearly uniform flow was altered as little as feasible by the blending of the two streams.

Total diffusivities of natural gas in air for the region near the center of the conduit were computed from the data for turbulent, steady, nonuniform flow. The total diffusivities were found to be rather complicated functions of the conditions of flow. Limitations in the configuration of the apparatus did not permit a study of the behavior of the total diffusivities to be made over as wide a range of flow rates as would be necessary to investigate the large-scale trends indicated by this study.

The transfer processes in a turbulent stream are considered here to result from a combination of the transport associated with the molecular migration of the components of the phase and the transport due to the relative macroscopic motions resulting from turbulence in the fluid as well as its gross motion across the section. Transfer of material through a unit area of surface by diffusional processes only may be expressed for radial transport as

$$\dot{m}_{Ad} = -D_A \frac{\partial \sigma_A}{\partial r} + \overline{\sigma_A' u_r'} \quad (1)$$

where \dot{m}_{Ad} is the weight of component A transported by diffusional processes per unit area and per unit time. For convenience Equation (1) is often expressed as

$$\dot{m}_{Ad} = -(\epsilon_{DA} + D_A) \frac{\partial \sigma_A}{\partial r} \quad (2)$$

where ϵ_{DA} is the eddy diffusivity for component A. The eddy diffusivity and molecular diffusivity, or Fick diffusion coefficient, may be combined in one term, the total diffusivity, ϵ_{DA} . Equation (2) may then be written as

$$\dot{m}_{Ad} = -\epsilon_{DA} \frac{\partial \sigma_A}{\partial r} \quad (3)$$

Likewise equations for momentum transfer in fluid flow may be developed. The corresponding result to compare with Equation (3) for the case of a fluid flowing uniformly through a straight, circular conduit is

$$\tau = \frac{\sigma}{g} \epsilon_m \frac{\partial u_x}{\partial r} \quad (4)$$

where τ is the shear stress in pounds per square foot. Reynolds (9) proposed that

ϵ_m , the eddy viscosity, and ϵ_r , the eddy conductivity, were equal. Experimental evidence (11) indicates that for practical

purposes a proportionality may be established between ϵ_m and ϵ_{DA} .

It was the intent of the present work to investigate further the nature of ϵ_{DA} in the initial mixing of two concentric streams where the turbulent-velocity profile of the central, main stream was altered as little as possible by the addition of the diffusing component. In particular it was desired to establish the behavior of ϵ_{DA} along the axis of the coaxial streams.

THEORY

For steady state the rate of accumulation of the diffusing component in a fixed element of volume is zero. Therefore the sum of the divergences of the convective and diffusional fluxes of the component is zero or, expressed analytically,

$$-\frac{\partial \sigma_A}{\partial t} = 0 = \nabla \cdot \sigma_A u + \nabla \cdot (-\epsilon_{DA} \nabla \sigma_A) \quad (5)$$

In Equation (5) it is implicitly assumed that there is isotropic turbulence and therefore isotropic eddy diffusivity. Also the Fick diffusion coefficient is assumed to be isotropic in character. The assumptions are not necessary in the development of the final expression for the radial eddy diffusivity but are made to simplify the writing of the equations. If cylindrical symmetry is assumed and diffusional transport in the direction of flow neglected, there is obtained for a perfect gas

$$r \epsilon_{DA} \frac{\partial n_A}{\partial r} = \frac{\partial}{\partial x} \int_0^r n_A u_x dr - n_A \frac{\partial}{\partial x} \int_0^r u_x dr = \frac{\sigma}{\sigma_{air}^0} \quad (6)$$

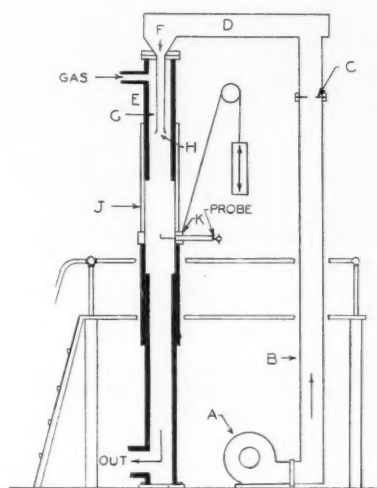


Fig. 1. Schematic diagram of turbulent-diffusion apparatus.

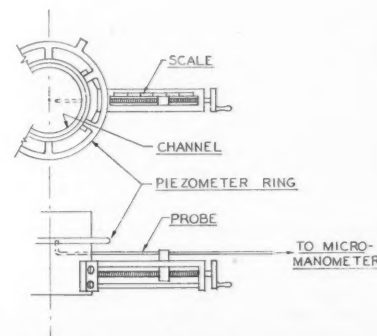


Fig. 2. Arrangement of probe and piezometer ring.

Equation (6) is more easily used in treating experimental data if the integrations are made with respect to $(r/r_0)^2$ where r_0 is the radius of the channel. The transformation then gives for the eddy diffusivity in the r direction

$$\epsilon_{DA} = \frac{\frac{\partial}{\partial x} \left[\left(\frac{r_0}{r} \right)^2 \int_0^{(r/r_0)^2} n_A u_x d \left(\frac{r}{r_0} \right)^2 \right] - n_A \frac{\partial}{\partial x} \left[\left(\frac{r_0}{r} \right)^2 \int_0^{(r/r_0)^2} u_x d \left(\frac{r}{r_0} \right)^2 \right]}{\frac{4}{r_0^2} \frac{\sigma}{\sigma_{air}} \frac{\partial n_A}{\partial \left(\frac{r}{r_0} \right)^2}} \quad (7)$$

The advantages of using the variable $(r/r_0)^2$ are twofold. Derivatives of the composition with respect to $(r/r_0)^2$ do not go to zero at the center of the channel, and the terms being differentiated with respect to x are seen to be simply the space-average values of the respective

integrands from the center of the channel to the point in question.

An expression for the eddy viscosity may be developed also. In the analysis it is assumed that there are cylindrical

symmetry, constant specific weight, and no effect of potential fields and that the time-average velocities in the θ and r directions are zero. With these assumptions, the Navier-Stokes equations, combined with the equation of continuity,

result in the following equation for steady state, turbulent flow:

$$u_x \frac{\partial \left(\frac{\sigma}{g} u_x \right)}{\partial x} = - \frac{\partial P}{\partial x} + \frac{1}{r} \frac{\partial}{\partial r} \left(r \frac{\sigma}{g} \frac{\partial u_x}{\partial r} \right) \quad (8)$$

By use of the same transformation as was applied to Equation (6), the expression for the total eddy viscosity is found to be

$$\epsilon_m = \frac{gr_0^2}{4\sigma} \frac{\partial P}{\partial x} + \frac{r_0^2}{8} \frac{\partial u_x}{\partial \left(\frac{r}{r_0} \right)^2} \quad (9)$$

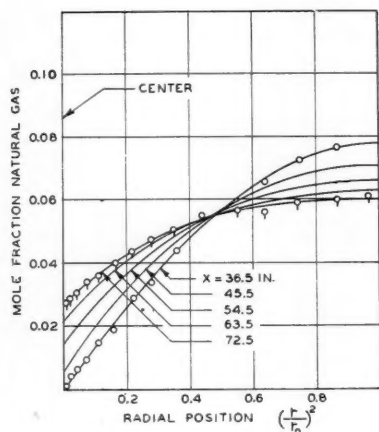


Fig. 3. Composition as a function of the square of the relative radial position—Reynolds number of 44,000.

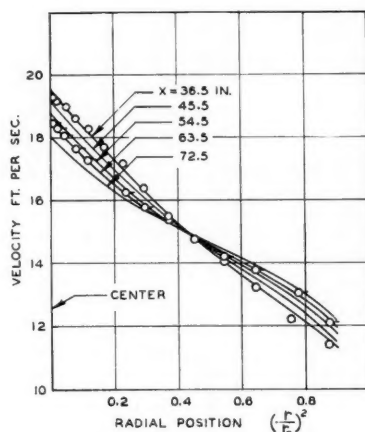


Fig. 5. Velocity as a function of the square of the relative radial position—Reynolds number of 44,000.

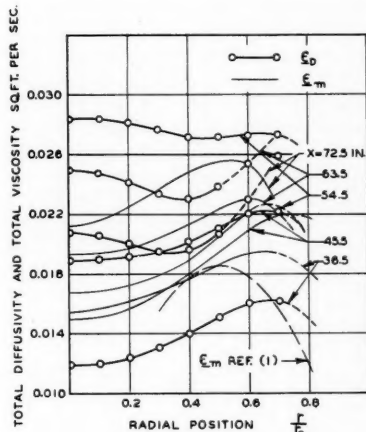


Fig. 6. Total diffusivity, ϵ_D , and total viscosity, ϵ_m , as functions of position—Reynolds number of 44,000.

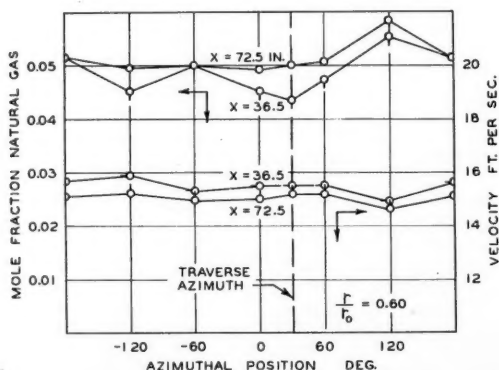


Fig. 4. Variation of velocity and composition with azimuthal position—Reynolds number of 44,000.

Since the pressure drop in gaseous streams at low Reynolds numbers is relatively small, $\partial P/\partial x$ may be approximated from generalized friction-factor data (6) as follows:

$$\frac{\partial P}{\partial x} = \frac{f \sigma (U_x)^2}{gr_0} \quad (10)$$

This expression neglects the effect of diffusion on the shear at the wall. The total eddy viscosity then becomes

$$\epsilon_m = \frac{-r_0^2}{4} \frac{\partial u_x}{\partial \left(\frac{r}{r_0} \right)^2} \left\{ \frac{(U_x)^2 f}{r_0} - \frac{1}{2} \frac{\partial}{\partial x} \left[\left(\frac{r_0}{r} \right)^2 \int_0^{(r/r_0)^2} u_x^2 d \left(\frac{r}{r_0} \right)^2 \right] \right\} \quad (11)$$

In Equation (11) the second term on the

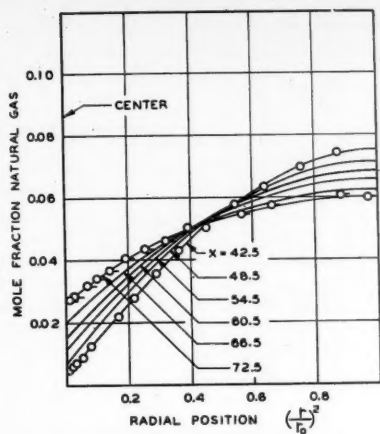


Fig. 7. Composition as a function of the square of the relative radial position—Reynolds number of 79,000.

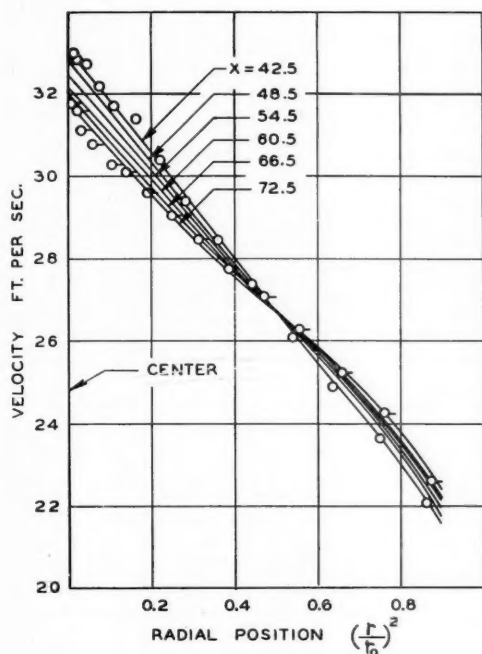


Fig. 8. Velocity as a function of the square of the relative radial position—Reynolds number of 79,000.

right-hand side is the derivative with respect to x of the space-average value of the square of the velocity from the center line to the point in question and becomes zero for uniform flow.

EXPERIMENTAL EQUIPMENT AND PROCEDURES

The equipment used in this study of turbulent diffusion was constructed for an earlier investigation of mass transfer between air and water droplets. Modifications were made to accommodate an annulus for the introduction of natural gas. It was realized that the upstream length from the

mixing section was not sufficient for full development of uniform flow before mixing, but the apparatus was used, nevertheless, because of interest in making at least a preliminary study of the nature of the eddy diffusivity along the center line of the flow channel.

A schematic diagram of the apparatus used in the diffusion measurements is shown in Figure 1. Air at ambient temperature was circulated by the blower *A* through a tube *B* and orifice section *C* to a plenum chamber *D* at the ceiling. Here the air changed direction and was passed down through the test section *E*, which was 6 in. in diameter. The central air stream *F* was concentric with an annulus *G* through which natural gas was introduced. Gas entered the annulus at ambient temperature and at a rate measured by a separate orifice meter. At section *H*, where the natural gas joined the central air stream, the annulus had a nominal width of $\frac{1}{8}$ in. but a difference in radius varying between 0.120 and 0.130 in. The volumetric flow rate of the

The Lucite test section could be moved through a vertical distance of 5 ft. and rotated through an angle of 180 deg. On the test section was mounted a brass sleeve *K* holding the sampling probe with an opening 0.065 in. in diameter. The probe served also as a Pitot tube and could be moved across the diameter of the test section. At the highest traverse position the probe opening was 36.5 in. below the exit of the annulus at *H* of Figure 1. The brass sleeve *K* also served as a piezometer ring for measuring static pressures as shown in Figure 2.

The composition of the flowing stream was established by measuring the specific weight of the phase by means of a special manometer (4) with gas columns 139 in. long. The difference in weight of gas in the two columns was obtained by observing the movement of a bubble in a horizontal capillary tube connecting the two sides of the manometer (3, 7). The equation of state of a perfect gas was assumed in converting the pressure measurements to composition data.

After the velocity and composition data were obtained, they were smoothed by plotting as functions of the square of the relative radial position, $(r/r_0)^2$. The slopes of the curves, $\partial u_x / \partial (r/r_0)^2$ and $\partial n_g / \partial (r/r_0)^2$, were smoothed with respect to $(r/r_0)^2$ and x . The smoothed slopes were integrated to obtain the recorded values of n_g and u_x . This procedure was followed in order to increase the consistency of the results but did not decrease the uncertainty.

EXPERIMENTAL RESULTS

Studies of the mixing of the coaxial streams of air and natural gas were made at ambient temperature. For the first set of measurements the mean gas temperature was 71.6°F., and the bulk velocity was 14.4 ft./sec. The composition of the gas stream was 0.0435 mole fraction natural gas, taken as a mixture of methane and ethane with a mean molecular weight of 18.8, and the remainder was air. The test section had a diameter of 6 in., and the Reynolds number for the run was 44,000.

The composition measurements at a Reynolds number of 44,000 are shown in Figure 3, which also includes experimental points for $x = 72.5$ and 36.5 in. The tabulated experimental data are available (5).

In the development of the composition data for a Reynolds number of 44,000 it was observed that the integral $\int_0^1 n_g u_x d(r/r_0)^2$ indicated a progressive increase in the weight rate of natural gas flowing in the vertical plane common to the traverses. The apparent increase was attributed to transports in the θ direction as a result of concentration gradients. Figure 4 shows the magnitude of the gradients. The composition and velocity data were collected in the vertical plane at $\theta = 30^\circ$, where the concentration gradients in the θ direction were close to a minimum.

It was desired to compute ϵ_D for the natural gas for the case of symmetrical

gas through the annulus was made to correspond roughly to the flow rate in the same annulus located downstream but in a full channel. Also just before reaching the $\frac{1}{8}$ -in. annulus shown in Figure 1, the cross section of the gas stream was contracted slightly to minimize the lateral velocity component of the gas when it joined the central air stream. As the air and gas stream passed through the Lucite test section *J*, measurements of velocity and concentration were made as functions of the radius of the channel and the distance downstream from the point of initial mixing at *H*. At the outlet of the flow apparatus the mixed gases were passed through a flame holder and burned.

flow. Consequently the composition profiles obtained experimentally were corrected. A reasonable basis for such corrections appeared to be an approach leaving the shape of the profiles unchanged as well as the concentration at the center of the channel. The experimental composition profiles were adjusted to follow the equation of continuity for the hydrocarbon constituent by equating the average concentration at each traverse to that at $x = 54.5$ in. The magnitude of the corrections to n_g did not exceed 7% of the local value.

Besides the corrections to n_g described it was also necessary to adjust the velocity 0.2 ft./sec. or about 1% of the center-line velocity at a downstream distance of $x = 72.5$ in. and a Reynolds number of 44,000 in order to satisfy the equation of continuity for the stream as a whole. The velocity data are shown in Figure 5.

From the symmetrical velocity and composition data, values of ϵ_D and ϵ_m were computed by use of Equations (7) and (11) respectively. Figure 6 shows the results. There is also included in Figure 6 a curve showing ϵ_m as obtained (1) for steady, uniform flow between parallel plates.

Another set of measurements was made at a Reynolds number of 79,000, which corresponded to a bulk velocity of 26.4 ft./sec. The mean temperature was 75.2°F. and the composition of the exit stream was 0.0481 mole fraction natural gas.

Smoothed composition data are shown in Figure 7 and Table 1. Figure 8 records the corresponding velocity data. As in the case of the lower Reynolds number, corrections were made to n_g in order to compute ϵ_D for symmetrical flow. Figure 9 depicts the variation of velocity and composition with azimuthal position. Figure 10 shows values of ϵ_D and ϵ_m for the Reynolds number of 79,000. Also shown in Figure 10 is a plot of ϵ_m as obtained for steady, uniform flow between parallel plates (1).

Random fluctuations in the compositions and velocities at a Reynolds number of 79,000 were initially much greater than for the measurements at the lower Reynolds number. To mitigate the condition a grid with triangular holes 0.25 in. on a side constructed from wires 0.1 in. in diameter was placed in the air channel 4.0 ft. above the exit of the annulus. The large-scale fluctuations were substantially reduced. The mean values of the point compositions were, however, essentially unchanged. Also the effect of the grid on the smaller scale turbulence in the stream should have been in a large measure damped out by the time an element of fluid reached the point of the discharge of the annulus (2).

It was observed that the axes of symmetry of the velocity and composition profiles did not correspond to the axis of the channel as they did at the lower

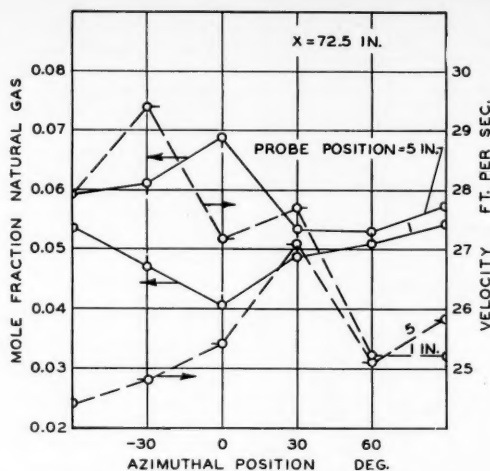


Fig. 9. Variation of velocity and composition with the azimuthal position—Reynolds number of 79,000.

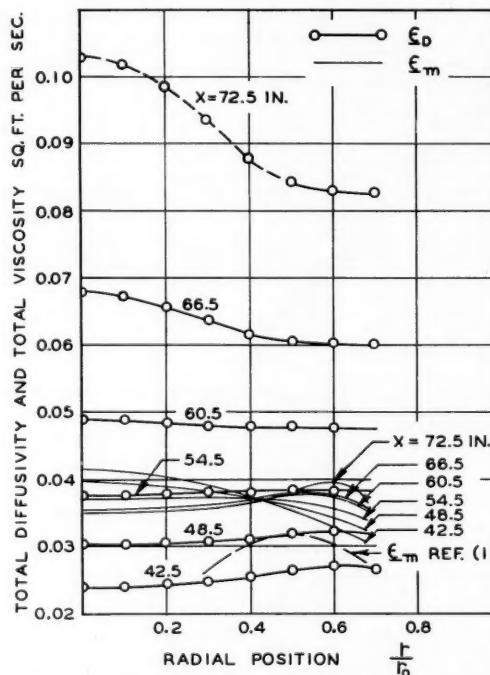


Fig. 10. Total diffusivity, ϵ_D , and total viscosity, ϵ_m , as functions of position—Reynolds number of 79,000.

Reynolds number. As the downstream distance increased, the displacement became greater. At $x = 72.5$ in. the displacement was approximately 0.2 in. The warping of the concentration and velocity profiles was thought to result primarily from eccentricity in both the annulus and the Lucite tube. The maximum variation from the nominal inside diameter of 6 in. for the Lucite tube was 0.03 in.

As a check on the slightly nonuniform flow when diffusion was occurring, velocity profiles were obtained for the case where no natural gas was flowing through the system. Figure 11 shows the results for the case where the total flow rate was approximately the same as for the diffusion experiment at a Reynolds number of 44,000. It can be seen that the nonuniformity was associated with the geometry of the channel and was not

a result of diffusion. The dashed lines represent the regions of greatest uncertainty in the measurements

DISCUSSION OF RESULTS

The Fick diffusion coefficient D for methane in air at 32°F. is 1.7×10^{-4} sq. ft./sec. (10) and the kinematic viscosity for air at 70°F. is 1.64×10^{-4} sq. ft./sec. (8). By comparison of these molecular quantities with the eddy quantities in Figures 6 and 10, the large contribution of turbulent exchange to material and momentum transfer may be observed.

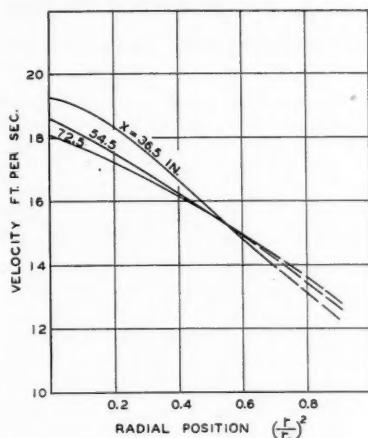


Fig. 11. Change of velocity with distance downstream in absence of diffusion—Reynolds number of 44,000.

Uncertainties in the values of ϵ_D for the particular experimental arrangement stem mainly from the effects of the slight eccentricities in the annulus section and the Lucite tube combined with an insufficient length of straight section before the mixing of the coaxial streams of air and natural gas. The short length of straight section did not allow satisfactory development of normal uniform flow in the central air stream, as the approach was only 8 diameters in length as compared with a recommended value of 45 diameters (12). As a result of the channel geometry there was a θ or azimuthal component of velocity as well as components in the r and x directions. The flow was not then just two-dimensional in the r and x directions. Even though suitable corrections were made for the lack of symmetry, use of a channel allowing strictly two-dimensional cylindrical flow would greatly improve the analysis of the results.

The values of the eddy diffusivity calculated from Equation (7) are sensitive to the change in composition with respect to distance along the flow channel. Eddy diffusivities in the present work are least reliable at the upper and lower ends of

the working section, as at these locations greater corrections were made in the measured composition of the stream. The values of the eddy diffusivity are not believed to involve probable errors greater than 15% for the conditions studied.

In the case of the eddy viscosity, part of the uncertainty arose from the fluctuations in the velocity data. The corrections to composition had no effect on the values of eddy viscosities. Since the pressure drop was not well defined, the error introduced by using data obtained from correlations for pipes has a direct influence on the eddy viscosities, as may be seen from Equation (9). It is estimated, however, that the eddy viscosities do not involve probable errors greater than 15%.

Both the eddy diffusivity and eddy viscosity are most reliable for values of (r/r_0) between 0.3 and 0.6, less reliable near the center of the channel, and least reliable at the walls. The regions of greatest uncertainty are indicated by the dashed curves. The gradation in uncertainty is partly the result of the corrections to the composition profiles and partly a natural consequence of the mathematical treatment of the terms in the equations for the eddy quantities.

CONCLUSIONS

From the consideration of composition and velocity as functions of $(r/r_0)^2$, values of the eddy diffusivity and the eddy viscosity may be established for the central portion of a nearly symmetrically flowing stream. Use of (r/r_0) as the independent variable does not permit direct ascertaining of the center-line values of the eddy properties.

The eddy properties are complicated functions of the particular conditions of flow and channel geometry. In particular, the eddy diffusivity is especially sensitive because of the association between mass transfer of a particular component and momentum transfer. When values of the eddy diffusivity are reported, they should be defined in terms of the particular transfer and channel conditions.

NOTATION

- A_A = Fick diffusion coefficient for component A, sq. ft./sec.
- d = differential operator
- f = Fanning friction factor
- g = gravitational constant, 32.2 ft./sec.²
- $\dot{m}_{A,d}$ = weight rate of component A transport by diffusional process, lb./(sq. ft.)(sec.)
- n_A = mole fraction of component A
- n_g = mole fraction natural gas
- P = pressure, lb./sq. ft.
- r = radial coordinate in the system of cylindrical coordinates, ft.
- r_0 = radius of channel, ft.

- t = time, sec.
- u = vector velocity
- u_r' = fluctuating component of radial velocity, u_r , ft./sec.
- u_x = time-average point velocity in x direction, ft./sec.
- U_x = bulk velocity, ft./sec.
- x = axial coordinate in the system of cylindrical coordinates, ft.
- ∇ = del, a vector operator
- ϵ_c = eddy conductivity, sq. ft./sec.
- ϵ_D = total diffusivity for natural gas, sq. ft./sec.
- $\epsilon_{D,A}$ = eddy diffusivity for component A, sq. ft./sec.
- $\epsilon_{D,A}$ = total diffusivity for component A, sq. ft./sec.
- ϵ_m = eddy viscosity, sq. ft./sec.
- ϵ_m = total viscosity, sq. ft./sec.
- θ = angular coordinate in the system of cylindrical coordinates, radians
- σ = specific weight of system, lb./cu. ft.
- σ_A = time-average point concentration of A, lb./cu. ft.
- σ_A' = fluctuating component of concentration of A, lb./cu. ft.
- $\overline{\sigma_A' u_r'}$ = time average of indicated product, lb./(sq. ft.)(sec.)
- σ_{air}^0 = specific weight of air at temperature and pressure for a given point, lb./cu. ft.
- τ = shear stress in x direction, lb./sq. ft.
- ∂ = partial-differential operator

LITERATURE CITED

1. Connell, W. R., W. G. Schlenger, and B. H. Sage, Document 3657 Am. Doc. Inst., Library of Congress, Washington, D. C. (1952). Price: \$1.00 for photoprint or \$4.65 for 35-mm. microfilm.
2. Davis, Leo, Report 3-17, Jet Propulsion Laboratory, Calif. Inst. Technol. (1952).
3. Henry, A., *Compt. Rend.*, **155**, 1078 (1912).
4. Lynn, Scott, W. H. Corcoran, and B. H. Sage, *Rev. Sci. Instr.*, **27**, 368 (1956).
5. Lynn, Scott, W. H. Corcoran, and B. H. Sage, Document 5122. Am. Doc. Inst., Library of Congress, Washington, D. C. (1957). Price: \$2.50 for photoprints or \$1.75 for 35-mm. microfilm.
6. McAdams, W. H., "Heat Transmission," McGraw-Hill Book Company, Inc., New York (1954).
7. Ower, E., *Reports & Mem. No. 1308*, Aeronaut. Research Comm., Gr. Brit. (1930).
8. Page, Franklin, Jr., W. H. Corcoran, W. G. Schlenger, and B. H. Sage, *Ind. Eng. Chem.*, **44**, 419 (1952).
9. Reynolds, O., *Proc. Manchester Lit. Phil. Soc.*, **14**, 7 (1874).
10. Sherwood, T. K., and R. L. Pigford, "Absorption and Extraction," McGraw-Hill Book Company, Inc., New York (1952).
11. Sherwood, T. K., and B. B. Woertz, *Trans. Am. Inst. Chem. Engrs.*, **35**, 517 (1939).
12. Towle, W. L., T. K. Sherwood, and L. A. Seder, *Ind. Eng. Chem.*, **31**, 462 (1939).

Study of Bubbling Performance in Relation to Distillation and Absorption

JU CHIN CHU, JOHN FORGRIEVE, ROBERT GROSSO, S. M. SHAH, and DONALD F. OTHMER

Polytechnic Institute of Brooklyn, Brooklyn, New York

One of the important factors affecting the efficiency of vapor-liquid contacting operations is the relationship between available interfacial area and contact time.

Because of the difficulties in measuring these quantities, little information has heretofore been made available on them. Previous studies have been confined to extreme oversimplifications of the turbulent type of contacting taking place in fractionation devices. The present investigation consisted of the determination of interfacial area and contact time for the formation of air bubbles submerged in water and aqueous solutions. The bubbles were produced at single vertical slots and rose through a flowing liquid. In order to complete the study on physical contacting, a companion study is concerned with vapor-liquid behavior in the froth and entrainment zones. The experimental technique in this study involved taking high-speed motion pictures of the bubbling action. Measurements of the area and volume of bubbles were made at intervals during the course of their growth, and values of total contact time and average interfacial area per unit volume of vapor are presented.

It was found that both the average interfacial area per unit volume of vapor a and the total contact time t_m were primarily affected by the head of flowing liquid on the slot. Below slot submergence of approximately 2.5 in. of liquid, interfacial area was shown to decrease with increasing slot submergence and increasing slot area. Above 2.5 in. of liquid, interfacial area was a function of skirt clearance, liquid viscosity, and surface tension.

Total contact time was found to increase with increasing slot submergence and to decrease with increasing vapor rate and skirt clearance.

Through the use of an integrated mass transfer-rate equation, the terms a and t_m can be used in conjunction with the appropriate mass transfer coefficient for predicting the point efficiencies on bubble-cap plates.

OBJECTIVES AND SIGNIFICANCE OF THE STUDY

One of the chief problems still confronting the designers of distillation and absorption columns is the accurate prediction of the degree of approach to equilibrium of the contact steps involved, better known as the *efficiency*. In the case of bubble-cap towers, plate efficiencies, as they are called, are expressed in one of the three following terms: (1) over-all plate efficiency, (2) Murphree plate efficiency, (3) point or local Murphree plate efficiency.

Murphree plate efficiency is an integrated average of local Murphree efficiencies at all points across a full plate.

Over-all plate efficiency represents the average of efficiencies for all the plates in a column. The calculation of plate or over-all values from point efficiencies has been well discussed (27).

Correlations for over-all plate efficiency have been proposed (2, 3, 9, 30). Extensive plate-efficiency studies have been reported (18, 19, 20, 32). Walter and Sherwood (43) have developed a useful correlation for local efficiency with the aid of certain simplifying assumptions. Because local efficiency is the "building block" from which the plate and over-all values are obtained, it was felt that the factors affecting this term should be determined.

The purpose of the present study is to investigate the factors affecting local Murphree plate efficiency at single, vertical bubble-cap slots. The factors involved are operating conditions, mechanical design of the tray and bubble

caps, and the physical properties of liquid and vapor of the system. A companion project (19, 26) is concerned with extending these results to the case of multiple slots, analogous to a "full tray" of a bubble-plate tower.

The instantaneous rate of transfer of a single component, present in concentration C , from a volume of vapor V_M to the liquid through which it is rising, can be represented by

$$K_{G,A}(C - C^*) dt = -V_M dC \quad (1)$$

By integrating Equation (1) over the liquid layer through which the vapor bubble rises, one obtains

$$\ln(1 - E_{LM}) = -\int_0^{t_m} \frac{K_{G,A} dt}{V_M} \quad (2)$$

The over-all mass transfer coefficient, $K_{G,A}$, can be assumed practically constant

John Forgrieve is with Esso Research & Engineering Co., Linden, New Jersey; Robert Grosso is with Esso Standard Oil Company, Bayonne, New Jersey; and S. M. Shah is at California Texas Oil Company, Bombay, India.

when the vapor is bubbled through the liquid (2, 3). Thus

$$\ln(1 - E_{LM}) = -K_{G_1} \int_0^{t_m} \frac{A \, dt}{V_M} \\ = -K_{G_1} a_1 t_m \quad (3)$$

For the purpose of the present studies, in which the investigation was divided into two parts of mass transfer phenomena at single and multiple slots, respectively, Equation (3) can be modified by the addition of a froth and entrainment term ($K_{G_2} a_2 t_m$) to

$$\ln(1 - E_{LM}) \\ = -K_{G_1} a_1 t_m - K_{G_2} a_2 t_m \quad (4)$$

Employment of single slotted caps made the extent of the froth and entrainment zones in this study negligible. The experimental portion of this work then involved only the determination and correlation of the terms K_{G_1} and $a_1 t_m$. The terms a and t_m were evaluated by means of high-speed motion pictures of the action of air bubbling through water and aqueous solutions. Mass transfer coefficients were evaluated and correlated from actual point-efficiency data obtained from a distillation system composed of various concentrations of acetone and water (14). These results, together with those for the multiple slot case in which froth and entrainment regions are involved, will provide considerably more insight into the physical mechanisms underlying vapor-liquid contacting on a bubble tray.

REVIEW OF LITERATURE

A search of the literature of the past thirty years reveals that there is considerable disagreement over the pertinent variables affecting bubble formation and that no universally acceptable correlations exist. For purposes of comparison, the previous work can be conveniently classified under two main headings: (1) bubble formation at circular orifices in a horizontal plane (13, 28, 31, 39 to 42) and (2) bubble formation at vertical slots (1, 2, 3, 5, 8, 17, 18, 19, 23, 34, 39, 40, 41). As only the latter topic is of specific interest in this work, a review of investigations of the former is omitted here.

In his semitheoretical treatment of local efficiency, Geddes (17) utilized both a modified form of the static formation equation to obtain bubble size and an empirical formula derived from O'Brien's and Gosline's (29) data to find the ascending velocity. His assumption was that the contact time of a bubble emerging from a slot into a turbulent liquid stream approaches that of an isolated bubble rising in a quiescent liquid column of the same static height. In addition to neglecting the growth period of the

bubble, during which its area is continually changing, Geddes also assumed the bubbles to be spherical in shape.

Davidson (8) presented some results of experiments on bubble formation at both orifices and single slots. Empirically, bubble size calculated by Geddes's equation and multiplied by a factor of three checked with Davidson's data. Davidson's theory that the area for bubbling at the slot is a function only of surface tension and liquid density would seem to apply only when the bubbles are in mechanical equilibrium with their surroundings during formation.

The works of Carey et al. (1) and Rogers and Thiele (34) seem to have confirmed the fact that slot opening is a function of gas rate, liquid density, and slot dimensions. Cross and Ryder (5) have recently improved the Rogers and Thiele equations by including the effect of surface tension.

The study of bubble formation at vertical slots, however, has been reported by Spells and Bakowski (39). Using a high-speed motion picture camera, they investigated the behavior of air bubbles produced at single slots submerged in water and concluded that bubble size was a function of vapor rate, the effect being stronger during the formation of the bubbles at the slot. Submergence not only helped to determine the mode of formation, but also affected the size in the latter case.

Although Spells and Bakowski's paper is of considerable value in providing the first reliable data in a relatively virgin field, their conclusions are subject to some doubt. Specifically, the statement that neither slot characteristics nor liquid properties influenced bubble development was based on a preliminary study which was not supported by quantitative evidence. Previous results on both the slot and orifice studies indicated that such was not the case. The air-flow rates employed were far below those which would be of commercial interest.

The results of a second investigation of bubble formation at submerged slots have recently been published by Spells and Bakowski (39). This study consisted of high-speed motion pictures of the formation of air bubbles in water at multiple vertical slots. It was noted that a vapor rate high enough to open the slots fully was never reached in this work.

From the results and analyses of previous studies, it seems clear that more data are required before an intelligent correlation of the factors affecting bubble formation can be made. Qualitatively, at least, there is an indication that the characteristics of bubbles formed at vertical slots are less dependent upon the physical and mechanical variables of the system than are those of bubbles formed at horizontal orifices.

If the effect of the vapor solubility on bubble size can be assumed negligible

because of the brief contact time, it appears that the gas rate, liquid rate, slot and cap design, liquid submergence, surface tension, and liquid viscosity are principal independent variables governing bubble formation at vertical slots. To a markedly smaller extent, liquid density and vapor properties may exert some effect (2, 3).

Based on this review, a program was set up to study the effect of these variables on the interfacial area and the contact time involved in vapor-liquid contacting. Because a fundamental approach to the type and mechanisms of mass transfer in the bubble-formation region was deemed impractical if multiple slot bubbling took place, the investigation was confined to single-slot behavior.

EXPERIMENTAL EQUIPMENT AND PROCEDURE

Description of Equipment

The experimental apparatus employed for the determination of the bubbling-area-time relationship, a t_m , was designed with the aim of permitting as large a variation in the operating and mechanical factors as possible. Although only the bubbling phenomena at single slots were studied in this program, the equipment is such that adaptations for further work on multiple-slot arrangements may easily be made. The bubble tray and its accessories were patterned, in general, after those used by the C. F. Braun Company for their film on bubble-plate action.

A diagrammatic layout and photograph of the equipment are presented in Figures 1 and 2. The "column" is seen to consist of a single, rectangular, aluminum plate *A* topped by transparent walls and resting on an angle-iron base. The experimental plate was made removable so that different types of caps and cap arrangements might be tested. The walls *B* are constructed of methyl methacrylate (Lucite) joined at the edges by angle iron and held to the plate by angle-iron flanges. Below the plate is a copper surge tank *C*, through which the air enters and the back-trapped liquid leaves. The tank and plate are held by four angle-iron legs *E* with suitable supporting struts welded to them.

Air is supplied by a blower *F* and is metered before being discharged into the tank by an orifice plate *G*, placed in the galvanized-iron duct. Liquid is recycled by pump *H* from the holdup tank *I*, passed through an orifice meter *J* and introduced to the test plate. The space behind the inlet weir is packed with fine-mesh screen *D*, which serves to distribute the liquid flow to the plate. After flowing across the plate, the fluid is finally discharged through the downspout *K* and back into the holdup tank, where it remains long enough to be deaerated.

A pressure tap was soldered to the side of the surge tank with a lead passing to one end of a U-tube water manometer. Since the other end of the U tube was open to the atmosphere, plate pressure drop was obtained directly.

In order to effect a variation in the plate liquid height, Lucite outlet weirs of 1, 1½, and 3 in. were used. These weirs were

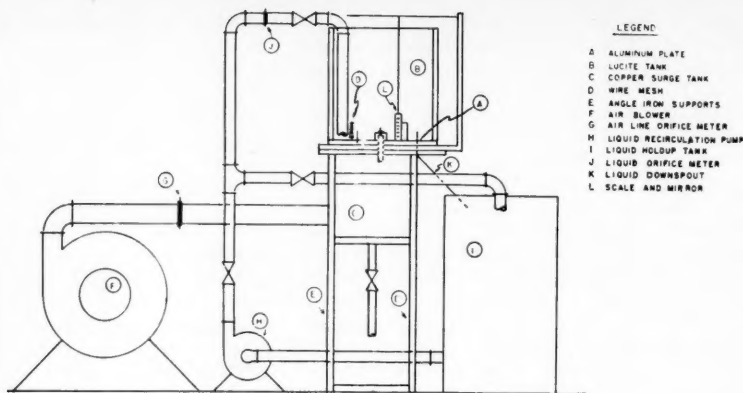


Fig. 1. Equipment for bubble-formation study.

bolted to the downstream end of the test plate.

Accessories

Two sizes of bubble caps were employed. The majority of the tests involved 1.5-in.-diam., 1/16-in. thick, spun-aluminum caps, 1.5 in. high. Various slot sizes were cut out by a milling machine. One set of runs was made by use of a commercial 3-in.-diam. cast-iron cap having a single 1¼- by ⅝-in. triangular slot exposed. The riser used in all runs consisted of a 4-in. length of 1-in. O.D. aluminum tubing threaded into the test plate and had a ⅝-in.-wide cross piece welded across its top. A machine screw, passing through holes in the cross piece and in the cap, served to attach the cap to the riser. An annular spool, having an inside diameter of 1 in., was fitted on top of the riser to reduce the annular flow area for the series of runs using the large cap. A plastic disk with an area 11/12 that of the riser was inserted into the riser for the small cap runs to equalize the riser and slot area. Although a comparison of several films of runs made with and without this riser constriction indicated that it had negligible effect on the results, all data reported here were obtained with the disk present. Drawings of the bubble caps and riser employed are given in Figure 12.

On the test plate itself, a mirror was placed at a suitable angle to the cap slot being photographed, so that two views of the emerging bubbles might be obtained. In addition, a scale was also included in the pictures, so that quantitative measurements were possible *L*.

In order to obtain a variation in viscosity, it was found desirable to elevate the temperature of the circulating water. For this purpose, a 5-kw. General Electric immersion heater was installed in the holdup drum for the series of runs listed under Results.

In another set of tests the effect of surface tension was determined. Surface tension was varied by the addition of a small amount of isoamyl alcohol to the circulating water. Concentrations of isoamyl alcohol were used up to a maximum of 2½%. In

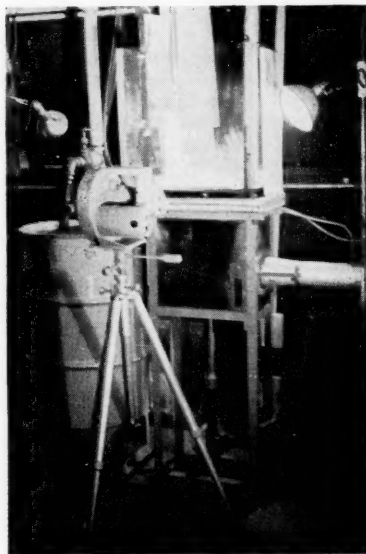


Fig. 2. Photograph of equipment for bubble-formation study.

order satisfactorily to disengage the entrained vapor from this liquid, it was necessary to install a 2-ft. length of 10-in.-diam. galvanized-iron duct in the holdup drum. The duct acted to reduce turbulence and churning in the drum, thereby allowing runs to be made at surface tensions as low as 32 dynes/cm. Surface tensions were measured by means of a duNuoy tensiometer.

For obtaining the data, a Wollensak Fastex 16-mm. high-speed motion picture camera was employed. At full voltage of 110 volts this machine has a top film speed of 7,000 frames/sec. Since maximum speed required in this work was 2,500 frames/sec.,

a Variac set at 70 volts was employed to obtain this speed. Illumination was provided by three RSP-2 photo spot lamps. The number and position of these lamps were determined by a trial-and-error method. The optimum conditions were found to consist of having one lamp behind and to the right of the subject and two in front, one on each side. Photographs of the equipment employed are shown in Figure 2.

EXPERIMENTAL PROCEDURE

The technique for obtaining data in this portion of the study was relatively simple. In a given run the mechanical features of weir height, cap and riser arrangement, and slot size were adjusted, and then the camera and lighting facilities arranged. Next the air blower and liquid-circulation pump were started and the air- and liquid-flow rates set at the desired values by means of damper and valve controls, respectively. The run, which consisted of taking the high-speed motion picture, was then made. At the film speed employed, the time required to expose 50 ft. of film was less than 1 sec. At the time of the film exposure, the following data were recorded: (1) air-flow rate, (2) liquid-flow rate, (3) air orifice temperature and pressure, (4) room temperature and pressure, (5) mechanical layout: (a) cap and slot and (b) weir height, (6) liquid employed—temperature and physical properties, (7) liquid height on plate, and (8) plate pressure drop.

Based both on the results of the literature review, which gave an indication of the factors possibly affecting bubble formation, and on the limits of the facilities available for the research, the variables and their ranges investigated were (1) vapor rate = superficial slot velocity, 15 to 50 ft./sec.; (2) liquid rate = 0.5 to 12.0 gal./min./in. of free plate width; (3) weir height = 1.0 to 3.0 in.; (4) slot submergence = 0.5 to 4.0 in.; (5) slot size = ⅜ to ½ to ⅝ by 1¼ in.; (6) cap size = 1½ to 3 in. diam.; (7) liquid surface tension = 30 to 72 dynes/cm.; (8) liquid viscosity = 0.4 to 1.0 centipoise. The results of the experiments involving these factors and the correlations developed are tabulated and explained in the sections on Results and Discussion of Results.

EXPERIMENTAL RESULTS AND DATA TREATMENT

A description of the procedure involved and the type of data obtained in this phase of the program has been given in the previous section. In order to understand and interpret the results obtained, it may be desirable to review the methods used in handling the data. The initial portion of this section is devoted to a discussion of these methods. Tabulations and plots of the actual results follow.

Data Treatment

The actual information on bubble size and contact time obtained from a frame-by-frame analysis of the films was a rather complex and time-consuming process. A preliminary study of several of

the early films indicated that, although the bubbles followed a rather regular pattern of development insofar as shapes were concerned, the actual sizes varied considerably. In order to make quantitative measurements, it was necessary to assign a particular geometric shape to each bubble in order to calculate its area and volume. It was found that as the bubble growth was initiated at the slot its shape closely approximated that of a paraboloid. When the bubble broke away from the slot, it assumed an ellipsoidal configuration. Because a mirror view of the bubbles was also included, it was not necessary to assume that the surfaces were figures of revolution. Indeed, later analysis showed that this assumption would have been considerably in error. Equations were derived expressing the surface area and volume of both an ellipsoid and a paraboloid as functions of the three principal diameters. Curves of area vs. diameter ratios were drawn up to facilitate computation. Copies of these curves were shown together with the derivation of the pertinent equations (14).

In a particular run it was found that five to six axial measurements of a bubble at various stages in the course of its development were sufficient to define its "growth curve." From the 50 ft. of film exposed in a run it was usually possible to make measurements on five or six bubbles. In all runs the results of all bubbles were averaged. Each set of measurements included the following data (14): (1) frame number after start of bubble (e.g., when bubble first emerges, frame number is zero); (2) axial measurements of height, width, and depth; (3) shape—whether paraboloidal or ellipsoidal. The diametrical measurements were taken with a centimeter scale. In order to convert these dimensions into "true" values, a scale factor referring to the centimeter scale to the scale photographed was calculated.

As all the pictures were taken at the same applied voltage to the camera, the speed at corresponding frames after the start of the film was the same. Thus generalized film-speed curves were derived, so that contact times might be easily obtained. These curves with a parameter of initial cumulative frame number related time elapsed from frame zero to any frame studied. Data for these curves were obtained by means of a time trace from a flashing neon light (60 cycles/sec.) in the film margin. Details of the camera speed curve were given (14). Contact-time data for a particular bubble were obtained by marking the frame in which the bubble started as frame zero so that the number of frames from the start of the film to any point might be measured, and by then going to the generalized camera speed curves to read off time values corresponding to the frame numbers re-

corded with the bubble-size data. The total time was that required for the bubble to disappear into the froth.

In the calculation of the interfacial area A , the pertinent diameter ratios were first obtained and A was then obtained directly from the previously mentioned computational curves. Maximum bubble volume V_M was next calculated from the measured diameters. The ratio A/V_M was plotted against contact time, t , for several of the early runs, and it was noted that these "growth" curves had a characteristic S shape.

Daniel (6) showed that these curves could be rectified by plotting

$$\ln \frac{A/V_M}{(A/V_M)_{\max} - (A/V_M)} \text{ vs. } t$$

where $(A/V_M)_{\max}$ is the asymptotic value reached by the ratio (A/V_M) . By this procedure the following mathematical expression, relating A/V_M to t , was evolved:

$$A/V_M = \frac{(A/V_M)_{\max} e^{j+bt}}{1 + e^{j+bt}} \quad (5)$$

where j and b are the intercept and slope, respectively, of the rectified curve.

The area at_m could then be obtained as

$$\begin{aligned} at_m &= \int_0^{t_m} (A/V_M) dt \\ &= \frac{(A/V_M)_{\max}}{b} \ln \frac{(1 + e^{j+bt_m})}{(1 + e^j)} \quad (6) \end{aligned}$$

When Equation (6) was applied, the following facts soon became apparent.

$$e^j \text{ is a very small value, approximately } e^{-5} \quad (7)$$

and so

$$1 + e^j \text{ is approximately equal to } 1$$

and as

$$e^{j+bt_m} \text{ is approximately equal to } e^{j2}$$

$$1 + e^{j+bt_m} \text{ is essentially equal to } e^{j+bt_m}$$

It was then found that Equation (6) could be simplified to the following term to within an accuracy of less than 1%:

$$\begin{aligned} at_m &= \int_0^{t_m} (A/V_M) dt \\ &= (A/V_M)_{\max} (t_m + j/b) \quad (8) \end{aligned}$$

In summary, the treatment of the data consisted of the following steps:

1. Calculation of bubble area A and maximum bubble volume V_M by means of the computational plots relating these terms to bubble-diameter ratios.
2. Calculation of bubble-contact time t and maximum time t_m .

3. Evaluation of "bubble-growth" equation (A/V_M) as a function of t , found by plotting

$$\ln \left(\frac{(A/V_M)}{(A/V_M)_{\max} - (A/V_M)} \right) \text{ vs. } t$$

4. Calculation of at_m by means of equation: $at_m = (A/V_M)_{\max} (t_m + j/b)$.
5. Calculation of a as $a = at_m/t_m$.

Description of Results

The results of this investigation, calculated as described in the previous paragraphs,* are presented in Figures 3 through 9. In the graphical presentation both interfacial area per unit volume of vapor a and total contact time t_m were plotted against static slot submergence s . The latter term was defined as the weir height minus slot height plus weir crest. For each of the plots one other independent variable has been employed as a parameter in order to show its effect. Where effects of the parameter were noted, the data have been cross plotted to illustrate the magnitude of the effects.

Effect of Liquid Rate and Weir Height

No direct relationships for either interfacial area or contact time with liquid rate or weir height were obtained. However, it was soon found that a third factor, dependent on these two, did correlate the former terms effectively. This intermediate factor is the static slot submergence. Because it exerted the major effect on the mechanism of bubble formation, static slot submergence was employed as the abscissa for most of the subsequent plots.

Effect of Air Rate

With the results tabulated*, Figure 3, interfacial area per unit volume of vapor vs. slot submergence, and Figure 4, total contact time vs. slot submergence, were constructed by means of the various air rates tested. Superficial slot velocities of 15 to 50 ft./sec. were used in the test work. The shape of the curve given in Figure 3 was unchanged by changes in any of the other variables studied. No significant effect of air rate on a , the interfacial area, can be detected from these runs.

The results depicted in Figure 3 were obtained from runs made with zero skirt clearance. To confirm these results, additional tests involving the variation of vapor rate were conducted by means of a 0.25-in. skirt clearance. Results of this set of experiments are presented in Figure 3A. These data also indicate that vapor rate has no effect on interfacial area.

*Tabular material has been deposited as document 5110 with the American Documentation Institute, Photoduplication Service, Library of Congress, Washington 25, D.C., and may be obtained for \$1.25 for photoprints or 35-mm. microfilm.

Figure 4 is typical of the contact-time-slot-submergence relationships found in the remainder of the work. The data indicate that air rate does exert some effect on contact time.

Since the effect of vapor rate on contact time is small, additional data from some of the later runs in which slot velocity was varied are shown in Figure 4A. The same small effect of vapor rate is shown in this curve.

A cross plot of the data on slot velocity is given in Figure 4B. It is interesting to note that contact time decreases with vapor rate and goes through a minimum at a slot velocity of approximately 30 ft./sec. The change in contact time between air rates of 30 and 50 ft./sec. is small at the higher slot submergences. It was observed that the slot became wide open at air rates of 30 and 50 ft./sec., depending mainly on the static head of liquid above the slot. It seems quite possible, therefore, that the effect of air rate on total contact time is reduced after the slot becomes fully open.

Effect of Skirt Clearance

The summary of results applicable to these determinations is given elsewhere.* Figure 5 shows the relationship between interfacial area and slot submergence for various values of skirt clearance. It is somewhat surprising to note that the data for skirt clearance of 0 and 0.5 in. fall on the same curve, while the results at a clearance of 0.25 in. are substantially higher. This point will be discussed under Results. Figure 5A is a cross plot of interfacial area vs. skirt clearance for submergences greater than 0.25 in. and shows the magnitude of the effect directly.

The contact time t_m is shown as a function of slot submergence and skirt clearance in Figure 6. As it had been shown that vapor rate has an effect on contact time, only those runs in which slot velocity = 30 ft./sec. were employed in this figure, which shows that there is a small but significant effect of skirt clearance on t_m .

Attempts to obtain data at values higher than 0.5 in. in the present study were unsuccessful owing to the action of vapor bubbling underneath the cap. It is more likely that this sort of bubble leakage occurs in the commercial towers operating at high vapor rate. However, extraneous bubbles formed in this manner were found to obscure the bubbles passing through the slot, thereby preventing measurement of the latter. In addition, it was felt that clearances of greater than 0.5 in. would be quite out of proportion to the 1.5-in.-diam. caps used.

Effect of Slot Area

Figure 7 contains plots of interfacial area vs. slot submergence for various slot sizes. The curves show that for slot

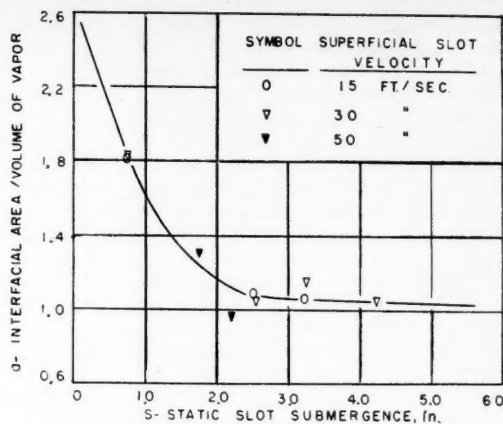


Fig. 3. Effect of vapor rate on interfacial area.

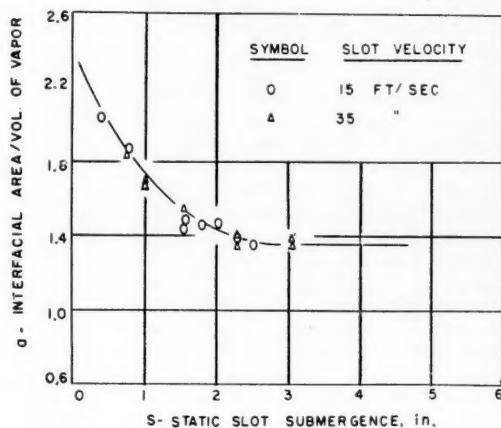


Fig. 3a. Effect of vapor rate on interfacial area.

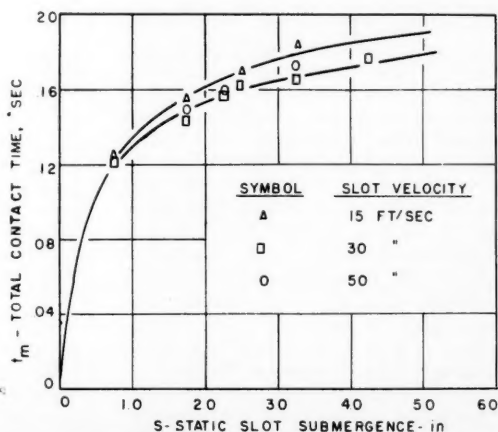
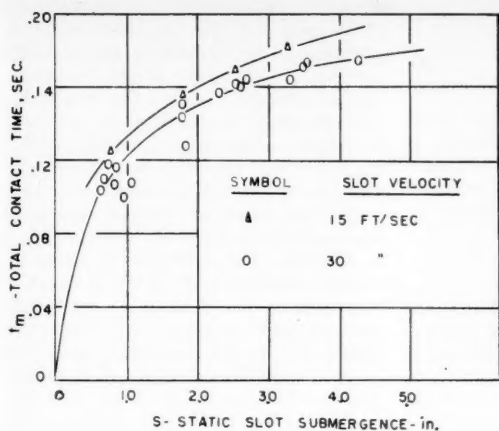


Fig. 4. Effect of vapor rate on contact time.

*See footnote on page 19.

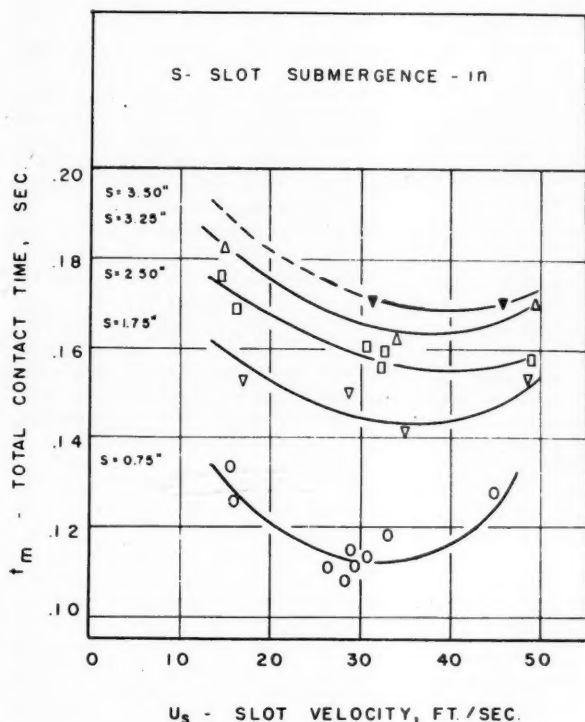


submergence lower than approximately 2.5-in. interfacial area is reduced by an increase in slot area. These results indicate that there is no effect of slot area on contact time.

Effect of Surface Tension

Results of runs in which surface tension was varied from 72, 60, 45 to 32 dynes/cm. are given elsewhere.* At slot submergences greater than 2.0 in. there appears to be an effect of surface tension on interfacial area, with the interfacial area being lowered by a reduction of surface tension. The data

Fig. 4a. Effect of vapor rate on contact time.



for slot submergences greater than 2.5 in. indicate the negligible effect of surface tension upon time of contact and interfacial area.

Effect of Viscosity

During the investigation, the viscosity values were varied, ranging from 0.95 to 0.66 and 0.40 centipoise. The relationship between interfacial area and liquid viscosity is shown directly in Figure 8 for slot submergences greater than 2.5 in. The data indicate that lowering the viscosity results in a reduction of interfacial area. Because viscosity was varied by raising the temperature of the circulating water, slight reductions in surface tension due to the higher temperatures were unavoidable. The change in surface tension is of insufficient magnitude to affect interfacial area. The change in interfacial area can be attributed only to viscosity. Figure 9 shows clearly that the contact time is not affected by liquid viscosity.

Since the results of the mass transfer study in the next section indicated that the bubble-formation region is of considerable importance in vapor-liquid

Fig. 4b. Total contact time vs. superficial slot velocity for various slot submergencies.

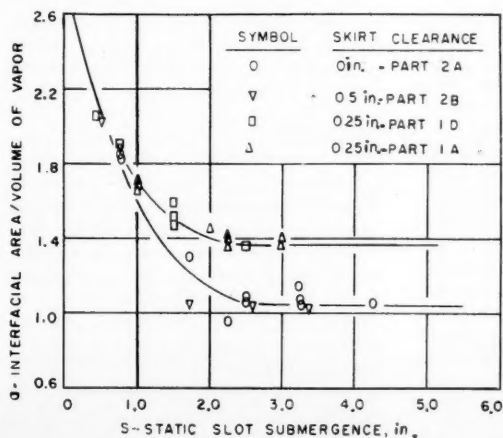


Fig. 5. Effect of skirt clearance on interfacial area.

contacting, an attempt at correlating these results in the form of useful design equations is described on the following pages.

Correlation of Bubble-formation Results

The tables and plots of the previous section illustrate the effects of the different variables tested on interfacial area and on contact time. Insofar as the attempt to provide a basis for future studies on commercial-sized equipment is concerned, this information demonstrates the variables to be considered. An attempt has also been made to include all these findings in a single correlation in a

*See footnote on page 19.

manner suitable for use by design engineers.

Interfacial Area per Unit Volume of Vapor a

It has been shown that two modes of formation are possible, depending upon slot submergence. Reference to the curves of interfacial area vs. slot submergence Figures 3 to 9 show that the horizontal portions of the curves consistently start in the range of slot submergence, 2.25 to 2.75 in. For correlation purposes, an average value of 2.5 in. has been taken as the point at which interfacial area becomes independent of slot submergence. For values of static slot submergence less than 2.5 in., the variables shown to influence a were slot submergence and slot area. Equations found to characterize this relationship are of the form

$$\frac{1}{a - a_0} = K_1 s - c \quad (8)$$

where a_0 , K_1 , and c are functions of slot area. A tabulation of the values of these constants for the slot areas considered is presented in Table 1. The constants are related to slot area, A_s , by the equations

$$a_0 = 5.88 A_s^{0.30} \quad (9)$$

$$K_1 = 985 A_s + 0.20 \quad (10)$$

$$c = 332 A_s - 0.40 \quad (11)$$

The final equation for interfacial area is

$$\frac{1}{a - 5.88 A_s^{0.30}} = A_s(985s - 332) + 0.20s + 0.40 \quad (12)$$

For values of slot submergence greater than 2.5 in., interfacial area has been shown to be a function of skirt clearance, liquid viscosity, surface tension, and, to a small extent perhaps, liquid density (2, 3). Expressing this relationship symbolically gives

$$a = (h, \mu, \sigma, \rho) \quad (13)$$

where h = skirt clearance.

Dimensional analysis reveals that the appropriate grouping of the variables in Equation (13) is

$$a = \frac{1}{h} F' \left[\frac{h \sigma \rho}{\mu^2 g_c} \right] \quad (14)$$

where F' represents a mathematical function.

Because skirt clearances of zero were employed for many of the tests, h must be redefined in order to prevent Equation (14) from degenerating. If h_c is taken as the maximum height of the slot measured from the tray floor, it maintains its directional significance on the term a , as it includes skirt clearance and has the advantage of not taking on a null value.

Equation (14) then becomes

$$a h_c' = F' \left[\frac{h_c' \sigma \rho}{\mu^2 g_c} \right] \quad (15)$$

Values of the group $(h_c' \sigma \rho) / \mu^2 g_c$ have been calculated for the various conditions employed in this study.* Interfacial areas for slot submergences greater than 2.5 in. may be predicted from the correlation curve, Figure 10.

Total Contact Time t_m

The variables shown to exert an influence on contact time were slot submergence, vapor rate, and skirt clearance. It was found that the contact-time data given on the previous pages could be rectified by plotting them against the dimensionless ratio s/h_c on logarithmic coordinate paper. A family of essentially parallel lines was obtained which followed the equation

$$t_m = d(s/h_c)^{0.27} \quad (16)$$

where h_c is skirt clearance + slot height, in., and d is a function of slot velocity, u_s , and of h_c' . The appropriate grouping is, by dimensional analysis,

$$d = f(h_c'/u_s) \quad (17)$$

A tabulation of the values of d calculated for various conditions of h_c'/u_s is given elsewhere.* A graphical relationship allowing the constant to be easily evaluated is presented in Figure 11.

In order to test the reliability of these equations, measured values of the product $a t_m$ were compared with values calculated by the foregoing techniques. The comparison is presented in Table 2. It will be noted that an average deviation between the measured and calculated values of 7.2% was obtained.

Error Analysis

This section deals with a discussion of the types and magnitudes of the errors introduced into the results of this study and their effects on the precision of the final correlation.

Interfacial Area

The characterization of the growing bubbles as either ellipsoids or paraboloids in order to calculate interfacial areas was discussed in a previous section. This hypothesis is considerably more realistic than the assumption of bubble sphericity used in earlier studies (2, 3, 17). The bubbles, however, were not always geometrically regular and it was necessary to neglect any additional surfaces formed by the irregularities. While these additional areas could not be accurately evaluated, they were estimated to be less than 10% of the measured values in the majority of runs. It is significant that

the errors introduced by neglecting these areas were of a more or less systematic nature, and so the results reported are consistent within themselves. An exception to this was noted in the tests made at reduced surface tension. In this case a certain amount of foaming at the bubble-liquid interface was observed; the actual values of interfacial area under these conditions therefore probably are higher than Figure 11 indicates.

While the diametrical bubble measurements were being made, it was found that a reproducibility of about 1 mm. in the scale reading was possible. Since the values of average interfacial area are most strongly affected by errors in the determination of bubble area when the bubbles have become large, this does not result in a serious error. In the latter phase of the bubble growth period, bubble diameter in an average case will be about 4 cm. The probable error in interfacial area, therefore, for a single bubble becomes about 2.5%, as measurement errors result in the same directional changes in both numerator and denominator of A/V_M . Measuring a number of bubbles in each run negated the effects of error measurement of this type.

The chief cause of error in the reported values of interfacial area is thought to be the fact that the bubbles themselves were not reproducible. During a given run the six to ten bubbles photographed showed frequently a large variation among their sizes. As successive diametrical measurements showed that each bubble followed a regular growth pattern, it was considered more advantageous to minimize the number of measurements on each bubble studied during a run. The emphasis was therefore placed on considering as many bubbles as possible. Except where poor photographing conditions prevailed, it was usually possible to average the values obtained from four to eight bubbles per film.

An example of the reproducibility of a series of runs is shown in the 0.25-in. skirt-clearance tests of Figure 5. Two sequences of runs were made at identical conditions to check the reproducibility of the technique. As can be seen, the two sets of data show excellent agreement. It can be concluded that the effects observed are significant and are not the result of random fluctuations.

Contact Time

The error analysis of contact-time values reported is somewhat easier to perform. This term was taken as the interval between the time a bubble first showed itself from under the slot and the time it disappeared into the froth region. Errors in this quantity arose from two sources: (a) finding the specific frames showing the appearance and disappearance of a bubble and (b) calculating the average film speed between the two points.

*See footnote on page 19.

Contact time was calculated by dividing the counted number of frames by the average film speed. In general, the initial and final frames of a sequence were readily located to within five frames at either point. If there was any question, the film was run slowly through the projector, backward and forward, at the approximate start or finish in order to locate the precise frame.

Film speed was evaluated from a time trace in the film margin resulting from a flashing (60 cycles/sec.) neon light in the camera. Based on the results of a number of films, a generalized curve was drawn up (14) and used to obtain film speed. Speed was thus calculated as

$$S = 120N \text{ (frames/sec.)}$$

where

N = number of frames between neon-lighted frames

S = film speed, frames/sec.

The number of frames n was evaluated to the nearest plus or minus one-half frame on each side.

The equation for contact time is

$$t_m = \frac{n}{120N} \quad (18)$$

where

n = number of frames between the start and finish of a bubble.

For a single bubble, the probable error in contact time for an average case of $n = 240$ and $N = 18$ is (14)

$$\begin{aligned} \text{p.e. } (t_m) &= 0.8453 \sqrt{\frac{2}{\pi} \left[\frac{s^2(n)}{n^2} + \frac{s^2(N)}{N^2} \right]} \\ &= 0.67 \sqrt{\frac{(10)^2}{(240)^2} + \frac{(1)^2}{(18)^2}} \\ &= 4.6\% \end{aligned} \quad (19)$$

The derivation of Equation (19) is given elsewhere (14).

Since an average of six bubbles per run was employed, the effect of this measured error is reduced less than 2% on the average reported.

As in the case of interfacial area, the lack of reproducibility is felt to be the major source of inaccuracy in the reported t_m values. The average standard deviation in t_m for the 6B runs is 0.013. For a typical value of $t_m = 0.13$ sec., averaged over six bubble measurements, a 90% confidence interval of 0.13 ± 0.010 is obtained. This is equivalent, on a percentage basis, to saying that it is 90% certain that the true value lies within a range of $\pm 7.7\%$ of the measured value of t_m .

DISCUSSION OF RESULTS

The results of this study as presented in the previous section indicate that static

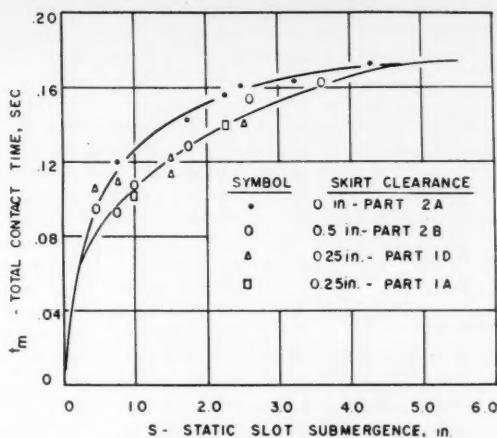


Fig. 6. Effect of skirt clearance on contact time.

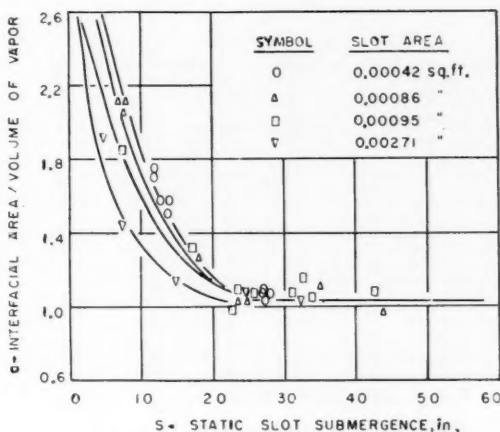


Fig. 7. Effect of slot area on interfacial area.

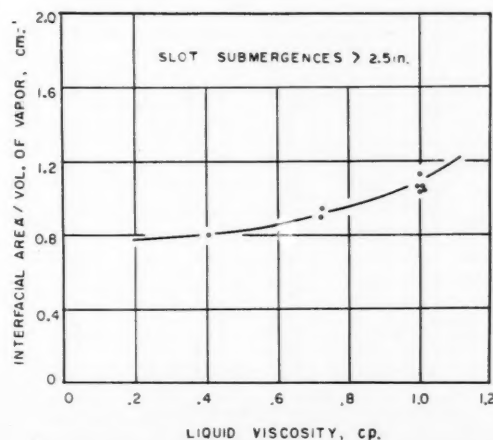


Fig. 8. Effect of liquid viscosity on interfacial area.

slot submergence had the greatest effect of all the variables tested on both the average interfacial area for mass transfer and the time of contact between the rising vapor and the liquid. Other variables showing smaller but nonetheless significant effect on one or both of these terms were vapor rate, slot area, skirt clearance, liquid viscosity, and surface tension. An attempt to explain these results and to compare them with the results of previous studies is given in the following paragraphs.

Effect of Slot Submergence

A study of several of the films showed that apparently two mechanisms of formation were possible, depending on the slot submergence. At low slot submergence the growth period was fairly short and the bubbles reached the liquid

surface while they were still relatively small. It is interesting to note that even at low submergences there was no significant jetting action and vapor flow was in the form of discrete bubbles. Thus a bubble emerging from the slot continued to grow until its top reached the liquid surface. As slot submergence was increased up to approximately 2 in., the bubble size also increased.

At higher slot submergences the mode of formation changed and a second growth period occurred after a bubble broke away from the slot. In this case a thin channel connected the bubble and the slot, and so the bubble continued to expand until the channel became unstable and broke. Because of the channel, larger bubbles were formed at the higher submergences with a subsequent reduction in area per unit volume of gas. Continued

increase in slot submergence above a value of about 3 in., however, resulted in no change in the average time required for the channel to collapse; i.e., bubble size then ceased to be a function of slot submergence.

The effect of slot submergence on contact time may be explained in the following manner. At slot submergences approaching zero, an emerging bubble is very small in size and leaves the slot almost instantaneously. As submergence is increased, a resistance is placed in the bubble path which it must overcome in order to escape. Therefore the bubble not only must expend energy to move against this resistance, but must also grow larger at the same time. More surface for the frictional drag of the water is thus provided. At high submergences bubbles have a chance to break away from the slot and rise, at constant size, through the liquid. A linear relationship between contact time and slot submergence should then exist, corresponding to a period of free rise. At the higher submergences the contact time can therefore be considered to consist of two periods: (1) a period of formation where velocity is low because energy must be expended to create new surface and (2) a period of free rise. The higher the submergence, the more dominant will be the latter period. The relationship between contact time and interfacial area will approximate linearity.

Effect of Air Rate

The data in Figure 3 show that air rate has no significant effect on the interfacial area. At first glance this result appears to contradict some of the earlier studies in which vapor rate was shown to influence final bubble size (8, 29, 39, 41). Spells and Bakowski (40) reported that the combination of vapor rate and slot submergence completely characterized the mode of formation and the final bubble size. Their findings on the effect of slot submergence and their explanation of formation mechanism are in complete agreement with the results presented here. Data showing the effect of air rate on bubble volume for both studies have been plotted in Figure 13. Although the range of air rates and the test equipment employed differed substantially, the results show fairly good agreement. In Figure 13 the present results show that final bubble size is influenced by air rate at the lower air rates. This conclusion is in qualitative agreement with the findings of other investigators (8, 29) but appears contradictory in view of the lack of effect on α , the interfacial area.

West et al. (44) reported values of effective surface area per unit volume of gas in the foam region above perforated plates. With the data of the previous investigators (18) they made a similar calculation for bubble-cap plates. No direct measurements of interfacial area

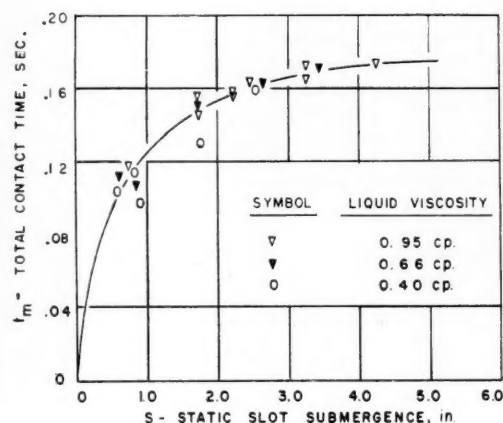


Fig. 9. Effect of liquid viscosity on contact time.

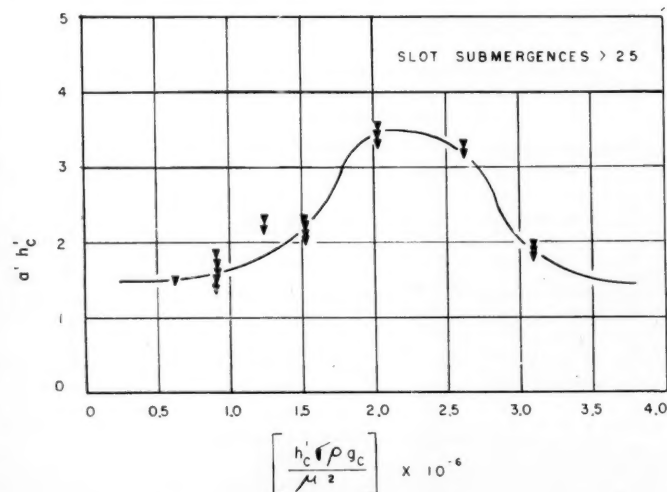


Fig. 10. Determination of interfacial area.

However, still to be accounted for is the somewhat paradoxical conclusion that air rate in the low range exerts an effect on final bubble size and does not appreciably influence the average interfacial area per unit volume a . Two reasons can be advanced to account for this result. The mathematical expression for a derived by dividing Equation (8) by t_m is

$$a = at_m/t_m$$

$$= (A/V_M)_{max}(1 + j/bt_m) \quad (20)$$

The interfacial area a is proportional to the ratio $(A/V_M)_{max}$. It is approximately inversely proportional to the cube root of V_M , and for a sphere the proportionality is exact. Thus large increases in V_M result in very much smaller changes in $(A/V_M)_{max}$, and small changes in V_M could easily be lost in the process of evaluating the more insensitive interfacial area a . It was shown that, as air rate was increased to 30 ft./sec., total contact time was found to decrease (Figure 7). The small decreases in $(A/V_M)_{max}$ resulting from an increase in air rate are consequently offset by the decrease in t_m , insofar as the determination of a is concerned.

Effect of Slot Area

At low submergences slot area was shown to exert a considerable influence on the size of the bubbles produced and consequently on their average surface area. Above submergences of about 3 in., slot area ceased to affect interfacial area. The result may be explained as follows. At low slot submergences the average bubble size will be determined largely by the manner in which it is formed, as there is no secondary growth period and

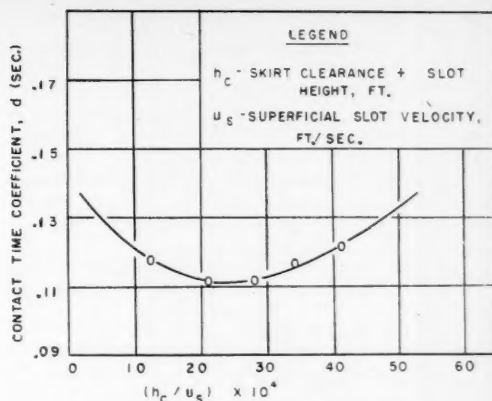


Fig. 11. Correlation of contact-time coefficient d .

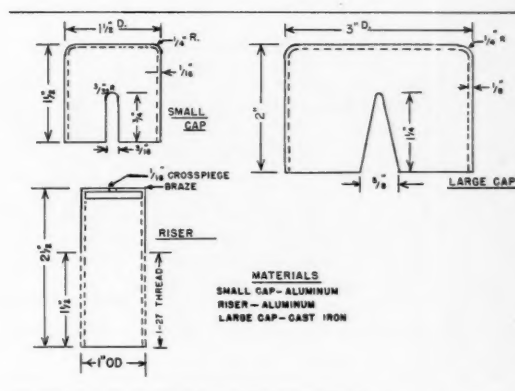


Fig. 12. Details of caps and riser, bubble-formation study.

no period of free rise. Thus a stream of gas emanating from a large nozzle would be expected to be dispersed into large bubbles, with a resultant low value of interfacial area. As slot submergence is increased, however, the period of secondary channel feeding starts. In this region both the final size and the average size depend largely on what happens to the bubble after it has emerged from the slot. Slot size would therefore be expected to play a markedly smaller role in the over-all contacting process. Experimentally it was found that at low slot submergences increasing slot size resulted in a decrease in interfacial area equivalent to an increase in bubble size. On the other hand, bubble size was virtually unaffected by slot area at higher submergences.

The lack of effect of slot size on contact time again indicates that the period of free rise is appreciable only at the higher slot submergences. During free rise, bubble velocity is a function of

its size. Since the bubble size is constant at higher submergences, velocity and contact time are therefore not functions of slot size.

Effect of Skirt Clearance

The effect of skirt clearance on interfacial area shown in Figure 5 was rather anomalous. At 0- and at $\frac{1}{2}$ -in. clearances the data fell approximately on the same curve, indicating no significant variation. However, a substantially higher curve was obtained at a skirt clearance of 0.25 in. In order to substantiate this result, as well as to check on the reproducibility of the technique, a second series of tests was made at the latter clearance. As Figure 5 clearly shows, the data lined up perfectly with those of the first tests. In Figure 6 it can be seen that an increase in skirt clearance at constant slot submergences causes a reduction in contact time, but the irregular effects noted in the case of interfacial area at the slot submergence of 0.25 in. were not

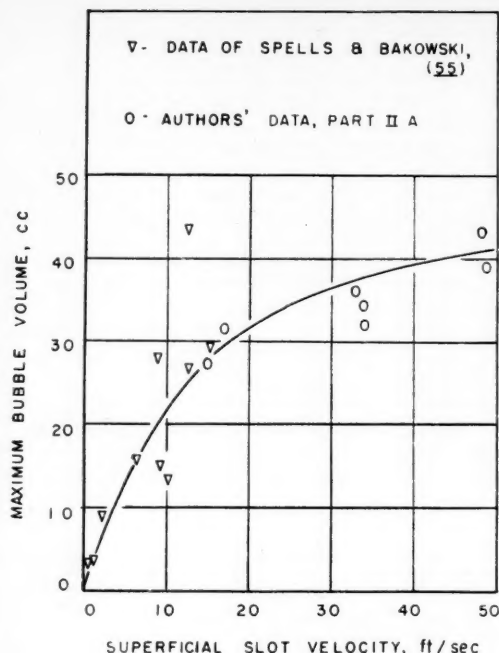


Fig. 13. Maximum bubble volume vs. superficial slot velocity.

detected. Smolin, Goldberg, and Welsh (26) in their study on froth heights and densities used the same cap and riser design that was used in this study and also observed significantly different tray hydraulic properties at this skirt clearance.

It is reasonable to presume that the cause of this strange behavior at 0.25-in. skirt clearance is related to the effect of the flowing liquid on bubble formation. At zero clearance all liquid streams contacting the emerging bubble can be assumed to possess approximately the same velocity. When the cap is raised above the tray floor, however, an additional liquid stream flowing under the cap contacts the vapor. At low skirt clearance of about $\frac{1}{4}$ in. the liquid passing under the cap apparently reaches a fairly high velocity. An additional drag force is thereby exerted on the emerging bubble, pulling it away from the slot before it has the opportunity to reach full size. This mechanism also explains the reduction in contact time, since the bubbles which have been removed from the slot earlier also reach the liquid surface earlier.

At half-inch skirt clearances the constriction is much larger. The velocity of the liquid stream contacting the base of a growing bubble is therefore not so great. Substantially smaller effects on the resultant bubble size would be postulated for this condition.

The large increase in interfacial area found at skirt clearance of 0.25 in. indicates that further study is warranted. It is probable that in a given case the

optimum skirt clearance for high interfacial area is a function of the geometry of the cap and tray design.

Effect of Surface Tension

The values of interfacial area are affected by surface tension only at the higher values of slot submergence. In this region the average values of A/V_M are independent of submergence. This finding is in sharp contrast to that noted in the case of the slot size tests. In this case the effects were of importance at low liquid heights. The influence of surface tension, therefore, must be related to the period of secondary bubble growth, a region not existing at low submergences. In effect, what must happen is that a lowering of surface tension allows the channel to become somewhat larger, which consequently enables it to feed more vapor into the connected bubble. By this means, bubble size is increased and the ratio A/V_M decreased.

Measurements in this phase of the study were complicated by the amount of froth that existed in the liquid. This was partially due to the creation of additional surface area by a slight decomposition of the rising bubbles, thus introducing some error into the calculation of interfacial area. Most of the froth was carried over from the holdup drum due to poor vapor-disengaging characteristics of the liquid. It was only because of the installation of a 3-ft.-long, 8-in.-diam. galvanized duct, through which the downcomer liquid had to pass in a tortuous path, that it was possible to

make runs at surface tensions of 45 and 32 dynes/cm. Without this duct the flowing liquid became almost opaque from the entrained vapor. Even with the duct in place it was necessary to maintain low liquid flow rates in order to obtain satisfactory photographic conditions. Variation in slot submergence for these runs was obtained largely by the use of different weir heights.

There was no significant variation in contact time with static surface tension measured, although more than usual scattering of the data points occurred. The latter phenomenon appears to be due chiefly to the difficulty in interpreting the films of these tests. The heavy froth carryover made measurements both of size and time somewhat unreliable. In cases of low surface tension the application of the correlations here alone to predict point efficiency is not recommended because of the possible effects of the froth layer. It is hoped that the combination of these results with those obtained in the companion study on froth characteristics by Smolin (38) will prove valuable.

Effects of Liquid Viscosity

A small effect of liquid viscosity on average interfacial area, a did exist, with lower values of a resulting from viscosity decrease. The relations are similar to those obtained in the surface-tension tests and again indicate that the major influence of viscosity is felt during the channel-feeding period. Apparently vapor escapes into the bubble at a faster rate as viscosity is decreased.

The literature shows considerable disagreement over the effect of viscosity on bubble size. Schnurmann (35) investigated the size of gas bubbles produced in a variety of liquids, including alcohols, acids, sugar solution, and certain electrolytes. He found that bubble size was independent of the method of bubble production but tended to vary inversely with liquid viscosity. Datta, Napier, and Hewitt (?), on the other hand, investigated the formation of gas bubbles at circular orifices and noted that a hundred-fold increase in viscosity resulted in only a 10% reduction in bubble volume. Their study involved aqueous glycerine solutions of various concentrations.

The other indication of the effect of viscosity on the size of bubbles formed at bubble-cap slots was obtained from the work of Keyes and Byman (23). These authors reported that an increase in bubble-cap plate efficiency was found when liquid viscosity was raised. The higher efficiency was attributed to a reduced bubble size.

It is significant to note that all investigators have found that bubble size is reduced by an increase in liquid viscosity. The disagreement is on the magnitude of the effect. While the results of the present study tend to

TABLE 1.
TABULATION OF CONSTANTS IN INTERFACIAL-AREA EQUATION (SLOT SUBMERGENCE < 2.5 in.)

Part*	Slot size, in.	a_0	K_1	c	A_s , sq. ft.
3B	$\frac{1}{2} \times \frac{1}{8}$	0.52	0.60	-0.20	0.000422
3C	$\frac{1}{2} \times \frac{1}{8}$	0.52	0.60	-0.20	0.000422
3D	$\frac{1}{2} \times \frac{1}{8}$	0.52	0.60	-0.20	0.000422
2A	$\frac{3}{4} \times \frac{1}{8}$	0.71	1.15	-0.25	0.00095
3A	$\frac{3}{4} \times \frac{1}{8}$	0.58	0.99	-0.10	0.00086
5A	$1\frac{1}{4} \times \frac{1}{8}$	0.85	2.89	-0.50	0.00271

General equation

$$\frac{1}{a - 588A_s^{0.30}} = A_s(985s - 332) + 0.20s + 0.40$$

*Refer to the original data in reference 14.

TABLE 2.
COMPARISON OF PREDICTED AND MEASURED VALUES OF at_m

Run	Predicted	Measured	% Error	Run	Predicted	Measured	% Error
1A6	0.172	0.175	1.7	3A5	0.166	0.170	2.4
1A18	0.161	0.155	3.7	3A6	0.173	0.166	4.2
1A25	0.204	0.230	12.5	3A7	0.170	0.182	6.6
1A36	0.234	0.194	17.0				
1A37	0.189	0.175	7.4	3B1	0.228	0.231	1.3
1A38	0.173	0.153	11.5	3B2	0.238	0.208	14.5
				3B4	0.195	0.224	12.9
1D1	0.218	0.216	0.9	3B5	0.211	0.188	12.2
1D2	0.187	0.206	9.2	3B6	0.202	0.190	6.3
1D4	0.167	0.178	6.2				
1D4A	0.167	0.169	1.2	4A1	0.250	0.278	10.0
1D4B	0.246	0.243	1.2	4A2	0.170	0.163	4.3
				4A4	0.177	0.165	7.3
2A1	0.215	0.226	4.9	4A5	0.165	0.180	8.3
2A2	0.211	0.219	3.6	4A7	0.166	0.176	5.7
2A6	0.174	0.150	16.0				
2A10	0.211	0.190	11.0	4B4	0.140	0.152	8.5
2A11	0.194	0.186	4.3	4B5	0.127	0.129	1.6
2A12	0.202	0.180	12.2	4B6	0.133	0.139	2.9
2A13	0.192	0.180	4.4	4B8	0.140	0.120	16.7
2A14	0.180	0.171	5.3	4B9	0.147	0.133	10.5
2B1	0.206	0.188	9.5	5A1	0.191	0.203	5.9
2B2	0.183	0.172	6.4	5A2	0.165	0.154	7.1
				5A3	0.159	0.151	5.3
				5A5	0.163	0.155	5.2

Average error = 7.2

An average error of 7.2% in at_m is equivalent to an error of 2.5% in the calculated point efficiency.

confirm those of Schnurmann (25) and Keyes and Byman (23), all three investigations dealt with a relatively turbulent contacting operation. Since Datta et al. (7) employed a fairly quiescent bubbling zone, the difference in the magnitude of the effects of viscosity may be due to the presence of turbulence caused by a flowing liquid.

The lack of effect of liquid viscosity on contact time shown in Figure 9 is at first glance surprising. For free-rise conditions, Stokes's Law would predict that decreasing viscosity should result in an increase in velocity or a decrease in contact time. Because of the liquid turbulence, however, large deviations from Stokes's Law are to be expected. Available evidence from the other tests, especially the small effect of vapor rate on contact time, indicates that free rise does take place. A more complicated

mathematical expression than Stokes's Law will be required to characterize this motion.

CONCLUSIONS

As part of a program to investigate the factors affecting point efficiency in distillation, a study was made of the formation of air bubbles at single bubble-cap slots immersed in aqueous solutions. An analysis of high-speed motion pictures of the bubbling action enabled both the average interfacial area for mass transfer and the total contact time to be determined under a variety of conditions. Variables tested included vapor rate, liquid rate, weir height, static slot submergence, slot size, liquid viscosity, and surface tension. The principal effects of these variables and the derived correlation for predicting interfacial area and

contact time are summarized in the following sections.

1. The static slot submergency, or liquid seal on the slot, was found to exert a great effect on both interfacial area and contact time. With respect to interfacial area, the existence of two zones was established.

a. At slot submergences lower than approximately 2.5 in. interfacial area was found to decrease with slot submergence, according to the equation

$$\frac{1}{a - a_0} = K_1 s - c \quad (8)$$

b. At slot submergences above 2.5 in. interfacial area was unaffected by variations in slot submergence.

Total contact time of a bubble was found to increase with slot submergence, according to the equation

$$t_m = d \left(\frac{s}{h_c} \right)^{0.27} \quad (16)$$

where d is a function of slot velocity and skirt clearance plus slot height.

2. Slot size was the only other variable shown to affect interfacial area in the low slot-submergence region. The constants in Equation (11) were found to correlate with slot area.

3. In the high slot-submergence region (above 2.5 in.) interfacial area was found to be influenced by liquid viscosity, surface tension, and skirt clearance. Interfacial area was lowered by reductions in surface tension and liquid viscosity. Skirt clearances of from 0 to 0.5 in. were tested. Interfacial area was found to reach a maximum at a clearance of 0.25 in.

4. In addition to slot submergence, other variables found to affect total contact time were skirt clearance and vapor rate. Increase in both of the terms resulted in a decreased time of contact between vapor and liquid. An attempt is made to explain these results in the light of previous investigations.

5. Correlations for predicting interfacial area as a function of the variables studied were developed and took the form:

a. Interfacial area per unit volume of vapor:

(1) Slot submergences less than 2.5 in. of liquid:

$$\frac{1}{a - 588A_s^{0.30}} = A_s(985s - 332) + 0.20s + 0.40 \quad (12)$$

2. Slot submergences greater than 2.5 in. of liquid:

$$ah_c' = F \left[\frac{h_c' \sigma \rho}{\mu^2 g_c} \right] \quad (15)$$

where the functional relationship F is graphically represented by Figure 10.

b. Total contact time:

$$t_m = d(s/h_c)^{0.27} \quad (16)$$

where d is determined from Figure 11 to be a function of h_c'/u_s .

c. Point efficiency, E_{LM} , is related to interfacial area and contact time through the equation

$$\ln(1 - E_{LM}) = -0.00848K_G a t_m \quad (3)$$

ACKNOWLEDGMENT

Grateful acknowledgment is made to Research Corporation for financial assistance, to Professor G. Daniel for his advice on statistical treatment, to Dr. M. J. P. Bogart, A. S. Brunjes, J. A. Davies, J. Middleton, W. C. Schreiner, and W. F. Schurig for their helpful comments.

NOTATION

a	= average interfacial area per unit volume of vapor, ft. ⁻¹
a_0	= function of slot area = $5.88A_s = 0.30$
A	= interfacial area for mass transfer, sq. ft.
A_s	= area per slot, sq. ft.
b	= slope of rectified bubble-growth curve
C	= concentration of component in vapor, lb. moles/cu. ft.
C^*	= concentration of component in vapor in equilibrium with liquid, lb. moles/cu. ft.
c	= function of slot area = $332A_s - 0.40$
d	= function of (h_c'/u_s) , sec.
E_{LM}	= Murphree point efficiency
F', F	= Representation of mathematical function
g_c	= consistency factor, (lb. mass) (ft.)/(lb. force)(sec. ²)
h	= skirt clearance, ft.
h_c	= skirt clearance = slot height, in.
h_c'	= skirt clearance + slot height, ft.
j	= intercept of rectified bubble-growth curve
KG	= over-all mass transfer coefficient, $\frac{\text{lb. moles}}{(\text{hr./sq. ft.})(\text{lb. moles/cu. ft.})}$
kG	= vapor-film mass transfer coefficient, $\frac{\text{lb. moles}}{(\text{hr./sq. ft.})(\text{lb. moles/cu. ft.})}$
k_L	= liquid-film mass transfer coefficient, $\frac{\text{lb. moles}}{(\text{hr./sq. ft.})(\text{lb. moles/cu. ft.})}$
L	= liquid flow rate, ga./min. (in. of free-plate width, free plate width defined as plate width minus bubble-cap diameter)
m	= slope of vapor-liquid-equilibrium curve, dC_V/dC_L
M	= molecular weight
N	= number of bubbles measured per run

n	= number of frames between neon-lighted frames
P	= pressure, lb./sq. ft.
p.e.	= probable error of the mean of a series of measurements
r	= bubble radius, ft.
R	= gas-law constant, $\frac{\text{lb./ft.}}{(\text{lb. mole})(^\circ\text{C.})}$

S	= film speed, frames per sec.
s	= static slot submergence, in.
t	= contact time, hr.
T	= temperature, $^\circ\text{C.}$
u_s	= slot velocity, ft./sec.
V	= vapor velocity, cu. ft./sec.
V_c	= superficial column velocity, ft./sec.
V_M	= instantaneous volume of vapor bubble, cu. ft.
V_s	= continuous-phase velocity-bubble velocity
W_h	= weir height, in.
y	= vapor composition, mole fraction
y^*	= vapor composition in equilibrium with liquid
Z	= length of bubble travel, liquid head on plate minus one-half slot height
μ	= viscosity, lb./ft. (sec.) or centipoises
ρ	= density, lb./cu. ft.
ρ'	= molar density, lb. moles/cu. ft.
σ	= surface tension, lb. force/ft.

Subscripts

L	= liquid
V	= vapor
1	= bubbling zone
2	= froth and entrainment zone

LITERATURE CITED

- Carey, J. S., J. Griswold, W. K. Lewis, and W. H. McAdams, *Trans. Am. Inst. Chem. Engrs.*, **30**, 504 (1934).
- Chu, J. C., *Petroleum Processing*, **5**, 39 (1951).
- Chu, J. C., J. R. Donovan, B. C. Boswell, and L. C. Fuhrmeister, *ibid.*, **1**, 524 (1951).
- Chu, J. C., J. Kalil, and W. A. Wetteroth, *Chem. Eng. Progr.*, **39**, 141 (1953).
- Cross, C. A. and H. Ryder, *J. Appl. Chem. (London)*, **2**, 51 (1952).
- Daniel, C., personal communication (1952).
- Datta, R. L., D. H. Napier, and D. M. Hewitt, *Trans. Inst. Chem. Engrs. (London)* (Feb. 14, 1950).
- Davidson, Leon, paper presented at A.I.Ch.E. New York meeting (1948).
- Davies, J. A., *Petroleum Refiner* (Aug. and Sept., 1950).
- , personal communication (1950).
- Dixon, W. J., and F. J. Massey, "Introduction to Statistical Analysis," McGraw-Hill Book Company, Inc., New York (1951).
- Drickamer, R. O., and J. R. Bradford, *Trans. Am. Inst. Chem. Engrs.*, **39**, 319 (1943).

- Eversole, W. G., G. H. Wagner, and E. Stackhouse, *Ind. Eng. Chem.*, **33**, 1459 (1941).
- Forgrieve, John, Robert Grosso, S. M. Shah, and G. C. Papacosta, thesis, Polytech. Inst. Brooklyn (1953).
- Garner, F. H., *Trans. Inst. Chem. Engrs. (London)*, **28**, 88 (1950).
- and A. P. Skelland, *ibid.*, **29**, 315 (1951).
- Geddes, R. L., *Trans. Am. Inst. Chem. Engrs.*, **42**, 79 (1946).
- Gerster, J. A., A. P. Colburn, W. E. Bonnett, and T. W. Carmody, *Chem. Eng. Progr.*, **45**, 716 (1949).
- Grohse, E. W., R. F. McCartney, H. J. Hauer, J. A. Gerster, and A. P. Colburn, *ibid.*, **45**, 725 (1949).
- Higbie, R., *Trans. Am. Inst. Chem. Engrs.*, **31**, 365 (1935).
- Hougen, O. A., and K. A. Watson, "Chemical Process Principles," Part II, p. 502, John Wiley and Sons, Inc., New York (1947).
- "International Critical Tables," Vol. 5, p. 32.
- Keyes, D. B., and L. Byman, *Univ. Ill. Eng. Expt. Sta. Bull. No. 328* (1941).
- Kharbada, O., D. Ch. E. thesis, Polytechnic Inst. Brooklyn (1953).
- Klinkenberg, A., and H. H. Moy, *Chem. Eng. Progr.*, **45**, 17 (1948).
- Lange, N. A., ed., "Handbook of Chemistry and Physics," Handbook Publishers, Inc., Sandusky, Ohio (1950).
- Lewis, W. K., Jr., *Ind. Eng. Chem.*, **28**, 399 (1936).
- Maier, C. G., *U. S. Bur. Mines Bull.*, **206**, 62 (1927).
- O'Brien, M. P. and J. E. Gosline, *Ind. Eng. Chem.*, **27**, 1936 (1935).
- O'Connell, H. E., *Trans. Am. Inst. Chem. Engrs.*, **42**, 741 (1946).
- Pattle, R. E., *Trans. Inst. Chem. Engrs. (London)* (Feb. 14, 1950).
- Peavy, C. C. and E. M. Baker, *Ind. Eng. Chem.*, **29**, 1056 (1937).
- Perry, J. H., "Chemical Engineers Handbook," 3 ed., p. 610-18, McGraw-Hill Book Company, Inc., New York (1950).
- Rogers, M. C., and E. W. Thiele, *Ind. Eng. Chem.*, **26**, 524 (1934).
- Schnurmann, R., *Z. physik. Chem.*, **143**, 456 (1929).
- Sherwood, T. K., "Absorption and Extraction," McGraw-Hill Book Company, New York (1937).
- and R. E. Reed, "Applied Mathematics in Chemical Engineering," McGraw-Hill Book Company, Inc., New York (1939).
- Smolin, W., I. Goldberg, and H. Welsh, thesis, Polytech. Inst. Brooklyn (1956).
- Spells, K. E., and S. Bakowski, *Trans. Inst. Chem. Engrs. (London)*, **28**, 38 (1950).
- ibid.*, **30**, 189 (1952).
- Van Krevelen, D. W., and J. J. Hoftijzer, *Chem. Eng. Progr.*, **46**, 29 (1950).
- Vershoor, H., *Trans. Inst. Chem. Engrs. (London)* (Feb. 14, 1950).
- Walter, J. F., and T. K. Sherwood, *Ind. Eng. Chem.*, **33**, 493 (1941).
- West, F. B., W. D. Gilbert, T. Shimizu, *Ind. Eng. Chem.*, **44**, 247 (1952).

Presented at A.I.Ch.E. St. Louis meeting

Calculated Performance of a Dissolved— gas-drive Reservoir by a Phase-behavior Method

F. H. BRINKMAN and C. F. WEINAUG

University of Kansas, Lawrence, Kansas

A phase-behavior approach to the prediction of the performance characteristics of a dissolved-gas-drive reservoir is unique in that the problem of choosing flash, differential, or composite-solution gas-oil ratios and formation-volume factors has been circumvented. Data required are a compositional analysis of the reservoir fluid, the bubble point of this fluid, and the relative-permeability curves for the reservoir rock.

Gas-oil ratios and formation-volume factors were calculated under conditions duplicating the performance of the reservoir. A comparison was then made between these results and those obtained by calculations involving a differential, a flash, and a composite process. A vital factor in the solution of the problem is the accuracy of the calculated equilibrium constant. Agreement within 3% was obtained when a calculated differential formation-volume curve was compared with an experimentally determined curve.

Many reservoir engineering calculations depend for their solution on laboratory pressure, volume, and temperature measurements of formation-volume factors and solution gas-oil ratios. How to determine these factors experimentally for the best duplication of the conditions under which reservoir oil is produced to the stock tank has been a matter of disagreement and much speculation in the oil industry.

Three methods are in general use today: the *differential process*, which assumes that as the pressure on an oil is lowered, the gas being liberated from the oil phase is continuously removed from contact with it; the *flash process*, which assumes that all the gas being liberated from the oil phase remains in contact with it; and the *composite process*, which assumes that a differential process occurs in the reservoir and a flash process occurs upon the liquid portion being produced to the stock tank. Each laboratory process has decided limitations and does not represent accurately conditions under which reservoir oil is produced.

A fourth method, a calculative process duplicating the performance characteristics of a dissolved-gas-drive reservoir, is presented here. This process largely escapes the deviations from actual field performance of the other three methods. It may be used to predict recoveries from dissolved-gas-drive reservoirs and may also serve as a tool for the comparison of present methods of determining formation-volume factor and solution gas-oil ratios with the values calculated from any process which duplicates the conditions of either the reservoir or production to the stock tank.

THEORY

Development of Equation

In the hypothetical reservoir chosen for this problem, the oil is assumed to

be at its bubble point at original conditions of temperature and pressure. Upon pressure depletion the relative permeabilities of the oil and gas phases are assumed to follow the curves illustrated in Figure 1.

Over an infinitesimal pressure drop a certain number of moles of fluid produced. The number of moles produced from the liquid phase for each component are given by the following equation:

$$x_n \Delta L_t = \Delta L_n \quad (1)$$

and from the vapor phase,

$$y_n \Delta V_t = \Delta V_n \quad (2)$$

The moles of component n remaining in the reservoir are then

$$C_{n_1} - \Delta L_n - \Delta V_n = C_{n_2} \quad (3)$$

The number of moles remaining over a pressure drop $P_2 - P_1$ may be expressed as

$$C_{n_1} - \int_{P_1}^{P_2} x_n dL_t - \int_{P_1}^{P_2} y_n dV_t = C_{n_2} \quad (4)$$

Since the variables x_n and y_n cannot be expressed in terms of L_t and V_t , respec-

tively, Equation (4) has no direct solution but must be solved by a trial-and-error procedure. Over small pressure increments Equation (4) may be expressed in the form

$$C_{n_1} - \frac{1}{2}[x_{n_1} + x_{n_2}]\Delta L_t - \frac{1}{2}[y_{n_1} + y_{n_2}]\Delta V_t = C_{n_2} \quad (5)$$

Equation (5) has a direct solution. The mole fractions of each component in the liquid phase and in the vapor phase are assumed at a pressure (P_2), averaged with the known mole fractions in the respective phases at (P_1), and multiplied by the assumed number of moles produced from the liquid or vapor phase. To check the assumptions made, however, three conditions must be satisfied. First, at P_2 the conditions of equilibrium equation (6) must be met:

$$\sum y_{n(P_2)} = \sum \left(\frac{K_n C_n}{(L/V + K_n)V} \right)_{P_2} = 1 \quad (6)$$

The actual mole fractions of the liquid and vapor phases may be calculated and checked against the assumed mole fractions in Equation (5). Second, the total number of moles of vapor and liquid remaining in reservoir are obtained also from Equation (6). Conversion of these moles to a volume at reservoir conditions by the use of empirical correlations (2) will result in a check upon the total number of moles withdrawn. If the volume calculated at P_2 is equal to the original reservoir volume calculated for 100 moles of liquid (in this case), then the total mole withdrawal ($\Delta L_t + \Delta V_t$) was estimated correctly. The third check to be made is for the assumed ratio $\Delta V_t/\Delta L_t$. From the assumed $\Delta V_t/\Delta L_t$ and the mole fraction of the produced fluids, the volumes of gas flowing per volume of liquid at reservoir conditions may be calculated from Equation (7):

$$\frac{\bar{V}_g}{\bar{V}_o} = \frac{ZRT}{P_{(avg)}} \frac{\rho_o}{M_o} \frac{\Delta V_t}{\Delta L_t} \quad (7)$$

This assumed \bar{V}_g/\bar{V}_o is compared with the average \bar{V}_g/\bar{V}_o calculated from the two instantaneous formations $(\bar{V}_g/\bar{V}_o)_{(1)}$ associated with the liquid saturations at P_2 and P_1 . This latter value is calculated by the use of Equation (8).

$$\frac{\bar{V}_g}{\bar{V}_o} = \left(\frac{\mu_o}{\mu_g} \right) \left(\frac{k_g}{k_o} \right) \quad (8)$$

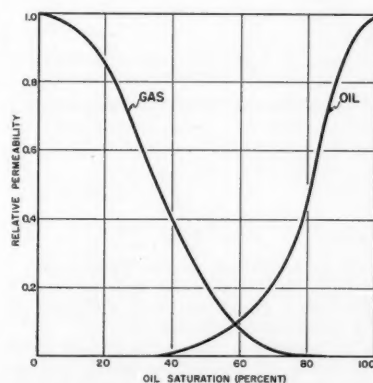


Fig. 1. Relative permeability.

F. H. Brinkman is at present with Carter Oil Company, Tulsa, Oklahoma.

If the assumed values of the mole fractions of each component, the total mole withdrawals, and the relative volume ratio of vapor to liquid withdrawals at reservoir conditions are in agreement with the corresponding calculated values, then Equation (5) is satisfied and the next pressure drop may be attacked.

PROCEDURE

Calculation of the Performance of a Dissolved-gas-drive Reservoir: Phase-behavior Method

Initial Data. The initial composition of an oil sample (5) for which a differential-formation-volume-factor curve was experimentally obtained was determined to be as follows:

Component	Mole fraction
Methane	0.3290
Ethane	0.1489
Propane	0.0393
Isobutane	0.0092
n-Butane	0.0283
Isopentane	0.0108
n-Pentane	0.0171
n-Hexane	0.0358
Heptanes plus	0.3816
	1.0000

Heptanes plus Saturation pressure
Molecular wt.-217 2,575 lb./sq. in. abs.
Sp. gr.-0.84 at 149°F.

Computed Data. Equilibrium constants, needed for the complete pressure range from the saturation pressure to atmospheric pressure, were calculated by the following sequence of steps:

1. The critical temperature of 810°F., the critical pressure of 265 lb./sq. in. abs., and the molal average boiling point of 502°F. of the heptanes plus (C_7+) fraction were determined by the methods recommended by Brown et al. (2).

2. The convergence pressure, 5,500 lb./sq. in. abs., was determined by Hadden's method (3).

3. The minimum K values shown in Figure 2 were computed by the procedure presented by G. G. Brown (2).

4. The equilibrium vaporization constants for methane shown in Figure 2 were obtained from the tables published by Hanson (4), and the constants for the constituents ethane through normal hexane were obtained from Brown's charts (2).

5. The values for the C_7+ fraction were obtained when the values for ethane through normal hexane were plotted against their respective normal boiling points and the molal average boiling point of the C_7+ fraction was extrapolated from this curve.

6. By the use of these values and the general shape of equilibrium-vaporization-constant curves for known systems, the curves were extended to the convergence pressure. A final adjustment in the curves made it possible for the computing, through equilibrium-vaporization constants, of a bubble point at 2,575 lb./sq. in. abs. by use of the equation

$$\sum (K_n C_n) = 1 \quad (9)$$

7. The volumes of the liquid and the vapors, both within the reservoir and at stock-tank conditions, were computed by the procedures of Brown (2).

8. Viscosity of reservoir oil was calculated by Beal's (1) correlation charts, and gas viscosity was obtained from the correlation charts of Muskat (6).

9. Relative permeabilities to each phase were determined from Figure 1, a hypothetical relative-permeability graph chosen for this problem.

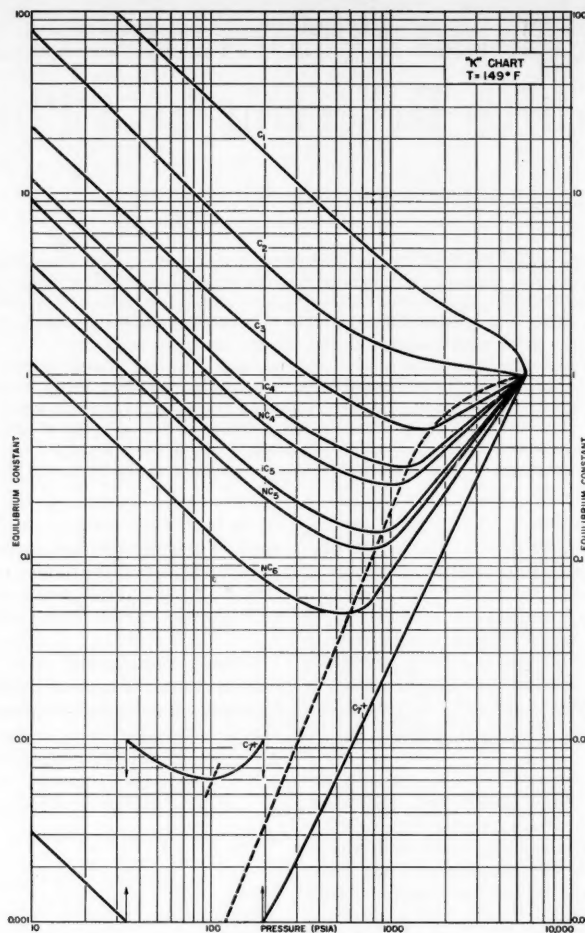


Fig. 2. Equilibrium constants.

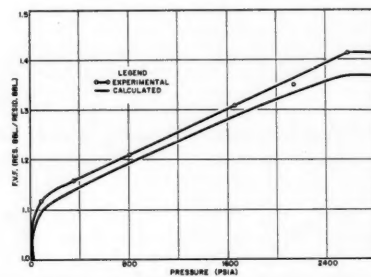


Fig. 3. Differential formation-volume factors.

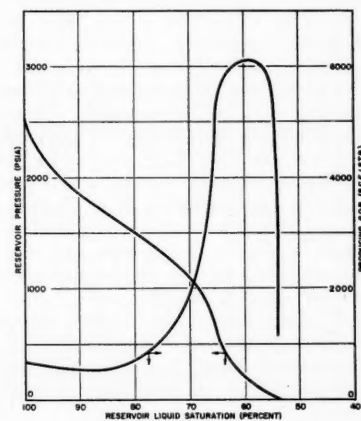


Fig. 4. Calculated pressure and gas-oil-ratio history.

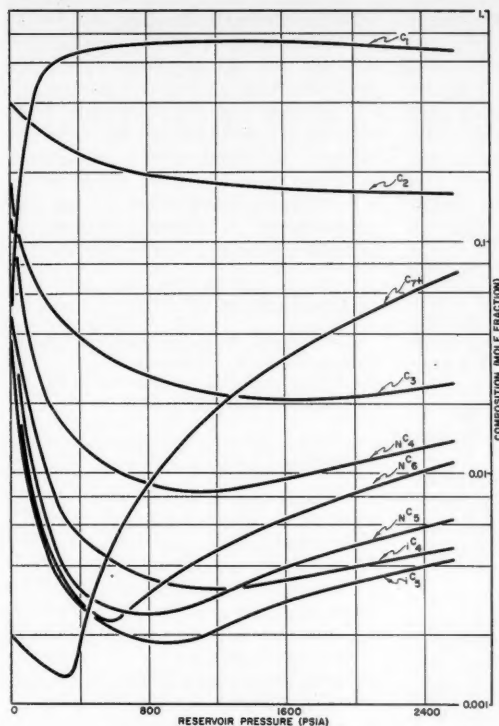


Fig. 5. Calculated reservoir-gas composition.

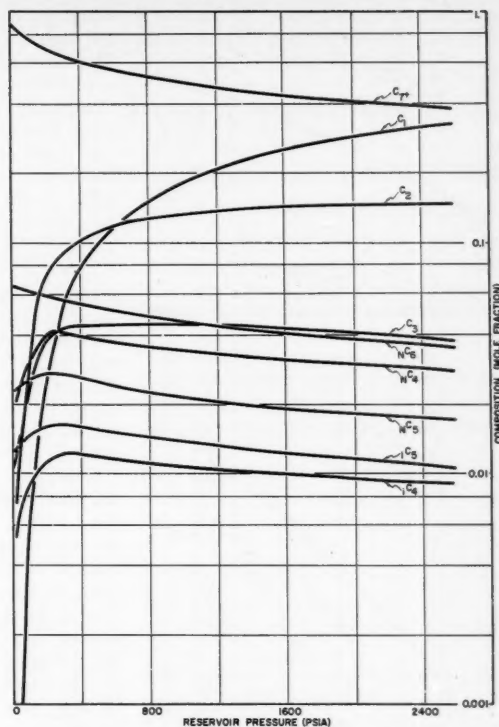


Fig. 6. Calculated reservoir-liquid composition.

The equations presented in the section on theory were solved for the pressure steps of 2,575, 2,000, 1,700, 1,400, 1,100, 700, 300, and 14.7 lb./sq. in. abs. by use of the procedures indicated above. Brinkman's dissertation (7) presents the calculations in tabular form for each of the pressure steps. It must be understood that the time required to make these involved calculations can be considerably shortened by the use of digital computing machines.

Calculation of Formation-volume Factors and Solution Gas-oil Ratios Characteristic of the Three Laboratory Processes

Differential Vaporization Process. The development of the equation

$$Wx_n - y_n dW = (W - dW)(x_n - \hat{x}_n) \quad (10)$$

which mathematically duplicates the differential vaporization process follows.

Simplifying Equation (10) and substituting $K_n x_n$ for y_n , one derives the equation

$$W dx_n = K_n x_n dW - x_n dW \quad (11)$$

Separating variables and integrating results in the equation

$$\int_{x_{n2}}^{x_{n1}} \frac{dx}{x_n(K_n - 1)} = \int_{W_2}^{W_1} \frac{dW}{W} \quad (12)$$

If the equilibrium constant in Equation (12) is taken at the mean effective pressure between the upper and lower limits of x_1 and x_2 , corresponding to a small pressure increment, then the term $1/(K_n - 1)$ may be considered a constant, and the resulting integration will lead to the equation

$$x_{n2} = x_{n1} \left(\frac{W_2}{W_1} \right)^{(K_n - 1)} \quad (13)$$

The summation of this equation results in the following final equation:

$$\sum x_{n2} = 1 = \sum (x_{n1}) \left(\frac{W_2}{W_1} \right)^{(K_n - 1)} \quad (14)$$

When the correct mean effective pressure is obtained, Equation (14) is satisfied. As the resultant liquid is at its bubble point, the bubble-point pressure may be calculated by multiplying the computed x_{n1} by equilibrium constants of pressures below the mean effective pressure until the following equation is satisfied:

$$\sum x_{n2} K_n = 1 \quad (15)$$

Equation (14) was solved repeatedly by the use of about 9/10 for the ratio of W_2 to W_1 until a liquid with a bubble point of 14.7 lb./sq. in. abs. at 149°F. resulted. This residual liquid was then cooled to 60°F., and the residual volume was calculated. From residual "liquid"

and the liquid volumes calculated at the various reservoir pressures obtained in the repetitive solution of Equation (14), the formation-volume-factor curve in Figure 3 was drawn.

Composite Process. The composite method of determining formation-volume factors and solution gas-oil ratios is similar to the differential method. The liquids obtained at the various pressures in the solution presented above, however, are flashed to 60°F. and 14.7 lb./sq. in. abs. The formation-volume factor is calculated when the volume of liquid at the high pressure and 149°F. is divided by the volume of liquid remaining after it has been flashed to 14.7 lb./sq. in. abs. and 60°F. The moles of gas formed in this flashing process are used in computing the solution gas-oil ratio.

Flash Process. A flash process is one in which the gas evolved from a liquid undergoing a pressure reduction is kept in continuous contact with the liquid. The procedure followed here is to flash the original liquid to various reservoir pressures and then the resulting liquid to stock-tank conditions.

Computed-field-performance Process. This method of obtaining formation-volume factors and solution gas-oil ratios involves the duplication of all the conditions of temperature, pressure, and gas-liquid associations for oil both in the reservoir and on the way to the stock tank. Reservoir volumes of oil at various

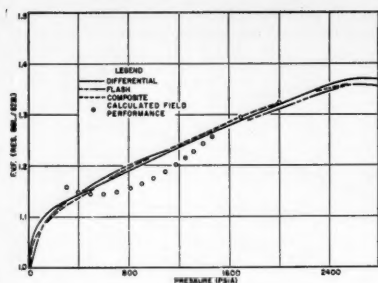


Fig. 7. Calculated formation-volume factors.

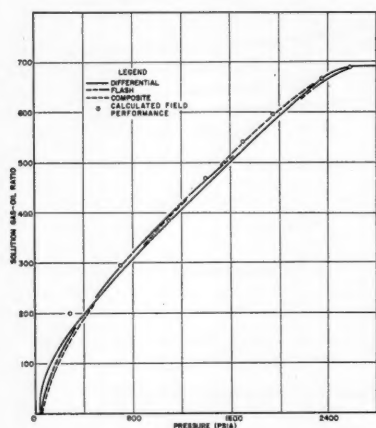


Fig. 8. Calculated solution gas-oil ratios.

pressures may be obtained from the calculations of the performance characteristics of the reservoir. The stock-tank volume of a unit reservoir volume of oil is then obtained by flashing to atmospheric conditions this reservoir oil with any gas flowing with it (the $(\bar{V}_g/\bar{V}_o)_{(i)}$ relationship existing at the specified reservoir pressure). The ratio of these volumes is the formation-volume factor. The solution gas-oil ratio is obtained when the stock-tank volume of oil is divided into the volume of solution gas released. This quantity is the difference between the total volume of vapor released and the volume of vapor initially flowing with the oil from the reservoir, all gas volumes being measured at atmospheric conditions. Incidental to the calculations is the fact that the producing gas-oil ratios may also be found when the total equilibrium volume of gas at the stock tank is divided by the equilibrium volume of oil at the stock tank.

DISCUSSION OF RESULTS

The calculated reservoir pressure and producing gas-oil ratios are shown in Figure 4 as functions of liquid saturation in the reservoir. The curves illustrate the typical characteristics associated with dissolved-gas-drive reservoirs. Figures 5

and 6 show the compositional changes in the gas and liquid phases in the reservoir. The most radical changes in compositions occur between 300 and 14.7 lb./sq. in. abs. Conversely, the first 900 lb./sq. in. drop from the saturation pressure produces only slight compositional changes in both the liquid and the gaseous phases. This latter result is a function of the relative permeabilities of the flowing phases. At 1,700 lb./sq. in. abs. the gas phase begins to flow, producing increasing compositional changes; these changes, however, are not radical but gradual. Initially, the fluid being produced comes entirely from the liquid phase. But when the gas saturation in the reservoir reaches a certain minimum value, the gas becomes mobile and production is then obtained from both phases.

The excess gas being produced with the oil may yield one of two effects: (a) at the lower pressures associated with separators and stock tanks the gas may become undersaturated and vaporize some of the associated liquid or (b) the gas may pass through a retrograde region, especially upon the lowering of temperature associated with production. In this second case the volume of liquid is augmented by the condensing liquid from the gas phase. Both these effects are illustrated in this problem.

Figures 7 and 8 show the formation-volume factors and solution gas-oil ratios calculated by the differential, the flash, the composite, and the phase-behavior-flash processes. Essentially the formation-volume factors for the early stages of pressure reduction check one another. Below 1,700 lb./sq. in. abs., the pressure at which gas begins to flow, condensation from the excess gas being produced with the oil causes a lowering of the formation-volume factor for the computed phase-behavior-flow process below formation-volume factors for the other processes. At the reservoir pressure of 300 lb./sq. in. abs., however, a change in the nature of the excess gas causes liquid vaporization and results in a higher formation-volume factor for the calculated phase-behavior-flow method.

The authors realize that the uncertainties of predicting equilibrium constants, etc., as well as the amount of work required, seriously limit the general application of this method. However, an examination of the formation-volume factors calculated by the various methods will show that serious deviations from actual behavior could result from the use of the type of equations developed by Turner (8) and Muskat (9) and the data from the present laboratory procedures. It is worth reiterating also that an ordinary desk-size calculating machine is of no help in making the involved computations that are needed. The method is practicable only where a multielement digital computer of the most recent type is available. The prediction, nevertheless,

of the laboratory differential data within 3% indicates that equilibrium constants, etc., do describe the behavior of this particular system. For this reason and for the fact that the deviations noted between the methods can be explained logically, the trends shown are believed to be real. It is hoped that these results will stimulate more effort toward the improvement of present methods of measuring formation-volume factors.

ACKNOWLEDGMENT

The authors wish to thank the State Geological Survey of Kansas for preparing the figures and making time available for the preparation of this article.

NOTATION

- x = liquid mole fraction
- y = vapor mole fraction
- C = total moles in reservoir
- L = moles of liquid in reservoir
- V = moles of vapor in reservoir
- M = molecular weight
- \bar{V}_g = flowing volume of vapor at reservoir conditions
- \bar{V}_o = flowing volume of liquid at reservoir conditions
- Z = compressibility factor
- R = gas constant
- T = absolute temperature
- P = absolute pressure
- K = vapor-liquid-equilibrium constant
- k = relative permeability
- μ = viscosity
- ρ = density
- W = moles of liquid present during differential vaporization

Subscripts

- n = component number
- t = total
- 1 = initial condition
- 2 = final condition
- i = instantaneous
- 0 = liquid
- g = gas

LITERATURE CITED

1. Beal, Carlton, *Petroleum Technol.*, T. P. 2018 (March, 1946).
2. Brown, G. G., D. L. Katz, G. G. Oberfell, and R. C. Alden, "Natural Gasoline and the Volatile Hydrocarbons," Natural Gas. Assoc. America, Tulsa, Okla. (1948).
3. Hadden, S. T., *Chem. Eng. Progr.*, **44**, No. 2 135 (February, 1948).
4. Hanson, G. H., M. J. Rzasa, and G. G. Brown, *Ind. Eng. Chem.*, **37** 1216 (1945).
5. Lindly, B. E., *Petroleum Engineer*, **7**, No. V, 34 (February, 1936).
6. Muskat, Morris, "Physical Principles of Oil Production," 94-95, (1949).
7. Brinkman, F. H., M.S. thesis, Univ. Kansas (1954).
8. Turner, J., *Oil Weekly*, 114, 32 (June 12, 1944).
9. Muskat, M., *J. Appl. Phys.*, **16**, 147 (1945).

Vapor-liquid Equilibria for Hydrogen-light-Hydrocarbon Systems at Low Temperatures

ALVIN L. BENHAM and DONALD L. KATZ

University of Michigan, Ann Arbor, Michigan

Experimental equilibrium vapor and liquid compositions are reported for the hydrogen-methane system at -150° , -200° , and -250°F . and at pressures of 500 to 4,000 lb./sq. in. The ternary system hydrogen-methane-propane was studied at 0° , -100° , and -200°F . at 500 and 1,000 lb./sq. in. Phase compositions were determined for a limited number of similar conditions for the hydrogen-methane-propylene and hydrogen-methane-ethylene-ethane-propylene-propane systems.

It has been noted that although low-temperature processing of hydrogen-containing light-hydrocarbon systems is becoming increasingly important, there is a deficiency in our knowledge of the behavior of these systems. Aroyan and Katz (1) and later Williams and Katz (10) have reviewed the available binary data for hydrogen-light hydrocarbon systems. Data are available for hydrogen with methane (4, 5, and 7), ethylene (10), ethane (10), propylene (10), propane (2 and 10), isobutane (3), and *n*-butane (1 and 9) and also for the hydrogen-

methane-ethylene (8) and hydrogen-methane-ethane (7) systems.

Since a study of the available hydrogen-methane data revealed internal scatter and inconsistency, new data were obtained for this system. Ternary-system data were obtained for the hydrogen-methane-propylene and the hydrogen-methane-propane systems. As an indica-

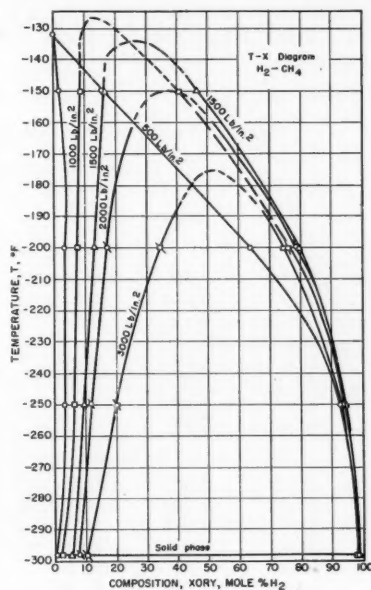
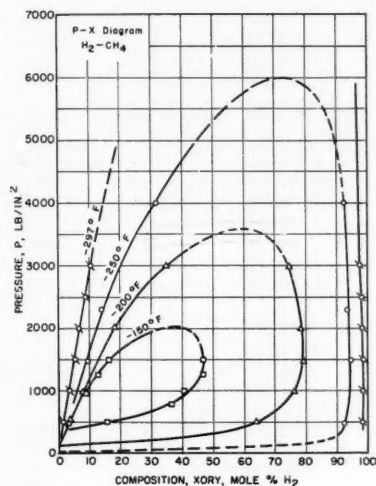


Fig. 2. ↑ Temperature-composition diagram for hydrogen-methane binary system.

Fig. 1. ← Pressure-composition diagram for hydrogen-methane binary system.

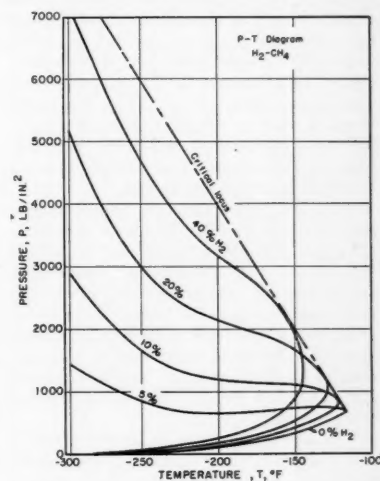


Fig. 3. Pressure-temperature diagram for hydrogen-methane binary system.

TABLE 1. ORIGINAL DATA FOR HYDROGEN-METHANE SYSTEM

Run	Temperature, °F.	Pressure,* lb./sq. in.	Phase compositions	
			Vapor mole % H ₂	Liquid mole % H ₂
3	-150	500	15.83	1.70
4	-150	1,000	40.60	8.77
8	-150	1,280	46.31	12.55
9	-150	1,500	46.78	16.22
2A	-200	500	63.92	3.43
5	-200	1,000	76.18	7.81
11	-200	1,490	79.31	13.10
2B	-200	1,990	78.23	18.05
15	-200	3,000	74.57	34.99
12	-250	490	92.79	3.18
13	-250	1,490	94.66	9.50
14	-250	2,300	93.83	13.94
16	-250	4,000	92.89	31.70

*All pressures are absolute pressures.

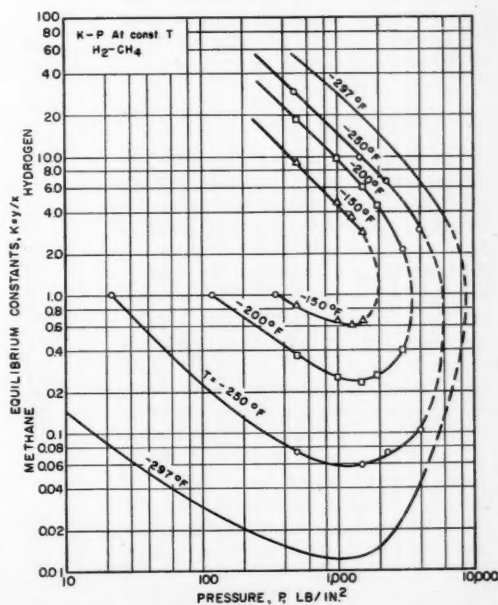


Fig. 4. Equilibrium constants vs. pressure for the hydrogen-methane system.

tion of the behavior of hydrogen in complex systems, some data were obtained for the hydrogen-methane-ethylene-ethane-propylene-propane system.

EQUIPMENT AND PROCEDURES

The equipment used for obtaining the experimental data was the same as previously described (1 and 10). Essentially it consisted of a high-pressure stainless steel cell in a constant-temperature air bath. An external circulating system took vapor from the top of the cell and returned it to the bottom of the cell.

The temperature in the cell was measured by a three-junction copper-constantan thermopile. The error in temperature measurement is believed to be within $\pm 1.0^\circ\text{F}$. at -300°F . and $\pm 0.1^\circ\text{F}$. at room temperature. Pressures are believed to be within $\pm 0.5\%$ of the true pressure. During measurements temperatures and pressures were held constant from 2 to 8 hr. within these limits. Samples of liquid phases were analyzed at intervals until two successive samples gave a constant composition. A thermal-conductivity cell was used to indicate the constancy of composition for the hydrogen-methane system.

Analyses of vapor and liquid phases, made with a CEC 21-103B mass spectrometer, are generally accurate to within $\pm \frac{1}{2}\%$ of the component composition except at low concentrations, where the error may be somewhat larger. Many of the analyses for the hydrogen-methane binary system were made by means of the gas-density method described by Williams and Katz (10) and are also believed to be accurate to within $\pm \frac{1}{2}\%$.

The gases used in this investigation as they existed in their containers were shown by the mass spectrometer to have a minimum purity of 99.0% (H_2 99.5%). Hydrogen and methane were both purified further by passing them through a train containing silica gel, Ascarite, and activated charcoal. The ethylene, ethane, propylene, and propane were purified further by a partial-differential vaporization.

HYDROGEN-METHANE SYSTEM

The hydrogen-methane system was studied at temperatures of -150° , -200° , and -250°F . and at pressures from 500 to 4,000 lb./sq. in. as given in Table 1. The pressure-composition diagram is given in Figure 1, in which the data of Freeth (5) at -297°F . have been included. The critical regions of the envelopes as shown in the illustrations are extrapolations. The reverse-order solubility of hydrogen is shown in the temperature-composition diagram, Figure 2. The envelopes terminate with the formation of a solid phase at about -300°F . The pressure-temperature plot of the data in Figure 3 shows that at low concentrations of hydrogen the phase envelopes contain a minimum and that at higher concentrations the slope of the bubble-point curve is always negative. The phenomenon was first noted by Kay (6) for the hydrogen-petroleum-

naphtha system. The equilibrium constants for hydrogen and methane have been plotted as a function of pressure in Figure 4.

HYDROGEN-METHANE-PROPANE SYSTEM

The hydrogen-methane-propane system was studied at temperatures of 0° , -100° , and -200°F ., Table 2, and at pressures of 500 and 1,000 lb./sq. in. Selected triangular plots of the phase compositions are given in Figures 5, 6, and 7. At -100°F . and 1,000 lb./sq. in., Figure 6, liberty was taken to extrapolate the phase-composition curves since a three-component critical point is known to lie on a curve connecting the liquid and vapor lines.

The equilibrium constants for hydrogen in the hydrogen-methane-propane system taken from smoothed triangular diagrams are plotted in Figure 8 as a function of the mole percentage of propane in the liquid phase. As shown, composition does have an effect upon the equilibrium constant for hydrogen, the effect being that addition of methane to the hydrogen-propane system results in decreasing the hydrogen equilibrium constant. Figure 9 contains the methane equilibrium constants taken from smoothed triangular diagrams and plotted as a function of the mole percentage of propane in the liquid phase. Figure 10 contains a similar plot of the propane equilibrium constants as a function of the mole percentage of propane in the liquid

TABLE 2. ORIGINAL DATA FOR HYDROGEN-METHANE-PROPANE SYSTEM

Run	Liquid composition			Vapor composition		
	Mole % H_2	Mole % CH_4	Mole % C_3H_8	Mole % H_2	Mole % CH_4	Mole % C_3H_8
Temperature = 0°F . Pressure = 500 lb./sq. in.						
25	0.15	25.83	74.02	3.98	84.08	11.94
26	0.329	23.57	76.10	8.31	80.26	11.43
27	0.717	20.98	78.30	13.96	73.29	12.75
28	0.907	16.13	82.96	27.90	60.70	11.40
29	1.13	13.67	85.20	37.26	52.08	10.66
30	1.31	11.72	86.98	45.76	43.37	10.87
31	1.00	7.97	91.03	58.75	31.66	9.59
(46)	2.30	0.00	97.70	90.70	0.00	9.30
Temperature = -100°F . Pressure = 500 lb./sq. in.						
(1)	0.00	62.0	38.0	0.0	98.70	1.30
20	0.452	49.58	49.97	14.36	84.43	1.21
21	0.645	44.99	54.36	22.13	76.73	1.14
22	0.683	42.38	56.94	24.57	74.21	1.22
19	1.09	24.93	73.98	59.80	39.25	0.95
18	1.22	21.40	77.38	68.72	30.46	0.82
24	1.16	16.07	82.77	67.83	31.04	1.13
(46)	1.55	0.00	98.45	99.02	0.00	0.976
Temperature = -200°F . Pressure = 500 lb./sq. in.						
(46)	0.86	0.0	99.14	99.9+	0.00	
46	0.789	8.59	90.62	95.73	3.79	0.48
44	1.79	43.67	54.54	83.40	15.92	0.68
48	2.85	87.07	10.08	—	—	
2A	3.43	96.57	0.00	63.92	36.08	0.00
Temperature = 0°F . Pressure = 1,000 lb./sq. in.						
(1)	0.00	53.00	47.0	0.00	90.30	9.70
32	2.02	32.77	65.21	25.54	66.09	8.37
33	2.67	25.70	71.63	45.49	47.77	6.74
34	2.75	24.30	72.95	46.89	45.78	7.33
35	3.09	17.90	79.01	58.95	34.57	6.48
36	3.79	13.03	83.18	66.57	26.57	6.86
(46)	4.75	0.00	95.25	94.08	0.00	5.92
Temperature = -100°F . Pressure = 1,000 lb./sq. in.						
(46)	3.02	0.00	96.98	99.31	0.00	0.69
37	2.76	14.70	82.54	85.62	13.39	0.99
38	3.27	34.28	62.45	61.82	36.81	1.37
39	3.27	46.37	50.36	—	—	
40	3.66	58.44	37.90	43.23	53.01	3.76
Temperature = -200°F . Pressure = 1,000 lb./sq. in.						
(46)	1.63	0.00	98.37	99.9+	0.00	
45	1.79	10.14	88.07	99.00	0.37	0.63
43	3.00	55.93	41.07	87.70	12.04	0.26
42	2.96	57.84	39.20	87.70	12.04	0.26
41	3.12	59.14	37.74	86.66	13.07	0.27
47	5.97	81.22	12.81	80.08	19.61	0.31
5	7.81	92.19	0.00	76.18	23.82	0.00

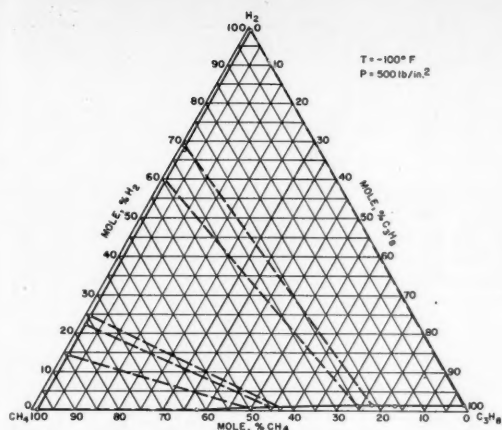


Fig. 5. Triangular composition diagram for hydrogen-methane-propane system at -100°F. and 500 lb./sq. in.

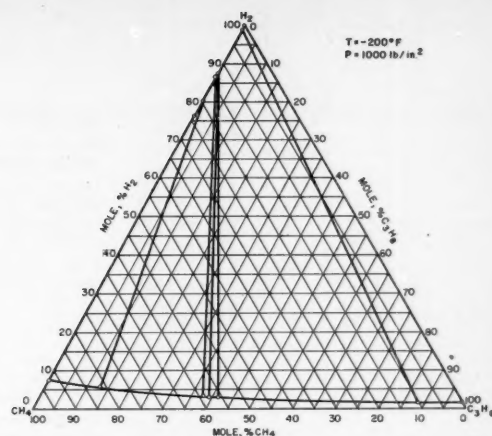


Fig. 7. Triangular composition diagram for hydrogen-methane-propane system at -200°F. and $1,000\text{ lb./sq. in.}$

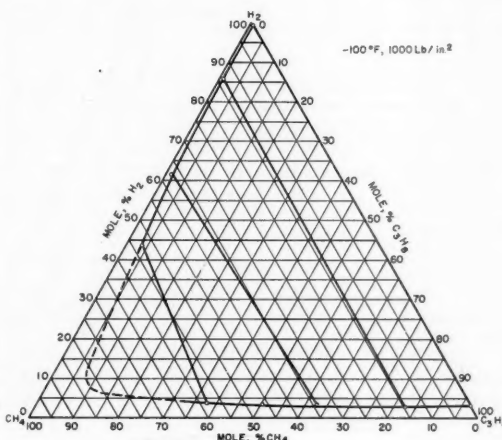


Fig. 6. Triangular composition diagram for hydrogen-methane-propane system at -100°F. and $1,000\text{ lb./sq. in.}$

TABLE 3. ORIGINAL DATA FOR HYDROGEN-METHANE-PROPYLENE SYSTEM

$-100^{\circ}\text{F.}, 500\text{ lb./sq. in.}$

Run	Liquid composition			Vapor composition		
	x_{H_2}	x_{CH_4}	$x_{\text{C}_3\text{H}_6}$	y_{H_2}	y_{CH_4}	$y_{\text{C}_3\text{H}_6}$
49	0.728	51.26	48.01	14.93	83.37	1.70
50	0.986	41.15	57.86	29.33	69.09	1.58
(46)	1.36	0.00	98.64	98.72	0.00	1.28

TABLE 4

ORIGINAL DATA FOR COMPLEX SYSTEM CONTAINING HYDROGEN, METHANE, ETHYLENE, ETHANE, PROPYLENE, AND PROPANE

Run		52	53	54	55	56	
Temperature, °F.		0	-100	-100	0	-100	
Pressure, lb./sq. in.		500	500	500	1,000	1,000	
Liquid phase compositions, mole %	}	H ₂	1.04	1.34	1.48	2.36	1.97
		H ₁	7.67	14.84	12.77	16.45	17.82
		C ₂ H ₄	9.42	9.06	18.23	17.32	17.97
		C ₂ H ₆	5.07	4.66	4.21	4.02	3.74
		C ₃ H ₆	8.39	7.77	7.07	6.67	6.00
		C ₃ H ₈	68.41	62.33	56.24	53.18	52.50
Vapor- phase compositions, mole %	}	H ₂	38.28	65.79	68.60	46.93	77.26
		CH ₄	31.37	30.45	25.45	35.18	19.66
		C ₂ H ₄	8.56	2.00	4.06	9.64	2.09
		C ₂ H ₆	3.44	0.65	0.60	1.73	0.38
		C ₃ H ₆	2.63	0.26	0.24	0.86	0.10
		C ₃ H ₈	15.72	0.85	1.05	5.66	0.51

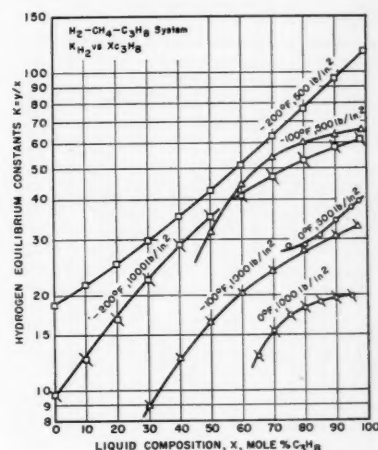


Fig. 8. Equilibrium constants for hydrogen in the hydrogen-methane-propane system as a function of mole percentage of propane in the liquid phase—cross plots.

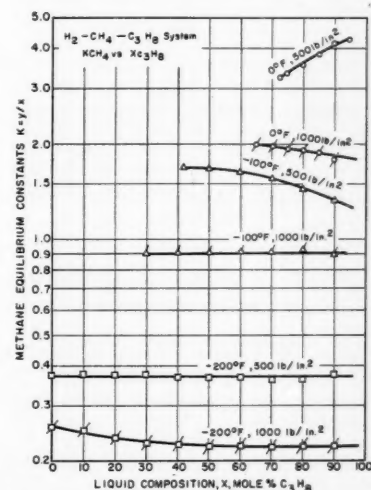


Fig. 9. Equilibrium constants for methane in the hydrogen-methane-propane system as a function of mole percentage of propane in the liquid phase—cross plots.

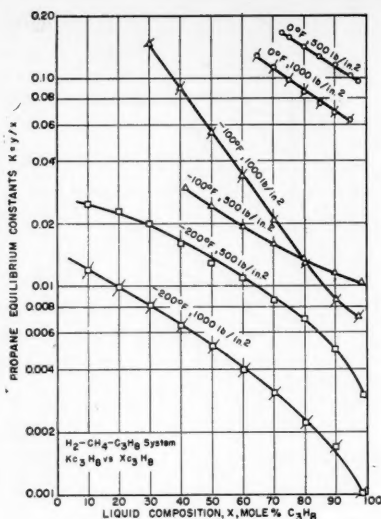


Fig. 10. ← Equilibrium constants for propane in the hydrogen-methane-propane system as a function of mole percentage of propane in the liquid phase—cross plots.

Fig. 12. → Constituent equilibrium constants in the hydrogen-methane-ethylene-ethane-propylene-propane system as a function of the normal boiling point.

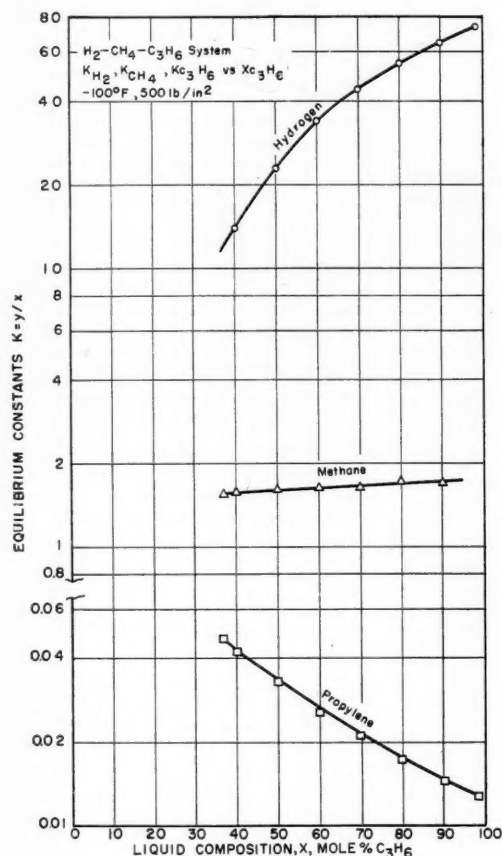


Fig. 11. ← Hydrogen, methane, and propylene equilibrium constants in the hydrogen-methane-propylene system as a function of the mole percentage of propylene in the liquid phase—cross plots.

phase. The effect of adding methane to the hydrogen-propane system is to increase the equilibrium constant for propane.

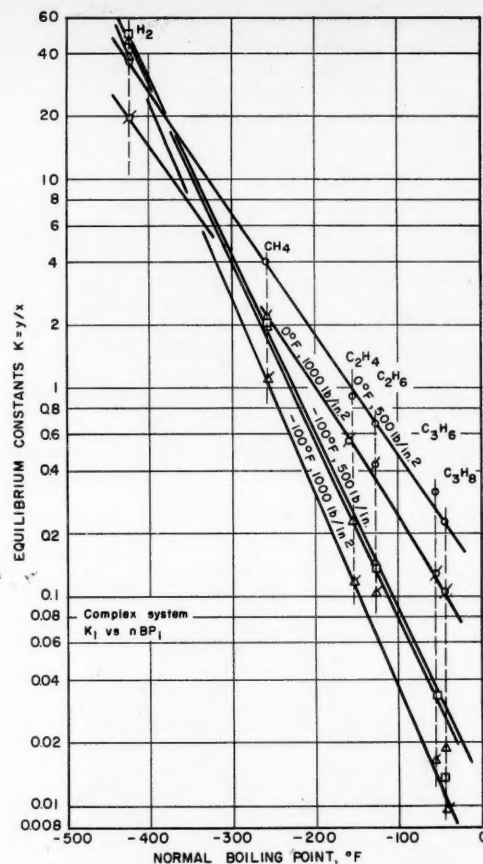
HYDROGEN-METHANE-PROPYLENE SYSTEM

Table 3 contains the phase compositions for two equilibria of the hydrogen-methane-propylene system at -100°F . and 500 lb./sq. in. These two equilibria along with the binary systems were

sufficient to establish the ternary diagram. Figure 11 shows equilibrium constants for the ternary system taken from this triangular diagram.

HYDROGEN-METHANE-ETHYLENE-ETHANE-PROPYLENE-PROPANE SYSTEM

Six equilibria were determined for the six-component system. Data were obtained at temperatures of 0° and -100°F . and at 500 and 1,000 lb./sq. in. (Table 4).



A plot of the equilibrium constants for the constituents as a function of their normal boiling points, Figure 12, indicates the consistency of the results.

ACKNOWLEDGMENT

This work was made possible by a fellowship grant from the Phillips Petroleum Company. The pure hydrocarbons were also donated by the Phillips Petroleum Company.

LITERATURE CITED

1. Aroyan, H. J., and D. L. Katz, *Ind. Eng. Chem.*, **43**, 185 (1951).
2. Burris, W. L., N. T. Hsu, H. H. Reamer, and B. H. Sage, *Ind. Eng. Chem.*, **45**, 210 (1953).
3. Dean, M. R., and J. W. Tooke, *Ind. Eng. Chem.*, **38**, 389 (1946).
4. Fastowsky, M. G., and V. G. Gonikberg, *J. Phys. Chem. (U.S.S.R.)*, **14**, 427 (1940).
5. Freeth, F. A., and T. T. H. Verschöyle, *Proc. Roy. Soc. (London)*, **130A**, 453 (1931).
6. Kay, W. B., *Chem. Revs.*, **29**, 501 (1941).
7. Levitskaya, E. P., *J. Tech. Phys. (U.S.S.R.)*, **11**, 197 (1941).
8. Likhter, A. I., and N. P. Tikhonovich, *ibid.*, **10**, 1201 (1940).
9. Nelson, E. E., and W. S. Bonnell, *Ind. Eng. Chem.*, **35**, 204 (1943).
10. Williams, R. B., and D. L. Katz, *ibid.*, **46**, 2512 (1954).

Mass Transfer at Low Pressures

THOMAS K. SHERWOOD and NORMAN E. COOKE

Massachusetts Institute of Technology, Cambridge, Massachusetts

Data are reported for the evaporation of spheres of naphthalene into air, helium, carbon dioxide, and Freon-12, and of liquid diethyl adipate into air at pressures from 0.1 to 3,000 μ Hg and at Reynolds numbers from 0 to 1.37. By use of suitable values of the surface-evaporation coefficient and the assumption of additivity of surface evaporation and diffusional resistances, the data are well correlated. The results lend semiquantitative support to the theory of sublimation of crystals developed by Stranski.

Mass transfer between a solid or liquid and a gas at low pressure is a subject of wide scientific and technological interest. Vacuum sublimation of ice ("freeze-drying") has been developed in recent years as a useful process for drying antibiotics, sera, blood plasma, and other heat-sensitive materials (52, 22, 16, 17, 18). Metals and inorganic salts are evaporated at low pressures to coat plastics, lenses, and other parts. Objects moving at high velocities in the upper atmosphere attain high temperatures and tend to sublime; for scientific purposes it is desirable to estimate the rate of sublimation of meteors and satellites.

The subject is also one of considerable interest in conjunction with various mass transfer operations in chemical engineering, as knowledge of evaporation at low pressures throws considerable light on the *interfacial*, or surface, resistance to mass transfer, about which relatively little is known.

THEORETICAL BACKGROUND

It is well known that solids and liquids evaporate at a *finite* rate in the absence of any gas-phase diffusional resistance. This rate is given by

$$\begin{aligned} -\frac{dW}{d\theta} &= \alpha A \sqrt{\frac{Mg_0}{2\pi RT}} (P_V - P_A) \\ &= \alpha AK_1(P_V - P_A) \end{aligned} \quad (1)$$

for which it is convenient, as indicated in the table of nomenclature, to express the gas constant R , the pressures P_V and P_A , and the conversion factor g_0 , in pressure units of microns Hg. Equation (1) with P_A equal to zero gives the rate of vaporization into an absolute vacuum.

This expression was first derived by Hertz (23) and later by Knudsen (32) and by Langmuir (33). The same relation has been derived (42) from statistical thermodynamics without the assumption of a particular model of gas behavior, such as the kinetic theory. It follows from a consideration of the rate of impingement of gas molecules on the surface as given by the kinetic theory for saturated vapor and of the assumption that the fraction $1-\alpha$ of the molecules hitting the surface does not condense. At equilibrium the rates of evaporation and condensation are assumed to be equal, whence it follows that the rate of vaporization into an absolute vacuum must be proportional to the *evaporation coefficient* α . As applied to the case of evaporation, Equation (1) is an expression for the rate of escape of molecules from the surface; no diffusional resistance, as of the vapor through air, is involved.

The difficulty with Equation (1) is the uncertainty regarding the evaporation coefficient α , which has been the subject of a great deal of experimental and theoretical investigation. A few of the many experimental values of α found in the literature are listed in Tables 1 and 2. Considerable evidence exists that α varies greatly with the purity of the material and the degree of surface contamination. Several investi-

gators have reported values of α increasing in successive tests as continuing efforts were made to remove minute traces of impurities, and Hickman (24) postulates that α should be unity for pure liquids with absolutely clean surfaces, in support of which he and Trevo (25) have induced water and glycerol to evaporate at rates corresponding to values of α from 0.5 to 1.0, which is twenty to forty times greater than rates reported by earlier workers who took less care to obtain clean surfaces. Evidently the effect of trace contaminants is so great that reported values of α may often be lower than the characteristic values for the substances tested.

All the values of α found in the literature were obtained with essentially pure substances. Data on solutions are completely lacking, though Emmert and Pigford (15) deduced a value of α of $1.8 - 7.4 \times 10^{-6}$ for the absorption of carbon dioxide by water and $3.7 - 9.1 \times 10^{-8}$ for oxygen in water.

Attempts to develop useful theoretical expressions for α have met with little success. Thus Polanyi and Wigner (4) relate α to the vibrational frequency of the molecules F , the molecular spacing r , and the enthalpy of vaporization L :

$$\alpha = \frac{L}{\pi F^2 r^3} = \frac{1.338L}{S^2} \quad (2)$$

The second form follows from the relation between F and the speed of sound in the liquid, S . Table 1 lists values of α calculated by means of this expression; it is evident that these compare very poorly with the experimental values. Though the two are not equal, Figure 1 suggests the possibility of a functional relationship with a sharp peak near a value of 0.08 for the right-hand side of Equation (2).

More recently Wyllie (59) has proposed that α should be numerically identical to the "free angle ratio" of Kincaid and Eyring (30). Table 1 lists this ratio for a number of liquids; it may be seen that these do not agree with the reported values of α .

By virtue of their more ordered structure, the sublimation of solids is more complex

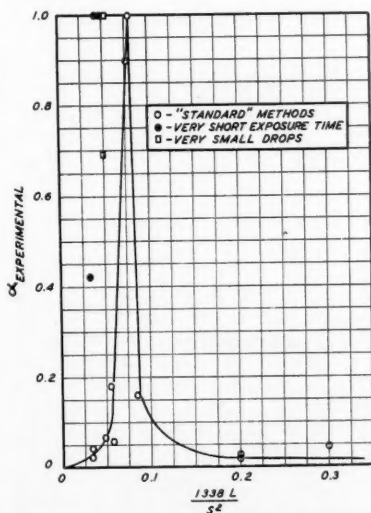
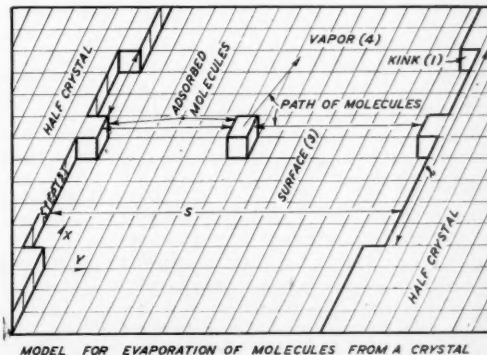


Fig. 1. Comparison of evaporation coefficients with theory of Polanyi and Wigner.

Fig. 2. Diagram illustrating process of separation of molecules from crystal surface.



than the evaporation of liquids. With increasing understanding of crystal growth and structure it has become evident that molecules can join and leave the crystal only at certain definite points on the surface and that diffusion of molecules over the surface occurs when crystals form, evaporate, or dissolve. The fact that the molecule must diffuse over the surface before it can pass into the vapor can materially reduce the rate of sublimation (51).

In Figure 2 the incomplete layer of molecules on top of complete layers is the *half crystal*. The boundary of the half crystal is a *step*, which contains *kinks* due to the incompleteness of the row of molecules. As the crystal sublimates, the molecule separates at the kink, moves out across the step, leaves the step to move across the plane, and finally leaves the plane and enters the vapor phase. The sequence is one of diffusional processes, each of which involves a resistance.

With this general picture as a model, Knacke, Stranski, and Wolff (31) derived an expression for α in terms of the several diffusional resistances:

$$\frac{1}{\alpha} = \frac{K_{pp}}{K_{sp}} \left[1 + \frac{K_{ks}}{K_{ks}} \right] + \frac{1}{K_{pp}} \quad (3)$$

Here K is a rate coefficient; subscript pv refers to the path from plane to vapor, sp to the path from step to plane, ks to that from kink to step, and pp to that across the plane. This result is of little practical use but represents the beginning of a valid theory. It explains the low value of 10^{-6} for α for claudetite (As_2O_3), since a primary valence bond must be broken and K_{ks} is very small. It suggests that α might increase with ambient gas velocity in cases where K_{pp} is small, as impinging gas molecules may assist transfer across the plane. As will be shown, this is the case for naphthalene, the flat molecules of which lead to small values of K_{pp} (as compared with the other K 's).

DIFFUSIONAL RESISTANCE

The molecular resistance to diffusion away from the evaporating surface becomes dominant at pressures above a few millimeters of mercury, and various empirical equations involving dimensionless groups have been developed for application to flow over surfaces of different shapes. For spheres the Frössling (19) equation with the constant recommended by Ranz and Marshall (48) is

$$\begin{aligned} -\frac{dW}{d\theta} &= \frac{2D_0MA}{PRTD} \\ &\cdot (1 + 0.30 Re^{1/2} Sc^{1/3})(P_v - P_A) \\ &= \frac{K_2A}{P} (P_v - P_A) \end{aligned} \quad (4)$$

where D_0 is the molecular diffusion coefficient at atmospheric pressure, sq. cm./sec.; D is the diameter of the sphere, cm.; Re is the Reynolds number based on the sphere diameter; Sc is the Schmidt group, $\mu/\rho D_0$; and P is the total pressure in microns Hg.

In the general case molecules must first escape from the surface and then be transported by molecular diffusion into the main body of the gas stream. It would appear to be a logical assumption that the resistances to both rate processes should be additive, with the individual resistances determined by Equations (1) and (4):

$$-\frac{A(P_v - P_A)}{dW/d\theta} = \frac{1}{\alpha K_1} + \frac{P}{K_2} \quad (5)$$

Because of the diffusional resistance, the rate will be less than the absolute rate of escape from the surface; let this fraction be β :

$$\frac{1}{\beta} = \frac{1}{\alpha} + \frac{K_1}{K_2} P \quad (6)$$

Here β is the ratio of the actual rate of evaporation to the absolute rate of

escape as given by Equation (1) for an α of unity; K_1 is defined by Equation (1); and K_2 is defined by Equation (4).

If K_1 is small, the rate of escape from the surface becomes controlling and the ratio β approaches the evaporation coefficient α . If K_2 is small or the pressure large, diffusion away from the surface becomes controlling, and the value of α is not important. The diameter of the sphere appears in the denominator of K_2 , and so the diffusional resistance may be relatively unimportant for very small spheres or drops, when the rate of evaporation is determined primarily by α , which conceivably varies with the radius of curvature. It may be noted that the ratio β does not depend on the vapor pressure and should not be affected by the increase in vapor pressure as the drop becomes very small.

The concept of additivity of diffusional

TABLE 1. VALUES OF THE EVAPORATION COEFFICIENT OF LIQUIDS

Substance	α experimental	α calc. by Eq. (2)	Free angle ratio, ψ	Remarks	Reference
Benzene	0.9	0.078	0.85		5
Carbon tetrachloride	1.0	0.079	1		3, 5, 47
Chloroform	0.16	0.086	0.54		5
Dibutyl phthalate	1.0	0.052	6.8×10^{-4}	Very small droplets	7
Diethyl adipate	0.18	0.050	0.54		This work
Diethyl hexylphthalate	1.0	0.042	6.1×10^{-5}	Short exposure time	25
Ethanol	0.24	0.20	0.020		10
Mercury	1.0	0.047	1	Short exposure time (32); small droplets (58)	32, 58
Methanol	0.045	0.30	0.05		5
Potassium	1.0	—	1		43, 45
Water	0.42	0.033	0.04	Very short exposure time	24
Water	0.04	0.033	0.04		1, 4

TABLE 2. VALUES OF THE EVAPORATION COEFFICIENT FOR SOLIDS

Substance	α Experimental	Notes	Reference
Ammonium chloride	3.9×10^{-4}	*	53
Benzoic acid	0.09-0.51		2
Cadmium	0.388-0.65	$T = 417.6^\circ$ to 507.6°C .	6
Camphor	0.139-0.190		
Ice	0.94 ± 0.06	-85° to -60°C . Very careful work	57
Ice	0.44	$T = -54.8^\circ\text{C}$.	56
Iodine	0.055-0.208	$40^\circ\text{C} \leq T \leq 70^\circ\text{C}$.	35
Mercuric bromide	0.64		39
Mercurous chloride	10^{-4}	*	41
Mercury	0.85-0.94	$-64^\circ\text{C} \leq T \leq -41.5^\circ\text{C}$.	58
Monoclinic arsenic oxide	10^{-6}	*	54, 55
Naphthalene	0.036-0.135	$40^\circ\text{C} \leq T \leq 70^\circ\text{C}$.	35
Naphthalene	0.0562-0.162	Variation due to nature of ambient gas and flow conditions. 0°C .	This work
Nickel	$0.75 < \alpha < 1$	Ring heated by an induction current	28
Phosphorous (red)	1.57×10^{-9}	$480^\circ\text{C} \geq T \geq 305^\circ\text{C}$.	37, 38
	4.67×10^{-3}	*	
Platinum	1	Hot-wire technique	29
Potassium	1	Vapor pressure of some faces greater than saturation vapor pressure	26
Potassium perrhenate	0.80	$T = 768^\circ$ to 742°K .	44
Sulfur	1	α varied from crystal face to crystal face as did vapor pressure of each face	49

*These four substances all apparently exist in one form in the solid and in an entirely different form in the vapor.

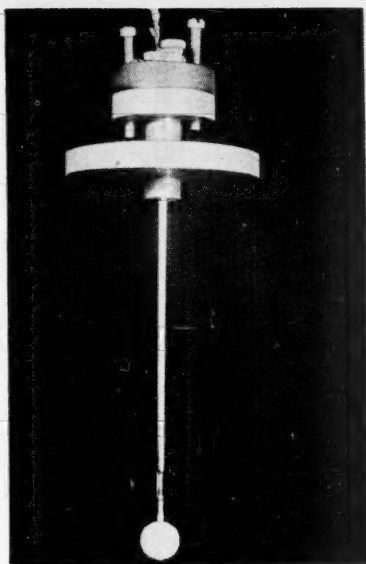


Fig. 3. Test sphere of naphthalene.

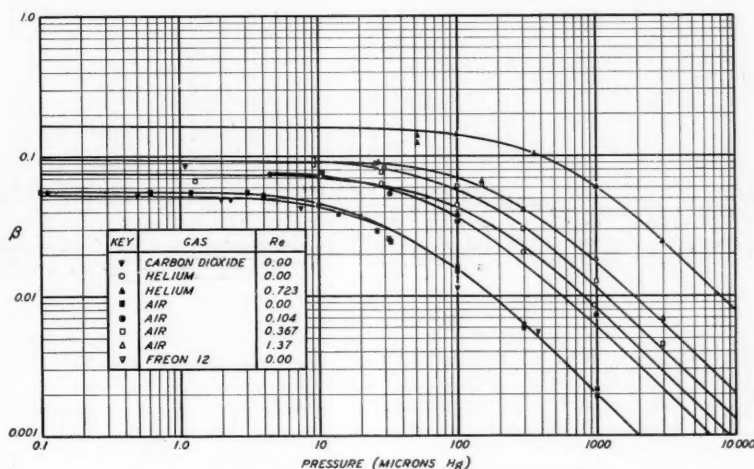


Fig. 4. Relative sublimation rates for naphthalene.

and surface-escape resistances has been employed previously by Langmuir and Langmuir (34), Carman (11), and others but never properly tested. Fuchs (20) and later Bradley and co-workers (7, 8) introduced a modification to allow for the ratio of the molecular mean free path to the dimensions of the experimental equipment. Monchick and Reiss (40) developed equations based on the non-equilibrium character of the gas phase and suggested that the apparent evaporation coefficient should change as drop size or pressure become very small.

Crout (14, 21, 50) showed that as

evaporation occurs the distribution of molecular velocities near the surface could not be the same as the equilibrium distribution and that, as a consequence, the rate of evaporation from a flat surface should be limited by the speed of sound in the vapor. Crout's theory would appear to apply only when the space above the evaporating surface has a minimum dimension of at least three mean free paths, since this length of travel by the molecules is necessary to reestablish a normal equipartition of energy in the vapor molecules. For the naphthalene used in the present work the mean free path at the lowest pressures was 16 cm., or more than three times the diameter of the tube employed, and so Crout's theory was not tested.

Application of Equation (5) requires that the ambient partial pressure P_A be known. In many cases there is an additional resistance to transport of vapor from the space surrounding the evaporating material to the point at which P_A is measured or controlled. Data are re-

ing but reradiating walls, and the numerical results are the same.

EXPERIMENTAL PROCEDURE

Small (1.0 cm.) spheres of naphthalene were sublimed at pressures from 0.1 to 3,000 μ total pressure in air, helium, carbon dioxide, and Freon-12. Rates of evaporation were measured in stagnant gas and in gas flowing over the sphere at Reynolds numbers up to 1.37.

The principal part of the apparatus consisted of a 5.08-cm. I.D. copper tube in which the test spheres were mounted. Dried gas entered through a controlled leak to an intermediate-pressure chamber, then through a sonic orifice to a flow-straightening section upstream of the test position. The latter consisted of a 12-cm. bundle of 0.63-cm. copper tubes each 12.8 cm. long. Downstream from the bundle of tubes the gas entered the 5.08-cm. copper tube through a reducing nozzle. Both nozzle and copper test section were internally polished.

The test sphere was centered in the test section 26 cm. downstream from the nozzle and 22.9 cm. upstream from the discharge into a 15.3-cm. steel pipe. The latter was evacuated by means of a large oil-diffusion pump (15.3-cm. throat) in series with a 100-cu. ft./min. mechanical pump. The entire flow-measuring, flow-straightening, and test sections were surrounded by a water bath maintained at 0°C. Pressure was measured by means of two McLeod gauges and one Alphatron gauge at taps 3.8 cm. downstream from the test sphere.

The naphthalene spheres were formed on a stainless steel stock carrying a thermocouple and were machined smooth. One of these is shown in Figure 3. When a test was made, the sphere was weighed and placed in the apparatus, the pressure adjusted, and the sphere removed and reweighed after approximately 0.178 g. had been estimated to be evaporated. Test periods varied from 0.4 to 29.1 hr. The weight-time relationship having been established, the observed times were adjusted to a constant weight loss of 0.1779 g., this being the observed loss in 1 hr. in the case of naphthalene at 0.10 μ with no gas flow.

Since both the rate of evaporation and gas flow were very small, the evaporative cooling of the surface was negligible, and both gas and sphere surfaces were within 0.1° of 0°C. in all tests. At this temperature the vapor pressure of the naphthalene as used was measured by the effusion technique and found to be 5.74 μ , agreeing well with an extrapolation of the data of Bryant (9) obtained by an air-saturation method at higher temperatures. The vapor pressure of diethyl adipate was found similarly to be 1.46 μ at 0°C. The diffusion coefficient for naphthalene in air at 1 atm. was taken (12) to be 0.0639 sq. cm./sec. and that for diethyl adipate as 0.0199 sq. cm./sec.

RESULTS

The data obtained were compared with Equation (6), as it was anticipated that the concept of additivity of surface-

escape and diffusional resistances might prove valid.

The rate was found to be independent of pressure below about 1μ , and so the results at 0.1μ were assumed to involve no diffusional resistance. The adjusted test time θ_2 is the ratio of the time at pressure P to the time for the same weight loss at 0.1μ (1 hr. for naphthalene), whence from Equations (5) and (6),

$$\theta_2 = \frac{\alpha}{\beta} = 1 + \alpha \frac{K_1}{K_2} P \quad (7)$$

The data were found to fall on straight lines when plotted as θ_2 vs. P , an indication that α was independent of pressure. In the case of stagnant air, α was found from the intercept to be 0.0625 and from the slope to be 0.0561; the latter is doubtless the better value.

Figure 4 summarizes the data on naphthalene in the form of a graph of β ($0.0561/\theta_2$) vs. pressure. The asymptotes at low pressure are the indicated values of the evaporation coefficient α , listed in Table 3. Decrease in β with increase in pressure indicates the increasing importance of the diffusional resistance.

The solid curves of Figure 4 are calculated from the theory of additivity of resistances, by use of Equation (6), with K_1 as defined by Equation (1). For finite gas flow the Ranz and Marshall value of K_2 was used, as given by Equation (4). With zero gas flow the naphthalene escaped by diffusion down the copper tube from the test sphere to the large exhaust conduit, where its partial pressure was essentially zero. In this case K_2 was obtained by adding the resistance to diffusion through the 22.9-cm. stagnant gas column to the diffusional resistance to evaporation from the sphere, as given by Equation (4).

The only data from the present study used in placing the lines on Figure 4 are the values of α obtained as described above. (Vapor pressure is not involved in β .) The excellent agreement with the experimental points would seem to be convincing proof of the additivity of surface evaporation and diffusional resistances. An alternative analysis is shown in Figure 5, where the observed and calculated values of β are compared directly.

Figure 6 shows similar results for the

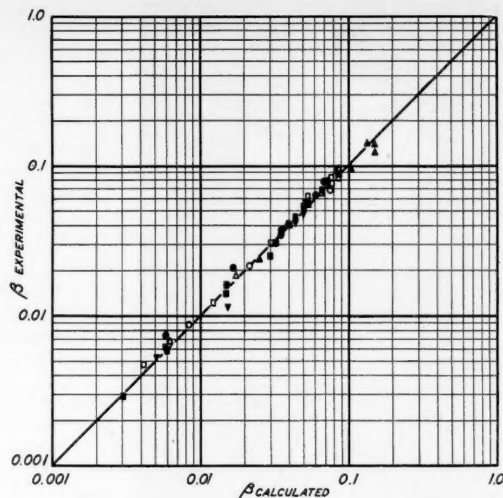


Fig. 5. Comparison of experimental and calculated sublimation rates.

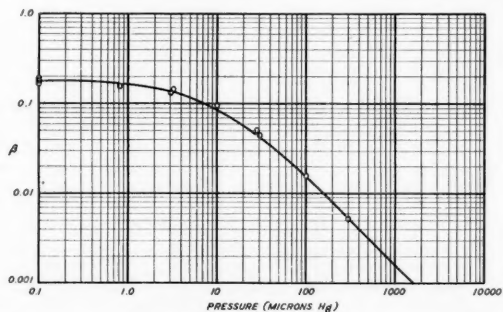


Fig. 6. Data on relative evaporation rates for diethyl adipate.

evaporation of carefully degassed liquid diethyl adipate from a stainless steel cup 1.11 cm. deep and 1.19 cm. in diameter. The calculated curve is based on a value of α of 0.177, with allowance for the reflection of molecules from the sides of the cup. This last effect corresponded to a resistance of 8 to 22% of that at the liquid surface, depending on the liquid level.

Monchick and Reiss (40) report data on the evaporation of very small drops of diamyl sebacate in a cloud chamber, and Birks and Bradley (7) give data on

the evaporation of small drops of dibutyl phthalate. These data are plotted in Figure 7 as

$$\frac{\alpha}{\beta} \text{ vs. } \alpha \frac{K_1}{K_2} P = \frac{\alpha DP}{2D_0} \sqrt{\frac{g_c RT}{2\pi M}}$$

with the values of α , P_v , and D_0 reported by these investigators. The results of this investigation for evaporation of naphthalene into stagnant air, helium, and carbon dioxide are also replotted, along with the theoretical line representing Equation (6). The general agreement of the data is good, and the results lend additional support to the basic theory represented by Equation (6). Only in the lower left corner of Figure 7 is the indicated agreement with theory sensitive to the value assumed for α . There is no evident trend indicating α to vary with the radius of curvature.

Several observations regarding the results of the present study may be made, in addition to an appraisal of the validity of the resistance theory. As the curves shown in Figure 4 are each based on a single value of α , it is evident that this coefficient is independent of pressure

TABLE 3. SUMMARY OF EXPERIMENTAL VALUES OF THE EVAPORATION COEFFICIENT

Evaporating substance	Gas	Reynolds number	α
Naphthalene	Air	0.00	0.0561
Naphthalene	Air	0.104	0.0773
Naphthalene	Air	0.367	0.0947
Naphthalene	Air	1.37	0.0960
Naphthalene	Helium	0.00	0.0758
Naphthalene	Helium	0.723	0.162
Naphthalene	Carbon dioxide	0.00	0.0526
Naphthalene	Freon-12	0.00	0.086 approx.
Diethyl adipate	Air	0.00	0.177

over the experimental range. Furthermore, the constancy of α over months of time for numerous test samples suggests that surface contamination, if present, was at least constant. The inference is that the values obtained are characteristic of the materials.

As shown in Table 3, α for naphthalene in air increases regularly from 0.0561 to 0.0960 as Re increases from 0 to 1.37; a somewhat greater effect of Re is indicated for naphthalene in helium. In line with the theory of Stranksi and co-workers, this result indicates that the flow of ambient gas may assist the transfer of molecules across the plane of the crystal (increase K_{pp}), the resistance to which is relatively large in the case of the flat naphthalene molecules. If K_{pp} is assumed to be a function of Re , Equation (3) may be put in the form

$$\frac{1}{\alpha} = A_1[1 + A_2 A_3] + A_4 f(Re) \quad (8)$$

where A_1 , A_3 , and A_4 depend only on the nature of the evaporating surface, and A_2 is a function of the interaction of foreign molecules with those of the crystal surface. Taking $f(Re)$ as 1.0 when Re is zero yields

$$\frac{1}{\alpha_0} - \frac{1}{\alpha} = A_4[1 - f(Re)] \quad (9)$$

where α_0 is the value of α with no gas flow. Figure 8 is a plot of the left-hand side of this expression vs. $1/Re$, from which the empirical form of $f(Re)$ may be developed. The intercept of 8.0 suggests that the highest values of α with flow over naphthalene are about 0.1 in air and 0.19 in helium.

It is also noted that α is smaller in air or carbon dioxide than in helium or Freon-12, the values for the latter two gases differing by less than 15%. It is difficult to imagine a mechanism by which the very dissimilar molecules helium and Freon-12 might produce nearly the same effect if both interfered with surface diffusion by adsorption on the surface. One can only speculate that neither helium nor Freon-12 affects the rate at all, but that air and carbon dioxide interfere in some way.

Recent chemical engineering literature has been concerned with the *interfacial*, or surface-evaporation, resistance, and it is of interest to note the magnitude of this effect in the case of evaporation into air at 1 atm. Figure 9 is a graph showing the surface-evaporation resistance as a percentage of the total resistance to mass transfer for air flow over a 1-cm. sphere of naphthalene, α being taken as 1.0. Corresponding values of the surface resistance for other values of α may easily be obtained: at 1 atm. the percentage is seen to be 2.5 at $Re = 10^7$; if α were 0.1 the value would be $2.5(1/0.1)/(0.975 + 0.25)$, or 20.4%. Evidently α must be very much smaller than the

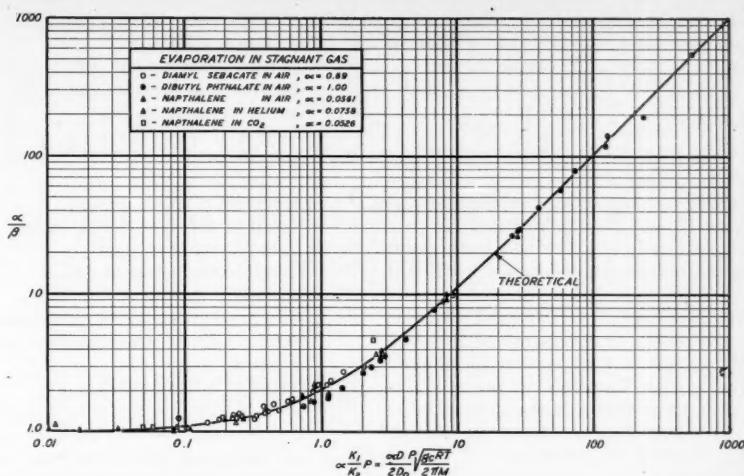


Fig. 7. Comparison of present data on naphthalene with data from the literature on small liquid drops.

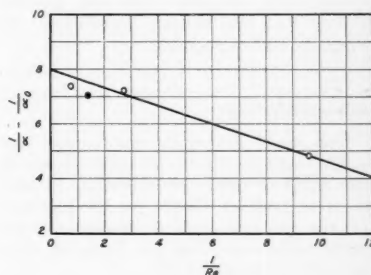


Fig. 8. Effect of gas-flow rate on evaporation coefficient.

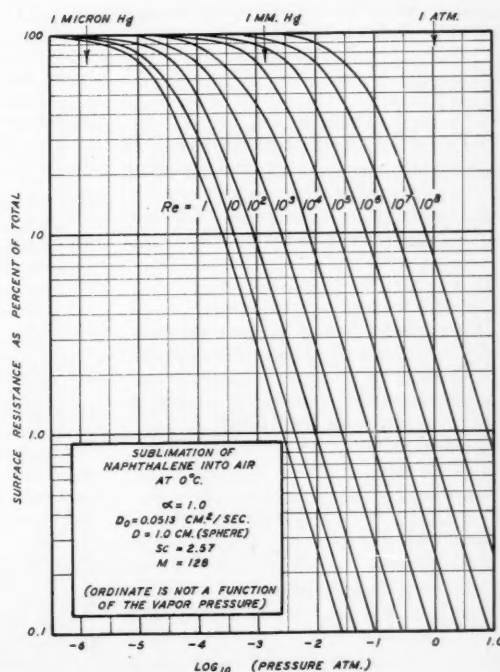


Fig. 9. Illustration of the relative importance of surface-evaporation and diffusional resistances.

values here reported for the surface resistance to be important at 1 atm. in the usual range of Reynolds numbers.

SUMMARY

Values of the evaporation coefficient α were measured for naphthalene subliming into air, helium, carbon dioxide, and Freon-12, and for liquid diethyl adipate evaporating in air. The results are given in Table 3. The evaporation coefficient was found to be independent of pressure over the range 0.1 to 3,000 μ of mercury, but to be higher in helium and Freon-12 than in air or carbon dioxide. Results obtained at Reynolds numbers up to 1.37 indicate that α increases with Re .

The data lend excellent support to the concept of additivity of surface evaporation and diffusional resistances, being capable of prediction on the basis of the available correlations for evaporation from single spheres together with experimental values of evaporation coefficients. The results agree in a semi-quantitative fashion with the general theory of sublimation developed by Stranski and coworkers.

ACKNOWLEDGMENT

The work described was carried out under contract DA-19-020-ORD-3244 with the Office of Ordnance Research, Department of Defense. Funds for the purchase of the vacuum pumps employed were supplied by the National Research Corporation Scientific Trust.

NOTE:—The original data are not tabulated, but are on file as the 1956 Sc.D. thesis of Norman E. Cooke in the Library of the Massachusetts Institute of Technology, Cambridge, Massachusetts. Photostat or microfilm copies may be ordered from the library.

NOTATION

A = surface area, sq. cm.

A_1, A_2, A_3 = functions of the nature of the surface of the evaporating solid substance

A_2 = function of interaction of foreign molecules with those of the crystal surface

D = diameter of sphere, cm.

D_v = diffusivity, sq. cm./sec.

D_0 = diffusivity at 1 atm., sq. cm./sec.

F = vibrational frequency of molecule, sec.⁻¹

g_c = conversion factor = 1.333 g. mass/(μ Hg)(cm.)(sec.²)

G = mass flow rate, g./sec.)(sq. cm.)

$$K_1 = \sqrt{\frac{Mg_c}{2\pi RT}}$$

$$K_2 = \frac{2D_0M}{RTD} (1 + 0.30 Re^{1/2} Sc^{1/3});$$

see Equation (4)

$K_p, K_{sp}, K_{ks}, K_{pp}$ = rate constants in Equation (3)

L = enthalpy of vaporization, g. cal./g.

M = molecular weight, g./g. mole

P = pressure, μ Hg

P_A = partial pressure of evaporating substance in ambient gas, μ Hg

P_v = vapor pressure, μ Hg

r = molecular spacing, cm.

R = gas constant = $62.37 \times 10^6 \mu$ Hg/(cc.)(g./mole)(°K.)

Re = Reynolds number, DG/μ

S = speed of sound in liquid, m./sec.

Sc = Schmidt number, $\mu/\rho D$

T = absolute temperature, °K.

W = mass, g.

α = evaporation coefficient (sometimes referred to as accommodation coefficient)

α_0 = value of α in stagnant gas

β = ratio of actual rate of mass transfer (evaporation) to the limiting rate of escape of molecules from the surface, as given by Equation (1) for $\alpha = 1.0$

μ = gas viscosity, g./sec.)(cm.)

ψ = free-angle ratio

ρ = gas density, g./cc.

θ = time, sec.

θ_2 = ratio of the time of evaporation of 0.1779 g. at pressure P to the time for the same weight loss at 0.1 μ

LITERATURE CITED

- Alty, T., *Phil. Mag.*, **15**, 82 (1933).
- , *Proc. Roy. Soc. (London)*, **A161**, 68 (1937).
- , and C. A. McKay, *ibid.*, **A149**, 104 (1935).
- Alty, T., and F. H. Nicoll, *Can. J. Research*, **4**, 547 (1931).
- Baranaev, M., *J. Phys. Chem. (U.S.S.R.)*, **13**, 1635 (1939).
- Bennewitz, K., *Ann. Phys.*, **59**, 193 (1919).
- Birks, J., and R. S. Bradley, *Proc. Roy. Soc. (London)*, **A198**, 226 (1949).
- Bradley, R. S., M. G. Evans, and R. W. Whytlaw-Gray, *Proc. Roy. Soc. (London)*, **A186**, 368 (1946).
- Bryant, H. S., Jr., Sc.D. thesis, Mass. Inst. Technol., Cambridge (1956).
- Bucka, H., *Z. physik. Chem.*, **195**, 260 (1950).
- Carman, P. C., *Trans. Faraday Soc.*, **44**, 529 (1948).
- Chipolone, M. D., S. M. thesis, Mass. Inst. Technol., Cambridge (1955).
- Clausing, P., *Ann. Phys.*, **5F12**, 961 (1932).
- Crout, P. D., *J. Math. and Phys.*, **15**, 1 (1936).
- Emmert, R. E., and R. L. Pigford, *Chem. Eng. Progr.*, **50**, 87 (1954).
- Flösdorf, E. W., "Biological Applications of Freezing and Drying," Chap. 2, Academic Press, Inc., New York (1954).
- , "Freeze-Drying," Reinhold Publishing Corp., New York (1949).
- , and S. Mudd, *J. Immunol.*, **29**, 389 (1935).
- Froessling, N., *Gerlands Beitr. Geophys.*, **52**, 170 (1938).
- Fuchs, N., *Physik. Z. Sowjetunion*, **6**, 224 (1934).
- Giddings, H. A., and P. D. Crout, *J. Math. and Phys.*, **15**, 124 (1936).
- Harris, R. J. C., ed., "Biological Applications of Freezing and Drying," Academic Press, Inc., New York (1954).
- Hertz, H., *Ann. Phys.*, **17**, 177 (1882).
- Hickman, K. C. D., *Ind. Eng. Chem.*, **46**, 1442 (1954).
- , and D. J. Trevo, *Ind. Eng. Chem.*, **44**, 1882 (1952).
- Hock, F., and K. Neumann, *Z. physik. Chem.*, **NF2**, 241 (1954).
- Hottel, H. C., and J. D. Keller, *Trans. Am. Soc. Mech. Engrs.*, **55-56**, 39 (1933).
- Johnston, H. L., and A. L. Marshall, *J. Am. Chem. Soc.*, **62**, 1382 (1940).
- Jones, H. A., I. Langmuir, and G. M. Mackay, *Phys. Rev.*, **30**, 201 (1927).
- Kincaid, J. F., and H. Eyring, *J. Chem. Phys.*, **6**, 620 (1938).
- Knacke, O., I. N. Stranski, and G. Wolff, *Z. physik. Chem.*, **198**, 157 (1951).
- Knudsen, M., *Ann. Phys.*, **47**, 697 (1915).
- Langmuir, I., *Phys. Rev.*, **2**, 329 (1913).
- , and D. B. Langmuir, *J. Phys. Chem.*, **31**, 1719 (1927).
- Marcellen, R., *Compt. Rend.*, **158**, 1674 (1914).
- Marshall, A. L., K. W. Dornte, and F. J. Norton, *J. Am. Chem. Soc.*, **59**, 1161 (1937).
- Melville, H. W., and S. C. Gray, *Trans. Faraday Soc.*, **32**, 271 (1936).
- Ibid.*, 1026 (1936).
- Metzger, F., and E. Miescher, *Nature*, **142**, 572 (1938).
- Monchick, L., and H. Reiss, *J. Chem. Phys.*, **22**, 831 (1954).
- Neumann, K., *Z. physik. Chem.*, **A191**, 284 (1942).
- ibid.*, **A196**, 16 (1950).
- Ibid.*, **NF2**, 215 (1954).
- , and V. Costeanu, *Z. physik. Chem.*, **A185**, 65 (1939).
- Neumann, K., and K. Schmoll, *Naturwissenschaften*, **39**, 131 (1952).
- Polanyi, M., and E. Wigner, *Z. physik. Chem.*, **A139**, 439 (1928).
- Pruger, W., *Z. Physik*, **115**, 202 (1940).
- Ranz, W. E., and W. R. Marshall, *Chem. Eng. Progr.*, **48**, 173 (1952).
- Rideal, E., and P. M. Wiggins, *Proc. Roy. Soc. (London)*, **A210**, 291 (1951).
- Schrage, R. W., "A Theoretical Study of Interphase Mass Transfer," Columbia Univ. Press, New York (1953).
- Sears, G. W., *J. Chem. Phys.*, **24**, 868 (1956).
- Shackell, L. F., *Am. J. Physiol.*, **24**, 325 (1909).
- Spingler, H., *Z. physik. Chem.*, **B52**, 90 (1942).
- Stranski, I. N., and U. Winkler, unpublished, quoted in Knacke, O., I. N. Stranski, and G. Wolff, *Z. Elektrochem.*, **56**, 476 (1952).
- Stranski, I. N., and G. Wolff, *Z. Elektrochem.*, **53**, 1 (1949).
- Strickland-Constable, R. F., and E. W. Bruce, *Trans. Inst. Chem. Engrs. (London)*, **32**, 192 (1954).
- Tschudin, K., *Helv. Phys. Acta*, **19**, 91 (1946).
- Volmer, M., and I. Estermann, *Z. Physik*, **7**, 1 (1921).
- Wyllie, G., *Proc. Roy. Soc. (London)*, **A197**, 383 (1949).

Mass and Heat Transfer to Single Spheres and Cylinders at Low Reynolds Numbers

S. K. FRIEDLANDER

Columbia University, New York, New York

Rates of mass and heat transfer to single spheres and cylinders at low Reynolds numbers are predicted from boundary-layer theory. The velocity distributions which are assumed to exist are those derived from the linearized Navier-Stokes equations by Tomotika and Aoi.

In the case of the sphere the Nusselt number is found to be a function only of the Peclet group when the Stokes streamline function is assumed to apply. Experimental data for mass and heat transfer to single spheres fall 10 to 40% higher than predicted from the theory. Experimental data for heat and mass transfer to single cylinders at large N_{Pe} check the theory.

Curves are also plotted for the efficiency of removal of colloidal particles by combined direct interception and diffusion for both spheres and cylinders.

This paper deals with the theory of mass and heat exchange between single spheres or cylinders and fluids when the relative motion is laminar and natural convection can be neglected. Transfer of this type is of importance in extraction from drops or in the solution of solid particles (continuous phase a liquid) when diameters are smaller than 200 to 500 μ . It is of interest in spray drying and aerosol scrubbing (continuous phase a gas) when the drops are smaller than about 100 μ in diameter. For cylinders the problem is receiving considerable attention because of its application to aerosol filtration by fibrous filters. In addition, the phenomenon is of importance in the case of low velocity measurements by hot-wire anemometers.

For steady state mass transfer with low concentrations and constant diffusivity, the equation describing diffusion in a moving fluid takes the form

$$u' \frac{\partial c'}{\partial x'} + v' \frac{\partial c'}{\partial y'} + w' \frac{\partial c'}{\partial z'} = D \left[\frac{\partial^2 c'}{\partial x'^2} + \frac{\partial^2 c'}{\partial y'^2} + \frac{\partial^2 c'}{\partial z'^2} \right] \quad (1)$$

A similar expression can be written for heat transfer provided viscous dissipation can be neglected. These expressions apply to any flow regime, but solutions vary depending on the form of the velocity distribution. No general solution appears to exist for laminar flow around spheres or cylinders, although Kronig and Bruijsten (6) and Frisch (4) have obtained expressions for N_{Nu} for the sphere at very small values of N_{Pe} by use of perturbation methods. For the case of the cylinder Langmuir (7) has derived an equation

for N_{Nu} by a rough method of approximation.

Heat transfer from flat plates and cylinders at very high Reynolds numbers has been investigated theoretically by use of boundary-layer theory and the Von Karman integral relation. A number of calculations of this type are reported by Eckert (2). The approach involves the assumption of the existence of a thermal boundary layer, that is, a limited region of the flow which is affected by the presence of the heated surface. At the edge of the layer the temperature reaches the main-stream value and all the temperature derivatives (with respect to the normal to the surface) vanish. If a temperature distribution is assumed, the heat transfer rate can be calculated by use of the known velocity distribution and a simple heat balance. The velocity profile is usually calculated from momentum-boundary-layer theory, which applies at high Reynolds numbers. The Nusselt number obtained in this way is insensitive to the form of the original temperature distribution, and the theoretical results compare well with experiment up to the point of separation of the boundary layer (2). The success of the method together with its simplicity are its principal justification as it lacks rigor in several respects.

In this paper a similar approach is taken but the velocity distribution which is assumed to exist is that derived from the linearized Navier-Stokes equations by Tomotika and Aoi (9). Stream functions derived in this way apply for $N_{Re} \leq 5$. In the case of the sphere the method permits evaluation of N_{Nu} over the entire N_{Pe} range in contrast with the perturbation methods (4, 6) which can be used only for small N_{Pe} . For the

cylinder a simplified stream function correct only near the surface is used and the results are limited to large N_{Pe} , i.e., to thin boundary layers as in aerosol diffusion and heat and mass transfer in liquids. Again the primary justifications for the attack are the success attending its application and its simplicity.

Few experimental data have been reported in the literature for the low N_{Re} range. Ranz and Marshall (8) and Kramers (5) have obtained data for mass and heat transfer to spheres. In the high N_{Pe} range, data on heat transfer to cylinders have been obtained by Davis (1) and recalculated by Ulsamer (10), and data on mass transfer by Dobry and Finn (3).

DIFFUSION FROM SINGLE SPHERES

A fluid flows in the positive x direction around a sphere from which material (or heat) diffuses. The steady state has been reached, and resistance to transfer is present only in the fluid. It is assumed that a concentration (or thermal) boundary layer exists around the sphere with a radius b' , which is a function only of the angle θ between the radius vector and the positive x axis. It is not necessary that $b' - a$ be small. At the boundary the concentration has attained the main-stream value. A mass balance (mass transfer will be referred to in the rest of the paper although the results are equally applicable to heat transfer) is written for the region between the surface of the sphere and the boundary layer, diffusion being neglected in the θ direction. (The latter is 0 for $N_{Pe} = 0$ and is very small for very large values of N_{Pe} .)

At any angle θ the total amount of

material which has diffused from the surface is given by the expression

$$F' = \int_0^{\psi'} 2\pi c' d\psi' \quad (2)$$

where $2\pi\psi'$ is the volumetric flow rate of the fluid and $c' = C - C_M$. If no diffusion occurs in the θ direction, the change in F' with θ is due only to the mass diffusing from the surface:

$$\begin{aligned} -\frac{dF'}{d\theta} \delta\theta \\ = -D \left(\frac{\partial c'}{\partial r} \right)_{r'=a} 2\pi a \sin \theta \delta\theta \quad (3) \end{aligned}$$

or

$$\begin{aligned} -\frac{d \left[\int_0^{\psi'} c' d\psi' \right]}{d\theta} \\ = -D \left(\frac{\partial c'}{\partial r} \right)_{r'=a} a^2 \sin \theta \quad (4) \end{aligned}$$

This equation can also be obtained by partial integration of Equation (1) when diffusion in the θ direction is assumed negligible. For $N_{Re} \ll 1$, ψ' is given by Tomotika and Aoi (9) as

$$\psi' = \frac{1}{2} U r'^2 \left(1 - \frac{3}{2} \frac{a}{r'} + \frac{1}{2} \frac{a^3}{r'^3} \right) \sin^2 \theta \quad (5)$$

Equation (5) will be recognized as the Stokes stream function for the sphere. When

$$r = \frac{r'}{a}, \quad \psi = \frac{\psi'}{a^2 U}, \quad (6)$$

and

$$c = \frac{C - C_M}{C_0 - C_M}$$

then

$$\begin{aligned} -\frac{dF}{d\theta} &= -\frac{d \left[\int_0^{\psi} c d\psi \right]}{d\theta} \\ &= -\frac{2}{N_{Pe}} \left(\frac{\partial c}{\partial r} \right)_{r=1} \sin \theta \quad (7) \end{aligned}$$

The boundary conditions which must be satisfied by c and its derivatives are obtained from the definition of the boundary layer and from (1):

at $r = 1$,

$$c = 1, \quad \frac{\partial \left(r^2 \frac{\partial c}{\partial r} \right)}{\partial r} = 0 \quad (8)$$

at $r = b(\theta)$,

$$c = 0, \quad \frac{\partial c}{\partial r} = 0, \quad \frac{\partial \left(r^2 \frac{\partial c}{\partial r} \right)}{\partial r} = 0$$

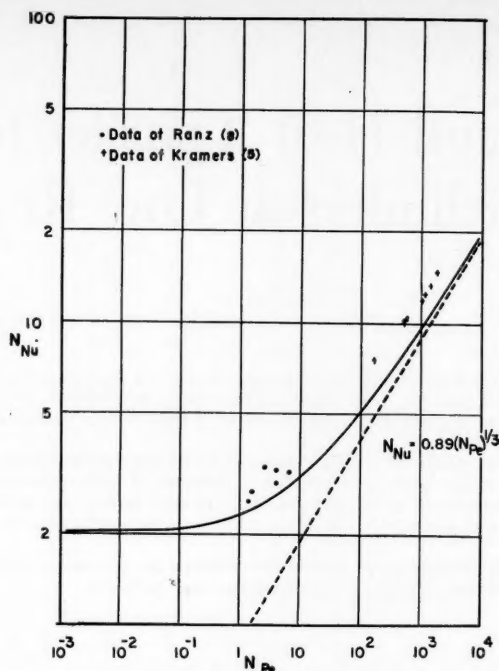


Fig. 1. Transfer to single spheres.

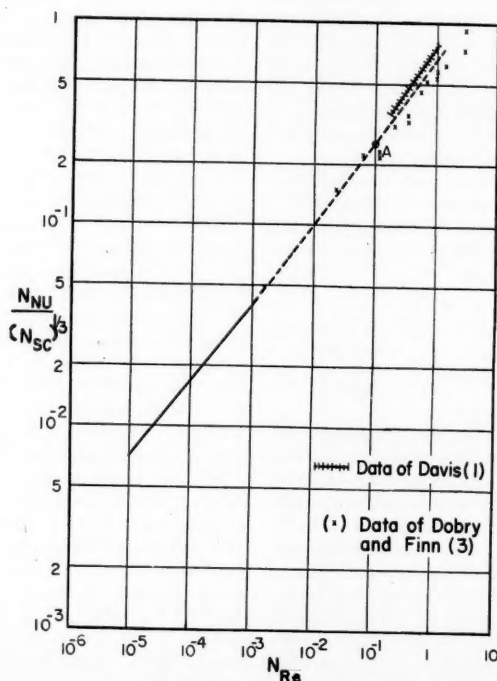


Fig. 2. Transfer to single cylinders.

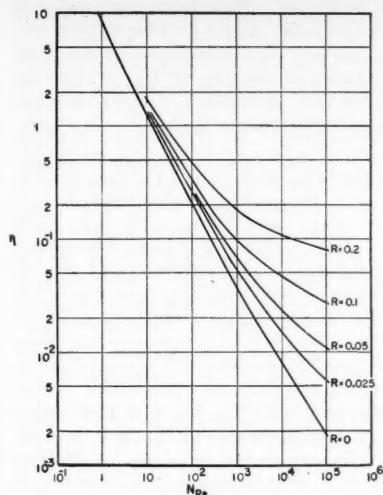


Fig. 3. Removal efficiency for spheres by combined diffusion and direct interception.

In the manner often used in boundary-layer problems, a distribution is assumed for c which satisfies as many boundary conditions as possible. A particularly simple form is

$$c = 1 - \left[\frac{1 - \frac{1}{r}}{1 - \frac{1}{b}} \right] = 1 - \left[\frac{1 - \frac{1}{h}}{\frac{r}{h}} \right] \quad (9)$$

This expression satisfies all the foregoing conditions with the exception of $\partial c / \partial r = 0$ at $r = b$; it has the additional advantage of reducing to the stagnant distribution when $b = \infty$; viz., $c = 1/r$. Now

$$F = \int_0^{\psi_b} c \, d\psi = \int_0^{(c\psi)_{r=b}} d(c\psi) - \int_1^{c_{r=b}} \psi \, dc \quad (10)$$

or with (8)

$$F = - \int_1^0 \psi \, dc \quad (11)$$

Substituting (5) and (9) gives

$$F = \frac{1}{h} \int_1^b \frac{1}{2} \left(1 - \frac{3}{2r} + \frac{1}{2r^3} \right) \sin^2 \theta \, dr = \frac{1}{h} \left(\frac{b}{2} - \frac{3}{4} \ln b - \frac{1}{8b^2} - \frac{3}{8} \right) \sin^2 \theta \quad (12)$$

Substituting in (7) results in

$$\frac{dF}{d\theta} = \frac{d \left[\frac{1}{h} \left(\frac{b}{2} - \frac{3}{4} \ln b - \frac{1}{8b^2} - \frac{3}{8} \right) \sin^2 \theta \right]}{d\theta}$$

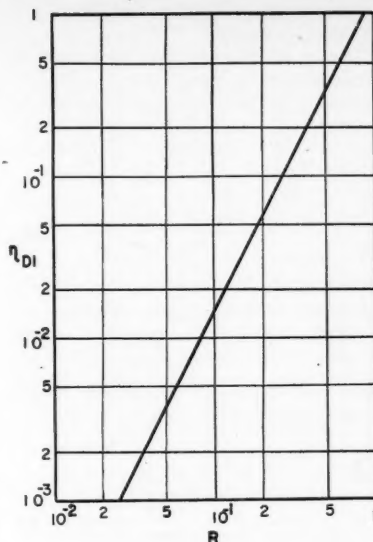


Fig. 4. Removal efficiency by direct interception for single spheres.

$$= \frac{2 \sin \theta}{N_{Pe} h} \quad (13)$$

An analytical solution of this equation can be obtained for very large or very small N_{Pe} , but for the intermediate region it is necessary to integrate numerically.

For very large N_{Pe} (very thin boundary layers), F may be expanded as a function of h and then all high-order terms dropped:

$$\begin{aligned} \frac{F}{\sin^2 \theta} &= \frac{1}{h} \left[\frac{1}{2} (1 + h + h^2 + h^3 + h^4 + \dots) - \frac{3}{4} \left(h + \frac{h^2}{2} + \frac{h^3}{3} + \frac{h^4}{4} + \dots \right) - \frac{1}{8} + \frac{1}{4}h - \frac{1}{8}h^2 - \frac{3}{8} \right] \\ &= \frac{h^2}{4} + \frac{5}{16}h^3 + \dots \quad (14) \end{aligned}$$

or

$$F \cong \frac{h^2}{4} \sin^2 \theta$$

Rearranging (13) gives

$$\left(\frac{h \sin \theta}{2} \right) \frac{dF}{d\theta} = - \frac{\sin^2 \theta}{N_{Pe}} \quad (15)$$

and integrating between $F = 0$ at $\theta = \pi$ and $F = F_\infty$ at $\theta = 0$ gives

$$F_\infty = \left(\frac{3\pi}{4N_{Pe}} \right)^{2/3} \quad (16)$$

Now

$$N_{Nu} = - \int_0^\pi \left(\frac{\partial c}{\partial r} \right)_{r=1} \sin \theta \, d\theta \quad (17)$$

$$= \int_\pi^0 \frac{N_{Pe}}{2} \frac{dF}{d\theta} \, d\theta = \frac{N_{Pe} F_\infty}{2} = 0.89 (N_{Pe})^{1/3} \quad (18)$$

If, instead of (9), a polynomial in three terms is used for c , one obtains

$$N_{Nu} = 0.975 (N_{Pe})^{1/3} \quad (19)$$

For very small N_{Pe} , $b \rightarrow \infty$ (stagnant case)

$$F \cong \frac{b}{2} \sin^2 \theta \quad (20)$$

Then

$$\frac{d \left(\frac{b}{2} \sin^2 \theta \right)}{d\theta} = - \frac{2 \sin \theta}{N_{Pe}} \quad (21)$$

whence

$$b = \frac{4}{N_{Pe}(1 - \cos \theta)} \quad (22)$$

Substituting in (17) gives

$$N_{Nu} = \frac{4}{N_{Pe}} \ln \left(\frac{1}{1 - N_{Pe}/2} \right) \quad (23)$$

$$= 2 \left(1 + \frac{N_{Pe}}{4} + \frac{N_{Pe}^2}{12} + \dots \right) \quad (24)$$

The first two terms in this expansion were obtained by Kronig and Bruijsten (6) in their perturbation solution for small N_{Pe} .

For the intermediate N_{Pe} range it was necessary to integrate (13) numerically. This was done by the method of isoclines, plotting $N_{Pe} F / 2$ vs. $\cos \theta$ with lines of constant slope = $1/h$.

The entire curve is plotted in Figure 1 with the few experimental data available in the low N_{Pe} range. In general, the data are from 10 to 40% higher than the theoretical prediction. Three possible explanations for the low trend of the theory are

1. The data were all taken in the range $1 < N_{Re} < 5$, which is somewhat higher than the limit of applicability of (5). At higher N_{Re} small eddies are set up to the rear of the sphere and transfer is increased. (Compare the calculations for the cylinder below.)

2. The theory does not take diffusion in the θ direction into account; this would tend to increase transfer.

3. Similarity hypotheses of the type (9) break down for thick boundary layers.

DIFFUSION FROM THE CYLINDER

The cylinder is treated in a manner analogous to that for the sphere. The fluid flows in the positive x direction and a thermal or concentration boundary

layer exists around the cylinder of radius b' . Diffusion in the θ direction is considered negligible, and a mass balance is written for the region between the surface of the sphere and the boundary layer.

At any angle θ the total amount of material which has diffused from the surface is given by the equation

$$F' = \int_0^{\psi'} c' d\psi' \quad (25)$$

where ψ' is the volumetric flow rate in the positive x direction. The change in F' with a small change in angle $\delta\theta$ is

$$\begin{aligned} -\frac{dF'}{d\theta} \delta\theta &= -\frac{d \left[\int_0^{\psi'} c' d\psi' \right]}{d\theta} \delta\theta \\ &= -D \left(\frac{\partial c'}{\partial r'} \right)_{r=a} a \delta\theta \quad (26) \end{aligned}$$

This equation can also be obtained by partial integration of Equation (1), on the assumption that diffusion in the θ direction is negligible.

For $N_{Re} < 1$, ψ' is given by Tomotika and Aoi (9) as

$$\begin{aligned} \psi' &= -AaU \left[\left(\frac{r'}{a} - \frac{a}{r'} - \frac{2r'}{a} \ln \frac{r'}{a} \right) \sin \theta \right] \\ &\quad - \frac{N_{Re}}{16} aU \left[\left(\frac{r'^2}{a^2} - \frac{a^2}{r'^2} \right) \right. \\ &\quad \left. - 2A \frac{r'^2}{a^2} \ln \frac{r'}{a} \right] \sin 2\theta \quad (27) \end{aligned}$$

[It should be noted that the A of (27) is the negative of the A used by Tomotika and Aoi.]

Unlike Equation (5), the stream function for the sphere, this expression applies only in the region fairly near the cylinder, as it does not approach $\psi' = Ur' \sin \theta$ as r' approaches infinity. Thus the treatment which follows is necessarily limited to larger values of N_{Pe} , i.e., to boundary

layers contained within the region for which (4) is valid.

If $\psi = \psi'/aU$, (26) may be written in dimensionless terms:

$$\begin{aligned} -\frac{dF}{d\theta} &= -\frac{d \left[\int_0^{\psi} c d\psi \right]}{d\theta} \\ &= -\frac{2}{N_{Pe}} \left(\frac{\partial c}{\partial r} \right)_{r=1} \quad (28) \end{aligned}$$

Rearranging (25) gives

$$F = -\int_1^0 \psi dc \quad (29)$$

since the boundary conditions which must be satisfied by c are

$$\begin{aligned} \text{at } r = 1, \quad c &= 1, \quad \frac{\partial \left(r \frac{\partial c}{\partial r} \right)}{\partial r} = 0 \quad (30) \\ \text{at } r = b(\theta), \quad c &= 0, \quad \frac{\partial \left(r \frac{\partial c}{\partial r} \right)}{\partial r} = 0. \end{aligned}$$

These conditions except for $\partial c/\partial r = 0$ at $r = b$ are satisfied by

$$c = 1 - \frac{\ln r}{\ln b} \quad (31)$$

Substituting in Equation (6) yields

$$\begin{aligned} F &= -\frac{1}{\ln b} \int_1^b \left[A \left(1 - \frac{1}{r^2} - 2 \ln r \right) \sin \theta \right. \\ &\quad \left. + \frac{N_{Re}}{16} \left(r - \frac{1}{r^3} - 2A r \ln r \right) \sin 2\theta \right] dr \\ &= \frac{1}{\ln b} \left\{ A \left(4 + 2b \ln b - 3b - \frac{1}{b} \right) \sin \theta \right. \\ &\quad \left. + \frac{N_{Re}}{16} \left[\frac{1}{2} \left(b^2 + \frac{1}{b^2} - 2 \right) \right. \right. \\ &\quad \left. \left. + A \left(b^2 \ln b - \frac{b^2}{2} + \frac{1}{2} \right) \right] \sin 2\theta \right\} \quad (32) \end{aligned}$$

In general, (28) must be integrated numerically; however, when N_{Re} is very small and N_{Pe} very large, an analytical solution is possible. If $N_{Re} < 10^{-3}$ the term with the coefficient $N_{Re}/16$ becomes negligible. Also

$$\begin{aligned} \ln b &= \left(1 - \frac{1}{b} \right) + \frac{1}{2} \left(1 - \frac{1}{b} \right)^2 \\ &\quad + \frac{1}{3} \left(1 - \frac{1}{b} \right)^3 + \dots \\ &= (b-1) + \frac{(b-1)^2}{2} + \frac{(b-1)^3}{3} \\ &\quad + \dots \text{ for } b \text{ near } 1 \end{aligned}$$

For very large N_{Pe} , i.e., very thin boundary layers, all except the first term in series expansions of $1 - (1/b)$ and $(b-1)$ may be dropped. Substituting in (28) gives

$$(b-1) \frac{d}{d\theta} \left[\frac{2}{3} A (b-1)^2 \sin \theta \right] = -\frac{2}{N_{Pe}} \quad (33)$$

Integrating between $F = 0$ at $\theta = \pi$ and $F = F_\infty$ at $\theta = 0$ gives

$$F_\infty = \left[\left(\frac{2A}{3} \right)^{1/2} \frac{3\pi^{1/2}}{N_{Pe}} \frac{\Gamma\left(\frac{3}{4}\right)}{\Gamma\left(\frac{5}{4}\right)} \right]^{2/3} \quad (34)$$

For the cylinder

$$\begin{aligned} N_{Nu} &= -\frac{1}{2\pi} \int_0^\pi \left(\frac{\partial c}{\partial r} \right)_{r=1} d\theta \\ &= \int_\pi^0 \frac{N_{Pe}}{\pi} \frac{dF}{d\theta} d\theta = \frac{N_{Pe}}{\pi} F_\infty \quad (35) \\ &= 1.035 (AN_{Pe})^{1/3} \\ &= 1.035 (A \cdot N_{Re})^{1/3} (N_{Se})^{1/3} \quad (36) \end{aligned}$$

For $N_{Re} > 10^{-3}$ it is necessary to integrate (28) numerically, as the term in (32) with the coefficient $N_{Re}/16$ becomes important. The numerical inte-

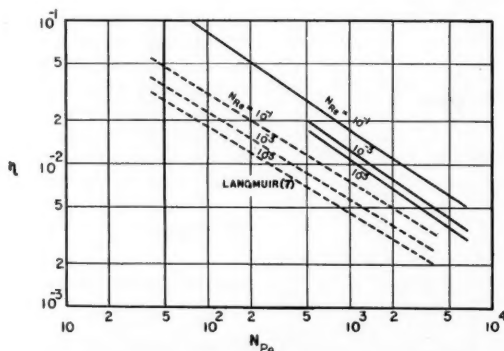


Fig. 5. Removal efficiency by diffusion for cylinders.

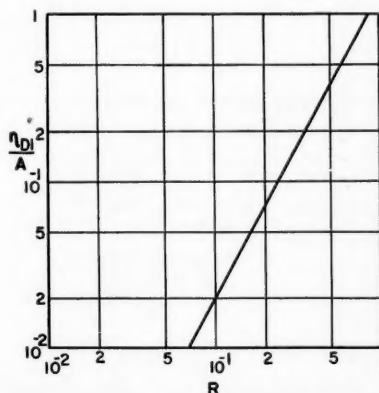


Fig. 6. Removal efficiency by direct interception for single cylinders.

gration was carried out for $N_{Re} = 10^{-1}$ and for this value of N_{Re} , the Nusselt number took the form

$$N_{Nu} = 0.557(N_{Pe})^{1/3} \quad (37)$$

In Figure 2 $N_{Nu}/(N_{Sc})^{1/3}$ is plotted vs. N_{Re} ; for $N_{Re} > 10^{-3}$, the curve represents an extrapolation of (36) through the $N_{Re} = 10^{-1}$ point, A , determined by numerical integration. The data of Dobry and Finn (3) for mass transfer and the range of the data of Davis (1) for heat transfer to oils, as recalculated by Ulsamer (10), are also shown. The agreement is good.

The asymptotic solution, Equation (36) is admittedly on the edge of the region applying to problems of present interest. However, its extrapolation through the point determined numerically shows that it is not too much in error over a wider region; moreover, it serves to "hang" the rest of the curve through the numerically evaluated point.

To recapitulate, Equation (36) was derived for $N_{Re} < 10^{-3}$ and $N_{Pe} \gtrsim 10^2$ and (37) was obtained numerically for $N_{Re} = 10^{-1}$ and $N_{Pe} \gtrsim 10$. The large values required for N_{Pe} limit the applicability of Figure 2 to diffusion in liquids and to colloidal-particle transfer.

DIFFUSION AND DIRECT INTERCEPTION OF COLLOIDAL PARTICLES BY THE SPHERE

For the diffusion of a colloidal particle with finite diameter, the concentration falls to zero at $r' = a + a_p$ or $r = 1 + R$ instead of at the surface of the sphere. This is the effect known as *direct interception*. The form assumed for c is

$$c = 1 - \frac{\frac{1}{1+R} - \frac{1}{r}}{\frac{1}{1+R} - \frac{1}{b}} \quad (38)$$

and Equation (7) becomes

$$\frac{d}{d\theta} \left[\frac{\sin^2 \theta}{\left(\frac{1}{1+R} - \frac{1}{b} \right)} \int_{1+R}^b \frac{1}{2} \left(1 - \frac{3}{2r} + \frac{1}{2r^3} \right) dr \right] = - \frac{2 \sin \theta}{N_{Pe} \left(\frac{1}{1+R} - \frac{1}{b} \right)} \quad (39)$$

It would be necessary to solve this equation numerically for each value of R , a tedious process. The combined effect of diffusion and direct interception can, however, be estimated in the following manner.

In Figure 3 the efficiency of removal for pure diffusion ($R = 0$) is plotted vs. N_{Pe} . The removal efficiency is defined as the fraction of the volume swept out by the sphere from which all the diffusing material is removed. For a sphere,

$$\eta = 4 \frac{N_{Nu}}{N_{Pe}} \quad (40)$$

For the case of pure interception the efficiency of removal can be calculated from the stream function. The rate of flow of fluid is given by

$$2\pi\psi' = \pi U a^2 r^2 \sin^2 \theta \left(1 - \frac{3}{2r} + \frac{1}{2r^3} \right) \quad (41)$$

The point of closest approach of a streamline or particle path to the sphere occurs at $\theta = \pi/2$. Thus the volume of fluid from which particles of radius R are completely removed in unit time is

$$2\pi\psi'(\theta = \pi/2) = \pi U a^2 (1+R)^2 \cdot \left[1 - \frac{3}{2(1+R)} + \frac{1}{2(1+R)^3} \right] \quad (42)$$

and the removal efficiency by interception

$$\begin{aligned} \eta_{DI} &= \frac{\text{volume cleaned}}{\text{total volume swept out}} \\ &= (1+R)^2 \cdot \left[1 - \frac{3}{2(1+R)} + \frac{1}{2(1+R)^3} \right] \end{aligned} \quad (43)$$

The efficiency η_{DI} is plotted in Figure 4 as a function of R . It is interesting to note that the log-log relationship is linear with

$$\eta_{DI} = 1.45R^2 \quad (44)$$

It is assumed that the removal by diffusion alone is due to the existence of a pseudo particle radius, an inherent diffusion radius, which can be obtained

from Figure 4, the plot of η_{DI} vs. R ; to each value of η from Figure 3 ($R = 0$) there corresponds a value of R_0 , the "diffusion radius," in Figure 4. If to the diffusion radius is added the actual radius, one can then find a new value for η from Figure 4. Values for η as a function of N_{Pe} with R as the parameter were obtained in this way and plotted in Figure 3. Unfortunately, there are no experimental data available with which to check the theory.

DIFFUSION AND DIRECT INTERCEPTION OF COLLOIDAL PARTICLES BY THE CYLINDER

Again the concentration falls to zero at $r = 1 + R$ and the form assumed for c is

$$c = 1 - \frac{\ln \left(\frac{1+R}{r} \right)}{\ln \left(\frac{1+R}{b} \right)} \quad (45)$$

To determine η as a function of R , it would be necessary to substitute (45) in (28) and then to integrate numerically for each value of N_{Re} and R from $r = 1 + R$ to $r = b(\theta)$. To avoid this tedious process, one estimates the combined removal by interception and diffusion in a manner similar to that in the preceding section:

For the cylinder,

$$\eta = \pi \frac{N_{Nu}}{N_{Pe}} \quad (46)$$

In Figure 5 the removal efficiency η for pure diffusion ($R = 0$) is plotted vs. N_{Pe} with N_{Re} as the parameter. The curve for $N_{Re} = 10^{-1}$ was obtained by

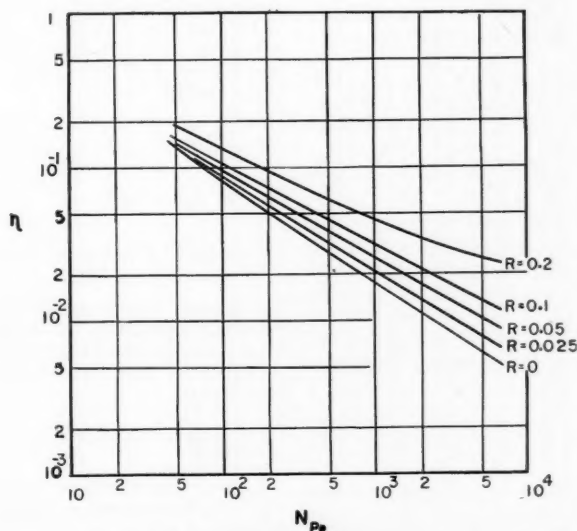


Fig. 7. Removal efficiency by diffusion and direct interception for single cylinders at $N_{Re} = 10^{-1}$.

numerical integration of (26), and the rest of the curves were obtained from the approximate solution (35). Shown also are the theoretical curves of Langmuir (7), which lie below those of the boundary-layer theory and which have a greater slope.

The efficiencies determined by taking the $N_{Re}/16$ term into account are somewhat greater than those calculated from (36) for $N_{Re} = 10^{-1}$. This probably results from the eddies set up behind the cylinder, which are described by the $N_{Re}/16$ term. The efficiency of removal by direct interception,

$$\eta_{DI} = \psi(\theta = \pi/2) = -A \left[(1+R) - \frac{1}{(1+R)} - 2(1+R) \ln(1+R) \right] \quad (47)$$

In Figure 6, η_{DI}/A is plotted vs. R , and, as in the case of the sphere, the log-log relationship is linear. The equation for the curve is

$$\eta_{DI} = 1.25AR^{1.82} \quad (48)$$

and for $N_{Re} = 10^{-1}$

$$\eta_{DI} = 0.1455R^{1.82} \quad (49)$$

Also for pure diffusion ($R = 0$) and $N_{Re} = 10^{-1}$, from Figure 5

$$\eta = \frac{1.75}{N_{Pe}^{2/3}} \quad (50)$$

The existence of a pseudo particle radius R_0 is assumed, such that

$$\eta_{DI} = \eta_{R_0(\text{diffusion})} \quad (51)$$

$$\frac{1.75}{N_{Pe}^{2/3}} = 0.1455R_0^{1.82} \quad (52)$$

Solving for R_0 and assuming

$$\eta = 0.1455(R + R_0)^{1.82} \quad (53)$$

one obtains

$$\eta = 0.1455 \left[R + \frac{3.96}{N_{Pe}^{0.367}} \right]^{1.82} \quad (54)$$

Values for η obtained in this way are plotted in Figure 7 as a function of N_{Pe} with R as the parameter. This set of curves applies only to $N_{Re} = 10^{-1}$. For values of $N_{Re} < 10^{-3}$ the removal due to the combination of interception and diffusion can be estimated by use of Equation (27):

$$\eta = 1.25A \left[R + \frac{1.69}{(AN_{Pe})^{0.367}} \right]^{1.82} \quad (55)$$

No data available are sufficiently accurate to check the theory; however, it should be noted that the $R = 0$ line (pure diffusion) is equivalent to point A of Figure 2, which agrees well with the data.

CONCLUSIONS

Rates of heat and mass transfer from single spheres or cylinders to fluids in laminar motion can be predicted with some success by means of boundary-layer theory.

Values of N_{Nu} for the sphere can be obtained as a function of the Peclet number alone over the entire N_{Pe} range by numerical integration. For $N_{Pe} > 10^3$ the equations can be solved analytically to give

$$N_{Nu} = 0.89(N_{Pe})^{1/3} \quad (18)$$

For $N_{Pe} \ll 1$ an analytical development gave

$$N_{Nu} = \frac{4}{N_{Pe}} \ln \left(\frac{1}{1 - N_{Pe}/2} \right) \quad (23)$$

For $N_{Pe} < 10^{-1}$, $N_{Nu} \cong 2$, the value for stagnant diffusion.

The few experimental data available in the low N_{Re} range for heat and mass transfer fall from 10 to 40% higher than the theory.

For the case of particles of finite diameter diffusing to a single sphere, efficiencies of removal can be calculated from boundary-layer theory, but a tedious numerical integration would be required for each value of R . Thus an approximate method is used to determine η as a function of R . No experimental data are available to check the theory.

Values of N_{Nu} for the cylinder were obtained as a function of N_{Sc} and N_{Re} for large values of N_{Pe} (thin boundary layers). For $N_{Re} < 10^{-3}$ the equations can be solved analytically to give

$$N_{Nu} = 1.035(AN_{Pe})^{1/3} \quad (36)$$

For $N_{Re} = 10^{-1}$, a numerical integration gave

$$N_{Nu} = 0.557(N_{Pe})^{1/3} \quad (37)$$

With these expressions a plot was made of $N_{Nu}/(N_{Sc})^{1/3}$ as a function of N_{Re} . The theory compared very well with the few experimental data for large N_{Pe} .

For the case of diffusion of particles, efficiencies by combined direct interception and diffusion were estimated by an approximate method. For $N_{Re} = 10^{-1}$

$$\eta = 0.1455 \left[R + \frac{3.96}{N_{Pe}^{0.367}} \right]^{1.82} \quad (54)$$

and for $N_{Re} < 10^{-3}$

$$\eta = 1.25A \left[R + \frac{1.69}{(AN_{Pe})^{0.367}} \right]^{1.82} \quad (55)$$

In general, efficiencies determined from boundary-layer theory fall somewhat higher than those calculated by Langmuir (7). No experimental data are available to check the theory.

NOTATION

a = sphere or cylinder radius, cm. or μ
 a_p = colloidal-particle radius, cm. or μ
 $A = \frac{1}{2(2.00223 - \ln N_{Re})}$
 $b = b'/a$, dimensionless

b' = boundary-layer radius, cm. or μ
 $c = (C - C_M)/(C_0 - C_M)$, dimensionless
 $c' = C - C_M$, g., g. moles, or particles/cc.
 C = concentration, g., g. moles, or particles/cc.
 C_M = main-stream concentration, g., g. moles, or particles/cc.
 C_0 = concentration at surface of cylinder or sphere, g., g. moles, or particles/cc.
 D = diffusivity, sq. cm./sec.
 F = quantity of diffusing material, dimensionless
 F' = quantity of diffusing material, g., g. moles, or particles
 $h = 1 - 1/b$
 k = mass transfer coefficient, cm./sec.
 N_{Nu} = Nusselt number, $2ka/D$, dimensionless
 N_{Pe} = Peclet number, $2aU/D$, dimensionless
 N_{Re} = Reynolds number, $2aUp/\mu$, dimensionless
 N_{Sc} = Schmidt number, $\mu/\rho D$, dimensionless
 $r = r'/a$, dimensionless
 r' = radial distance, cm. or μ
 $R = a_p/a$, dimensionless
 R_0 = diffusion radius, dimensionless
 u' = velocity in x direction, cm./sec.
 U = main-stream velocity, cm./sec.
 v' = velocity in y direction, cm./sec.
 w' = velocity in z direction, cm./sec.
 η = removal efficiency by diffusion and direct interception, dimensionless
 η_{DI} = removal efficiency by direct interception, dimensionless
 ρ = fluid density, g./cc.
 θ = angular displacement from positive x axis
 μ = fluid viscosity, g./cm.(sec.)
 ψ = stream function, dimensionless
 ψ' = stream function, cc./sec.
 ψ_b = stream function at boundary, dimensionless
 ψ_b' = stream function at boundary, cc./sec.

LITERATURE CITED

1. Davis, A. H., *Phil. Mag.*, **47**, 1057 (1924).
2. Eckert, E., *V.D.I.-Forschungsheft*, **416**, 1942.
3. Dobry, Reuven, and R. K. Finn, *Ind. Eng. Chem.*, **48**, 1540 (1956).
4. Frisch, H. L., *J. Chem. Phys.*, **22**, 123 (1954).
5. Kramers, H., *Physica*, **12**, 61 (1946).
6. Kronig, R. and J. Bruijsten, *Appl. Sci. Research*, **A2**, 439 (1951).
7. Langmuir, Irving, *O.S.R.D. Rept.* 865 (Sept. 4, 1942).
8. Ranz, W. E., and W. R. Marshall, Jr., *Chem. Eng. Progr.*, **48**, 141, 173 (1952).
9. Tomotika, S., and T. Aoi, *Quart. J. Mech. Appl. Math.*, **3**, 140 (1950).
10. Ulsamer, J., *Forsch. Gebiete Ingenieurw.*, **3**, 94 (1932).

Presented at A.I.Ch.E. Detroit meeting

Heat Transfer in the Critical Region

R. P. BRINGER and J. M. SMITH

Purdue University, Lafayette, Indiana

Heat transfer coefficients were measured experimentally for carbon dioxide in turbulent flow in an 0.18-in. I.D. pipe. The pressure was 1,200 lb./sq. in. abs. and the bulk temperature varied from 70° to 120°F. In this critical region the coefficients between fluid and tube wall ranged from 300 to 2,600 B.t.u./(hr.)(sq. ft.)(°F.) over a Reynolds number interval of 30,000 to 300,000.

Existing empirical and semitheoretical correlations were found inadequate in this region, where the thermal conductivity, viscosity, density, and specific heat are all varying rapidly and nonuniformly with temperature. A method of integrating the heat and momentum transfer equations with variable physical properties, recently proposed by Deissler, was applied to the experimental data and found to fit well. The application required extensive calculations, which were carried out with an Electrodata digital computer.

A simplified procedure was proposed for estimating heat transfer coefficients in the critical region by using a semitheoretical equation developed for zero heat flow. Simple rules were suggested for estimating the temperature at which to evaluate the physical properties when this equation is applied to the real case of finite heat transfer. The method worked well when compared with the computed heat transfer coefficients of Deissler for supercritical water but showed about 30% deviation when compared with the carbon dioxide results. This discrepancy is believed due to the fact that the carbon dioxide was very close to the critical point (reduced pressure = 1.1) but the water was somewhat further removed (reduced pressure = 1.6).

Empirical correlations of heat transfer coefficients for fluids flowing in circular tubes have been available for many years (9, 20, 21), and semitheoretical methods based upon relating the transfer of momentum and heat have also been developed (1, 27). Both procedures give dependable results when the physical properties of the fluid do not vary greatly from the center of the conduit to the tube wall. This condition prevails when the temperature change across the tube diameter is negligible, and hence the correlations often have been described as applying at isothermal conditions. Perhaps the first practical problem in which deviations from this condition were severe was in the heating or cooling of viscous petroleum fractions, where the viscosity change across the tube was large and the conventional correlations did not apply. An empirical modification, using the ratio $(\mu_0/\mu_b)^{0.4}$, was successfully introduced by Sieder and Tate (24) to handle this case.

With the development of gas turbines, rocket motors, and high-pressure steam power plants, the problem of variable physical properties has become much more severe. Large temperature differences between the fluid and the tube wall at ordinary pressure can cause severalfold changes in the thermal conductivity, viscosity, and specific heat (except for diatomic gases); however, as long as the critical pressure is not approached the variations are uniform and exhibit no

unusual characteristics. The most severe case is encountered when the fluid is in the critical region, for here the changes in properties are both irregular and large for small variations in temperature.

The purpose of this investigation was to measure heat transfer coefficients in the critical region and to develop a method of correlating the results so that predictions might be made without heat transfer measurements. Carbon dioxide was chosen as the fluid because of its intermediate critical temperature and because its physical and thermal properties are fairly well established.

EXPERIMENTAL METHOD

The experimental method consisted of measuring the energy transferred to carbon dioxide flowing through a tube. The large variation in physical properties combined with entrance effects makes it impossible to maintain a constant heat transfer coefficient along a finite length of tube. Hence measurements taken over a section of tube would lead to average values of h which would have little significance. It was accordingly necessary to determine a local or point heat transfer coefficient defined by the expression

$$q_0 = h(t_0 - t_b) \quad (1)$$

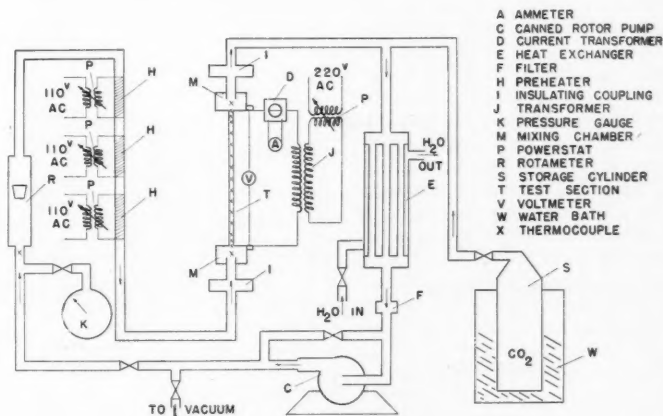


Fig. 1. Experimental apparatus.

R. P. Bringer is at present with Dow Chemical Company, Midland, Michigan, and J. M. Smith is at the University of New Hampshire, Durham, New Hampshire.

where q_0 is the local rate of heat transfer per unit area at the wall and t_0 and t_b are the wall and bulk fluid temperatures. The measurement of the heat transfer rate at any point is facilitated by electrical heating, with the current passed directly through the tube wall. If, in addition, a material is used which has an electrical resistivity independent of temperature, q_0 for a given voltage becomes the same at any point along the tube. This is important because it means that the variations in wall temperature along the tube length will be reduced and be caused by only the change in fluid temperature and heat transfer coefficient. With a variable electrical resistivity q_0 becomes a function of wall temperature and the interpretation of the results is more difficult.

The bulk fluid temperature was determined by the following heat balance

$$I^2 R_z \left(\frac{z}{L} \right) = w(H_b - H_1) \quad (2)$$

where H_b represents the enthalpy of the carbon dioxide at the bulk-mean temperature at the point z distance from the entrance to the test section of the tube. The temperature t_b can be found after H_b is determined from Equation (2) by reference

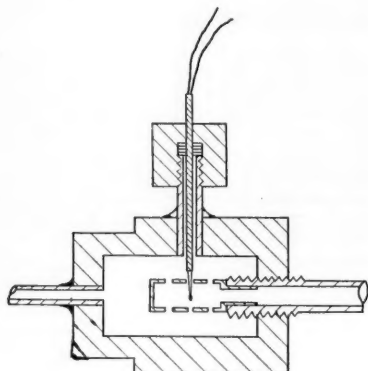


Fig. 2. Mixing chamber.

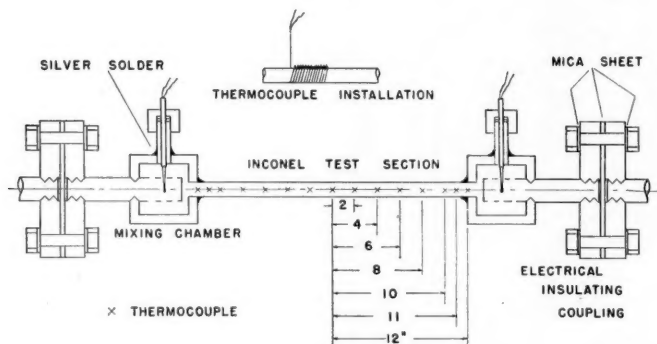


Fig. 3. Assembled test section.

to the thermodynamics properties of carbon dioxide.

The wall temperature was measured directly by thermocouples attached to the tube wall as described in the next section.

APPARATUS

The complete equipment, illustrated in Figure 1, consists of a closed circuit in which carbon dioxide is heated in the test section T and cooled in the heat exchanger E . The canned-rotor pump C was constructed according to the design developed by the Oak Ridge National Laboratory for a high-suction-pressure, high-temperature, totally enclosed unit (28). The pump was made from type 300 stainless steel materials, except for the bearings of Graphitar No. 14 and the chrome plate in the journal of the rotor. The unit was entirely satisfactory for the service required in this study.

The test section consisted of an Inconel tube 0.25 in. O.D., 0.035 in. of wall thickness and 24.0 in. long. The high tensile strength of Inconel made it possible to use a thin-walled tube and thus to obtain the desired heat input. Also the temperature coefficient of electrical resistivity (0.00069 ohm ft./°F.) was sufficiently low that temperature variations along the tube had no appreciable effect on its resistance. Identical mixing chambers were silver soldered to each end of the Inconel tube. The chambers were fashioned from 2-in.-diam. steel stock bored with a circular hole 1 in. in diameter. The details of a chamber fitted with thermocouple and shield are shown in Figure 2. The shield provided an adiabatic section for temperature measurement in addition to providing for mixing of the fluid. The thermocouples were made from 30-gauge copper-constantan wire and inserted into the center of the mixing space, thus providing a $\frac{1}{2}$ -in. isothermal length before the metal wall was reached. Electrical insulation was provided by insulating couplings made by inserting sheets of mica between stainless steel flanges as shown in Figure 3, where the complete test section is illustrated.

Outer surface temperatures of the tube wall were measured with fifteen copper-constantan glass-insulated thermocouples

located at 0, 1, 2, 4, 6, 8, 10, 12, 14, 16, 18, 20, 22, 23, and 24 in. from the tube entrance, as indicated in Figure 3. The couples were spot-welded to the tube wall and then the lead wires wound around the tube for several turns before leaving the test section through the Fiberglas insulation (2 in. thick). The measured values were corrected to inside surface temperatures (commonly referred to as wall temperatures) by use of the known heat flux, tube thickness, and diameter, and thermal conductivity of Inconel as a function of temperature.

SCOPE OF INVESTIGATION

In order to simplify the comparison of the experimental results for the heat transfer coefficient with theoretical predictions, it was desirable to operate the test section at essentially constant pressure and constant wall temperature. The wall temperature does not remain constant along the entire length of tube (see Figure 8). However it was possible to obtain h at a constant wall temperature since the coefficient could be computed at any point along the tube. All that was necessary was to calculate h at a location where the inside-wall temperature was equal to the desired value. Unless this point occurred in the central 10 in., where entrance and exit effects were negligible, the run was not used. This situation is illustrated in Figure 4, where the temperature profiles for run 59 are plotted. In this instance an inside-surface-wall temperature of 110°F. was required, corresponding to a measured outer surface value of 115°F. Reference to the figure (solid line) indicates that this temperature occurred a little beyond the midway point along the tube. The dotted line shows the approximate fluid temperature (bulk mean) profile.

Since the heat input per unit length was constant for the whole tube, Figure 4 can be used to illustrate how the heat transfer coefficient varies with position. At the entrance h has a very high value and then decreases as entrance thermal effects disappear. In the central section variations in h are less and are due to the effect of changes in the physical properties of carbon dioxide.

The equipment was then operated at constant heat flux, and at a pressure of 1,200 lb./sq. in. abs. (the critical value is 1,070 lb./sq. in. abs.). The heat fluxes were chosen so as to give wall temperatures, in the central portion of the test section, of 100, 110, 130, and 150°F. The heat input and entrance temperature and flow rate of

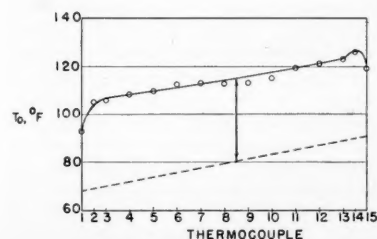


Fig. 4. Wall temperature profile for run 59.

carbon dioxide were varied to give the following range of conditions:

Reynolds number	30,000 to 300,000
Heat transfer rate, B.t.u./hr.(sq. ft.)	10,000 to 100,000
Carbon dioxide tem- perature, °F.	70-120 (critical value 88°F.)

PHYSICAL PROPERTIES

In order to calculate h from Equation (1) and to obtain the values of the Prandtl, Nusselt, and Reynolds numbers for correlation purposes, one or more of the following properties of carbon dioxide are required: density, enthalpy, specific heat, viscosity, or thermal conductivity.

Michels and Michels (15) have very carefully determined the P - V - T relations in the critical region and their results were used to establish the density as a function of temperature at 1,200 lb./sq. in. abs.

The most accurate enthalpy data appear to be those calculated by Michels and DeGroot (16) from the P - V - T results previously mentioned. These results rather than the earlier work of Plank and Kuprianoff (19) were used here. A plot of the enthalpy data at 1,200 lb./sq. in. abs. was used in connection with the solution of Equation (1) for the heat transfer coefficient.

The viscosity of carbon dioxide at elevated pressures has been studied by Phillips (18), Stakelbeck (25), Comings and Egly (3), and Schroer and Becker (22). Also Kiyama and Makita (12) made measurements over a wide range of conditions, 1 to 96 atm. and 50° to 300°C. Naldrett and Maass (17) carried out excellent determinations in a narrow range near the critical point. Most of the data compare favorably in overlapping regions, though carried out in different types of equipment. For this work a plot of all the data except those of Schroer and Becker was used in preparing the viscosity curve at 1,200 lb./sq. in. abs. shown in Figure 5. A specific heat curve is shown on the same graph.

Much less attention has been given to the study of thermal conductivity at high pressures. The first reliable investigation reported was that of Sellschopp (23), who made measurements in the range of 50° to 120°F. and 700 to 1,325 lb./sq. in. abs. His results were admittedly erroneous in the critical region because of free convection, and a curve of density vs. thermal conductivity confirms this by indicating a pronounced hump near the critical point. Krausschold (13) has applied a correction to these data to offset the effect of convection, and the corrected data give a smooth increasing curve of conductivity vs. density as expected. Lenoir and Comings' (14) independent measurements are about 15% higher than those of Sellschopp but

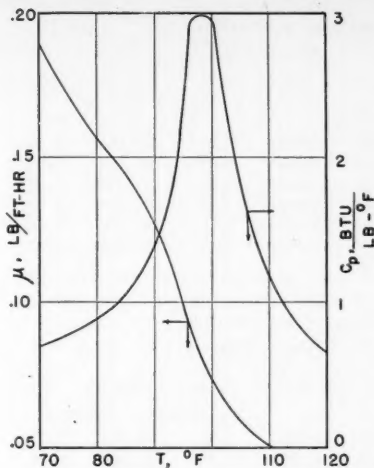


Fig. 5. Viscosity and specific heat of CO_2 at 1,200 lb./sq. in.

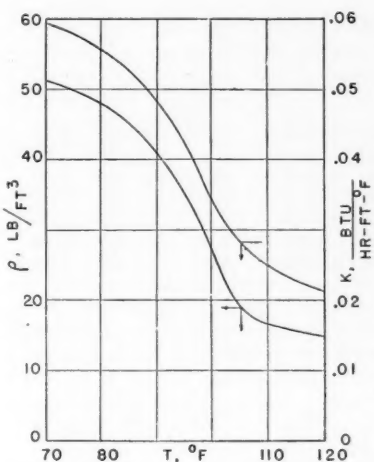


Fig. 6. Density and thermal conductivity of CO_2 at 1,200 lb./sq. in.

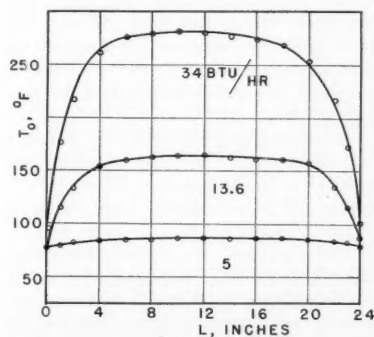


Fig. 7. Wall temperature profiles with no flow.

give a smooth k vs. p curve which parallels Krausschold's corrected curve. Franck (11) combined additional data by Stoljarow, et al. (26) with what were considered the most reliable points in the previous investigations and proposed a composite set of data. It was found that these results compared well with the values predicted by applying the law of corresponding states in the manner suggested by Lenoir and Comings (14). Franck's work was used in this investigation and the 1,200 lb./sq. in. abs. results are shown along with the density in Figure 6.

EXPERIMENTAL RESULTS

Equating the electrical energy input to the value of q_0 in Equation (1) is based upon the assumption of negligible heat losses radially and longitudinally from a point in the test section. To test this assumption wall-temperature profiles were measured for conditions of no flow. The results, illustrated in Figure 7, show that for a wall temperature in the central section of the tube wall in this study, the loss is about 12 B.t.u./hr. Since the minimum value of the total heat transferred in the runs at $t_0 = 150^\circ\text{F}$. was 1,430 B.t.u./hr., the heat loss amounted to but 0.8%.

The flat portions of the curves in Figure 7 also show that the temperature in the central section of the tube wall is unaffected by end losses. Heat transfer coefficients for all the runs were computed from data taken in the section 7 to 17 in. from the entrance. Even at 280°F . wall temperature, far beyond the 150°F . maximum employed in the runs, the profile in the center portion is almost flat.

Analogous wall-temperature profiles with carbon dioxide flowing through the tube are shown in Figure 8 for four of the runs described in Tables 1 to 4. The central flat portions are again present. Their slope, in these cases with flow, is not zero but finite, the value depending upon the temperature rise of the carbon dioxide.

In a series of preliminary tests with water at 80° to 150°F . and low pressures, heat transfer coefficients were obtained which agreed well with the Dittus-Boelter equation. For twenty-four runs the average absolute difference between the electrical energy input to the whole test section and the heat transferred to the water, as determined by the measured inlet and outlet temperatures, was 2.4%, with twelve positive deviations and nine negative values. The maximum value was 5.0%. Water was used in these tests because its properties are well established and the heat-balance deviations would reflect the uncertainties in the equipment operation rather than in the property data.

For the carbon dioxide runs the maximum deviation was also less than 5%

TABLE 1. SAMPLE RESULTS AT $t_0 = 100^\circ\text{F}$.
($Pr_0 = 6.30$)

Run	h_i B.t.u./(hr.)($^\circ\text{F}$./sq. ft.)	Nu_0	Re_0	β	Nu_b	Re_b	Pr_b
66	650	290	50,400	0.00055	174	39,600	2.42
71	1,240	551	112,000	0.00054	328	87,000	2.37
94	825	367	49,500	0.00040	248	41,700	3.30
95	870	387	66,000	0.00044	248	55,000	2.82
99	1,625	722	145,000	0.00036	471	121,000	2.98
102	2,060	920	183,000	0.00038	595	152,000	2.97

TABLE 2. SAMPLE RESULTS AT $t_0 = 110^\circ\text{F}$.
($Pr_0 = 2.85$)

Run	h_i B.t.u./(hr.)($^\circ\text{F}$./sq. ft.)	Nu_0	Re_0	β	Nu_b	Re_b	Pr_b
46	635	382	44,000	0.0022	172	48,000	2.43
55	583	350	32,200	0.0027	157	37,000	2.44
56	1,450	873	87,500	0.0028	388	94,500	2.43
59	975	585	62,500	0.0024	266	69,000	2.54
111	2,660	1,600	155,000	0.0016	970	202,000	5.52
145	1,050	629	63,000	0.0015	382	83,000	5.64
151	2,320	1,390	158,000	0.0014	905	233,000	6.35
154	880	530	76,000	0.0007	420	97,000	5.31

TABLE 3. SAMPLE RESULTS AT $t_0 = 130^\circ\text{F}$.
($Pr_0 = 1.68$)

Run	h_i B.t.u./(hr.)($^\circ\text{F}$./sq. ft.)	Nu_0	Re_0	β	Nu_b	Re_b	Pr_b
77	620	475	36,400	0.0084	172	49,600	2.64
83	1,700	1,300	93,000	0.0096	473	127,000	2.67
84	1,770	1,350	104,000	0.0087	501	143,000	2.85
116	1,310	1,010	89,000	0.0063	510	151,000	6.40
123	488	373	36,800	0.0047	237	55,500	5.05
126	740	567	80,000	0.0032	415	102,000	3.62
128	360	276	54,000	0.0025	186	71,500	4.35

TABLE 4. SAMPLE RESULTS AT $t_0 = 150^\circ\text{F}$.
($Pr_0 = 1.43$)

Run	h_i B.t.u./(hr.)($^\circ\text{F}$./sq. ft.)	Nu_0	Re_0	β	Nu_b	Re_b	Pr_b
85	458	380	32,000	0.0112	148	51,500	4.10
89	1,080	897	63,500	0.0143	319	103,500	3.16
93	1,710	1,420	108,000	0.0130	550	175,000	4.05
133	333	276	49,500	0.0052	172	75,000	4.29
137	900	745	117,500	0.0063	453	182,000	4.64
142	432	358	41,000	0.0078	200	75,600	5.85

for all runs except those with inlet or outlet temperatures between 95° and 100°F . This temperature corresponded to the region where the enthalpy was changing most severely and, on the basis of the water results, was due to errors in the enthalpy values rather than in the temperature measurements.

The heat transfer coefficients computed from Equation (1) are tabulated for a few sample runs in Tables 1 to 4 for the four wall temperatures.* Corresponding

values of the Nusselt and Reynolds numbers evaluated at both the wall and bulk fluid temperature are also shown. These numbers were obtained by use of the fluid properties given in Figures 5 and 6.

The quantity β shown in the tables is proportional to the heat transfer rate and is useful in applying Deissler's (7) theory of heat transfer with variable physical properties.

The heat transfer coefficients are seen from the tabular values to be large, particularly in Table 2, where the carbon dioxide was closest to the critical point in most runs. The results are plotted as Nu_0 vs. Re_0 in Figures 9 to 12, where the points refer to the experimental results

and the lines to theoretical predictions described in the following section.

PREDICTION OF HEAT TRANSFER COEFFICIENTS

The results were first compared with the dimensionless correlations of the Dittus-Boelter, Sieder and Tate, and Chilton types. In the Dittus-Boelter equation all fluid properties were evaluated at the bulk temperature. The data showed a systematic deviation (as high as 50%) with the heat transfer rate. In the Sieder and Tate equation the properties are all evaluated at the bulk temperature except the viscosity used in the ratio $(\mu_0/\mu_b)^{0.14}$. The agreement was also unsatisfactory, the deviations again being systematic with β and actually somewhat larger than for the Dittus-Boelter relationship. In the Colburn correlation all the properties except c_p are evaluated at a film temperature midway between the bulk and wall values. This approach showed deviations as large as +127 and -74%; in this case they were not systematic with respect to β .

If the temperature and velocity profiles across the tube can be computed, the bulk mean temperature can be evaluated and used in Equation (1) to determine h for comparison with the experimental results. The following equations for the rates of momentum and heat transfer have been used in this way to predict semitheoretical expressions for the heat transfer coefficient.

$$\tau = \frac{\mu}{dy} + \rho\epsilon \frac{du}{dy} \quad (3)$$

$$q = -k \frac{dt}{dy} - \rho\epsilon_h c_p \frac{dt}{dy} \quad (4)$$

Most of these developments have been based upon constant fluid properties and therefore are applicable only for the hypothetical case of no heat transfer. Although some of the resulting correlations have been satisfactory for small variations in physical properties, they would not be expected to apply for a fluid in the critical region.

Recently this method of approach has been expanded in an attempt to handle the case of large variations in properties. What is necessary is a fundamental relationship between temperature and property accurate enough to represent the data and still simple enough to allow the solution of Equations (3) and (4). Deissler in a series of papers (4 to 8) has proposed a logarithmic relationship for viscosity of the form $\mu/\mu_0 = b(t/t_0)^{\alpha_2}$, where b and α_2 are constant. Assumptions are required in handling Equations (3) and (4) and the set proposed by Deissler is as follows:

The eddy diffusivities for heat and momentum transfer ϵ_h and ϵ are the

*Tabular material has been deposited as document 5118 with the American Documentation Institute, Photoduplication Service, Library of Congress, Washington 25, D.C., and may be obtained for \$1.25 for photoprints or 35-mm. microfilm.

same. In the carbon dioxide data reported here, the Reynolds number was always above 30,000 and the Prandtl number greater than unity. Hence the Peclet number ($Pe = Re Pr$) exceeded 30,000. Under these conditions this assumption is probably a good one. Fortunately, also, the ratio ϵ_h/ϵ can vary considerably about unity and not significantly affect the computed profiles.

Assumptions are necessary for the variation of eddy diffusivity with distance from the tube wall and many have been suggested by various investigators. Deissler (6, 8) proposed the following expressions which were used for this investigation:

$$\epsilon = (n^2)uy \left[1 - \exp \left(-\frac{n^2 uy}{\mu/\rho} \right) \right] \quad (5)$$

for flow close to wall;

$$\epsilon = m^2 \frac{(du/dy)^3}{(d^2u/dy^2)^2} \quad (6)$$

for flow at a distance from the wall.

$$n = 0.124$$

$$m = 0.36$$

The variation in shear stress τ and heat transfer rate q across the tube has a negligible effect on the velocity and temperature profiles. These quantities do vary with radial position. However, there is evidence to indicate that this variation does not significantly affect the profiles.

With the three assumptions, Equations (3) and (4) may be written in the following dimensionless forms:

$$1 = \left\{ \frac{\mu}{\mu_0} + \frac{\rho}{\rho_0} n^2 u^* y^* \right\} \quad (7)$$

$$\cdot \left[1 - \exp \left(-\frac{n^2 u^* y^*}{(\mu/\mu_0)(\rho_0/\rho)} \right) \right] \frac{du^*}{dy^*}$$

$$1 = \left\{ \frac{k}{k_0 Pr_0} + \frac{\rho}{\rho_0} \frac{c_p}{c_{p_0}} n^2 u^* y^* \right\} \quad (8)$$

$$\cdot \left[1 - \exp \left(-\frac{n^2 u^* y^*}{(\mu/\mu_0)(\rho_0/\rho)} \right) \right] \frac{dt^*}{dy^*}$$

for flow close to the wall (up to a distance parameter of $y^* = 26$).

Analogous expressions are obtained for flow at a distance from the wall by use of Equation (6).

The dimensionless velocity and distance parameters are defined in the conventional way:

$$u^* = \frac{u}{(\tau_0/\rho_0)^{1/2}} \quad (9)$$

$$y^* = \frac{(\tau_0/\rho_0)^{1/2}}{\mu_0/\rho_0} y \quad (10)$$

The dimensionless temperature has been defined by Deissler as follows:

$$t^* = \frac{(t_0 - t)c_{p_0}\tau_0}{q_0(\tau_0/\rho_0)^{1/2}} = \frac{1}{\beta} \left(1 - \frac{t}{t_0} \right) \quad (11)$$

and so

$$\beta = \frac{q_0(\tau_0/\rho_0)^{1/2}}{c_{p_0}\tau_0 t_0} \quad (12)$$

Thus β may be considered a dimensionless heat flux and is directly proportional to the heat transfer rate at the wall.

It is noted in Equations (7) and (8) that the fluid properties occur as ratios to the wall-temperature values. Hence the functional relationship

$$\left(\frac{\mu}{\mu_0} \right) = b \left(\frac{t}{t_0} \right)^a$$

and similar ones for specific heat and thermal conductivity are convenient. In applying this approach to the carbon dioxide data, it was necessary to use three different a and b values to cover the required temperature range. At a distance from the critical point the variation of properties with temperature would be more uniform and a single value of a and b might suffice.

Equations (7) and (8) and their counterparts for flow far from the wall were integrated by use of the property data given in Figures 5 and 6. Then bulk means values of temperature and velocity were computed. Finally Nusselt and Reynolds numbers were compiled. The stepwise operations necessary in obtaining the profiles, and their integration to obtain bulk values, necessitate a great number of numerical calculations. Thus the solutions and calculations were programed and carried out on an Electrodata model 30-201 digital computer.

Analysis of the equations shows that the solutions are obtained most conveniently for constant wall temperature and constant value of heat transfer rate or, more precisely, constant value of β . Hence the computations were made for the four wall temperatures studied experimentally and for a series of β values at each wall temperature. The β values were chosen to agree as closely as possible with the experimental range of heat transfer rates. Since it was possible to operate the equipment only at a constant heat transfer rate, q_0 , but not β , each experimental point corresponds to a different β . In Figures 9 to 12 the points are identified according to the range of β values to which they correspond.

The computed results are shown in Figures 9 to 12 as solid lines for specific values of β . The variation of the Nusselt number with β on these figures is particularly interesting. In Figure 9 both predicted and experimental results show a decrease in Nu with an increase in β ,

but the effect is small. Since the fluid temperature is always less than the wall value and the latter is 100°F. for this case, the fluid is not in the region (95° to 105°F.) of most pronounced change in properties with temperature. In Figure 10 the predicted curves show Nu first to increase then decrease as β increases. Examination of the data points out the same trend. This unusual variation is believed to be caused by the fact that now the wall temperature is such that the fluid properties are changing very rapidly, and indeed the specific heat passes through a maximum (Figure 5). Agreement between experimental and predicted results is not so good as in Figure 9 but is still satisfactory.

In Figure 11 for a wall temperature of 130°F. the data show a continuous increase in Nu with β and are in good agreement with the predicted curves for $\beta = 0.004$ and 0.008. The predicted results also show at $\beta = 0.012$ the reverse trend that was found in Figure 10. At this higher wall temperature of 130°F. the bulk fluid temperature would have to be low in order for the temperature profile to pass through the region of maximum change in physical properties. This means that the temperature difference between bulk fluid and wall would be large and lead to a high heat transfer rate. Hence the decrease in Nu with β (at high values of β) predicted in Figure 11 is expected. Experimentally it was not possible to operate at heat transfer rates high enough to reach β values above 0.0096, and so this reverse trend was not observed.

When the wall temperature has risen to 150°F., the fluid temperatures are above the critical range and a continuous increase in Nu with β is observed. The agreement between experimental and predicted results is quite satisfactory.

In summary, two points stand out in Figures 9 to 12. The first is that the solution of the rate of momentum and heat transfer equations proposed by Deissler has correctly predicted the variation in heat transfer coefficient in the critical range. The second is that in the critical region the Nusselt number changes with heat transfer rate or β and that the direction of this change depends upon which side of the critical temperature is involved. Thus in Figure 9, where the temperature was less than the critical value, the Nusselt number decreased with β but in Figure 12, where the temperature was above the critical, the opposite occurred.

It appears from this investigation that the theoretical method is adequate for handling heat transfer problems in the critical region. However, it is too complicated and requires too much time for most applications. Hence there is a need to develop a generalized and simplified substitute for the theoretical approach.

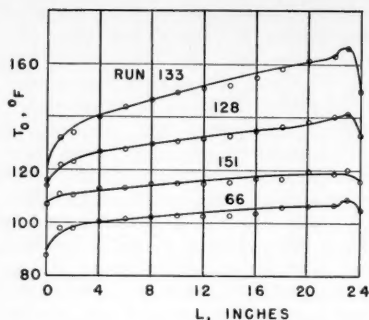


Fig. 8. Wall temperature profiles with flow.

GENERALIZED CORRELATIONS FOR ESTIMATING HEAT TRANSFER COEFFICIENTS

For the prediction of the Nusselt number from the curves in figures such as 9 to 12, the wall temperature and β must be known. Deissler (6) suggested that the effect of β could be eliminated by evaluating Nu and Re at a reference temperature t_x located between the wall and bulk values. In a later paper Deissler (7) computed, according to his theory, curves similar to these Figures 9 to 12 for water at 5,000 lb./sq. in. abs., about 1,800 lb./sq. in. abs. above the critical pressure. The reference temperature required to make all the separate curves coincide with the $\beta = 0$ line was then determined. The result was a plot of t_x vs. t_0/t_b with separate curves for each wall temperature. Eckert (10) suggested that the effect of t_0 might be eliminated by plotting x [equal to $(t_x - t_b)/(t_0 - t_b)$] vs. $(t_m - t_b)/(t_0 - t_b)$, where t_m is the transposed critical temperature. This latter quantity is the temperature, at a specified pressure, for which the specific heat is a maximum. Figure 13 is such a plot and does indicate that all the data for various wall temperatures is brought together on a single curve. Thus Figure 13 plus the $\beta = 0$ line for a given wall temperature may be used to replace the extensive calculations associated with the prediction method previously described. Additional simplification is obtained from the fact that the wall temperature affects the $\beta = 0$ curves only through the Prandtl number, Pr_0 . This follows from the condition that the temperature across the tube is constant at $\beta = 0$, the case of no heat transfer. This constant temperature is the wall temperature and is the one at which the Prandtl number should be evaluated. Since the $\beta = 0$ curves are essentially straight lines on the Nu vs. Re plots, this means that the prediction method can be reduced to Figure 13 and an equation of the form

$$Nu_x = a(Re_x)^b(Pr_0)^c \quad (13)$$

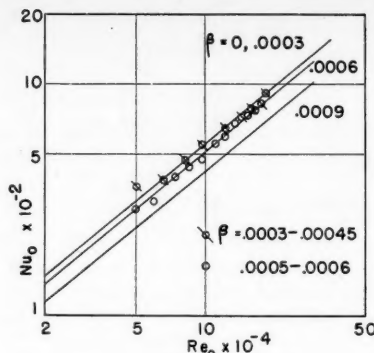


Fig. 9. $Nu_0 = f(Re_0, \beta)$, $T_0 = 100^\circ\text{F}$. experimental and theoretical results.

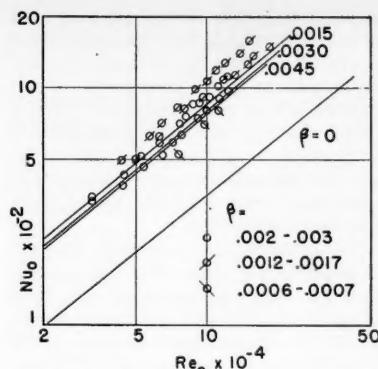


Fig. 10. $Nu_0 = f(Re_0, \beta)$, $T_0 = 110^\circ\text{F}$. experimental and theoretical results.

Finally it may be noted that Figure 13 can be divided approximately into three straight-line sections as shown in Table 5

TABLE 5.

$(t_m - t_b)/(t_0 - t_b)$	x
< 0	0
0 to 1.0	$(t_m - t_b)/(t_0 - t_b)$
> 1.0	1.0

Since $x = (t_x - t_b)/(t_0 - t_b)$, the three sections of the curve suggest the simple rules shown in Table 6 for t_x in terms of the relationship between t_m and t_0 and t_b .

TABLE 6.

$(t_m - t_b)/(t_0 - t_b)$	Reference temperature, t_x
< 0	t_b
0 to 1.0	t_m
> 1.0	t_0

It may be noted that these reference-temperature proposals suggest that when t_0 and t_b are both below the transposed critical value t_m , the reference temperature to use is the wall temperature.

In final form the simplified method consists of Equation (13) and the rules for evaluating the reference temperature shown in Table 6. Using the $\beta = 0$ lines computed by Deissler for water the constants a , b , and c in Equation (13) were numerically evaluated so that the equation takes the form

$$Nu_x = 0.0266(Re_x)^{0.77}(Pr_0)^{0.55} \quad (14)$$

Equation (14) and Table 6 were first tested by application to the computed points of Deissler for water. The results (Figure 14) show good agreement with Equation (14), an indication that the procedure is satisfactory for supercritical water at 5,000 lb./sq. in. abs. Next the reference temperature rules and Equation (14) were applied to the carbon

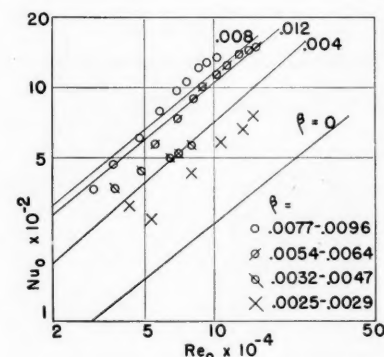


Fig. 11. $Nu_0 = f(Re_0, \beta)$, $T_0 = 130^\circ\text{F}$. experimental and theoretical results.

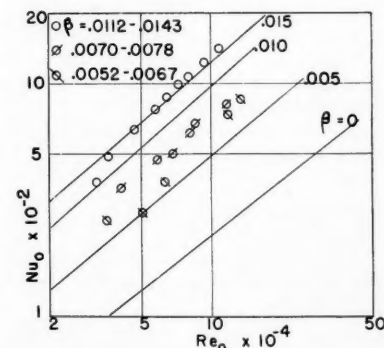


Fig. 12. $Nu_0 = f(Re_0, \beta)$, $T_0 = 150^\circ\text{F}$. experimental and theoretical results.

dioxide data obtained in this study. The comparison, shown in Figure 15, indicates that Equation (14) is about 30% low. The solid line obtained by keeping the

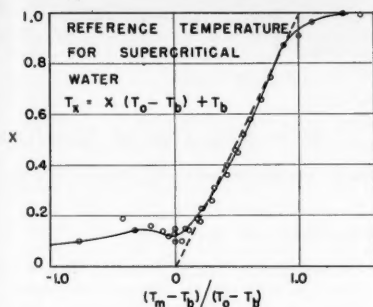


Fig. 13. Reference temperature for supercritical water; $T_x = X(T_o - T_b) + T_b$.

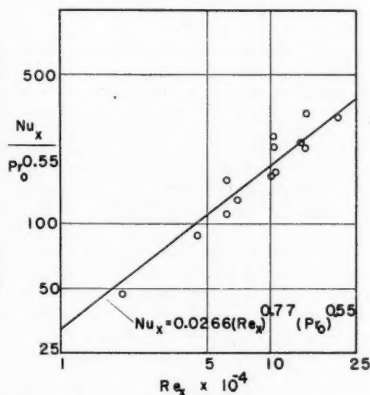


Fig. 14. Supercritical water data after application of reference temperature rule.

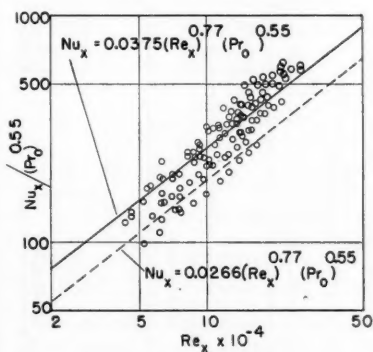


Fig. 15. CO₂ data after application of reference temperature rule.

same exponents on Re_x and Pr_o but increasing the coefficient fits the data much better, the average deviation being 16%.

Failure of Equation (14) to predict the carbon dioxide data accurately is believed

due to inadequacy of the mixture rule in the close proximity of the critical point. Thus the water results are at a reduced pressure of 1.6 and for carbon dioxide the reduced pressure is only 1,200/1,070 = 1.1. While Deissler's theory predicted the experimental results in this region very close to the critical point, the simplified approach based upon the reference temperature rule did not. It is concluded that the simplified approach may be satisfactory as long as the critical point is not approached too closely. More work with carbon dioxide and other fluids is necessary in order to define more definitely the region of applicability of the reference temperature rule.

ACKNOWLEDGMENT

J. W. Smith of the Statistical Department, Purdue University, assisted with the programing of the calculations on the computer. The Engineering Experiment Station and Purdue Research Foundation provided financial assistance.

NOTATION

- c_p = specific heat at constant pressure, B.t.u./lb. (°F.)
- h = local coefficient of heat transfer between fluid and tube wall, B.t.u./hr. (sq. ft./°F.)
- H = enthalpy of carbon dioxide, B.t.u./lb.
- H_1 = enthalpy at entrance to test section
- I = Electric current
- k = thermal conductivity, B.t.u./hr. (ft./°F.)
- L = length of test section, ft.
- Nu = Nusselt number, dimensionless
- Pe = Peclet number ($Pe = Pr Re$), dimensionless
- Pr = Prandtl number, dimensionless
- q = heat transfer rate per unit area.
- q_o = heat transfer rate per unit area at the tube wall, B.t.u./hr. (sq. ft.)
- R_t = total electrical resistance of test section, ohms
- Re = Reynolds number, dimensionless
- t = temperature, °F.
- t^* = dimensionless temperature defined by Equation (11)
- u = point velocity in direction of flow, ft./hr.
- u^* = dimensionless velocity defined by Equation (9)
- w = weight rate of flow of carbon dioxide in tube, lb./hr.
- z = distance from end of test section, measured in direction of flow, ft.
- y = radial distance in tube, measured from tube wall, ft.
- y^* = dimensionless distance defined by Equation (10)
- β = dimensionless parameter proportional to heat transfer rate, defined by Equation (12)

- ϵ = eddy diffusivity, sq. ft./hr.
- ϵ_h = eddy diffusivity for heat transfer, sq. ft./hr.
- μ = viscosity of fluid, lb./hr. (ft.)
- ρ = density of fluid, lb./cu. ft.
- τ = shear stress per unit area, pounds/(sq. ft.)

Subscripts

- o = wall conditions
- b = bulk mean conditions of fluid

LITERATURE CITED

1. Boelter, L. M. K., R. C. Martinelli, and F. Jonassen, *Trans. Am. Soc. Mech. Engrs.*, **63**, 447 (1941).
2. Colburn, A. P., *Trans. Am. Inst. Chem. Engrs.*, **29**, 174 (1933).
3. Comings, E. W., and R. S. Egly, *Ind. Eng. Chem.*, **33**, 1224 (1941).
4. Deissler, R. G., *Natl. Advisory Comm. Aeronaut. Tech. Note 2138* (1950).
5. ———, *Natl. Advisory Comm. Aeronaut. Rept. E52F05* (1952).
6. ——— and C. S. Eian, *Natl. Advisory Comm. Aeronaut. Tech. Note 2629* (1952).
7. Deissler, R. G., and M. F. Taylor, *Natl. Advisory Comm. Aeronaut. Rept. E53B17* (1953).
8. ———, *Natl. Advisory Comm. Aeronaut. Tech. Note 3145* (1954).
- 8A. Deissler, R. G., *Trans. Am. Soc. Mech. Engrs.*, **76**, 73 (1954).
9. Dittus, F. W., and L. M. K. Boelter, *Univ. Calif. (Berkeley), Publ. Eng.*, **2**, 443 (1930).
10. Eckert, E. R. G., Discussion, *Trans. Amer. Soc. Mech. Engrs.*, **76**, 83 (1954).
11. Franke, E. U., *Chem.-Eng.-Techn.*, **25**, 238 (1953).
12. Kiyama, R., and T. Makita, *Rev. Phys. Chem., Japan*, **22**, 49 (1952).
13. Krausschold, H., *Forsch. Gebeite Ingenieurw.*, **5B**, 186 (1934).
14. Lenoir, J. M., and E. W. Comings, *Chem. Eng. Progr.*, **47**, 223 (1951).
15. Michels, A., and C. Michels, *Proc. Roy. Soc. (London)*, **A153**, 201 (1935).
16. Michels, A., and S. R. de Groot, *Appl. Sci. Research*, **A1**, 94 (1948).
17. Naldrett, S. N., and O. Maass, *Can. J. Research*, **18B**, 322 (1940).
18. Phillips, P., *Proc. Roy. Soc. (London)*, **87**, 48 (1912).
19. Plank, R., and J. Kuprianoff, *Z. ges. Kälte-Ind.*, **36**, 41 (1929).
20. Prandtl, L., *Physik. Z.*, **11**, 1072 (1910).
21. Reynolds, Osborne, *Proc. Manchester Lit. Phil. Soc.*, **14**, 7 (1874).
22. Schroer, E., and G. Becker, *Z. physik. Chem.*, **173A**, 178 (1935).
23. Sellschopp, W., *Forsch. Gebeite Ingenieurw.*, **5B**, 162 (1934).
24. Sieder, E. N., and G. E. Tate, *Ind. Eng. Chem.*, **28**, 1429 (1936).
25. Stakelbeck, H., *Z. ges. Kälte-Ind.*, **40**, 33 (1933).
26. Stoljarow, E. A., *J. physik. Chem. (U.S.S.R.)*, **24**, 166 (1950).
27. Von Karman, T., *Trans. Am. Soc. Mech. Engrs.*, **61**, 705 (1939).
28. Zerby, C. D., "O.R.N.L. Pump Brochure," Oak Ridge Nat. Lab. (1954).

Liquid-liquid Extraction in a Pulsed Perforated-plate Column

W. H. LI and W. M. NEWTON

Georgia Institute of Technology, Atlanta, Georgia

Liquid extractions of benzoic acid-toluene solutions by means of water were studied under varying flow rates of both solvents in a 2-in. perforated-plate column to which pulsations of different frequencies and amplitudes were applied. Studies on reversal of the phase of the dispersion were made. With fixed flow rates of both solvents, the rate of extraction increased much more rapidly when the flow through the perforation became turbulent. The results are correlated by means of Reynolds number based on the flow through the perforations and are calculated from the product of the frequency and amplitude of the pulsations.

Since Sherwood, Evans, and Longcor (14) found in their study of extraction from single drops that 40 to 50% of the extraction is accomplished before a drop leaves the nozzle, frequent reformation of droplets of the dispersed phase should greatly improve the efficiency of extraction. A perforated-plate column should achieve this result, and a series of investigations on extraction in perforated-plate column was made by several investigators (1, 11, 12, 13, and 16).

Later, extraction from single drops was further studied. In a consideration of the mechanism of solute transfer in spray towers Licht and Conway (10) reported that the amounts of acetic acid extracted during drop formation by use of isopropyl ether, methyl isobutyl ketone, and ethyl acetate as solvent are 5, 8, and 17% respectively. These values are, however, less than those reported by Sherwood et al. Data on the extraction of acetic acid from benzene drops of known volume by water have been reported by West et al. (17), whose results have shown that approximately 14 to 20% extraction was obtained during drop formation.

The rate of emission of droplets through the perforations of the plate is limited by the physical properties of both phases and the size of perforations. Furthermore, each phase passes only once through each plate on its way through the column. It is thus believed that if pulsations were applied to the fluids in the column, so that the fluids would pass back and forth through the same plate before they leave for the next one, not only the frequency but also the speed of reformation of droplets through each plate would be greatly increased, depending on the frequency and amplitude of the pulsation applied. Dijk (6) was granted a patent on an agitated perforated-plate column for liquid-liquid extraction based on this principle. In Dijk's column the pulsation was achieved by a reciprocating mecha-

nism which lowered and raised the perforated plates in relation to the column and its liquid contents. Alternatively, the plates or the packing may be made stationary and the liquids reciprocated by means of an external piston and cylinder. A preliminary investigation on performance of a pulsed packed column for liquid-liquid extraction was reported by Feick and Anderson (8).

From the results reported by the previous investigators on perforated-plate towers and pulsed columns, it seems desirable to investigate a pulsed perforated-plate column for liquid-liquid extraction. Improvement of the performance of such a column should be expected.

The variables investigated in this work were flow rates of both phases, frequency and amplitude of pulsation, and the reversal of phase of dispersion. The effects of these variables on the performance of a pulsed perforated-plate column were studied.

EQUIPMENT AND MATERIALS

A schematic diagram of the extraction unit consisting of perforated-plate column, separators, rotameter, flow controls, pumps, storage tanks, and other auxiliary equipment is shown in Figure 1.

Extraction Column. The column consisted of eleven segments of Pyrex pipe spacers, 2 in. I.D., 2½ in. O.D., and 2 in. long, which were manufactured by the Corning Glass Company. The disengaging chambers at the top and bottom of the column were standard 2-in. cast iron crosses, between which the perforated plates and glass spacers were all held together by four ⅝-in. tie rods.

Perforated Plates. The brass plates were 5/32 in. thick and perforated with eighty-five holes of 1/16-in. diameter. The fraction of cross-sectional area of the column covered by these eighty-five holes was 8.51%. The center-to-center distance between the holes was 3/16-in., and the holes were arranged in an equilateral-triangular pattern. In order to reduce the pressure drop through the plates, all the holes on each plate were countersunk on both sides to a depth of 1/16 in. Sample above each plate was withdrawn from the column for analysis through a hole drilled horizontally through the plate and connected with a cock valve which was directly attached to the plate outside the column. Between the plate and the glass spacer a ⅝-in. asbestos gasket was used at each

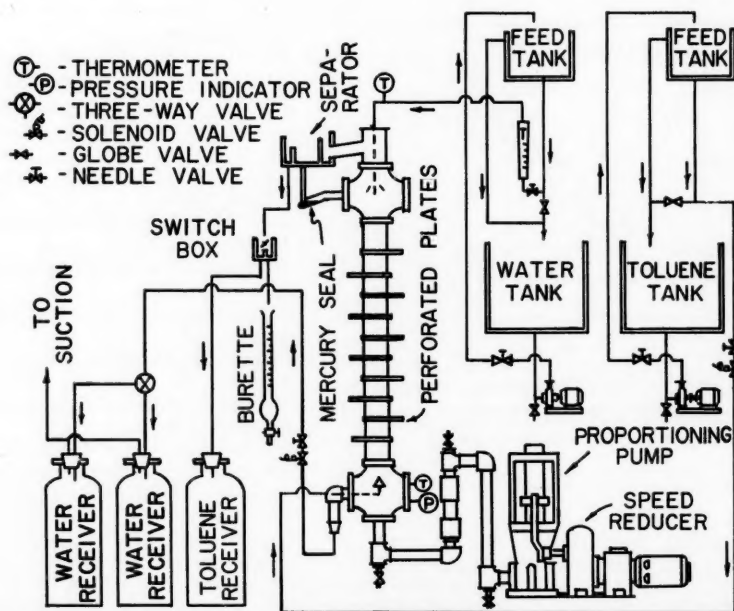


Fig. 1. Flow diagram of equipment.

W. H. Li is at present with E. I. du Pont de Nemours and Company, Inc., Chattanooga, Tennessee.

joint. A thin layer of graphite was pasted over the surfaces of the gaskets before they were assembled. In all this work ten plates were used, with a plate spacing of $2\frac{1}{4}$ in.

Separators. Two separators were used, one at each end of the column, to facilitate coalescence of all the droplets so as to separate completely the two liquid phases before they were withdrawn from the column. The top separator consisted of a rectangular brass box with a width, length, and height of 5, 7, and 3 in. respectively. The weir, with a height and width of $1\frac{1}{2}$ and 5 in. respectively, was located at a distance of 1 in. from the outlet end. A baffle was used near the entrance of the separator to prevent the emulsion from flowing straight through the separator. In the return line from the separator to the column for the heavier phase (water) a mercury seal was used to restrict the flow to one direction only. The bottom separator was made of a piece of 1-in. pipe, 4 in. long.

Feed Distributors. The distributor for toluene feed at the bottom of the column was made of 16-gauge aluminum sheet in the shape of a cone with a vertical angle of 60 deg. and a base $1\frac{1}{2}$ in. in diameter. On the surface of the cone seventy-eight holes $1/16$ in. in diameter were spaced in such a way that their projections on the base would give the same number of holes per unit area. In the center of the bottom disengaging chamber the cone was mounted so that its presence did not restrict the flow of the liquids through the column. A piece of $3/8$ -in. stainless pipe projecting down to the center of the top disengaging chamber was used to introduce the water feed.

Pulsing Unit. The pulsations were generated by a proportioning pump which was

connected with the motor through a variable-speed reducer covering an output speed range from 0 to 110 rev./min. The plunger diameter was $2\frac{1}{2}$ in.

In the U bend of the 1-in. line connecting the pump and the column a mercury seal was used to separate the fluid in the proportioning pump, water in this case, from the fluids in the column. A surge section was also provided in the pulsing line to prevent the possibility of mercury leaking into the pump. The amount of mercury used was carefully adjusted so that it was enough to stop the possible circulation of fluid from pump to the column or vice versa, but not sufficient to fill up the lower part of the bottom disengaging chamber. A vent was provided to purge any gas entrained in the pulsing line.

Feed Controls. Two $1/2$ -in. solenoid valves, full port type and normally closed, were used to control the streams fed into or taken out of the column. Two sets of switches for these solenoid valves were mounted on the revolving arm of the proportioning pump so that they were open only when the plunger of the pump came to its top and bottom positions respectively. The opening of the valves was thus synchronized with the strokes of the pump. The duration of opening each valve, as fixed by the length of contact of the switch, was about 7% of the time for a complete revolution. In other words, the volume of displacement by the pump was not appreciably affected by the number of streams added to or withdrawn from the column.

Feed Supplies and Other Accessories. All the lines for toluene solution containing benzoic acid were $3/8$ -in. stainless steel except the valves. Glass tanks were used for toluene-benzoic acid solution.

A constant head for both water and toluene feed was maintained by circulating the feeds from the storage to two constant-level tanks, which were located 20 ft. above the top of the column.

At the higher water flow rates it was found necessary to apply suction to the water-receiving bottles in order to maintain the desired flow rate of water through the solenoid valve, which was closed 93% of the time.

A pressure indicator was made of a piece of rubber tubing on which a slot approximately $3/8$ in. long was cut with a sharp blade. One end was plugged up, and the other was connected by glass tubing to the bottom disengaging chamber. This apparatus amounts to a Bunsen valve commonly used on laboratory wash bottles. The rubber tubing itself was enclosed in a glass tube, which was provided with a long glass tubing to indicate the height of the water column for pressure determination. The recorded pressure, therefore, was the maximum pressure at the center of the bottom disengaging chamber, including both the pressure to overcome the friction through the plates and the static head of the fluid mixture in the column. Actually the pressure-drop relationship was more or less sinusoidal and had both positive and negative peaks. The technique reported here was a measure of the peak pressure drop on the upstroke. Since some finite pressure differentials might have to be maintained for periods of time in order to open the split-tube valve to permit it to communicate pressure from inside to outside, the pressure drop obtained by this method might be slightly lower than the actual value. However, this method was used because of its simplicity.

Materials. Merck's reagent-grade toluene, Baker's C. P. grade benzoic acid, and Atlanta city water were used in determining the equilibrium-distribution curve and making the runs. The toluene solution after more benzoic acid had been added to make up the proper concentration was used over and over again; the water extract was discarded. The city water was saturated with toluene before use throughout this work.

EXPERIMENTAL

Equilibrium-distribution Curve

Equilibrium distribution of the system benzoic acid-toluene-water was determined for a temperature range from 74° to 91°F. The results were plotted in Figure 2. In the analysis an alcoholic solution of sodium hydroxide, 0.01N, was used for titration with phenolphthalein as the indicator.

Procedure

In starting up a run the column was filled with a water solution of benzoic acid from the previous run up to the top plate and the rest was filled with fresh water. The exact concentration of the initial water solution was immaterial because the purpose of charging the column with this water solution was to hasten the attainment of steady state. Both the fresh water and the toluene solution were then pumped into the overhead constant-level tanks, and the regulating valves were set for desired flow rates. The proportioning

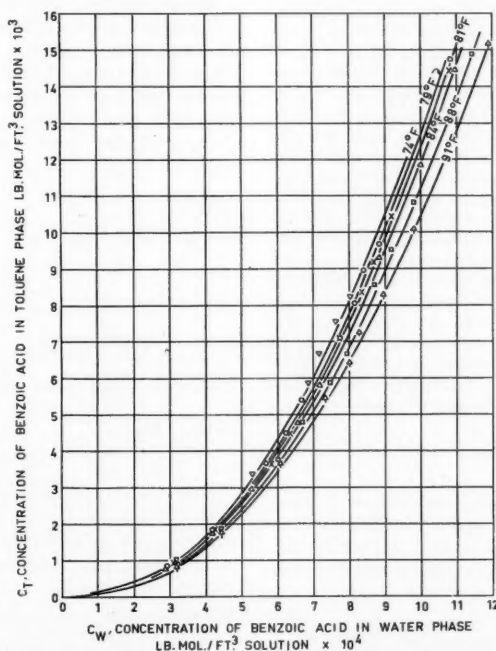


Fig. 2. Equilibrium distribution of benzoic acid-toluene-water system.

pump and the switches for the solenoid valves were turned on. By regulating the suction applied to the water-receiving bottles and the valve setting on the exit-water line, one could set the level of the interface and maintain it constant in the top separator for runs with water as the continuous phase. Constancy of the exit composition of both streams was tested by frequent titration of samples withdrawn at 5-min. intervals. A steady state was reached after a total throughput of three to four times the column volume, depending on the flow rates used. For the case with water as the discontinuous phase, the interface was set in the bottom-disengaging chamber.

When steady state was obtained, the by-pass for each stream was closed, the electric time recorder was started, and the exit streams were collected in the receivers provided for that purpose. At the conclusion of the run the time on the recorder was noted and the by-pass valves were opened.

During the run the exit toluene solution was periodically led off through the switch box into a graduated burette, where its flow was measured within a fixed time interval. The water rate was indicated by the rotameter.

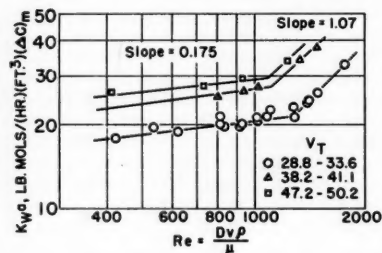


Fig. 3. Effect of pulsation on over-all transfer coefficient with constant flow rates, toluene dispersed.

At the end of a run the proportioning pump, solenoid valves, and water feed were turned off simultaneously. The thickness of toluene layer separated under each plate was measured and the water samples were withdrawn from each plate for titration. After all the toluene in the top separator had been decanted, the proportioning pump was run again with the water feed on, until all the toluene solution in the column rose and overflowed into a graduated cylinder, where its total volume in the column was measured as holdup. This total volume could be checked with the sum of all layers previously measured under each plate before they were combined. Holdup is therefore defined as the volume percentage of the dispersed phase in the liquid mixture which is present in the column during a steady operation.

Concentrations of both exit streams were analyzed by titrating the samples taken from the receivers with 0.01N alcoholic solution of sodium hydroxide with phenolphthalein as indicator. Blanks on fresh water which had been saturated with toluene were also determined. Plate concentrations of toluene layers were not analyzed but calculated by material balance after the

concentrations of water layers and flow rates were known.

The toluene solution containing benzoic acid was replaced by a fresh batch after every five or six runs, and the viscosity and surface tension of the used batch were determined. Throughout this investigation the viscosity of the toluene feed varied between 0.6230 and 0.6575 centipoise and the surface tension between 29.5 and 30 dynes/cm.; both properties were measured at 80.5°F.

The length of stroke traversed by the plunger of the proportioning pump was recorded by a tracing device attached to the upper end of the plunger.

CALCULATIONS

In this study all runs of which the error in material balance was greater than 5% were discarded.

The effective volume used in the calculation of $K_w a$ values from Equation (1) was 0.1015 cu. ft., which included the disengaging chambers, the top separator, and the glass column. The slope dC_T/dC_W of equilibrium curve at different temperatures was taken at an average toluene concentration. For each run this slope was determined according to the temperature.

The Reynolds number through the perforations was calculated by use of the density and viscosity of a two-phase liquid mixture containing 16% toluene by volume, which was the average analysis of the holdup of all the runs. Although a rigorous calculation of ρ and μ by use of the actual holdup analysis for each run was possible, nevertheless the variation in holdup analysis had little effect upon the ratio ρ/μ since both ρ and μ decreased with increasing toluene holdup. The average values of ρ and μ of the liquid mixture were calculated by taking the sum of individual density and viscosity of each pure component in proportion to their respective volumes. It might also be pointed out that during each flow wave the initial movement of liquid mixture through the perforations was probably streamline although the major portion of the flow was turbulent. With this fact that the viscosity of the liquid mixture varied not only with the composition but also with the manner of dispersion, this method of averaging the kinematic viscosity was only an approximation. For the same reason, an average of room temperature of 80°F. was used to calculate ρ/μ for all the runs. The term v , the arithmetic average velocity of liquid mixture through the perforations, was calculated from the volume of displacement of the plunger in the pump and the area of perforations on the plate. Table 1* summarizes the experimental data and calculated results.

THEORY

Colburn's H.T.U. method of correlation (4) has been applied by the previous authors (1, 13, 16) to their data on liquid-liquid extraction in perforated-plate col-

umn. The equations may be summarized as follows:

$$K_w a = \frac{N/\theta}{(\Delta C)_m V_T} \quad (1)$$

$$(H.T.U.)_{ow} = \frac{V_w}{K_w a} \quad (2)$$

$$(H.T.U.)_{ow} = H \frac{V_w}{V_T} (H.T.U.)_r + (H.T.U.)_w \quad (3)$$

In this investigation with the superimposition of pulsation on a perforated-plate column, the Reynolds number through the perforations was used to characterize the pulsation in the column.

Mass transfer film coefficients in wetted-wall columns have been shown by Gilliland and Sherwood (9) and Chilton and Colburn (3) to be functions of Reynolds and Schmidt numbers. Dodge and Dwyer (7), Comings and Briggs (5), and Brinsmade and Bliss (2) reported that mass transfer film coefficients are affected by the flow rates of both phases. The mass transfer film coefficients for liquid-liquid extraction in a given pulsed column under constant temperature and certain-sized perforations can be expressed through dimensional analysis as

$$k_T a = \phi_T (V_T)^n (V_w)^m (Re)^d \quad (4)$$

$$k_w a = \phi_w (V_T)^n (V_w)^m (Re)^d \quad (5)$$

Brinsmade and Bliss (2) pointed out that their method of correlation could be applied if either individual coefficient is independent of one flow rate. The exponent t in Equation (5) can be assumed to be zero. The effect of pulsation on both film coefficients is assumed to be same, that is, d equal to r . Equations (4) and (5) are combined to give the over-all coefficient

$$\frac{(Re)^d}{K_w a H} = \frac{1}{\phi_T (V_T)^n (V_w)^m} + \frac{1}{H \phi_w (V_w)^s} \quad (6)$$

or

$$(H.T.U.)_{ow} (Re)^d = \frac{H (V_w)^{1-m}}{\phi_T (V_T)^n} + \frac{1}{\phi_w (V_w)^{s-1}} \quad (7)$$

If the water film resistance is small—as is the case with the benzoic acid-toluene-water system—the second term on the right of Equation (6) can be omitted, and the following equation is obtained:

$$\frac{K_w a H}{(Re)^d} = \phi_T (V_T)^n (V_w)^m \quad (8)$$

*Table 1 has been deposited as document 5121 with the American Documentation Institute, Photoduplication Service, Library of Congress, Washington 25, D.C., and may be obtained for \$1.25 for photoprints or \$1.25 for 35-mm. microfilm.

DISCUSSION OF RESULTS

Unique Characteristics of a Pulsed Column with Toluene Dispersed

With constant flow rates of both phases, the effect of pulsation expressed in terms of Reynolds number Re on the rate of mass transfer is shown in Figure 3. Each curve shows a break in slope at a Reynolds number between 1,050 and 1,200 which divides the curve into two regions. The lower region, where the effect of Reynolds number on K_{wa} value is small, is called the *streamline* region and the other the *turbulent* region.

With varying flow rates of both phases, the slopes of both streamline and turbulent regions remain unchanged, as shown by curves A, B, and C in Figure 3. The critical Reynolds number, however,

by settling during the short interval of stroke reversal was slowly sucked downward through the perforations against a thin layer of toluene accumulated under the plate and then expanded into drops surrounded by a toluene film which has the lower surface tension. This phenomenon of forming cell-like structure by dispersion of large water drops between toluene films is similar to the formation of foams by blowing of air into a soap solution.

The toluene phase in the cell-like mixture began to coalesce into droplets after leaving the top plate and rose as a dispersed phase in the top disengaging chamber. In the lower end of the streamline region, therefore, the water phase was actually discontinuous in the space between plates. To avoid confusion with

number beyond 1,200, the toluene phase became clearly dispersed with vigorous turbulence in the water phase, as shown in Figure 6.

As the Reynolds number was further increased, the size of the dispersed droplets became finer and finer, until with a Reynolds number around 1,800 the fine toluene droplets in the exit water stream could not be settled out in the bottom separator. With all toluene and water rates investigated, flooding occurred at a Reynolds number of approximately 1,800. Curves in Figure 3, therefore, should not be extrapolated at the upper end.

When operating at the lower end of the streamline region with a Reynolds number around 400, the column was only partially filled with cell-like dis-

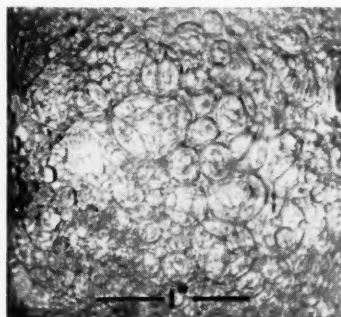


Fig. 4. Dispersion of toluene, $Re = 417$.

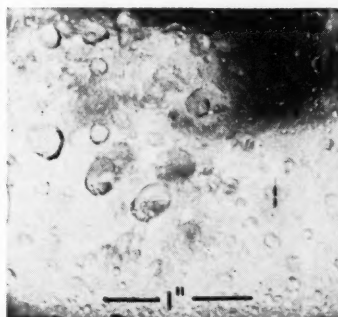


Fig. 5. Dispersion of toluene, $Re = 1029$.



Fig. 6. Dispersion of toluene, $Re = 1475$.

decreases slightly with increasing flow rates.

When the column was operating near the lower end of the streamline region with low Reynolds number, a cell-like formation with large drops of water phase surrounded by toluene films was observed as shown in Figure 4. The reason for this cell-formation phenomenon is that during the suction stroke a water layer which had been accumulated above the plate

the case to be described later where water was the true dispersed phase throughout the column, the water phase, despite its cell-like formation, was still considered as continuous in this lower part of the streamline region.

As the Reynolds number increased in the streamline region, the cell size became smaller and the cell-formation phenomenon gradually disappeared (Figure 5). Upon further increase of Reynolds

persions, the lower space of each column segment between plates being left mainly full of continuous water phase. The column seemed to be underloaded. For this reason, runs with Reynolds number less than 400 were not attempted.

When pressure drop across the column was plotted vs. Reynolds number in Figure 7, the same shape of curve was obtained as in Figure 3, with the same critical Reynolds number around 1,200.

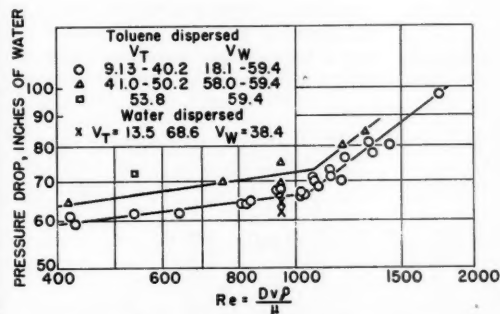


Fig. 7. Effect of pulsation on pressure drop.

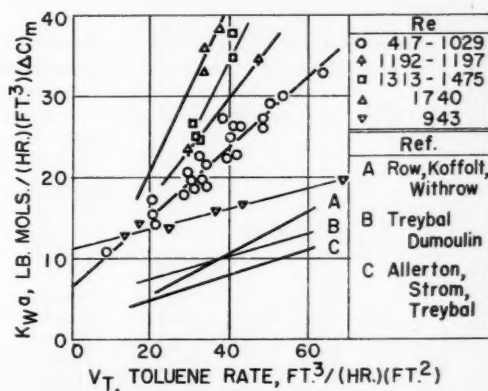


Fig. 8. Extraction coefficient in pulsed (curves with data points) and nonpulsed (curves A, B, and C) perforated-plate columns.

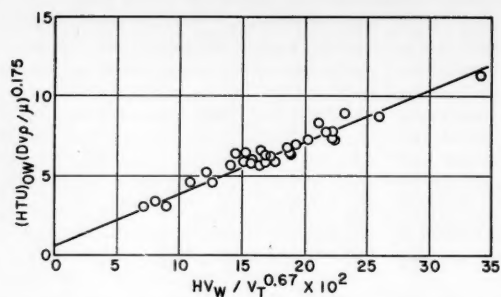


Fig. 9. Over-all $(H.T.U.)_{OW}$ in the streamline region, toluene dispersed.

To study the cause of the break of the curves in Figure 3 and 7, the column was operated with water alone under the same conditions as with both water and toluene. Water fed into the bottom of the column through the toluene feed line was kept at a rate of 40.2 cu. ft./ (sq. ft.)(hr.) for all the runs. A set of pressure-drop data was taken with varying Reynolds numbers and recorded in Table 2. These data, if plotted in Figure 7, showed the same shape of curve with a break at a Reynolds number around 1,200. It is evident that the break of curves in Figures 3 and 7 is due to the change of nature of flow of liquid mixture in the column, that is, from streamline to turbulent flow.

TABLE 2. PRESSURE DROP WITH WATER PHASE ALONE

Stroke length, in.	Frequency strokes/min.	Re	Pressure drop, in. of water
1.44	9.75	425	61.4
1.44	27.50	1197	75.3
1.44	30.40	1325	80.5
1.44	37.10	1615	89.3

Effect of Varying Pulsation

It may be seen from Figure 3 that the slopes are 0.175 and 1.07 for the streamline and turbulent regions respectively. The mass transfer coefficients were greatly increased by operation in the turbulent region. Similarly, the pressure drop across the column was increased in the same manner as the mass transfer coefficients, with slopes 0.155 and 0.85 for streamline and turbulent regions respectively.

For the data shown in Figure 3, different stroke length and frequencies were used. The effect of pulsation on transfer coefficients was found to be dependent on the product of the stroke length and frequency of the pulsation. For practical consideration, low frequency and long stroke length seem to be preferable; however, a constant inter-phase was more easily maintained during operation under short strokes. In this work a stroke length of 1.44 in. or a height of 2.25 in. of displacement in the column was found to be satisfactory; in other words, there was a linear displacement of one plate spacing.

Effect of Varying Flow Rates

With a constant Reynolds number, a series of runs was made to study the effect of flow rates of both phases on over-all mass transfer coefficients. In the streamline region the over-all mass transfer coefficient was only slightly affected by the water rate $[K_{wa} = \alpha(V_W)^{0.11}]$ with toluene rate held constant, but considerably more by the toluene rate $[K_{wa} = \beta(V_T)^{0.55}]$ with water rate held constant. In the turbulent region, the effect of water rate on the over-all mass transfer coefficient was still small $[K_{wa} = \gamma(V_W)^{0.23}]$, and the toluene rate had a large influence upon this coefficient $[K_{wa} = \delta(V_T)^{1.2}]$.

In Figure 8 K_{wa} is plotted vs. V_T with Reynolds number as the parameter. The over-all transfer coefficient increases more rapidly with toluene rate as the Reynolds number increases.

With water as the dispersed phase, the rate of increase of K_{wa} values with

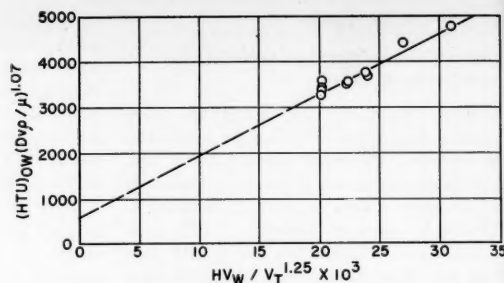


Fig. 10. Over-all $(H.T.U.)_{OW}$ in the turbulent region, toluene dispersed.

increasing toluene rate is small. It seems that with either phase being dispersed, the over-all transfer coefficient is affected mainly by the flow rate of the dispersed phase and slightly by the continuous phase.

H.T.U. Correlations

In the investigations (1, 13, 16) reported in the literature, the results on liquid-liquid extraction in a perforated-plate column were correlated by Equation (3) and values of $(H.T.U.)_w$, the intercept, and $(H.T.U.)_T$, the slope, were obtained from the plot of $(H.T.U.)_{OW}$ vs. $H(V_W/V_T)$. $(H.T.U.)_w$ and $(H.T.U.)_T$ values obtained from a similar plot by use of the present results are given in Table 3. Both $(H.T.U.)_w$ and $(H.T.U.)_T$ values or both film resistances decreased as the Reynolds number increased.

When $(H.T.U.)_{OW}$ was plotted vs. $H(V_W/V_T)$ with the present results, runs 5, 6, and 30, where the flow-rate ratio of water to toluene was high, did not fall on the straight line. This fact agrees with the finding of Row, Koffolt, and Withrow (13) that there was marked deviation from straight line with low toluene rate and high water rate.

The correlation of results by Equation (7) is more satisfactory. By trial and error, the best straight line was obtained when a value of n equal to 0.67 for the streamline region was used as shown in Figure 9. The intercept $1/(\phi_W(V_W)^{0.175})$ is 0.55 and the slope $1/\phi_T$ is 33.1. All the data fell on a straight line. Similarly for the turbulent region, the value of n was found to be 1.25, and the results are shown in Figure 10, giving an intercept

TABLE 3. COMPARISON OF H.T.U.'S IN PERFORATED-PLATE COLUMNS

Plate characteristics		Reference	Continuous phase	Dispersed phase	Flow rates, Cu. ft./ (hr.)(sq. ft.)		$(H.T.U.)_w$	$(H.T.U.)_T$	$Re, D_{wp}/\mu$
Spacing, in.	Hole Diam., in.				V_W	V_T			
6	3/32	13	Water	Toluene	11.8-37.1	12.5-47.7	0.25	106	
6	1/8	13	Water	Toluene	11.8-37.1	11.8-47.7	0.25	115	
3	3/16	16	Water	Toluene	15.1-32.5	9.7-81.8	0.65	30	
6	3/16	16	Water	Toluene	22.9-41.5	30.2-76.8	0.25	63	
9	3/16	16	Water	Toluene	23.2-38.9	35.8-78.6	0.25	68	
4 3/4	3/16	1	Water	Kerosene	24.7-13.6	33.8-16.2	0.65		
2 1/4	1/16	Present	Water	Toluene	18.1-38.4	9.13-63.6	0.50	26.6	417-1,150
2 1/4	1/16	data, pulsed column	Water	Toluene	38.4-58.0	30.7-41.1	0.42	20.4	1,300-1,500
2 1/4	1/16		Toluene	Water	38.4	13.5-68.6	1.85	10.0	943

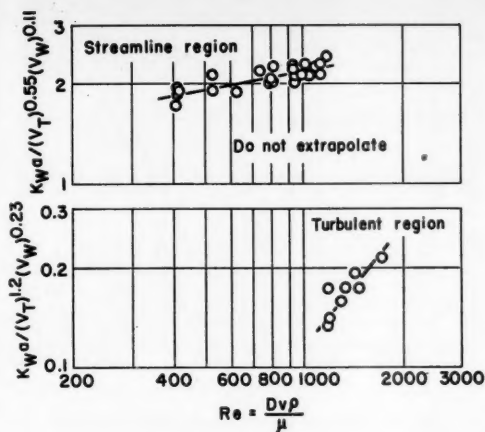


Fig. 11. Correlation of over-all transfer coefficient with Reynolds number, toluene dispersed.

550 and a slope 1.36×10^4 . Since the value of m is small, it is neglected in plotting Equation (7) on Figures 9 and 10.

According to Equation (7), a series of lines should be drawn in Figures 9 and 10 with each line representing one constant water rate. However, since all points within the range of the water rates studied fell so close to the same straight line, it is obvious that such procedure is not necessary. The intercept and the slope of the curves in Figures 9 and 10 were, therefore, obtained by use of an average water rate.

Approximate Correlation

The results are correlated by Equation (8) and plotted in Figure 11. It is seen that the value of exponent m is small compared with that of n , and so Figure 11 can be replotted without much error, as shown in Figure 12 by the following equation:

$$\frac{K_w a H}{(Re)^d} = \phi'_T (V_T)^n \quad (9)$$

Most of the data on liquid-liquid extraction in perforated-plate columns with the benzoic acid-toluene-water system reported in the literature were correlated fairly well by a log-log plot of H.T.U. vs. V_W/V_T as shown by Treybal (15). A similar plot was made in Figure 13 with the present results and the correlation was not so satisfactory as that obtained by using Equation (7).

Water as Dispersed Phase

In the operation with water as discontinuous phase, the interface was maintained in the bottom disengaging chamber, and all the other operating conditions remained the same. The droplet size of the dispersed water phase was found to be small, as shown in Figure 14.

The results with water as dispersed phase were plotted in Figure 8, which shows that with a high toluene rate

above 15 cu. ft./hr.(sq. ft.) a lower transfer coefficient was obtained by dispersing water in toluene, but at low toluene rate below 15 cu. ft./hr.(sq. ft.) a higher transfer coefficient was obtained. Whether the water or toluene phase should be dispersed in order to obtain the highest transfer coefficient will consequently depend on the toluene rate used. The low values of transfer coefficients with water as discontinuous phase and a toluene rate above 15 cu. ft./hr.(sq. ft.) were probably due to the fact that the increase of water film resistance more than offsets the decrease of toluene film resistance caused by the phase reversal.

Comparison of Results from the Literature

The results on perforated-plate columns using the system benzoic acid-toluene-water were taken from the literature for comparison. But owing to wide variation of conditions under which the results were obtained by different investigators, only a rough comparison of results to show relative magnitudes was possible.

Since the values of $(H.T.U.)_W$ and $(H.T.U.)_T$ reported in the literature were obtained as intercepts and slopes by plotting $(H.T.U.)_{OW}$ vs. HV_W/V_T according to Equation (3), the same procedure was followed in obtaining $(H.T.U.)_W$ and $(H.T.U.)_T$ values for the present work. The results are shown in Table 3.

The values of $(H.T.U.)_W$ reported by various investigators are not much different from those in this study, and they are all much smaller than the $(H.T.U.)_T$ values. The difference between $(H.T.U.)_T$ values reported in the literature and this study, however, was appreciable, and the $(H.T.U.)_T$ values from the present work are the lowest. Large increase of over-all transfer coefficients by superimposition of pulsation is evident from comparison of the present results with those of previous investigators, as shown in Figure 8.

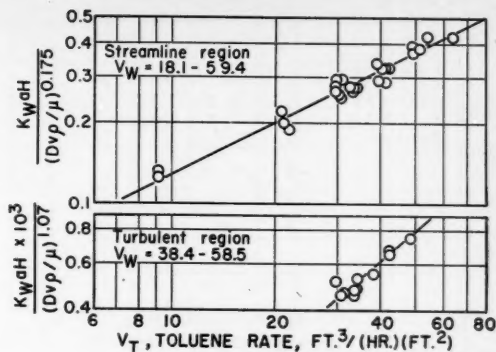


Fig. 12. Effect of toluene rate on $K_w a$, toluene dispersed.

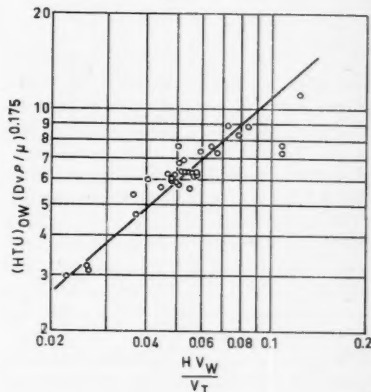


Fig. 13. Extraction in a pulsed column, toluene dispersed in streamline region.

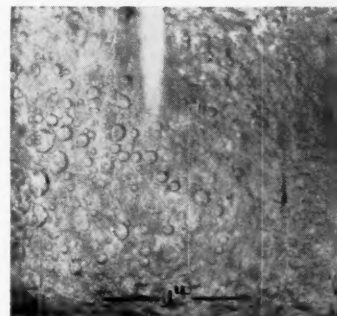


Fig. 14. Dispersion of water, $Re = 943$.

Holdup

Under constant pulsation the toluene holdup was increased by increasing the toluene rate and only slightly affected by the water rate. The results are plotted in Figure 15.

The effect of pulsation on holdup, shown in Figure 16, was large in both streamline and turbulent regions. As the Reynolds number increased, the size and the rising velocity of dispersed toluene in the column decreased, and so the toluene holdup increased. In transition from streamline to turbulent region

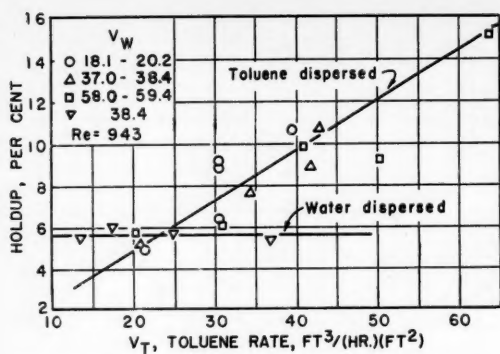


Fig. 15. Effect of toluene rate on holdup with constant pulsation, $Re = 943$.

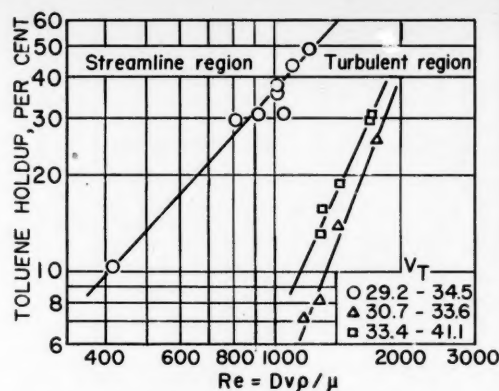


Fig. 16. Effect of pulsation on toluene holdup.

the toluene holdup suddenly dropped from 48 to 7%, as shown in Figure 16. This sudden drop of toluene holdup was due to the fact that the dispersed toluene changed its form from cell-like films into drops upon transition from the streamline to the turbulent region. Since the toluene drops would rise faster in the continuous-water phase than the toluene films, the toluene holdup in the column became less for the turbulent region than for the streamline region.

With water as the dispersed phase, the water holdup was found to be unaffected by the toluene rate. It seemed that the holdup was affected mainly by the flow rate of the discontinuous phase and was practically independent of the flow rate of the continuous phase.

CONCLUSIONS

The performance of the perforated-plate column for liquid-liquid extraction was greatly improved by superimposing pulsations. As compared with the results in literature, transfer coefficients found in this work are considerably higher.

A critical Reynolds number based on the average velocity through the perforations was found to be around 1,200, above which the rate of increase of the transfer coefficient was much more rapid with an increase in the Reynolds number. Pressure drop across the column increased with the Reynolds number in a similar manner.

Toluene-film resistance was found to be the controlling factor for the mass transfer.

Lower transfer coefficients were obtained with water as the discontinuous phase. This decrease was probably due to the increase of water film resistance, which was more than enough to offset the decrease of toluene film resistance.

A high flow-rate ratio of water to toluene gave abnormally low $(H.T.U.)_{OW}$ values, which could not be correlated by plotting $(H.T.U.)_{OW}$ vs. HV_W/V_T .

A modified H.T.U. method of correla-

tion is recommended and general equations including the effect of pulsation are presented.

The holdup increased with increasing flow rate of the discontinuous phase and independent of flow rate of the continuous phase. With constant flow rates holdup increased exponentially with an increase in the Reynolds number.

NOTATION

a	= interfacial area, sq. ft./cu. ft. of effective column volume
C	= concentration of benzoic acid, lb. moles/cu. ft. of solution
$(\Delta C)_m$	= logarithmic mean of concentration-difference driving force at the extremities of the column, lb. moles/cu. ft. of solution
D	= diameter of the perforations on the plate, ft.
H	= reciprocal of the slope of the equilibrium-distribution curve equal to dC_W/dC_T
H.T.U.	= height of transfer unit, ft.
k	= film transfer coefficient, lb. moles benzoic acid transferred/(hr.)(sq. ft.)(ΔC) _m
K	= over-all transfer coefficient, lb. moles benzoic acid transferred/(hr.)(sq. ft.)(ΔC) _m
N	= number of moles of benzoic acid transferred
Re	= Reynolds number through the perforations on the plate, equal to Dvp/μ
v	= velocity of toluene-water mixture through the perforations, ft./sec.
V'	= effective volume of the column, cu. ft.
V	= flow rate, cu. ft./(hr.)(sq. ft.)

$$\left. \begin{matrix} d \\ m \\ n \\ r \\ s \\ t \end{matrix} \right\} = \text{exponents} \qquad \left. \begin{matrix} \alpha \\ \beta \\ \gamma \\ \delta \\ \phi \\ \phi' \end{matrix} \right\} = \text{constants}$$

θ	= time, hr.
μ	= viscosity of the toluene-water mixture, lb./(sec.)(ft.)
ρ	= density of the toluene-water mixture, lb./cu. ft.

Subscripts

O	= over-all
T	= toluene phase
W	= water phase

LITERATURE CITED

- Allerton, Joseph, B. O. Strom, and R. E. Treybal, *Trans. Am. Inst. Chem. Engrs.*, **39**, 361 (1943).
- Brinsmade, D. S., and Harding Bliss, *ibid.*, p. 679.
- Chilton, T. H., and A. P. Colburn, *Ind. Eng. Chem.*, **26**, 1183 (1934).
- Colburn, A. P., *Trans. Am. Inst. Chem. Engrs.*, **35**, 211 (1939).
- Comings, E. W., and S. W. Briggs, *Trans. Am. Inst. Chem. Engrs.*, **38**, 143 (1942).
- Dijk, W. J. van, U. S. patent 2,011,186 (1935).
- Dodge, B. F., and O. E. Dwyer, *Ind. Eng. Chem.*, **33**, 485 (1941).
- Feick, G., and Anderson, H. M., *Ind. Eng. Chem.*, **44**, 404 (1952).
- Gilliland, E. R., and T. K. Sherwood, *Ind. Eng. Chem.*, **26**, 516 (1934).
- Licht, William, Jr., and J. B. Conway, *Ind. Eng. Chem.*, **42**, 1151 (1950).
- Moulton, R. W., and J. E. Walkey, *Trans. Am. Inst. Chem. Engrs.*, **40**, 695 (1944).
- Pyle, C., A. P. Colburn, and H. R. Duffy, *Ind. Eng. Chem.*, **42**, 1042 (1950).
- Row, S. B., J. H. Koffelt, and J. R. Withrow, *Trans. Am. Inst. Chem. Engrs.*, **37**, 559 (1941).
- Sherwood, T. K., J. E. Evans, and J. V. A. Longcor, *Ind. Eng. Chem.*, **31**, 1144 (1939).
- Treybal, R. E., "Liquid Extraction," 1 ed., McGraw-Hill Book Company, Inc., New York (1951).
- , and F. E. Dumoulin, *Ind. Eng. Chem.*, **34**, 709 (1942).
- West, F. B., P. A. Robinson, and A. C. Morgenthaler, Jr., T. R. Beck, and D. K. McGregor, *Ind. Engr. Chem.*, **43**, 234 (1950).

Mechanics of Vertical-moving Fluidized Systems

LEON LAPIDUS and J. C. ELGIN

Princeton University, Princeton, New Jersey

Fluidization, more specifically the fluidization of beds of solid particles and catalysts, has become a subject of wide interest in chemical engineering during the past few years. Its major practical application has thus far been in the catalytic cracking of petroleum fractions but it is being studied and developed as a technique for conducting a wide variety of other reactions involving solids and fluids, especially solids and gases. Its broad ramifications and its basic character have not as yet been widely appreciated.

The fundamental importance of the phenomenon of fluidization to the majority of chemical engineering operations and processes and hence to phase-change separations in which two phases must be brought into contact is now recognized. Any mass of particles, whether they be solid, liquid, or gas, which are suspended in a continuous fluid because of the motion of the fluid between the particles, represents and can be classified as a fluidized system (7).

This conclusion means that a multitude of operations involving masses of particles, droplets, or bubbles suspended in a fluid can be classified as fluidized systems. Examples are a liquid-liquid extraction tower, the fluidized catalytic-cracking bed of finely divided solids, a sieve-plate tower, mixing of two liquids or solid particles with liquid in an agitated tank, solids settling through a liquid (sedimentation), gas bubbles rising through a liquid (aeration), pneumatic transport of solids, and spray drying.

All such systems are controlled by and subject to the same fundamental combination of forces and their characteristics and behavior are determined basically by the same general principles. This is so irrespective of the relative direction of motion of the particles and fluid with respect to each other and to the walls of the containing vessel. The requirement is that relative motion or slip exist between particles and fluid. It is theoretically possible to generalize the basic properties of such systems in terms of the geometry,

the physical properties of the system, and the flow rates regardless of whether the particles are solid, liquid, or gaseous.

In the present paper the authors will define and develop in detail the basic relationships that characterize any ideal fluidized system, an ideal system being defined as one in which nonporous, rigid spheres are fluidized in a particulate manner by an incompressible fluid. This will serve as a model analogously to the perfect gas law or Raoult's law for solutions. This ideal case will, in general, be more closely approached for solid particles or very small liquid droplets where the density difference between particle and fluid is not too great.

With the relative direction of motion of particles and fluid with respect to each other and the containing walls as a basis, the possible types of vertical fluidized systems are formulated. The slip velocity is shown to be the fundamental variable in all types of systems.

Based upon the experimental determination of the fraction holdup (or void fraction) and the superficial fluid velocity for an unfed, bottom-restrained fluidized system, a graphical procedure is outlined for the preparation of a generalized operational diagram. This diagram can be used for predicting and comparing the operating mechanics and characteristics of all ideal vertical fluidized systems. Experimental data for the fluidization of small solid particles with water are presented as validation of the basic theories.

The fundamental concepts will not be altered by complications introduced by a departure from the spherical or distortion and expansion of liquid and gas bubbles in motion. While very important in many practical cases, they are secondary effects determined by particular interrelationships of the forces involved and do not change the basic concepts.

Since the development of the theory and the completion of the experimental work described in this paper, Mertes and Rhodes (4) have published a treatment of moving solids-fluid systems. Their work lends additional support to the

theory and generalizations presented in this paper.

BASIC QUANTITIES IN FLUIDIZATION

The void fraction ϵ and its opposite, the holdup $(1 - \epsilon)$, within a given volume are important characteristic properties of any fluidized system. To date they must be measured experimentally and correlated with the pertinent physical and flow factors, calculations that correspond to evaluating an equation of state. The upper limit of ϵ is the fully expanded bed, or 100% voids, conversely a holdup of zero. The lower limit, as will be seen later, depends upon the type of fluidized system.

The total pressure drop in a fluidized system is the sum of wall friction and hydrostatic head. On the basis of neglecting the very small amount of wall friction, the pressure drop per foot of height is given by

$$\frac{\Delta P}{z} = (1 - \epsilon)(\rho_d - \rho_f) \quad (1)$$

where

$\Delta P/z$ = pressure drop per unit height
 ρ_d = density of discontinuous phase
 ρ_f = density of continuous phase

If the subdivided phase is lighter than the continuous fluid, $\rho_d < \rho_f$, the pressure drop occurs in the opposite direction, i.e., from top to bottom of the bed. Thus the pressure drop and the holdup are linearly related.

Of further interest are the velocities of the two phases. V_f' may be called the *superficial fluid velocity* and V_d' the *net average superficial vertical-particle velocity*. Both these velocities are based upon the total cross section of the empty tube. The actual velocities are then given by

$$V_f = \text{fluid velocity} = V_f' / \epsilon$$

$$V_d = \text{average particle velocity}$$

$$= V_d' / (1 - \epsilon)$$

Also the vectorial difference between the

fluid velocity and the solids velocity (with the convention of upward flow as positive) may be defined as the slip velocity,

$$V_s = \text{slip velocity} = V_f - V_d \\ = V_f / \epsilon - V_d / (1 - \epsilon) \quad (2)$$

As can easily be shown, for spherical particles, the specific contact area varies with the fraction voids in the following way

$$\bar{a} = \frac{6(1 - \epsilon)}{D_p} \quad (3)$$

where

\bar{a} = specific contact area per unit volume

D_p = particle diameter

Since \bar{a} varies linearly with the amount of holdup $(1 - \epsilon)$, the holdup is a prime factor in determining the contact area for mass transfer or mass transfer efficiency in any particle-type contacting device. In addition \bar{a} is directly proportional to $\Delta P/z$ in such equipment. The importance of examining the behavior of the holdup for various operating conditions is immediately apparent.

TYPES AND CLASSIFICATION OF VERTICAL-MOVING FLUIDIZED SYSTEMS

The previous description of an ideal vertical fluidized system leads to the recognition of certain basic types and classes of systems. Two standard types may be postulated: (1) free and (2) mechanically restrained. The relative direction of motion of particle and fluid relative to the walls then leads to several types under each category. With the convention of upward flow assumed as a positive quantity and downward as negative and $\rho_d > \rho_f$, these categories and the slip velocity for each may be classed as follows:

Free Systems

Free systems require no constraint in the flow path with the particle feed rate controlled externally at the particle inlet. The rate of particle addition must be determined by the net movement of the volume of particles through the fluidizing zone.

Counter-current: $V_s = V_f - (-V_d)$. Particles and fluid are fed at opposite ends of the tower. The relative position of feed depends on the density values. If $\rho_d > \rho_f$, then particles are fed at the top of the tower and flow downward. Free settling is a special case of counter-current flow in which the fluid velocity V_f is set equal to zero. This assumes that the liquid being displaced by the accumulation of particles is removed without being allowed to pass through the dynamic contacting zone.

Concurrent Cogravity: $V_s = -V_f - (-V_d)$. This represents a relatively new

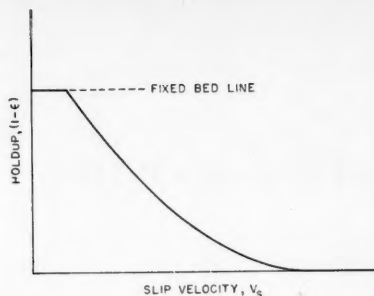


Fig. 1. Schematic representation of holdup $1 - \epsilon$ vs. the slip velocity V_s .

technique for contacting. If $\rho_d > \rho_f$, both particles and fluid are fed at the top of the tower and move downward together.

Concurrent Countergravity: $V_s = V_f - (V_d)$. This is generally referred to as *solids transport*. If $\rho_d > \rho_f$, both particles and fluid are fed at the bottom of the tower and move upward together.

Mechanically Restrained Systems

In these systems the flow path of the particles is mechanically restrained and the particle feed rate is externally controlled at the particle exit.

Unfed, Bottom Restraint: $V_s = V_f - (0)$. If $\rho_d > \rho_f$, the fluid is fed at the bottom of the tower and passes through a particle impermeable membrane or screen and then upward through a fixed quantity of particles. Even though there is motion of the particles within the bed, there is no net motion with regard to the walls. Thus the particle velocity V_d may be set equal to zero. This type of operation has received considerable experimental and theoretical study and represents in many people's minds the only form of fluidized system. If the restraining screen is removed, the operation degenerates into a free system, which could be maintained only by continuously feeding particles to the top of the tower.

This unfed system has one less degree of freedom than the previously described free systems. Whereas in countercurrent and concurrent flow both the fraction void and the particle velocity are variable, only fraction void can be changed in batch fluidization, as the net particle velocity is always zero. In terms of pressure drop, the nonfed bed always has a constant value of $\Delta P/z$. This is a result of the constant weight of the bed and the subsequent changes in z with V_f . For a continuously fed bed the length z is constant and the weight or holdup in the bed varies with V_d and V_f . Hence both $\Delta P/z$ and $1 - \epsilon$ vary with V_d and V_f .

Bottom Restraint, Downward Particle Feed: $V_s = V_f - (-V_d)$. This corresponds to feeding liquid at the bottom of the tower (if $\rho_d > \rho_f$) and feeding particles at the top. In the steady state

condition particles are withdrawn at the bottom at a controlled rate and fed at the top at the same rate to maintain a constant inventory of particles in the tower.

Bottom Restraint, Upward Particle Feed: $V_s = V_f - (V_d)$. For $\rho_d > \rho_f$, particles are continuously withdrawn at a controlled rate from the top of a bottom-restrained fluidized bed and constantly fed at the same rate at the bottom. This represents transport of the particles by the fluid.

Bottom Restraint, Concurrent, Cogravity Feed: $V_s = -V_f - (-V_d)$. Solid particles, $\rho_d > \rho_f$, are fed at the top of the bed with the fluid. Particles are withdrawn from the bottom at the same rate.

Top Restraint, Cogravity Particle Flow: $V_s = V_f - (0)$. For $\rho_d > \rho_f$, this case has significance only if V_f exceeds the transport velocity of an individual particle. Under these conditions a packed bed will be formed below the restraining screen. For conditions below the transport velocity the system will behave as if the screen were not present.

Top and Bottom Restraint, Fluid Upward: $V_s = V_f - (0)$. A variety of possible operations exists here: a fully packed bed between the two screens, a packed bed occupying only a part of the volume, or a fully fluidized system. The actual situation will depend on the total inventory of particles between the screens as compared with the available volume.

Slip Velocity as the Characterizing Parameter

The relationship between the operating mechanics of all types of systems is determined by the same basic laws. This can be illustrated by considering the behavior of a single particle suspended in a fluid. This is analogous to consideration of a very dilute solution or a high vacuum for a gas and can serve as a reference condition.

For a single spherical particle falling through a quiescent fluid, nonmoving with respect to the walls, an acceleration period is followed by a regime in which the particle moves at a constant velocity, which is the terminal, or free-fall, velocity V_f . By equating the vertical gravitational force downward to the vertical drag upward, this velocity may be calculated; i.e., for viscous flow

$$V_f = \frac{(\rho_d - \rho_f)gD_p^2}{18\mu_f} \quad (\text{Stokes's Law})$$

As V_f , the fluid velocity, is zero, this equation predicts the particle velocity relative to the walls.

If the fluid is set in motion counter-currently upward relative to the walls, the velocity of the particle with respect to the walls V_d is reduced and when $V_f = V_d$ the particle is stationary, or $V_d = 0$. This fluid velocity is known as the *transport velocity* and is identical with

the free-fall velocity V_f . This may be expressed as

$$V_d = V_f \text{ for } V_f = 0 \text{ (free-fall)}$$

and

$$V_f = V_t \text{ for } V_d = 0 \text{ (transport)}$$

At any intermediate value of V_f between zero and the transport velocity or, in fact, at any fluid velocity with respect to the walls, the relative or slip velocity of fluid past the particle is constant and equal to the free-fall, or transport, velocity. The slip velocity, as defined by Equation (2), is thus

$$V_s = V_f - V_d = \text{constant}$$

Thus the slip velocity, or the relative velocities of particle and fluid to each other, is the invariant parameter in determining the behavior and properties of the system. The particle knows the movement of only the fluid and not the walls and does not know whether it is moving relative to the latter or not.

For a mass of particles suspended in a fluid stream one may postulate the presence of a third group of forces, namely, the forces exerted by the particles on one another. This would cause an additional vertical component opposite to the fluid motion. In the present work it is proposed that even in a multiparticle fluidized system the invariant parameter of operation is still the slip velocity as defined by Equation (2). In other words, any one of the forms of a fluidized system described above will at the same value of the slip velocity have the same void fraction ϵ or the same holdup $(1 - \epsilon)$ for a given fluid-particle system.

In mathematical terminology this dependence of holdup on the slip velocity, no matter what the type of operation, can be expressed as

$$(1 - \epsilon) = \phi(V_s) \quad (4)$$

where $\phi(V_s)$ represents a functionality of V_s . Graphically Equation (4) can be schematically represented by Figure 1.

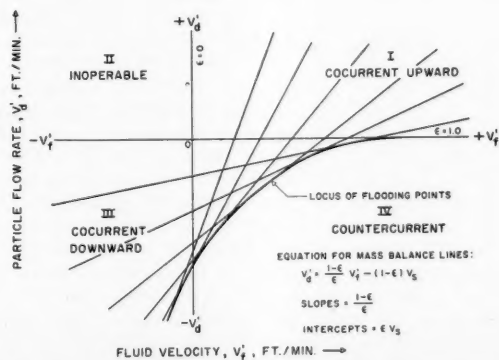


Fig. 2. Schematic diagram of superficial solids velocity V_d' vs. superficial fluid velocity V_f' at constant values of the holdup $1 - \epsilon$.

The upper limit of holdup on this curve is the fully packed bed and the lower limit is an empty bed.

Equations (2) and (4) can be combined and plotted graphically. The resulting diagram defines on a single plot the relation between holdup and flow rates existent over any flow regime for all types of vertical free or restrained systems. Furthermore, this diagram defines the limits of operation of each type of system and the range of fluid velocities over which each can exist. Any fluid-particle system will exhibit this characteristic diagram, which can be quantitatively plotted to scale if the relation expressed by Equation (4) is known.

PREPARATION OF GENERALIZED OPERATIONAL DIAGRAM

While there are a number of methods available for preparing a generalized operational diagram, the technique to be illustrated here is the most convenient and rapid. Equation (2)

$$V_s = \frac{V_f'}{\epsilon} - \frac{V_d'}{1 - \epsilon} \quad (2)$$

may be rearranged to yield

$$V_d' = \frac{1 - \epsilon}{\epsilon} V_f' - (1 - \epsilon) V_s \quad (5)$$

For any single value of the holdup there will be only one value of the slip velocity V_s ; therefore, for this value of the holdup Equation (5) represents a straight line, the slope of which will be $(1 - \epsilon)/\epsilon$ and the intercept on the V_f' axis ϵV_s .

In addition data are required for the system under consideration as represented by Equation (4). These could be obtained by experimentally determining $(1 - \epsilon)$ vs. the fluid velocity for a batch fluidization or a bottom-restrained, unfed bed. For this unfed operation $V_d' = 0$ and one may write

$$\left. \frac{V_f'}{\epsilon} \right|_{\text{batch}} = V_s = \phi^{-1}(1 - \epsilon)$$

Substituting into Equation (5) results in

$$V_d' = \frac{1 - \epsilon}{\epsilon} V_f' - (1 - \epsilon) \left. \frac{V_f'}{\epsilon} \right|_{\text{batch}} \quad (6)$$

For any value of $(1 - \epsilon)$ chosen, $(1 - \epsilon)/\epsilon$ can be calculated. With the value of $V_f'_{\text{batch}}$ corresponding to the chosen $(1 - \epsilon)$, the straight line as represented by Equation (6) is immediately defined. This procedure can be continued for all values of $(1 - \epsilon)$ from zero to the value for the fully packed bed. The result is a series of lines each at a constant value of the holdup. Figure 2 shows such a diagram for $\rho_d > \rho_f$. Each quadrant in this diagram is labeled as to the possible types of operation. The intercept described by ϵV_s is for $V_d' = 0$.

It is to be realized that Figure 2 holds only for one system, i.e., one particle size fluidized by a single fluid. There is partial experimental evidence that if the plot is made with V_f'/V_t vs. V_d'/V_t as coordinates then this chart becomes a general one for all types of systems although predicted on the basis of experimental data for only one system.

THE GENERALIZED HOLDUP—FLOW-VELOCITY CURVE

By use of Figure 2 a cross plot has been constructed in which the fraction holdup is plotted as ordinate vs. the superficial fluid velocity as abscissa with superficial solids velocity as the parameter. This diagram is represented in Figure 3 and is titled the generalized operational diagram for vertical moving fluidized systems. It shows the relationship among and the limits of all types of vertical fluidized systems.

The ordinate of holdup $1 - \epsilon$ has values from zero to the figure corresponding to a fully packed bed. The abscissa of superficial fluid velocity V_f' has both negative and positive values. The positive values may be classified as smaller or greater than the transport velocity of a single particle. Shown above the graph are schematic representations of the different regimes or zones of fluidization. All free-system operations are bounded by the area $\delta abd\delta$ and the area to the right of jqd . Any other area on the diagram represents operation with mechanical restraint of some type.

Before a discussion of the various regimes in this generalized diagram it may be best to note the significance of certain of the areas, points, and lines.

1. For negative values of V_f' the fluid moves downward and for positive values upward.
2. At $V_f' = V_t$ = point d , particles and fluid both move upward.
3. To the left of $V_f' = 0$ particles and fluid both move downward.
4. Point c is the commonly determined fluidizing velocity of an unfed supported

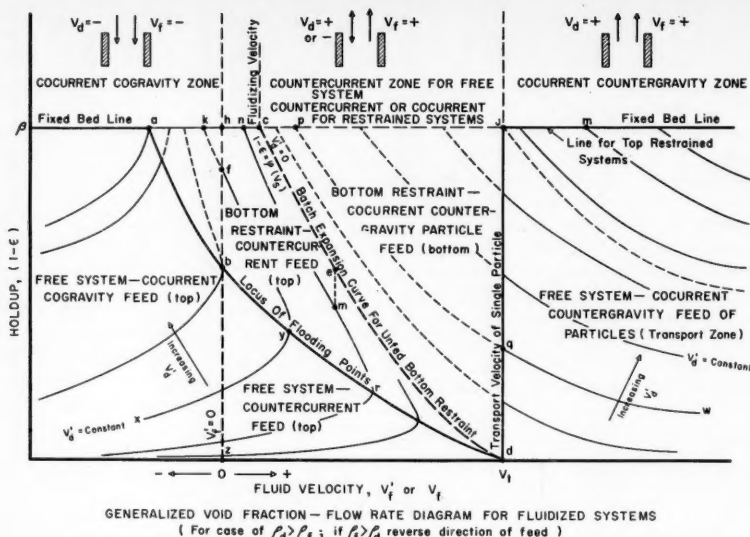


Fig. 3. Schematic generalized operational diagram for vertical-moving fluidized systems.

bed and the line cd represents the batch expansion curve.

5. No free system can exist above curve abd .

6. Curves such as xy or wqp show the variation in holdup for various combinations of fluid velocity, in each case at a constant particle velocity.

It is important to note that fluidization is a single continuous phenomenon extending from the fixed bed on one side through a region of increasing fluid velocity to a fixed bed at the other limit. Each of the different types of vertical flow systems represents a different regime within limits defined by the basic laws. Thus countercurrent unrestricted fluidization, e.g., the spray tower, has concurrent countergravity and cogravity fluidization as its limits. A mechanically supported bed has the fixed bed and transport as its limits.

The free concurrent-cogravity and free countercurrent systems are represented by the areas $\beta abz\beta$ and $bydzb$, respectively. In each area the lines of constant superficial solids rate increase in numerical value from bottom to top and from right to left. Thus a vertical line in either regime shows the change of holdup with changing particle feed rate at a constant fluid rate. Such towers are operable only in the region to the left of curve abd , which is termed the locus of the flooding points. Thus, point y represents the flooding point for the solids feed rate indicated by line xy . The flooding point is defined as the maximum fluid rate possible at a given solids rate in a free fluidized system. The significance of this flooding line will be discussed later. A further increase in V_f' causes $1 - \epsilon$ to decrease along yd and the particle throughput no longer equals the rate of

particle feed since a portion is rejected by the system. The rejection rate increases with increasing V_f' until it equals the rate of feed at V_t , which is equal to the free-fall velocity of a single particle. Point b represents the maximum holdup and particle feed possible in a stationary column of fluid. Note that the concurrent cogravity holdups may be much larger than the countercurrent-system holdups. This indicates a possible advantage for this type of contacting.

The area to the right of the line jqd represents the regime of concurrent-countergravity flow, commonly referred to as the transport region. Lines of constant superficial solids rate, such as wq , increase in numerical value from bottom to top and from left to right. In this case the holdup decreases as the fluid velocity increases for a fixed rate of particle feed. It is possible to have any combination of holdup from that of a packed bed to zero depending upon the particular combination of flow rates. A flooding point corresponding to that for countercurrent operation apparently does not exist.

Bottom-restraint-countercurrent operation is represented by the region bounded by $hcdhb$. This type of system can be achieved by starting with a nonfed fluidized bed and then adding solids at the top and withdrawing from the bottom. Initially a condition on the batch fluidization curve such as point e will be established. As the solids are fed the bed adjusts vertically downward to a new condition, say point m . For this particular solids rate, variations in the fluid velocity will cause the holdup to move either along mn or along mr . Point r represents a limiting point in both the countercurrent and the bottom-restrained-countercurrent feed systems.

At the same fluid velocity and the same particle velocity the bottom-restrained-countercurrent system gives higher holdups than the free system. Neither, however, give holdups as large as the nonfed-bottom-restrained condition at the same fluid velocity.

Bottom-restraint-concurrent-countergravity operation is represented by the region bounded by $cpjqdc$. By introduction of particles to the bottom of a batch-fluidized bed and withdrawing from the top, a bottom-restrained transport condition is achieved. The holdups in this case will be larger than for the batch-fluidized bed. Higher holdups at a lower fluid velocity than in the free system are also possible. The limits of operation of superficial fluid velocity are the fluidizing velocity, point c , and the transport velocity, point d . Above the transport velocity the presence or absence of a mechanical restraint will not influence the stability of the system.

Bottom restraint, concurrent-cogravity feed is represented by the region $ahba$. This system can be achieved by starting with a fixed bed sitting on a bottom restraint. Particles are then withdrawn from the bottom and added at the same rate. This corresponds to moving from point h to say point f , a fluidized bed. The particle rate must, of course, be greater than the rate at h . Adding fluid to the top of the bed will move the holdup along the line fh . The maximum fluid velocity possible is given by point a .

Consideration may be given to the case of top restraint or top and bottom restraint, but the practical implications of these types of operations are not apparent and so these operations will not be discussed.

Sedimentation can also be represented on such a chart. The constant rate-of-sedimentation curve would lie to the right of the zero velocity point, as the fluid is set in motion countercurrent to the walls by displacement as particles settle through it.

Any system in which the particles are fed at either terminal is restricted in operation to the flow conditions below the limiting void of the flooding point. If, however, the particles are fed at an intermediate point between the terminals, a restriction is removed or a degree of freedom added. This permits a tower of this design to operate either as a countercurrent or a concurrent fluidized bed. It may be transferred from one system to the other by an adjustment of either the fluid or particle flow. Wilhelm and Valentine (9) have studied a system of this type and have shown that it may be transferred from one or the other system at will. They also showed that the void-fraction-fluid-velocity relationship closely parallels that of screen-supported fluidization and passes through a minimum with gas flow for any solids flow in the

region where transition from one type of fluidization to the other occurs.

The reader's attention is called to the recent work of Flinn (1), who has summarized in detail many of the aspects of the operational diagram and the modes of operation discussed in this paper.

CONCEPT OF "MINIMUM VOID"—LIMITING FLOW OR FLOODING IN FREE COUNTERCURRENT SYSTEMS

The void fraction in a mechanically supported bed can vary from that of the fully packed bed (approximately 40% voids for most spherical solids) to the fully expanded condition of 100% voids. In contrast, in any continuously moving fluidized system there exists, for any particular size and combination of densities and fluid viscosities, a "minimum void" fraction (ϵ) which the system cannot exceed. This minimum void fraction varies slightly with the flow ratio of particles and fluid V_d'/V_f' and density difference $\Delta\rho$ and usually lies in the region from 100% to approximately 80 to 85% voids. In none of the countercurrent systems thus far observed in these studies have void fractions less than about 70 to 75% been obtained; in most they correspond to 90 to 95% voids. This minimum void corresponds to a definite minimum possible slip velocity and represents the limiting flow which can be obtained through such a system. In other words this represents the flooding point or flooding velocity. Mathematically, this point can be described by

$$\left. \frac{d(V_f')}{d(1-\epsilon)} \right|_{V_d'} = 0 \quad (7)$$

as can be seen in Figure 3. The locus of these points is represented by curve *abd* in Figure 3.

When the flow rates to the system exceed those corresponding to this minimum void, a portion of the particles fed is rejected by the system; this portion is refused by a tower of constant cross section and overflows the tower at the point of feed. If the feed terminal of the tower is surmounted by a section of expanding cross section (a funnel), thus reducing the fluid velocity at this point, the rejected portion of the feed forms a fluidized bed in the funnel supported by the fluid bed below. The height above the tower proper varies with the rate of feed above the flooding point. With high-density lead particles and proper funnel dimensions it is possible to form a fixed bed in the funnel above the flooding point. When this occurs, the feed rate to the system is reduced to that corresponding to the flow of particles through a fixed orifice and control of the fluidization is lost. Flooding will also be a phenomenon of free concurrent cogravity systems (Figure 3).

The so-called "rejection" or "carry-back" point employed by some authors has no fundamental significance and is peculiar to some particular combination of design and operating conditions of a certain tower. The well-known minimum escaping surface or area necessary for a boiling or gas-aerated system is directly related to the minimum void and the heterogeneity of fluidization. Likewise in the dispersion of an immiscible liquid or solid particles in a batch-agitated vessel there is a minimum void which is an exemplification of the same basic phenomena.

The characterization and general correlation of the flooding point for a fluidized system to permit prediction is of utmost importance. This can be accomplished by use of Figure 2, which represents a family of constant-void-fraction lines intersecting in the countercurrent and concurrent-cogravity regimes. Since the flooding point is defined as the maximum throughput of solids at a given liquid throughput, the flooding point will be located on the tangent to the family of constant-void-fraction lines. This tangent curve is called the *locus of flooding points* on Figure 2 and can be located by drawing a smooth curve tangent in turn to each constant-void-fraction line. Thus the entire flooding curve can be obtained from data for an unfed bottom-restrained bed.

An analytical expression for the flooding curve could be obtained if the equation-of-state curve, Equation (4), is known. By using Equations (4) and (5), and carrying out the differentiation indicated as the necessary condition at flooding, Equation (7), one can evolve an algebraic expression.

GENERAL CONCLUSIONS REGARDING FLUIDIZED SYSTEMS

1. Free countercurrent systems are generally restricted to a void range between $\epsilon = 100\%$ and approximately $\epsilon = 70$ to 80%.

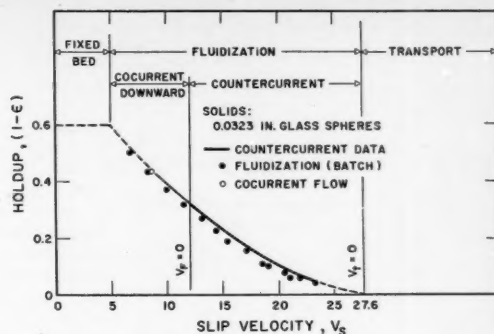


Fig. 4. Data of Price (5), holdup $(1 - \epsilon)$ vs. slip velocity V_s .

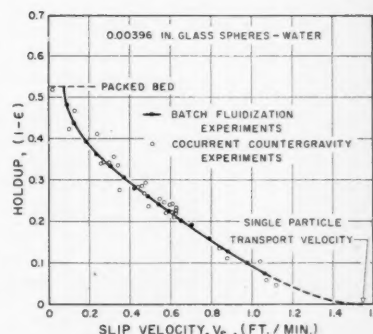


Fig. 5. Data of Struve (6), holdup $(1 - \epsilon)$ vs. slip velocity V_s .

2. Such systems can be formed only from the fully expanded or 100% void state and never from the fully packed state.

3. Similar restrictions exist at zero fluid feed rate, i.e., in a nonflowing column of fluid. Hence a bed of particles can never be passed through an unrestricted column of fluid in the fully packed condition. Only by introduction of a restriction in the column by a reduced opening or by concurrent-cogravity flow of the continuous fluid can a fully packed bed be formed. For a liquid-liquid system this would result in coalescence. This opening and not the fluid dynamic conditions or the particle feed rate would then control the discharge rate independently of the bed height.

4. A mechanically supported bed may have any void fraction between the fully packed and 100%.

5. Concurrent-cogravity systems may attain a holdup equal to the fully packed condition; i.e., passing fluid downward may fully pack the bed, and increase the holdup and hence the contact area.

6. It will be noted that these theoretical curves predict that there will not be a single invariant fluidizing velocity. Instead this velocity will be determined by

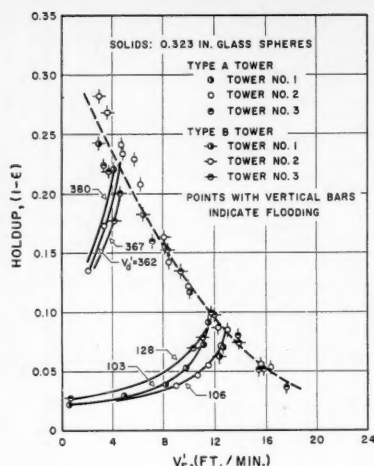


Fig. 6. Data of Price (5), holdup $(1 - \epsilon)$ vs. superficial fluid velocity V_f' .

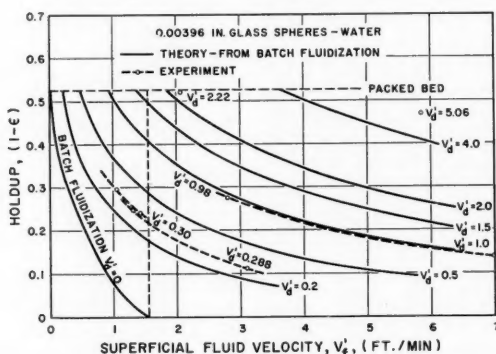


Fig. 7. Data of Struve (6), holdup $(1 - \epsilon)$ vs. superficial fluid velocity V_f' .

the flow rates and the mechanical arrangement of the system.

EXPERIMENTAL DATA

Until this point the present paper has dealt largely with the theoretical development of the behavior of ideal fluidized systems. Now some of the experimental data which have been collected in these laboratories will be examined to verify or disprove the validity of the theory. Only a brief resume of the experimental work will be presented, as detailed accounts will be the subject of further papers.

The systems under study were spherical glass beads fluidized by water. The ratio of the solid-particle diameter to the fluidizing-tower diameter was always small, i.e., at least 1/50, in order to minimize wall effects. These conditions represent a reasonable approach to the ideal system previously defined.

Figure 4 represents data of Price (5) with fraction holdup $(1 - \epsilon)$ plotted vs. the slip velocity V_s . The holdups fall on a continuous curve from $(1 - \epsilon)$ equal to approximately 0 to 60%. (This corresponds to void fractions of 99+ to 40%.) The solid curve represents a full range of

countercurrent data, the solid points represent batch-fluidization data, and the single unfilled point is concurrent flow downward. The points of zero fluid velocity ($V_f' = 0$) and zero particle velocity V_i are indicated. In the concurrent downward bed the holdup exceeds either of the other systems and may approach that of a fully packed bed. This is an important point for it means that much larger contact areas for mass transfer are possible under these conditions.

Figure 5 represents data of Struve (6) once again plotted as holdup vs. the slip velocity. Raw-data points are shown for concurrent-countergravity flow for both free and bottom-restrained systems. The holdups fall around the smooth continuous curve representing batch-fluidization operation. Least-square treatment of the data gives a series of points which fall almost exactly on the continuous curve.

The behavior of these same experimental data as predicted by the generalized operating chart, Figure 3, is also of interest.

being studied in terms of the theoretical predictions of the generalized operational diagram.

DESIGN CONSIDERATIONS

It is important to emphasize one phase of the results of the present theory. For known particle diameter, densities and viscosities, the holdup and hence ΔP may be predicted for any vertical-flow fluidized system from an experimental determination of holdup vs. fluid velocity for a mechanically supported unfed bed of particles and fluidizing fluid. Alternatively, any of the generalized correlations of holdup vs. slip velocity in the literature (2, 3, 8) may be used with due regard for the accuracy and region of fluidization for the particular measurements involved.

Either technique allows the complete determination of the generalized operational diagram from the data for the single type of fluidized system. Thus the design of a multitude of different types of moving fluidized systems may be easily achieved.

ACKNOWLEDGMENT

The development of the generalizations and theoretical considerations presented in this paper has been materially supported by the research and experimental investigations of B. G. Price, D. R. Flinn, and D. L. Struve. The authors wish to express their deep appreciation to these investigators for their contributions to many specific details and to the broad understanding of the properties of fluidized systems herein presented. Their thesis studies will be reported in detail in subsequent papers.

The authors also wish to thank the National Science Foundation and the E. I. duPont de Nemours and Company for their generous assistance in the form of fellowships granted to the Princeton Department of Chemical Engineering and held by two of the above-mentioned investigators during the course of the experimental studies and to the California Research Corporation for a research grant-in-aid which permitted certain of the important experimental work involved to be pursued.

LITERATURE CITED

1. Flinn, D. R., M.S. thesis, Princeton Univ., Princeton, N. J. (1954).
2. Lewis, E. W., and E. W. Bowerman, *Chem. Eng. Progr.*, **48**, 603 (1952).
3. Lewis, W. K., E. R. Gilliland, and W. C. Bauer, *Ind. Eng. Chem.*, **41**, 1104 (1949).
4. Mertes, T. S., and H. B. Rhodes, *Chem. Eng. Progr.*, **51**, 429, 517 (1955).
5. Price, B. G., Ph.D. thesis, Princeton Univ., Princeton, N. J. (1951).
6. Struve, D. L., Ph.D. thesis, Princeton Univ., Princeton, N. J. (1955).
7. Wilhelm, R. H., "Proc. Second Midwestern Conference on Fluid Mechanics," Ohio State Univ., p. 379 (1952).
8. ———, and Mooson Kwauk, *Chem. Eng. Progr.*, **44**, 201 (1948).
9. Wilhelm, R. H., and Stephan Valentine, *Ind. Eng. Chem.*, **43**, 1199 (1951).

Effect of Concentration Level on Mass Transfer Rates

L. E. WESTKAEMPER and ROBERT R. WHITE

University of Michigan, Ann Arbor, Michigan

Carbon tetrachloride was evaporated into a stream of air over ranges of gas concentration from 0 to 0.70 mole fraction carbon tetrachloride, Reynolds number from 600 to 15,000, and Schmidt number from 0.23 to 1.17. The data were correlated by an equation and also by a computer solution to the differential equation describing mass transfer from values of eddy viscosity and eddy diffusivity obtained from the literature.

Investigations of mass transfer have resulted in the development of methods for correlation and prediction of mass transfer rates in a variety of situations. The effect of Reynolds number, Schmidt number, and similar variables has been analyzed for many systems; however, the effect of concentration level has received little attention.

Various terms in mass transfer calculations contain concentration level as a variable. For example, the j factor for mass transfer has been defined by Colburn (2) as

$$j_D = \frac{k_g p_{Bm} Sc^{2/3}}{G_m}$$

where p_{Bm} is a log-mean concentration term.

Experimental studies on the effect of concentration level on mass transfer rates have been meager. Cairns and Roper (1) studied the concentration-level variable in the air-water system and correlated their data by the following equation:

$$\frac{k_g R T d}{D_r} \left(\frac{p_{Bm}}{P} \right)^{0.83} (Sc)^{-0.44} = 0.021 Re^{0.83} \quad (1)$$

the ratio (p_{Bm}/P) was varied from 0.15 to 0.99 by Cairns and Roper, and concentration level enters their correlation as an important variable.

The objectives of the present study were to collect mass transfer rate data in the air-carbon tetrachloride system over a wide range of concentration level and to study various methods of correlating the data.

EXPERIMENTAL WORK

Liquid carbon tetrachloride was evaporated from a plane surface in the bottom of a rectangular duct into a turbulent air stream passing through the duct.

Gas concentrations were varied from 0.00 to 0.70 mole fraction carbon tetrachloride. Reynolds number varied from 600 to 14,700 and the Schmidt number from 0.23 to 1.17. Gas temperatures varied from 68 to 91°C., and all experiments were conducted at atmospheric pressure. The ratio (p_{Bm}/P) varied from 0.29 to 0.81.

The test section is shown in Figure 1.

L. E. Westkaemper is at present with Rohm and Haas Company, Pasadena, Texas.

Liquid enters the section through a 1-in. pipe at A and is distributed over the test area by the perforated plate PP . The plate is perforated by 1/16-in. holes spaced on

1/2-in. equilateral triangle centers. Liquid leaves the test section at overflow weirs B and C and flows into a holding tank. Test-section details are given in Figure 2. The

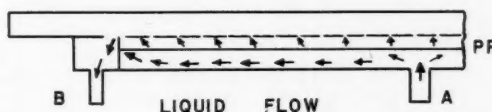


Fig. 1. Test section.

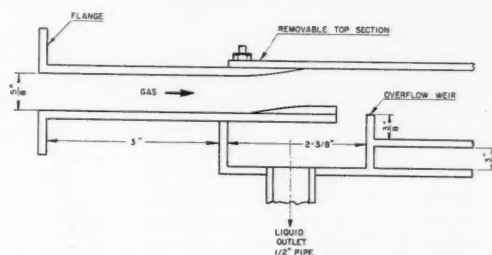


Fig. 2. Test section details; 1/8 in. sheet steel throughout inlet cross section and cross section for gas flow over liquid: 5/8- by 4 1/16-in. length, 48 in. between weirs.

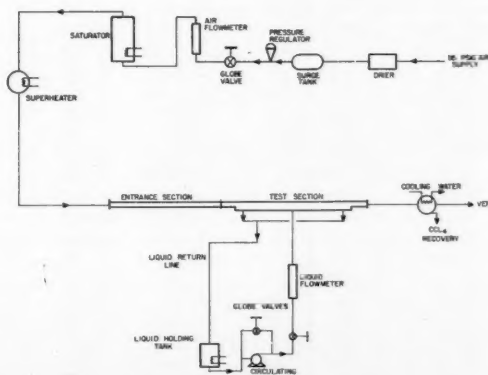


Fig. 3. Schematic flow sheet.

wetted area of the test section is 1.35 sq. ft.

The remaining experimental apparatus is identified in the flow sheet shown in Figure 3. The entrance section preceding the test section is a 36-in. length of rectangular duct of cross section 4 1/16 by 5/8 in., which is identical to the cross section for gas flow above the liquid in the test section.

The saturator shown in Figure 3 is a 36-in. length of 12-in. steel pipe provided with two 1,500-watt immersion heaters and a thermoregulator. A perforated plate in the base distributes incoming air through the liquid carbon tetrachloride in the saturator, and the air leaves saturated with carbon tetrachloride vapors.

The bottom of the liquid holding tank is made from 12-in. steel pipe. A sight glass was placed on a length of 2-in. pipe forming the top of the tank to increase the sensitivity of volume readings.

A steel top was used on the test section during the experimental runs. However, a glass top was used in preliminary runs to observe the maximum gas velocities with stable gas-liquid interfaces. It was observed that ripples appeared on the liquid surface when gas velocities exceeded 10 to 12 ft./sec. A small increase in gas velocity at this level caused the ripples to grow and become unstable; i.e., the ripples grew until entrainment of liquid in the gas resulted. When the surface was unstable, the entrained liquid was carried out into the exit lines, and thus the pressure drop through the vent lines was more than doubled.

In the evaporation experiments the pressure drop through the vent lines was carefully observed during the start-up

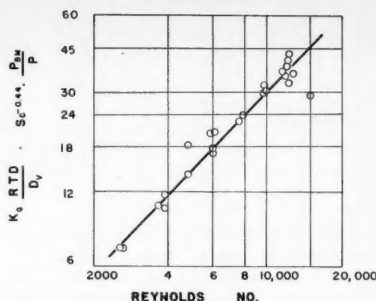


Fig. 4. Correlation of the data with a concentration term.

period, and if it was steady as the gas velocity was increased to operating conditions, the run was continued.

The compositions reported as experimental data were determined as follows. The inlet composition was calculated from the temperature and pressure of the gas by assuming that it was at its dew point when it left the saturator. The validity of this assumption was verified in preliminary runs by an analysis of the gas made by quantitative charcoal absorption of the carbon tetrachloride in a measured gas sample.

The change in the composition of the gas passing through the test section was relatively small; therefore error in gas analysis is magnified when the change in composition is taken. For this reason, it was felt that the exit-gas composition

would best be determined by calculation from the measured evaporation rate, the inlet-gas rate, and the inlet-gas composition.

Check runs showed that evaporation rates could be reproduced within 10%, as may be seen by comparing runs 12 and 14, 2 and 4, and 18 and 18a in Table 1.

Additional experimental details and data are available elsewhere (6).

CORRELATION OF THE DATA

Dimensionless Groups

Various methods of correlating the data have been used by previous investigators. For convenience in comparing the results with those from other sources, the data were correlated by plotting $[(k_g R T D / D_v) \cdot p_{Bm} / P \cdot Sc^{0.44}]$ as a function of Reynolds number. This term is equal to (j) (Re) where $j = (k_g p_{Bm} Sc^{0.44}) / G_m$. Figure 4 shows a correlation of the data for this investigation. The equation of the line shown is

$$\frac{k_g R T D}{D_v} \cdot \frac{p_{Bm}}{P} \cdot Sc^{-0.44} = 0.0014 Re^{1.08} \quad (2)$$

The standard deviation of the error is 16%.

Figure 5 shows the data plotted in a manner similar to that of Figure 4, except that the term (p_{Bm} / P) has been omitted from the ordinate. The equation of the line shown is

$$\frac{k_g R T D}{D_v} \cdot Sc^{-0.44} = 0.00012 Re^{1.42} \quad (3)$$

The standard deviation of the error is 15%. The ordinate of Figure 5 is equal to (j) (Re) when $j = (k_g P Sc^{0.56}) / G_m$.

Data taken by Cairns and Roper for the evaporation of water into air in a wetted-wall column may be plotted in a manner similar to that shown in Figure 4. A plot of Cairns and Roper's data is shown in Figure 6. The equation of the line shown is

$$\frac{k_g R T D}{D_v} \cdot \frac{p_{Bm}}{P} \cdot Sc^{-0.44} = 0.061 Re^{0.67} \quad (4)$$

The standard deviation of the error is 21%. Cairns and Roper improved the correlation of their data as shown in Figure 7 and used the following equation:

$$\frac{k_g R T D}{D_v} \left(\frac{p_{Bm}}{P} \right)^{0.83} Sc^{-0.44} = 0.021 Re^{0.83} \quad (1)$$

Here the standard deviation of the error is reduced to 10%. If the form shown by Equation (3) is used to correlate Cairns and Roper's data, the correlation is quite poor.

Equations (1) to (4) were determined from the data by the method of least squares.

Equations (2) and (3) show that the definition of the j factor influences the exponent of the Reynolds number in the

TABLE 1. CALCULATED DATA

Run	U_{avg} , ft./sec.	G_m , lb. mole/ (hr.)(sq. ft.)	Re	Sc	N , lb. mole/ hr.	p_{Bm}/P	k_g , lb. moles/ (hr.)(atm./sq. ft.)
2	6.90	53.5	11,900	0.385	0.121	0.533	0.585
3	6.80	53.0	11,800	0.386	0.116	0.529	0.538
4	6.72	52.3	12,200	0.382	0.114	0.531	0.588
5	6.15	47.5	11,200	0.364	0.106	0.514	0.530
6	5.37	40.0	9,800	0.350	0.097	0.499	0.457
7	5.20	39.5	9,500	0.355	0.085	0.511	0.471
8	6.44	49.8	11,800	0.348	0.074	0.502	0.421
9	5.87	45.0	12,200	0.315	0.076	0.466	0.489
10	5.21	39.3	11,400	0.295	0.078	0.423	0.473
11	5.56	42.0	11,600	0.308	0.079	0.651	0.583
12	4.26	32.7	5,980	0.471	0.0476	0.630	0.218
13	4.35	33.0	6,020	0.470	0.0586	0.625	0.273
14	4.25	32.4	5,790	0.478	0.0507	0.625	0.228
15	6.02	46.3	7,800	0.505	0.072	0.642	0.317
16	3.49	27.6	3,750	0.638	0.0249	0.722	0.116
17	5.32	41.6	5,570	0.640	0.0510	0.734	0.262
18	2.71	21.3	2,690	0.690	0.0218	0.732	0.093
18a	2.81	21.9	2,770	0.630	0.0231	0.733	0.098
19	4.24	32.6	3,770	0.722	0.0380	0.748	0.158
20	3.54	27.3	3,460	0.675	0.0300	0.743	0.127
21	4.74	36.4	4,470	0.700	0.0416	0.747	0.202
22	2.74	21.3	1,620	1.16	0.0312	0.810	0.077
23	1.70	13.5	1,110	1.11	0.0270	0.798	0.070
24	0.75	6.03	600	1.02	0.0276	0.782	0.060
25	3.25	25.3	1,910	1.17	0.0342	0.810	0.082
26	2.28	17.7	1,400	1.13	0.0309	0.802	0.076
27	6.88	53.0	11,800	0.432	0.116	0.471	0.519
28	4.62	34.1	13,100	0.230	0.0440	0.287	0.760
29	5.60	42.0	14,700	0.242	0.079	0.312	0.613
30	2.43	18.5	4,690	0.333	0.0185	0.520	0.190
31	4.05	30.9	7,490	0.353	0.0304	0.535	0.312
32	5.47	41.6	9,660	0.368	0.0467	0.551	0.411

Area of evaporating surface, 1.35 sq. ft.

correlation. An exponent of 1.08 appears on the Reynolds number in Equation (2), where $j = (k_p p_{Bm} Sc^{0.56})/G_m$.

An exponent of 1.42 appears on the Reynolds number in Equation (3), where $j = (k_p P Sc^{0.56})/G_m$.

Cairns and Roper were able to focus attention on the (p_{Bm}/P) term, since the Schmidt number was held constant in their research. The (p_{Bm}/P) must be included in the correlation of their data. The air-carbon tetrachloride data of this paper may also be correlated by use of the (p_{Bm}/P) term, as is shown by Equation (2). Hence the form shown by Equations (2) and (4) seems to be the more general, as the form given by Equation (3) will not correlate the data of Cairns and Roper. Since Equations (2) and (4) correlate the data of this investigation with deviations of 16 and 15% respectively, Equation (1) used by Cairns and Roper also will correlate the data as well.

Differential Equation

In the case of molecular transport processes, the transfer rates for momentum, heat, and mass are given by

$$\tau = \mu \frac{du}{dy} \quad (5)$$

$$q = -k \frac{dT}{dy} \quad (6)$$

$$N_A = -D_s \frac{dc}{dy} \quad (7)$$

Here the conductance terms are viscosity, thermal conductivity, and molecular diffusivity. The potential terms are the gradients of velocity, temperature, and concentration. Each potential term is in differential form.

Similar treatment is made in the case of turbulent transfer processes. Expanding the molecular transfer equations

$$\tau = \mu \frac{du}{dy} + \rho \epsilon_m \frac{du}{dy} \quad (8)$$

$$q = -k \frac{dT}{dy} - \rho c_p \epsilon_c \frac{dT}{dy} \quad (9)$$

$$N_A = -D_s \frac{dc}{dy} - E \frac{dc}{dy} \quad (10)$$

The foregoing equations serve to define ϵ_m , eddy viscosity; ϵ_c , eddy conductivity; and E , eddy diffusivity. In each case the units are (distance)² per unit time. The definitions take this form in the hope that the similarity of the definitions will result in simple relationships between eddy properties; that is, it is hoped that the eddy properties will be equal or proportional to one another.

In this work the primary interest is in the mass transfer rate equation (10). From this equation and a material balance, the equation for turbulent mass transfer is derived:

$$\begin{aligned} \frac{dc}{dt} = & \frac{\partial}{\partial x} (D_s + E) \frac{\partial c}{\partial x} - \frac{\partial (uc)}{\partial x} \\ & + \frac{\partial}{\partial y} (D_s + E) \frac{\partial c}{\partial y} - \frac{\partial (vc)}{\partial y} \\ & + \frac{\partial}{\partial z} (D_s + E) \frac{\partial c}{\partial z} - \frac{\partial (wc)}{\partial z} \quad (11) \end{aligned}$$

Equation (11) relates gas concentration to time, gas velocity, eddy diffusivity, molecular diffusivity, and position in the system. Under steady state conditions for turbulent gas flow between parallel plates in the x direction and mass transfer in the y direction normal to the plates, $dc/dt = 0$ and $w = 0$. For the experiments of this investigation $\partial u/\partial x$, $\partial/\partial x [(D_s + E)(\partial c/\partial x)]$, and v are negligible, and so Equation (11) simplifies to

$$u \frac{\partial c}{\partial x} = \frac{\partial}{\partial y} \left[(D_s + E) \frac{\partial c}{\partial y} \right] \quad (12)$$

In the experimental work only small changes in gas composition occurred in the 4-ft. length of the test section. Temperature changes in the gas were small, as were changes in the gas volume. Hence the assumptions that $\partial u/\partial x = 0$ and $(\partial/\partial x) [(D_s + E)(\partial c/\partial x)] = 0$ are justifiable.

The assumption that $v = 0$, however, is valid only over certain ranges of operation. This assumption was necessary in separating the variables in Equation (11). The comparison of the evaporation rates calculated by use of Equation (12) with the experimental rates is shown in Table 2. Mathematical details are available elsewhere (6). The calculated values are seen to be in error at low Reynolds numbers. Previous workers have shown that the presence of a velocity normal to the wall is important in momentum transfer studies.

Yuan and Finkelstein (9) have shown that the presence of a velocity normal to the surface 1/100 as great as the main-stream velocity increases the friction by 85%. The actual value of v in this work is given by N_A/c_t , the moles transferred per unit time per unit area divided by the total gas concentration in moles per unit volume. When main-stream velocity is lowered, this term becomes increasingly important for a given evaporation rate. Consequently, it is felt that the poor correlation of the data at low Reynolds numbers is caused by neglecting v .

The solution of Equation (12) requires that velocity u and eddy diffusivity E be known as a function of position. The variation of velocity with distance from the wall has been measured by Coreoran et al. (3) for air passing between parallel plates. The velocity distribution was measured in an isothermal as well as in a nonisothermal system. Temperature differences between the plates of 20°F. did not appreciably alter the velocity distribution observed. Dimensionless ve-

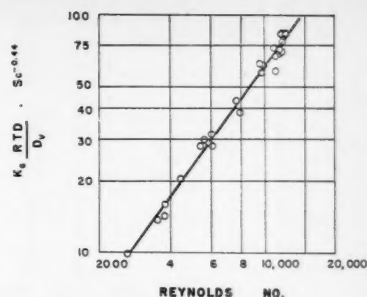


Fig. 5. Correlation of the data without a concentration term.

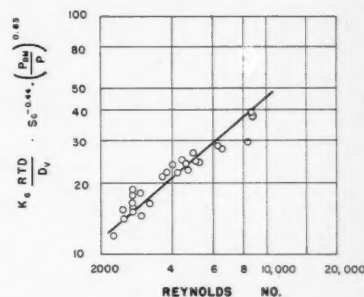


Fig. 6. Correlation of Cairns and Roper.

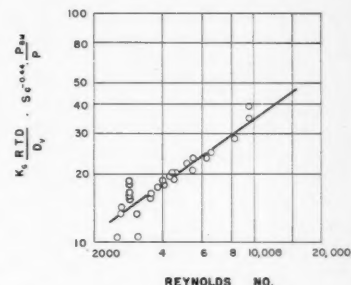


Fig. 7. Data of Cairns and Roper.

locity based on these data is shown in Figure 8.

Since the variation of eddy diffusivity with distance from the wall has not been reported in the literature, this information must be obtained indirectly.

It was noted that eddy viscosity, eddy conductivity, and eddy diffusivity were defined by Equations (8) to (10) in the hope that these quantities would be equal or proportional. Various researchers have conducted experiments to determine the relationship between the eddy properties.

Woertz (8) measured concentration distribution and mass transfer rates of water through air between parallel plates. Eddy-diffusivity values for the center region between the plates were obtained by differentiation of the concentration data and use of Equation (10).

Woertz also measured pressure drop and velocity distribution while the mass transfer process took place. Eddy-

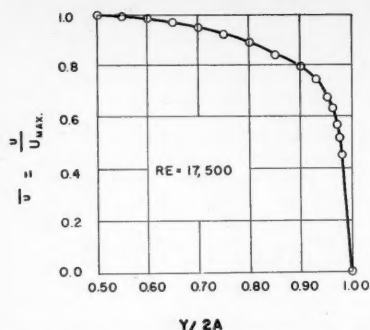


Fig. 8. Velocity distribution between parallel plates, (3).

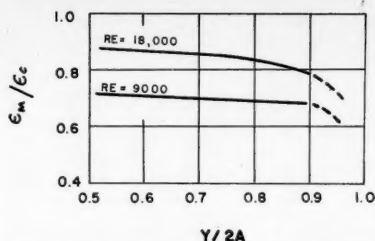


Fig. 9. Ratio of eddy viscosity to eddy conductivity, (3).

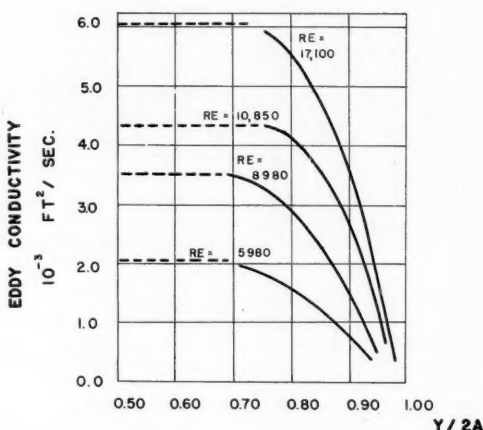


Fig. 10. Eddy conductivity values (3).

viscosity values for the center region between the plates were obtained by calculating the shear stress from the pressure drop, differentiating the velocity data, and using Equation (8).

Woertz found that the ratio of the eddy viscosity to eddy diffusivity in the center of the duct for Reynolds numbers up to 60,000 was 0.62; i.e.,

$$\epsilon_m/E = 0.62 \quad (13)$$

Further study of eddy properties was made by Sage and associates (3), who considered the relation between eddy viscosity and eddy conductivity.

Sage determined eddy viscosity for air passing between parallel plates by use of Equation (8), as shown above. Sage also measured heat flux and temperature distribution. Eddy conductivity values were obtained by differentiating the temperature data and using Equation (9).

Sage obtained more detailed distributions of velocity and temperature than did Woertz. Hence Sage compared eddy viscosity to eddy conductivity for various

Reynolds numbers. This comparison is shown in Figure 9, where the ratio of eddy viscosity to eddy conductivity is plotted vs. distance from the wall with parameters of Reynolds number.

There has been no experimental study relating eddy conductivity to eddy diffusivity; however, a relationship may be inferred from the studies of Sage and Woertz. Figure 9 shows that the ratio of eddy viscosity to eddy conductivity is approximately 0.7 for the center of the duct at a Reynolds number of 10,000. Hence,

$$\epsilon_m/\epsilon_c = 0.7 \quad (14)$$

The work of Woertz showed that $\epsilon_m/E = 0.62$ and hence

$$\epsilon_c/E = 1.1 \approx 1 \quad (15)$$

Equation (15) suggests that eddy conductivities may be taken as equal to eddy diffusivities when these quantities are defined by Equations (9) and (10). The units in each case are (distance)² per unit time. Figure 10 shows the eddy conductivity values calculated by Sage for air. The characteristic diameter in the Reynolds number used by Sage was twice the hydraulic radius, and this basis is used in Figure 10. Equation (15) and Figure 8 were used to calculate eddy diffusivity values for air from eddy conductivity values for air.

In this research, however, the gas was not air, but a mixture of air and carbon tetrachloride. Consequently, a method of predicting the effect of composition on eddy diffusivity must be used. As suggested by Deissler (4), this was done with the following expression:

$$\frac{\text{eddy diffusivity}}{\text{kinematic viscosity}} = \text{constant} \quad (16)$$

TABLE 2. COMPARISON OF COMPUTED AND EXPERIMENTAL RESULTS.

Run	(Re)	\bar{c} calc.	\bar{c} exp.	N calc.	N exp.	% Dev.
2	11,900	0.614	0.600	0.0110	0.0123	-10.6
4	12,200	0.608	0.595	0.0113	0.0115	-1.7
6	9,800	0.598	0.627	0.0107	0.0099	8.1
7	9,500	0.561	0.615	0.0101	0.0086	17.4
8	11,800	0.623	0.687	0.0093	0.0075	24.0
9	12,200	0.631	0.626	0.0077	0.0077	0.0
11	11,600	0.629	0.635	0.0083	0.0081	2.5
14	5,790	0.190	0.690	0.0155	0.0050	210
16	3,750	0.507	0.757	0.0052	0.0025	108
17	5,570	0.221	0.682	0.0139	0.0051	172
18	2,690	0.227	0.806	0.0080	0.0022	264
21	4,470	0.497	0.707	0.0085	0.0047	81
28	13,100	0.675	0.633	0.0039	0.0044	-11.4
29	14,700	0.670	0.684	0.0080	0.0079	1.9
30	4,690	0.865	0.530	0.0005	0.0018	-73
31	7,490	0.576	0.612	0.0036	0.0031	17.4

N, evaporation rate, std. cu. ft./sec.

\bar{c} , dimensionless outlet concentration, $(c - c_w)/(c_0 - c_w)$

% Dev. (exp. N - calc. N)/(exp. N) (100)

(Re), Reynolds number, characteristic radius equal to the clearance between plates

A similar relation was used by Woertz, who found that the product ($E\rho$) was the same for air, carbon dioxide, and helium at the same Reynolds number. Since the viscosities of air, carbon dioxide, and helium do not vary greatly, Woertz could have used the product ($E\rho/\mu$) = (E/ν) as Deissler suggested.

Equation (16) was used to calculate eddy diffusivity in air-carbon tetrachloride as a function of position from the eddy diffusivities in pure air, except for the value of eddy diffusivity at the liquid surface. The viscosity of the air-carbon tetrachloride mixtures was calculated by use of the correlation and data of Wilke and Bromley (7).

A final calculation was necessary to obtain the eddy diffusivity at the liquid surface. Since one of the "parallel plates" of this research was actually a liquid surface, it could not be considered as a fixed surface. The drag of the gas stream on the liquid surface causes a surface velocity in the liquid, as shown by Tek (5); hence the gas velocity does not drop to zero at the liquid surface but instead drops to a value equal to the surface velocity of the liquid.

Tek has developed equations which may be used to calculate the liquid surface velocity and the surface shear from the main-stream gas velocity and the properties of the liquid. This calculation involves the use of Equations (17) and (18), which were developed by Tek (5).

$$u_s = \frac{(dh/dx)a_1^2 g_c}{6\nu_1} \quad (17)$$

where $(dh/dx) = k_T U_{avg}^2 =$ surface inclination due to gas velocity,

and

$$g_c \tau_s = \frac{4\mu_1 u_s}{a_1} \quad (18)$$

Eliminating (u_s) from Equations (17) and (18) gives

$$\tau_s = \frac{4}{6} a_1 U_{avg}^2 k_T \frac{\mu_1}{\nu_1} \quad (19)$$

Equation (19) may be used to calculate the shear stress at the liquid surface, which is also given by Equation (8). For the case of the liquid surface, in units consistent with Equation (19), Equation (8) becomes

$$g_c \tau_s = (\mu + \epsilon_m \rho) \left(\frac{du}{dy} \right)_s \quad (20)$$

Combining (19) and (20) and solving for $(\mu + \epsilon_m \rho)_s$ gives

$$\begin{aligned} (\mu + \epsilon_m \rho)_s &= \frac{g_c \frac{4}{6} a_1 U_{avg}^2 k_T (\mu_1/\nu_1)}{du/dy} \\ &= \frac{2a_1 g_c U_{avg}^2 k_T \rho_l}{3(du/dy)_s} \quad (21) \end{aligned}$$

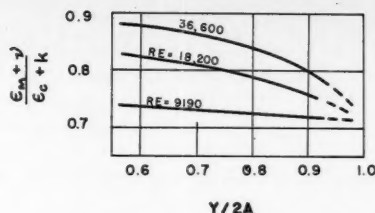


Fig. 11. Ratio of total viscosity to total conductivity (3).

and

$$(\nu + \epsilon_m)_s = \frac{2a_1 g_c U_{avg}^2 k_T \rho_l}{3\rho(du/dy)_s} \quad (22)$$

Equation (22) gives the "total" viscosity ($\nu + \epsilon_m$) at the surface as a function of the average velocity U_{avg} and the velocity gradient at the surface $(du/dy)_s$.

It was assumed that the velocity gradient at the liquid surface was equal to the velocity gradient at the wall in Sage's experiments. Accordingly, the values of $(du/dy)_s$ were calculated by differentiating the velocity data shown in Figure 8 and the total viscosities calculated from Equation (22).

Actually the velocity gradient at the liquid surface will be somewhat less than the velocity gradient at a fixed boundary, and therefore the values of total viscosity obtained by the foregoing procedure are low. As a result, the values of eddy conductivity or eddy diffusivity derived from the eddy viscosity will also be low and will tend to decrease the rate calculated from Equation (12).

Sage reports values of the ratio of total viscosity ($\nu + \epsilon_m$) to total conductivity $[k/(\rho\epsilon_m) + \epsilon_c]$, and these are shown as a function of Reynolds number and position in Figure 11. Thus Figure 11 can be used to evaluate the total conductivity at the surface from the total viscosity calculated from Equation (22). The total diffusivity at the surface was taken as equal to the total conductivity at the surface.

This step is somewhat inconsistent with the use of the data of Woertz and Sage to show that $\epsilon_c/E = 1$. Consistency would require that $(k/\rho\epsilon_m)$ be subtracted from total conductivity values to give eddy conductivity and eddy diffusivity. Total diffusivity would be obtained for use in Equation (12) by adding D_s to the eddy diffusivity.

However the equation $\epsilon_c/E = 1$ is verified only for the center region of gas flow, and the approximation of taking total conductivity equal to total diffusivity is probably as accurate as assuming that $\epsilon_c/E = 1$ throughout the flow domain. Once a total diffusivity at the liquid surface is known, it may be used as a limiting value for the total diffusivities (6) in the main gas stream, as shown in Figure 12.

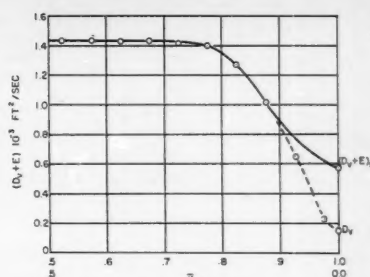


Fig. 12. Total diffusivity values for run 6.

The surface velocity of the gas was not high enough ($\bar{u} \approx 0.1$) to alter greatly the velocity profile shown in Figure 8. As this velocity distribution was approximated in a computer solution by a step function, accuracy was not improved by adding the correction at the wall.

An electronic differential analyzer was used to solve the ordinary differential equations (6) resulting from the separation of variables in Equation (12).

A summary of the outlet concentrations calculated by computer solution of Equation (12) is shown in Table 2, which also shows the experimental outlet concentration, which was calculated from the inlet-gas concentration, the inlet-gas rate, and the evaporation rate.

Table 2 shows good agreement between the calculated and experimental evaporation rates for Reynolds numbers over 7,000. The average deviation is 10.5% for these runs. Even though numerous approximations must be made in using Equation (11) to correlate mass transfer data, the outlet concentrations predicted by this equation agree closely with the experimental concentrations for Reynolds numbers over 7,000, as seen in Table 2. No arbitrary constants are used in the equation at any point. This suggests that Equation (11) may prove as useful in mass transfer as the Fourier-Poisson equation has in heat transfer.

Certain predictions may be made concerning the effect of concentration level on mass transfer by examination of Equation (12). In addition to the terms containing concentration gradient, this equation contains the term $(D_s + E)$, which is a function of concentration level. This term depends on concentration level because of the variation of E with concentration, as has been discussed.

Hence Equation (12) suggests that for a system in which there is no change in eddy diffusivity with concentration, there would be no effect of concentration level. Also if (eddy diffusivity)/(kinematic viscosity) = constant, a mixture with a kinematic viscosity independent of concentration should also have an eddy diffusivity independent of concentration.

The air-water system is one which has a gas kinematic viscosity largely inde-

TABLE 3. CORRELATION OF DATA OF CAIRNS AND ROPER WITH EQUATION (12)

Run	Reynolds No.	Gas ΔT , °F.	Outlet concentration, \bar{c} Equation (12)	Cairns and Roper
4	6520	251	0.29	0.43
9	9095	254	0.26	0.38
11	3273	342	0.15	0.39
18	4828	315	0.21	0.31

pendent of concentration. At 212°F. the kinematic viscosities of air and steam differ by only 7%. This system would be expected to show little effect of concentration level on mass transfer rates.

Extensive data in the air-water system have been taken by Cairns and Roper. While these data clearly require a concentration variable (p_{Bm}) in their correlation, this apparent contradiction of Equation (12) may be explained. Cairns and Roper operated a wetted-wall column in their investigation, and the temperature of the gas passing through the column changed by as much as 340°F. Furthermore, the inlet-gas temperatures varied from run to run. Hence there was a kinematic viscosity change, caused by temperature change. The variation in the kinematic viscosity of the inlet gas for various runs was over 30% and of the gas passing through the test section was as high as 80%. Most of the data taken by Cairns and Roper were for Reynolds numbers less than 7,000, where Equation (12) is not satisfactory. Nevertheless, four runs of Cairns and Roper were correlated by Equation (12) with the differential analyzer. Each calculated dimensionless outlet concentration for these runs was lower than that reported by Cairns and Roper (Table 3). Since the dimensionless concentration $\bar{c} = (c - c_w)/(c_0 - c_w)$, the mass transfer rate predicted by concentrations from Equation (12) would be high in each case. In the derivation of Equation (12) it was assumed that the eddy diffusivity was independent of x . The large change in kinematic viscosity and eddy diffusivity in the direction of flow in the work of Cairns and Roper makes it unlikely that Equation (12) is adequate to correlate their data.

If the air-water system is to be used to study the effect of concentration level, the temperature drop in the gas must be held at a minimum. This suggests that an apparatus similar to that used in this study might prove more successful than a wetted-wall column, where control of gas temperature is difficult.

CONCLUSION

In summary, the facts that data of this investigation may be correlated equally well by Equations (1), (2), and (3) and that the data of Cairns and Roper may be correlated best by Equation (1) and less satisfactorily by Equation (4), which is similar in form but not in

coefficients to Equation (2), lead one to suspect that functions of this type between the dimensionless groups may be too simple to represent adequately mass transfer data over a wide range in the level of concentration of the transferring component.

In a sense this is corroborated by the relatively successful result of applying the mass equation in differential form to the data correlation even though a considerable number of assumptions and the use of data on eddy properties from many sources were involved. Of particular interest is the fact that the correlation by the differential equation begins to fail exactly where it might be expected to fail at low flow rates, or Reynolds numbers less than 7,000, where the bulk motion normal to the axis of flow and in the direction is no longer negligible.

This suggests that, as further research makes available velocity distributions in turbulent-flow regimes of various geometries, the use of computing machines will make feasible the correlation and application of mass and heat transfer data in the form of the differential equations describing mass and energy balances as a more basic technique for treating many problems now being approached only through dimensional analysis.

NOTATION

A	= area
a	= one-half the clearance between parallel plates
a_l	= liquid depth
C_0	= concentration of the inlet gas to the test section
C_w	= concentration of the gas at the liquid surface
c	= concentration, moles per unit volume
\bar{c}	= dimensionless concentration, $(c - c_w)/(c_0 - c_w)$
c_p	= heat capacity
D_m	= molecular diffusivity
d	= characteristic diameter
E	= eddy diffusivity, (distance) ² per unit time
g_c	= conversion factor, (32.2 pounds mass/pound force)(feet/second) ²
G_m	= flow rate, moles per unit time per unit area
h	= heat transfer coefficient
j	= a modified j factor for mass transfer
j_D	= the j factor for mass transfer defined by Colburn, $(k_g p_{Bm} Sc^{2/3})/G_m$

k	= thermal conductivity, B.t.u. per unit time per unit area per degree Fahrenheit per foot
k_c	= mass transfer coefficient, moles per unit time per unit area per unit concentration difference
k_g	= mass transfer coefficient, moles per unit time per unit area per unit pressure difference
k_T	= a constant
N_A	= mass transfer rate, moles per unit time per unit area
P	= total pressure
p	= gas partial pressure
p_{Bm}	= logarithmic mean partial pressure of component B
p_i	= gas partial pressure at point i
Q	= heat flow rate, B.t.u. per unit time
q	= heat flow rate, B.t.u. per unit time per unit area
R	= the gas constant
Re	= the Reynolds number
Sc	= the Schmidt number
T	= temperature
t	= time
U_{avg}	= average gas velocity in direction of flow
U_{max}	= maximum gas velocity in direction of flow
u	= component of gas velocity in x direction
V_1	= kinematic viscosity of liquid
v	= component of gas velocity in y direction
w	= component of gas velocity in z direction
x	= coordinate axis; distance
y/y	= $y/2a$ = coordinate axis; distance
ϵ_c	= eddy conductivity, (distance) ² per unit time
ϵ_m	= eddy viscosity, (distance) ² per unit time
λ	= kinematic viscosity, (distance) ² per unit time
μ	= absolute viscosity
ϕ	= density
τ	= shear stress

LITERATURE CITED

1. Cairns, R. C., and G. H. Roper, *Chem. Eng. Sci.*, **3**, 97 (1954).
2. Colburn, A. P., and T. H. Chilton, *Ind. Eng. Chem.*, **26**, 1183 (1934).
3. Corcoran, W. H., F. Page, W. G. Schlinger, and B. H. Sage, *ibid.*, **44**, 410 (1952).
4. Deissler, R. G., *Natl. Advisory Comm. Aeronaut. Tech. Note* 3145, 15 (1954).
5. Tek, M. R., Ph.D. thesis, Univ. Mich., Ann Arbor (1953).
6. Westkaemper, L. E., Ph.D. dissertation, Univ. Mich., Ann Arbor (1955).
7. Wilke, C. R., and L. A. Bromley, *Ind. Eng. Chem.*, **43**, 1641 (1951).
8. Woertz, B. B., and T. K. Sherwood, *ibid.*, **31**, 1034 (1939).
9. Yuan, S. W., and A. B. Finkelstein, "General Proceedings of Heat Transfer and Fluid Mechanics Institute," Los Angeles, Am. Soc. Mech. Engrs. (1955).

Presented at A.I.Ch.E. New Orleans meeting

Vapor-liquid Equilibria of Nitrogen-argon-oxygen Mixtures

R. E. LATIMER

Linde Air Products Company, a Division of Union Carbide and Carbon Corporation, Tonawanda, New York

The equations and graphs presented here for the vapor-liquid equilibrium of the nitrogen-argon-oxygen low-temperature system are based on published binary and ternary experimental data involving mixtures of nitrogen, argon, and oxygen, and on careful thermodynamic study over a period of years of accurate plant-performance data on tall, large air-rectifying columns operating near the minimum reflux ratios. The plants have achieved separations that are impossible according to some of the published equilibrium data, and thus the plant data have made a major contribution toward the preparation of this paper.

The vapor-liquid equilibrium of the nitrogen-argon-oxygen low-temperature system is described in this paper over the range of pressure from 0.2 to 20 atm. by the simple equations for "regular" solutions and by simple equations for vapor pressures and for the ratio of fugacity coefficients. For convenience these equations are plotted on a large number of graphs, some of which are included in this paper and all of which are available.*

VAPOR PRESSURES

The vapor pressures of nitrogen-argon-oxygen liquid mixtures are represented by the equation

$$\log_{10} P = a - \frac{b}{T} \quad (1)$$

in which P is the vapor pressure in atmospheres, T is the absolute temperature in degrees Kelvin, and a and b are functions of the liquid composition. Table 1 shows values of a and b at 10% intervals of composition, from Clark, Din, and Robb (2) for argon-oxygen mixtures; from Dodge and Dunbar (3) for nitrogen-oxygen mixtures except

*Figures 13 to 32, and 34 to 49 are omitted from this paper owing to lack of space. The complete set of diagrams, Figures 1 to 49, is available as Document 5032 from the American Documentation Institute, Auxiliary Publications Service, Library of Congress, Washington 25, D.C., at \$8.75 for photoprints or \$3.00 for 35-mm. microfilm.

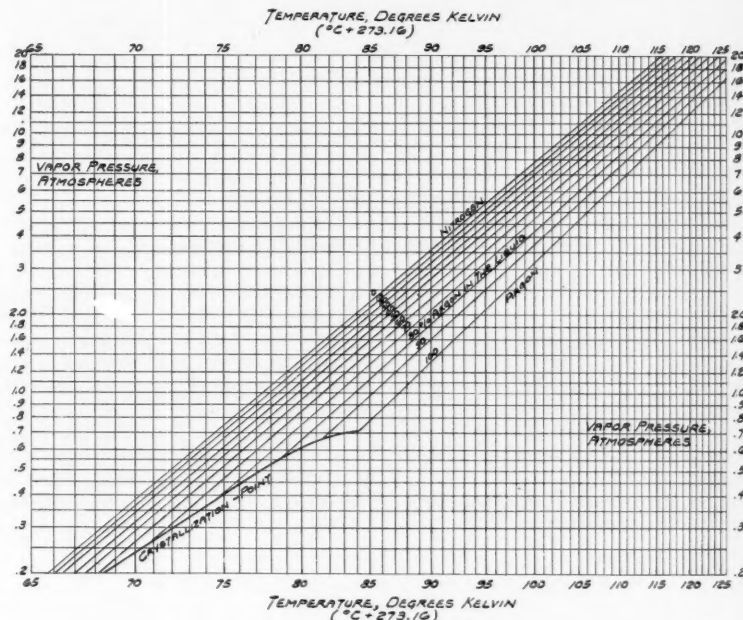


Fig. 1. Vapor pressure of N_2 -A liquid mixtures.

100% oxygen; and interpolated from the data of Holst and Hamburger (4) for nitrogen-argon mixtures except 100% nitrogen and 100% argon. Figures 1, 2,

and 3 show the vapor pressures according to Table 1 for nitrogen-argon, nitrogen-oxygen, and argon-oxygen mixtures, respectively, from 0.2 to 20 atm., as a

TABLE 1

VAPOR PRESSURES OF NITROGEN-ARGON, ARGON-OXYGEN, AND NITROGEN-OXYGEN BINARY LIQUID MIXTURES

$$\log_{10} P_{atm} = a - \frac{b}{T^{\circ}K.}$$

$$T^{\circ}K. = \frac{b}{a - \log_{10} P_{atm}}$$

Data of Clark, Din, and Robb for argon-oxygen

Data of Dodge and Dunbar for nitrogen-oxygen, except 100% oxygen

Data of Holst and Hamburger for nitrogen-argon, except 100% nitrogen and 100% argon

% N ₂	% O ₂	a	b	% N ₂	% A	a	b	% A	% O ₂	a	b
100	0	3.9335	304.49	100	0	3.9335	304.49	100	0	3.96370	346.000
90	10	3.9051	304.52	90	10	3.9164	305.0	90	10	3.96748	346.709
80	20	3.8818	305.35	80	20	3.9018	306.0	80	20	3.97276	347.782
70	30	3.8626	306.84	70	30	3.8881	307.5	70	30	3.97896	349.107
60	40	3.8493	309.21	60	40	3.8746	309.3	60	40	3.98603	350.661
50	50	3.8418	312.52	50	50	3.8610	311.5	50	50	3.99396	352.439
40	60	3.8444	317.32	40	60	3.8475	313.9	40	60	4.00279	354.445
30	70	3.8585	323.89	30	70	3.8405	317.0	30	70	4.01258	356.689
20	80	3.8915	333.18	20	80	3.8482	322.1	20	80	4.02340	359.189
10	90	3.9541	346.64	10	90	3.8743	330.36	10	90	4.03543	361.985
0	100	4.0490	365.19	0	100	3.96370	346.000	0	100	4.04898	365.186

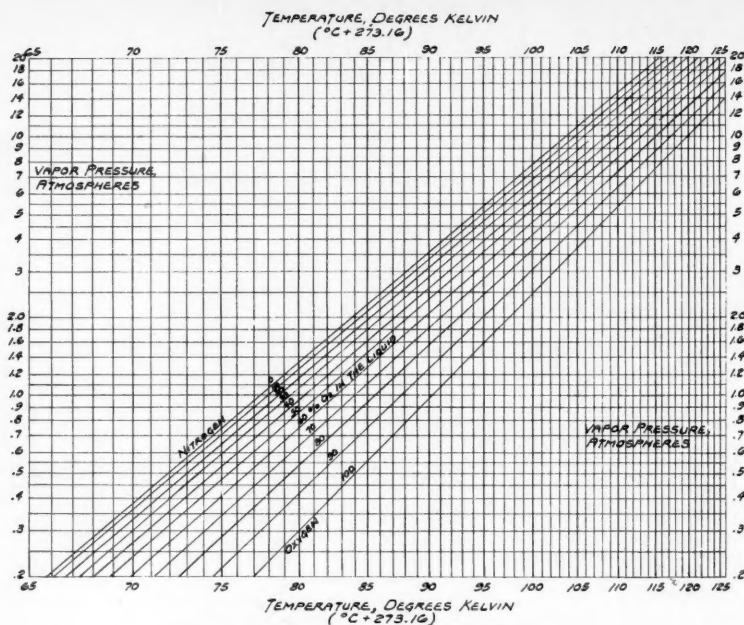


Fig. 2. Vapor pressure of N_2 - O_2 liquid mixtures.

function of absolute temperature, with lines at 10 or 20% intervals of liquid composition. The crystallization-point phase boundary is plotted on Figures 1 and 3 from the solid-liquid-equilibrium data reported by Ruhemann, Lichter, and Komarow (8).

As a fairly good approximation, straight-line interpolations of the con-

stants a and b are made in Figure 4 for ternary mixtures from the values for binary mixtures in Table 1. Values of the constants can be read from Figure 4 with sufficient accuracy for most purposes. Table 2 shows the bubble-point temperatures at 1,000 mm. of mercury as measured by Weishaupt (9) for forty-one mixtures of nitrogen-argon-oxygen, in

comparison with the temperatures computed by use of a and b constants read from Figure 4. The experimental temperatures have a mean absolute deviation of 0.19°C . and a mean algebraic deviation of 0.07°C . from those computed from Figure 4.

VAPOR-LIQUID EQUILIBRIUM AS A FUNCTION OF TEMPERATURE AND COMPOSITION

Raoult's Law states that the partial pressure of a component i in a liquid solution is equal to the vapor pressure of that component times its mole fraction in the liquid:

$$p_i = P_i x_i \quad (2)$$

Dalton's Law states that the partial pressure is also equal to the total pressure times the mole fraction in the vapor:

$$p_i = \pi y_i \quad (3)$$

Combining these two expressions gives

$$p_i = \pi y_i = P_i x_i \quad (4)$$

The relative volatility of component i with respect to component k can then be written as follows:

$$\alpha_{ik} = \frac{y_i/x_i}{y_k/x_k} = \frac{P_i/\pi}{P_k/\pi} = \frac{P_i}{P_k} \quad (5)$$

The foregoing equations apply only to "ideal" liquid solutions and "ideal" gases (at low pressure). Except at very low pressure, fugacities must be substituted for pressures in these equations, and thus Raoult's and Dalton's laws are converted into the Lewis and Randall equations:

$$f_i = f_{\pi i} y_i = f_{P_i}^0 x_i e^{v_{L_i}(\pi - P_i)/RT} \quad (6)$$

$$\alpha_{ik} = \frac{y_i/x_i}{y_k/x_k} = \frac{f_{P_i}^0 e^{v_{L_i}(\pi - P_i)/RT} / f_{\pi i}^0}{f_{P_k}^0 e^{v_{L_k}(\pi - P_k)/RT} / f_{\pi k}^0} \quad (7)$$

If the liquid solution is not ideal, the liquid-phase activity coefficient γ_i must be inserted into the Raoult's Law and the Lewis and Randall equations. Thus, at low pressures

$$p_i = \gamma_i P_i x_i \quad (8)$$

$$p_i = \pi y_i = \gamma_i P_i x_i \quad (9)$$

$$\alpha_{ik} = \frac{y_i/x_i}{y_k/x_k} = \frac{\gamma_i P_i}{\gamma_k P_k} \quad (10)$$

And at higher pressures, with negligible deviation of the vapor phase from the Lewis and Randall equation assumed,

$$f_i = f_{\pi i} y_i = \gamma_i f_{P_i}^0 x_i e^{v_{L_i}(\pi - P_i)/RT} \quad (11)$$

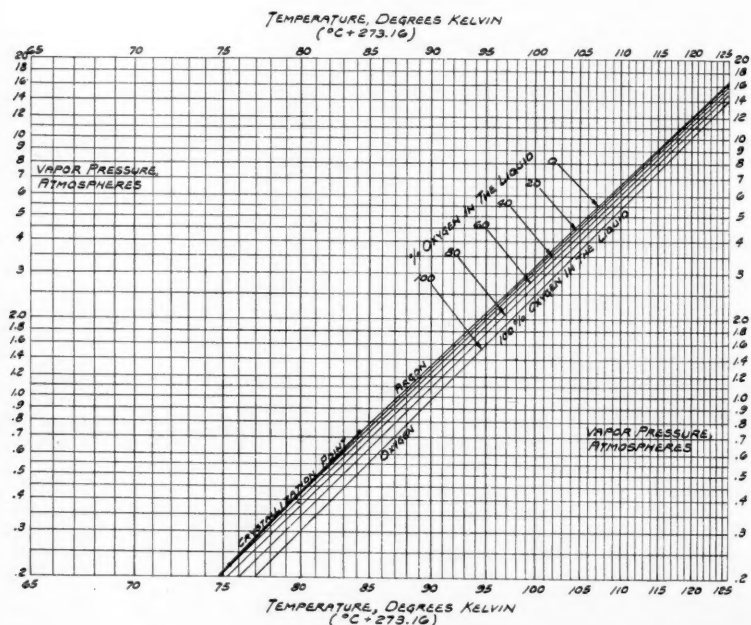


Fig. 3. Vapor pressure of A - O_2 liquid mixtures.

$$\alpha_{ik} = \frac{y_i/x_i}{y_k/x_k} = \frac{\gamma_i f_{Pi}^0 e^{\int_{L_i}^{\infty} (\pi - P_i)/RT / f_{\pi i}^0}}{\gamma_k f_{Pk}^0 e^{\int_{L_k}^{\infty} (\pi - P_k)/RT / f_{\pi k}^0}} \quad (12)$$

Further in this paper, evidence is presented to show that nitrogen-oxygen, argon-oxygen, and nitrogen-argon liquid binary mixtures are "regular" solutions (3a), for which the entropy of mixing is the same as for ideal-liquid solutions; that is, the excess entropy of mixing is zero. For a regular binary solution of components i and k , the equations for the liquid-phase activity coefficients are

$$T \log_{10} \gamma_i = c x_k^2 \quad (13)$$

$$T \log_{10} \gamma_k = c x_i^2 \quad (14)$$

The constant c is the same for both components and is likely to be independent of the temperature; therefore,

$$\begin{aligned} T \log_{10} \frac{\gamma_i}{\gamma_k} &= c(x_k^2 - x_i^2) \\ &= c(x_k - x_i)(x_k + x_i) \\ &= c(x_k - x_i) \end{aligned} \quad (15)$$

For regular binary solutions at a liquid composition of 50% of each component, x_i equals x_k equals 0.50, and γ_i equals γ_k . Thus, for regular binary solutions at 50-50 liquid composition Equation (12)

reduces to Equation (7). And for binary regular solutions—if it is known or may be presumed that they are regular solutions—the relative volatility at 50-50 composition can be evaluated as a function of temperature from vapor-pressure data, from data as to density of the pure-component liquids, and from the Hougen and Watson (5) generalized fugacity chart.

Since

$$\log P_i = a - \frac{b}{T} \quad (1)$$

then

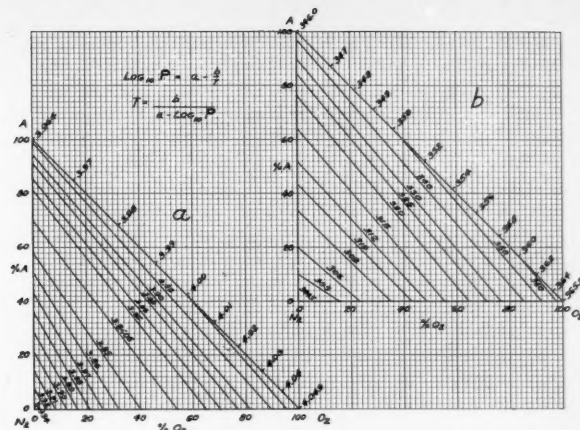


Fig. 4. Constants α and b in the vapor-pressure equation for N_2 -A- O_2 liquid mixtures.

$$\log \alpha_{ik(\text{ideal})} = \log \frac{P_i}{P_k} = a' - \frac{b'}{T} \quad (16)$$

Likewise, $\log \alpha_{ik(50-50)}$ can be approximated by the same form of equation:

$$\log \alpha_{ik(50-50)} = a'' - \frac{b''}{T} \quad (17)$$

Equation (7) has been evaluated for the three binary 50-50 mixtures at a number of temperatures and pressures, and these values of $\alpha_{ik(50-50)}$ are accurately represented from 0.2 to 20 atm. in the manner of Equation (17), as follows:

TABLE 2
COMPARISON OF WEISHAUPT EXPERIMENTAL NITROGEN-ARGON-OXYGEN EQUILIBRIUM DATA AT 1,000 MM. HG WITH WEISHAUPT'S EQUATIONS AND THE WRITER'S EQUATIONS

Run	Subscripts: x Weishaupt experimental data,										r recommended equations of this paper														
	Experimental					Weishaupt equations					Experimental					Weishaupt equations					Writer's equations				
	x_O	x_A	x_N	T_x	T_r	y_O	y_A	y_N	y_O	y_N	α_{NO}	α_{AO}	α_{NA}	α_{NO}	α_{AO}	α_{NA}	α_{NO}	α_{AO}	α_{NA}	α_{NO}	α_{AO}	α_{NA}			
8	0.1159	0.1115	0.7726			81.32	0.0331	0.0453	0.9216	0.0385	0.0505	0.9110	4.177	1.422	2.935	3.555	1.362	2.605	3.573	1.456	2.455				
9	0.1496	0.1447	0.7057			81.80	0.0531	0.0771	0.8698	0.0524	0.0690	0.8786	3.470	1.501	2.310	3.552	1.362	2.604	3.615	1.449	2.492				
10	0.2058	0.1939	0.6003	83.21		82.70	0.0840	0.1214	0.7946	0.0787	0.1011	0.8202	3.25	1.536	2.12	3.577	1.361	2.629	3.611	1.430	2.525				
12	0.2047	0.1130	0.6823	82.27		82.08	0.0726	0.0655	0.8619	0.0729	0.0558	0.8713	3.56	1.633	2.18	3.590	1.388	2.590	3.622	1.469	2.466				
13	0.3403	0.1317	0.5280	83.71		83.37	0.1401	0.0744	0.7855	0.1386	0.0765	0.7849	3.61	1.371	2.63	3.651	1.427	2.560	3.758	1.479	2.541				
14	0.3092	0.2497	0.4411	84.48		84.00	0.1366	0.1538	0.7096	0.1378	0.1535	0.7087	3.74	1.392	2.68	3.601	1.381	2.605	3.709	1.407	2.636				
15	0.2659	0.3597	0.3744	85.00		84.00	0.1224	0.2309	0.6467	0.1278	0.2311	0.6411	3.75	1.395	2.69	3.563	1.337	2.665	3.697	1.370	2.699				
16	0.4461	0.0887	0.4652	84.51		84.29	0.1896	0.0533	0.7571	0.1931	0.0566	0.7503	3.83	1.413	2.71	3.726	1.474	2.528	3.769	1.512	2.493				
17	0.4402	0.1640	0.3958	85.38		84.94	0.2112	0.1103	0.6785	0.2054	0.1108	0.6838	3.57	1.401	2.55	3.703	1.448	2.557	3.745	1.473	2.542				
18	0.3935	0.3081	0.2984	86.21		86.14	0.2095	0.2208	0.5637	0.2063	0.2244	0.5693	3.55	1.382	2.57	3.639	1.389	2.620	3.730	1.404	2.657				
19	0.4955	0.3142	0.1903	87.68		87.80	0.3027	0.2710	0.4263	0.3019	0.2709	0.4272	3.66	1.411	2.60	3.685	1.415	2.604	3.751	1.411	2.658				
20	0.5143	0.1144	0.3713	85.55		85.33	0.2498	0.0823	0.6679	0.2473	0.0818	0.6709	3.70	1.480	2.50	3.758	1.487	2.527	3.800	1.507	2.522				
21	0.4697	0.4027	0.1276	88.68		88.00	0.0930	0.3776	0.3019	0.3150	0.3729	0.3122	3.46	1.373	2.52	3.647	1.381	2.642	3.697	1.367	2.704				
22	0.5885	0.1624	0.2691	86.79		86.67	0.3110	0.1329	0.5561	0.3117	0.1323	0.5560	3.78	1.494	2.53	3.769	1.486	2.536	3.810	1.489	2.559				
23	0.5816	0.2992	0.1192	89.08		89.19	0.4016	0.2948	0.3036	0.3990	0.2960	0.3050	3.69	1.427	2.59	3.730	1.442	2.586	3.733	1.421	2.627				
24	0.6065	0.0041	0.3894	85.57		85.33	0.2879	0.0043	0.7078	0.2876	0.0030	0.7094	3.83	1.842	1.553	2.474	1.839	1.571	2.443	1.839	1.571	2.443			
25	0.6152	0.1115	0.2733	86.80		86.80	0.2675	0.3423	0.0929	0.5648	0.3370	0.0927	0.5703	3.71	1.496	2.48	3.810	1.518	2.510	3.834	1.518	2.526			
26	0.0873	0.0808	0.8319	81.10		80.87	0.0289	0.0386	0.9325	0.0278	0.0350	0.9372	3.38	1.442	2.34	3.538	1.360	2.601	3.514	1.465	2.399				
28	0.2309	0.0046	0.7645	81.69		81.48	0.0760	0.0019	0.9221	0.0761	0.0022	0.9217	3.66	1.459	2.37	3.559	1.451	2.521	3.614	1.523	2.373				
29	0.0846	0.0723	0.8431	80.98		80.80	0.0261	0.0315	0.9424	0.0267	0.0311	0.9432	3.62	1.412	2.56	3.541	1.363	2.598	3.512	1.468	2.392				
30	0.4391	0.0058	0.5551	83.59		83.37	0.1735	0.0042	0.8223	0.1749	0.0034	0.8217	3.75	1.496	2.48	3.716	1.472	2.525	3.768	1.553	2.426				
31	0.2376	0.2095	0.5529	83.27		83.18	0.0984	0.1133	0.7883	0.0947	0.1146	0.7907	3.45	1.308	2.64	3.588	1.373	2.614	3.674	1.432	2.566				
32	0.0077	0.1064	0.8859	80.52		80.42	0.0022	0.0395	0.9583	0.0024	0.0436	0.9540	3.66	1.412	2.56	3.456	1.315	2.628	3.467	1.442	2.404				
33	0.0121	0.7902	0.1977	86.68		86.46	0.0076	0.5759	0.1953	0.0076	0.5746	0.4178	3.36	1.160	2.90	3.365	1.158	2.906	3.551	1.175	3.022				
34	0.0104	0.6547	0.3349	84.93		84.88	0.0041	0.4022	0.5937	0.0054	0.4047	0.5899	3.85	1.416	2.72	3.918	1.583	2.476	3.841	1.552	2.475				
36	0.0190	0.2344	0.6576	82.04		81.90	0.0064	0.1525	0.8411	0.0070	0.1525	0.8405	3.82	1.487	2.57	3.991	1.608	2.482	3.765	1.553	2.424				
37	0.0183	0.2643	0.7174	81.85		82.26	0.0056	0.1269	0.8675	0.0065	0.1298	0.8737	3.78	1.458	2.59	3.820	1.595	2.395	3.792	1.489	2.547				
42	0.7347	0.2475	0.0178	91.47		91.47	0.0370	0.3216	0.0414	0.6269	0.3151	0.0580	1.500	2.72	3.429	1.276	2.687	3.595	1.374	2.595	2.616				
43	0.8249	0.1559	0.0192	91.79		91.76	0.7453	0.2048	0.0499	0.7231	0.2113	0.0656	1.454	2.72	3.918	1.583	2.476	3.841	1.552	2.475	2.475				
44	0.7849	0.0616	0.1535	88.91		89.31	0.3362	0.0596	0.4042	0.3290	0.0657	0.4053	3.85	1.416	2.72	3.991	1.583	2.476	3.841	1.552	2.475				
45	0.9035	0.0509	0.0456	91.43		91.63	0.1601	0.7833	0.0657	0.1510	0.7740	0.0701	0.1559	3.82	1.487	2.57	3.918	1.608	2.482	3.765	1.553	2.424			
46	0.6780	0.1711	0.1509	88.77		89.02	0.4526	0.1666	0.3808	0.4439	0.1787	0.3774	3.78	1.458	2.59	3.820	1.595	2.395	3.792	1.489	2.547				
47	0.7883	0.1519	0.0598	90.73		90.77	0.6415	0.1813	0.1772	0.6282	0.1868	0.1850	3.64	1.468	2.48	3.882	1.543	2.516	3.752	1.499	2.503				
48	0.7922	0.1942	0.0136	91.74		91.76	0.0606	0.7154	0.0302	0.0945	0.7094	0.0302	1.450	2.72	3.429	1.276	2.687	3.595	1.374	2.595	2.616				
49	0.6895	0.3165	0.0140	91.32		91.32	0.127	0.5822	0.0306	0.3872	0.5663	0.3892	0.0445	1.407	2.72	3.429	1.276	2.687	3.595	1.374	2.595	2.616			
50	0.6814	0.0773	0.2413	87.40		87.38	0.3983	0.0670	0.5347	0.3933	0.0691	0.5376	3.79	1.485	2.55	3.861	1.549	2.492	3.846	1.540	2.497				
51	0.5988	0.3813	0.0199	90.90		90.81	0.5062	0.4381	0.0557	0.4938	0.4454	0.0608	1.360	2.72	3.429	1.276	2.687	3.595	1.374	2.595	2.616				
52	0.2014	0.7834	0.0152	90.18		89.97	0.1721	0.7887	0.0392	0.1672	0.7909	0.0419	1.178	2.72	3.429	1.276	2.687	3.595	1.374	2.595	2.616				
53	0.0621	0.9269	0.0110	89.87		89.27	0.0552	0.8979	0.0469	0.0533	0.9147	0.0320	1.088	2.72	3.429	1.276	2.687	3.595	1.374	2.595	2.616				
54	0.1966	0.6573	0.1461	87.87		87.87	0.2602	0.1300	0.5302	0.2602	0.1300	0.5302	3.52	1.220	2.88	3.473	1.251	2.799	3.595	1.230	2.899				
55	0.3852	0.5520	0.0628	89.62		89.77	0.2915	0.5354	0.1731	0.5843	0.1677	0.5843	3.64	1.283	2.84	3.567	1.316	2.710	3.618	1.296	2.793				
56	0.0901	0.7733	0.1368	87.74		87.74	0.0621	0.6148	0.3231	0.0612	0.6224	0.3164	3.42	1.154	2.97	3.405	1.185	2.874	3.554	1.188	2.992				
57	0.1634	0.4456	0.3910	84.81		84.57	0.0790	0.2678	0.6532	0.0777	0.2721	0.6502	3.46	1.246	2.78	3.497	1.284	2.723	3.635	1.321	2.752				

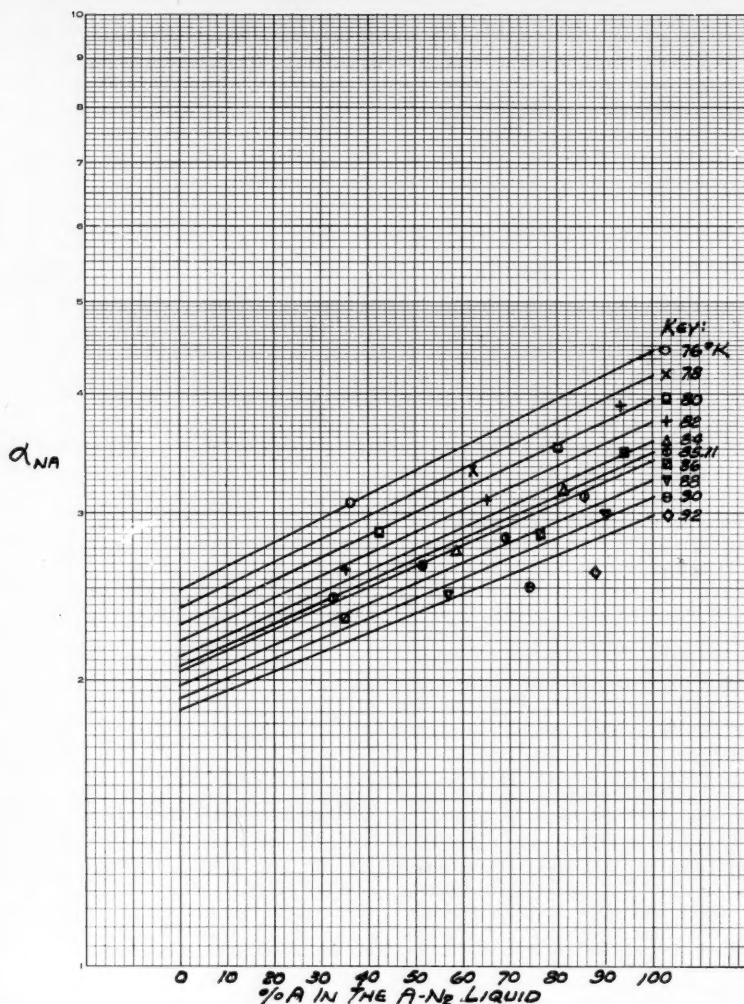


Fig. 5. Experimental α_{NA} binary data of Holst and Hamburger compared with author's correlation isotherms.

$$\begin{aligned} \log \alpha_{NO(50-50)} &= \log \frac{f_{PN}^0 e^{v_{LN}(\pi - P_N)/RT} / f_{\pi N}^0}{f_{PO}^0 e^{v_{LO}(\pi - P_O)/RT} / f_{\pi O}^0} \\ &= -0.470 + \frac{88.4}{T} \end{aligned} \quad (18)$$

$$\begin{aligned} \log \alpha_{AO(50-50)} &= \log \frac{f_{PA}^0 e^{v_{LA}(\pi - P_A)/RT} / f_{\pi A}^0}{f_{PO}^0 e^{v_{LO}(\pi - P_O)/RT} / f_{\pi O}^0} \\ &= -0.132 + \frac{23.1}{T} \end{aligned} \quad (19)$$

$$\begin{aligned} \log \alpha_{NA(50-50)} &= \log \frac{f_{PN}^0 e^{v_{LN}(\pi - P_N)/RT} / f_{\pi N}^0}{f_{PA}^0 e^{v_{LA}(\pi - P_A)/RT} / f_{\pi A}^0} \\ &= -0.338 + \frac{65.3}{T} \end{aligned} \quad (20)$$

$$\begin{aligned} \log \alpha_{NA(50-50)} &= \log \alpha_{NO(50-50)} - \log \alpha_{AO(50-50)} \\ &= \log \frac{\alpha_{NO(50-50)}}{\alpha_{AO(50-50)}} \end{aligned} \quad (21)$$

The fugacity ratios of Equations (18), (19), and (20) actually can be represented as a function of temperature by those equations over the entire binary-composition ranges, as these fugacity ratios are functions of temperature almost exclusively and are virtually unaffected by the limited pressure variation with composition at constant temperature. Therefore, by substituting these expressions for the fugacity ratios into Equation (12) and then combining Equation (15) with Equation (12), one obtains the following equations:

$$\log \alpha_{NO} = -0.470 + \frac{88.4 + c(x_O - x_N)}{T} \quad (22)$$

$$\log \alpha_{AO} = -0.132 + \frac{23.1 + c'(x_O - x_A)}{T} \quad (23)$$

$$\log \alpha_{NA} = -0.338 + \frac{65.3 + c''(x_A - x_N)}{T} \quad (24)$$

Thus for each binary combination, $\log \alpha$ is linear with liquid composition for each isotherm. By plotting $\log \alpha_{ik}$ against x_i for every experimental point along each isotherm for which experimental data are available, one can then select the value of constant c that results in a family of straight isotherms that reasonably well correlate the experimental data. This was done for Figures 5, 6, and 7, on which the families of straight lines are graphs of the following equations:

$$\log \alpha_{NO} = -0.470 + \frac{88.4 + 8.3(x_O - x_N)}{T} \quad (25)$$

$$\log \alpha_{AO} = -0.132 + \frac{23.1 + 7.5(x_O - x_A)}{T} \quad (26)$$

$$\log \alpha_{NA} = -0.338 + \frac{65.3 + 9.5(x_A - x_N)}{T} \quad (27)$$

These are the equations for relative volatilities of the respective binary mixtures. The 50-50 midpoint of each isotherm in Figures 5, 6, and 7 was established by Equations (18), (19), and (20) from vapor-pressure data and the generalized fugacity chart. Only the slope of each isotherm on Figures 5, 6, and 7 is dependent on the value assigned to the constant c in Equations 22, 23, and 24, which is determined from the experimental equilibrium data shown on those figures.

Figure 6 shows that a wealth of experimental equilibrium data are available for nitrogen-oxygen mixtures. The data at 65°, 70°, and 77.5°K. are by Armstrong, Goldstein, and Roberts (1). The data at 74.7° and 79.07°K. are by Inglis (6), and the data for 90.5°, 99.44°, 110.05°, 119.92°, and 125.0°K. are by Dodge and Dunbar (3). Figure 6 shows that Equation (25) represents all these data fairly well except those points approaching the 126.2°K. critical point of nitrogen (33.5 atm.).

Figure 7 shows the family of lines that was obtained by using a value of 7.5 for the constant c' in Equation (23) for argon-oxygen mixtures, resulting in Equations

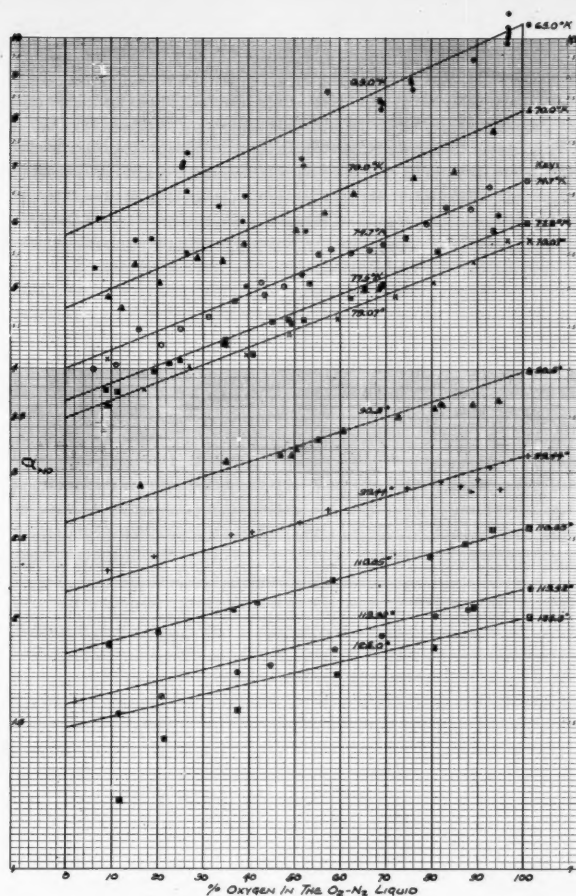


Fig. 6. Experimental α_{NO} binary data of Inglis, of Dodge and Dunbar, and of Armstrong et al. compared with author's correlation isotherms.

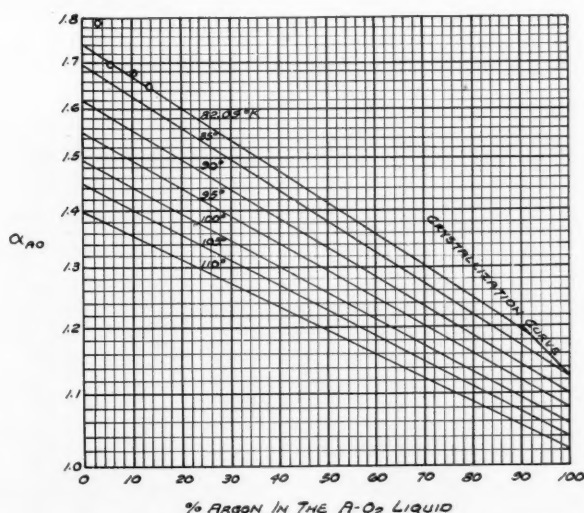


Fig. 7. Experimental α_{AO} binary data of Inglis compared with author's correlation isotherms.

tion (26). The straight lines for Figure 7 are plots of this equation. By selection of 7.5 for the numerical value of the constant, the 82.09°K. isotherm was made to pass through the fragmentary experimental data of Inglis (6) at 0 to 14% argon for that temperature. This value of the constant also resulted in location of the 90°K. isotherm so as to agree identically near 100% argon with carefully taken plant data. This value of the constant also resulted in location of the 95°K. isotherm on Figure 7 so as to agree reasonably satisfactorily with performance data from 0 to 15% argon in the liquid on ordinary and on very tall upper columns of air separating double columns, evaluated by the writer for cases for which the reflux ratio could be computed with considerable accuracy and for which a pinch condition was reached in this composition range. In this same composition and temperature range the Linde rectifying columns achieve separations which would be impossible, even with a very large number of trays, according to the experimental equilibrium data of Clark, Din, and Robb. The data of Clark, Din, and Robb therefore are not shown on Figure 7. The 100°, 105°, and 110°K. isotherms according to Equation (26) are plotted on Figure 7 for reference, although no Inglis or Linde data are available for checking them.

Equation (25) and the lines on Figure 6, which are plots of this equation, have been used for rectifying-column design since 1950 and Equation (26) and the lines plotted therefrom on Figure 7 have been used for design since 1954. They do not, however, differ greatly from the previous design data.

Figure 5 shows lines that resulted from selecting a value of $c'' = 9.5$ in Equation (24) for nitrogen-argon mixtures, resulting in Equation (27), so that the lines would agree on Figure 5 with Holst and Hamburger's (4) experimental data at 76° to 82°K. Unfortunately, data at temperatures increasing from 84° to 92°K. give relative volatility values differing increasingly downward from the lines for Equation (27). These look like systematic error in the Holst and Hamburger data, as Equation (20), on which Equation (27) is partly based, is believed to be accurately established by the Holst and Hamburger vapor-pressure data and by the Hougen and Watson (5) generalized fugacity chart. The midpoints of the isotherms shown on Figure 5 are established by the above-mentioned vapor-pressure data and fugacity chart, and the slopes of all the isotherms are established by choice of the constant 9.5 so as to agree with the low-pressure 76°-to-82°K. equilibrium data.

If Equations (25), (26), and (27) and the straightness of the isotherms on Figures 5, 6, and 7 are accepted as adequately established by the experi-

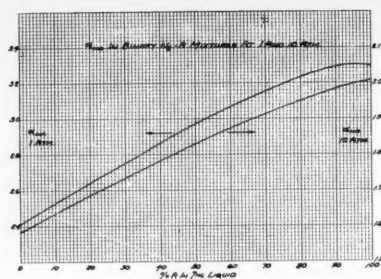


Fig. 8. α_{NA} in binary N_2 - A mixtures at 1 and 10 atm.

mental points on Figures 5, 6, and 7 and by the foregoing discussion, this acceptance verifies that the three binary systems nitrogen-oxygen, argon-oxygen, and nitrogen-argon form "regular" solutions and that in addition to Equations (25), (26), and (27) the following equations are also correct for these binary systems:

For nitrogen-oxygen mixtures:

$$T \log \frac{\gamma_N}{\gamma_O} = 8.3(x_O - x_N) \quad (28)$$

$$T \log \gamma_N = 8.3x_O^2 \quad (29)$$

$$T \log \gamma_O = 8.3x_N^2 \quad (30)$$

For argon-oxygen mixtures:

$$T \log \frac{\gamma_A}{\gamma_O} = 7.5(x_O - x_A) \quad (31)$$

$$T \log \gamma_A = 7.5x_O^2 \quad (32)$$

$$T \log \gamma_O = 7.5x_A^2 \quad (33)$$

For nitrogen-argon mixtures:

$$T \log \frac{\gamma_N}{\gamma_A} = 9.5(x_A - x_N) \quad (34)$$

$$T \log \gamma_N = 9.5x_A^2 \quad (35)$$

$$T \log \gamma_A = 9.5x_N^2 \quad (36)$$

In accordance with the equations in Wohl's (10) paper on liquid-phase activity coefficients for multicomponent mixtures, Equations (25) to (36) for the binary systems can be combined in a thermodynamically correct manner into the following equations for nitrogen-argon-oxygen ternary mixtures in general:

$$T \log \gamma_N = 9.5x_A^2 + 8.3x_O^2 + (9.5 + 8.3 - 7.5)x_Ax_O \quad (37)$$

$$T \log \gamma_A = 7.5x_O^2 + 9.5x_N^2 + (7.5 + 9.5 - 8.3)x_Ox_N \quad (38)$$

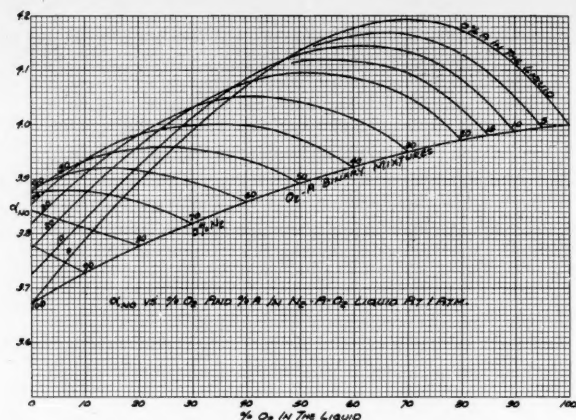


Fig. 9. α_{NO} vs. % O_2 and % A in N_2 - A - O_2 liquid at 1 atm.

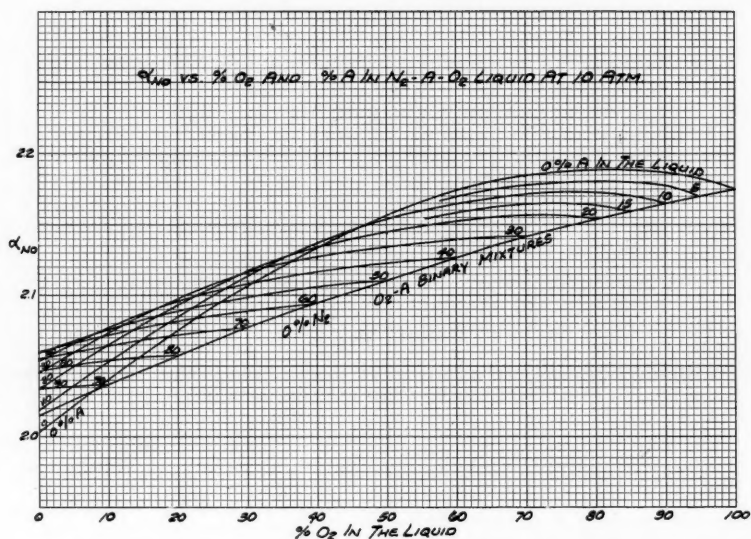


Fig. 10. α_{NO} vs. % O_2 and % A in N_2 - A - O_2 liquid at 10 atm.

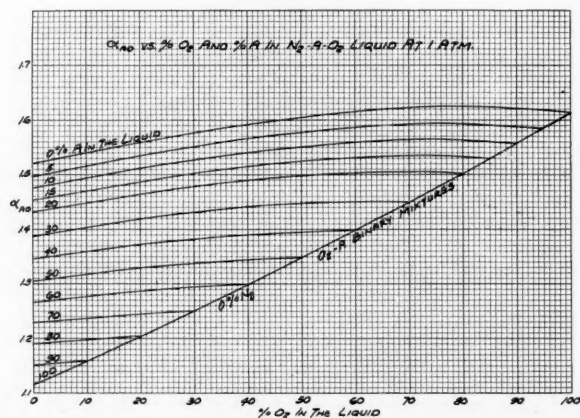


Fig. 11. α_{AO} vs. % O_2 and % A in N_2 - A - O_2 liquid at 1 atm.

$$T \log \gamma_O = 8.3x_N^2 + 7.5x_A^2 + (8.3 + 7.5 - 9.5)x_Nx_A \quad (39)$$

$$T \log \frac{\gamma_N}{\gamma_O} = 8.3(x_O - x_N) + 2x_A \quad (40)$$

$$T \log \frac{\gamma_A}{\gamma_O} = 7.5(x_O - x_A) + 1.2x_N \quad (41)$$

$$T \log \frac{\gamma_N}{\gamma_A} = 9.5(x_A - x_N) + 0.8x_O \quad (42)$$

$$\log \alpha_{NO} = -0.470 + \frac{88.4 + 8.3(x_O - x_N) + 2x_A}{T} \quad (43)$$

$$\log \alpha_{AO} = -0.132 + \frac{23.1 + 7.5(x_O - x_A) + 1.2x_N}{T} \quad (44)$$

$$\log \alpha_{NA} = -0.338 + \frac{65.3 + 9.5(x_A - x_N) + 0.8x_O}{T} \quad (45)$$

Binary Equations (25) to (27) and ternary Equations (43) to (45) are consistent with the following identity:

$$\alpha_{NO}/\alpha_{AO} = \alpha_{NA} \quad (46)$$

The preceding equations are equations for "regular" solutions of nitrogen, argon, and oxygen.

VAPOR-LIQUID EQUILIBRIUM AS A FUNCTION OF PRESSURE AND COMPOSITION

The operation of a rectifying column is more nearly isobaric throughout than

isothermal. Therefore, it is convenient for design purposes to combine the ternary vapor-pressure equations and graph of Figure 4 with the ternary equations for relative volatility as a function of temperature [Equations (43) to (45)], in order to get for design use equations and graphs of relative volatility as a function of pressure.

Equations (43) to (45) are of the form

for each liquid composition. Combining Equations (47) and (48) gives

$$\log \alpha_{ik} = f + \frac{g}{a - \log \pi}$$

Rearranging gives

$$\log \alpha_{ik} = f + \frac{g}{b} (a - \log \pi) \quad (49)$$

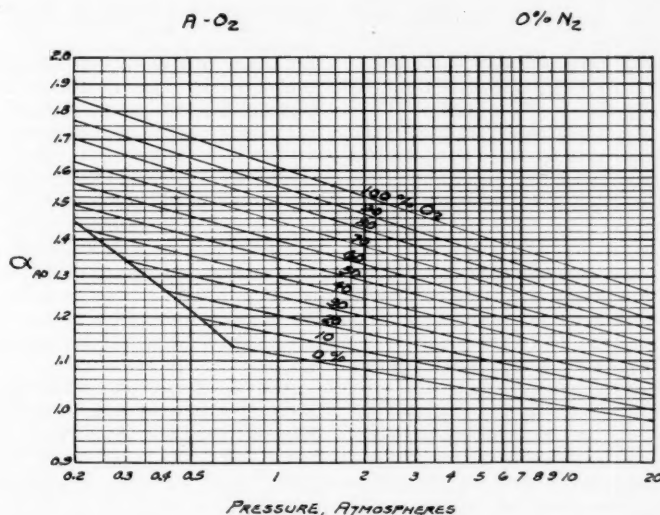


Fig. 33. α_{AO} vs. pressure and % O_2 in liquid for A- O_2 mixtures. (Figures 13 to 32 and 34 to 49 are plotted similarly to cover the entire N_2 -A- O_2 composition range for α_{NO} , α_{AO} , and α_{NA} vs. pressure and liquid composition.)

$$\log \alpha_{ik} = f + \frac{g}{T} \quad (47)$$

for each liquid composition. The vapor-pressure equation is of the form

$$\log \pi = a - \frac{b}{T} \quad (48)$$

Combining constants reduces this to

$$\log \alpha_{ik} = h - m \log \pi \quad (50)$$

Thus, the relative volatility is plotted vs. total pressure as a straight line on logarithmic graph paper for each liquid composition.

Therefore, from Figure 4 and Equations (43) to (45) the relative volatilities α_{NO} and α_{AO} , and α_{NA} for nitrogen-argon mixtures, were computed at 1 and 10 atm. and are plotted as a function of liquid composition on Figures 8 to 12 as the basis for construction of logarithmic graphs.

Figures 13 to 49* are logarithmic plots of α_{NO} and α_{AO} , and α_{NA} for the nitrogen-argon mixtures, against the total pressure in atmospheres absolute from 0.2 to 20 atm., with separate straight lines for each liquid composition. The entire ternary-composition range is covered, with separate lines for each 10% interval of percentage of argon and oxygen in the liquid. However, the α_{AO} graphs cover 5% intervals of percentage of argon, from 0 to 20% argon in the liquid. The points on each line for 1 and 10 atm. are plotted from Figures 8 to 12, and straight

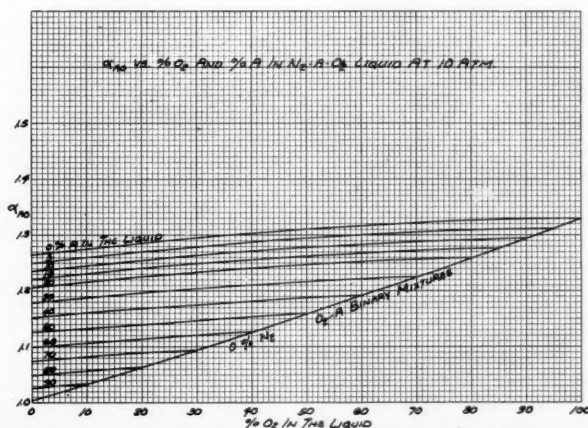


Fig. 12. α_{AO} vs. % O_2 and % A in N_2 -A- O_2 liquid at 10 atm.

*See footnote on page 75.

TABLE 3
MEAN DEVIATIONS OF WEISHAUP'T'S NITROGEN-ARGON-OXYGEN EXPERIMENTAL DATA FROM THE EQUATIONS

	Deviation of experimental data from writer's equations					Deviation of experimental data from Weishaupt's equations				
	ΔT	$\Delta\alpha_{NO}$	$\Delta\alpha_{AO}$	$\Delta\alpha_{NA}$	$\Delta\alpha_{all}$	$\Delta\alpha_{NO}$	$\Delta\alpha_{AO}$	$\Delta\alpha_{NA}$	$\Delta\alpha_{all}$	
Absolute mean deviation	0.194°C.	0.122	0.047	0.109	0.091	0.106	0.060	0.114	0.092	
Algebraic mean deviation	0.074°C.	-0.050	-0.024	-0.0006	0.025	-0.019	-0.012	0.004	0.012	
Root mean square deviation		0.168	0.062	0.156	0.135	0.160	0.081	0.171	0.141	

lines are drawn through these points from 20 down to 0.2 atm., or the crystallization curve.

The phase boundary between liquid and solid, that is, the crystallization point curve, is plotted on the diagrams from the experimental nitrogen-oxygen, argon-oxygen, and nitrogen-argon data of Ruhemann, Lichter, and Komarow (8) by use of straight-line interpolation of crystallization temperatures across the ternary diagram, as was done for the constants a and b in Figure 4.

Figures 13 to 49 are the working graphs of relative volatility for rectifying column design. However, it is convenient for the user to pick off values of relative volatilities at the pressure of his proposed rectifying column, and to plot them against percentage of oxygen, with separate curves for 0, 5, 10, etc., % argon, for the range of composition that he is concerned with. Then, in the tray-to-tray multicomponent rectification calculations [Lewis and Matheson (7)] values of the respective relative volatilities are read off the graphs and entered in the calculation for each tray for the liquid composition that exists at that point.

COMPARISON WITH WEISHAUP'T'S NITROGEN-ARGON-OXYGEN EXPERIMENTAL DATA AND EQUATIONS

Weishaupt (9) measured the equilibrium vapor and liquid compositions for forty-three nitrogen-argon-oxygen mixtures at 1,000 mm. Hg and measured the saturation temperatures thereof. In Table 2 are tabulated the equilibrium liquid and vapor compositions and the measured temperatures compared with the temperatures computed by Figure 4. The measured relative volatilities α_{NO} , α_{AO} , and α_{NA} are compared for each point with the values from Equations (43) to (45).

Weishaupt presented approximate equations for the equilibrium vapor compositions at 1,000 mm. Hg only. It is of interest to compare at only this one pressure the experimental relative volatilities, the relative volatilities computed from Weishaupt's single-pressure equations, and the relative volatilities computed by the writer's general equations which cover the range from 0.2 to 20

atm. This is done in Table 2, and the results tend to confirm for ternary mixtures the reasonable degree of accuracy of the writer's equations.

The mean deviations of the experimental data from the writer's equations and from Weishaupt's equations are listed in Table 3, which shows that the writer's equations describe Weishaupt's experimental data approximately equally as well as Weishaupt's own equations do. The writer's equations have been shown to describe the vapor-liquid equilibrium not only at 1,000 mm. Hg, as Weishaupt's do, but over a wide range of pressure, insofar as binary equilibrium data are available with which to test them. The writer's equations, furthermore, have a sound thermodynamic basis, which is the safest way to describe such a system over a wide range of composition and pressure from a limited amount of available data.

ACKNOWLEDGMENT

A very large number of calculations were made by Phyllis M. Turner, who also plotted the computed points on the many diagrams. The drafting was done by Edna H. Saylor. The writer extends his appreciation to these coworkers and also wishes to thank Linde Air Products Company, in particular L. I. Dana and G. J. Boshkoff, for encouraging him to prepare this work for publication and for authorizing its publication.

NOTATION

e = base of the natural logarithms, 2.7182 ---
 f = fugacity of a component in a liquid or vapor solution
 f_P^o = fugacity of a pure component at its vapor pressure P
 f_x^o = fugacity of a pure component at the total pressure π of the mixture
 p = partial pressure of a component in the vapor
 P = vapor pressure of a pure component liquid or liquid mixture, atm. abs.
 R = gas constant
 T = absolute temperature, °K.
 v_L = average molar volume of a pure liquid between its vapor pressure P and the total pressure π
 x = mole fraction of a component in the liquid

y = mole fraction of a component in the vapor, especially the vapor in equilibrium with the liquid of composition x

α = relative volatility; defined by the following equation:

$$\alpha_{ik} = \frac{y_i/x_i}{y_k/x_k}$$

γ = activity coefficient of a component in the liquid phase

π = total pressure, atm. abs.

Subscripts

N = nitrogen

O = oxygen

A = argon

i and k = any components

Two subscripts for components used together, such as NO or ik , indicate that the property is for the first component listed relative to the second.

(50-50) = subscript indicating a liquid composition of 50% of each of the two components of a binary mixture

$a, a', b, b', c, c', f, g, h$, and m = arbitrary constants

Notation occurring only in Tables 2 and 3:

Subscripts r and x refer to the recommended equations of this paper and to Weishaupt's experimental data, respectively.

$\Delta\alpha$ = difference in relative volatility of one component with respect to another, according to two different sources of information.

The compositions shown in Table 1 and in all the graphs are liquid compositions.

LITERATURE CITED

- Armstrong, G. T., J. M. Goldstein, and D. E. Roberts, *J. Research Natl. Bur. Standards*, **55**, 265 (1955).
- Clark, A. M., F. Din, and J. Robb, *Proc. Roy. Soc. (London)*, **A221**, 517 (1954).
- Dodge, B. F., and A. K. Dunbar, *J. Am. Chem. Soc.*, **49**, 591 (1927).
- Hildebrand, J. H., *ibid.*, **51**, 66 (1929).
- Holst, G., and L. Hamburger, *Z. physik. Chem.*, **10**, 513 (1916).
- Hougen, O. A., and K. M. Watson, "Chemical Process Principles," Part 2, 1 ed., p. 622, John Wiley and Sons, New York (1947).
- Inglis, J. K. H., *Phil. Mag.*, **11**, 640 (1906).
- Lewis, W. K., and G. L. Matheson, *Ind. Eng. Chem.*, **24**, 494 (1932).
- Ruhemann, Martin, A. Lichter, and P. Komarow, *Physik. Z. Sowjetunion*, **8**, 326 (1935).
- Weishaupt, Josef, *Angew. Chem.*, **B20**, 321 (1948).
- Wohl, Kurt, *Trans. Am. Inst. Chem. Engrs.*, **42**, 215 (1946).

Presented at A.I.Ch.E. Pittsburgh meeting.

Axial Mixing of Binary Gas Mixtures Flowing in a Random Bed of Spheres

K. W. McHENRY, JR., and R. H. WILHELM

Princeton University, Princeton, New Jersey

Measurements are reported on axial mixing of binary gas mixtures at room temperature and atmospheric pressure in a random bed of spherical particles. By means of the Fick's Law equation for diffusion an axial Peclet number, $d_p U/E_z$ (where d_p is particle diameter, U is interstitial velocity, and E_z is axial eddy diffusivity), was computed in terms of the ratio of the amplitudes of a sinusoidal concentration wave at the inlet and outlet of the bed. An experimental method was devised to eliminate end effects in the system. For the gas systems H_2-N_2 and $C_2H_4-N_2$ and for Reynolds numbers between 100 and 400 the mean of twenty-one determinations of axial Peclet number was 1.88 ± 0.15 . This value is in excellent agreement with a value of 2.0 predicted theoretically on the assumption that the bed acts as a series of n perfect mixers, where n is the number of particles traversed between inlet and outlet.

Axial diffusivity for turbulent flow of gases among particles is about sixfold larger than radial diffusivity, previously determined. It is suggested that axial diffusivity may not, perhaps, be neglected in contacting devices, such as adsorbers and catalytic reactors.

The development of rational design methods for fixed-bed reactors, heat exchangers, and adsorbers presupposes a knowledge of the extent of fluid-phase mixing which occurs in the spaces between the packing. In pursuit of this requirement, measurements of eddy-diffusion coefficients for mixing perpendicular to the direction of flow now account for a substantial part of the literature. Made by a technique involving the determination of concentration profiles downstream from a point source of tracer material, these measurements have included liquid and gaseous systems over wide flow conditions. On the other hand, mixing in the direction of flow has received much less attention. In most design methods it is neglected because of the absence of steep axial gradients or perforce because of a lack of knowledge of the magnitude of the axial eddy diffusion coefficient involved. Recent studies by Ogburn (10) have indicated that such neglect may not always be justified. In studying the hydrogenation of ethylene in a fixed bed of catalyst with isothermal wall, this author found that experimentally determined axial temperature profiles showed several departures from those calculated with all major effects except axial diffusion taken into account. The initial temperature gradient was not so steep as the predicted gradient; the measured peak temperature did not reach the calculated peak; the temperature downstream of the peak fell more rapidly than was anticipated from the calculations. All three effects point to the presence of an important heat leak away from the temperature peak and hence possibly to axial mixing.

Previous literature on axial mixing includes the following studies. Danckwerts (2)

K. W. McHenry, Jr., is at present with Standard Oil Company (Indiana), Whiting, Indiana.

measured an axial diffusion coefficient for the flow of water through Raschig rings at one value of Reynolds number. The method involved the response function of the system to a step change in concentration at the inlet. Using the response to a sinusoidally varying input Kramers and Alberda (7) determined axial mixing properties of water in a bed similar to that used by Danckwerts. Two values of flow rate were investigated in this study. Deisler and Wilhelm (4) reported a single value of the axial eddy diffusivity characteristic of a range of Reynolds numbers. The system was gaseous, with flow occurring through a bed of fused-alumina spheres. The frequency-response technique was employed.

Work on axial diffusion here reported was undertaken to include flow rates of laboratory and plant-scale interest. Independence of the results of the particular gases used in the experiments was established. A generalized correlation for use in fixed-bed equipment design is presented. Essentially an extension of the work of Deisler and Wilhelm (4), present high gas-flow-rate requirements led to experimental problems of producing, analyzing, and recording relatively high-frequency concentration waves of sinusoidal form. The earliest work of frequency response applied to mass diffusion problems is that of Winsche and Rosen (12).

THEORY

The first part of this discussion relates to the theory underlying the experimental method, the second, to a possible mechanistic approach to axial mixing in packed beds.

Experimental Method

When a fluid passes through the interstices of a packed bed, macroscopic particles of fluid will be subjected to splitting, acceleration, deceleration, and trapping. If these individual modes of mixing are repeated a large number of times in random order, the resulting

over-all mixing process may be described by a law similar to Fick's Law for molecular diffusion. Practically, in a bed of sufficient length-to-diameter ratio and tube-to-particle ratio this law has been found to hold.

Making the assumptions listed below and combining Fick's Law with a material balance on a flowing system, one may write

$$E_z \frac{\partial^2 x}{\partial z^2} - U \frac{\partial x}{\partial z} = \frac{\partial x}{\partial t} \quad (1)$$

where x is the mole fraction of one gas in a binary mixture, E_z is the eddy-diffusion coefficient for diffusion in the axial direction, U is the intergranular velocity, z is the axial coordinate, and t is time. The assumptions are (1) that x is a function of z and t only, there being no radial gradients, (2) that U is everywhere constant, and (3) that x may be related to the volumetric concentration usually used with Fick's Law through the constant molar density. The first term in Equation (1) represents migration of material along the tube axis in a diffusionlike manner, the second term represents transport due to gross flow, and the third term represents holdup.

Two boundary conditions are applied as follows: (1) at the inlet of the bed ($z = 0$) concentration is given by

$$x(0) = x_M + A(0) \cos \omega t \quad (2)$$

where $x(0)$ is the inlet mole fraction, x_M is the mean mole fraction about which the concentration oscillates, $A(0)$ is the amplitude of the inlet concentration wave, and ω is the angular frequency of the oscillations; (2) at sufficiently long distance down the bed the amplitude approaches zero ($A \rightarrow 0$ as $z \rightarrow \infty$). An alternate choice of boundary conditions has been reported (7) leading to the same approximate solution as Equation (5) below. However, those conditions chosen here seem more suitable in view of bed continuity maintained across the boundaries used in these experiments.

Introducing complex notation, one

assumes a solution to Equation (1) of the form

$$\mathbf{x} = \mathbf{A}e^{i\omega t} \quad (3)$$

where \mathbf{x} is a complex mole fraction, the real part of which gives $x - x_M$, and \mathbf{A} is a complex amplitude containing in its real part both the amplitude and the phase shift compared with $z = 0$ of the concentration wave. Substitution of Equation (3) into Equation (1) yields an ordinary differential equation in \mathbf{A} and z which may be solved by standard methods. With the introduction of boundary conditions this solution is

$$\mathbf{A} = \mathbf{A}(0)$$

$$\cdot \exp \left[1 - \left(1 + \frac{4i\omega E_z}{U^2} \right)^{1/2} \right] \frac{Uz}{2E_z} \quad (4)$$

Expansion of the square root leads to the following approximate solution:

$$\mathbf{A} \approx \mathbf{A}(0) \exp \left[-\frac{i\omega z}{U} - \frac{\omega^2 E_z z}{U^3} \right] \quad (5)$$

Equation (5) is valid if the group $5\omega^2 E_z^2 / U^4 \ll 1$. The maximum error in amplitude due to the use of Equation (5) in the present experimental work is 1.4%, well within the error of measurement.

Several pertinent dimensionless groups are defined as follows: dimensionless bed length $L/d_p = L$, where L is the bed length and d_p the particle diameter; dimensionless frequency number $d_p \omega / U = N_f$; and Peclet number, $d_p U / E_z = N_{Pe}$. Using these groups, substituting Equation (5) into Equation (3), and taking the real part yields

$$x(L) \approx x_M + A(0) \exp \left[-\frac{N_f^2 L}{N_{Pe}} \right] \cdot \cos(\omega t - N_f L) \quad (6)$$

$x(L)$ is the mole fraction at bed length L , $N_f L = \phi_{rate}$ is the phase shift referred to the bed entrance, and $A(0) \exp [-N_f^2 L / N_{Pe}] = A(L)$ is the amplitude at bed length L . The ratio of outlet to inlet amplitudes leads to the equation

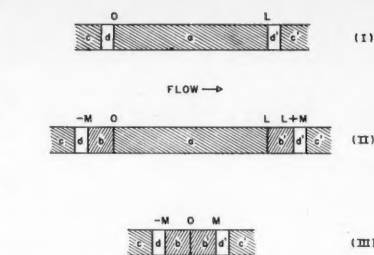
$$\frac{A(L)}{A(0)} \approx \exp \left[-\frac{N_f^2 L}{N_{Pe}} \right] \quad (7)$$

or

$$-\ln \left[\frac{A(L)}{A(0)} \right] \approx \frac{1}{N_{Pe}} N_f^2 L \quad (8)$$

If the system is described by Equation (1) and the condition necessary to give Equation (5) is met, then a plot of $-\ln [A(L)/A(0)]$ vs. $N_f^2 L$ is a straight line through the origin, the slope being the reciprocal of the Peclet number.

Two methods for obtaining amplitude ratios for the reduction of data through Equation (8) were considered. The first is the direct method. In part I of Figure 1, devices for measuring the concentration of the flowing stream are placed at d



abb'cc': Packed Section
dd': Analytical Cell

Fig. 1. Experimental arrangement of end sections and test section.

and d' and the bed length between them, $0-L$, is the length used in Equation (8). The peak-to-peak concentration difference shown by device d is taken as the amplitude $A(0)$, at point 0, and similarly with respect to device d' and point L . In practice several difficulties were encountered in using the direct method. For the determination of the concentration at point 0 (or L), the measuring device must approach infinitesimal length in the direction of flow. If it does not, the concentration determined is an average over the length of the measuring unit. No technique for measuring gas-phase concentrations in a negligible length, say less than one packing-element diameter, was available which did not require removal of the packing in the interior of the measurement section. The resulting unpacked space undoubtedly influenced flow conditions immediately downstream of d and immediately upstream of d' , resulting in a false picture of the extent of axial mixing in an undisturbed section of packed bed. Finally, the boundary conditions associated with Equation (1) require a constant value of the diffusivity across the system boundaries. It is doubtful, however, that the mixing which occurs in the empty measuring sections can be described by Fick's Law, and, if it were the case, the diffusivity would not have the same value as in the adjacent packed sections.

To circumvent these problems the indirect method was developed. In this method concentration-wave-amplitude measurements are made at points removed from the system boundaries and experimentally determined corrections applied to the ratios in order to identify the true amplitudes at these boundaries. Figure 1, part II, shows schematically the arrangement for measurement at points remote from the test section a , and Figure 1, part III, the arrangement for determination of corrections. The theory of the indirect method is as follows. $A(z)$ is the concentration-wave amplitude as a function of dimensionless bed length z , M is the dimensionless length of sections b and b' , and ψ , a variable characterizing mixing in the analytical cells. The subscripts *in* and *out* refer to inlet

and outlet and subscripts a, b, b' refer to sections in position during measurements. Then

$$A(0)_{abb'} = f[A(-M)_{abb'}, \omega, M, U, \psi_{in}] \quad (9)$$

where f is an undefined function. If the system under consideration is linear (amplitude independent), then

$$A(0)_{abb'} = A(-M)_{abb'} f_{in}(\omega, M, U, \psi_{in}) \quad (10)$$

Similarly,

$$A(L+M)_{abb'} = A(L)_{abb'} f_{out}(\omega, M, U, \psi_{out}) \quad (11)$$

or

$$A(L)_{abb'} = \frac{A(L+M)_{abb'}}{f_{out}} \quad (12)$$

Therefore

$$\left[\frac{A(L)}{A(0)} \right]_{abb'} = \left[\frac{A(L+M)}{A(-M)} \right]_{abb'} \frac{1}{f_{in} f_{out}} \quad (13)$$

when the ratio of Equations (12) and (10) is taken. The amplitude ratio at the boundaries of the test section in Equation (13) is expressed in terms of the ratio of amplitudes at points upstream and downstream of the test section and a correction factor, $1/f_{in} f_{out}$.

If the test section a is removed, then the following equations hold for the arrangement shown in Figure 1, part III:

$$A(0)_{bb'} = A(-M)_{bb'} f_{in} \quad (14)$$

and

$$A(M)_{bb'} = A(0)_{bb'} f_{out} \quad (15)$$

or

$$A(0)_{bb'} = \frac{A(M)_{bb'}}{f_{out}} \quad (16)$$

Therefore, equating the right-hand sides of Equations (14) and (16) and rearranging yields

$$\frac{1}{f_{in} f_{out}} = \left[\frac{A(-M)}{A(M)} \right]_{bb'} \quad (17)$$

Then substituting Equation (17) into Equation (13) gives

$$\left[\frac{A(L)}{A(0)} \right]_{abb'} = \left[\frac{A(L+M)}{A(-M)} \right]_{abb'} \cdot \left[\frac{A(-M)}{A(M)} \right]_{bb'} \quad (18)$$

provided that frequency ω , velocity U , length of end sections M , and the analytical-cell mixing characteristics ψ_{in} and ψ_{out} are retained at constant values during the experiments with and without the test section in place. The first three

variables are under direct control of the experimenter. The mixing characteristics of the analytical cells depend on the geometry of the cells and flow conditions within them and presumably may be kept constant from experiment to experiment. Thus the natural logarithm of Equation (18) can be substituted into Equation (8) to obtain a value of the Peclet number which characterizes axial mixing in the test section free from end effects or anomalies due to unknown amounts of mixing in the regions of the concentration-measuring devices. This method of experimentation and calculation was used in the work reported here.

Axial Mixing in Packed Beds

Any type of mixing process which is found experimentally to obey Fick's Law may be thought of as taking place as a series of individual steps repeated a large

For n such mixers in series it may be shown (9) that for a sinusoidal input of amplitude A_0 to the first mixer, the amplitude ratio is given by

$$\ln \frac{A_n}{A_0} \approx -\frac{n\omega^2 L^2}{2U^2}, \quad \frac{\omega L}{U} \ll 1 \quad (20)$$

But

$$\lambda = \frac{L}{n} \quad (21)$$

Therefore

$$\ln \frac{A_n}{A_0} \approx -\frac{\omega^2 L^2}{2U^2}, \quad \frac{\omega L}{nU} \ll 1 \quad (22)$$

where A_n is the amplitude of the sinusoidal concentration wave leaving the n th mixer. Or, if $L = L/d_p$ is substituted,

$$\ln \frac{A_n}{A_0} \approx -\frac{N_f^2 L^2}{2n}, \quad \frac{N_f L}{n} \ll 1 \quad (23)$$

If it is assumed that perfect mixing

over the cross section of the flow system at the inlet and removed (e.g., by adsorption or chemical reaction) at the outlet. Second, a rapid gas-analysis system (3) was available which made possible measurements of concentration oscillations of as high as 20 cycles/sec.

Equipment

Figure 2 shows the flow system. Two gases pass through two stages of pressure regulation to rotameters. Needle valves downstream of the rotameters regulate gas flow to the concentration-wave generator. Leaving the wave generator, the mixed gas stream flows through a conical expansion section into the test column. Static pressure is adjusted with a valve beyond the column.

The gas pairs were hydrogen-nitrogen and ethylene-nitrogen. The electrical heater and room-temperature bath are used to bring the ethylene temperature, as measured by a thermometer in the gas line upstream of the flow meter, to within a few degrees

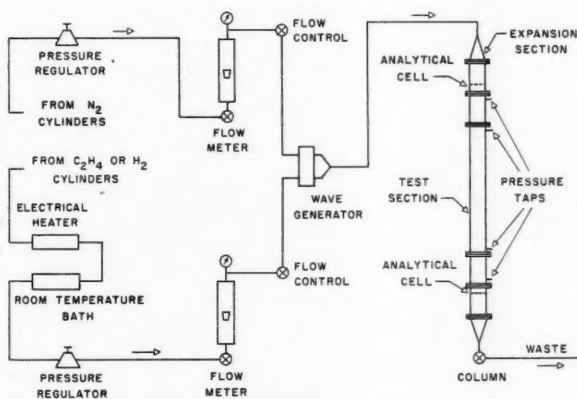


Fig. 2. Experimental flow system.

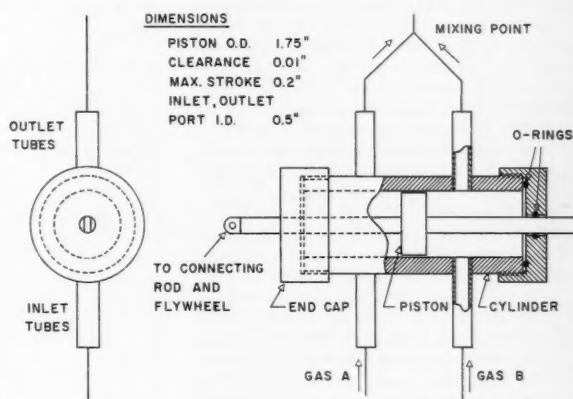


Fig. 3. Composition sine wave generator.

number of times. In molecular diffusion the individual step is the movement of a molecule along its mean free path, and in radial mixing in a packed bed it is the side-stepping motion of a parcel of fluid of uniform concentration as it encounters a packing element (8). It is useful to think of the individual step in the axial-eddy-diffusion process as a complete mixing, such as would be approached in a well-stirred vessel.

The similarity between the frequency response of a series of perfect mixers and of a system which combines plug flow and axial diffusion has already been considered by Kramers and Alberda (7). It is interesting to investigate this similarity more closely. The packed column may be considered to be divided into incremental lengths λ such that within each λ complete mixing occurs. The equation describing such mixing is

$$c_i = c_o + \frac{\lambda}{U} \frac{dc_o}{dt} \quad (19)$$

where c_i is the concentration at the beginning of length λ , c_o is the uniform concentration throughout λ , and λ/U is the average residence time for length λ .

occurs over the length represented by one particle diameter, then

$$n = L \quad (24)$$

and

$$-\ln \frac{A_n}{A_0} \approx \frac{N_f^2 L^2}{2}, \quad N_f \ll 1 \quad (25)$$

But the left-hand side of Equation (25) for the mixing model is identical with the left-hand side of Equation (8) for the differential equation solution. Therefore

$$N_{Pe}' = 2 \quad (26)$$

when complete mixing is achieved at every particle position down the tube. It will be shown that this value of N_{Pe}' is secured quite closely through experiment.

EXPERIMENTAL

A frequency-response method was chosen for the measurement of axial mixing for two reasons. First, this technique offers advantages of simplicity over two other possible choices, namely, measurement of the response of the flow system to a concentration step function, in which the production of a sharp step exactly at the bed entrance is difficult, or measurement of axial mixing in the steady state, in which a tracer material must be introduced uniformly

of room temperature. Joule-Thomson cooling is not so severe with nitrogen and hydrogen so that the length of copper tubing between the pressure regulators and the flow meter offers enough heat transfer surface to assure these gases being at or near room temperature.

In addition to pressure reducers on the gas cylinder, diaphragm pressure regulators are installed upstream of the flow meters. Thus the flow-meter pressure could be kept constant for the entire range of flows required in the experiments. The flow meters are rotameters in banks of two (overlapping ranges) for each gas stream. They were calibrated against wet-test meters and a certified dry-gas meter. Calibrations were run with the meters at the same pressure as used in subsequent experiments. Corrections for small variations in room temperature and atmospheric pressure were made as directed by the flow-meter manufacturer.

The concentration-wave generator, shown in Figure 3, consists of a piston driven by a connecting rod from an eccentrically mounted pin on a flywheel. A connecting rod of sufficient length to ensure sinusoidal motion is used. The flywheel has adjustable counterweights mounted on its periphery to provide dynamic balancing. A sliding bar carrying the crank pin is bolted to the flywheel face, allowing changes in amplitude

of the concentration wave. Through a variable-speed drive and interchangeable gears, a frequency range from a few cycles per minute to 30 cycles/sec. is available. Frequency is determined by timing a revolution counter geared to the flywheel shaft.

In operation, the motion of the piston, which does not travel far enough to reach the inlet and outlet ports, varies the capacity of the flow paths for the two gases in such a way that the concentration downstream of the mixing point is given by

$$x = x_M + \frac{\pi V f}{Q_T} \sin 2\pi f t \quad (27)$$

where x is the mole fraction of one gas in the binary mixture, x_M the mean mole fraction, V the volume displaced by a full stroke of the piston, f the frequency, Q_T the total volumetric flow rate, and t , time. Equation (27) was derived on the assumption of ideal gases. It was found that the amplitude of the concentration wave actually observed at the inlet of the test column was much less than $\pi V f / Q_T$. This decrease was thought to be due to mixing in the flow system between the generator and the column, especially at the point where the flow area increased as the $\frac{1}{8}$ -in. connecting line met the column. A special conical expansion section was provided to decrease this mixing as much as possible. Although the loss in amplitude necessitated construction of a wave generator with four times the theoretical displacement volume, mixing which occurred in the approach lines assured damping of higher harmonics that might be present in the wave.

The column is comprised of seven sections flanged together. Following the expansion section is a 4-in. length of 2-in. Pyrex pipe. This section and a similar one at the lower end of the column carry the analytical cells and are packed above the top cell and below the bottom cell with the same packing material as the test section. Electrical leads for each cell are brought out between two layers of sheet rubber serving as gasket material for the upper and lower flanges. Coating the rubber with silicone fluid prevented current leakage to the grounded flanges due to moisture picked up from the surrounding air. Similar gasket material of single thickness is used for the remaining flanges.

The test section and the sections above and below it are made of 1.94-in. I.D. brass tubing. These three sections correspond to sections a , b , and b' in Figure 1. The length of b and b' is 0.5 ft., and test sections of 0.92, 1.99, and 2.91 ft. are available. Glass spheres 0.127 in. in diameter are used as packing for all sections. Micrometer measurements on sixty beads gave a standard deviation of 0.005 in. Fraction voids, as measured in the same column, are 0.388. The same method of packing, i.e., pouring a small volume of beads and tapping the column to promote settling, was used each time the column was repacked. A machined grid at the lower end of the bottom 6-in. section supports the packing, and a heavy screen held in place by a spring clip at the upper end of the top 6-in. section keeps the top level of the packing constant between repackings. No screens are used between the end sections and the test section and gaskets are cut to maintain a smooth wall across the

joint. Pressure taps, located as shown in Figure 2, are connected to mercury manometers reading static pressure at the points indicated. Pressure drop across the test section could be correlated by use of Ergun's equation (5).

The rapid gas-analysis system used has been described in detail elsewhere (3). A radium- D source of alpha particles rolled onto a silver strip serves as one electrode of an ionization chamber. The strip is mounted axially in a brass cylinder, which is the other electrode and through which the gases to be analyzed flow. When a voltage is applied to the electrodes, an ion current flows which is directly proportional, over a short composition range, to the mole fraction of one of the gases in the mixture. A 100-megohm resistor between the center electrode and ground provides a voltage drop proportional to the current. Since the output impedance of the cell-resistor combination is very high, an impedance-matching circuit must be inserted between the resistor and a conventional cathode-ray oscilloscope. The circuit used in the triode-follower of Krakauer (6), with a balancing cathode-follower added to provide zero shift and minimize drift due to plate and filament battery-voltage changes. The necessary high-input, low-output impedance is provided by this circuit, which also has a frequency response flat to greater than 2,500 cycles/sec. In order to prevent stray capacitance from harming the frequency response, the cell leads were kept short by mounting a separate triode-follower for each cell at the point on the column where the lead emerged. A switching circuit allows the output from either triode-follower to be displayed on either a Leeds and Northrup Speedomax recorder or a DuMont 304A oscilloscope. The change in output for a 10 mole % change in gas composition is about 0.3 volt for both gas systems used. A fixed resistor voltage divider is used to attenuate the input to the recorder, which has a maximum range of 0 to 20 mvolt.

A disadvantage of the analysis system is the presence of a large amount of random noise in the ionization current. Three possible causes of this noise may be listed: trickle currents leaking between the high-(-900 volts, outer electrode) and low-voltage (~-3 volts, center electrode) portions of the cell; actual fluctuations in concentration within the cell; and random emission of alpha particles from the source. The possible presence of the first cause was shown by purposely adding moisture to the cylinder gases normally used, which led to a tenfold increase in noise. However, careful drying of the gases gave no improvement in noise level over that found when the gases were used directly from their cylinders. A simple guard ring made of a layer of grounded metal foil inserted between the two layers of Teflon separating the center electrode from the arm holding it, which is part of the outer electrode, was unsuccessful in lowering noise. Thus the first possible cause is either not important or cannot be eliminated by simple measures.

That turbulent concentration fluctuations do occur in a flowing system which has concentration gradients is certain; however, the noise level and noise frequency were the same in a quiescent as in a flowing system, and so the second possibility was eliminated.

The third cause, which was thought to be the major one, also could not be eliminated simply. Stronger radium- D sources than originally installed, 2.5 vs. 0.5 curie., improved the signal-to-noise ratio somewhat but still left the high noise level shown in Figure 4. The resulting increase in signal strength, however, made it possible to use a band-pass filter between the triode-follower and the oscilloscope. The filter used is a Krohnkite ultralow-frequency model with continuously variable upper and lower cutoffs. For the present use both upper and lower cutoff are set at the concentration-wave frequency. Since the cutoffs are not sharp, this practice results in some loss of signal but also in almost complete elimination of noise, even that at frequencies near the signal frequency. Figure 5 is the wave of Figure 4 after insertion of the filter. Noise at the signal frequency could not, of course, be repressed by this method. Because of this limitation, at the higher signal frequencies some variation in observed amplitude from wave to wave was noted, necessitating the averaging of amplitudes over several waves as described below. Noise amplitude below about two cycles per second is negligible, resulting in waves of uniform observed amplitude as shown by the one cycle per second waves in Figure 5. It should be noted that the use of the band-pass filter eliminates higher harmonics from the observed wave that may actually be present in the concentration wave. This in no way invalidates its use as long as the flow system is described by a linear differential equation. By superposition theory each concentration-wave frequency is attenuated as if it were present alone. That the flow system is linear is assured by the results, below, of experiments carried out at different concentration-wave amplitudes.

A further property of the analytical system is its pressure dependence. The ion current is directly dependent on the stopping power of the gas, which in turn depends on the pressure at constant temperature. Thus at constant composition more current is produced from the inlet cell than from the outlet cell owing to pressure drop across the intervening column. The same is true, to a lesser extent, with regard to the difference in current for a given concentration difference. Since it is this difference that is used as a measure of the concentration-wave amplitude, it is necessary to calibrate the cells under the same pressure conditions as those to be met in any given experiment with sinusoidally varying concentration. The technique of this calibration is discussed below.

Procedure

The data required for the determination of the axial Peclet number at any given Reynolds number can be conveniently divided into two static (without imposed concentration waves) and two dynamic (with imposed concentration waves) experimental results.

Static calibrations were run both with and without the test section of the column in place, as the pressure drop between the inlet and outlet cells was different in the two cases. Calibration factors in terms of change in cell output per unit change in gas composition for the inlet cell divided by the same ratio for the outlet cell were

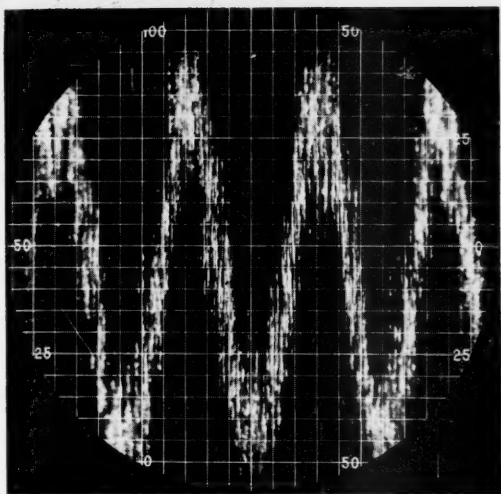


Fig. 4. Oscilloscope trace of one cycle per second concentration wave: unfiltered.

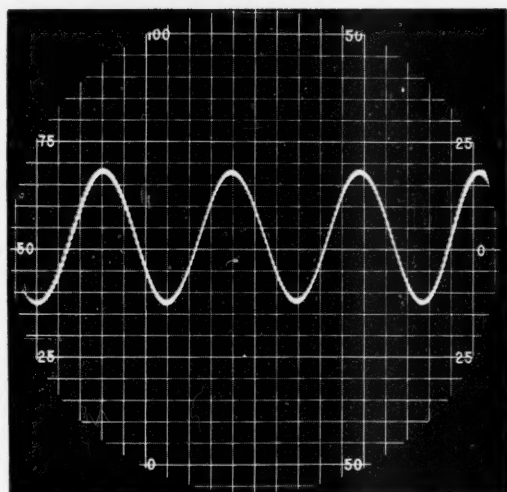


Fig. 5. Oscilloscope trace of one cycle per second concentration wave: filtered.

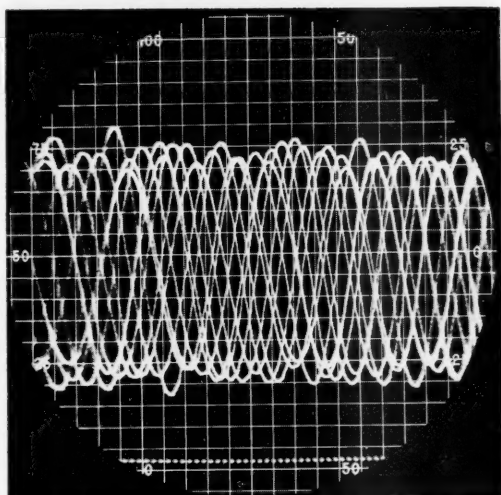


Fig. 6. Typical oscilloscope trace for concentration wave amplitude measurement.

obtained in the following manner. Flow rates of each of the two gases were set to the same value as that to be used in the succeeding dynamic experiment and the pressures of the two cells noted.

With the cell pressures kept the same by increasing the flow of one gas while decreasing the flow of the other, the gas composition was changed by roughly 5 mole % from the mean composition to be used in the dynamic

portion of the run. The output from each cell was set to near zero on the recorder. The gas composition was then adjusted, with the aid of the flow meters, to a value roughly 5 mole % on the other side of the mean. Since the change in gas composition was the same for both cells, dividing the output change for the inlet cell, as taken from the recorder chart, by the change for the outlet cell gave the desired factor. This procedure was repeated three times for each of the conditions (1) test section and end sections in place and (2) end sections only in place. The factors so obtained were always near unity and the 95% confidence limits for a typical mean of 3 were ± 0.04 . Scatter was due to analytical cell noise and a certain amount of amplifier drift which could not be eliminated.

Dynamic runs were made under the same two conditions of test section in place and no test section as were the static runs. Preliminary tests were made to determine the proper length of wave-generator stroke to give about 10 mole % peak-to-peak waves at the inlet cell. The concentration amplitude of the inlet wave was determined by comparing the wave height on the oscilloscope face with a rough calibration of the oscilloscope similar to the static cell calibrations. No record of the inlet amplitudes for any given frequency and flow rate was kept, as initial experiments showed the Peclet number to be independent of amplitude. A single run usually covered a range of flow rates and always included three or more frequencies at each flow rate. Data were obtained for the various frequency-flow combinations in random order so as to include any unknown time-dependent effects with the experimental error. Replicates of each combination were made in all runs to give a good measure of this error.

Dynamic run procedure was as follows. After a suitable warm-up of electronic components the cell outputs were switched to the oscilloscope and the band-pass filter was adjusted to the desired frequency. The wave generator was started and frequency set by means of a Strobotac. An initial reading of the revolution counter was recorded and the stopwatch started. Gas flow was adjusted and readings of flow meters, cell pressures, test-section pressures, and room temperature recorded. With the inlet-cell output shown on the face of the oscilloscope a photograph of the trace was taken. This was repeated for the outlet cell, flows were rechecked, and the final reading of the revolution counter and elapsed time were recorded.

Figure 6 shows a typical photograph of the oscilloscope trace. By operating the oscilloscope so that the signal was slightly out of synchronization with the sweep, multiple exposures could be made in which individual waves did not superimpose and could be picked out for amplitude measurement. In the section of Figure 6 covered by the center fifty horizontal units, twenty waves can be distinguished. Averaging the maxima and minima of these waves gives an average amplitude of 52 ± 1 at a 95% confidence level. The variation in amplitude from wave to wave is caused by random noise at the same frequency as the signal frequency.

As the phase angle does not contain the

diffusivity until higher order terms than those in Equation (6) are reached, phase-angle measurements do not provide an accurate method of determining axial Peclet numbers. However, in a few runs phase angles were measured as a check on the validity of Equation (6). Lissajous patterns on the oscilloscope were used in phase-angle determination. At a given flow rate frequencies were adjusted to give the easily discernible patterns of 90, 180, 270, and 360 deg. Frequency, flow rates, and pressures were recorded to allow calculation of phase angles for comparison with the measured angles.

Treatment of data consisted of the following three operations: calculation of Reynolds number, calculation of Peclet number, and, where applicable, calculation of phase angle.

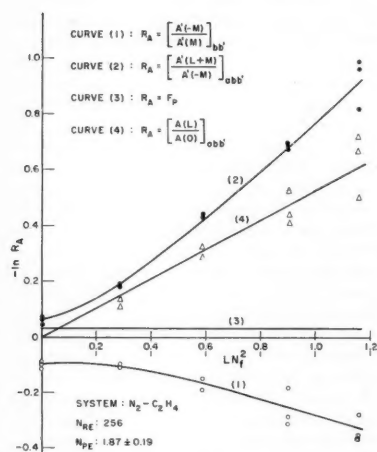


Fig. 7. Example of relative importance of various experimental corrections.

Reynolds number was calculated from the measured flow rates converted to mass velocity in the unpacked column, measured particle diameter, and viscosity as determined by the Wilke (11) correlation for gas mixtures. All values were taken at the mean gas composition.

Peclet number was calculated as follows. By comparison of the photographs of the traces from inlet and outlet cells amplitude ratios $[A(L+M)/A(-M)]_{abb'}$, from the portion of the run with test section in place, and $[A(-M)/A(M)]_{bb'}$, from the portion with only end sections in place, were determined for each frequency-flow combination. Since replicates of each combination were made, a pair of each of the ratios was calculated. Based on the original random order of data taking, a random choice of the two ratios to be used together as in Equation (18) was made. With this method of calculation a fair picture of the experimental error in both portions of the dynamic runs is reflected in the final Peclet numbers. Consistent use of the high values of one ratio with the low values of the other would have unduly minimized error, and pairing high with high and low with low would have increased the spread of Peclet numbers beyond the true error. To convert the amplitude ratios as measured

in oscilloscope units to the corresponding concentration ratios, use was made of the results of the static calibrations. The factor $[\Delta R_{in}/\Delta R_{out}]_{abb'}$, which is the change in recorder output for unit change in mole fraction for the inlet cell divided by the same ratio for the outlet cell, when multiplied by the measured amplitude ratio with the test column in place gives that amplitude ratio in concentration units. The similar factor from the static calibration with end sections only multiplied by the corresponding amplitude ratio gives that ratio in concentration units. In practice the logarithms of the two amplitude ratios were determined along with that of the pressure correction and the three added to give the desired amplitude ratio:

$$\ln \left[\frac{A(L+M)}{A(-M)} \right]_{abb'} + \ln \left[\frac{A(-M)}{A(M)} \right]_{bb'} + \ln F_p = \ln \left[\frac{A(L)}{A(0)} \right]_{abb'} \quad (28)$$

where

$$F_p = \frac{[\Delta R_{in}/\Delta R_{out}]_{abb'}}{[\Delta R_{in}/\Delta R_{out}]_{bb'}} \quad (29)$$

The use of recorder units in the case of the static factor and oscilloscope units in dynamic amplitude ratios is not inconsistent, as both measure voltage. The factor relating the two measurements is constant and cancels when used in ratios. The negative of the right-hand side of Equation (28) is the experimental ordinate of the plot described by Equation (8). The abscissa, $N_f^2 L$, was calculated directly from experimental values of flow rate, converted to velocity by use of the density of the mean gas mixture at the mean column pressure, frequency, particle diameter, and test-section length.

The plot of Equation (8) having been formed for each value of Reynolds number, the slope, $1/N_{Pe}$, and the 95% confidence limits on the slope were determined from a least squares fit of the data. Taking the reciprocal of the slope gives the Peclet number and expressing the confidence limits as percentage of slope equals percentage of Peclet number gives the limits on the Peclet number.

Runs involving phase-angle measurement were made before the indirect method of amplitude-ratio measurement was developed. This is not a drawback to the validity of the results, however, for two reasons. First, as has been mentioned, under the conditions in which the expansion of Equation (4) to Equation (5) is allowable, phase angle is not a function of axial mixing; hence the unknown amount of mixing caused by entrance and exit effects is not a factor. Second, a correction involving the transit time of a wave through the analytical cells can be applied to take into account the finite thickness of the cells. The objections to the use of the direct method which were raised in the case of amplitude determination are thus circumvented. Phase-angle calculations then simply involve comparison of measured phase angles with the calculated values, $N_f L$,

corrected for cell transit time. The correction is

$$\phi_{trans} = \frac{\omega L_c}{2} \left[\frac{U_{in} + U_{out}}{U_{in} U_{out}} \right] \quad (30)$$

where ϕ_{trans} is the phase angle due to transit time of one-half inlet cell + one-half outlet cell, L_c is the length of each cell, and U the velocity through the cell calculated from the flow rate and density at the cell pressure. Then

$$\phi_{calc} = N_f L + \phi_{trans} \quad (31)$$

RESULTS

The variables investigated in determining the correlation of Peclet number vs. Reynolds number and the ranges covered are shown in Table 1.

TABLE 1
VARIABLES INVESTIGATED

Variables of measuring technique	Range
1. Frequency	0.21-10.4 cycles/sec.
2. Amplitude	5 and 10 peak-peak mole %
3. Column length	0.92, 1.99, 2.91 ft.
Variables affecting axial diffusion	
1. Reynolds number	10.4-379
2. Gas system	C ₂ H ₄ -N ₂ , H ₂ -N ₂
3. Mean composition of gas	20, 50 mole % C ₂ H ₄ , 50 mole % H ₂

Factors affecting axial mixing which were held constant were column diameter, 0.161 ft.; packing type, spherical random; and packing diameter, 0.0106 ft.

Confirming Experiments

Several experiments were performed to check the validity of the use of an equation based on Fick's Law, Equation (1), to describe axial mixing in packed beds, and to determine whether the indirect method of amplitude ratio measurement summarized in Equation (18) was effective in eliminating end effects. The criteria for validity of Fick's Law were (1) linearity and zero intercept of the plot of $-\ln [A(L)/A(0)]_{abb'}$ vs. LN_f^2 , (2) independence of calculated Peclet numbers from initial concentration wave amplitude, Equation (1) being a linear differential equation, and (3) agreement between calculated and measured phase angles. Criteria for the soundness of the experimental method also included amplitude independence as well as independence of the Peclet number of the column length.

A typical plot of $-\ln [A(L)/A(0)]_{abb'}$ vs. LN_f^2 is shown in curve 4 of Figure 7. The actual variable in the abscissa is the frequency, as column length, particle diameter, and flow rate were kept constant throughout the experiment. The plotted points determining curve 4 result from the random combinations of

points at the same abscissa from curves 1 and 2, as mentioned above, plus the constant pressure and cell strength correction shown in curve 3. The results of the static calibrations for the flow conditions shown are plotted on the ordinate. Since the correction factor, F_p , is determined from the same static calibrations, addition of curves 1, 2, and 3 at the origin gives curve 4 a zero intercept by definition. For this reason no points are plotted for curve 4 on the ordinate and only the triangular points shown were used in checking the validity of Fick's Law.

A general equation for the best line through the ten points may be written:

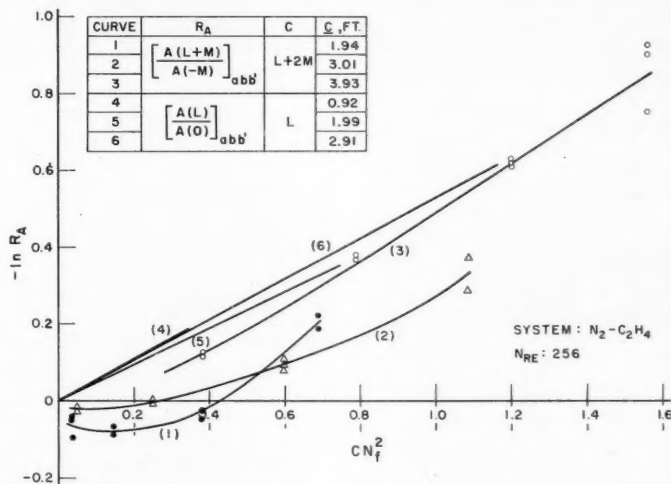


Fig. 8. Experimental demonstrations of effectiveness of correction for end effects.

$$-\ln \left[\frac{A(L)}{A(0)} \right]_{abb'} = a + b_1(LN_f^2) + b_2(LN_f^2)^2 + b_3(LN_f^2)^3 + \dots \quad (32)$$

where a, b_1, b_2, \dots are coefficients to be determined by least squares. Forming the least squares quadratic one obtains

$$-\ln \left[\frac{A(L)}{A(0)} \right]_{abb'} = -0.0313 + 0.543(LN_f^2) + 0.0275(LN_f^2)^2 \quad (33)$$

The linear regression line may also be determined:

$$-\ln \left[\frac{A(L)}{A(0)} \right]_{abb'} = -0.0432 + 0.583(LN_f^2) \quad (34)$$

And, finally, the best straight line through the origin is determined:

$$-\ln \left[\frac{A(L)}{A(0)} \right]_{abb'} = 0.536(LN_f^2) \quad (35)$$

An analysis of variance which tests the difference between deviations from the lines represented by Equations (33) and (34) against the deviations from the

quadratic indicates that the quadratic term is not significant at the 75% level. A similar test of the difference between deviations from Equations (34) and (35) against deviations from Equation (34) shows no significance of the nonzero intercept at the 75% level. The 75% confidence level was chosen rather than the more usual 95% level to ensure that if a quadratic term or a nonzero intercept were present in the data they would not be missed by requiring 95% certainty of their existence. Similar checks made on

all experiments substantiated the assumption that within the precision of the data the plots of amplitude ratio vs. LN_f^2 were linear with zero intercept.

A complete factorial design of experiments covering several initial amplitudes, the three available column lengths, and the entire Reynolds number range was not a feasible method of determining whether the assumptions of amplitude independence and column-length independence were valid. Instead, one experiment was designed to check the amplitude effect and another the column-length effect, both being run at the same Reynolds number. In addition, simultaneous checks were made on the effect of interchanging the two analytical cells, which are identical in dimensions and differ only in the strength of the radium-D alpha-particle sources, one being about 6% stronger than the other.

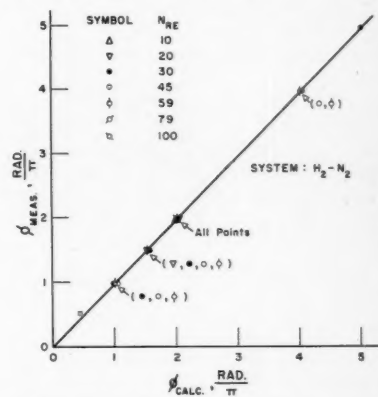


Fig. 9. Comparison of measured and calculated compositional phase angles.

Table 2 shows the results of the experiments designed to confirm the assumptions of the theory and the experimental method.

The details of statistical computations are reported elsewhere (9). The conclusion reached from the statistical calculations is that there are no significant effects of column length, initial amplitude, and analytical cell strength on the Peclet numbers determined in the runs shown in Table 2. All remaining runs were made with the longest column, approximately 10 mole % peak-to-peak initial amplitude, and analytical cells in the "normal" positions.

Figure 8 is another demonstration of the effectiveness of the correction for end effects embodied in the indirect method of amplitude measurement. Curves 1, 2, and 3 show the observed amplitude ratios plotted against N_f^2 times total column length (test section plus end sections) for the three columns used. These plots represent the data uncorrected for end effects. However, curves 4, 5, and 6 show the least square lines through the same data to which the corrections derived from measurements

TABLE 2
RESULTS OF CONFIRMING EXPERIMENTS*

Run	Amplitude†	Test-section length, ft.	Cell positions‡	Peclet number	Limits** on N_{Pe}'
E-34	High	2.91	Normal	1.32	± 0.12
E-35A	High	0.92	Normal	1.83	± 1.49
E-35B	High	1.99	Normal	2.14	± 0.42
E-37H	High	2.91	Reversed	2.14	± 0.27
E-37L	Low	2.91	Reversed	2.30	± 0.53
E-38	High	2.91	Reversed	2.28	± 0.26
E-40	High	2.91	Normal	1.87	± 0.19
			Mean	1.98	± 0.32 ††

* $N_{Re} = 256$, 20 mole % C_2H_4 in N_2 for all runs.

† High amplitude = approximately 10 mole % peak to peak. Low amplitude = one-half high amplitude.

‡ Normal = cell with stronger source at column inlet.

** 95% confidence.

†† Limits on a mean of seven runs.

with end sections alone are applied. The Peclet numbers listed in Table 2 for runs E-35A, E-35B, and E-40 were calculated from the slopes of curves 4, 5, and 6, respectively. It may be seen that the end-effect correction is greatest for the shortest column (cf. curves 1 and 4) and least for the longest column (cf. curves 3 and 6). This type of behavior is expected.

The effect of pressure drop and the resulting difference in mean gas density between inlet and outlet of the test section was not tested experimentally. However, an approximate solution of Equation (1) with sinusoidal boundary conditions in which the velocity U was replaced by G/ρ and ρ was allowed to vary with distance was formulated. No significant effect of pressure drop on amplitude ratio, for a given Peclet

Prime Results

The final correlation of Peclet number and Reynolds number is shown in Figure 10. The ordinate is Peclet number, written $d_p U/D + E$, where d_p is particle diameter, U is interstitial velocity, E is eddy diffusivity, either axial or radial, and D is molecular diffusivity. The ordinate is Reynolds number $d_p G_0/\mu$, where G_0 is superficial mass velocity, based on the empty-column cross section, and μ is viscosity. The choice of a log-log plot is based on ease of data presentation only.

Precision of the present data is indicated by a vertical line joining two plotted points which represent the 95% confidence limits on the Peclet number value for each experiment. The precision indicated is believed to be due primarily to random noise in the analytical system.

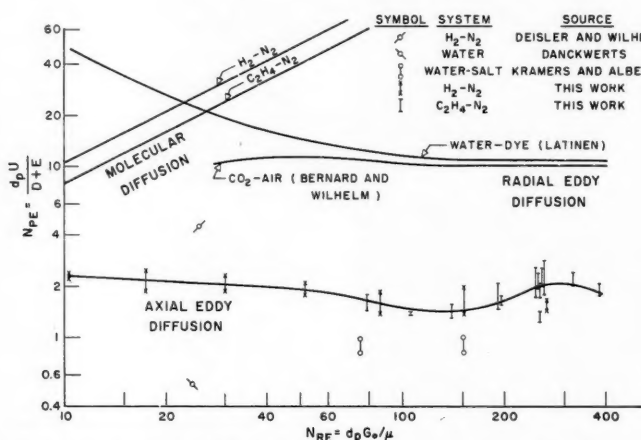


Fig. 10. Diffusion in packed beds in terms of Peclet number vs. Reynolds number.

number, in the range of pressure drops met with in the present work was found. (Maximum density difference between inlet and outlet of the test section was 14.5% for the H_2-N_2 system and 12.2% for the $C_2H_4-N_2$ system.) Hence, it is believed that pressure drop has no effect on the validity of the experimental method.

The final point in the proof of the validity of Fick's Law for packed beds is the correlation of measured and calculated phase angles in Figure 9. While the excellent agreement does not exclude the possibility that a packed bed follows a non-Fickian law, if it does follow Fick's Law the correlation is required.

The conclusions reached from the confirming experiments are these:

1. The experimental method provides reliable estimates of a parameter, the Peclet number, in the Fick's-Law equation for axial diffusion in a packed bed.
2. This equation, while giving no insight into the details of axial mixing, is a sufficiently precise means for describing the gross behavior of such a bed.

Each pair of points represents a determination of Peclet number based on a slope such as in Figure 7, and includes at least twelve amplitude-ratio measurements, six on test column plus end sections and six, for calibration purposes, on end sections alone. At least three different frequencies, with replication of each, were involved.

The effect of Reynolds number may be seen in the line drawn through the plotted points. The curvature shown is perhaps arbitrary. However, under the assumption that axial and radial mixing are similar processes a break in the curve in the 100 to 200 Reynolds-number range might be expected. An alternative procedure is to find the best straight line through the plotted points by least squares. This line is found to have essentially zero slope, and hence a mean of all values may be used. An exact statement as to the significance of this mean follows.

For twenty-one determinations of Peclet number in the Reynolds-number range from 10 to 400: $Pr (2.03 > \nu_{Pe} > 1.73) = 95\%$, where Pr is read as "the

probability of" and ν_{Pe} is the true mean of twenty-one determinations.

The effect of gas system may be noted by comparing the points shown for the two systems tested. In the Reynolds-number range where the data overlap, no significant difference exists between Peclet numbers for the 20 mole % C_2H_4 in N_2 and 50 mole % H_2 in N_2 systems. In addition, the Peclet number for the 50 mole % C_2H_4 in N_2 system was determined at $N_{Re} = 191$. It was found to be the same, within experimental error, as that for the 20% C_2H_4 mixture at $N_{Re} = 194$. The 50% C_2H_4 data were less precise because of a higher noise level in the analytical-cell output at the higher C_2H_4 concentration. It may be inferred that there is no major effect of gas composition on Peclet number. In comparing the two gas systems tested it is well to note that there is a fourteenfold density difference between nitrogen and hydrogen, whereas the densities of nitrogen and ethylene are the same. Thus any effects of density difference on axial mixing may be ruled out, at least in the overlapping Reynolds-number range. Extension of the correlation to untested gas pairs therefore may be made with more assurance.

DISCUSSION

A graphical comparison of data of three other investigators with present measurements of axial Peclet numbers is given in Figure 10. The experimental method of Deisler and Wilhelm (4) most closely approximates that of this work. The same analytical system as well as frequency-response technique was used. The axial Peclet number shown here was calculated from their value of D_L , the longitudinal diffusivity, measured over the Reynolds-number range from 3.8 to 48.4, and is plotted vs. the mean N_{Re} . In their work prime interest was in measuring the intraparticle diffusivity of porous pellets. The value of longitudinal diffusivity was a by-product of the main work and could be obtained only as a single value characteristic of a range of Reynolds numbers. It is believed that the present method, in which there is no added effect of porous packing, has more utility for axial-diffusion measurements as such.

Kramers and Alberda (7) also used the frequency-response method. In their system the sinusoidally varying salt concentration was followed by means of electrical conductivity. The packing consisted of Raschig rings and there was a particle-to-tube ratio of 0.13 and a length-to-diameter ratio of 4.6. The equation solved by these authors and its approximate solution were the same as Equations (1) and (6), respectively, although different boundary conditions were used. The Peclet numbers shown in Figure 10 were calculated from their values of D/Ud_p , where D is axial diffu-

sivity. The limits of accuracy and the Reynolds number range over which these authors state that the Peclet numbers are valid are shown in the figure. It would be fortuitous if these data, for a liquid system, agreed exactly with those for gas systems. However, it may be pointed out that it was found in the present work that short columns gave incorrect results owing to end effects. In addition, the high particle-to-tube ratio and the hollow packing might lead to extensive by-passing. The effect of by-passing would be to show more axial mixing and hence a lower N_{Pe} than was found in the present investigation.

The value of Peclet number for a Reynolds number of 24 calculated from the data of Danckwerts (2) also is shown. In Danckwerts's work an equation similar to Equation (1) was solved for a concentration step introduced at zero time at the inlet of the bed. Axial diffusivity could then be calculated by matching experimental outlet concentration vs. time curves with those given by the solution to the equation. The lack of agreement between these and present data may be due to differences in system alone. Here too, however, Raschig rings were used in a column of such size that the particle-to-tube ratio was 0.20. By-passing might account for the low value observed.

It is interesting also to compare axial mixing with the data in the literature on radial mixing. A radial Peclet number of about 12 in the Reynolds-number range from 100 up has been found by several investigators, and curves for two cases (1, 8) are shown in the figure. Present data indicate that axial mixing is about six times as efficient as radial mixing in a packed bed. It is presumed that axial mixing is the consequence of more complex events, such as local trapping, by-passing, acceleration, and deceleration, than the stream-splitting, or "random-walk," mechanism that has served well in explaining radial mixing. Implications of more efficient axial mixing to the designer of chemical reactors are, however, apparent. In most reactor designs axial diffusion is neglected because axial gradients are not steep. This may, in some cases, be an unsafe assumption, as even a small gradient multiplied by a large coefficient in a differential equation can lead to an important element in the solution of the equation.

The curves for molecular diffusion for the two gas systems make up the final portion of Figure 10. These curves serve to point out the greater than thirtyfold increase in axial mixing efficiency for a turbulent system in the N_{Re} range from 100 up. If other effects, such as natural convection, could be eliminated at very low flows, it would be expected that the curves for eddy and molecular diffusion

would merge at a low value of Reynolds number.

A final comparison is made between the Peclet numbers obtained in this work and the number predicted when it is assumed that as each particle of packing is traversed complete mixing takes place. The excellent agreement found between the predicted value of 2.0 and the experimental of 1.88 ± 0.15 is suggested to provide a basis for still further and more detailed investigations of fundamental aspects of mixing.

An assessment of the importance of axial mixing in chemical reactors has not yet been completed.

ACKNOWLEDGMENT

The authors express their appreciation to the General Electric Company, the duPont Company, and the Shell Development Company for support of graduate fellowships during the course of this work.

The authors wish also to acknowledge with thanks guidance provided by Professor J. C. Whitwell in statistical aspects of the work.

NOTATION

Dimensions of the quantities listed are given as m = mass, l = length, t = time. Any consistent system may be used.

a, b_1, b_2, \dots	= coefficients in regression equations
c_1	= inlet concentration to perfect mixer, moles/l ³
c_o	= uniform concentration within perfect mixer, moles/l ³
d_p	= packing element diameter, l
f	= frequency, t ⁻¹
f	= function of
f_{in}	= function of for inlet analytical cell
f_{out}	= function of for outlet analytical cell
n	= number of perfect mixers in series
t	= time, t
x	= mole fraction
x_M	= mean mole fraction about which concentration oscillates
x	= complex mole fraction
z	= axial coordinate, l
A	= amplitude of concentration wave, mole-fraction units
A_n	= amplitude of concentration wave in n th perfect mixer of series, moles/l ³
A_o	= amplitude of concentration wave entering first perfect mixer of series, moles/l ³
A	= complex amplitude
D	= molecular diffusivity, l ² /t
E	= eddy diffusivity, l ² /t
E_z	= eddy diffusivity, axial direction, l ² /t
F_p	= pressure and cell strength correction for analytical system, dimensionless
G	= mass velocity, based on interstitial area, m/l ² t

G_o	= mass velocity, based on empty-column cross section, m/l ² t
L	= dimensionless bed length = L/d_p
L	= bed length, l
L_c	= length of analytical cell, l
M	= dimensionless length of end sections = M/d_p
M	= length of end sections, l
N_f	= frequency number = $d_p\omega/U$
N_{Pe}	= Peclet number, axial direction = $d_p U/E_z$
N_{Pe}	= generalized Peclet number = $d_p U/(E + D)$
N_{Re}	= Reynolds number = $d_p G_o/\mu$
Q_T	= total volumetric flow through wave generator, l ³ /t
R_A	= amplitude ratio, dimensionless
ΔR_{in}	= change in output of inlet analytical cell for unit mole percentage of change in gas composition, volts/mole %
ΔR_{out}	= ditto for outlet cell
U	= interstitial velocity, l/t
V	= volume displaced by full stroke of wave generator piston, l ³
λ	= length assigned to single perfect mixer, l
μ	= viscosity, m/l ² t
ν_{Pe}	= true mean axial Peclet number
ρ	= density, m/l ³
ϕ_{calc}	= calculated phase angle, radians
ϕ_{meas}	= measured phase angle, radians
ϕ_{trans}	= phase angle due to transit time of concentration wave through analytical cells, radians
ψ_{in}	= variable characterizing mixing in inlet analytical cell
ψ_{out}	= ditto for outlet cell
ω	= angular frequency, radians/t

Subscripts

a, b, b' = sections of column (Figure 1) in place when measurements are made

LITERATURE CITED

- Bernard, R. A., and R. H. Wilhelm, *Chem. Eng. Progr.*, **46**, 233 (1950).
- Danckwerts, P. V., *Chem. Eng. Sci.*, **2**, 1 (1953).
- Deisler, P. F., Jr., K. W. McHenry, Jr., and R. H. Wilhelm, *Anal. Chem.*, **27**, 1366 (1955).
- Deisler, P. F., Jr., and R. H. Wilhelm, *Ind. Eng. Chem.*, **45**, 1219 (1953).
- Ergun, Sabri, *Chem. Eng. Progr.*, **48**, 89 (1952).
- Krakauer, Stewart, *Rev. Sci. Inst.*, **24**, 496 (1953).
- Kramers, H., and G. Alberda, *Chem. Eng. Sci.*, **2**, 173 (1953).
- Latinen, G. A., Ph.D. dissertation, Princeton Univ., Princeton, N. J. (1951).
- McHenry, K. W., Jr., Ph.D. dissertation, Princeton Univ., Princeton, N. J. (1957).
- Ogburn, Hugh, Ph.D. dissertation, Princeton Univ., Princeton, N. J. (1954).
- Wilke, C. R., *J. Chem. Phys.*, **18**, 517 (1950).
- Rosen, J. B., and W. E. Winsche, *J. Chem. Phys.*, **18**, 1587 (1950).

Presented at A.I.Ch.E. Pittsburgh meeting

Heat Transfer to Non-Newtonian Fluids

A. B. METZNER, R. D. VAUGHN and G. I. HOUGHTON

University of Delaware, Newark, Delaware

This paper presents the first theoretical analyses combined with an experimental study of the variables controlling heat transfer rates to non-Newtonian fluids in the streamline-flow region. The theoretical analyses, for the limiting types of non-Newtonian materials, were related to the intermediate case of Newtonian behavior to form a coherent theory applicable to Newtonian and non-Newtonian fluids alike.

The experimental data covered Graetz numbers between 100 and 2,000 and were correlated with a mean deviation of 13.5%. The flow-behavior indexes of the three non-Newtonian fluids used varied from 0.18 to 0.70.

Some preliminary non-Newtonian results are presented on the problems of nonisothermal fluid-flow pressure losses and heat transfer outside the laminar-flow region. Further theoretical work is recommended in both these areas. Additional experimental data would be of value in all of the problems discussed.

The industrial importance of non-Newtonian behavior is generally known and the types of non-Newtonian behavior encountered have been discussed by many authors (1 and 13, for example); nevertheless, not a single proved method is available for prediction of heat transfer rates to highly non-Newtonian fluids such as viscous slurries, gels, and polymeric melts and solutions. The object of this investigation was to develop a quantitative understanding of at least a part of this problem. The streamline-flow region was chosen for study to enable a rigorous theoretical analysis and to take advantage of the usual high consistency of these materials, which make the streamline region of primary importance in many industrial applications.

It has been shown (13) that previous experimental work in the area of heat transfer to suspensions and other non-Newtonian materials may be divided into two categories.

One category consists of publications devoted to a study of suspensions of relatively inert (i.e., nonsolvated) solids or of dilute suspensions of other solids. The work of Miller (16), Orr and Dalla-Valle (18), and Winding and coworkers (23) and parts of the work of Bonilla and coworkers (2) and of Salamone and Newman (21) fall into this category. Such suspensions are usually nearly Newtonian in behavior; hence the peculiarities due to the non-Newtonian properties are difficult to evaluate experimentally. Most of these investigators made some attempt to consider this problem, but the purposes of their work usually did not include the presentation of broad defining equations which might apply to highly non-Newtonian systems as well as to the inert suspensions studied. Accordingly, this part of the prior art sheds relatively little light on the problem under consider-

ation here, although the publications are of considerable interest in the field for which they were primarily intended.

The second of the categories deals with empirical correlations of experimental data on more highly non-Newtonian systems. The publication of Chu and coworkers (5) and an appreciable part of the Bonilla et al. (2) and Salamone and Newman (21) data fall into this group. It has been shown elsewhere (12, 13) that the empirical correlations proposed by these authors are unrealistic and in two cases may even lead to prediction of negative heat transfer coefficients. Attempts to recorelate the experimental results (4, 13) have been only partially successful, possibly owing to limitations of the rheological data. Accordingly, prior to this work, reliable heat transfer estimates could be made only if an industrial problem dealt with one of the few fluids which have been studied experimentally. This would enable use of the raw data rather than of any correlation, but such estimates would, of course, be limited to the specific experimental conditions which had been studied.

As the over-all problem was not well understood, the need for as rigorous a theoretical approach as possible was indicated. Pigford (19) recently published the first theoretical study of heat transfer to non-Newtonians in the laminar-flow region. This work represents a generalization of Leveque's method (11) for predicting forced-convection heat transfer coefficients for Newtonian fluids.

Leveque's solution of the simplified Fourier-Poisson equation for heat conduction to a moving fluid assumes that the temperature-boundary layer for the important case of high mass flow rates through short tubes is confined to a thin region near the heated surface. In this region it may be assumed that the velocity varies linearly with the distance

from this surface. If this is true, the velocity distribution in this region may be represented by

$$u = \alpha(R - r) \quad (1)$$

where α is the velocity gradient at the wall. Leveque's final result was

$$\frac{h_a D}{k} = 1.615 \left(\frac{\alpha C_p \rho D^3}{8kL} \right)^{1/3} \quad (2)$$

For a Newtonian fluid $\alpha = 8V/D$ and Equation (2) reduces to the familiar Leveque solution where the term in brackets becomes the product of $4/\pi$ and the Graetz number.

For a non-Newtonian fluid the value of α differs from $8V/D$ but may be obtained from the Mooney-Rabinowitsch equation for flow in circular conduits (1, 14, 17, 20). Pigford has rewritten the Leveque equation in the form

$$\frac{h_a D}{k} = 1.75 \delta^{1/3} \left(\frac{w C_p}{kL} \right)^{1/3} \quad (3)$$

where

$$\delta = \frac{\alpha}{8V/D} \quad (4)$$

Physically the term δ represents the ratio of the velocity gradients at the walls of the tubes and hence is related to the ratio of the heat transfer rates for a non-Newtonian fluid compared with that for a Newtonian. Pigford (19) showed that this ratio may be evaluated as follows, if the basic assumptions of the Leveque approach are valid, For Bingham plastic fluids:

$$\delta = \frac{1 - \tau_y/\tau_w}{1 - 4/3 \tau_y/\tau_w + 1/3 (\tau_y/\tau_w)^4} \quad (5)$$

For pseudoplastic fluids:

$$\delta = \frac{3n' + 1}{4n'} \quad (6)$$

Evaluation of δ by means of Equation (6) actually does not require assumption of pseudoplastic-fluid behavior. The term n' is the flow-behavior index of the fluid (13, 14) and quantitatively defines the behavior of any type of non-Newtonian material. Accordingly, Equation (6) may be used with Bingham plastic and dilatant fluids as well as with pseudoplastics.

As the limiting cases of "infinite," or ultimate, Bingham-plastic or pseudoplastic behavior are approached, τ_y/τ_w

R. D. Vaughn is at present with Shell Development Company, Emeryville, California.

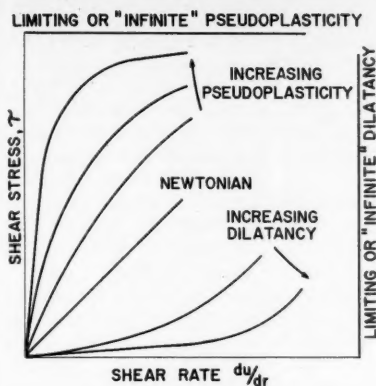
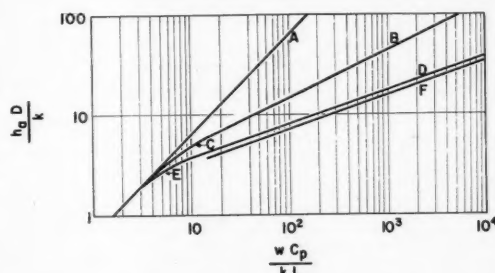


Fig. 1. Shear-stress-shear-rate diagram indicating various types of fluid behavior.

Fig. 2. Summary of theoretical heat transfer relationships for various types of fluid behavior; curve *CB*: plug flow ("infinite" pseudoplasticity); curve *ED*: parabolic velocity profile (Newtonian fluid); curve *F*: conical velocity profile ("infinite" dilatancy).



approaches a value of unity and n' approaches zero. Accordingly, the values of δ predicted by Equations (5) and (6) approach infinity, causing the heat transfer coefficients predicted by Equation (3) to do the same. The source of this difficulty lies in the assumptions underlying the Leveque approximation. In either of these limits, plug flow is approached (13, 22), and hence the region near the wall for which the velocity distribution may be assumed linear [Equation (1)] becomes smaller than the region in which there is a temperature gradient. Accordingly, the velocity gradient in the fluid near the wall has ceased to be a determining factor in the rate of heat transfer; hence the basic premise of the Leveque approach no longer is valid. In the limit of complete "plug" flow of the fluid the problem is identical to that of conduction into a solid cylinder initially at a uniform temperature. The rate of heat transfer in this case is determined solely by the rate of molecular conduction. As this can give only a finite rate of heat transfer, the foregoing equations rather evidently need some modifications near this limiting case of plug flow.

THEORETICAL DEVELOPMENT

In many studies of complex problems the mathematical equations describing the physical situation are too difficult to solve, and the number of simplifying assumptions necessary to obtain an

analytical solution may appreciably reduce the applicability of the results. A generally simpler and often as satisfying method of attacking such problems from an engineering point of view is to study the limiting cases which the problem may be shown to approach. This is the method of attack used in the present paper.

The limiting situations which encompass all types of steady state fluid behavior may be defined by reference to Figure 1. As a fluid becomes progressively more pseudoplastic, the shear stress-shear rate relationship progressively approaches the indicated horizontal line more closely. At this limit, the shear stress becomes independent of shear rate and the flow behavior index n' (13) approaches zero. At the other extreme of increasing dila-

ptic fluids would normally be reduced to conditions under which the time-dependent effects would no longer manifest themselves. Under such conditions design for these materials would be identical with the procedure outlined here for other types of non-Newtonian behavior.

The remainder of the theoretical development consists of two distinct steps: (1) development of theoretical equations for the cases of infinite pseudoplasticity ($n' = 0$) and infinite dilatancy ($n' = \infty$) and (2) development of a method of interpolation for cases of finite degrees of non-Newtonian behavior. This second problem is appreciably simplified by virtue of the extensive analyses available for the intermediate case of Newtonian behavior ($n' = 1.00$).

Infinite Pseudoplasticity

As the flow-behavior index n' decreases toward zero the velocity profile of a fluid flowing through a round tube progressively flattens until a perfectly flat profile or plug flow is reached at the limit of n' equal to zero (13, 22). A solution of the Fourier-Poisson heat-conduction equation for this limit was made by Graetz (7) and was reviewed in detail by Drew (6). This solution, shown as curve *C* of Figure 2, becomes unwieldy for values of the Graetz number (wC_p/kL) above about 500; however, for values of wC_p/kL above 100 an asymptotic solution extending the one given by Boussinesq (3) is possible (22). This solution may be written

$$\frac{h_a D}{k} = \frac{8}{\pi} + \frac{4}{\pi} \left(\frac{wC_p}{kL} \right)^{1/2} \quad (7)$$

and is shown as line *B* on Figure 2.

For values of wC_p/kL below about 5 the theoretical curves for plug flow approach the limiting case of an outlet fluid temperature equal to the wall temperature of the tube. This limit is shown as curve *A* of Figure 2 and may be described (12) by the heat-balance equation:

$$\frac{h_a D}{k} = \frac{2}{\pi} \frac{wC_p}{kL} \quad (8)$$

Infinite Dilatancy

For this case ($n' = \infty$) the velocity profile of a fluid flowing in a round tube is conical (13, 22). This velocity profile accordingly is especially well suited to the use of a Leveque-type approximation, as Equation (1) is obeyed at all radii. Placing $n' = \infty$ into Equation (6) and substituting the result into Equation (3) gives

$$\frac{h_a D}{k} = 1.590 \left(\frac{wC_p}{kL} \right)^{1/3} \quad (9)$$

This equation is shown as curve *F* of Figure 2.

A theory of heat transfer to Newtonian fluids in laminar flow was first given by Graetz (8). The assumptions upon which his solution is based, as well as the solution itself, are adequately presented by Drew (6), Jakob (10) and McAdams (12) and need not be repeated here. The resulting equation is plotted as curve *E* in Figure 2. Below Graetz numbers of about 3 the results are identical with curve *A*; i.e., the exit-fluid temperature approaches the wall temperature very closely.

Generally speaking, one is interested in high mass flow rates and relatively short tubes, i.e., in high Graetz numbers. For Graetz numbers above about 100 the Graetz equations become unwieldy. Leveque (11) noted this deficiency and proceeded to develop his asymptotic equation. An outline of the development and a thorough review is given by reference 6. Leveque's equation describing the transfer of heat to a Newtonian fluid flowing in streamline motion through round tubes is shown as curve *D* of Figure 2 and may be obtained by placing $\alpha = 8V/D$ in Equation (4) and substituting the result into Equation (3):

$$\frac{h_a D}{k} = 1.75 \left(\frac{w C_p}{k L} \right)^{1/3} \quad (10)$$

The equation most recently recommended by McAdams (12) for this situation (high Graetz number, laminar flow) is

$$\frac{h_a D}{k} \left(\frac{\mu_w}{\mu} \right)^{0.14} = 1.75 \left[\frac{w C_p}{k L} + 0.04 \left(\frac{D}{L} N_{Gr} N_{Pr} \right)^{0.75} \right]^{1/3} \quad (11)$$

Its similarity to the above Leveque equation is obvious. The viscosity-ratio term represents the familiar Sieder-Tate correction factor to account for the distortion of the assumed velocity distribution by the radial temperature gradient. Presumably a similar correction factor will be required in all the non-Newtonian work; this will be discussed later. The last group of terms on the right-hand side of Equation (11) corrects for changes in heat transfer rate due to natural convection currents caused by the temperature gradients. For the viscous gels studied in the present work, as with most non-Newtonian fluids likely to be processed in the laminar region, this term may be assumed negligible.

Pigford (19) has recently developed a series of equations which theoretically account for the effects of both natural convection and radial viscosity variations (due to the temperature gradient) upon the Newtonian heat transfer rate. The simpler empirical approach of the Sieder-Tate correction factor was used in this work, however, to avoid the mathematical complications due to these factors, and

the complex problem of non-Newtonian behavior were considered theoretically.

In summary of this section, the limiting cases of non-Newtonian behavior have been defined and the solution to the heat transfer problem corresponding to each has been given. A brief discussion was also devoted to the theory of heat transfer to Newtonian fluids as Newtonian behavior may be thought of as a special intermediate case of non-Newtonian behavior. The results are summarized in Figure 2. Heat transfer coefficients for all pseudoplastic and Bingham plastic non-Newtonian fluids should lie between the curves for a parabolic velocity distribution (AED) and those for uniform velocity distribution, or plug flow (curves ACB). Similarly, all coefficients for dilatant fluids should lie between curves AED for a parabolic velocity distribution and curve *F* for a conical velocity distribution. The remainder of this theoretical section will be devoted to finding methods of interpolating between

Inspection of these equations (or of curves *D* and *F* of Figure 2) shows that even in the case of infinite dilatancy $n' = \infty$ the heat transfer coefficient is still 90.9% of that for a Newtonian fluid at the same Graetz number. Experimental verification of Equation (12) for fluids of reasonable dilatancy (n' in the neighborhood of 2.0) is therefore probably impractical since the difference between the results for Newtonian and dilatant fluids is within the usual experimental error.

Below Graetz numbers of 20 an even closer similarity between heat transfer rates for Newtonian and dilatant fluids may be expected to exist. For this reason, the tentative design procedure for dilatant fluids at all Graetz numbers may be stated as

$$\delta^{1/3} = \frac{\left(\frac{h_a D}{k} \right)_{\text{dilatant}}}{\left(\frac{h_a D}{k} \right)_{\text{Newtonian}}} = \left(\frac{3n' + 1}{4n'} \right)^{1/3}$$

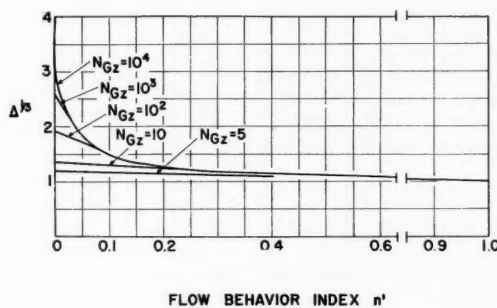


Fig. 3. Theoretical ratio of non-Newtonian to Newtonian heat transfer rates in laminar-flow pseudoplastic fluids.

these limiting cases for intermediate amounts of non-Newtonian behavior.

Dilatant Fluids ($1.00 < n' < \infty$)

Above a Graetz number of about 20 the Leveque approximation may be used to predict heat transfer rates for both Newtonian fluids ($n' = 1.00$) and infinitely dilatant fluids ($n' = \infty$) in laminar flow. Accordingly it is obviously a valid assumption that the same method may be used to calculate heat transfer coefficients within the entire region between these limits. From Equations (6) and (3), therefore,

$$\frac{h_a D}{k} = 1.75 \left(\frac{3n' + 1}{4n'} \right)^{1/3} \left(\frac{w C_p}{k L} \right)^{1/3} \quad (12)$$

or

$$\frac{h_a D}{k \delta^{1/3}} = 1.75 \left(\frac{w C_p}{k L} \right)^{1/3} \quad (13)$$

where

$$\delta^{1/3} = \left(\frac{3n' + 1}{4n'} \right)^{1/3} \quad (6)$$

Below Graetz numbers of about 20 this procedure is not exact but will probably be slightly conservative. Above $N_{Gr} = 20$ this relationship is identical to that given by Equations (12) and (13) and hence is indicated as being theoretically exact under these conditions.

Pseudoplastic Fluids ($0 < n' < 1.00$)

The problem in this case is one of interpolation between curves *C-B* ($n' = 0$) on one hand and curves *E-D* ($n' = 1.00$) on the other. For this purpose a correction factor Δ may be defined as follows:

$$\Delta^{1/3} = \frac{\left(\frac{h_a D}{k} \right)_{\text{non-Newtonian}}}{\left(\frac{h_a D}{k} \right)_{\text{Newtonian}}}$$

When $n' = 0$, $\Delta^{1/3}$ is given by the ratio of the ordinates of the aforementioned curves at any chosen value of the Graetz number. At values of n' close to unity, the value of Δ will coincide with that of δ as given by Equation (6), provided the Leveque approximation is also valid (N_{Gr} above about 100). Any method of interpolation between curves *CB* and *ED* must, therefore, satisfy the following

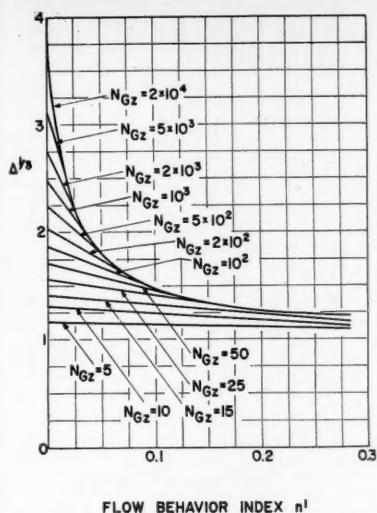


Fig. 4. Theoretical ratio of non-Newtonian to Newtonian heat transfer rates for extremely pseudoplastic fluids in laminar flow.

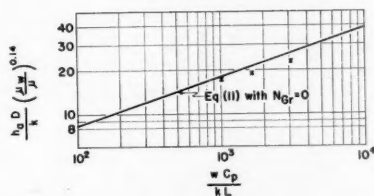


Fig. 5. Proof of equipment: comparison of Newtonian data with recommended (12) equation.

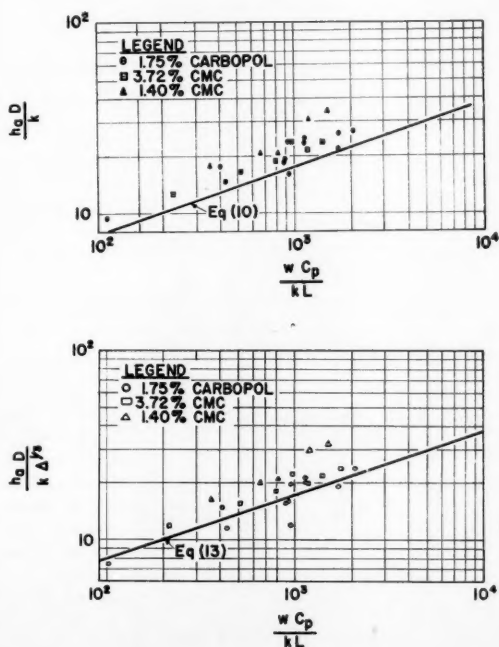


Fig. 6. Comparison of experimental non-Newtonian data with theoretical Newtonian curve.

Fig. 7. Comparison of data with theoretical curve for non-Newtonian fluids.

conditions: (a) the method must give the correct value of Δ when $n' = 0$ and (b) it must give $\Delta = \delta$ when n' approaches unity, where Equations (13) and (6) are known to be either rigorously valid or a very close approximation ($N_{Gz} > 100$).

The simplest possible interpolation procedure was arbitrarily chosen in this work; viz., a linear interpolation was made between the value of $\Delta^{1/3}$ at $n' = 0$ and the point at which this straight line first became tangent to $\delta^{1/3}$ at higher values of n' at selected values of the Graetz numbers. These interpolating curves are shown in Figures 3 and 4.

In Figure 3 the uppermost curve represents Equation (6) to an n' as low as 0.02; in Figure 4 the corresponding value of n' to which the Leveque theory is valid is about 0.01 at $N_{Gz} = 2 \times 10^4$.

The most significant conclusion indicated by these two figures is that at the higher Graetz numbers Equations (13) and (6) are valid to extremely low values of the flow-behavior index n' . Even at as low a value of the Graetz number as 100, the interpolation follows Equation (6) until n' drops below about 0.10. The importance of the assumed validity of a linear interpolation is therefore not critical in view of the small range of the flow-behavior index over which this is used. At lower values of the Graetz number, on the other hand, while the linear interpolation is used over a wide range of values of n' the value of $\Delta^{1/3}$ is so near unity that the exact choice of interpolation procedures is still not critical. The fact that high Graetz numbers and values of n' above 0.10 are usual

industrial practice means that only rarely will Figures 3 and 4 be used under conditions such that Equation (6) is not applicable. The chief value of Figures (3) and (4) may therefore be considered to be that of having defined the limits within which Equation (6) is valid.

The theoretical methods of predicting heat transfer coefficients for non-Newtonian fluids in laminar flow may be summarized as follows:

(a) For wC_p/kL above 100 and n' between 0.10 and infinity,

$$\frac{h_a D}{k} = 1.75 \delta^{1/3} \left(\frac{wC_p}{kL} \right)^{1/3} \quad (13)$$

where

$$\delta = \frac{3n' + 1}{4n'} \quad (6)$$

(b) For values of n' below 0.10 at all values of wC_p/kL , and for n' between 0.10 and 1.00 when wC_p/kL is below 100,

$$\frac{(h_a D/k)_{\text{non-Newtonian}}}{(h_a D/k)_{\text{Newtonian}}} = \Delta^{1/3}$$

where $\Delta^{1/3}$ is obtained from Figure 3 or 4. The term $(h_a D/k)_{\text{Newtonian}}$ may be obtained from Figure 2 under all conditions.

(c) If n' is above unity and wC_p/kL below 100, procedure b is also followed, but the correction factor is taken as

$$\delta^{1/3} = \left(\frac{3n' + 1}{4n'} \right)^{1/3}$$

This procedure appears to be rigorous down to values of the Graetz number of about 20.

These three alternatives encompass all ranges of Newtonian and non-Newtonian behavior considered in this paper. Most industrial problems may be expected to fall into procedure a.

As the foregoing theoretical conclusions have been based on a number of assumptions, experimental proof must be obtained to show their validity and to define the need for a Sieder-Tate type of correction factor. Since the equipment and materials used were chosen to simulate industrial practice, experimental data were obtainable to verify only the first of the three design procedures.

EXPERIMENTAL EQUIPMENT

A gravity-fed, variable-speed Moyno "progressing-cavity" type of pump was used in this work. Upon leaving the pump the fluid passed through an orifice mixer fitted with a thermocouple for temperature equalization and measurement. The mixer was followed in turn by a 20-diam.-long calming section and a 19-ft.-long heat transfer test section. This exchanger had an inside diameter of 1.368 in. and was surrounded by 3- and 5-in.-diam. copper water tubes. The inner annulus thus formed

served as a steam jacket for the test section itself and the outer annulus acted as an isothermal insulator since the same steam was admitted to both annuli. Upon leaving the test section the fluid was passed through a second orifice mixer for measurement of the exit-fluid temperature. Heat balances were obtained to check the measured temperature rise of the fluid against the rate of steam condensation. The wall temperature of the 1.368-in. test section was measured by seven thermocouples distributed along its length. This exchanger was generally similar to that described in detail by Bonilla and coworkers (2). Auxiliary equipment was conventional.

To measure the isothermal-fluid-flow properties, both a Stormer concentric-cylinder viscometer and a capillary-tube viscometer were used; both were calibrated with National Bureau of Standards oils. The capillary-tube viscometer was equipped with a constant-temperature bath to allow operation at elevated temperatures. Operating pressures were supplied by compressed nitrogen controlled by a Grove regulator and measured by calibrated laboratory-test pressure gauges. The Stormer viscometer was used primarily for purposes of comparison with the capillary-viscometer room-temperature results. Methods of converting these experimental viscometric data to the rheological parameters K' (or γ) and n' have been described elsewhere (13, 15).

The thermal conductivities of the fluids were measured by the steady state method with two chambers in series. The upper chamber contained the fluid of unknown conductivity and the lower a fluid of known conductivity (water). A thermocouple at the center of the plate below and above each cell indicated the surface temperature there. A constant-temperature bath above the two chambers supplied the heat flux which passed through the two chambers to an ice-water bath below. Downward heating was used to minimize convection effects. The entire apparatus was insulated and could easily be disassembled.

Fluid heat capacities were measured by adding a known amount of electrical energy to an insulated, agitated bath containing the fluid of unknown heat capacity in six 1-in.-diam. by 10-in.-long sample tubes. The rise in the temperature of the entire bath was measured by a calibrated thermometer and the heat capacity of the fluid calculated after subtracting the capacity of the bath (other than the sample fluid) as determined by calibration with water and checked with benzene.

Fluid densities were measured by a modified pycnometric method. Full experimental details are available (22).

RESULTS

Proof of the absence of unusual experimental conditions and of any calculational or procedural errors was obtained by first taking heat transfer data on molasses, a Newtonian fluid. Comparison of the experimental results with Equation (11) is shown in Figure 5. The maximum deviation of an experimental data point from the curve was -10%.

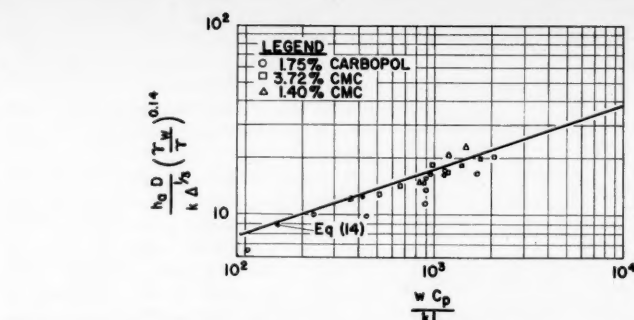


Fig. 8. Comparison of data with theoretical relationship after introduction of the Sieder-Tate correction factor.

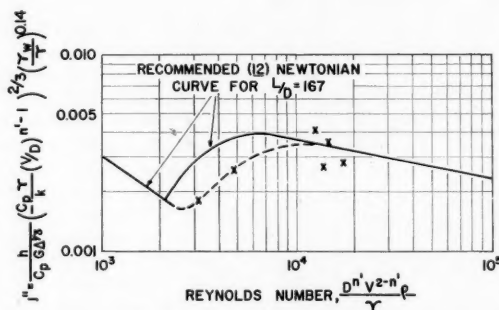


Fig. 9. Non-Newtonian heat transfer in the transition and turbulent-flow regions.

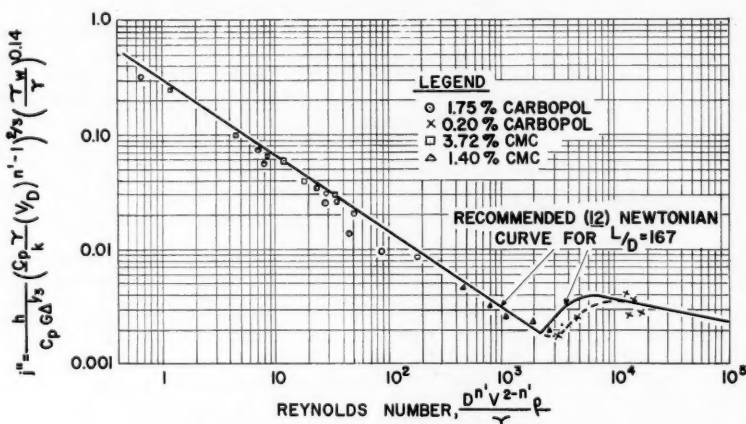


Fig. 10. Non-Newtonian heat transfer: summary and correlation of all data.

In view of the fact that maximum deviation of prior-art data was $\pm 30\%$ (12), it was concluded that all procedural details of the present work were entirely satisfactory.

Heat Transfer to Non-Newtonian Fluids: Laminar Flow

Heat transfer data were taken on the following three non-Newtonian fluids: (1) a 1.75% solution of Carbopol in

water (the flow behavior index n' of this fluid varying between 0.18 and 0.40, depending upon the temperature and shear rate), (2) a 3.72% solution of sodium carboxymethylcellulose (CMC) in water (n' varying between 0.43 and 0.51 for this fluid), and (3) a 1.40% CMC solution with a flow-behavior index of 0.70.

A plot of the original data on these fluids is shown in Figure 6. Since no factor is included here to correct for the

deviation of the fluids from Newtonian behavior, the data fall, as would be expected, considerably above the curve. Introduction of the correction factor $\Delta^{1/3}$ ($= \delta^{1/3}$), as in Figure 7, brings the data more nearly in line with the theoretical curve. There is still much scatter, however, the maximum deviations being +35 and -30%.

It is instructive at this point to compare these results with those reported for Newtonian fluids. McAdams (12), in reviewing the Newtonian data, has pointed out that the scatter in that case is as great as $\pm 100\%$. The causes of this great scatter are the distortion of the velocity profile and the free-convection effects resulting from the temperature gradient in the fluid. For fluids of high consistency, which certainly includes these highly non-Newtonian fluids, free convection effects are very small and may be neglected. The distortion of the velocity profile for Newtonian fluids is usually allowed for empirically by introduction of the Sieder-Tate viscosity ratio: $(\mu/\mu_w)^{0.14}$.

As will be shown later, the flow properties of the 1.75% Carbopol-water system were least dependent on temperature and the 3.72% and 1.40% CMC-water systems have an increasing dependence of the flow properties on temperature in the order given. Inspection of Figure 7 shows the trend of data away from the curve to be in the same order. These facts suggest that a correction factor analogous to the viscosity ratio (μ/μ_w) would aid in correlation of the data. The denominator γ of the generalized Reynolds number seems a plausible substitute for the viscosity of Newtonian fluids, as it uniquely defines the consistency of non-Newtonian fluids of any given flow-behavior index.

The data including the empirical correction factor $(\gamma/\gamma_w)^{0.14}$ are plotted in Figure 8. With the exception of a few of the points for the Carbopol-water system, this empirical correction factor adequately correlates the experimental results. Thus the final correlating equation (for wC_p/kL above 100) adopted in this work for both Newtonian and non-Newtonian fluids is

$$\frac{h_a D}{k \Delta^{1/3}} = 1.75 \left(\frac{wC_p}{kL} \right)^{1/3} \left(\frac{\gamma}{\gamma_w} \right)^{0.14} \quad (14)$$

For wC_p/kL below 100, the procedures previously outlined are recommended upon introduction of the $(\gamma/\gamma_w)^{0.14}$ term to account for distortion of the theoretically assumed velocity profile.

The significance of each of the non-Newtonian terms in Equation (14) has already been discussed. For Newtonian fluids, $\Delta^{1/3} = 1.00$, γ reduces to μ and γ_w to μ_w . Accordingly the foregoing equation reduces to the one usually recommended for this special case when natural-convection effects are absent.

The mean deviation of the non-Newtonian data from Equation (14) is 13.5%. The two points furthest from the curve were for those runs having the greatest error in the heat balances; hence the presence of some experimental errors is indicated. The fact that most of the

data points fall below the curve may be related to the fact that all heat transfer coefficients were based upon the input heat flux as measured by the steam-condensation rate. This was considered to be the most direct, hence accurate, procedure. Nevertheless, these values were usually somewhat lower than those calculated from the temperature rise of the fluid. In any case, all deviations are within experimental error and no adjustment of the curve is felt warranted on the basis of these data alone.

Heat Transfer Outside the Laminar Flow Region

It has been shown that the conventional Newtonian-friction-factor-Reynolds-number curve is useful for interpretation of non-Newtonian data upon generalization of the Reynolds number (14). More recently the utility of this generalized Reynolds number has been shown to extend to the problem of mixing-power requirements (15) as well. Its use in correlation of non-Newtonian heat transfer data is therefore suggested by the close analogy between these three problems for Newtonian fluids.

For the case of Newtonian heat transfer, the relevant dimensionless groups are the Reynolds number $(DV\rho/\mu)$, the Prandtl number, $C_p\mu/k$, and either the Nusselt (hD/k) or Stanton (h/C_pG) numbers. In addition the Sieder-Tate $(\mu/\mu_w)^{0.14}$ factor is required. Finally, the L/D ratio is important if data in the laminar and transition regions are considered.

Generalization of the foregoing dimensionless groups for applicability to non-Newtonian as well as to Newtonian fluids involves, in addition to the Sieder-Tate factor already considered, the Prandtl and Reynolds numbers—as both contain the Newtonian viscosity. Unquestionably, both may be used in their present form if a judiciously chosen apparent viscosity μ_a is used to replace the true Newtonian viscosity. A possible method of determining this apparent viscosity is to equate the Newtonian Reynolds number to the generalized one, as follows:

If

$$\frac{DV\rho}{\mu_a} = \frac{D^{n'} V^{2-n'} \rho}{\gamma}$$

then

$$\mu_a = \gamma(V/D)^{n'-1}$$

Substitution into the conventional Prandtl number gives

$$\frac{C_p \mu_a}{k} = \frac{C_p \gamma}{k} (V/D)^{n'-1}$$

Accordingly, the relevant non-Newtonian dimensionless groups become

the generalized Reynolds number:

$$\frac{D^{n'} V^{2-n'} \rho}{\gamma}$$

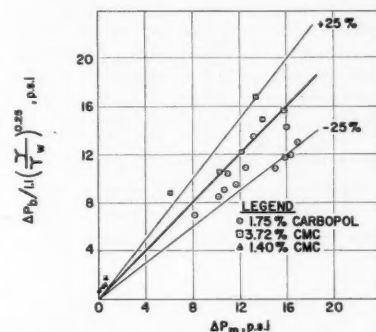


Fig. 11. Comparison of corrected bulk-temperature pressure drop with measured values.

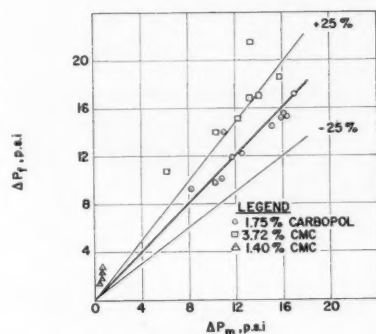


Fig. 12. Comparison of pressure drops calculated at the film temperature with measured values.

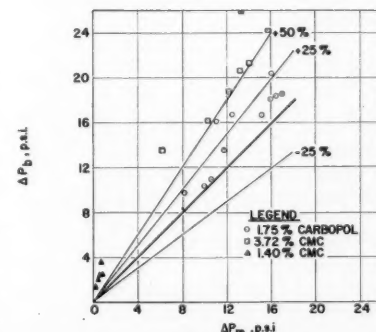


Fig. 13. Comparison of pressure drop calculated for isothermal conditions with non-isothermal measured values.

the generalized Prandtl number:

$$\frac{C_p \gamma}{k} (V/D)^{n'-1}$$

either the Nusselt or Stanton numbers:

$$\frac{hD}{k} \text{ or } \frac{h}{C_p G}$$

the dimensionless consistency ratio:

$$\frac{\gamma}{\gamma_w}$$

In the laminar and transition regions the L/D term as well as the correction factor $\Delta^{1/3}$ (or $\delta^{1/3}$) is also relevant. Presumably the latter would decrease in importance much as the L/D term as the flow becomes fully turbulent and the non-Newtonian fluid loses its peculiar identity.

If these generalizations are both valid and adequate, the functional relationships between the dimensionless groups must be the same as found in conventional Newtonian heat transfer. If this were not the case, the generalized correlations for non-Newtonian fluids would not reduce to the well-established Newtonian formulas upon substitution of $n' = 1.00$ (and $\gamma = \mu$) into the generalized Reynolds and Prandtl numbers. The only expected exception to this consideration would occur in the transition region, as it has been established (14) that the transition from laminar to fully developed turbulent flow is more gradual for highly pseudoplastic fluids, for example, than for Newtonians. For a fluid with a flow-behavior index of about 0.80, these considerations indicate a transition region extending to Reynolds numbers of about 10,000 although quantitative data are not available.

In order to preview this important problem of heat transfer outside the laminar region, a small number of data were taken with a dilute (0.2%) Carbopol solution having a flow-behavior index varying between 0.74 and 0.82. These data are shown in Figure 9 on a conventional j -factor-Reynolds-number plot using the aforementioned dimensionless groups. The solid line represents the conventional Newtonian relationship recommended by McAdams (12) and the dashed line is intended to represent a curve through the data points.

It is seen that the experimental data are in perfect confirmation of all the expected trends. The experimental errors (leading to a scatter of $\pm 20\%$) and the paucity of data, however, prevent any very firm conclusions. In particular, the flow-behavior index of the fluid was sufficiently high that the non-Newtonian correction factor $\Delta^{1/3}$ (Figure 3) could be taken equal to unity within experimental error; hence no information is available on its importance outside the laminar region.

Figure 10 summarizes all the experimental data on the conventional j -factor type of plot. In view of the good agreement between the theoretical analysis and the experimental data in the laminar region, heat transfer estimates may be made with considerable certainty here. Outside the laminar region the present results may be considered indicative primarily of a method of approach, which may be either refuted or confirmed by more extensive work. Up to Reynolds numbers of 15,000 to 20,000 Figure 10 may be used for order-of-magnitude estimates, however, and as such represents some improvement on the prior art.

Nonisothermal-pressure-drop Calculations

McAdams (12) suggests two methods for correlation of nonisothermal-pressure-drop data for Newtonian fluids.

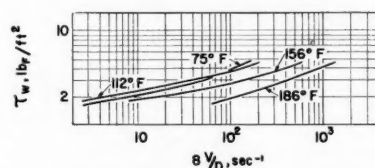


Fig. 14. Rheological properties of the 1.75% Carbopol-water system.

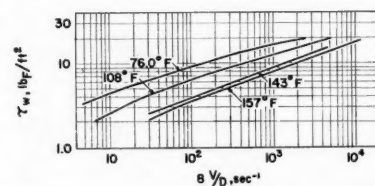


Fig. 15. Rheological properties of aqueous 3.72% CMC (sodium carboxymethylcellulose) solution.

The most recent edition of this book recommends that the actual pressure drop may be calculated from the usual laminar-flow equations upon substitution of the fluid viscosity at a film temperature defined by

$$t_f = t_b + \frac{t_w - t_b}{4} \quad (15)$$

The older second edition of this book recommended either use of this procedure or consideration of the pressure drop calculated at the bulk temperature as the product of the nonisothermal pressure drop and the factor $1.1 (\mu/\mu_w)^{0.25}$.

The results shown in Table 1 for the Newtonian fluid, molasses, indicate that neither method predicts the nonisothermal pressure drop very accurately, and these data accordingly leave little basis for choice of one method over the other.

For non-Newtonian fluids, the method corresponding to the first of these approaches involves evaluating the fluid consistency, γ and the flow-behavior index n' at the film temperature defined by Equation (15). These are then used with the generalized Reynolds number to calculate the friction factor or may be substituted directly in the generalized equivalent of Poiseuille's law (14):

TABLE 1.
NONISOTHERMAL PRESSURE-DROP DATA
FOR MOLASSES

Velocity, ft./sec.	Measured pressure drop, lb./sq. in.	Calculated pressure drop, lb./sq. in., with viscosity evaluated at film tempera- ture	Bulk viscosity divided by $1.1(\mu/\mu_w)^{0.25}$
3.22	2.6	2.2	2.4
1.90	0.5	1.0	1.2
5.82	4.5	3.3	3.4

I.D. of pipe: 1.368 in.
Distance between pressure taps: 19.07 ft.

$$\Delta P = \frac{32\gamma LV^{n'}}{g_c D^{n'+1}} \quad (16)$$

McAdams's older recommendation, involving the one-quarter power of the viscosity ratio, was adopted by calculating the bulk-temperature pressure drop by means of Equation (16) and dividing the result by

$$1.1 \left(\frac{\gamma}{\gamma_w} \right)^{0.25}$$

Figure 11 compares the results obtained upon calculating the nonisothermal pressure drop in the last manner with the actual measured pressure drop. Figure 12 shows a similar comparison for the case in which the calculated pressure drop was based upon Equations (15) and (16). The improvement obtained by either method may be noted by comparison with Figure 13, in which the calculated pressure drop was obtained by use of bulk-temperature physical properties. If one neglects the 1.4% CMC data, for which the measured pressure drops were too small to be determined accurately, all but five data points are within 25% of the 45° line of equivalence in both Figures 11 and 12. The mean deviation of the data from the line of equivalence is 14% in Figure 11 and 18% in Figure 12. Thus there is very little basis for choice of one method over the other; in general the data are overcorrected in Figure 11 and undercorrected in Figure 12. Fortunately the $\pm 25\%$ uncertainty in use of these methods, although large, is frequently not prohibitive.

As the problem of nonlaminar fluid pressure drop is not yet entirely clear for non-Newtonian fluids flowing isothermally, it is not fruitful to discuss noniso-

thermal flow outside the laminar region at this time.

Rheological Properties of Fluids Used

The fundamental flow groups for interpretation of the capillary-viscometer data, $D\Delta p/4L$ and $8V/D$, are plotted in Figures 14 to 17 for the four fluids used. To avoid confusion, the experimental

i.e. the liquid was slightly non-Newtonian at this temperature. At the higher temperatures used in the heat exchanger, however, no non-Newtonian behavior could be detected.

Other Physical Properties

The thermal conductivities of the four non-Newtonian fluids used ranged from

$$\frac{h_a D}{k \delta^{1/3}} = 1.75 \left(\frac{w C_p}{k L} \right)^{1/3} \left(\frac{\gamma}{\gamma_w} \right)^{0.14}$$

where

$$\delta = \frac{3n' + 1}{4n'}$$

As shown by Figures 8 and 10, this equation has been checked with three non-Newtonian fluids over the following ranges of variables:

$$n' : 0.18 \text{ to } 0.70$$

$$\frac{w C_p}{k L} : 100 \text{ to } 2050$$

$$N_{Re} : 0.65 \text{ to } 2100$$

The Newtonian equation recommended by McAdams (12) represents the special case obtained by substitution of $n' = 1.00$

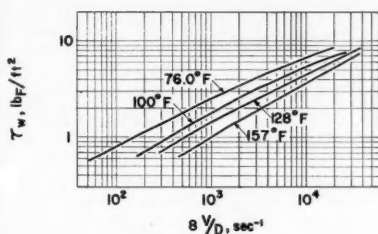


Fig. 16. Rheological properties of aqueous 1.40% CMC solution.

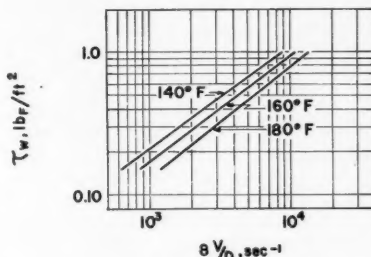


Fig. 17. Rheological properties of aqueous 0.20% Carbopol solution.

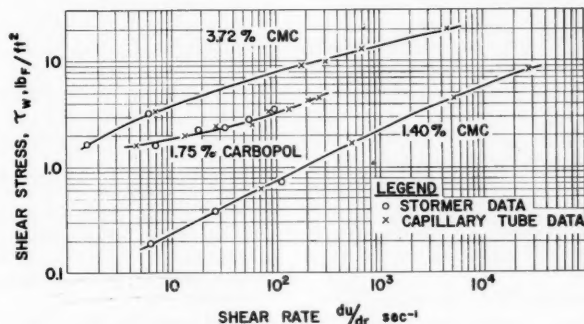


Fig. 18. Equivalence of rheological data as obtained with rotational and capillary-tube viscometers.

data points have been omitted. However, the individual curves are well supported in that the maximum deviation from any curve was only 14% and the mean deviation was less than 2%. On these logarithmic plots the slope of the tangent to the curve gives the value of the flow-behavior index n' at the particular value of $8V/D$ chosen.

In order to show the validity of the capillary-tube data, the 75° to 76°F. capillary-tube data for the three viscous fluids were compared with similar shear-stress-shear-rate data measured with a Stormer rotational viscometer by means of the usual relationships (13) for calculation of the shear rates. As Figure 18 shows, the agreement between the two viscometers is excellent.

Experimental viscosity data for the molasses used are shown in Figure 19. The three points shown at 72.5°F. correspond to three different shear rates;

the conductivity of water to as much as 25% below water. The heat capacities for these same fluids were found to be within 3% of the value for water at the same temperature. Since this was approximately equal to the reliability of the measurements, the heat capacity of water was used in the calculations. Similarly, the densities of the non-Newtonian fluids were found to be equal to the density of water.

SUMMARY

The recommended design procedure for calculation of laminar-region heat transfer coefficients for fluids in which natural-convection effects are not present may be summarized as follows:

1. For most fluids likely to be encountered (n' above 0.10) at reasonably high flow rates ($w C_p / k L$ above 100)

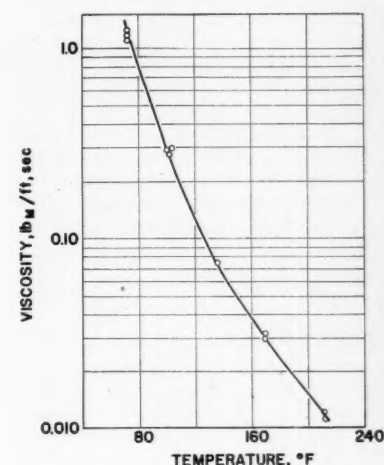


Fig. 19. Viscosity-temperature relationship for molasses.

($\delta = 1.00$ and $\gamma = \mu$) into the foregoing equation. The mean deviation of the non-Newtonian data from this equation was 13.5% and the maximum deviation 30%. These figures compare very favorably with those usually reported for Newtonian fluids.

2. For extremely highly pseudoplastic fluids (n' below 0.10) and for all pseudoplastics at low flow rates ($w C_p / k L$ below 100), the ordinate of curve AED of Figure 2 at any given value of the Graetz number is taken as equal to $[(h_a D) / (k \Delta^{1/3})] (\gamma_w / \gamma)^{0.14}$. The term $\Delta^{1/3}$ is evaluated from Figure 3 or 4.

3. For dilatant fluids the ordinate as read from curve AED of Figure 2 is equated to the quantity $[(h_a D) / (k \delta^{1/3})] (\gamma_w / \gamma)^{0.14}$, where $\delta = 3n' + 1/4n'$. At higher flow rates ($w C_p / k L$ above 100) this procedure is identical to that of part 1.

The procedures outlined under 2 and 3 have not been verified experimentally

but may be recommended as being at least good approximations in view of the excellent agreement between theory and experiment found in part 1. It should be noted that pseudoplastic and Bingham-plastic fluids have higher transfer coefficients in the laminar region than do Newtonians. The reverse is true for dilatant materials, for which, as a matter of fact, the foregoing recommendations predict heat transfer coefficients which are always within 10% of those for Newtonian fluids.

Heat transfer rates outside the laminar-flow region may be estimated from Figures 9 and 10. As the importance of the term $\Delta^{1/3}$ has not been established outside the laminar region, the conservative procedure of assuming it to be equal to unity for pseudoplastic fluids is recommended.

The usual Newtonian methods for nonisothermal-pressure-drop calculations in laminar flow may be applied to the non-Newtonian fluids studied with an accuracy of about $\pm 25\%$. No attempt has been made to predict nonisothermal pressure drops outside the laminar region.

Attention must be drawn to the strong need for additional data for all the problems discussed. In particular, the limitations of the present work are that only one tube size and length has been studied and all the data have been for heating of the fluids.

ACKNOWLEDGMENT

This work was started on funds provided by a duPont Fellowship and continued under sponsorship of the Office of Ordnance Research, U. S. Army. The Continental-Diamond Fibre Division of The Budd Company made available the Stormer viscometer used.

NOTATION

C_p = fluid heat capacity, B.t.u./
(lb._M)(°F.)
 du/dr = velocity gradient or shear rate,
sec.⁻¹ (du/dr)_i refers to the
shear rate at the (inner) bob of
a viscometer and (du/dr)_w to
the shear rate at the wall of a
tube
 D = tube diameter, ft.
 g = acceleration of gravity, ft./sec.
 g_c = dimensional conversion factor,
32.2 (ft.) (lb._M) / (sec.²) (lb._F)
 G = mass velocity, lb._M / (hr.) (sq. ft.)
or lb._M / (sec.) (sq. ft.) $G = V\rho$
 h = heat transfer film coefficient,
B.t.u. / (hr.) (sq. ft.) (°F.)
 h_a = a film coefficient based upon an
arithmetic-mean temperature
difference
 j'' = grouping of dimensionless terms:

$$j'' = \frac{h}{C_p G \Delta^{1/3}}$$

$\left[\frac{C_p \gamma}{k} (V/D)^{n'-1} \right]^{2/3} \left(\frac{\gamma_w}{\gamma} \right)^{0.14}$
 k = thermal conductivity, B.t.u. /
(hr.) (ft.) (°F.)
 K' = fluid-consistency index, (lb._F)
(sec.^{n'}) / sq. ft. If the fluid hap-
pens to be Newtonian $K' = \mu/g_c$
 L = tube length, ft.
 n' = flow-behavior index, dimension-
less. The numerical value of n'
lies between zero and unity for
pseudoplastic and Bingham-
plastic fluids, is equal to unity
for Newtonians, and is greater
than unity for dilatant fluids.
The flow-behavior index at a
given shear stress is equal to the
slope of the logarithmic curves
of Figures 14 to 17
 ΔP = pressure drop, (lb._F) / (sq. ft.) or
(lb._F) / (sq. in.). ΔP_b refers to a
pressure drop calculated at the
fluid bulk temperature, ΔP_f to
that calculated at the film tem-
perature, and ΔP_m to the
measured pressure drop
 r = radial distance, ft.
 R = radius of tube, ft.
 t = temperature, °F. (t_b denotes the
fluid bulk temperature, t_f the
film temperature, and t_w the
temperature at the wall.)
 Δt = temperature difference or driv-
ing force, °F.
 u = local velocity, ft./sec.
 V = average or bulk velocity, ft./sec.
 w = mass flow rate, lb._M / hr. or
lb._M / sec.
 α = velocity gradient at wall of tube,
sec.⁻¹
 β = coefficient of expansion, °F.⁻¹
 γ = fluid consistency, lb._M / (ft.)
(sec.^{2-n'}) γ_w refers to the term
evaluated at the wall tempera-
ture. $\gamma = g_c K' s^{n'-1}$. For a New-
tonian fluid, $\gamma = g_c K' = \mu$.
 δ = ratio of non-Newtonian to New-
tonian shear rates, $\delta = \alpha/8V/D$
 $= (3n' + 1)/4n'$ dimensionless
 $\Delta^{1/3}$ = ratio of non-Newtonian to New-
tonian heat transfer rates, di-
mensionless. In regions for
which the Leveque theory is
valid, $\Delta^{1/3} = \delta^{1/3}$.
 μ = Newtonian viscosity, lb._M / (sec.)
(ft.). μ_w denotes viscosity evalu-
ated at the wall temperature and
 μ_a the "apparent" viscosity of a
non-Newtonian fluid.
 π = 3.14 . . .
 ρ = density, lb._M / cu. ft.
 τ = shear stress, lb._F / sq. ft. τ_w de-
notes the shear stress at the wall
of a tube and τ_i that at a vis-
cometer bob.
 τ_y = yield value of a Bingham-plastic
fluid, lb._F / sq. ft.

Dimensionless Groups

N_{Gr} = Grashof number, $(\beta \Delta t D^3 \rho^2 g) / \mu^2$
 N_{Ga} = Graetz number, $w C_p / k L$

N_{Nu} = Nusselt number, taken as
 $hD/k\Delta^{1/3}$ or $hD/k\delta^{1/3}$ in the
laminar region. For Newtonian
fluids $\Delta^{1/3} = \delta^{1/3} = 1.00$; hence
 $N_{Nu} = hD/k$.
 N_{Pr} = generalized Prandtl number,
 $(C_p \gamma / k) (V/D)^{n'-1}$. For New-
tonian fluids $n' = 1.00$ and
 $\gamma = \mu$; hence $N_{Pr} = C_p \mu / k$.
 N_{Re} = generalized Reynolds number,
 $(D^n V^{2-n} \rho / \gamma)$. For Newtonians,
this reduces to $DV\rho/\mu$.
 N_{St} = Stanton number, taken as
 $h/(C_p G \Delta^{1/3})$ in the laminar re-
gion

LITERATURE CITED

- Alves, G. E., D. F. Boucher, and R. L. Pigford, *Chem. Eng. Progr.*, **48**, 385 (1952).
- Bonilla, C. F., Armando Cervi, Jr., T. J. Colvin, Jr., and S. J. Wang, *Chem. Eng. Progr. Symposium Ser.* No. 5, **49**, 127 (1953).
- Boussinesq, J., "Théorie Mathématique de la Chaleur," Bachelier, Paris (1835). See also reference 6.
- Branch, R. E., M. Ch. E. thesis, Univ. Delaware, Newark (1954) (described in reference 13).
- Chu, J. C., Frank Brown, and K. G. Burrige, *Ind. Eng. Chem.*, **45**, 1686 (1953).
- Drew, T. B., *Trans. A.I.Ch.E.*, **26**, 26 (1931).
- Graetz, L., *Ann. Physik*, **18**, 79 (1883).
- Ibid.*, **25**, 337 (1885).
- Hedstrom, B. O. A., *Ind. Eng. Chem.*, **44**, 651 (1952).
- Jakob, Max, "Heat Transfer," Vol. 1, John Wiley and Sons, Inc., New York (1949).
- Leveque, M. A., *Ann. Mines*, **13**, 201 (1928).
- McAdams, W. H., "Heat Transmission," McGraw-Hill Book Company, Inc., New York (2 ed.: 1942, 3 ed.: 1954).
- Metzner, A. B., in "Advances in Chemical Engineering," Vol. 1, T. B. Drew, ed., Academic Press, Inc., New York (1956).
- , and J. C. Reed, *A.I.Ch.E. Journal*, **1**, 434 (1955).
- Metzner, A. B., and R. E. Otto, *ibid.*, **3**, 3 (1957).
- Miller, A. P., Jr., Ph.D. thesis, Univ. Washington, Seattle (1953).
- Mooney, Melvin, *J. Rheology*, **2**, 210 (1931).
- Orr, Clyde, Jr., and J. M. DallaValle, *Chem. Eng. Progr. Symposium Ser.* No. 9, **50**, 29 (1954).
- Pigford, R. L., *ibid.*, No. 17, **51**, 79 (1955).
- Rabinowitsch, B., *Z. physik. Chem.*, **A145**, 1 (1929).
- Salamone, J. J., and Morris Newman, *Ind. Eng. Chem.*, **47**, 283 (1955).
- Vaughn, R. D., Ph.D. thesis, Univ. Delaware, Newark (1956).
- Winding, C. C., F. W. Dittman, and W. L. Kranich, "Thermal Properties of Synthetic Rubber Latices," Report to Office of Rubber Reserve, Cornell Univ., Ithaca, N. Y. (1944).

Presented at A.I.Ch.E. Los Angeles meeting

Spray-extraction-tower Studies

A. I. JOHNSON, G. W. MINARD, CHEN-JUNG HUANG, J. H. HANSULD, and V. M. McNAMARA

University of Toronto, Toronto, Canada

This paper describes further research on a 4-in. I.D. by 8-ft. spray tower of Elgin design. Previous work concerned limiting flow and holdup in this tower. Owing to its high capacity and low cost, the spray tower would have much greater commercial application in liquid-liquid extraction if its conditions of transient operation could be predicted and if it could be operated to yield low H_i values. This research attempts to show that transient conditions can be predicted and that low H_i values for both mass and heat transfer can be realized near the limiting flow conditions.

Theoretical equations for rate of approach to steady state derived and tested for the systems ethylene dichloride-water-propionic acid and ethylene dichloride-water-acetic acid show that the approach depends on the ratio of the phase flow rates. This study is important for the prediction of start-up time for industrial towers.

With the same systems the extraction capacity of the spray tower was investigated up to the condition of rejection. The results were correlated as K_{EA} and $H_{i,OE}$ vs. a function of the ratio of the phase flow rates. The dispersed-phase flow rate was found to have primary significance.

The heat transfer rates between water as continuous phase and solvents of various densities were correlated as H_i values plotted against a function of the ratio of the phase flow rates. The advantages of operation near rejection were demonstrated, and the effect of direction of heat transfer was found to be significant.

Continuous extraction utilizes the countercurrent flow under the influence of gravity of the two phases in a vertical tower. In industry this has usually been carried out in packed, baffled, or sieve-plate towers. Spray towers, which have no packing and in which one phase passes through the second as drops, have been the subject of several investigations (2, 3, 7, 8, 9, 12, 14, 16, 19, 20). Such

towers are inexpensive in construction and if operated near their flooding point have large throughputs and large interfacial areas.

This present discussion continues the first studies on the same apparatus, which were concerned with determining the conditions of flooding (16), and includes studies of the rate of approach to steady state along with extraction and heat

transfer investigations. The studies were directed especially at operations near limiting flow conditions.

Since the experimental work in this paper was completed, two excellent researches have been reported (8, 9). Both of these were for a much smaller diameter column, 2 in., compared with 4 in. for the present study. The experimental results of the study on the rate of approach to steady state are believed to be the first for extraction operations.

APPARATUS

The apparatus has been discussed elsewhere in detail (16) and will be treated only briefly here, with reference to the flow diagram, Figure 1, and the column diagram, Figure 2.

The column was of Elgin design (3), which has been used extensively for recent spray- and packed-tower work. The main dimensions are shown in Figure 2. The column proper was an 8-ft. section of standard 4-in. Pyrex pipe. The flanges were machined from cast iron, then were heavily nickel plated. All piping and supply tanks were copper.

Although the tower may be easily

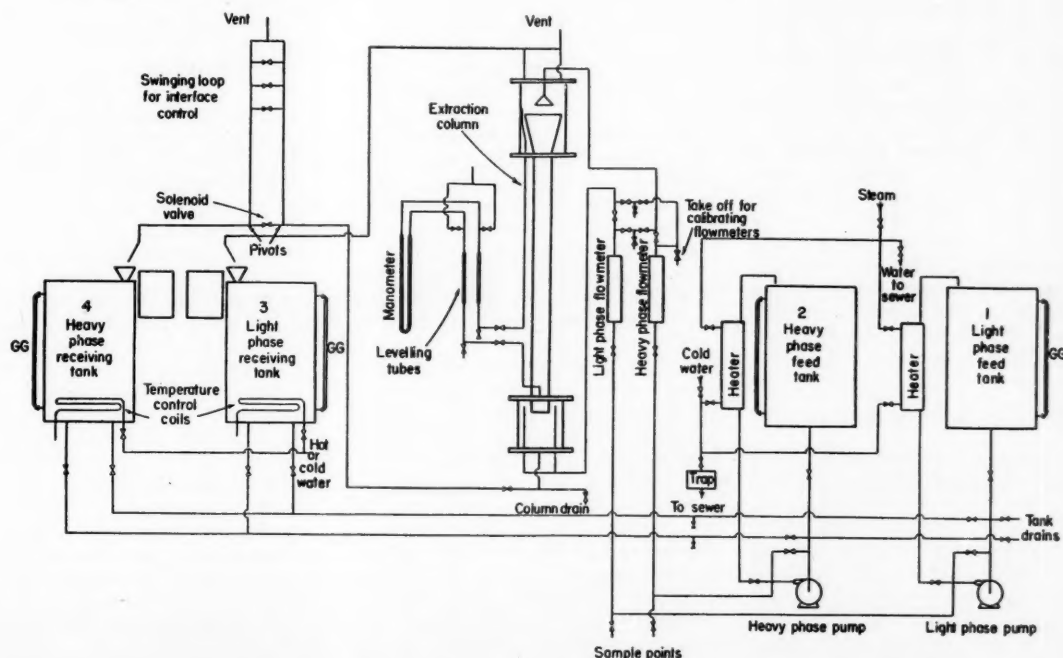


Fig. 1. Flow diagram for liquid-liquid-extraction apparatus spray-tower operation; heavy phase dispersed.

reversed, for all runs reported here the heavy phase was discontinuous. The dispersed phase enters through the spray nozzle in the upper spray section and enters the column proper through the conical entry piece. The drops of dispersed phase from the column proper settle in the lower chamber and are drawn off through the overflow loop. The continuous phase enters the column proper by means of the circular weir, passes countercurrent to the flow of dispersed phase, and overflows from the top of the column.

For studies of rate of approach to steady state and of mass transfer the feed and solvent solutions were made up in tanks 1 and 2, mixing and temperature adjustment being achieved by circulation of the liquid by the feed pumps through the small heat exchangers. The solutions were then pumped through the column at predetermined flow rates measured by the rotameters. The raffinate from the tower was collected in tank 4 and the extract was drained to the sewer. The unsteady state operation of the tower will be described in more detail later.

For the heat transfer studies tanks 3 and 4 were fitted with coils of $\frac{1}{2}$ -in. tubing. The heavy and light phases were circulated to and from these tanks where the heat exchanged in the column was added to or removed from the liquid as desired. The insulation and heating of the column for the heat transfer work are discussed in more detail later.

DEFINITION OF FLOODING AND REJECTION

In a spray tower of design similar to that used in this study the condition of flooding as originally defined by Elgin and Blanding (3) can be somewhat extended. Because there is a spray chamber and an entry cone of larger diameter than the tower proper, the bubbles of dispersed phase can entirely fill the entry cone and the tower will still operate smoothly even after flooding has occurred. On this basis Minard and Johnson (16) defined the absolute limiting flow as rejection, that condition at which the drops of dispersed phase overflow the entry cone into the annular space between the cone and the spray chamber. At this point the operation must be discontinued, as the annulus will soon fill with dispersed phase and eventually the drops will be prevented from forming properly at the spray nozzle or else they will pass off from the top of the tower with the continuous phase.

RATE OF APPROACH TO STEADY STATE

Most of the investigations in diffusional operations are concerned with the steady state condition, that is the condition when the operation of any equipment is independent of time. In any countercurrent mass transfer operation the initial concentrations of the exit streams will differ from the steady state conditions. The rate at which these concentrations approach the steady state conditions is of interest because in

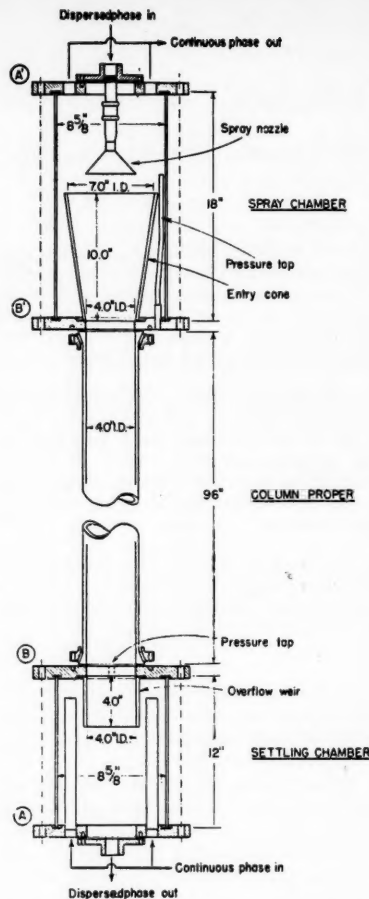


Fig. 2. Spray-extraction column; heavy phase dispersed.

determinations of apparatus efficiency the operation must be continued long enough to allow initial variations to disappear before final measurements are taken. In some apparatus it may not be feasible to achieve fully steady state conditions and some means of predicting the final steady state conditions from the transient conditions may be desirable.

The most advanced work in the field of unsteady state behavior in countercurrent operations has been done by Lapidus and Amundson (13), who considered the unsteady behavior of stage-wise absorption and extraction equipment for both cross-current and countercurrent flow. Their treatment was entirely mathematical and no experimental data were presented. They assumed that the plate-type absorber was fed with a fat gas stream and a lean oil stream at a constant rate of the inert material and that the compositions of the entering streams to an absorber were functions of time. In other words, although the previous works were based on the constant compositions of the streams entering the tower, they considered the problems of

unsteady feed concentrations. It was assumed further that initially any arbitrary composition can exist on the plate. Formulas were developed to show how the outgoing fat-gas and lean-oil compositions would vary with time. With these formulas, it is possible to compute the composition on any plate at any time for the countercurrent stagewise operation. A further mathematical treatment of transient behavior in stagewise operations which should be mentioned is that of Aerivos and Amundson (1).

The first part of the present study describes the development and testing of simpler formulas for differential continuous countercurrent extraction.

Theoretical Considerations

The method of attacking the problems involves first setting up simplified conditions which include the more important variables but disregard others and then applying material-balance equations. Since the terminal positions of the flows are fixed by the construction of the tower, it is apparent that the composition of the exit stream from a tower must be only a function of time. Flow rates of the two feed streams q_D for the dispersed phase and q_C for the continuous phase, in cubic feet per minute, will be considered to remain constant during the operation.

In order to simplify the problem, the time θ in minutes will be considered to be zero when the amount of the holdup of the dispersed phase in the column has reached a steady value. Then the amount of the holdup of the dispersed phase in the column will be constant during the operation because the flow rates are constant. Therefore any arbitrary compositions of the exit streams can exist initially because extraction has occurred to some extent during formation of the holdup in the column. It is assumed further that in this research the compositions of the two feed streams are invariable with time. As the mutual solubility between the solvent and the diluent is assumed to be zero, the amount of inert component in either the continuous or the dispersed stream is invariable in the process. Therefore the only variables with time are the concentrations of the two exit streams during the operation.

$C_{Ci}(\theta)$ and $C_{Di}(\theta)$ represent the time-dependent concentrations of the inlet continuous and dispersed phases, respectively, and $C_{Co}(\theta)$ and $C_{Do}(\theta)$ the equivalent concentrations in the outlet streams in pound moles of acid per cubic foot of phase at time (θ) , minutes. As mentioned above, the concentrations of the inlet or outlet streams are functions of the time only. The continuous phase is the extract phase for the runs to be described.

The net inflow of the solute component to the column at the moment (θ) may

be set equal to the rate of accumulation of the solute in the column. The resulting differential equation will be

$$q_D[C_{Di}(\theta) - C_{Do}(\theta)] + q_C[C_{Ci}(\theta) - C_{Co}(\theta)] = H \frac{d}{d\theta} [C_c(\theta)] + h \frac{d}{d\theta} [C_D(\theta)] \quad (1)$$

where H and h represent the steady state values of the holdup in the continuous and dispersed phases respectively, and $C_c(\theta)$ and $C_D(\theta)$ are the respective average column concentrations. In order to simplify the following equations all concentrations of either phase are to be read as transient concentrations; steady state values will be indicated as C' ; initial values will be denoted as $C(0)$ with the appropriate subscript.

In order to relate the two dependent variables C_{Do} and C_{Co} , linear equilibrium relationships will be assumed at any moment; that is,

$$C_{Co} = \alpha C_{Do} + \beta \quad (2)$$

Similarly for the average concentrations,

$$C_D = \gamma C_{Do} + \delta \quad (5)$$

$$C_C = \gamma C_{Co} + \delta \quad (6)$$

These assumptions will result in the expression

$$[q_D C_{Di}] + [q_C C_{Ci}] - [q_D C_{Do} + \alpha q_C C_{Do} + q_C \beta] = \gamma(H\alpha + h) \frac{d}{d\theta} [C_{Do}] \quad (7)$$

Substituting for the solute-free inlet concentration of continuous phase $C_{Ci} = 0$ reduces Equation (7) to a linear equation of the first order:

$$q_D C_{Di} - q_C \beta = [q_D + \alpha q_C] C_{Do} + \gamma(H\alpha + h) \frac{d}{d\theta} [C_{Do}] \quad (8)$$

This equation may be solved for C_{Do} thus:

$$C_{Do} = \left[\frac{q_D C_{Di} - q_C \beta}{q_D + q_C \alpha} \right] + [k e^{-B\theta}] \quad (9)$$

where $B = [(q_D + q_C \alpha) / (\gamma(H\alpha + h))]$ and k is the integration constant.

$$+ \left[C_{Do}(0) - \frac{q_D C_{Di} - q_C \beta}{q_D + q_C \alpha} \right] e^{-B\theta} \quad (11)$$

When operating conditions have reached steady state,

$$\frac{d}{d\theta} [C_{Do}] = 0 \text{ and } \frac{d}{d\theta} [C_{Co}] = 0 \quad (12)$$

Then C_{Do}' , the concentration of the exit dispersed (raffinate) phase at steady state, will be calculated from Equation (1) by substitution of Equation (12):

$$q_D [C_{Di} - C_{Do}'] + q_C [C_{Ci} - C_{Co}'] = 0$$

and by use of Equation (3) with $C_{Ci} = 0$,

$$C_{Do}' = \frac{q_D C_{Di} - q_C \beta}{q_D + q_C \alpha} \quad (13)$$

Introducing C_{Do} into Equation (11) gives

$$C_{Do}(\theta) = C_{Do}' + [C_{Do}(0) - C_{Do}'] e^{-B\theta} \quad (14)$$

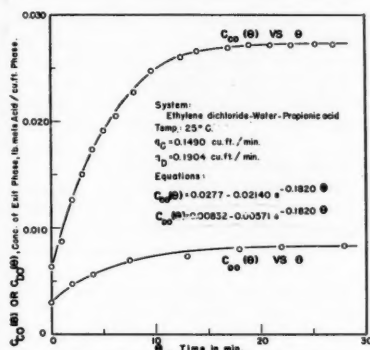


Fig. 3. Rate of approach to steady state.

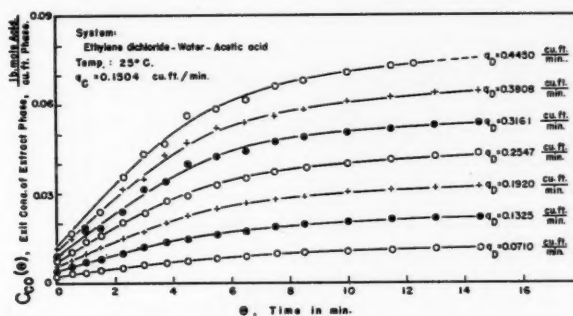


Fig. 4. Rate of approach to steady state.

$$C_C = \alpha C_D + \beta \quad (3)$$

These assumptions will result in the expression

$$q_D [C_{Di} - C_{Do}] + q_C [C_{Ci} - \alpha C_{Do} - \beta] = (H\alpha + h) \frac{d}{d\theta} [C_D] \quad (4)$$

Although the concentrations of the phases accumulated in the column are unknown, it has been assumed that the average concentration of each of these phases at any moment is a linear function of the instantaneous concentration of each exit stream from the tower. This may be expressed mathematically as

The integration constant k can be evaluated when the value of C_{Do} is known at $\theta = 0$:

$$k = C_{Do}(0) - \left[\frac{q_D C_{Di} - q_C \beta}{q_D + q_C \alpha} \right] \quad (10)$$

Here $C_{Do}(0)$, the concentration of the exit dispersed phase at $\theta = 0$, can be determined either by experiment or by computation from the linear relationship:

$$C_{Co} = C_{Do} + \beta$$

when C_{Co} is measured. Therefore, Equation (9) will become

$$C_{Do} = \left[\frac{q_D C_{Di} - q_C \beta}{q_D + q_C \alpha} \right]$$

Therefore

$$C_{Co}(\theta) = \alpha C_{Do}' + \alpha [C_{Do}(0) - C_{Do}'] e^{-B\theta} + \beta$$

$$C_{Co}(\theta) = C_{Co}' + [C_{Co}(0) - C_{Co}'] e^{-B\theta} \quad (15)$$

where C_{Co}' is the concentration of the outlet continuous (extract) phase at steady state.

Equations (14) and (15) determine the concentrations of the exit streams at any moment under unsteady state conditions for the postulated differential continuous countercurrent extraction. As shown, these equations involve the relationship between the concentrations of

the exit streams at any moment and their concentrations at steady state. Equation (13) shows that the concentration of the dispersed phase or the continuous phase at steady state varies with the flow rates of both streams. Then it may be concluded that the concentrations of the exit streams at any moment are influenced by the flow rates of both streams. Theoretically, these equations should be applicable right up to the limiting flow condition of the tower.

Method of Operation

The extraction tower system was operated as described in the general introduction for all the experimental runs made, the acid,

either propionic or acetic, being extracted from an ethylene dichloride solution by means of water. The spray nozzle used had ninety-seven holes each 0.120 in. in diameter.

For most runs tanks 1 and 3 were filled with water, the temperature in tank 1 being adjusted to exactly 25°C. by the water circulating through the heat exchanger, and in tank 3 by the solenoid valve and temperature control coils installed in that tank. Both of these tanks were used as light phase feed to allow a longer run time at high flow rates to ensure that the desired steady state conditions would be attained. Tank 2 was filled with ethylene dichloride, recovered from the previous run in tank 4, and the acid was added until the desired concentration was attained.

The temperature of this solution was adjusted to 25°C. in a manner similar to that used for the water in the tank.

The run proper began by filling the tower with water, the flow rate being adjusted to the desired value and maintained constant at the flow meter. As soon as water began flowing from the top of the tower to the sewer, the heavy phase was pumped to the top of the tower, its predetermined flow rate being quickly attained and maintained constant. The dispersed phase settled at the bottom of the tower and when the interface level had risen to the 3-in. mark on the scale, the settled liquid was drawn off at the bottom at such a rate that the interface level remained constant.

When the amount of the holdup of the dispersed phase in the column had reached a constant value, the sampling of the exit phases was started and continued at regular intervals until the run was ended. When the mass transfer between phases had reached steady state, the run was deemed complete. The time to start taking the first samples was arbitrarily taken as the time when the pressure difference across the column reached a constant value, because the pressure difference was assumed to be due only to the dispersed-phase holdup in the tower proper (16). In most runs approximately 1 min. was required for the holdup of the dispersed phase to reach a steady value after the first drops left the spray nozzle.

As steady state conditions were approached, there was less fluctuation in the flow-meter readings and in the level of the interface, until finally the apparatus ran virtually by itself. Terminal compositions of the extract and raffinate phases were determined by manual sampling, titrations being carried out against standardized sodium hydroxide solution by use of phenolphthalein as the indicator.

For each set of runs made, a constant continuous-phase flow rate was selected. The lowest dispersed-phase flow rate used was 0.0710 cu. ft./min. and this rate was increased run by run until rejection occurred or until the run time was so short that steady state conditions could not be attained. The higher the continuous-phase flow rate used, the lower the dispersed-phase flow rate required for rejection to occur. As soon as rejection occurred for one constant continuous-phase flow rate, a new rate was selected and another set of runs begun.

Discussion of Results

Running Log of Exit Streams Concentrations. The concentrations of the exit phases plotted against time for Run III-B-3 are shown in Figure 3, and the data are given in Table 1.* This information is typical of the results obtained. At the beginning of the extraction operation the plot exhibits the general appearance of an exponential curve, but as steady state is attained the curve becomes asymptotic to some value on the ordinate axis. The time necessary to reach this certain value is theoretically

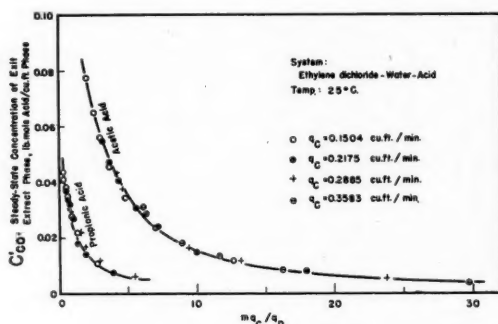


Fig. 5. Steady state concentration.

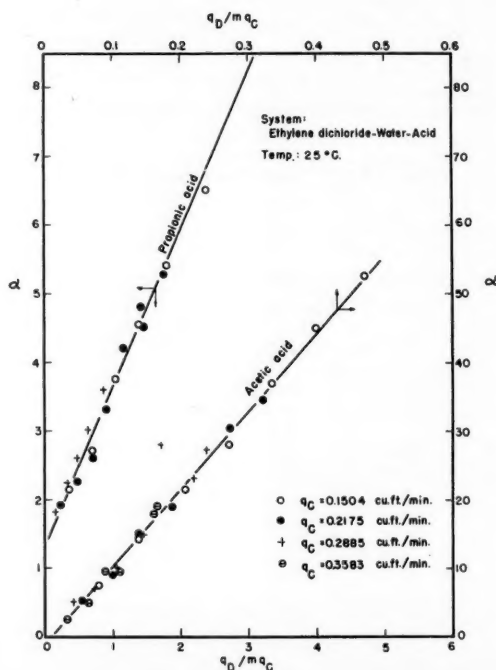


Fig. 6. Correlation of constant α .

*Tabular material has been deposited as document 5120 with the American Documentation Institute, Photoduplication Service, Library of Congress, Washington 25, D. C., and may be obtained for \$3.75 for photoprints or \$2.00 for 35-mm. microfilm.

infinite, as shown in Equations (14) and (15).

On the basis of the exit dispersed-phase composition, it requires about 6 min. to come within 5% of the steady state value. The equivalent time for the extract phase is 14 min. Before the concentration of the extract phase has reached a steady value, the concentration of the raffinate phase leaving the bottom of the settling chamber is approximately constant. This phenomenon can be explained by the fact that in the main body of the settled dispersed phase, mixing by

convection and turbulence is so rapid that the concentration of the solute is essentially uniform at all points. Thus, although raffinate droplets of varying composition are continuously reaching the surface of the settled dispersed phase, there is negligible effect upon the concentration of the raffinate leaving the bottom of the tower. This is probably the reason for the shorter time of transient behavior in the raffinate phase as compared with the extract phase.

Figure 4 shows curves of $C_{CO}(\theta)$ vs. θ employing a continuous-phase flow rate

of $q_C = 0.1504$ cu. ft./min. Each curve shows the transient behavior of the exit extract stream for a different flow rate of dispersed phase. For a constant flow rate of the continuous phase, the distance between the curves is proportional to the increase of the flow rate of the dispersed phase. The interval between any two adjoining curves is approximately constant because the flow rate of the dispersed phase was increased by the same amount for each run. When the operation approached flooding or rejection, the points deviated from the curve more than when the flow rate of the dispersed phase was low.

Proposed Correlation of Results.

GENERAL. There is no recognized way to correlate the experimental results under discussion. It is suggested, however, by analogy with relations developed for distillation and absorption that the constants α , β , and B in the theoretical equations and the steady state concentrations of exit phases C_{DO} and C_{CO} can be correlated with the relation obtained by multiplication of the slope of the equilibrium distribution line and the flow ratio of the two phases: $m(q_C/q_D)$. The equilibrium distribution data for the systems employed in this research are presented in Table 2.

STEADY STATE EXIT CONCENTRATION OF EXTRACT PHASE. The results shown in Figure 5 indicate that at steady state conditions the concentration of the exit continuous phase increases with increasing flow ratio of dispersed to continuous phases. The deviation of the observed value of the steady state concentration from that calculated from Equation (15) was within 5%. This implies the validity of the derived theoretical equations. The plot of C_{CO}' vs. $m(q_C/q_D)$ for both the systems studied as presented in Figure 5 produces a hyperbolic curve. From the graph the smaller the magnitude of the ratio $m(q_C/q_D)$ the higher will be the concentration of continuous phase leaving the top of the column. This concentration depends not upon the individual magnitudes of the flow rates but upon the relative ratio of the flow rates of the two phases. There is a practical limit to the individual values of q_C and q_D at the point of "rejection." Therefore it is suggested that the extraction operation should be carried out near this limiting flow condition with a low flow rate of continuous phase, in order to get a high concentration of exit continuous phase close to the equilibrium value C_{CO} .

EQUATION CONSTANTS. As originally postulated, Equations (14) and (15) are based on the assumption of a linear relation between the instantaneous concentrations of the extract and raffinate phases. A plot of $C_{CO}(\theta)$ against $C_{DO}(\theta)$ on ordinary coordinates produces an essentially straight line, an indication that the assumption is very nearly true. The constants α and β can then be deter-

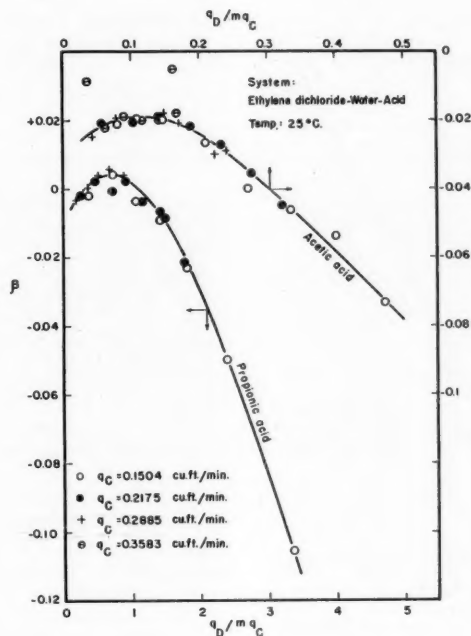


Fig. 7. Correlation of constant β .

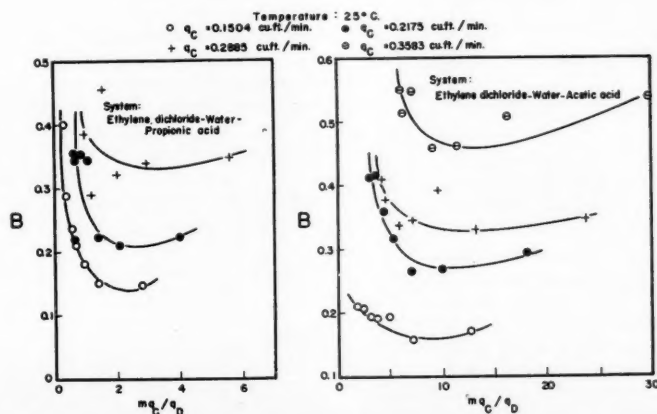


Fig. 8. Correlation of constant B .

mined by measuring the slope and intercept of the straight line. The constants so determined have been correlated for convenience with q_D/mq_C in Figures 6 and 7.

For the systems studied, the constant α bears a linear relation to the ratio q_D/mq_C . The magnitude of α is different for different systems owing to the fact that the equilibrium concentration of the extract phase for any fixed concentration of raffinate phase will be different.

On the other hand, the plot of β against q_D/mq_C on ordinary coordinates results in downward concave parabolic curves. In this case the constant has

magnitudes specific for the system. At this stage both α and β can be evaluated only empirically.

Because of the difficulty of measuring the contact area, the holdup, and the concentrations of the phases at any moment in the column, the constant B in the derived equations could not be evaluated from these individual factors. Its value was obtained empirically by plotting $[C_{co}' - C_{co}(\theta)]$ against θ on semi-log coordinates. The slope of the resulting line is equal to the constant B , as could be deduced from Equation (15).

In all the curves shown on Figures 5, 6, and 7, individual flow rate was not

an independent parameter. However, in the case of correlation of the constant B , flow rate does appear as a parameter, as is apparent in Figure 8, where the plots of B vs. mq_C/q_D give separate parabolic curves for each different dispersed-phase flow rate.

Validity of Proposed Equations. The validity of the equations derived in this study is indicated in Table 1. Listed are the percentage deviations of each calculated concentration from the equation for the corresponding observed value for run III-B-3. The discrepancy between observed and calculated values was within 10%, which is acceptable for most engineering estimation. The numerical results of all runs are summarized in Tables 3 and 4.

It should be pointed out that the proposed equations are still valid even though an apparently large deviation from observed values occurs at high values of the time θ . This deviation exists because the ordinate values are the logarithms of the difference values $[C_{co}' - C_{co}(\theta)]$, and small experimental errors in either of the concentrations involved will result in large errors in the ordinate value.

Applications of the Equations. If the degree of approach to steady state is defined as ξ , the ratio of steady state concentration driving force to the instantaneous driving force, it may be expressed mathematically as

$$\xi = \frac{C_{co}^* - C_{co}'}{C_{co}^* - C_{co}(\theta)}$$

where C_{co}^* represents the concentration of the exit continuous phase in equilibrium with the feed dispersed-phase concentration. Therefore, ξ can be evaluated analytically, by substitution of the equivalence of $C_{co}(\theta)$ from the proposed Equation (15) into the foregoing expression.

MASS TRANSFER STUDIES

The results of several investigations of extraction capacities of spray columns have been reported (2, 7, 8, 10, 11, 12, 15, 17); however, except for the work of Fleming and Johnson (8), little emphasis has been placed on extraction near limiting flow conditions, where larger extraction coefficients would be expected owing to the greater surface area per unit volume and the greater turbulence in both phases. The purpose of this part of the present study was to investigate extraction coefficients, especially in the region of rejection.

Apparatus

The apparatus was the same as that discussed above. The runs reported here were carried out in conjunction with the unsteady state runs reported for the rate of approach to steady state.

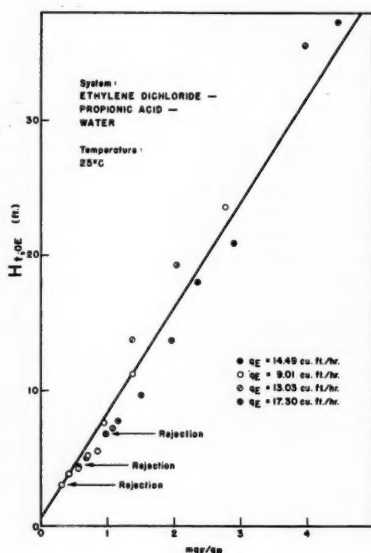


Fig. 9. Height-of-transfer-unit correlation.

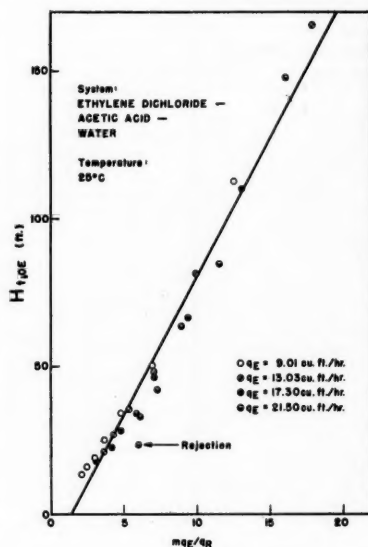


Fig. 10. Height-of-transfer-unit correlation.

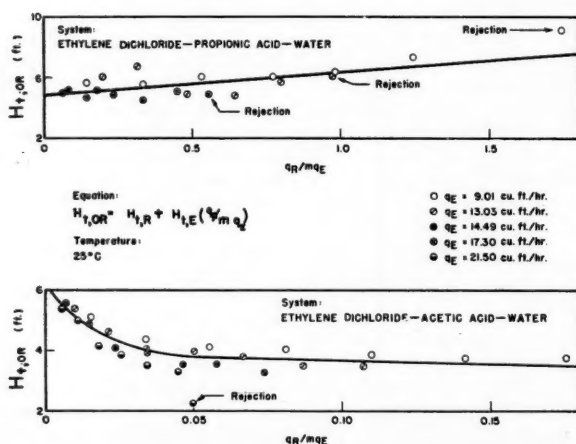


Fig. 11. Height-of-transfer-unit correlation.

Theory

The extraction results in this paper were correlated by use of both the transfer-unit concept and extraction coefficients. The transfer-unit concept for dilute solutions involves the defining equations suggested by Colburn (4):

Over-all number of transfer units based on extract phase

$$N_{t,OE} = \int_{C_{E1}}^{C_{E2}} \frac{dC_E}{(C_E^* - C_E)} \quad (16)$$

Over-all height of a transfer unit based on extract phase

$$H_{t,OE} = \frac{Z}{(N_{t,OE})} \quad (17)$$

Relation between over-all and film values of the heights of transfer units,

$$H_{t,OE} = H_{t,E} + H_{t,R} \left(\frac{mq_E}{q_R} \right) \quad (18)$$

Graphic integration between the limits C_{E1} and C_{E2} in Equation (16) gives a value for $N_{t,OE}$ which when used in the relation of Equation (17) gives in turn a value of the over-all height of a transfer unit for the particular situation which gives the values of C_{E1} and C_{E2} used. Equation (18) may be used then to obtain the film values, as this relation represents a straight line when plotted with $H_{t,OE}$ as ordinate and mq_E/q_R as abscissa. The slope of this line will be $H_{t,R}$ and the ordinate intercept ($mq_E/q_R = 0$) will be $H_{t,E}$. Similar relations are available for the raffinate phase.

The value of m in Equation (18) may be determined by the exact method proposed by Colburn (4), which requires a time-consuming graphical integration across the entire tower height Z . The value of m may also be evaluated by use of the approximate method suggested by Duncan, Koffolt, and Withrow (6), which gives an integrated average value from the expression

$$m_a = \frac{\int_{C_{R1}^*}^{C_{R2}^*} m dC_R}{C_{R2}^* - C_{R1}^*} \quad (19)$$

This is the value of m used in correlation of data in this present study. The value of m for use in Equation (18) may be evaluated by still another approximate method suggested by Colburn (4). Since the majority of transfer units are required in the dilute end of this countercurrent diffusional operation, a value of the slope of the distribution curve corresponding to C_{R1} is fairly accurate. For the specific case of a linear distribution curve all these methods reduce to equivalent expressions which are easily evaluated.

The mass transfer coefficient is related to the value of the H_t by the expression based on the extract phase

$$K_E a = q_E / (H_{t,OE})(S) \quad (20)$$

A similar relation may be presented for the raffinate phase. In the present study the mass transfer coefficient data have been presented as a plot of the values of Ka for the continuous phase as ordinate against the flow velocity q/S of the dispersed phase.

Discussion of Results

Figures 9 and 10 illustrate the correlation of the data as $H_{t,OE}$ vs. the group mq_E/q_R . In general a straight-line relationship is observed as predicted by Equation (18). There is one obvious difference in the H_t data obtained for the

of all the data was obtained up to the point of rejection; the curvature exhibited by the data for the system ethylene dichloride-acetic acid-water again indicates the limitation of the method.

Figures 12 and 13 show typical data for the systems involved plotted with extraction coefficient $K_E a$ as a function of the phase flow rates.

The main observation in these results is that normal operation up to the point of rejection was obtained. In general H_t values continued to decrease and $K_E a$ values continued to increase with increasing dispersed-phase flow rate for a given continuous-phase flow rate beyond Elgin flooding up the limiting

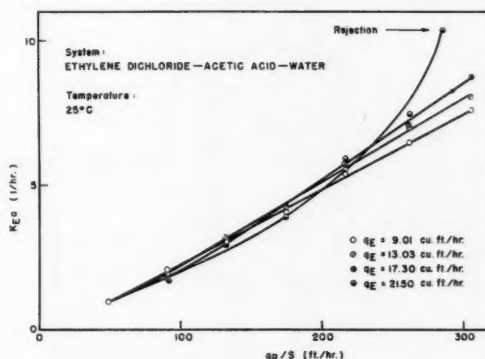


Fig. 12. Mass transfer coefficient correlation.

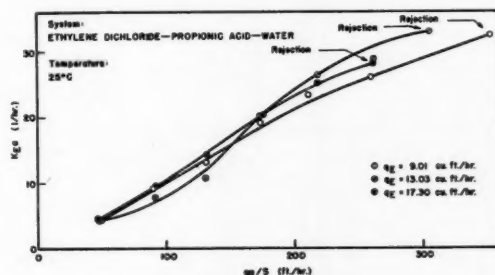


Fig. 13. Mass transfer coefficient correlation.

systems studied. The plot in Figure 9 gives an ordinate intersection resulting in a positive value for $H_{t,E}$, which is to be expected. On the other hand, the plot in Figure 10 gives an unlikely negative value for $H_{t,E}$. This discrepancy indicates some limitation in this method of correlation. It should be pointed out, however, that this method correlates the particular data up to rejection.

Figure 11 shows $H_{t,OR}$ values correlated as a function of the group q_R/mq_E and shows that a satisfactory correlation

flow condition described as rejection. No coalescence of the dispersed phase was observed in any of the runs made in this study.

HEAT TRANSFER STUDIES

Extraction studies on a tower as large as the one used in this series of investigations can be carried out using many different systems only at considerable expense. In order to study the effect of varying physical properties of the solvent

pairs on the operation of a spray column, it was decided to study the dynamically similar operation of extraction of heat. Preliminary heat transfer studies have been reported by Treybal (20) and by Garwin and Smith (9). This latter study used a single system and a 2-in.-diam. column.

Theoretical Principles

Equations for applying the transfer-unit concept to heat transfer may be set up in exactly the same manner as for mass transfer. For the over-all number of transfer units based on the continuous

For height of transfer unit,

$$H_t' = \frac{Z}{N_t'} \quad (23)$$

Furthermore there is a similar relationship between the over-all and film values of H_t' . Therefore

$$H_{t,oc}' = H_{t,c}' + \left(\frac{V_c c_c}{V_d c_d} \right) (H_{t,d}') \quad (24)$$

and

$$H_{t,od}' = H_{t,d}' + \frac{V_d c_d}{V_c c_c} (H_{t,c}') \quad (25)$$

Since c_c and c_d may be assumed constant, the expression for N_t' may be simplified to

$$N_{t,oc}' = \frac{t_{c1} - t_{c2}}{(t_d - t_c)_{\log \text{ mean}}} \quad (26)$$

Equations (23) to (26) were used for calculation and correlation in this part of the investigation.

Apparatus

The apparatus was essentially the same as shown in Figure 1. However, as indicated in Figure 14, the column was insulated by means of 2 in. of 85% magnesia-block insulation. The first inch of insulation on the column proper was wound with Nichrome heating wire, four turns to the inch, to form eleven separate heating circuits. Each heating circuit was controlled by a rheostat. A pair of thermocouples was installed at each heating circuit, one thermocouple touching the glass wall of the column and one just below the heating wire. The current to the heating wire was adjusted to maintain the column adiabatic.

Other thermocouples were placed in wells as indicated on Figure 14. These measured inlet and outlet temperatures of both phases. One long well extended through the column proper.

The two phases were recirculated to tanks 3 and 4, where copper heat exchange coils removed or returned the heat transferred in the column by circulation of cold or hot water inside the coils as required. Tanks 3 and 4 were also fitted with fume hoods to carry off fumes given off by the warm solutions.

Operation

The operation was very similar to that described by Minard and Johnson for flooding studies (16). For all runs the continuous phase was water. The dispersed phase consisted of carbon tetrachloride and carbon tetrachloride-naphtha mixtures. The properties of the mixtures are shown in Table 5. Either phase could be selected as the hot phase so that the transfer of heat in both directions was studied.

The continuous-phase flow rate was fixed, but the dispersed-phase flow rate was increased by small increments. About 1½ hr. were required for the temperature to become steady at each flow condition and for the column to become adiabatic. Thermocouple readings were taken and the dispersed-phase flow rate was again increased. This procedure was repeated until rejection was observed.

Two different spray heads were used. For most runs the nozzle used had twenty-one orifices 0.228 in. in diameter. Photographs of many of the runs were taken to record drop shape, size, and uniformity.

Discussion of Results

Figures 15, 16 and 17 illustrate typical results of the runs made in this part of the investigation. In general, runs were continued up to the point of rejection. This condition was chosen because it is easily reproduced and represents the highest possible throughput for the column. The terminal points on the plots represent rejection unless the run apply-

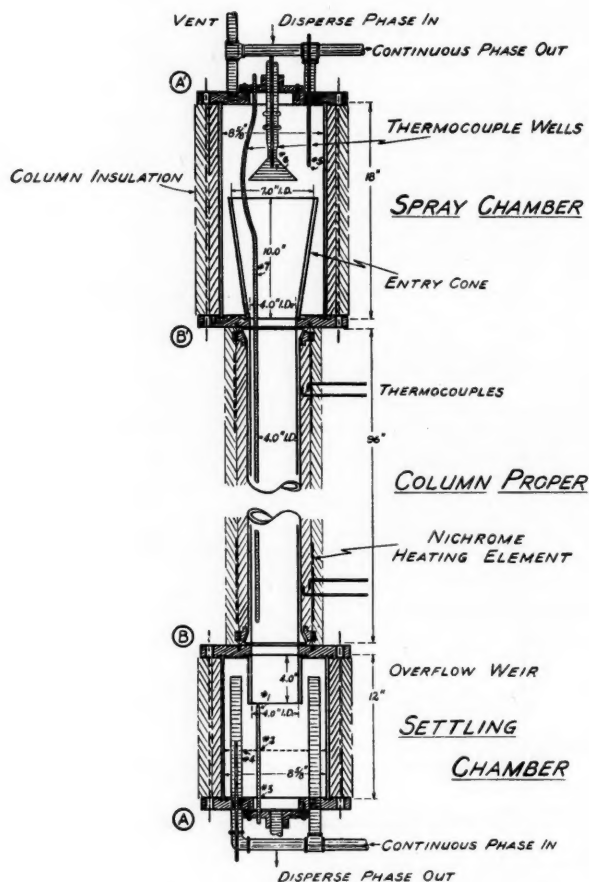


Fig. 14. Spray-tower; heavy phase dispersed.

phase,

$$N_{t,oc}' = \int_{t_{c1}}^{t_{c2}} \frac{dt_c}{t_d - t_c} \quad (21)$$

For dispersed phase,

$$N_{t,od}' = \int_{t_{d1}}^{t_{d2}} \frac{dt_d}{t_d - t_c} \quad (22)$$

In Equations (24) and (25) V_c and V_d are the continuous- and the dispersed-phase flow rates in cubic feet per hour per square foot and c_c and c_d are the respective heat capacities of the continuous and dispersed phases. The ratio of these latter variables is comparable to the slope of the equilibrium curve in mass transfer.

ing is starved; these runs were not carried beyond flooding.

The values of $H_{i,c'}$ decreased until rejection was attained, an indication that the most efficient operation of the tower corresponds to limiting flow conditions. No coalescence of drops was observed in any of the runs. It must be emphasized that no difference in drop size was observed between the two types of heat transfer operation.

The dispersed-phase rate at rejection for each continuous phase rate could be predicted with a maximum deviation of 15% by the original correlation of Minard and Johnson (16) an indication that those results hold for a wide range

of temperatures of the phases and the resulting changes in physical properties.

The maximum hot-phase temperatures ranges from 126° to 140°F., higher temperatures causing excessive evolution of fumes.

Runs which gave heat balance differences greater than 10% were discarded.

Figure 18 shows the results of plotting $H_{i,D'}$ as a function of the ratio of the flow rates, V_D/V_C . These results are analogous and very similar to the results for $H_{i,OR}$ for extraction in the system ethylene dichloride-water-acetic acid shown in Figure 11. These curves show the influence of the direction of heat transfer on the observed results.

Figure 19 shows the results of all the runs for the three different solvent pairs used and for the two different nozzles. All calculated points fall along one or the other of a pair of parallel straight lines with a slope of approximately -1. The eight series of runs made in this investigation were analyzed by the method of least squares. This analysis also showed that if a normal allowance is considered for experimental error only, the direction of heat flow to or from the continuous phase was important in influencing the $H_{i,c'}$ values observed at a given V_D/V_C value.

The influence of direction of flow of heat or mass has been a controversial

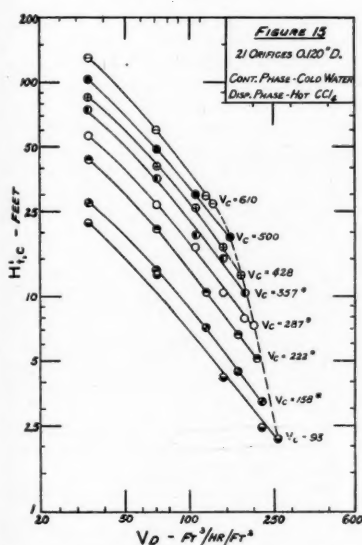


Fig. 15. Twenty-one orifices 0.120-in. diam.; continuous phase, cold water; dispersed phase, hot CCl_4 .

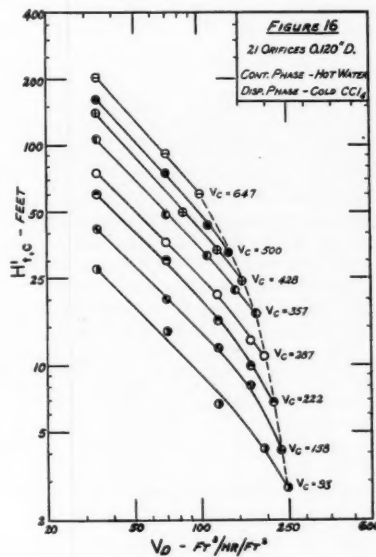


Fig. 16. Twenty-one orifices 0.120-in. diam.; continuous phase, hot water; dispersed phase, cold CCl_4 .

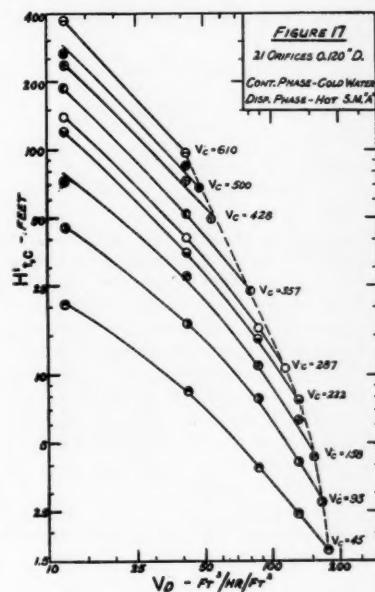


Fig. 17. Twenty-one orifices 0.120-in. diam.; continuous phase, cold water; dispersed phase, hot S.M. "A".

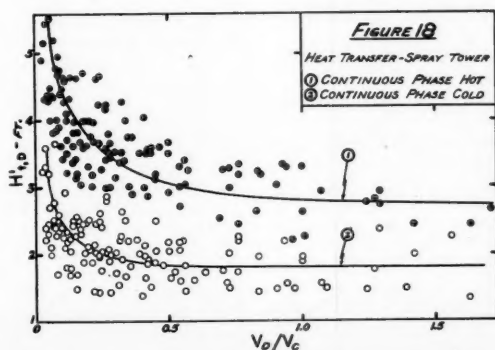


Fig. 18. Heat transfer, spray tower; (1) continuous phase hot, (2) continuous phase cold.

issue in recent years. It is believed that these results demonstrate rather conclusively that an effect of direction of heat transfer does exist. If the continuous phase can be said to have the controlling resistance as indicated by the high $H_{i,c'}$ values observed and correlated in Figure (19), then this effect could be explained qualitatively as being due to the lower viscosity of the continuous phase in the continuous-phase film near the drop. The heat transfer coefficient would be increased when the dispersed phase was hot and decreased when the dispersed phase was cold. This effect appears similar to the wall correction factor used to correlate heat transfer coefficients for fluids flowing in pipes, introduced by Sieder and Tate (18).

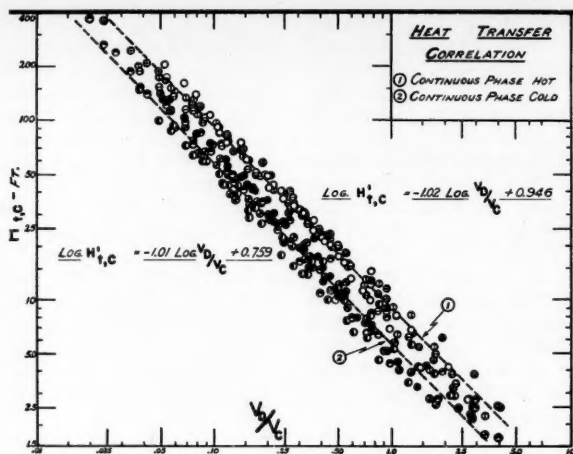


Fig. 19. Heat transfer correlation; (1) continuous phase hot, (2) continuous phase cold.

Perhaps a more plausible explanation stems from the work of Conkie and Savic (5), who showed theoretically that the coefficient for heat transfer from drops should vary as the ratio of the heat transfer coefficient for the boundary layer of the surrounding film to the viscosity of the droplet fluid. If the conditions of turbulence of the drops and the continuous phase in the present investigation agree with the conditions set up in the theory of Conkie and Savic, and this seems likely, then it would be expected that the heat transfer coefficient would be greater when the continuous phase is cold, as was observed.

These explanations, of course, require further examination and further experimental measurements.

CONCLUDING REMARKS

This investigation has attempted to present in concise form an intensive study of the rate of approach to steady state in extraction, mass transfer in extraction, and rate of heat transfer in an Elgin type of spray tower. Combined with the previous study of holdup and limiting flow, this series of investigations permits a more thorough understanding and prediction of spray-tower behavior.

The results are all for a 4-in.-diam. tower giving a large ratio of tower diameter to drop size. The results on the rate of approach to steady state are believed to be the first reported for a spray tower. The simplified equations proposed for transient conditions permit extrapolation to steady state conditions. The constants required in these equations may be correlated as functions of the ratio of the flow rates of the two phases. This ratio is also the most useful quantity for correlating mass transfer and heat transfer data.

During extraction the tower was shown to give stable operation up to and beyond flooding conditions. The H_i values continue to decrease for any given continuous-phase rate as the limiting flow condition is approached, including operation up to rejection. Results are presented for two systems not previously studied.

The heat transfer data show the advantages of using the transfer of heat rather than transfer of mass to study tower performance. Over rather wide ranges of operating conditions, no influence of the density of the dispersed phase was observed. The effect of changing drop size was small; however, the effect of the direction of heat flow was pronounced. Tentative explanations for this effect are suggested, but further study of this phase of work is required.

NOTATION

B	= correlating parameter
c	= specific heat, B.t.u./lb. (°F.)
C'	= steady state solute concentration, lb.-moles/cu. ft.
$C(\theta)$	= time-dependent solute concentration, lb.-moles/cu. ft.
C^*	= equilibrium solute concentration, lb.-moles/cu. ft.
h	= absolute holdup of dispersed phase, cu. ft.
H	= absolute holdup of continuous phase, cu. ft.
H_i	= height of transfer unit-mass transfer, ft.
H_i'	= height of transfer unit-heat transfer, ft.
k	= integration constant
Ka	= volumetric mass transfer coefficient, 1/hr.
m	= slope of equilibrium distribution curve
N_i	= number of transfer units-mass transfer

N_i'	= number of transfer units-heat transfer
q	= flow rate, cu. ft./min. or cu. ft./hr. as indicated
S	= cross-sectional area of column proper, sq. ft.
t	= temperature, °F.
V	= phase flow rate, cu. ft./hr. (sq. ft.)
Z	= height of column, ft.
$\alpha, \beta, \gamma, \delta$	= correlating parameters
θ	= time, min.
ξ	= degree of approach to steady state

Subscripts

a	= average value
C	= continuous phase
D	= dispersed phase
E	= extract phase
i	= inlet to column
o	= outlet from column
O	= over-all value
R	= raffinate phase
1	= inlet condition of phase
2	= outlet condition of phase

LITERATURE CITED

1. Acrivos, Andrew, N. R. Amundson, *Ind. Eng. Chem.*, **47**, 467 (1953).
2. Appel, F. J., and J. C. Elgin, *ibid.*, **29**, 451 (1937).
3. Blanding, F. H., and J. C. Elgin, *Trans. Am. Inst. Chem. Engrs.*, **38**, 305 (1942).
4. Colburn, A. P., *ibid.*, **35**, 211 (1939).
5. Conkie, W. R., and P. Savic, *Rept. MT23*, Natl. Research Council Canada (October, 1953).
6. Duncan, D. W., J. H. Koffolt, and J. R. Withrow, *Trans. Am. Inst. Chem. Engrs.*, **38**, 259 (1942).
7. Elgin, J. C., and F. M. Browning, *ibid.*, **31**, 639 (1935).
8. Fleming, J. F., and H. F. Johnson, *Chem. Eng. Progr.*, **49**, 497 (1953).
9. Garwin, Leo, and B. D. Smith, *Chem. Eng. Progr.*, **49**, 591 (1953).
10. Geankoplis, C. J., and A. N. Hixson, *Ind. Eng. Chem.*, **42**, 1141 (1950).
11. Hayworth, C. B., and R. E. Treybal, *ibid.*, **42**, 1174 (1950).
12. Johnson, H. F., and Harding Bliss, *Trans. Am. Inst. Chem. Engrs.*, **42**, 331 (1946).
13. Lapidus, Leon, and N. R. Amundson, *Ind. Eng. Chem.*, **42**, 1071 (1950).
14. Licht, William, and J. B. Conway, *ibid.*, **42**, 1151 (1950).
15. Meissner, H. P., C. A. Stokes, C. M. Hunter, and G. M. Morrow, *ibid.*, **36**, 917 (1944).
16. Minard, G. W., and A. I. Johnson, *Chem. Eng. Progr.*, **48**, 62 (1952).
17. Row, S. B., J. H. Koffolt, and J. R. Withrow, *Trans. Am. Inst. Chem. Engrs.*, **37**, 559 (1941).
18. Sieder, E. N., and G. E. Tate, *Ind. Eng. Chem.*, **28**, 1429 (1936).
19. Sherwood, T. K., J. E. Evans, and J. V. A. Longcor, *ibid.*, **31**, 1144 (1939).
20. Treybal, R. E., "Liquid Extraction," McGraw-Hill Book Company, Inc., New York (1951).

Viscosity of Suspensions of Spherical and Other Isodimensional Particles in Liquids

ANDREW PUSHENG TING and RALPH H. LUEBBERS

University of Missouri, Columbia, Missouri

The viscosity of a suspension is related to the properties of the suspending liquid and the suspended particles by measuring the viscosity of suspensions made up of closely sized materials such as glass spheres, plastic Zeolite spheres, blasting sand, and salt cubes in a wide range of concentrations in liquids of varying properties made up of castor oil, tetrabromoethane and carbon tetrachloride, or corn syrup and water. The measurements were made under carefully controlled conditions by means of a Brookfield viscometer, and the reproducibility of results was demonstrated by repetitive runs.

Equations are derived to describe the viscosities of these various suspensions in terms of the viscosity and density of the suspending liquid and of the shape, size distribution, density, and concentration of solid particles. The range of concentration covered is from infinite dilution to near infinite viscosity.

The results obtained can best be explained by postulating nonuniform distribution of particles in a suspension in a network of tetrahedral and simple cubical packings.

The control of viscosity of suspensions of solid particles in liquids is an important industrial problem. Although the number of factors influencing the viscosity is large, mechanical interference of the suspended particles undoubtedly is of major importance. The ultimate solution of this problem will probably be expedited by first clearing up the problem of mechanical interference. The purpose of this investigation is to throw some light on this phase of the question.

Historic Review

The first piece of fundamental theoretical work on the viscosity of suspensions was done by Einstein (6), who obtained the following equation:

$$\mu = (1 + 2.5x_c)\mu_0 \quad (1)$$

Bingham and Durham (2) measured fluidities of various suspensions with concentrations up to 5 to 9%. The fluidity

decreased rapidly and linearly as the volume concentration of the solids increased. Drucker and Kassel (5) and White (18) found that fluidities are normally additive in homogeneous mixtures and fine suspensions. The fact that suspensions of rigid spherical particles exhibited the same anomaly as lyophilic sols, viz., a decrease of viscosity with increasing rate of shear, was explained by McDowell and Usher (10) and supported by striking evidence.

Smith, Toote and Busang (14) made an interesting investigation of the packing of homogeneous spheres. Although the actual packing of spheres was of a very irregular and distorted pattern, they showed that for statistical purposes the arrangement may be treated as a mixture of close-hexagonal and simple-cubical packings only, in the proportion required to yield the observed porosity. Manegold, Hofmann, and Solf (11) calculated voids for packing with spheres of uniform or different sizes.

The shape and surface characteristics of particles naturally affect viscosity. Studies of DeVaney and Shelton (4) verified this fact.

Vand (16) derived a formula for spheres in liquids,

$$\mu = (1 + 2.5c + 7.17c^2 + 16.2c^3)\mu_0 \quad (2)$$

Robinson (12) found that the specific viscosity of the suspension is directly proportional to the volume fraction of the spheres and inversely proportional to the volume fraction of the free liquid in suspension. His data showed that packed-sediment volume appears to be approximately the effective volume of the particles at any concentration. The viscosity showed some decrease as the rate of shear increased, but the suspension was assumed to be Newtonian in his treatment.

MATERIALS AND EXPERIMENTAL METHODS

Solid Particles

Glass spheres, mustard seeds, and Nalcite resin were used as spherical particles. Crystals of common salt and blasting sands were used as cubes and rounded particles, respectively. All samples of particles were sized through standard fourth-root testing sieves. All samples of particles used were free flowing except one sample of glass spheres which was used to illustrate its effect on viscosity.

Andrew Pusheng Ting is at present with Chemical Construction Corporation, New York, New York.

In the study of polydisperse suspensions, binary and ternary mixtures of glass spheres were investigated. In the binary mixtures used, the particle-diameter ratios covered the range from 0.59 to 0.85, and the volume ratio of the large particles to the small ones from 0.10 to 10. In the ternary mixtures studied, the diameter ratios of the medium particles to the large ones varied between 0.42 and 0.84, and the diameter of the small particles to the medium ones was 0.84. The volume ratios among the large, medium, and small particles were either 1:4:2 or 3:4:2.

Liquid Media

Dense media blended to match the density of the solids: carbon tetrachloride and *s*-tetrabromoethane; castor oil and tetrabromoethane. Viscous media were castor oil and corn syrup.

Viscometer

A Brookfield Synchro-Lectric viscometer was used. For each measurement in this investigation the slowest permissible spindle speed was used and the reading taken as soon as its change began to be slow and steady. Ten to fifteen seconds was normally sufficient to obtain a reading.

Control of Temperature

All the viscosity determinations were made at $20.0^\circ \pm 0.1^\circ\text{C}$.

Experimental Procedure

Liquid was poured into a beaker large enough to eliminate wall and end effects. After the viscosity of the liquid was determined, a known weight of solid particles was added to the liquid. The mixture was stirred to form a "uniform" suspension. Air bubbles introduced into the suspension were removed in a vacuum chamber. After one viscosity test had been completed, more solids were added, and this procedure was repeated until the suspension became so concentrated that the viscosity readings were erratic and not reproducible.

EXPERIMENTAL RESULTS

The complete data on the suspension of various types of isodimensional solid particles in various types of liquids are presented in reference 15. A representative run for a monodisperse suspension is shown in Table 1. In Figure 6, data from two typical viscosity runs were plotted against the volume fraction of glass spheres for illustration. The rate of change of viscosity with volume fraction increases rapidly until the viscosity is nearly infinite at a volume fraction of 0.5. In order to obtain a linear relationship, all viscosity data were plotted as x_v/μ_{sp} vs. x_v graphs, as shown in Figures 7 and 8. Several conclusions are immediately apparent:

1. The data fall on straight lines. This indicates that the form of the linear relationship is valid over the entire range of concentration tested.

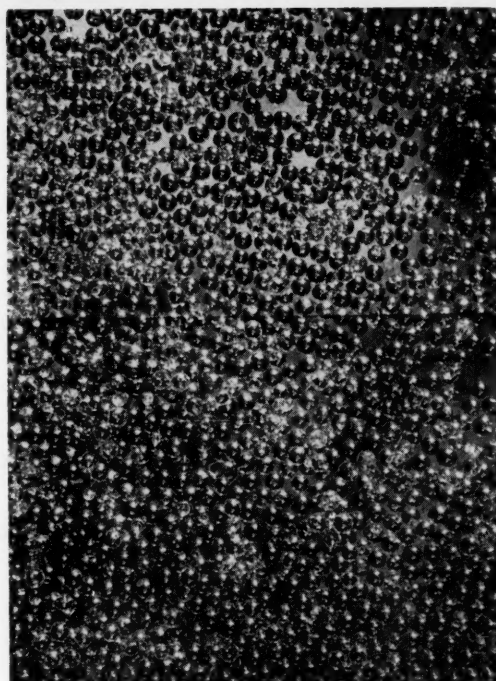


Fig. 1. Glass spheres, 390μ .

TABLE 1
VISCOSITY OF SUSPENSION OF GLASS SPHERES IN HEAVY LIQUID

Run: 6

Spheres: 3M#10, 60/70 mesh, 230μ
Density, 2.47 g./ml.

Liquid: Castor oil and *s*-tetrabromoethane
Density, same as for spheres
Weight, 731.3 g.

Viscometer spindle: #1

Spheres, g.	x_v	μ , cp., at rev./min.				μ_{sp}	x_v/μ_{sp}
		6	12	30	60		
0	0				29.6		
5.3	0.0072				29.9	0.010	0.719
15.8	0.021				30.8	0.040	0.526
31.4	0.041				32.0	0.080	0.513
40.3	0.052				32.9	0.110	0.472
65.8	0.083				35.2	0.189	0.439
86.6	0.106				37.6	0.270	0.392
103.5	0.124				39.7	0.342	0.362
120.4	0.141				41.8	0.412	0.342
163.5	0.183				47.1	0.591	0.310
184.8	0.202				50.6	0.710	0.285
206.9	0.221				53.5	0.808	0.274
230.8	0.240				57.7	0.950	0.253
261.3	0.263				63.9	1.160	0.227
315.3	0.301				76.9	1.598	0.198
343.4	0.319				89.3	2.02	0.158
384.3	0.345			105.2		2.56	0.135
413.8	0.361			118.3		3.00	0.120
458.7	0.385	150	146	142.0		3.78	0.102
543.9	0.426	218	217			6.32	0.067
614.1	0.456	308	296			9.00	0.051
698.6	0.489	572				18.30	0.027
766.8	0.512	700					

→ 500 The reading decreased with the time while the spindle was rotating in the suspension.

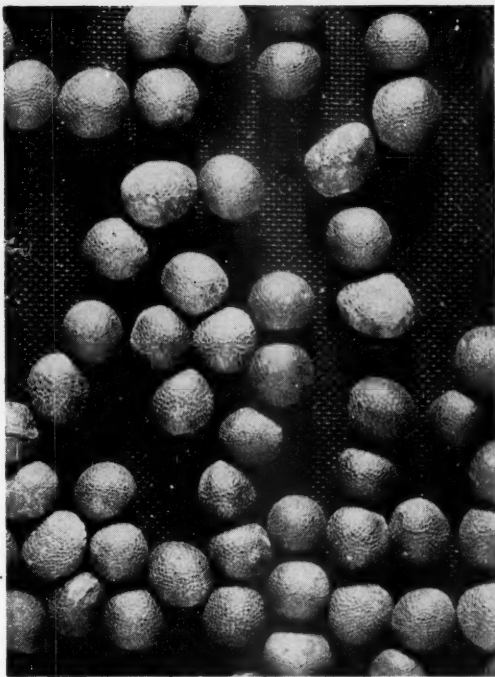


Fig. 2. Mustard seeds, 1,545 μ , on 200-mesh screen.

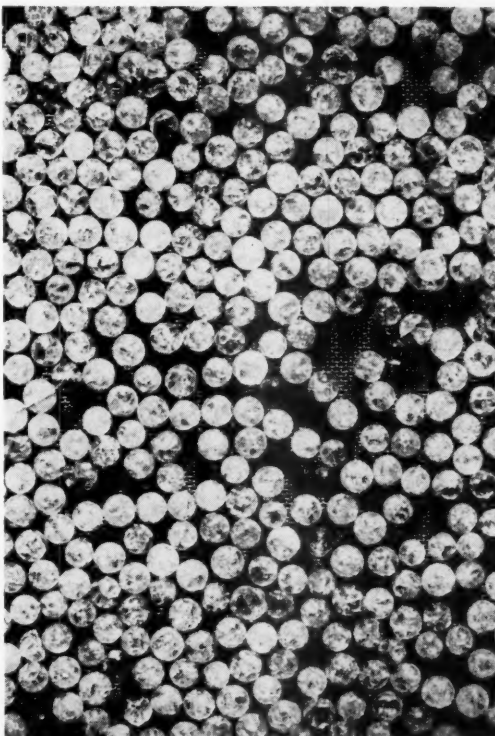


Fig. 3. Nalcite SAR., 920 μ , on 200-mesh screen.

2. The slopes of the linear graphs are primarily -1 and the intercepts on both axes equal each other for free-flowing monodisperse suspensions, regardless of the particle shape.

3. The intercepts of the linear graphs for spherical particles on the x_v axes ($x_{v,\infty}$, volume fraction of the solids when the viscosity of the suspension would approach infinity) vary with the attraction between particles, the viscosity of the pure liquids, and the relative density of the liquids to the particles. For free-flowing spheres there is no attraction between particles and the value of $x_{v,\infty}$ depends only upon the ratio of the viscosity of the pure liquid to the relative density of the liquid with respect to the solids, μ_0/R as shown in Figure 9. For cubes and grains with rounded corners, $x_{v,\infty}$ does not vary with the function μ_0/R but seems to remain constant regardless of the liquids used.

4. When the concentration of the solids became very high and close to the infinite-viscosity concentration, the viscometer readings decreased with continued shearing owing to the rotation of the viscometer bob, regardless of the shearing rate. The viscosity returned to its original value upon standing for a certain length of time. Therefore, structural thixotropy was definitely indicated. However, its effect was not obvious until the solids concentration was very high, as shown in Table 1.

For these thixotropic suspensions the first or second reading was taken as the viscosity at zero time. Only those viscometers which permit very rapid readings can be relied on for the reproducible results with suspensions. Continued shearing results in a change in viscosity. If the measurements were continued for a suspension of 0.5 solids fraction, the viscosity readings often decreased by as much as 30% in one hour with no evidence of a minimum value being reached even then.

CORRELATION

Derivation of Equation

If fluidity is additive and there is no interference between the liquid and the solids in a suspension, and as the fluidity of rigid solids is zero, the fluidity of the suspension would be

$$\phi = (1 - x_v)\phi_0 \quad (3)$$

where ϕ_0 is the fluidity of the liquid and x_v the volume fraction of the solids in the suspension. However, solids suspended in liquid media do not form uniform suspensions but "clusters," or a certain type of packings, even though they are inert and free flowing before being put into the liquids. The authors believe that only the portion of liquid

719
526
513
472
439
392
362
342
310
285
274
253
227
198
158
135
120
102
067
051
027

which is not occluded can move freely. Therefore the preceding equation does not represent the true picture, and the actual fluidity of a suspension should be that of the free liquid only; i.e.,

$$\phi = (1 - x_{e,eff})\phi_0 \quad (4)$$

where $x_{e,eff}$ is the effective volume fraction of the solids, i.e., the sum of the actual volume fraction of the solids plus the volume fraction of the occluded liquid. When solids concentration becomes so high as to form a complete ramifying aggregate or network of some rigidity, all the liquid is occluded in the particle packing and is no longer free. Under such conditions $x_{e,eff}$ equals unity, fluidity equals zero, viscosity approaches infinity, and x_e equals $x_{e,\infty}$, the volume fraction when the viscosity would equal infinity. Since $x_{e,eff}$ is proportional to x_e , $x_{e,eff}$ must equal $x_e/x_{e,\infty}$.

In terms of viscosity, Equation (4) becomes

$$\mu = \frac{\mu_0}{1 - \frac{x_e}{x_{e,\infty}}} = \frac{x_{e,\infty}}{x_{e,\infty} - x_e} \mu_0 \quad (5)$$

where μ and μ_0 are viscosities of the suspension and the liquid, respectively.

To simplify the equation and make it more convenient to use, one may express it in terms of specific viscosity,

$$\mu_{sp} = \frac{\mu - \mu_0}{\mu_0} = \frac{x_e}{x_{e,\infty} - x_e} \quad (6)$$

and

$$\frac{x_e}{\mu_{sp}} = x_{e,\infty} - x_e \quad (7)$$

When x_e/μ_{sp} is plotted against x_e , a line with a slope of -1 should be obtained. If the viscosity of a particular solids concentration is available, $x_{e,\infty}$ can be calculated by means of Equation (7) and viscosities for the complete concentration range can be predicted without further experiments. If no viscosity data are available, a correlation between $x_{e,\infty}$ and physical properties of the liquid-solids system will be very helpful for the prediction of viscosities of the suspension without any experiment.

Evaluation of $x_{e,\infty}$

Although the packing of spherical particles in suspension is very irregular and distorted, the authors suggest that it may be considered statistically as consisting only of the two most open types: the simple cubical and the tetrahedral packings, wherein there are six and four spheres, respectively, in contact with each sphere in consideration. The

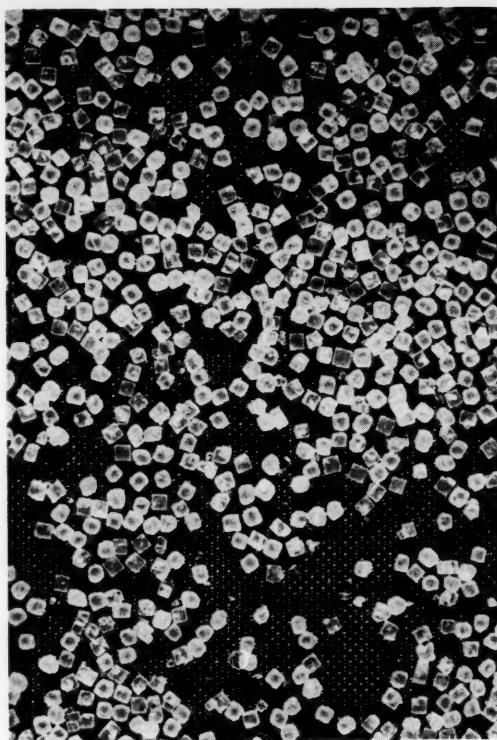


Fig. 4. Salt cubes, 385 μ , on 200-mesh screen.

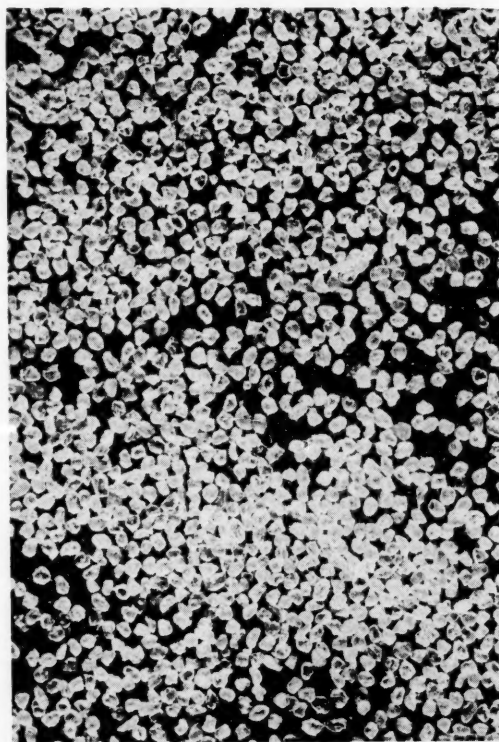


Fig. 5. Blasting sand, 274 μ , on 200-mesh screen.

volume
and 0
types o
The
for any
is relat
ing to

$$F_4 = \frac{0}{0}$$

where

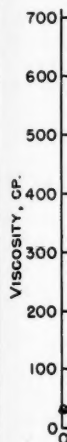


Fig. 6.

packing

For p
type o
packing
only, I

Evaluation

If t
flowing
thems
the di
packing
interac
packing
The fo
relative
and th
by μ_0 .
tetrah
ratio o
to the
curved
given

$$F_4 = 8$$

where
averag
is 7.4%

volume fractions of the solids are 0.524 and 0.34, respectively, for these two types of packings.

The fraction of each type of packing for any suspension of spherical particles is related to the value of the $x_{e,\infty}$ according to the following equation:

$$F_4 = \frac{0.524 - x_{e,\infty}}{0.524 - 0.34} = \frac{0.524 - x_{e,\infty}}{0.184} \quad (8)$$

where F_4 is the fraction of the tetrahedral

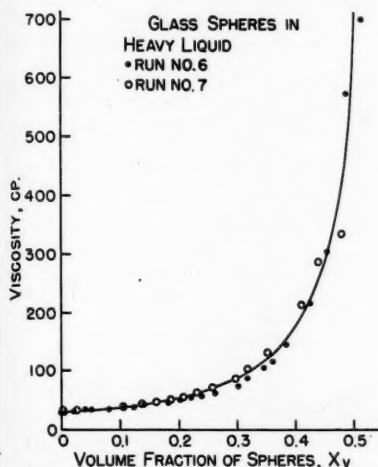


Fig. 6. Viscosity of suspensions of glass spheres in heavy liquid.

packing. Thus

$$x_{e,\infty} = 0.524 - 0.184F_4 \quad (9)$$

For packing consisting of tetrahedral type only, $F_4 = 1$ and $x_{e,\infty} = 0.34$. For packing consisting of simple cubical type only, $F_4 = 0$ and $x_{e,\infty} = 0.524$.

Evaluation of F_4

If the spherical particles are free-flowing, have negligible attraction among themselves, and are inert to the liquid, the distribution of the two types of packing should be determined by the interaction of the force causing closer packing and the resistance to movement. The force may be represented by R , the relative density of the liquid to the solids, and the resistance may be represented by μ_0 . A log-log plot of F_4 , the fraction of tetrahedral packing, against μ_0/R , the ratio of the viscosity of the pure liquid to the relative density, results in a slightly curved line, Figure 9. The relationship is given by the following equation:

$$F_4 = 8.59 \times 10^{-3} \left(\frac{\mu_0}{R} \right)^{0.469} + 0.350 \quad (10)$$

where μ_0 is expressed in centipoises. The average deviation from Equation (10) is 7.4% and the maximum 22%.

Monodisperse Suspensions

The viscosity of a monodisperse spherical suspension can be calculated from the physical constants of the solids and liquid. From Equations (9) and (10),

$$x_{e,\infty} = 0.460 - 1.58 \times 10^{-3} \left(\frac{\mu_0}{R} \right)^{0.469} \quad (11)$$

The average deviation from Equation (11) is 1.90% and the maximum 8.3%. Combining Equations (5) and (11) gives

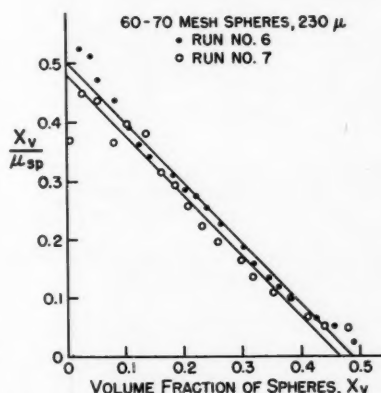


Fig. 7. Viscosity of suspensions of glass spheres in heavy liquid; 60- to 70-mesh spheres, 230 μ.

suspension higher than that of a monodisperse suspension. This was found experimentally to be true.

The intercepts on the x_e/μ_{sp} axes for polydisperse suspensions of spherical particles were found to be the same as the intercepts on the x_e/μ_{sp} axes for monodisperse suspensions. The intercepts on the x_e axis were found to be 1.26 times higher, and the slopes 1/1.26, or 0.79, times lower. Therefore, Equation (7) for monodisperse systems may be

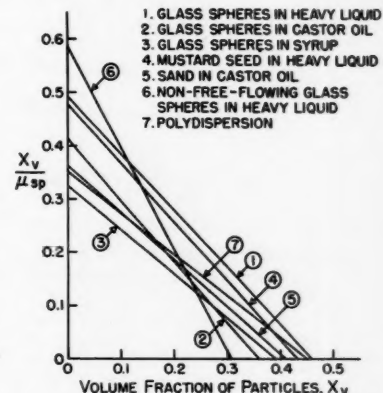


Fig. 8. Typical curves of mono- and poly-dispersed suspensions.

$$\mu = \frac{\mu_0}{1 - \frac{x_{e,\infty}}{0.460 - 1.58 \times 10^{-3} \left(\frac{\mu_0}{R} \right)^{0.469}}} \quad (12)$$

where the viscosities are in centipoises. For a solids fraction of 0.1, the average deviation from Equation (12) is 0.63% and the maximum 3.5%. For solids fraction of 0.3, the average deviation is 6.9% and the maximum 59%.

For cubes and grains with rounded corners, value of the $x_{e,\infty}$ for the monodisperse suspensions is not appreciably affected by the liquid viscosity and remains almost constant at 0.403. From Equation (5)

$$\mu = \frac{0.403}{0.403 - x_{e,\infty}} \mu_0 \quad (13)$$

Polydisperse Suspensions

If the particles are all of the same size, no more particles can enter into the network without changing the type of packing and consequently the viscosity. However, smaller particles can fill into the voids without changing the type of the primary packing. These additional smaller particles make the $x_{e,\infty}$ of a polydisperse

adapted to polydisperse systems simply by changing the coefficient of x_e ,

$$x/\mu_{sp} = (x_{e,\infty})_m - 0.79x_e \quad (14)$$

where $(x_{e,\infty})_m$ is the $x_{e,\infty}$ for the corresponding monodisperse system as calculated from Equation (11).

DISCUSSION

If the Einstein equation is expressed in terms of specific viscosity, it becomes

$$\frac{\mu - \mu_0}{\mu_0} = \mu_{sp} = kx_e$$

or

$$\frac{x_e}{\mu_{sp}} = \frac{1}{k}$$

where k is a constant independent of the concentration of the solids. As the suspension concentration approached zero, Equation (7), the relationship proposed by the authors, approaches the Einstein equation:

$$\frac{x_e}{\mu_{sp}} = x_{e,\infty}$$

Since $x_{e,\infty}$ is constant for any given system, $k = 1/x_{e,\infty}$. From Figure 7, the value of $1/x_{e,\infty}$ (or μ_{sp}/x_e when x_e ap-

proaches zero) is seen to be 2.0, against the Einstein shape factor of 2.5 for the spheres.

Vand and Robinson did not use glass spheres of a uniform size, but a wide distribution of size. As it was found that the size distribution did affect the two intercepts on the viscosity graphs, their conclusion would be good only for polydispersions and inaccurate for monodispersions.

According to the authors' hypothesis of the most open particle packing in

tion between particles becomes a controlling factor and the value of $x_{s,\infty}$ becomes much less than predicted by the suggested method. This accounts for the high $1/x_{s,\infty}$ values found by Harrison (8), 4.75, during investigation of aqueous suspensions of starch granules. Other seeming disagreement in values given in the literature may be explained by the fact that the effect of a wide size distribution of the particles on the value of $x_{s,\infty}$ might have been counteracted by nonfree-flowing properties.

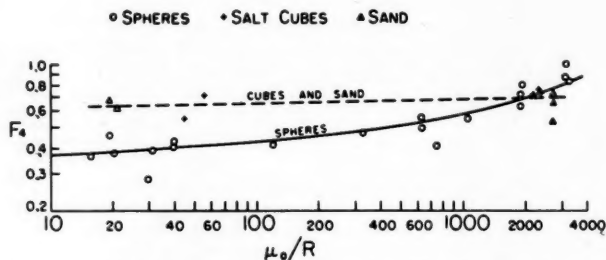


Fig. 9. Relation between the fraction of tetrahedral packing, F_4 , and the ratio of liquid viscosity to the relative density, μ_0/R , for monodisperse suspensions.

suspension, $x_{s,\infty}$ varies between 0.34 and 0.524 and hence $1/x_{s,\infty}$ varies between 1.9 and 2.9. This figure agrees with the work of Bancelin (1), 2.9; of Einstein, 2.5; of Eirich, Bunzl, and Margaretha (7), 2.5; of Broughton and Windebank (3), 2.5; and of Robinson (12), 2.4. It also accounts well for the discrepancies among these investigators. Therefore, the authors' equation is not only equivalent to the well-established Einstein's equation at negligible concentrations, but offers a useful expression and prediction for the viscosity of suspensions ranging from infinite dilution to infinite viscosity.

Few workers in this field have emphasized the effect of the size distribution of the solid particles on the viscosity of a suspension. This is probably due to the fact found by Einstein and supported by many others, that the viscosity of a monodisperse suspension is independent of the size of the particles. However, it does not follow that viscosity is independent of size distribution. The effect of particle-size distribution has not been seriously considered until recently (13, 17).

The linear relationship between x_s/μ_{sp} and x_s also holds for the monodisperse suspension of isodimensional particles of other than spherical shape. However, owing to the complexity introduced by their shapes, their packing would be entirely different from that of the spherical particles. Up to the present time there is no satisfactory method of describing their packing.

All these correlations, however, can be applied only to free-flowing particles. With nonfree-flowing particles the attrac-

It has always been difficult to obtain steady viscometer readings when the solid concentration became extremely high. Owing to the gradual change of the pattern of packing of the solids by the rotation of the viscometer, it would not be surprising to see the viscosity decreased with time during measurements. This thixotropic phenomenon of decreasing viscosity with continued shearing can be clearly explained by the authors' hypothesis of particle packing.

SUMMARY

A hypothesis for describing the viscosity behavior of suspensions of spherical particles is proposed—the hypothesis of the most open particle packing in suspensions.

The authors are of the opinion that solid spherical particles suspended in liquids do not form uniform suspensions, even though they are inert to the liquids and there is negligible attraction between particles. Instead, they form a network consisting of tetrahedral and simple cubical packings. The extent of each type of packing depends on a function of the viscosity of the pure liquid and the relative density of the liquid to that of the solids.

The extent to which each type of packing occurs determines the porosity of the suspension at the yield point and the concentration of the solids at infinite viscosity.

An equation describing the viscosities of suspensions of spherical particles was derived. The concentration range covered by this equation is from infinite dilution to infinite viscosity. The same equation may be used for polydisperse spherical suspensions if a proper coefficient is used. An equation describing the viscosities of monodisperse suspensions of other isodimensional particles is also given.

NOTATION

c	= concentration of solids in a suspension, the ratio of the volume of the particles to that of the liquid
k	= an empirical constant
R	= ratio of the liquid density to the solid density in a suspension (or the reciprocal if the liquid is heavier)
x_s	= volume fraction of solids in a suspension
$x_{s,\infty}$	= volume fraction of solids in a suspension when its viscosity would reach infinity if plastic flow did not come into play
$(x_{s,\infty})_m$	= $x_{s,\infty}$ for monodisperse suspension
μ	= viscosity of a suspension, centipoise, cp.
μ_0	= viscosity of the pure liquid making up a suspension, cp.
μ_{sp}	= specific viscosity, the ratio of the increase in viscosity of the suspension over that of the liquid to that of the liquid, $(\mu - \mu_0)/\mu_0$
ϕ	= fluidity of a suspension, $1/\mu$, cp.^{-1}
ϕ_0	= fluidity of pure liquid, $1/\mu_0$, cp.^{-1}
F_4	= fraction of the tetrahedral packing

LITERATURE CITED

- Bancelin, Von M., *Kolloid-Z.*, **9**, 1954 (1911).
- Bingham, E. C., and T. C. Durham, *Am. Chem. J.*, **46**, 278 (1911).
- Broughton, G., and C. S. Windebank, *Ind. Eng. Chem.*, **30**, 407 (1938).
- DeVaney, F. D., and S. M. Shelton, *U. S. Bur. Mines Rept. Invest.* 3469B (1940).
- Drucker, K., and R. Kassel, *Z. physik. Chem.*, **76**, 367 (1911).
- Einstein, Albert, *Ann. Physik*, **19**, 289 (1906), **34**, 591 (1911).
- Eirich, F., M. Bunzl, and M. Margaretha, *Kolloid-Z.*, **74**, 276 (1936).
- Harrison, W., *J. Soc. Dyers Colourists*, **27**, 84 (1911).
- Hatschek, Emil, *Kolloid-Z.*, **7**, 301 (1910).
- McDowell, C. M., and F. L. Usher, *Proc. Roy. Soc. (London)*, **A131**, 409, 564 (1931).
- Manegold, Erich, Remigius Hofmann, and Karl Solf, *Kolloid-Z.*, **56**, 142 (1931).
- Robinson, J. V., *J. Phys. Colloid Chem.*, **53**, 1042 (1949).
- Roscoe, R., *Brit. J. Appl. Phys.*, **3**, No. 8, 267 (1952).
- Smith, W. O., P. D. Toote, and P. F. Busang, *Phys. Rev.*, **34**, 1271 (1929).
- Ting, Andrew Pusheng, Ph.D. thesis, Univ. Missouri, University Microfilm, Ann Arbor, Mich. (1952).
- Vand, Vladimir, *J. Phys. Colloid Chem.*, **52**, 277, 300, 314 (1948).
- Ward, S. G., and R. L. Whitmore, *Brit. J. Appl. Phys.*, **1**, 286 (1950).
- White, G. F., *Ind. Eng. Chem.*, **4**, 267 (1912).

Presented at A.I.Ch.E. St. Louis meeting

An Empirical Correlation for Velocity Distribution of Turbulent Fluid Flow

B. F. RUTH and H. H. YANG

Lamar State College of Technology, Beaumont, Texas

PRANDTL, VON KARMAN, AND NIKURADSE EQUATIONS

The velocity distribution of a fluid flowing in a circular pipe has long been recognized as a problem of fundamental importance in mass and heat transfer. For the turbulent flow of an incompressible fluid, Prandtl (3) postulated that the shearing stress within the fully established turbulent core in a smooth pipe could be expressed by the following equation:

$$\tau = \rho l^2 \left(\frac{\partial u_m}{\partial y} \right)^2 \quad (1)$$

where l is a small increment in distance from the pipe wall and is usually called the *mixing length*. The total shearing stress of the fluid will equal the sum of apparent viscous and turbulent shearing stresses, as shown by Equation (2).

$$\tau = \mu \frac{du_m}{dy} + \rho l^2 \left(\frac{\partial u_m}{\partial y} \right)^2 \quad (2)$$

Since the viscous shearing stress is of negligible magnitude beyond the laminar boundary layer, Equation (2) may be simplified to include the turbulent shearing stress only and becomes

$$\sqrt{\tau} = l \frac{\partial u_m}{\partial y} \quad (3)$$

The term $\sqrt{\tau/\rho}$ has a dimension of velocity and is called the *shear velocity*, u_* . For further derivation, Prandtl made the following assumption for the vicinity of pipe wall:

$$l = ky \quad (4)$$

Therefore

$$u_* = ky \frac{\partial u}{\partial y} = ky \frac{du}{dy} \quad (5)$$

Upon integration, Equation (5) becomes

$$\frac{u_s - u}{u_*} = \frac{1}{k} \ln \frac{r}{y} \quad (6)$$

which is known as the *Prandtl equation for velocity distribution of turbulent fluid*

The material presented in this paper is taken from unpublished notes of B. F. Ruth, who until his death on January 1, 1954, was professor of chemical engineering at Iowa State College. The coauthor has selected and revised the original notes and developed some of the correlations.

in smooth pipes. The constant k is usually taken as 0.4 according to the experimental data of Nikuradse (2) for the turbulent region and 0.417 for the boundary region. For the turbulent core, therefore, Equation (6) becomes

$$\frac{u_s - u}{u_*} = 5.75 \log \frac{r}{y} \quad (6a)$$

Instead of Equation (4), Von Karman proposed to use the following expression to define the Prandtl mixing length:

$$l = k \frac{du}{dy} / \frac{d^2u}{dy^2} \quad (7)$$

This leads to the derivation of Equation (8), which also describes the velocity distribution of a turbulent core.

$$\begin{aligned} \frac{u_s - u}{u_*} &= -\frac{1}{k} \left[\sqrt{1 - \frac{y}{r}} \right. \\ &\quad \left. + \ln \left(1 - \sqrt{1 - \frac{y}{r}} \right) \right] \quad (8) \\ &= -\frac{1}{k} [\sqrt{x} + \ln(1 - \sqrt{x})] \end{aligned}$$

where $x = 1 - y/r$, the fractional radial distance from the axis of the pipe.

It may be seen that both Equations (6) and (8) indicate that $(u_s - u)/u_*$ is a function of y/r alone. A universal velocity-distribution curve may consequently be obtained by eliminating the term of maximum velocity u_s . An accepted correlation of this kind is that given following Equation (1).

$$\frac{u}{u_*} = 5.5 + 2.5 \ln \frac{yu_*\rho}{\mu} \quad (9)$$

or more conveniently expressed as

$$u^+ = 5.5 + 2.5 \ln y^+ \quad (10)$$

To examine the validity of these equations, $(u_s - u)/u_*$ vs. y/r was plotted in Figure 1, according to Equation (6a). Considerable discrepancy is indicated between this curve and the shaded experimental data of Nikuradse. The Nikuradse data cover a wide range of Reynolds number from 23,300 to 3,240,000. Equation (8) by Von Karman shows even greater deviation from the experimental data when plotted in the same manner as shown in Figure 1. In the derivation of Equation (6) the shearing stress τ and consequently u_* are assumed to be constant for all values of the radial distance y , i.e., from $y = 0$ to $y = r$. This assumption is certainly not in agreement with the actual behavior of fluids in turbulent flow and may be the cause of the discrepancy in both Equations (6) and (9).

The discrepancy is minimized by applying the law of linear stress distribution. Thus, the shearing stress to a fluid in turbulent flow in a smooth pipe is assumed proportional to the distance from the pipe wall,

$$\tau_x = \tau_r x \quad (11)$$

where τ_x is the shearing stress at a distance rx from the center of the pipe,

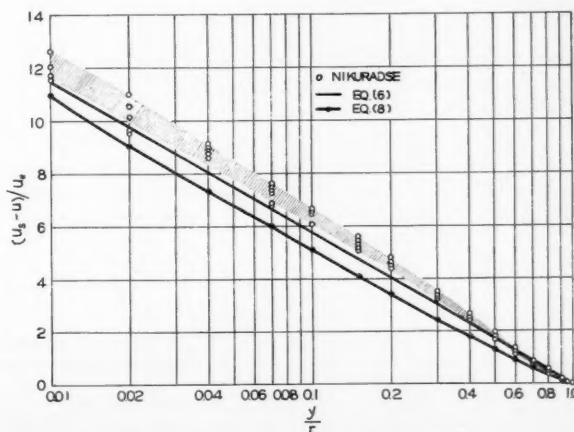


Fig. 1. Plot of $(u_s - u)/u_*$ vs. y/r .

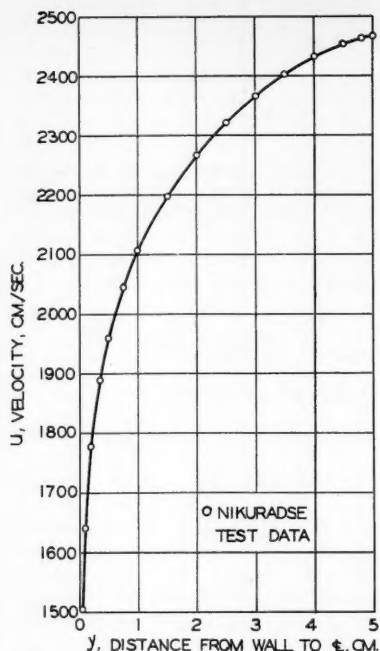


Fig. 2. Plot of u vs. y , using data of Nikuradse test No. 120.

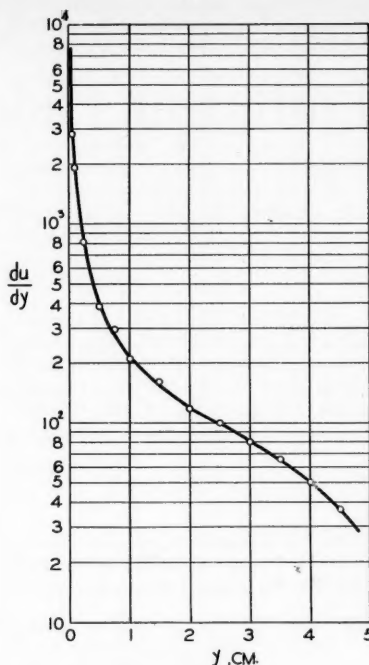


Fig. 3. Plot of du/dy vs. y , using data of Nikuradse test No. 120.

TABLE I
EMPIRICAL CORRELATION OF PRANDTL MIXING LENGTH

x	l/r	$x^{3/2}$	$\phi = 1 - x^{3/2}$	$(1/r)(dl/d\phi)$
1.00	0	1.00	0	0.273
0.98	0.0081	0.97	0.03	0.2586
0.96	0.0154	0.941	0.059	0.25
0.93	0.0250	0.897	0.103	0.2418
0.90	0.0355	0.854	0.146	0.2175
0.85	0.0507	0.7835	0.2165	0.1932
0.80	0.0627	0.715	0.285	0.1739
0.70	0.0834	0.586	0.414	0.1482
0.60	0.0995	0.465	0.535	0.1252
0.50	0.112	0.354	0.646	0.099
0.40	0.122	0.253	0.747	0.0895
0.30	0.129	0.1642	0.8358	0.0809
0.20	0.134	0.0892	0.9108	
0.10	0.138	0.0316	0.9684	
0.04	0.1395	0.00802	0.9919	
0.02	0.1398	0.00283	0.9972	
0	0.140	0	1.00	0.9591

and τ_r that in the vicinity of the pipe wall. Substituting $\tau_r x$ for τ in Equation (3) then gives

$$\sqrt{\frac{\tau_r x}{\rho}} = u_* \sqrt{x} = l \frac{du}{dy} \quad (12)$$

or

$$\frac{du}{dy} = \frac{u_* \sqrt{x}}{l} \quad (13)$$

Since

$$y = r(1 - x) \\ dy = -r dx$$

Equation (13) may be written as

$$\frac{du}{u_*} = -\frac{\sqrt{x} dx}{l/r} \quad (14)$$

It can be seen that if the dimensionless ratio of l/r could be expressed as a function of x , the foregoing equation could be integrated to form a new equation representing the velocity distribution for turbulent fluid inside a smooth pipe.

EMPIRICAL CORRELATION OF VELOCITY DISTRIBUTION

To determine l/r in terms of x , a set of typical velocity data of Nikuradse

test 120 was applied. The experimental data of velocity distribution were plotted in Figure 2 and differentiated graphically to yield du/dy as shown in Figure 3. Experimental values of l/r were then calculated according to Equation (13) as below:

$$\frac{du}{dy} = \frac{u_* \sqrt{x}}{l}$$

Hence,

$$\frac{l}{r} = \frac{u_* \sqrt{x}}{r \left(\frac{du}{dy} \right)} \quad (15)$$

The results were plotted against y in Figure 4.

An empirical correlation was made by Ruth, assuming l/r to be a function of $\phi = 1 - x^{3/2}$. Such a correlation was tabulated in Table 1 by use of the data of Figure 4. Values of l/r were first plotted against $1 - x^{3/2}$ in Figure 5. This curve has an exponentially decreasing slope $(1/r)(dl/d\phi)$ with respect to increasing ϕ as shown in Figure 6. This property enabled the development of an empirical equation which expresses l/r as a function of ϕ .

From Figure 6 it is seen that $(1/r)(dl/d\phi)$ has the following boundary values:

$$\frac{1}{r} \frac{dl}{d\phi} = 0.27 \text{ at } \phi = 0$$

$$\frac{1}{r} \frac{dl}{d\phi} = 0.06 \text{ at } \phi = 1$$

Hence

$$\log \left(\frac{1}{r} \frac{dl}{d\phi} \right) = \log 0.27 - 0.653\phi$$

$$\frac{1}{r} \frac{dl}{d\phi} = 0.27(10^{-0.653\phi}) = 0.27e^{-1.504\phi}$$

$$\frac{dl}{r} \cong 0.27e^{-1.5\phi} d\phi$$

Integrating the foregoing equation yields

$$\int_0^1 \frac{dl}{r} = \int_0^{\phi} 0.27e^{-1.5\phi} d\phi$$

$$\frac{l}{r} = \frac{0.27}{1.5} (1 - e^{-1.5\phi})$$

$$\frac{l}{r} = 0.18[1 - e^{-1.5(1-x^{3/2})}] \quad (16)$$

Equation (16) is an universal expression for the Prandtl mixing length l . A graphical correlation of l/r vs. x according to this equation is presented in Figure 7.

Substituting Equation (16) into (14) gives

$$\frac{du}{u_*} = \frac{-\sqrt{x} dx}{0.18[1 - e^{-1.5(1-x^{3/2})}]}$$

Integration again gives

$$\int_u^{u_*} \frac{du}{u_*} = \int_x^0 \frac{-\sqrt{x} dx}{0.18[1 - e^{-1.5(1-x^{3/2})}]}$$

One has then the following expressions for velocity difference $(u_* - u)/u_*$ similar to Equations (6) and (8):

$$\frac{u_* - u}{u_*} = 3.08$$

$$- 5.695 \log [e^{1.5(1-x^{3/2})} - 1] \quad (17)$$

Equation (17) is considered as the final form of this empirical derivation based on Prandtl's theory of mixing length. It was analyzed and graphically presented in Figure 8 so that it might be compared with the Nikuradse experimental data of test 120. A close agreement may be seen between the two curves for the entire range of y/r . Some deviation exists in the vicinity of the pipe wall where viscous shearing stress predominates. Although the correlated curve falls within the covered area of the Nikuradse data, Equation (17) may be regarded as a satisfactory expression for the behavior of a turbulent fluid. The correlation bears slight resemblance to Equations (6) and (8) in that they all have an exponential slope of 2.5, $k = 0.4$ being taken for the latter two.

GENERALIZED CORRELATION

For a more generalized correlation of velocity distribution, the term u_* in Equation (17) has to be excluded. Nikuradse's data were analyzed with an attempt to express u_*/u_* as a function of the modified Reynolds number $ru_*\rho/\mu$. This resulted in a semilogarithmic linear plot as shown in Figure 9. The straight line may be represented by the following equation:

$$\frac{u_*}{u_*} = 6.0 + 5.7 \log \frac{ru_*\rho}{\mu} \quad (18)$$

Combination of Equations (17) and (18) then yields the following equation

$$\frac{u}{u_*} = 2.92 + 5.7 \log \left\{ \frac{ru_*\rho}{\mu} [e^{1.5(1-x^{3/2})} - 1] \right\} \quad (19)$$

Thus u/u_* is no longer a function of $yu_*\rho/\mu$ or y^+ alone as is Equation (9) or (10). The velocity distribution of a turbulent fluid in terms of u/u_* is consequently not a linear function of $yu_*\rho/\mu$ on a semilogarithmic plot. This was confirmed by a careful plot of u/u_* vs. $yu_*\rho/\mu$ in Figure 10, which shows a series of wavy curves at various shearing-stress velocities. These curves propagate along the Nikuradse line with increasing Reynolds number and shearing-stress velocity. Equation (19) indicates a satisfactory agreement with the experi-

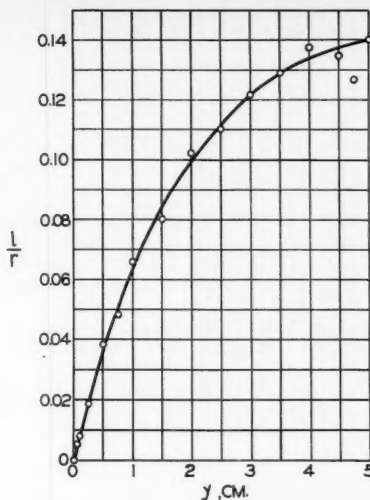


Fig. 4. Correlation of l/r vs. y , using data of Nikuradse test No. 120.

Fig. 6. Correlation of $(1/r) (dl/d\phi)$ vs. ϕ .

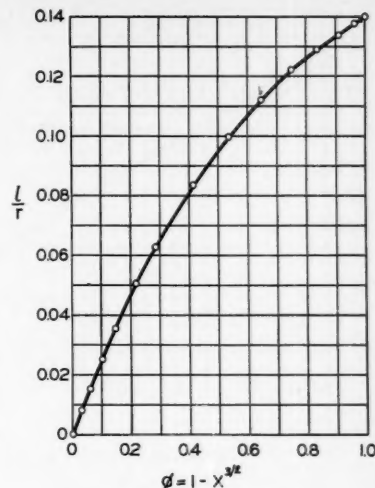
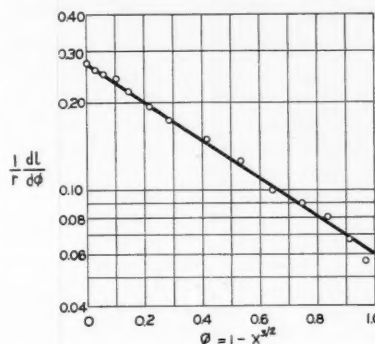
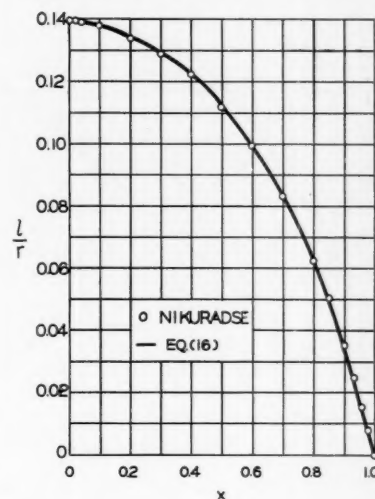


Fig. 5. Correlation of l/r vs. ϕ .

Fig. 7. Generalized correlation of l/r .



mental data of Nikuradse as can be seen in Figure 10. Equation (9) is good but only as an average throughout the turbulent region. Its deviation from actual data is approximately ± 0.5 of the u/u_* scale.

In regard to the average velocity of fluid through a pipe, Equation (17) may be transformed to give the following:

$$\begin{aligned} \frac{u_* - u_m}{u_*} &= \frac{1}{A} \int_0^A \{3.08 - 5.695 \\ &\quad \cdot \log [e^{1.5(1-x^{3/2})} - 1]\} dA \\ &= 2 \int_0^1 \{3.08 - 5.695 \\ &\quad \cdot \log [e^{1.5(1-x^{3/2})} - 1]\} x dx \quad (20) \end{aligned}$$

Numerical integration of Equation (2) and examination of fifty Nikuradse tests

on velocity distribution showed that

$$\frac{u_* - u_m}{u_*} = 4.07 \quad (21)$$

When u_*/u_* is substituted with Equation (18), Equation (21) becomes

$$\left(6.0 + 5.7 \log \frac{ru_*\rho}{\mu}\right) \left(1 - \frac{u_m}{u_*}\right) = 4.07$$

$$\frac{u_m}{u_*} = 1 - \frac{4.07}{6.0 + 5.7 \log \frac{ru_*\rho}{\mu}} \quad (22)$$

Although u_m/u_* could be expressed as a function of the modified Reynolds number given in Equation (22), the correlation is not so conveniently applicable as that of Senecal and Rothfus (4). Equation (22) indicates values of u_m/u_* ranging from 0.819 at $ru_*\rho/\mu = 1,080$

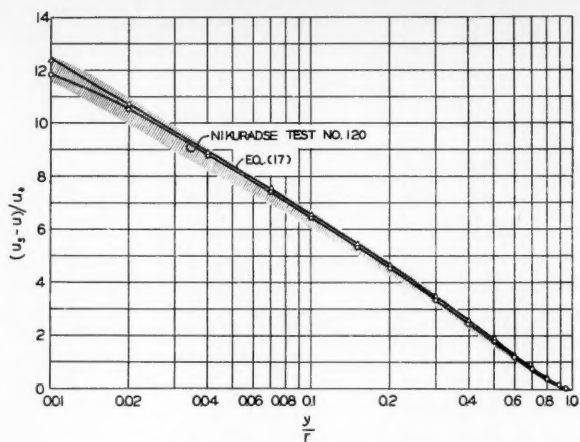


Fig. 8. Plot of $(u_s - u)/u_*$ vs. y/r .

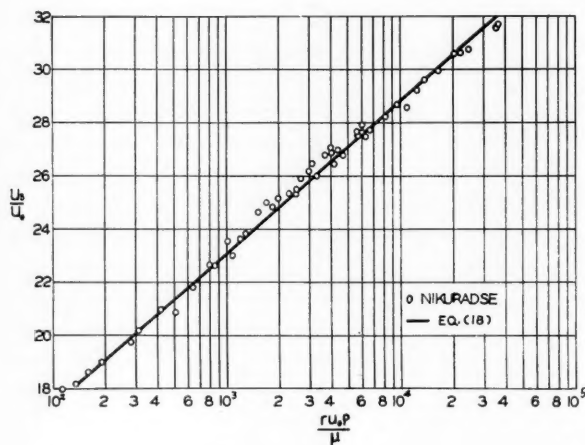


Fig. 9. Plot of u_s/u_* vs. $ru_*\rho/\mu$.

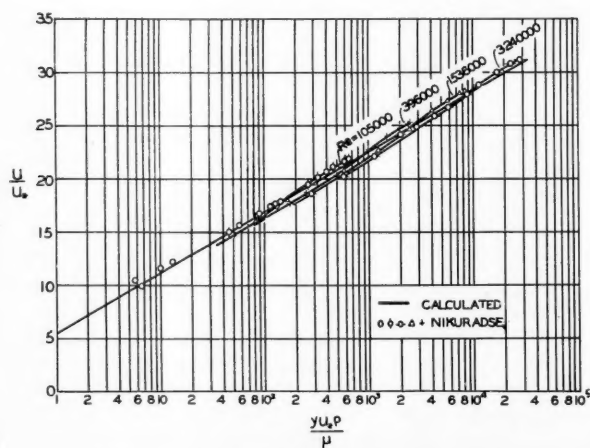


Fig. 10. Velocity distribution of turbulent fluid.

to 0.8725 at 55,900, which are in excellent agreement with the experimental values.

CONCLUSION

The foregoing empirical correlation of RUTH has established Equation (19) as a universal expression for fully developed turbulent flow in a smooth pipe. The equation shows that the velocity ratio u/u_* could be correlated against $ru_*\rho/\mu$ with the fractional radial distance x as a parameter. A plot of this equation would show a characteristic series of pulsating curves for fully developed turbulence similar to those shown in Figure 10. A generalized empirical equation for the Prandtl mixing length was also derived. Equation (16) shows the relationship between the ratio of l/r and the fractional radial distance x . The empirical correlation made possible a generalized expression for the ratio of average velocity of a turbulent fluid to its maximum velocity in terms of the modified Reynolds number $ru_*\rho/\mu$, which is given in Equation (22).

It must be stressed that the mixing-length correlation is valid only for Reynolds numbers over 100,000. This presumably restricts the final correlation to the same extent, i.e., fully developed turbulence.

NOTATION

- A = internal transverse area of pipe, sq. cm.
- k = proportionality constant
- l = Prandtl mixing length, cm.
- r = inside radius of pipe, cm.
- Re = Reynolds number = $(Du_m\rho)/\mu$
- u = velocity of fluid, cm./sec.
- u_m = mean velocity of fluid, cm./sec.
- u_s = maximum velocity of fluid, cm./sec.
- u_* = shearing-stress velocity of fluid, cm./sec. = $\sqrt{\tau/\rho}$
- x = fractional radius inside pipe = $1 - y/r$
- y = radial distance from pipe wall = $r(1 - x)$, cm.
- μ = viscosity of fluid, g./(cm.)(sec.)
- ρ = density of fluid, g./cc.
- τ = total shearing stress of fluid, g. force/sq. cm.
- τ_r = local shearing stress of fluid at pipe wall, g. force/sq. cm.
- τ_x = local shearing stress of fluid at a fractional distance x to center of pipe
- $\phi = 1 - x^{3/2}$

LITERATURE CITED

1. Martinelli, R. C., *Trans. Am. Soc. Mech. Engrs.*, **69**, 947 (1947).
2. Nikuradse, J., *V.D.I. Forschungsheft* 356 (1932).
3. Prandtl, Ludwig, "Essentials of Fluid Dynamics" [original text in German, translated into English by W. M. Deans], Hafner Publishing Company, New York (1952).
4. Senecal, V. E., and R. R. Rothfus, *Chem. Eng. Progr.*, **49**, 10, 533 (1953).

Studies of Thermal Conductivity of Liquids

BYRON C. SAKIADIS and JESSE COATES

Louisiana State University, Baton Rouge, Louisiana

Part III

Values of thermal conductivity and temperature coefficients for thirty-five pure organic liquids, in addition to those previously reported, obtained with a previously described apparatus (Part I), are presented. Values of thermal conductivity or temperature coefficients for twenty-eight of these liquids have not been reported before. The experimentally determined maximum error is $\pm 1.0\%$.

The two methods for predicting the thermal conductivity of liquids previously proposed (Parts I and II) are extended to cover the types of compounds studied in this investigation, in particular ring compounds.

The temperature coefficient of thermal conductivity was observed to decrease rapidly, approaching zero as the freezing point is approached. The existence of a transition temperature or region within the liquid state is shown and identified with the onset of molecular rotation.

This part of the series presents the results of a continuing study of the thermal conductivity of liquids and associated phenomena. The experimental apparatus was described in Part I, where the results of tests on fifty-three pure organic liquids, chain-type compounds, were reported. In this part the study was extended to new types of compounds, in particular to cyclic compounds, aromatics, and naphthenes, with side chains.

The data were correlated with the two methods previously proposed in Parts I and II. These methods represent different approaches to the problem. The method involving the theoretical equation throws light on the effect of molecular structure on thermal conductivity. The method involving a correlation of thermal conductivity as a function of reduced temperature emphasizes the effect of the functional atom or group in the molecule.

It was considered important also to investigate the variation of thermal conductivity with temperature in the regions close to the boiling and freezing points. The results are direct evidence of a new kind in support of the relatively recent idea on the existence of a transition temperature in the liquid state.

Experimental

The thermoconductimetric apparatus used in this study was described in detail in earlier publications (9, 10), where the results of a number of tests were also presented. The experimental procedure and method of calculation remain unchanged.

Results

The results obtained from the experimental determinations are presented in

Parts I and II appeared in the *A.I.Ch.E. Journal*, vol. 1, No. 3, p. 275 (1955).
B. C. Sakiadis is with E. I. du Pont de Nemours and Company, Inc., Wilmington, Delaware.

Table 1. The purity and sources of the chemicals are also indicated. The thermal conductivity of most liquids was determined at three temperatures equally spaced over the indicated temperature range, and the temperature coefficient was calculated from the results.

The experimentally determined maximum error in the value of thermal conductivity of liquids is $\pm 1.0\%$.

Comparison with Literature Values

An extensive literature survey has been made (7, 8), and values of thermal conductivity for numerous liquids have been collected, classified, and evaluated. Excluding the results of Bridgman, Daniloff, and Smith (7), determined with the same thin-film apparatus, which are high, the more dependable results fall mainly in two groups differing consistently by about 5%. The first group comprises the results of Riedel and Mason (7, 8) determined with similar but not identical thin-film apparatus. The second group comprises the results of Bates and Slawewski (7, 8), determined with thick- and thin-film apparatus respectively. The reported results differ in two respects. The values of thermal conductivity of the first group are low by about 5%, and the values of the temperature coefficient of thermal conductivity are also low. The results of the authors determined with a variable-film-thickness apparatus agree with the results of the second group.

It was shown by the authors (9, 10) that the consistent difference in the values of thermal conductivity of the two groups is due to surface effects and irregularities which were not accounted for by Riedel and Mason in the measurements of the liquid-film thickness by direct measurements.

In the apparatus used by Bates the liquid layer was about 2 in. thick, and the liquid-film thickness was measured directly within the liquid layer. Hence

the results should be free of any surface effects. Slawewski used a concentric type of thin-film apparatus but measured the liquid-layer thickness with electrical capacitance methods, thus obtaining a more representative average thickness. In the apparatus used by the authors the liquid-layer thickness is variable, and by means of a special method of calculation (10) the effect of surface films and irregularities is eliminated.

A comparison of reported values of the temperature coefficient of thermal conductivity with the authors' results shows that in all concentric types of thin-film apparatus, including that used by Slawewski, consistently low values are obtained. These are probably due to the expansion of the copper cylinders, at the higher operating temperatures, in the concentric type of apparatus used by these investigators. The results of Bates are consistently higher, but the effect has been traced (10) to the effects of heat transfer by radiation across the liquid layer, which were neglected by Bates.

DISCUSSION OF RESULTS

The thermal conductivity of liquids has been observed to vary linearly with temperature. In condensing apparatus the thermal conductivity of the liquid film at the boiling point is usually estimated by extrapolation of low-temperature data. It is important that this procedure be verified experimentally. Accordingly, the thermal conductivity of cyclopentane, cyclohexane, and ethyl alcohol was determined at temperatures close to the boiling point:

Liquid	Highest observed temperature, °F.	Boiling point, °F., at 1 atm.
Ethyl alcohol	167.0	173.1
Cyclopentane	116.7	120.7
Cyclohexane	168.7	177.4

The results show that the thermal conductivity varies linearly with temperature near the boiling point.

The region close to the freezing point is equally important. The thermal conductivity of *n*-dodecane, *n*-tetradecane, *n*-hexadecane, and *n*-octadecane was therefore determined at temperatures close to the freezing point. (*n*-Octadecane is a solid at room temperature.) The results are shown in Figure 1. The scatter of the data is within the maximum experimental error of $\pm 1.0\%$. The results show that the thermal conductivity is not a linear function of temperature as the freezing point is approached. Although *n*-dodecane does not show such behavior,

it is clear that at sufficiently low temperatures, outside the range of this apparatus, it could be expected to behave similarly.

The plots of Figure 1 bring up a number of interesting points. As the freezing point is approached, the temperature coefficient of thermal conductivity decreases rapidly toward zero. The thermal conductivity is observed to vary little with temperature in the region above the freezing point (14.7, 41.9, 64.6 and 81.9°F. for C_{12} , C_{14} , C_{16} , and C_{18} respectively).

Another point of interest is the shape of the curves in Figure 1. The curves show that there is a region where the

thermal conductivity drops sharply—about 4%—with a small temperature increase. In view of the fact that the temperature drop across the liquid layer in this apparatus is about 10°F., it is not certain whether this rapid drop extends over a range or whether it indicates transition phases with a sudden discontinuity. The idea of transition phases within the solid state is not new. A number of solid paraffins (3, 5, 13), alcohols (1), esters (2), and bromides (4) exhibit discontinuous changes in a number of physical properties at a transition temperature which have been attributed to the onset of hindered molecular rotation. The idea of transition phases within the liquid state is more recent. Moore, Gibbs and Eyring (6) conclude that far from being an amorphous and random aggregation of molecules, liquids not only possess a substantial degree of order, but many exhibit several recognizable transitions in addition to the solid-to-liquid and liquid-to-gas transitions. By considering the molecules in the liquid state to be arranged in a way similar to that adopted by the authors for the prediction of thermal conductivity (11), they suggest that many physical properties, when plotted against temperature, show abrupt discontinuities or transition temperatures. To confirm these ideas the authors have plotted properties for a large number of liquids as suggested by Moore, Gibbs, and Eyring. Careful consideration of the results leads to the conclusion that although there is some evidence for transition temperatures, it is far from being conclusive and the transition temperatures are difficult to establish. The authors believe that any transition temperatures present in the liquid state should be related to the transition temperatures observed in the solid state. Plots of freezing and transition points as functions of temperature for the solid paraffins (3, 5) show that transition temperatures appear only for the C_{25} to C_{38} paraffins. For paraffins with fewer than twenty-five carbon atoms the transition-temperature curve crosses the freezing-point curve. Transition temperatures in the solid state have been observed also for the first three members of the paraffin series. It is possible then that for the C_3 to C_{25} paraffins the transition temperature exists in the liquid state. The evidence on thermal conductivity presented by the authors appears to substantiate this idea. The observed transition region may then be identified with the onset of molecular rotation above which the molecules can rotate about their long axis or are "rotationally active." Qualitatively this may be visualized as follows. At a given temperature above the freezing point the molecules have a certain capacity to absorb energy for transfer. At the transition temperature part of this energy must be

TABLE 1.
OBSERVED VALUES OF THERMAL CONDUCTIVITY

Liquid	k at 100°F., B.t.u./(hr.) sq. ft.)/(°F./ft.)	$dk/dt \times 10^{-4}$, B.t.u./(hr.) sq. ft.)/(°F./ft.)	Temperature range, °F.	Source purity
Methyl ethyl ketone	0.0850	-1.68	103-152	4-c
Diethyl ketone	0.0830	-1.40	96-169	4-c
Methyl <i>n</i> -propyl ketone	0.0807	-1.40	102-169	4-c
2-Heptanone	0.0785	-1.20	107-169	2-b
3-Heptanone	0.0792	-1.13	110-169	2-e
4-Heptanone	0.0792	-1.22	103-169	2-e
2-Octanone	0.0796	-1.20	92-169	2-e
<i>n</i> -Butyl-ethyl ether	0.0725	-1.30	104-169	2-b
Di- <i>n</i> -butyl ether	0.0748	-1.30	101-169	2-b
Di- <i>n</i> -hexyl ether	0.0786	-1.12	101-169	2-b
1, 2-Bis (2-methoxy ethoxy) ethane	0.0942	-1.40	91-167	2-b
Ethylene glycol monomethyl ether	0.1064	-1.27	96-170	1-e
Ethylene glycol monoethyl ether	0.0982	-1.30	96-164	1-e
Ethylene glycol monobutyl ether	0.0904	-1.20	95-165	1-e
Diethylene glycol mono- methyl ether	0.1048	-0.95	101-165	1-e
Diethylene glycol monoethyl ether	0.1109	-0.88	101-164	1-e
Diethylene glycol monobutyl ether	0.0930	-0.90	101-165	1-e
Cyclopentane	0.0729	-1.09	90-117	5-a
Methyl cyclopentane	0.0666	-1.00	102-138	5-a
Cyclohexane	0.0686	-1.03	97-169	5-a
Methyl cyclohexane	0.0629	-0.97	104-168	5-a
Cyclohexene	0.0747	-1.20	98-165	5-a
Cyclohexanone	0.0817	-1.33	98-169	4-c
<i>i</i> -Propyl benzene	0.0715	-1.35	89-134	5-a
<i>n</i> -Butyl benzene	0.0758	-1.19	89-133	5-a
<i>n</i> -Dodecane	0.0797	-1.17	100-167	4-c
<i>n</i> -Tetradecane*	0.0794	-0.95	110-167	3-d
<i>n</i> -Hexadecane*	0.0819	-0.90	110-167	3-d
<i>n</i> -Octadecane*	0.0844	-0.85	110-167	3-d
Heptene-3	0.0749	-1.25	92-138	3-d
2, 4-Dimethyl pentane	0.0587	-1.00	100-152	5-a
<i>t</i> -Amyl alcohol	0.0682	-0.90	104-169	2-d
Heptanol-3	0.0801	-1.00	92-167	1-e
<i>n</i> -Decyl acetate	0.0818	-1.28	96-168	4-c
1-Bromododecane	0.0669	-0.86	98-169	2-b

*The given value of thermal conductivity is at 110°F. This value can be extrapolated to higher temperatures only. For values at lower temperatures see Figure 1.

- Source
1. Carbide and Carbon Chemicals Co.
 2. Eastman Organic Chemicals
 3. Humphrey-Wilkinson, Inc.
 4. Matheson Coleman and Bell, Inc.
 5. Phillips Petroleum Co.

- Purity
- a. Pure—99 mole % min.
 - b. "Eastman"—highest purity
 - c. Research—98% highest feasible purity
 - d. 95% min.
 - e. Practical

retained by the molecules to initiate rotation. As a result, the net energy transfer and thermal conductivity decrease sharply.

Two other points should be mentioned. (1) The position of the OH group in the alcohol molecule seems to play an important role: the thermal conductivity of heptanol-3 is much lower than that of *n*-heptyl alcohol. (2) The position of the functional group in a molecule (ether, ketone, or ester) having the same total number of carbon atoms does not affect the thermal conductivity.

The value of thermal conductivity of diethylene glycolmonoethyl ether is much higher than either the monomethyl or monobutyl member. This liquid is specified as low gravity by the supplier, and the effect is probably due to impurities. Literature data (8) confirm this observation.

CORRELATIONS OF THERMAL CONDUCTIVITY

Correlations of thermal conductivity are important for process calculations. Two general methods of predicting the thermal conductivity as a function of temperature were proposed by the authors (10, 11). In this paper the methods are extended to include the new data.

Correlation Based on a Modified Statement of the Theory of Corresponding States

According to this method the ratio of the thermal conductivity of two members of a given homologous series, at a given reduced temperature, is the same as that of the corresponding two members of any other homologous series at the same reduced temperature. The reduced pressure is omitted from the correlation, as at 1 atm. the effect of differences in reduced pressure on thermal conductivity is small.

The thermal conductivity of different homologous series was correlated as a function of reduced temperature with the number of effective carbon atoms as a parameter. The contribution to the thermal conductivity of a given functional group or atom in the molecule was determined by using the *n*-aliphatic hydrocarbons as a basis and taking the difference between it and the series in question at a reduced temperature $T_r = 0.6$. This temperature was selected in order to reduce the extrapolation of the experimental data. The contributions to the thermal conductivity were determined for ethers, ketones, monoglycol ethers, diglycol ethers, tertiary alcohols, naphthenes, and aromatic hydrocarbons. The results are shown in Table 2. The generalized chart for *n*-aliphatic hydrocarbons is shown in Figure 2. In this chart the line marked 12-18 should be used only if the molecules are "rotationally active," or about 70°F. above the freezing point. The convergence

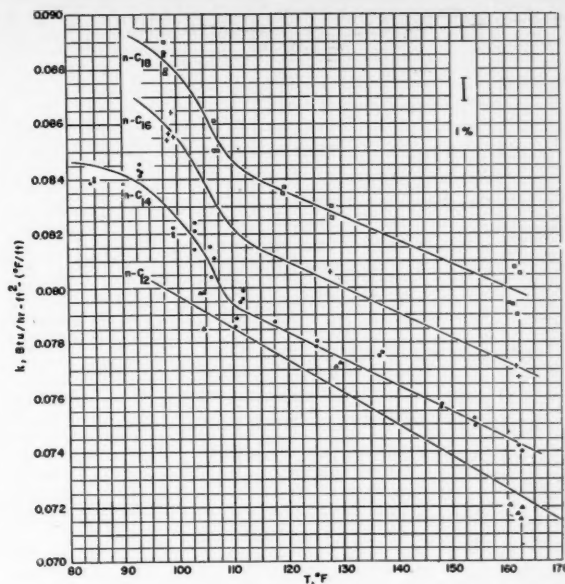


Fig. 1.

TABLE 2

STRUCTURAL CONTRIBUTION TO THE THERMAL CONDUCTIVITY OF LIQUIDS AT $T_r = 0.6$

A. Straight chain, saturated Basis: <i>n</i> -Aliphatic hydrocarbons		dk , B.t.u./ (hr./sq. ft.) (°F./ft.)	Effective number of carbon atoms, x
Series			
Hydrocarbons, C_nH_{2n+2}		0	$x = n$
Alcohols, $C_nH_{2n+1}OH$		+0.0070*	$x = n$
Esters, $C_nH_{2n}O_2$		-0.0070	$x = n - 2$
Halides, $C_nH_{2n+1}Cl$		-0.0168	$x = n$
$C_nH_{2n+1}Br$		-0.0248	$x = n + 1$
$C_nH_{2n+1}I$		-0.0310	$x = n + 2$
Nitro, $C_nH_{2n+1}NO_2$		0*	$x = n$
Ethers, $C_nH_{2n+2}O$		-0.0061	$x = n - 2$
Ketones, $C_nH_{2n}O$		-0.0041	$x = n - 2$
Monoglycol ethers, $C_nH_{2n+2}O_2$		0	$x = n - 2$
Diglycol ethers, $C_nH_{2n+2}O_3$		+0.0082	$x = n - 2$
B. Cyclic compounds			
I. Aromatic hydrocarbons			
Basis: Benzene† $k = 0.0800$ B.t.u./ (hr./sq. ft.) (°F./ft.)			
For contribution of added $-CH_2-$, $-CH_3$ groups in straight chain, consider benzene as ethane and determine contribution of groups as for <i>n</i> -aliphatic hydrocarbons.			
II. Naphthenes			
Basis: Cyclopentane. $k = 0.0738$ B.t.u./ (hr./sq. ft.) (°F./ft.)			
Contribution for each additional $-CH_2-$, or $-CH_3$ in ring or straight chain = -0.0083 B.t.u./ (hr./sq. ft.) (°F./ft.)			
C. Isomerization			
Type		dk , B.t.u./ (hr./sq. ft.) (°F./ft.)	
For one $-CH_3$ group		-0.0060	
For two $-CH_3$ groups		-0.0104	
For three $-CH_3$ groups		-0.0142	
Tert-alcohols $C \begin{array}{c} \text{C} \\ \\ \text{C} - \text{C} - \text{O} \\ \\ \text{C} \end{array}$		-0.0155	
D. Bonding (chain compounds)			
One double bond =		+0.0010	

*The first members of the high-polarity series, such as alcohols and nitrated alkanes, have a specific line as shown in Figure 2.

†This value for benzene has been obtained by extrapolation from the higher members.

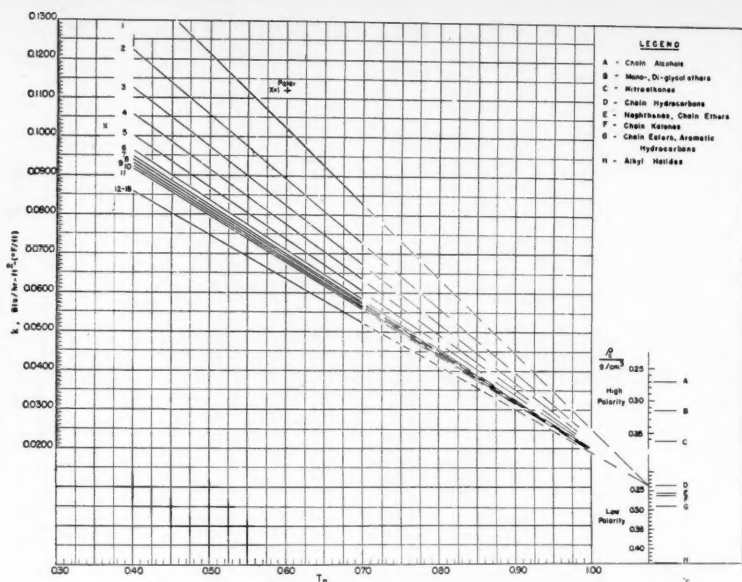


Fig. 2. Thermal conductivity vs. reduced temperature.

points of the different series are marked by letters but can be located also from

TABLE 3

A. Reference Points for Thermal Conductivity

Effective No. of carbon atoms, x	k , B.t.u./hr./sq. ft. (°F./ft.) at $T_r = 0.6$
1*	0.1022
2	0.0894
3	0.0822
4	0.0776
5	0.0738
6	0.0709
7	0.0700
8	0.0693
9	0.0687
10	0.0681
11	0.0675
12-18	0.0635

B. Coordinates for Critical-density Scales

1. Low-polarity series

ρ_c , g./cc.	k , B.t.u./hr./sq. ft. (°F./ft.) at $T_r = 1.075$
0.20	0.0145
0.25	0.0095
0.30	0.0045
0.35	-0.0005
0.40	-0.0055
0.45	-0.0105

2. High-polarity Series

ρ_c , g./cc.	k , B.t.u./hr./sq. ft. (°F./ft.) at $T_r = 1.075$
0.25	0.0411
0.30	0.0328
0.35	0.0245

*For the first members of the high-polarity series, such as methyl alcohol, the reference point is 0.1120 B.t.u./hr./sq. ft. (°F./ft.) at $T_r = 0.6$.

the critical density of the series. Although the critical density varies somewhat from member to member, an average value for two or three members is sufficient to locate the point. In this way the thermal conductivity for an entire series of liquids, at any temperature, can be estimated from a single known value. This value can be estimated by the previously presented (11) theoretical method.

The only data required in drawing Figure 2 are the reference values of k at $T_r = 0.6$ for the hydrocarbon series and the coordinates of the critical-density scales. These data are given in Table 3.

This method of calculation will be illustrated by two examples.

ILLUSTRATION 1. Calculate the thermal conductivity of *i*-propyl benzene at 120°F.

Data: $T_c = 1,145^\circ\text{R}$.

Basis: Benzene at $T_r = 0.6$

For contribution of *i*-propyl group, consider benzene as ethane; take the difference in k between ethane and *n*-pentane (or three carbon groups) at $T_r = 0.6$ from chart.

The difference is subtracted since the thermal conductivity decreases with increasing molecular size.

-[0.0894 (ethane) - 0.0738

(*n*-pentane)] =

1 isomerization

k

0.0800

-0.0156

-0.0060

0.0584

In Figure 2 locate this point at $T_r = 0.6$ and connect it with the convergence point for aromatic hydrocarbons by a straight line.

Read the value of thermal conductivity at $T_r = 0.506$ (120°F.).

$$k = 0.0689 \text{ B.t.u./hr./sq. ft.}(^\circ\text{F./ft.})$$

The observed value at the same temperature is 0.0688 B.t.u./hr./sq. ft. (°F./ft.).

ILLUSTRATION 2. Calculate the thermal conductivity of 3-heptanone at 140°F.

Data: $T_c = 1058^\circ\text{R}$. (estimated from the boiling point)

Effective number of carbon atoms $x = n - 2 = 7 - 2 = 5$

Structural contribution (Table 2) -0.0041

In Figure 2 locate the reference point for pentane, at $T_r = 0.6$, 0.0738. Subtract -0.0041 and locate new point, 0.0697. Connect the new point with the convergence point for ketones by a straight line. Read the value of thermal conductivity at $T_r = 0.566$ (140°F.).

$$k = 0.0742 \text{ B.t.u./hr./sq. ft.}(^\circ\text{F./ft.})$$

The observed value at the same temperature is 0.0747 B.t.u./hr./sq. ft. (°F./ft.).

This method of correlation was used to predict the thermal conductivity of the liquids tested in this investigation. The average deviation of the calculated from the observed values of thermal conductivity for a total of seventy-seven liquids (Parts I and II) is $\pm 1.3\%$. The maximum deviation is about $\pm 6.0\%$. The method of correlation was tested with respect to both the thermal conductivity and its temperature coefficient.

Correlation Based on Theoretical Equation

An equation, based on a simplified model of liquid state, for predicting the thermal conductivity of pure organic liquids and its temperature coefficient has been derived (Part II) and tested on a large number of straight-chain and branched liquids. Methods were also given for predicting the variables involved where no data are available (11, 12).

The equation is applicable to both normal and associated liquids. The only assumption involved in its derivation is a particular molecular arrangement in the liquid, which is in agreement with conclusions reached from X-ray diffraction studies. The equation is

$$k = C_p U_s \rho L \quad (1)$$

where

C_p = specific heat at constant pressure, B.t.u./lb. (°F.)

U_s = velocity of sound in the liquid, ft./hr.

ρ = liquid density, lb./cu. ft.

L = available intermolecular distance, ft.

k = thermal conductivity of liquid, B.t.u./hr./sq. ft. (°F./ft.)

In the calculation of the available intermolecular distance L for chain compounds, the assumption is made that the molecules, like rods in a bundle, are

TABLE 4

COMPARISON OF SOME EXPERIMENTAL VALUES OF THERMAL CONDUCTIVITY WITH VALUES CALCULATED BY THEORETICAL EQUATION AT 68°F.

Liquid	$k_{obs.}$ B.t.u./ (hr./sq. ft.) (°F./ft.)	C_p B.t.u./ (lb.)(°F.)	U ft./ sec.	ρ lb./ cu. ft.	$L \times 10^{-3}$ ft.	$k_{calc.}$ B.t.u./ (hr./sq. ft.) (°F./ft.)	% Dev.
Cyclopentane	0.0764	0.428	4290*	46.50	0.257	0.0790	+3.41
Methyl cyclopentane	0.0698	0.446	3980*	46.60	0.236	0.0703	+0.72
Cyclohexane	0.0719	0.442	3740*	48.50	0.252	0.0726	+0.97
Methyl cyclohexane	0.0660	0.442	3583	47.90	0.251	0.0685	+3.79
Cyclohexene	0.0785	0.429	3920*	50.50	0.251	0.0767	-2.29
Cyclohexanone	0.0859	0.433	4731	59.00	0.190	0.0827	-3.72
<i>i</i> -Propyl benzene	0.0758	0.388*	4365*	53.70	0.236	0.0772	+1.84
<i>n</i> -Butyl benzene	0.0796	0.403*	4430*	53.60	0.236	0.0813	+2.14

*Estimated values.

aligned perpendicular to the direction of heat flow.

The equation will be applied here to ring compounds. The available intermolecular distance for ring compounds is calculated on the assumption that the rings are stacked like coins with their longest dimension perpendicular to the direction of heat flow. As an example the benzene molecule will be considered. The thickness of the ring as determined by X-ray diffraction measurements (11) is 5.3 Å. = 1.738×10^{-9} ft. For purposes of calculation the shape of the ring will be taken as a square. The size of the edge can then be calculated readily from the critical density and the ratio of critical molecular volume and volume at absolute zero. For benzene:

$$v_c = 15.1 \times 10^{-27} \text{ cu. ft.}$$

$$v_c/v_0 = 3.94$$

$$v_0 = 3.83 \times 10^{-27} \text{ cu. ft.}$$

$$d = \left(\frac{v_0}{t}\right)^{1/2} = 1.485 \times 10^{-9} \text{ ft.}$$

The benzene ring then appears as a short parallelepiped with its thickness as the longer dimension. Hence the rings will be stacked with their thickness perpendicular to the direction of heat flow. The procedure for evaluating the available intermolecular distance for ring compounds is

1. Obtain v_c , v
2. Calculate v_c/v_0 and v_0
3. Obtain t [X-ray diffraction data (5)]
4. Calculate d and X
5. $L = X - d$

The necessary equations for obtaining these data are

$$v_c = \frac{M}{\rho_c \times 2.73 \times 10^{26}} \quad (2)$$

M = molecular weight

ρ_c = critical density, lb./cu. ft.

v_c = critical molecular volume, cu. ft.

$$v = \frac{M}{\rho \times 2.73 \times 10^{26}} \quad (3)$$

ρ = density at 68°F., lb./cu. ft.

v = molecular volume at 68°F., cu. ft.

$$n = \frac{v_c}{v_0} = 2 \left\{ 1 + \frac{(\rho_{f/2} - \rho_c)(T_c)}{(\rho_c)(T_c - T_f)} \right\} \quad (4)$$

ρ_f = density at freezing point, lb./cu. ft.

v_0 = molecular volume at absolute zero, cu. ft.

T_c = critical temperature, °R.

T_f = freezing point, °R.

$$v_0 = \frac{v_c}{n} \quad (5)$$

$$d = \left(\frac{v_0}{t}\right)^{1/2} \quad (6)$$

t = thickness of ring, ft. (Figure 3)

d = molecular width at absolute zero, ft. (Figure 3)

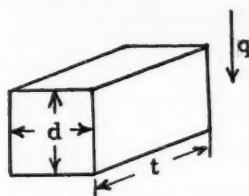


Fig. 3. Molecular model for simple ring compounds.

$$x = \left(\frac{v}{t}\right)^{1/2} \quad (7)$$

X = molecular width at 68°F., ft.

$$L = X - d \quad (8)$$

The correction for isomerization in the ratio n used for chain compounds is not necessary here. This method of evaluating the available intermolecular distance assumes that there is little or no empty space between molecules lined end to end or that the t dimension is the same at all temperatures. The same idea was used for chain compounds where the molecular length (equivalent to t here) l was taken as constant.

This method of evaluating the available intermolecular distance is strictly applicable to simple ring molecules such as benzene, cyclopentane, etc. The presence

of side carbon atoms introduces a complication. When the side chain is long enough, the question arises whether to consider the molecule as a ring or a chain. The problem is solved readily by considering the molecule first as a simple ring, that is, evaluating the side chain as an equivalent ring width, then as simple chain, that is, evaluating the ring as an equivalent chain length. The correct intermolecular distance is obtained by calculating a weighted average of the two. In taking the average the following dimensions are necessary.

Ring	Thickness, t , ft.
Benzene	1.485×10^{-9}
Cyclopentane	1.494×10^{-9}
Cyclohexane	1.588×10^{-9}
Chain	Incremental length
$-\text{CH}_2-$ or $-\text{CH}_3$	0.300×10^{-9} ft.

The method of calculation will be illustrated by an example.

ILLUSTRATION 3. Calculate the thermal conductivity of *n*-butyl benzene at 68°F.

Data:

$M = 134.21$

$T_c = 1190^\circ\text{R.}$

$T_f = 334^\circ\text{R.}$

$\rho = 53.60$ lb./cu. ft. at 68°F.

$\rho_f = 59.00$ lb./cu. ft. at T_f [estimated by Watson's relation (14)]

$\rho_c = 16.78$ lb./cu. ft. at T_c

$U = 4,430$ ft./sec. at 68°F. [estimated by method given in (11)]

$C_p = 0.403$ B.t.u./lb.(°F.) at 68°F. [estimated by method given in (12)]

Consider molecule as a ring.

$t = 5.30$ Å. (for benzene ring) + 0.42 Å.
(for side chain) = 5.72 Å. (11)

$t = 1.876 \times 10^{-9}$ ft.

$$n = v_c/v_0$$

$$= 2 \left\{ 1 + \frac{(29.50 - 16.78)}{16.78} \left(\frac{1,190}{856} \right) \right\} = 4.108 \quad (4)$$

$$v_c = \frac{134.21}{2.73 \times 10^{26} \times 16.78} = 29.30 \times 10^{-27} \text{ cu. ft.} \quad (2)$$

$$v_0 = \frac{29.30 \times 10^{-27}}{4.108} = 7.132 \times 10^{-27} \text{ cu. ft.} \quad (5)$$

$$d = \left(\frac{7.132 \times 10^{-27}}{(1.876 \times 10^{-9})^{1/2}} \right)^{1/2} = 1.951 \times 10^{-9} \text{ ft.} \quad (6)$$

$$v = \frac{134.21}{2.73 \times 10^{26} \times 53.60} = 9.172 \times 10^{-27} \text{ cu. ft.} \quad (3)$$

$$X = \left(\frac{9.172 \times 10^{-27}}{1.876 \times 10^{-9}} \right)^{1/2}$$

$$= 2.211 \times 10^{-9} \text{ ft.} \quad (7)$$

$$L = (2.211 - 1.951) \times 10^{-9}$$

$$= 0.260 \times 10^{-9} \text{ ft.} \quad (8)$$

Consider molecule as a chain (11).

$X = 1.771 \times 10^{-9}$ ft. [for straight-chain hydrocarbons (11)] (molecular length)

$$1 = \frac{v}{X^2} = \frac{9.172 \times 10^{-27}}{(1.771 \times 10^{-9})^2}$$

$$= 2.924 \times 10^{-9} \text{ ft.}$$

$$d = \left(\frac{v_0}{1} \right)^{1/2} = \left(\frac{7.132 \times 10^{-27}}{2.924 \times 10^{-9}} \right)^{1/2}$$

$$= 1.562 \times 10^{-9} \text{ ft.}$$

$$L = X - d$$

$$= (1.771 - 1.562) \times 10^{-9}$$

$$= 0.209 \times 10^{-9} \text{ ft.}$$

Weighted average available intermolecular distance

Thickness of ring	1.485 × 10 ⁻⁹
Length of chain	4 × 0.300 × 10 ⁻⁹
	= 1.200 × 10 ⁻⁹
	2.685 × 10 ⁻⁹ ft.

Contribution of ring =	
1.485 × 0.260 ×	
10 ⁻⁹ /2.685	= 0.1438 × 10 ⁻⁹
Contribution of chain =	
1.200 × 0.206 ×	
10 ⁻⁹ /2.685	= 0.0921 × 10 ⁻⁹

Weighted average available intermolecular distance

$$0.2359 \times 10^{-9} \text{ ft.}$$

Thermal conductivity

$$k = C_p U_s \rho L \quad (1)$$

$$k = 0.403 \times 4,430 \times 3,600 \times 53.60 \times 0.236 \times 10^{-9} = 0.0813 \text{ B.t.u.}/(\text{hr.}/\text{sq. ft.})$$

$$\text{C}^\circ\text{F.}/\text{ft.})$$

The observed value at the same temperature is 0.0796 B.t.u./(hr.)(sq. ft.)(°F./ft.). The temperature coefficient of thermal conductivity may be estimated by the method given in Part II. It can also be estimated as follows. Locate the calculated value of conductivity at 68°F. on Figure 2. Estimate the critical density of the liquid and locate convergence point. Connect the two points by a straight line.

This method of correlation was used to predict the thermal conductivity of the ring compounds tested in this investigation. The results are presented in Table 4. The average deviation of the calculated from the observed values of thermal conductivity for a total of fifty liquids, chain and ring compounds, is ±2.6%. The maximum deviation is about ±6.0%. This method of calculation is more tedious than the method based on the modified theory of correspond-

ing states. However, it has the advantage that it requires no experimental data on thermal conductivity. A better example of its usefulness would be its application to the case of 1,2-bis (2-methoxy ethoxy) ethane, which is polyether. The compound is relatively new, and few data are available on its properties. Further, it cannot be classified into any of the types of liquids so far studied. Consequently the theoretical analysis is required. All the necessary data have to be estimated.

$M = 178.22$	$\rho_c = 19.67 \text{ lb.}/\text{cu. ft.}$
$T_b = 882.2^\circ\text{R.}^*$	$\rho_f = 63.6 \text{ lb.}/\text{cu. ft.}^*$
$T_c = 1194^\circ\text{R.}^*$	$U_s = 4,100 \text{ ft.}/\text{sec.}^*$
$T_f = 460^\circ\text{R.}^*$	$C_p = 0.498 \text{ B.t.u.}/(\text{lb.})(^\circ\text{F.})^*$

*Estimated values.

The only property that could not be estimated with the required accuracy was the density at 68°F. Actual measurements on the compound gave a value of 61.50 lb./cu. ft. The result is

$k = 0.0973 \text{ B.t.u.}/(\text{hr.}/\text{sq. ft.})(^\circ\text{F.}/\text{ft.})$	calculated
$k = 0.0987 \text{ B.t.u.}/(\text{hr.}/\text{sq. ft.})(^\circ\text{F.}/\text{ft.})$	observed

In view of the errors introduced by the necessity of estimating all but one of the required variables, the observed deviation is satisfactory.

SUMMARY

Observed values of thermal conductivity and temperature coefficients are presented for thirty-five pure organic liquids, in addition to those reported in Part I. Values of thermal conductivity or temperature coefficients for twenty-eight of these liquids have not been previously reported.

The experimental results were correlated by two previously proposed methods. The method based on a theoretical equation, previously used for chain compounds (Part II), was adapted here for calculations on cyclic compounds. The method based on a modified statement of the theory of corresponding states (Part I) was extended to cover the new types of organic compounds studied in this investigation.

The thermal conductivity of three liquids was observed to vary linearly with temperature up to about the boiling point, at 1 atm., of the liquids. In the region close to the freezing point, it was observed, for the higher *n*-paraffins, that the thermal conductivity ceases to be a linear function of temperature. The temperature coefficient of thermal conductivity approaches zero as the freezing point is approached. A transition temperature or region within the liquid state was observed and identified with the onset of molecular rotation.

ACKNOWLEDGMENT

The authors wish to acknowledge the assistance of George Linder, a research

fellow, who performed part of the experimental work.

This research was conducted under National Science Foundation Grants G-221 and 558. The Department of Chemical Engineering and the Engineering Experiment Station provided additional funds and facilities.

NOTATION

- C_p = specific heat at constant pressure, B.t.u./(lb.)(°F.)
 d = molecular diameter at absolute zero, ft.
 k = thermal conductivity, B.t.u./(hr./sq. ft.)(°F./ft.)
 L = mean available intermolecular distance, surface to surface, ft.
 l = molecular length, ft.
 M = molecular weight
 n = number of carbon atoms in molecule, ratio of critical to minimum molecular volume
 q = heat flow
 T, t = temperature, °R., °F.
 t = molecular thickness, ring compounds, ft.
 U_s = velocity of sound in liquid, ft./sec.
 v = molecular volume at given temperature, cu. ft.
 X = molecular diameter at given temperature, ft.
 x = effective number of carbon atoms

Greek Symbols

- ρ = density, lb./cu. ft.

Subscripts

- b = boiling point
 c = critical
 f = freezing point
 0 = absolute zero
 r = reduced

LITERATURE CITED

- Baker, W. O., and C. P. Smyth, *J. Am. Chem. Soc.*, **60**, 1229 (1938).
- Crowe, R. W., and C. P. Smyth, *ibid.*, **73**, 5401 (1951).
- Fontana, B. J., *J. Phys. Chem.*, **57**, 222 (1953).
- Hoffman, J. D., *J. Chem. Phys.*, **20**, 541 (1952).
- Hoffman, J. D., and B. F. Decker, *J. Phys. Chem.*, **57**, 520 (1953).
- Moore, R. J., P. Gibbs, and H. Eyring, *ibid.*, **57**, 172 (1953).
- Sakiadis, B. C., and Jesse Coates, *Louisiana State Univ. Eng. Exp. Sta. Bull. No. 34*, Baton Rouge (1952).
- Ibid.*, No. 48 (1954).
- Ibid.*, No. 45 (1954).
- , *A.I.Ch.E. Journal*, **1**, 275 (1955).
- Ibid.*, p. 281.
- Ibid.*, **2**, 88 (1956).
- Seyer, W. F., R. F. Patterson, and J. L. Keays, *J. Am. Chem. Soc.*, **66**, 179 (1944).
- Watson, K. M., *Ind. Eng. Chem.*, **35**, 398 (1943).

Presented at A.I.Ch.E. Houston meeting

Mass and Heat Transfer from Drops in Liquid-liquid Extraction

A. E. HANDLOS and T. BARON

Shell Development Company, Emeryville, California

Mass and heat transfer rates in extraction are studied theoretically and experimentally for the practical range of the variables involved. For the particular but typical case of liquid drops moving through another liquid a simple correlation for the over-all mass transfer coefficient is presented, which holds with a probable error of 20%.

Included are systems in which the rate is limited by either coefficient, as well as systems in which both coefficients are significant. The correlation, valid for both directions of transfer with either phase dispersed, is useful for the extrapolation of performance from system to system in a given piece of equipment. Also, together with correlations for transfer area and effective driving force, it is part of the information needed for design.

The rate of transfer in any exchange process depends on three factors: the area of contact, the effective driving force, and the transfer coefficient. Occasionally these factors can be evaluated with comparative ease; for example, in a heat exchanger the area is determined solely by the geometry of design, the local driving force is the temperature difference, which may be easily found, and the transfer coefficient in the form of a Nusselt number is known from experiment as a function of the Reynolds and Prandtl numbers.

In principle, rates of mass transfer in an extraction device can be calculated in the same way. The source of the difficulty is that the three factors discussed above cannot be evaluated easily. For instance, no simple relation is known for the contact area and such design variables as throughput of the phases and geometry of distributor and contactor. Actually, the average contact area depends on the frequency distribution of sizes of the dispersed phase and the rate of rise (or fall) of the latter relative to the continuous phase, as well as on the circulation rates of the continuous phase. All these factors are determined by fluid-mechanical processes which are too complicated to be subject to theoretical evaluation. At the same time the large number of experiments necessary for an empirical attack have not yet been carried out.

Similar difficulties are encountered in averaging whatever driving force determines the rate of mass transfer at a given point, because in most extraction apparatus the circulation of the continuous phase results in flow patterns which are neither truly countercurrent nor truly concurrent. The circulation patterns are rarely known and even if they were known, the evaluation of the proper average driving force would be difficult mathematically.

In contrast to the large amount of experimental and theoretical work on transfer coefficients for heat transfer, the experimental and theoretical information available on mass transfer coefficients in extraction is inadequate. This lack of information is due partly to the discouraging results of the earlier investigators. Correlations along patterns well established in heat transfer and simple mass transfer situations have been unsuccessful. Slight differences in experimental conditions have unexplainably large effects. Furthermore, investigators in different laboratories obtain occasionally divergent results.

The three factors controlling extraction rates—the area, the average driving force, and the transfer coefficient—are best considered separately. This paper is a study of the mass transfer coefficient, which was chosen as the first step because simple conditions can be devised in which the transfer area and average driving force are controlled. Specifically, the study is restricted to mass or heat transfer to single drops. In the first phase of the work described below, the data in the literature were examined and correlated on the basis of mathematical models set up for this purpose. These correlations were promising, but some further work was necessary because the range of experimental conditions covered in the literature was small and in some cases the conditions were incompletely specified. The new data agree satisfactorily with the correlations derived, the root mean square percentage error being approximately 30%.

MASS TRANSFER AND THE THERMODYNAMICS OF IRREVERSIBLE PROCESSES

The object of this paper is to study the mass transfer from a liquid drop to the

continuous phase of another liquid in which it is freely rising or falling. Observation and theory indicate that during the course of their motion the drops execute small vibrations about an approximately spherical equilibrium configuration. Although this motion may play a significant role in determining the rate of mass transfer, it is hardly significant as far as the area of transfer is concerned. In the range of drop diameters of interest, say from 2 to 5 mm., the amplitude of this motion is small and therefore the area of the drop may be taken as that of a sphere of equivalent volume. If desired, small distortions may be taken into account in the transfer coefficient.

The problem of choosing a proper driving force is a more subtle one. Two general schemes are known for the treatment of irreversible phenomena: the kinetic theory of matter and the thermodynamics of irreversible processes. Unfortunately, the kinetic theory of liquids is not sufficiently advanced to furnish a reliable guide in the evaluation of diffusion in liquids. One must turn, therefore, to the theory of irreversible thermodynamics, which, at least at first glance, appears to furnish a considerable amount of information. In the absence of cross effects, the diffusion flux calculated from the rate of entropy production can be shown to be (6)

$$\bar{J}_1 = -L_1 \nabla(\bar{G}_1 - \bar{G}_2) \quad (1)$$

where J_1 is the diffusion flux of species 1, and \bar{G}_1 and \bar{G}_2 are the chemical potentials of species 1 and species 2, respectively; L is a coefficient for which the theory furnishes no information. Equation (1) can be put into a more attractive form by use of the Gibbs-Duhem equation,

$$x_1 d\bar{G}_1 + x_2 d\bar{G}_2 = 0; P, T \text{ constant} \quad (2)$$

and the material-balance relation,

$$x_1 + x_2 = 1 \quad (3)$$

Equation (1) may be put into either one of the following forms:

$$\bar{J}_1 = -\frac{L_1}{x_2} \nabla \bar{G}_1 \quad (4)$$

or

$$\bar{J}_1 = -\frac{L_1}{x_2} \left(\frac{\partial \bar{G}_1}{\partial x_1} \right)_{P,T} \nabla x_1 \quad (5)$$

The difficulty with these apparently useful equations is that the phenomenological coefficient L can by no means be assumed to be constant. This limitation is illustrated by applying the same theory to the familiar process of heat conduction in a solid. In this case the heat flux calculated from the rate of entropy production is given by

$$\bar{Q} = -\frac{L_2}{\theta^2} \nabla \theta \quad (6)$$

which, when compared to Fourier's law of heat conduction,

$$\bar{Q} = -k \nabla \theta \quad (7)$$

yields the following expression for the phenomenological coefficient L_2 :

$$L_2 = k \theta^2 \quad (8)$$

In most solids the thermal conductivity k is known to increase with the temperature; therefore, the coefficient for heat transfer in these cases increases faster than the square of the temperature.

Similarly, the coefficient L_1 may well depend on the chemical potential as well as on other parameters such as the viscosity. In this case the gradient of any "well-behaved" function of the chemical potential may be used as a driving force, as (46, 53)

$$\left. \begin{aligned} \bar{J}_1 &= -L_3 \nabla f(\bar{G}_1) \\ &= -L_3 \frac{df(\bar{G}_1)}{d\bar{G}_1} \nabla \bar{G}_1 \\ L_3 &= \frac{L_1}{x_2} \left[\frac{df(\bar{G}_1)}{d\bar{G}_1} \right]^{-1} \end{aligned} \right\} \quad (9)$$

is equivalent to Equation (4).

From a practical point of view, the function $f(\bar{G}_1)$ is best chosen in such a way that the quantity

$$L_3 \frac{df(\bar{G}_1)}{d\bar{G}_1}$$

remains as nearly constant as possible. The most convenient relationship is $f(\bar{G}_1) = c_1$, where c_1 is the concentration, because the concentrations can be calculated easily and are particularly suitable in the construction of various mathematical models especially when convec-

tion phenomena play an important role. On the other hand, as shown below, when the driving force is based on the gradient of activities the correlations improve significantly.

DEVELOPMENT OF CORRELATIONS

The method of correlation by dimensional analysis also has severe limitations in the present case. This is evident when one considers the variables which may be of significance in the mass transfer process. If mass transfer across both "films" is considered as a single problem, the variables are the diameter of the drop; the densities, viscosities, and diffusivities of the two phases; the relative velocity; interfacial tension; distribution ratio; and mass transfer coefficient. Since there are only three fundamental dimensions, one obtains from the Buckingham Pi theorem a relation among eight dimensionless numbers, such as

$$Nu = Nu(Re, Sc, We, \frac{\rho'}{\rho}, \frac{\mu'}{\mu}, \frac{D'}{D}, m) \quad (10)$$

The form of the functional relationship is unknown. The difficulty with this approach is apparent when one realizes that the number of dimensionless relationships involved is of the order of magnitude of the number of sets of independent data available. Another difficulty arises because the dimensionless ratios cannot be varied independently. Hence the number of combinations to be studied is very large. This difficulty remains when one considers the transfer across the inside and outside films separately. It is still necessary to determine two relations, each of which has the same form as Equation (10) except that the ratio of the diffusivities is eliminated.

In order to overcome these difficulties, it is convenient to construct simple mathematical models of transfer and to test these against the available data. It was recognized that the hydrodynamics of the flow pattern is markedly different in the regions inside and outside the drop. Accordingly, the inside and outside regions, i.e., the so-called "inside and outside films," are best treated separately. Of the various models tested, only the most successful ones for each film are presented.

First the transfer from the main body of the continuous phase to the interface of the drop is considered. A simple expression for the outside coefficient may be obtained in two different ways. If one considers a volume element of the continuous phase coming into contact with the drop at the forward stagnation point, as did Higbie (20), and calculates the unsteady state mass transfer for this volume element as it flows around the drop, the mass transfer coefficient turns out to be

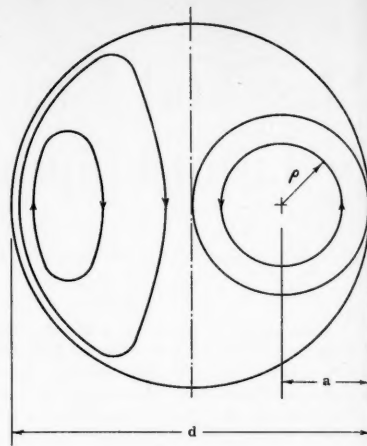


Fig. 1. Circulation patterns in drop.

$$Nu_0 = c \sqrt{Pe_0} \quad (11)$$

the constant c is determined by the time of contact between the two phases; this procedure is uncertain as the peripheral velocity is not known. On the other hand, the problem may be treated as a steady state boundary-value problem, in which the mass transfer coefficient can be calculated from the solution of the appropriate Fourier-Poisson equations. The difficulty here is that the steady state velocity distribution in the continuous phase is not known exactly and that furthermore the equations can be solved only when the velocity distribution follows some rather simple pattern. One may assume, as Pigford (23) did, that the radial velocity at any point is negligible and that the tangential velocity is everywhere equal to the velocity of the drop. With this assumption, the equations may be solved and one again obtains Equation (11) for the transfer coefficient. The constant c depends on the choice of the magnitude of the tangential velocity. Satisfactory agreement with the data are obtained when, as West (50) suggests, one calculates the time of contact between phases from the ratio d/\bar{V} . In this case Equation (11) becomes

$$Nu_0 = 1.13 \sqrt{Pe_0} \quad (12)$$

In the correlation presented below, the mass transfer coefficient for the outside film is always evaluated from this equation.

The problem of mass transfer within the drop is much more difficult. The simplest approach is to assume that the drop is stagnant and to calculate the rate of mass transfer by solving the ordinary equations of diffusion. Unfortunately, the mass transfer coefficients calculated in this way are usually an order of magnitude too small. The reason for this discrepancy must be that there is motion within the

drop. Kronig and Brink (25) have solved the Fourier-Poisson equations, using Hadamard's (19) circulation patterns, which were obtained on the assumption of viscous flow. The results show little improvement, as the only effect of treating the problem this way is to reduce the effective diameter of the drop (by a factor of approximately two) to a length characteristic of the circulation pattern.

The difficulty here is that the motion is highly turbulent. (The Reynolds numbers are about 1,000.) Thus attempts to set up exact equations are futile. A schematic model which takes into account the vibrations of the drop as well as the circulation patterns within the drop is necessary. In the following exposition the tangential motion caused by circulation is combined with the assumed random radial motions due to vibrations in the evaluation of an eddy diffusivity which, with a simplified circulation pattern, is used in the solution of the appropriate Fourier-Poisson equations. While the model may indeed represent the salient physical features of the transfer process within the drop, the justification is, of course, the agreement with experimental data.

The existence of circulation inside the drop has been inferred from a comparison of the drag coefficients of rising (or falling) drops with those of solid spheres at the same Reynolds number (2, 22). Circulation has also been observed directly (12, 13, 39, 42) as well as oscillations of the drop (21, 27), which would increase mixing within the drop. Garner, Skelland, and Hale (11) have shown that some trace impurities can retard circulation and that the transfer of a solute can promote circulation.

All these observations may be summarized by stating that the circulation which can be inferred from the usual equations of motion (19) has been frequently observed; however, in many instances, circulation did not develop. Whether this unexpected occasional rigidity is caused by trace impurities or some other surface effects is not known. No satisfactory criterion for the onset of circulation exists. The extraction model developed below is based on the assumption that the circulation in the drop is fully developed. Examination of the mass and heat transfer data in the light of this correlation showed no evidence of deviations that could be attributed to a lack of circulation.

Figure 1 shows a schematic drawing of the drop in which the streamlines of Hadamard are replaced by a system of tori shown in the cross section at the right. A particle is considered initially at a radius ρ . After a time sufficient for one circuit along a streamline, the particle is displaced to a point ρ' as a result of the assumed random radial motions. In the limiting case of complete mixing in one circulation period, the

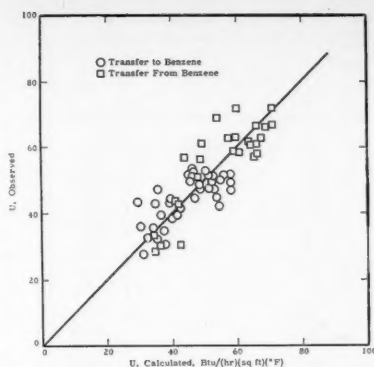


Fig. 2. Correlation of over-all heat transfer coefficients for benzene drops in water.

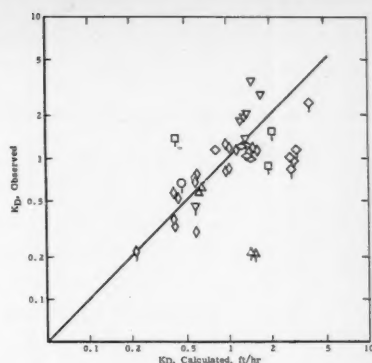


Fig. 3. Correlation of over-all mass transfer coefficients based on literature data; see Table 1 for key.

probability that a particle is found between ρ' and $\rho' + d\rho'$ is the ratio of the differential element of volume at ρ' to the total volume of the torus.

$$P(\rho') d\rho' = \frac{32\rho'}{d^2} d\rho' \quad (13)$$

With the substitution

$$r = \frac{4\rho}{d} \quad (14)$$

Equation (13) becomes

$$P(r') dr' = 2r' dr' \quad (15)$$

Accordingly, the square of the displacement is

$$z^2 = \frac{d^2}{16} (r' - r)^2 \quad (16)$$

If this experiment with the particle is repeated often, the mean square displacement is simply the expectation value of z^2 , which is

$$\begin{aligned} \bar{z}^2 &= \int_0^1 z^2(r') P(r') dr' \\ &= \frac{d^2}{8} \int_0^1 r'(r' - r)^2 dr' \\ &= \frac{d^2}{96} (6r^2 - 8r + 3) \quad (17) \end{aligned}$$

The characteristic time for the average displacement, i.e., the average circulation time is given by Kronig and Brink (25):

$$t = \frac{16d}{3V} \left(1 + \frac{\mu_i}{\mu_0} \right) \quad (18)$$

If the transfer process can be described by eddy diffusion, the transfer process is also represented by the Einstein equation, which connects the mean square deviation for a given time to the effective diffusivity:

$$E(r) = \frac{\bar{z}^2}{4t} = \frac{dV}{2,048} \frac{(6r^2 - 8r + 3)}{(1 + \mu_i/\mu_0)} \quad (19)$$

Multiplying and dividing by the molecular diffusivity, one obtains

$$E(r) = \frac{D \cdot Pe_i'}{2,048} (6r^2 - 8r + 3) \quad (20)$$

where

$$Pe_i' = \frac{Pe_i}{(1 + \mu_i/\mu_0)} \quad (21)$$

The equation of continuity in the chosen coordinate system is

$$\frac{\partial c}{\partial t} = \frac{16}{d^2} \frac{1}{r} \frac{\partial}{\partial r} \left(E \cdot r \frac{\partial c}{\partial r} \right) \quad (22)$$

If

$$r = 1 - y \quad (23)$$

then substituting Equations (20) and (23) into (22) yields

$$\begin{aligned} \frac{2,048d^2}{16DPe_i'} \frac{\partial c}{\partial t} \\ = \left[\frac{1}{1-y} \frac{\partial}{\partial y} (1-5y+10y^2-6y^3) \frac{\partial c}{\partial y} \right] \quad (24) \end{aligned}$$

The boundary conditions are

$$\begin{aligned} c &= c_0 \text{ at } t = 0, 0 \leq y \leq 1 \\ c &= 0, y = 0, t > 0 \end{aligned} \quad (25)$$

The problem is thus reduced to one of finding the solution of Equation (24) with the boundary conditions given by Equations (25). This can be done by the method of separation of variables. If

$$c = T(t)Y(y) \quad (26)$$

Equation (25) can be separated into two ordinary differential equations:

$$\frac{dT}{dt} = -\frac{16\lambda DPe_i'}{2,048d^2} \cdot T \quad (27)$$

and

$$\begin{aligned} \frac{d}{dy} (1 - 5y + 10y^2 - 6y^3) \frac{dY}{dy} \\ + \lambda(1 - y)Y = 0 \quad (28) \end{aligned}$$

TABLE 1. SUMMARY OF PUBLISHED MASS TRANSFER DATA

Solute	Continuous Phase	Dispersed Phase	Transfer to:	d cm.	V cm/sec	K_D obs	K_D calc.	Ref.	Symbol ^{a)}	
						ft/hr				
Acetic Acid	Methyl iso-butyl ketone	Water	Water	.161	9.9	1.16	1.02	(29)	◇	
	"	"	"	.161	9.9	0.83	1.01			
	"	"	"	.161	9.9	0.81	0.98			
	"	"	"	.161	9.9	1.23	0.98			
	"	"	"	.094	4.9	0.76	0.60			
	"	"	"	.094	4.9	0.30	0.59			
	"	"	"	.094	4.9	0.66	0.58			
	"	"	"	.094	4.9	0.70	0.58			
	"	"	"	.069	3.2	0.52	0.44			
	"	"	"	.069	3.2	0.33	0.42			
	"	"	"	.069	3.2	0.37	0.41			
	"	"	"	.069	3.2	0.57	0.41			
	"	"	"	.206	12.8	1.12	1.14			
	"	"	MIBK	.202	13.2	1.19	1.28			
	Water	MIBK	MIBK	.170	7.5	0.66	0.46			◇
Water	MIBK	Water	.220	10.4	1.39	0.42	□			
Acetic Acid	MIBK	Water	MIBK	.406	12.3	0.97	1.46	(26)	◇	
	"	"	"	.342	11.6	1.00	1.40			◇
	Ethyl Acetate	"	Ethyl Acetate	.406	8.7	1.06	0.82			◇
	Isopropyl Ether	"	Isopropyl Ether	.452	15.9	0.56	0.61			△
	Isopropyl Ether	"	Isopropyl Ether	.344	15.1	0.61	0.64			△
Acetic Acid	MIBK	Water	Water	.295	13.2	1.11	1.62	(34)	◇	
	"	"	"	.354	12.5	1.18	1.51			◇
	"	"	"	.418	11.9	1.09	1.42			◇
Acetic Acid	Water	Benzene	Water	.576	11.7	1.12	3.09	(44)	◇	
	"	"	"	.557	11.1	0.93	2.94			
	"	"	"	.536	10.7	0.81	2.83			
Diethylamine	"	"	"	.554	11.4	0.21	1.53		△	
	"	"	"	.378	9.4	0.21	1.44			
Acetic Acid	Water	Benzene	Water	.576	13.0	2.42	3.45	(4)	◇	
	"	MIBK	"	.320	10.3	0.87	1.93			□
Pyridine	"	Benzene	"	.552	12.4	0.45	0.58	▽	◇	
Acetone	"	"	"	.552	12.9	1.18	1.40			
Benzoic Acid	"	"	"	.550	12.4	0.22	0.22	◇		
Ethyl Acetate	Ethyl Acetate	Water	Water	.432	9.9	1.91	1.33	(24)	▽	
	"	"	"	.426	10.1	2.03	1.37			
	"	"	"	.472	9.3	1.82	1.26			
	"	"	"	.284	12.9	2.81	1.75			
	"	"	"	.370	11.0	3.54	1.49			◇
	"	"	"	.350	10.0	1.38	1.36			◇
Acetic Acid	Water	MIBK	Water	.290	11.1	1.52	2.08	(40)	□	
	"	Benzene	"	.390	10.6	0.98	2.83			◇

a) Applies only to Figure 3.

where λ represents any one of an infinite number of eigen values. Accordingly, the general solution of Equation (24) is

$$c(y, t) = c_0 \sum_1^{\infty} A_n Y_n$$

$$\cdot \exp \left(-\frac{16\lambda_n D P e_i'}{2,048 d^2} \right) \quad (29)$$

where c_0 is the initial concentration in the drop, A_n is constants to be evaluated from the boundary conditions, and Y_n is the eigen functions corresponding to λ_n .

It turns out that for the purpose of calculating mass transfer coefficients, the evaluation of the functional form of Y_n is unnecessary, as may be seen from the following argument. The ratio of the mass of solute at any time t to that at time 0 is

$$\frac{M(t)}{M(0)} = 2 \sum_1^{\infty} A_n^2 \exp \left(-\frac{16\lambda_n D P e_i'}{2,048 d^2} \right) \quad (30)$$

A film coefficient may be defined by means of the material-balance relation:

$$\frac{d}{dt} \frac{dc_i}{dt} = k_i (c_{i,\infty} - c_i) \quad (31)$$

which, according to the boundary conditions expressed in Equations (25), may also be written as

$$\frac{d}{dt} \frac{dc_i}{dt} = -k_i c_i \quad (32)$$

the solution of which is

$$\frac{M(t)}{M(0)} = \exp \left(-\frac{6k_i t}{d} \right) \quad (33)$$

Now, according to the general theory of eigen-value problems, each successive eigen value in Equation (30) is larger than the preceding one. In the present case the second eigen value is already large enough to permit use of the first term only in Equation (30) for the free-rise period. Then, by comparison of Equations (30) and (33), the mass transfer coefficient may be expressed as a function of the first eigen value:

$$k_i = \frac{16\lambda_1 D P e_i'}{(6)(2,048)d} \quad (34)$$

The problem is thus reduced to finding the lowest eigen value of Equation (28). This may be done conveniently by the Ritz method (28),

$$Y_n = \sum_1^i c_i y^i \quad (35)$$

being used as an approximate eigen function. With $j = 5$, the value obtained for the lowest eigen value is $\lambda_1 = 2.88$. Equation (34) then becomes

$$k_i = \frac{0.00375V}{(1 + \mu_1/\mu_0)} \quad (36)$$

which may be rearranged into the more convenient form

$$Nu_i = 0.00375Pe_i' \quad (37)$$

which is used in the correlation.

Equation (37) indicates that the Nusselt number for the inside is proportional to the Peclet number. In correlating the data, it was found that this proportionality holds and that the proportionality constant is that expected from the model. This unexpected agreement is probably fortuitous.

DISCUSSION OF RESULTS

In the models discussed above, the tacit assumption was made that the driving force for mass transfer in either phase is identified with the gradient of concentration. Although this is convenient in the formulation of the models, the choice of concentration gradients as driving forces in mass transfer may not be the best choice. The mass transfer problem is also complicated by possible resistances associated with transfer across the interface for which no allowance has been made. In the case of heat transfer to or from liquid drops, these difficulties probably do not exist. The driving force is clearly the temperature gradient. Furthermore, the models developed are directly applicable, with the simple substitution of temperature for concentration and thermal diffusivity for diffusivity.

Garwin and Smith (14) present data which may be directly compared with the models used here. In this case heat was transferred to and from benzene droplets rising in water and the results were reported as over-all coefficients of heat transfer. In Figure 2 the over-all coefficients of heat transfer are compared with those calculated from the individual coefficients given by Equations (12) and (37) by use of the usual relation:

$$\frac{1}{U} = \frac{1}{C_{p,0}\rho_0k_0} + \frac{1}{C_{p,i}\rho_i k_i} = \frac{1}{h_0} + \frac{1}{h_i} \quad (38)$$

The agreement is highly satisfactory; actually it is about as good as it is in the simple case of heat transfer to solid boundaries. There is no effect of the direction of transfer, which justifies the influence of the viscosity ratio in the mass transfer coefficient as it appears in Equations (37) and (21).

In Figure 3 the literature data on extraction from single drops are compared with values predicted from the correlations. A summary of these data is given in Table 1. The calculated values of the over-all coefficient were evaluated for the mass transfer equivalent of Equation (38):

$$\frac{1}{K_D} = \frac{m_{i,0}}{k_0} + \frac{1}{k_i} \quad (39)$$

With some notable exceptions, the cor-

TABLE 2. SUMMARY OF EXPERIMENTAL RESULTS

Solute	Continuous Phase	Dispersed Phase	Transfer to:	d _{3,2} cm	V cm/sec	\bar{m}_{in} a)	Concentration		Activity		Calc. K_D ft/hr	Percent Inside Control	Symbol d)
							Observed K_D ft/hr	$R_{N,t}$	Observed K_D ft/hr	$R_{N,t}$			
Acetic Acid	Water	Benzene	Water	.503	11.3	.023	.63	.972	2.51	.998	3.02	95	○
	"	"	Benzene	.440	13.9	.043	2.17	.991	2.57	.981	3.60	94	○
	Benzene	Water	Water	.407	10.8	13.8	.17	.891	.35	.487	.22	14	□
Benzoic Acid	"	"	Benzene	.409	10.8	37.7	.13	.974	.13	.922	.09	5	□
	Water	Benzene	Water	.521	13.8	9.86	.12	.925	-	-	.18	5	□
	"	"	Benzene	.533	13.1	3.55	.44	.991	-	-	.12	12	□
Phenol	Benzene	Water	Water	.414	16.6	1.00	1.92	.944	-	-	2.52	92	◇
	Water	Benzene	Water	.511	11.4	2.69	.63	.991	.56	.981	.59	19	◇
	"	"	Benzene	.505	11.2	2.76	.33	.978	.33	.978	.19	33	◇
Acetone	"	"	Water	.526	14.4	2.58	.59	.987	.57	.988	.63	16	◇
	Benzene	Water	Water	.527	15.1	2.56	.68	.993	.65	.946	.72	17	◇
	"	"	Benzene	.422	11.3	.362	2.53	.975	1.45	.971	1.68	82	◇
Salicylic Acid	Benzene	Water	Water	.416	12.2	.394	1.56	.999	2.45	.999	1.58	84	◇
	Water	Benzene	Water	.481	10.6	.939	1.12	.999	1.49	.998	1.29	44	◇
	"	"	Benzene	.503	10.8	.970	.68	.949	1.17	.946	1.31	43	◇
Acetic Acid	Water	Benzene	Water	.525	12.9	2.12	.54	.999	-	-	.69	19	◇
	"	"	Benzene	.525	12.8	1.91	.59	.991	-	-	.75	21	◇
	Water	Ondina 17 ^{b)}	Water	.616	13.4	.0012	.69	.975	.27	.945	.28	100	◇
Acetic Acid	Water	A oil ^{c)}	Water	.581	14.0	.0015	1.11	.996	.59	.995	.66	100	◇

a. $m = c_i/c_0$; b. Ondina 17, $\rho = 0.87$, $\mu = 20$ centipoises; c. mixture of Ondina 17 and kerosene, $\rho = 0.837$, $\mu = 5.9$ centipoises; d. applies only to Figures 4 and 5.

relation appears to be promising. The discrepancies between some of the experimental points and the correlation may be due, at least in part, to any of the following causes:

1. The experimental over-all coefficients were evaluated from the slopes of the curves for the number of transfer units vs. time. For most of the experimental points shown in Figure 3, only two points on the curve were available. Under these circumstances, the accuracy of the observed over-all coefficients cannot be estimated. Moreover, it is not always certain that the data were actually taken in the free-rise period rather than during the period of formation.

2. The distribution coefficient which enters in Equation (39) is often a function of concentration and temperature. The temperature control in the experiments was frequently inadequate, and in many cases the temperature was not even reported. Also, many authors fail to provide information concerning the variation of the distribution coefficient with concentration. This information is necessary in the evaluation of the proper average driving force. In these cases, the single distribution ratio given by the authors has been used and the average driving force evaluated from the logarithmic mean.

3. Failure of the correlation because the concentration gradient is not the true driving force.

4. There may be significant interfacial effects.

In addition to these uncertainties, the data used are not comprehensive. For a given solute and solvent pair, four cases are possible depending on the choice of the dispersed phase and the direction of transfer. For most of the systems only one of these has been studied. Additional experiments under controlled conditions were necessary.

The authors' data, given in Table 2, are compared with the correlation in Figures 4 and 5. In Figure 4 the observed over-all coefficients are evaluated on the basis of concentration differences for the driving force. As shown in Table 2, the new data cover all possible transfer situations and also represent a greater range of the viscosity ratio than the earlier data.

Figure 5 shows that the activity difference is a more suitable driving force than concentration difference. Unfortunately, activity data are not available for all systems used in these experiments. Consequently, there are fewer points in Figure 5 than in Figure 4. It is evident that for those systems for which activity data are available agreement of the experimental data with the theory is much better. Since the data include all possible transfer situations and there is a large range of physical properties and distribution coefficients, the agreement between the experimental and predicted

TABLE 3. EFFECT OF ADDITIVES ON MASS TRANSFER COEFFICIENT

Solute: acetic acid
Continuous phase: water
Dispersed phase: benzene
Transfer to: water

Additive	Concentration, wt. %*	d_s , cm.†	V , cm./sec.	$m_{in, avg.}$	K_D , ft./hr.	N , initial†
None		0.483	10.6	0.026	2.17	1.09
Dioctyl phthalate	0.05-0.005	0.490	11.5	0.023	2.50	1.07
Santicizer 141	0.05-0.005	0.498	11.3	0.023	1.73	1.06
Dibutyl tin dilaurate	0.05-0.005	0.481	10.6	0.024	0.81	0.74
Barium ricinoleate	0.0002	0.500	10.8	0.024	0.41	0.67

*In benzene phase.
†Based on activity.

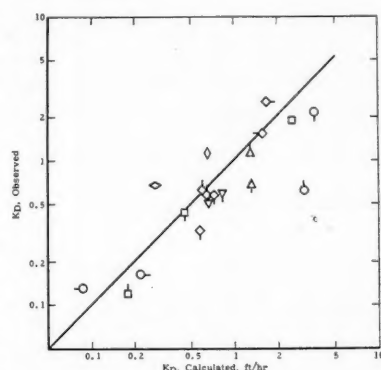


Fig. 4. Correlation of over-all mass transfer coefficients based on concentration; see Table 2 for key.

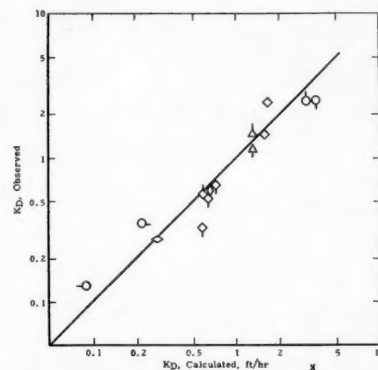


Fig. 5. Correlation of over-all mass transfer coefficients based on activity; see Table 2 for key.

values of the over-all transfer coefficient as shown in Figure 5 and the simplicity of the correlations recommend the methods presented. However, the correlations are limited to the period of free rise and do not apply to the transfer during the formation and coalescence of the drop, which is different from the free-rise period and requires separate study.

EFFECT OF ADDITIVES ON EXTRACTION RATES

The possibility of an additional resistance to transfer at the interface has been mentioned. One type of interfacial resistance is indicated in the work of Drickamer (9), who measured in a static system the rates of self-diffusion of sulfur dioxide between normal heptane and sulfur dioxide and of sulfuric acid between phenol and water. A second kind of interfacial resistance is shown by the work of West (50, 52, 31, 44, 47) and Coulson and Skinner (5). West, who attempted to repeat the work of Sherwood (40) on the transfer of acetic acid from benzene drops to water, observed transfer coefficients which were about one-third those reported by Sherwood.

Apparently the reported reduction in over-all transfer coefficients was caused by the presence of certain benzene-soluble substances that were extracted from a Tygon tubing used in the appa-

atus. Accordingly in the correlations presented here no data obtained in apparatus containing Tygon tubing were used. To study this effect quantitatively, however, the authors obtained data which show the effect of certain high-molecular-weight materials representative of components of Tygon. The data are shown in Table 3, for the extraction of acetic acid from benzene drops to water. There is a marked difference between the extraction rate in the presence of barium ricinoleate as compared with that in the presence of dioctyl phthalate. The data for other additives lie between these two extremes. While all these additives are surface-active agents and reduce the interfacial tension between benzene and water, the concentrations of the additives were kept at such a low level that the reduction in interfacial tension seems hardly significant. Recent experimental work by Garner and Hale (11) confirms that the effect of additives is not one of change in interfacial tension.

EXPERIMENTAL METHODS

The experimental techniques used in extraction studies are simple and apart from minor variations are essentially the same for all investigators. A comparison of the data in Figures 3 and 4 suggests that the experimental techniques themselves are not important. In general, the

drops are formed at a submerged capillary orifice and rise or fall through a column of the continuous phase. The dispersed phase after collection, is analyzed for the amount of solute transferred from the continuous phase. The drop size is determined by measuring the volume of a known number of drops or by other means, such as photographing the drops and comparing them to a reference scale. Usually an amount of dispersed phase just sufficient for analytical purposes is passed through the column, on the assumption that the concentration of the solute in the continuous phase does not change significantly.

In analyzing their data, previous investigators generally assumed that the distribution coefficient and hence the over-all coefficient of transfer are constants for the system. The equation for transfer is

$$\frac{dc_i}{dt} = -\frac{6K_D}{d}(c_i - c^*) \quad (1a)$$

where c^* is defined in terms of the concentration of solute in the bulk phase. For a constant K_D simple integration gives

$$N = \frac{6K_D}{d} t = \ln \frac{(c_i - mc_{0,i})}{(c_i - mc_{0,2})} \quad (2a)$$

As the number of transfer units calculated in this way includes the end effects, at least two column heights must be studied to permit an evaluation of K_D . The over-all transfer coefficient for the free-rise period is then determined by

$$K_D = \frac{d}{6} \left(\frac{\Delta N}{\Delta t} \right) \quad (3a)$$

When only two column heights are studied, the constancy of the over-all film coefficient, which is implicitly assumed in Equation (3a), cannot be examined. K_D may vary because of a choice of column heights such that the formation period is included in the free-rise period or because of variations in the distribution coefficients. Moreover, with only two column heights the accuracy of the data cannot be estimated. The assumption that the concentration in the continuous phase does not change in the course of the experiment is often not valid. While the total amount of solute transferred is usually too small to change the bulk concentration significantly, the possibility of high local concentrations in the path of the drops must be considered. It is surprising that no one has taken two or more samples of dispersed phase in succession and attempted an extrapolation to zero time. When three or more column heights were studied, a regression line of the number of stages against time can be obtained by statistical methods and the slope can be used in Equation (3a).

In derivation of Equation (1a) the assumption was that the drop is spherical

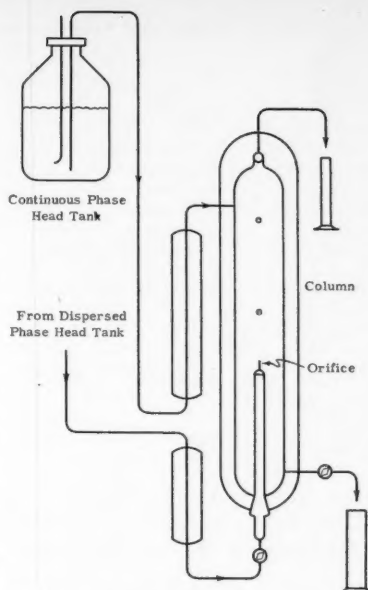


Fig. 6. Schematic drawing of equipment.

and the ratio $6/d$ is the ratio of area to volume. The validity of this assumption has been examined by several authors. In general, the observed deviations from the sphere do not change the volume-surface ratio by more than 10%, and it is agreed that this error is a secondary one.

The data on the transfer of heat between benzene and water were obtained from data on spray-tower operation. In the calculation of the over-all transfer coefficients the calculated relative velocity of the dispersed phase to the continuous phase was used and it was assumed that there was no circulation within the column. The end effects were avoided by measuring the rate of heat transfer to the continuous phase in the column. A similar technique has been applied to mass transfer (15, 16, 38).

The present data were obtained in the equipment which is shown schematically in Figure 6. The extraction column was 3 in. in diameter. Countercurrent flows of the continuous and dispersed phases were used, the flow rate of continuous phase (3 to 5 liters/hr.) being controlled by means of pressure drop in the lines and the constant head supply and dispersed rate being adjusted to give a rate of drop formation of 30 ± 1 drops/min. The exchangers and the column jacket were maintained at constant temperature by circulating water from a thermostat at $25.0 \pm 0.1^\circ\text{C}$.

Four column heights were studied, 35, 55, 75, and 85 cm., obtained by interchanging the orifice support tubes. A glass-capillary orifice, 0.041 in. I.D., was used when the organic phase was dispersed and an orifice of hypodermic tubing, 0.028 in. O.D., was used when the aqueous phase was dispersed. Reference marks were fired on the inner jacket of the column for measurement of the velocity of the drops and as an aid in

maintaining the level of dispersed phase. The velocity of the drops was measured by timing ten drops across a distance of 60 cm.

Samples of the dispersed and the continuous phases were taken after 1 and after $1\frac{3}{4}$ hr. of operation. Analytical results showed that steady state conditions prevailed between the two sample periods. During the sample period the drops were counted.

The acetic, benzoic and salicylic samples were titrated with 0.1 or 0.5N sodium hydroxide. The oil-phase samples were diluted with isopropyl alcohol to homogenize them. Acetone was analyzed with hydroxylamine hydrochloride, and phenol by a modification of the method of Koppeschaar (45).

The entire apparatus was made of glass and no stopcock grease was used in the system. Distilled water was used and the oil phases, benzene, Ondina 17, and A oil, were passed over silica gel to remove surface-active agents. These precautions were taken to avoid the effect of additives such as were described earlier. All solutes were chemically pure grades.

In spite of the precautions taken to obtain reproducible drop sizes, a 5 to 10% variation in drop volume was observed. A part of this variation was caused by errors in measuring the total volume of the drops sampled. The Sauter mean diameter (39) was used as the average diameter. The root mean square deviation of the observed drop diameters was 2 to 3%.

TREATMENT OF DATA

When the distribution coefficient was independent of concentration the over-all coefficient was calculated by Equation (3a). In the general case the distribution coefficient is dependent on concentration and Equation (1a) is not valid. The equation of transfer is

$$\begin{aligned} \frac{d}{6} \frac{dc_i}{dt} &= -k_i(c_i - c_{i,in}) \\ &= -k_o(c_{0,in} - c_o) \end{aligned} \quad (4a)$$

The following self-explanatory steps indicate the method of elimination of the interfacial concentrations $c_{i,in}$ and $c_{0,in}$:

$$-k_i(c_i - c_{i,in}) = -k_o(c_{0,in} - c_o) \quad (5a)$$

$$m_{in} = \frac{c_{i,in}}{c_{0,in}} \quad (6a)$$

$$c_{0,in} = \frac{k_o c_o + k_i c_i}{k_i m_{in} + k_o} \quad (7a)$$

$$\begin{aligned} \frac{d}{6} \frac{dc_i}{dt} &= -k_o(c_{0,in} - c_o) \\ &= -k_o \left[\frac{k_o c_o + k_i c_i}{k_i m_{in} + k_o} - c_o \right] \end{aligned} \quad (8a)$$

or

$$\begin{aligned} \frac{d}{6} \frac{dc_i}{dt} &= -\frac{k_o}{\kappa + m_{in}} (c_i - m_{in} c_o) \\ &= -K_D(c_i - m_{in} c_o) \end{aligned} \quad (9a)$$

where

$$K_D = \frac{k_0}{\kappa + m_{in}} \quad (10a)$$

and

$$\kappa = \frac{k_0}{k_i} \quad (11a)$$

It is necessary to relate m_{in} , the distribution coefficient at the interface to the bulk concentrations c_i and c_0 . For many systems in which the organic phase is dispersed, the effect of concentration on the distribution coefficient may be described adequately by an equation of the form

$$m = \frac{c_i}{c_0} = m_\infty + \alpha c_0 \quad (12a)$$

Therefore, also

$$m_{in} = \frac{c_{i,in}}{c_{0,in}} = m_\infty + \alpha c_{0,in} \quad (13a)$$

Combining Equations (5a), (11a), and (13a) one obtains the quadratic

$$m_{in}^2 + m_{in}(\kappa - m_\infty) - (m_\infty \kappa + \alpha c_i + \alpha \kappa c_0) = 0 \quad (14a)$$

The physically acceptable solution of this is

$$m_{in} = \frac{m_\infty - \kappa}{2} + \left[\frac{(m_\infty - \kappa)^2}{4} + m_\infty \kappa + \alpha c_i + \alpha \kappa c_0 \right]^{1/2} \quad (15a)$$

A number of stages is defined by integrating Equation (9a):

$$N' = \int_{c_{i,1}}^{c_{i,2}} \frac{(\kappa + m_{in}) dc_i}{(c_i - m_{in} c_0)} = -\frac{6}{d} k_0 \int_1^2 dt = -\frac{6}{d} k_0 t \quad (16a)$$

The integration must be performed with the aid of Equation (15a).

For a given set of values $c_{i,1}$, $c_{i,2}$, c_0 , α , m_∞ and t , Equations (15a) and (16a) can be used to calculate either coefficient if the other is known. Values of m_∞ and α for the systems which are reported here are given in Table 4. No single set of data can give information by which both the inside and outside coefficients can be found. However, consistent correlations can be developed by relying on experiments in which either the inside or the outside resistance is controlling.

For the purpose of comparing the data with the correlations an average experimental over-all coefficient was calculated in the following way. First κ was calculated from the correlations. With this, a series of values of N' were calculated from Equations (15a) and (16a) for various values of the time t . With the coefficient k_0 , evaluated from the relation $k_0 = (d/6) dN'/dt$, an average over-all

TABLE 4. DISTRIBUTION-DATA PARAMETERS FOR TRANSFER SYSTEMS AT 25°C.

Solute	Solvents*	m_∞	α
Acetic acid	Methyl isobutyl ketone	0.510	0.051
Acetic acid	Isopropyl ether	0.182	0.023
Acetic acid	Benzene	0.0113	0.017
Acetic acid	Ondina 17	0.00119	0.00957
Acetic acid	"A" oil	0.00150	0.00120
Benzoic acid	Benzene	1.52	912
Salicylic acid	Benzene	1.31	237
Acetone	Benzene	0.899	0.114
Phenol	Benzene	2.54	6.53
Pyridine	Benzene	2.59	313
Diethylamine	Benzene	0.583	11.6

*Other solvent is water.

coefficient was calculated from the expression

$$\bar{K}_D = \frac{k_0}{n+1} \sum_n \frac{1}{\kappa + m_{in,n}} \quad (17a)$$

where n refers to the n th value of t .

When the aqueous phase is dispersed, an analogous procedure may be followed. If

$$m' = \frac{c_0}{c_i} = m_\infty' + \beta c_i \quad (18a)$$

and therefore also

$$m_{in}' = \frac{c_{0,in}}{c_{i,in}} = m_\infty' + \beta c_{i,in} \quad (19a)$$

then Equation (20a),

$$m_{in}' = \frac{(m_\infty' - 1/\kappa)}{2} + \left[\frac{(m_\infty' - 1/\kappa)^2}{4} + \frac{m_\infty'}{\kappa} + \frac{\beta c_i}{\kappa} + \beta c_0 \right]^{1/2} \quad (20a)$$

and Equation (21a),

$$N'' = \int_{c_{i,1}}^{c_{i,2}} \frac{(m_{in}' + 1/\kappa) dc_i}{m_{in}'(c_i - c_0/m_{in}')} = -\frac{6}{d} k_i t \quad (21a)$$

take the place of Equations (15a) and (16a) respectively. In Table 2 N' and N'' are listed as N as the choice of Equation (16a) or (21a) is definite.

The use of the activity as the potential in the equations for transfer causes certain difficulties. The transfer equations are derived on the basis of the concentration as the potential, and integration of the equations is possible only because the flux and the potential are expressed in terms of the same conserved quantity. However, the following plausible (although essentially empirical) approach was found to result in a successful correlation.

The activities of the solute in each phase being assumed the same at equilibrium, it is possible to write the transfer equation in terms of the activities at a point. Since the distribution ratio at the interface is approximately equal to the

ratio of the activity coefficients $\bar{\gamma}_0/\bar{\gamma}_i$, where $\bar{\gamma}$ is an average coefficient in a given phase,

$$\begin{aligned} \bar{J} &= \frac{1}{\bar{\gamma}_i} k_i (a_i - a_{in}) \\ &= \frac{1}{\bar{\gamma}_0} k_0 (a_{in} - a_0) \\ &= \frac{1}{\bar{\gamma}_i} K_D (a_i - a_0) \end{aligned} \quad (22a)$$

and

$$\frac{1}{K_D} = \frac{m_{in}}{k_0} + \frac{1}{k_i} \quad (23a)$$

At this point the number of transfer units is defined as

$$N = \int_{a_{i,1}}^{a_{i,2}} \frac{da_i}{a_i - a_0} = -K_D \cdot \frac{A}{v} \int_1^2 dt \quad (24a)$$

Since the activity of the solute in the continuous phase in the experiments changes very little, a simpler form of Equation (24a) is

$$N = \ln \frac{(a_0 - a_i)_1}{(a_0 - a_i)_2} \quad (25a)$$

The advantage of defining N by Equations (23a) and (24a) depends on the possibility of a successful correlation for K_D . As Figures 4 and 5 show, these definitions are preferable to the less empirical definitions contained in Equations (2a), (16a), and (21a).

The correlation coefficients R for regression lines of the number of stages against time are given in Table 2. In no case has the last significant figure been rounded upward. In general, the values of R are close to unity, an indication of a good correlation. As a measure of the agreement between the observed and the calculated values of K_D based on activity, the root mean square of the percentage error, 100 (observed—calculated)/calculated, was found to be 30%. The correlation coefficient of the observed value of K_D on the calculated K_D is 0.932 and the corresponding standard error of estimate is 0.32.

For the systems with acetic acid as solute, the liquid-liquid equilibrium data were measured. The liquid-vapor data

of Othmer, Silvis, and Spiel (32) and the infinite-dilution data of Pierotti (36) for acetic acid in water were fitted by a Van Laar equation to give activity coefficients. The equilibrium data were used to obtain activity coefficients in the acetic acid-benzene system.

Data for activities for water-acetone were calculated from the liquid-vapor data of Beare, McVicar, and Ferguson (1) and correlated in the dilute region by $\ln \gamma_1 = 1.89x_2^2$. The distribution data of Gross and Schwarz (18) were used.

In the calculation of activities the effect of mutual solubility of the solvents was neglected. For the system phenol-water-benzene the phases were treated as three component mixtures in terms of the three binary systems. Data for the phenol-benzene system are given by Dickinson and Lassetre (8), distribution data are given by Philbrick (35), and data for the benzene-phenol system are given by (7). The water-phenol system and the water-benzene system were fitted by Van Laar equations from solubility data which are given in the International Critical Tables.

No consistent set of activity data could be developed for the benzoic acid in the benzene-water system in spite of available solubility, freezing-point (3, 37), and liquid-vapor data (48, 49). The freezing-point data show a molecular weight of 150 to 160 (formula weight = 122) even at the lowest concentrations. Water is reported to increase the association of benzoic acid (54), but the distribution data indicate a reduction in degree of association. The distribution data were obtained from Smith (41) and Farmer (10).

For salicylic acid between water and benzene the distribution data of von Szyskowski (43) were used. This solute-solvent system is interesting from the standpoint that the solubility of salicylic acid in benzene increases 31% when the benzene is saturated with water. Available data were insufficient for a calculation of activities.

Diffusivities were calculated by the correlation of Wilke (52). In addition, some experimental values for diffusivities were obtained by the diaphragm-cell method, which is described by Gordon

(17). These data are shown in Table 5 with the values calculated by the Wilke correlation. The correlation proposed by Othmer and Thakar (33) was also examined, and the deviation of the calculated values from the experimental values was found to be about the same for both correlations.

ACKNOWLEDGMENT

The authors gratefully acknowledge the contributions of R. L. Maycock, whose early studies of extraction from single drops provided them with useful data and thoughtful observations.

NOTATION

A	= drop area
a	= activity
C_p	= specific heat
c	= concentration, mass/unit volume
D	= diffusivity
d	= drop diameter
E	= eddy diffusivity
\bar{G}	= chemical potential
h	= transfer coefficient in heat transfer
\bar{J}	= generalized flux
K	= over-all mass transfer coefficient
k	= transfer coefficient in mass transfer
k	= thermal conductivity
m	= phase-distribution ratio
r	= $\rho/(d/4)$
t	= time
v	= drop volume
x	= mole fraction
z	= displacement or distance
L	= generalized conductivity
N	= number theoretical stages
N', N''	See Equations (16a) and (21a).
\bar{Q}	= heat flux
R	= correlation coefficient

U	= over-all heat transfer coefficient
V	= drop velocity
α	See Equation (12a).
β	See Equation (18a).
γ	= activity coefficient
κ	= k_0/k_i
λ	= eigen value of Equation (28)
ρ	= radius of circulation patterns, also density
θ	= temperature
μ	= viscosity
Nu	= Nusselt number, kd/D or hd/k
Pe_i	= inside Peclet number, dV/D
Pe_i^1	= modified inside Peclet number, $Pe_i/(1 + \mu_i/\mu_0)$

Subscripts

i	= inside, or dispersed, phase
0	= outside, or continuous, phase
∞	= at interface
∞	= at infinite dilution
1, 2	= inlet and outlet of column; used as $i, 1$ to indicate dispersed phase at inlet
D	= based on dispersed phase

Superscripts

— = average

LITERATURE CITED

1. Beare, W. G., G. A. McVicar, and J. B. Ferguson, *J. Phys. Chem.*, **34**, 1310 (1930).
2. Bond, W. N., and D. A. Newton, *Phil. Mag.*, **5**, No. 7, 794 (1928).
3. Bury, C. R., and H. O. Jenkins, *J. Chem. Soc.*, p. 688 (1934).
4. Clark, R. O., B.S. thesis, Univ. Washington, Seattle (1951).
5. Coulson, J. M., and S. J. Skinner, *Chem. Eng. Sci.*, **1**, 197 (1952).
6. De Groot, S. R., "Thermodynamics of Irreversible Processes," pp. 101-105, Interscience Publishers, Inc., New York (1951).
7. Derr, E. L., private communication.
8. Dickinson, R. G., and E. N. Lassetre, *J. Am. Chem. Soc.*, **61**, 54 (1939).
9. Drickamer, H. G., and L. H. Tung, *J. Chem. Phys.*, **30**, 6, 10 (1952).
10. Farmer, R. C., *J. Chem. Soc.*, **83**, 1446 (1903).
11. Garner, F. H., and A. R. Hale, *Chem. Eng. Sci.*, **2**, 157 (1953).
12. Garner, F. H., and A. H. P. Skelland, *Trans. Inst. Chem. Engrs.*, **29**, 315 (1951).
13. —, *Chem. Eng. Sci.*, **4**, 149 (1955).
14. Garwin, Leo, and B. D. Smith, *Chem. Eng. Progr.*, **49**, 591 (1953).
15. Geankoplis, C. J., and N. A. Hixson, *Ind. Eng. Chem.*, **42**, 1141 (1950).
16. Gier, T. E., and J. O. Hougen, *Ind. Eng. Chem.*, **45**, 1362 (1953).
17. Gordon, A. R., *Ann. N. Y. Acad. Sci.*, **46**, 285 (1945).
18. Gross, P., and K. Schwarz, *Monatsh. Chemie.*, **55**, 287 (1930).
19. Hadamard, J., *Compt. rend.*, **152**, 1735 (1911).

$$= \frac{n \sum N_i t_i - \sum N_i \sum t_i}{\sqrt{[n \sum N_i^2 - (\sum N_i)^2][n \sum t_i^2 - (\sum t_i)^2]}}$$

20. Higbie, Ralph, *Trans. Am. Inst. Chem. Engrs.*, **31**, 365 (1935).
21. Hu, Shengen, and R. C. Kintner, *A.I.Ch.E. Journal*, **1**, 42 (1955).
22. Hughes, R. R., and E. R. Gilliland, *Chem. Eng. Progr.*, **48**, 497 (1952).
23. Johnstone, H. F., R. L. Pig-ord, and J. H. Chapin, *Trans. Am. Inst. Chem. Engrs.*, **37**, 95 (1941).
24. Kopinsky, S., M.S. thesis, Mass. Inst. Technol., Cambridge (1949).
25. Kronig, R., and J. C. Brink, *Appl. Sci. Research*, **A2**, 142 (1950).
26. Licht, William, Jr., and J. Conway, *Ind. Eng. Chem.*, **42**, 1151 (1950).
27. Licht, William, Jr., and G. S. R. Narasimhamurthy, *A.I.Ch.E. Journal*, **1**, 366 (1955).
28. Margenau, Henry, and G. M. Murphy, "The Mathematics of Chemistry and Physics," pp. 253-259, D. Van Nostrand Company, New York (1943).
29. Maycock, R. L., private communication.
30. Mugele, R. A., and H. D. Evans, *Ind. Eng. Chem.*, **43**, 1317 (1951).

TABLE 5. DIFFUSIVITIES FOR TRANSFER SYSTEMS AT 25°C.

Solute	Solvent	D , sq. cm./sec. $\times 10^6$ *
Acetic acid	Benzene	2.78 (1.97)
	Water	1.15 (1.14)
Acetone	Benzene	2.62 (2.53)
	Water	1.07 (1.25)
Benzoic acid	Benzene	1.76 (1.34)
	Water	0.75 (1.02)
Phenol	Benzene	2.16 (3.27)
	Water	0.88 (0.96)
Salicylic acid	Water	0.75

*Figures in parentheses are experimental values; other values are based on Wilke correlation.

31. Oberholtzer, W., B.S. thesis, Univ. Washington, Seattle (1951).
32. Othmer, D. F., S. J. Silvis, and A. Spiel, *Ind. Eng. Chem.*, **44**, 1864 (1952).
33. Othmer, D. F., and M. S. Thakar, *Ind. Eng. Chem.*, **45**, 589 (1953).
34. Pansing, W. F., Ph.D. thesis, Univ. Cincinnati, Cincinnati, Ohio.
35. Philbrick, F. A., *J. Am. Chem. Soc.*, **56**, 2581 (1934).
36. Pierotti, G. J., private communication.
37. Rodebush, W. H., and J. M. Peterson, *J. Phys. Chem.*, **32**, 709 (1928).
38. Ruby, C. L., Ph.D. thesis, Princeton Univ., Princeton, N. J. (June, 1952).
39. Savic, P., Nat. Research Lab., Rept. MT-22, Ottawa, Canada (1953).
40. Sherwood, T. K., J. E. Evans, and J. V. A. Longcor, *Ind. Eng. Chem.*, **31**, 1144 (1939).
41. Smith, H. W., *J. Phys. Chem.*, **26**, 256 (1922).
42. Spells, K. E., *Proc. Phys. Soc. (London)*, **B65**, 541 (1952).
43. von Szyszkowski, B., *Z. physik. Chem.*, **131**, 175 (1928).
44. Tanaka, T., B.S. thesis, Univ. Washington, Seattle (1951).
45. Treadwell, F. P., and W. T. Hall, "Analytical Chemistry," 9 ed., Vol. II, p. 633, John Wiley and Sons, New York (1942).
46. Ubbelohde, A. R., *Trans. Faraday Soc.*, **33**, 599 (1937).
47. Vinkenes, R. A., B.S. thesis, Univ. Washington, Seattle (1951).
48. Wall, F. T., and F. W. Banes, *J. Am. Chem. Soc.*, **67**, 898 (1945).
49. Wall, F. T., and P. E. Rouse, Jr., *ibid.*, **63**, 3002 (1941).
50. West, F. B., A. J. Herrman, A. T. Chong, and L. E. K. Thomas, *Ind. Eng. Chem.*, **44**, 621 (1952).
51. West, F. B., P. A. Robinson, A. C. Morgenthaler, Jr., T. R. Beck, and D. K. McGregor, *Ind. Eng. Chem.*, **43**, 234 (1951).
52. Wilke, C. R., *Chem. Eng. Progr.*, **45**, 219 (1949).
53. Wirtz, K., *Z. Naturforsch.*, **3a**, 672 (1948).
54. Wright, W. G., *J. Chem. Soc.*, 683 (1949).

Void Fractions in Two-phase Steam-water Flow

H. S. ISBIN, NEIL C. SHER, and K. C. EDDY

University of Minnesota, Minneapolis, Minnesota

The pressure-drop characteristics associated with one liquid and one gaseous phase flowing concurrently in a pipe or tube have yet to be understood. The operation of evaporators, boilers, and condensers has long stimulated interest in the pressure drop of steam-water mixtures, and more recently this specialized case of one-component, two-phase flow has received even greater attention from the applications in cooling nuclear reactors. The two-phase-flow problems have not been amenable to thorough theoretical analyses, and therefore empirical and semiempirical correlations have attained unusual prominence in practical applications. The present investigation employs a new research tool for the study of two-phase-flow structure.

A variety of geometric flow patterns is possible. Bergelin, Alves, and others have classified these patterns according to visual appearance; whereas the Martinelli classifications were based upon whether the flow in each phase was termed *viscous* or *turbulent*. The distinction between viscous and turbulent flow in either phase is rather arbitrary, and if the Reynolds number for one phase, calculated on the basis of the total tube diameter, is greater than 2,000, the flow in the phase is called *turbulent*. This investigation is confined to the study of annular flow, in which most of the liquid is found in an annular ring surrounding the central vapor core and the flow in each phase is turbulent.

Boiling or flashing occurs when superheated water rises in an insulated vertical tube at atmospheric pressure. For a separated two-phase flow geometry, the mean linear steam velocity may exceed that of the water. The fraction of the tube occupied by the steam (void fraction) at a given cross section cannot be obtained directly from a determination of the thermodynamic quality. Void fractions, however, must be known for the estimation of the pressure drops due to head and momentum changes.

Void fractions and pressure drops for steam-water flows were measured in an 0.872-in. I.D. vertical tube at atmospheric pressure over a quality range of 0 to 4%. The test section was the hot leg of a natural-circulation loop, and the inlet liquid flow rate ranged from 1 to 3 ft./sec. A new technique for measuring void fractions was used, and the method utilizes the difference between the gamma-ray absorption coefficients of water and steam.

A comprehensive survey of two-phase frictional pressure drops has been prepared by Isbin, Mosher, and Moen (9), and an additional brief survey is given by Marchaterre (13). The experimental data of this investigation are compared with the predictions of the homogeneous and Martinelli models.

The treatment of the vapor-liquid mixture as a homogeneous fluid is called the homogeneous, fog, or Woods model (12). The two phases are assumed to be in equilibrium, average specific volume and viscosity properties are used, and

the mean linear velocities of the vapor and the liquid are assumed to be equal. For example, the total pressure drop for a steam-water mixture flowing vertically upward in a channel of uniform cross section is approximated by the following equation for steady-state conditions:

$$p_n - p_{n+1} = \underbrace{\left(\frac{z_{n+1} - z_n}{\bar{v}} \right) \frac{g}{g_c}}_{\text{static pressure drop}} + \underbrace{\frac{G^2}{g_c} (v_{n+1} - v_n)}_{\text{head pressure drop}} + \underbrace{\frac{\bar{f} G^2 \bar{v} (z_{n+1} - z_n)}{2g_c D}}_{\text{momentum pressure drop}} + \underbrace{\frac{\bar{f} G^2 \bar{v} (z_{n+1} - z_n)}{2g_c D}}_{\text{frictional pressure drop}} \quad (1)$$

where

$$v_n = q_n v_{sn} + (1 - q_n) v_{wn} \quad \text{and} \quad \frac{1}{\mu_n} = \frac{q_n}{\mu_s} + \frac{1 - q_n}{\mu_w}$$

Neil C. Sher is now at Westinghouse Atomic Power Division, Pittsburgh, Pennsylvania, and K. C. Eddy is at Esso Standard Oil Company, Linden, New Jersey.

eters involve the ratio of the two-phase frictional pressure drop to single-phase frictional pressure drop and the ratio of the single-phase frictional pressure drop of the gas to the corresponding value for the liquid. Parameters similar to those of Martinelli were derived by Levy (10), who carried out a theoretical analysis for annular flow, and by Gazley (7), who also developed a semiempirical method. In general, the Martinelli correlation was developed from extensive studies of two-component, two-phase flow with no mass transfer between phases. The adaptation of the correlation to the flow of flashing steam-water mixtures and the introduction of an empirical pressure dependency were carried out by Martinelli and Nelson (14).

The total pressure drop for a steam-water mixture flowing vertically upward in a channel of uniform cross section is approximated by the following equation by use of the Martinelli correlation:

$$p_n - p_{n+1} = \left(\frac{z_{n+1} - z_n}{\bar{v}} \right) \frac{g}{g_c} + \frac{G^2}{g_c} \left\{ \left[\frac{v_w(1-q)^2}{R_l} \right]_{n+1} + \left[\frac{v_s q^2}{R_g} \right]_{n+1} - \left[\frac{v_w(1-q)^2}{R_l} \right]_n - \left[\frac{v_s q^2}{R_g} \right]_n \right\}$$

static head
pressure drop pressure drop momentum pressure drop

$$+ \phi_{t,1}^2 \left[\frac{\bar{f} G^2 (1-\bar{q})^2}{2g_c D} v_w \right] [(z_{n+1} - z_n)]$$

frictional pressure drop

\bar{f} is the Fanning friction factor evaluated for the average liquid

Reynolds number over interval n to $n+1$,

$$\overline{Re} = \frac{(1-\bar{q})GD}{\mu_{\text{sat liquid}}}$$

$$\bar{q} = \frac{1}{2}(q_n + q_{n+1})$$

$\phi_{t,1}^2$, the Martinelli two-phase frictional pressure-drop factor, is evaluated for the

MINNESOTA NATURAL CIRCULATION LOOP NO.3

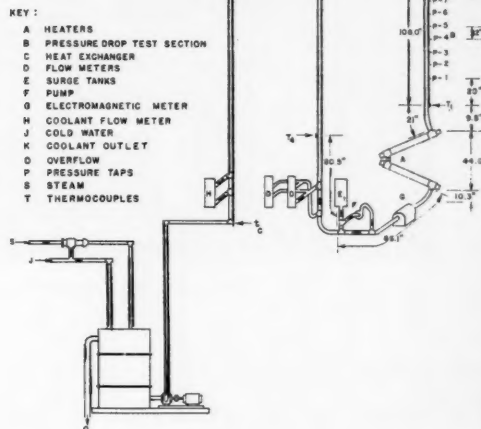


Fig. 1. The natural-circulation loop.

where

$$\frac{2}{\bar{v}} = \left(\frac{R_g}{v_s} + \frac{R_l}{v_l} \right)_n + \left(\frac{R_g}{v_s} + \frac{R_l}{v_l} \right)_{n+1}$$

TABLE 1

HOMOGENEOUS, MARTINELLI, AND EXPERIMENTAL PRESSURE DROPS

Run	q' , %	W , lb./sec.	Homogeneous model, lb./(sq. ft.)(ft.)				Martinelli correlation, lb./(sq. ft.)(ft.)				Experimental, lb./(sq. ft.)(ft.)	
			$(\Delta P/\Delta L)_H$	$(\Delta P/\Delta L)_M$	$(\Delta P/\Delta L)_{TPF}$	$(\Delta P/\Delta L)_{TP}$	$(\Delta P/\Delta L)_H^*$	$(\Delta P/\Delta L)_M^*$	$(\Delta P/\Delta L)_{TPF}$	$\phi_{t,1}$	$(\Delta P/\Delta L)_{TP}$	
22	0.75	0.707	5.2	19.4	22.0	46.6	16.2	4.2	22.1	3.34	42.5	
23	1.26	0.521	3.1	11.8	22.2	37.1	12.7	1.3	18.0	3.91	32.0	
24	0.78	0.342	4.6	3.7	6.9	15.2	15.8	0.4	7.8	3.78	24.0	
25	1.29	0.704	3.0	37.2	38.8	79.0	12.6	4.1	36.2	4.18	52.9	
26	1.17	0.520	3.1	10.6	21.2	34.9	13.2	1.4	16.0	3.59	30.6	
27	1.03	0.347	3.4	4.4	8.0	15.8	14.0	0.4	7.7	3.73	22.1	
28	0.39	0.706	10.2	18.3	11.2	39.7	21.2	2.4	18.1	3.03	41.7	
29	0.48	0.523	7.9	8.8	8.5	25.2	19.5	2.0	11.2	3.08	32.7	
30	0.44	0.343	8.1	2.8	3.9	14.8	20.3	1.2	5.5	3.19	27.0	
31	0.39	0.358	9.0	3.7	3.8	16.5	21.2	1.3	5.6	3.08	28.1	
32	0.48	0.527	7.9	8.3	8.4	24.6	19.5	2.0	11.5	3.20	33.0	
33	0.36	0.670	10.8	12.7	9.8	33.3	22.1	4.7	15.1	2.90	41.9	
34	0.40	0.750	10.3	20.6	12.2	43.1	20.9	2.9	18.4	2.90	42.2	
35	2.44	0.478	1.9	8.6	27.4	37.9	9.2	8.4	18.1	4.49	35.7	
36	4.26	0.352	1.0	7.5	41.5	50.0	6.2	3.6	21.5	6.37	31.3	
38	0.86	0.534	4.7	7.8	14.7	27.2	15.2	1.0	14.4	3.48	30.6	
39	1.29	0.346	3.1	2.6	10.0	15.7	12.6	1.0	9.2	4.10	22.8	
40	1.24	0.666	3.0	24.8	33.5	61.3	12.8	2.7	30.5	4.17	46.0	
41	1.28	0.532	2.9	10.2	23.7	36.8	12.6	1.3	18.2	3.92	32.1	
42	1.69	0.338	2.2	2.9	13.7	18.8	10.2	5.1	8.8	4.11	24.1	
43	1.35	0.711	2.8	26.5	40.7	70.0	12.3	2.6	37.1	4.33	52.0	
44	1.18	0.573	3.1	10.0	25.0	38.1	13.1	1.1	24.1	3.54	38.3	
45	4.18	0.352	0.9	16.2	32.8	49.9	6.3	1.4	25.9	6.93	33.6	

*Computed from experimental R_l .

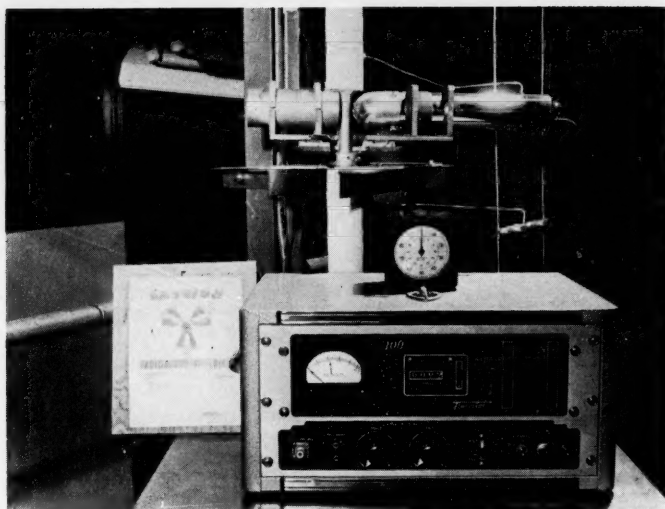


Fig. 2. Gamma absorption equipment.

flow conditions averaged over interval n to $n + 1$.

One assumes that the use of a mean velocity for each phase will describe adequately the momentum contributions.

The Martinelli correlation includes the evaluation of the liquid holdup based upon experimental measurements, most of which were made by trapping the liquid in the flow channel (11). In recent years radioactive methods have been employed for the measurement of liquid holdup. Studies at the University of Minnesota and elsewhere were carried out independently. Tomlinson (17) studied the application of a gamma-ray absorption technique, and Eddy (6) designed and constructed the gamma-absorption equipment used for studying steam-water flows. Dengler (5) added a radioactive

tracer to water and calculated the liquid holdup from measurements of the radiation intensity. A thulium gamma source has been used by the investigators at the Argonne National Laboratory, and the results are presented by Marchaterre (13). Zmola and Bailey (19) report the use of iridium 192 for measurement of densities of a boiling liquid. Schwarz (15) measured liquid holdups by a gamma-absorption method using iridium 192. Measurements were made with horizontal and vertical steam-water flows at pressures as high as 80 atm. A beta-ray-absorption technique (with strontium 90 employed as a source) has been used by Anson, Belin, and Horlor (3) to measure the density of steam-water mixtures in the throat of a critical-flow nozzle. The use of X-ray techniques is not included in this sur-

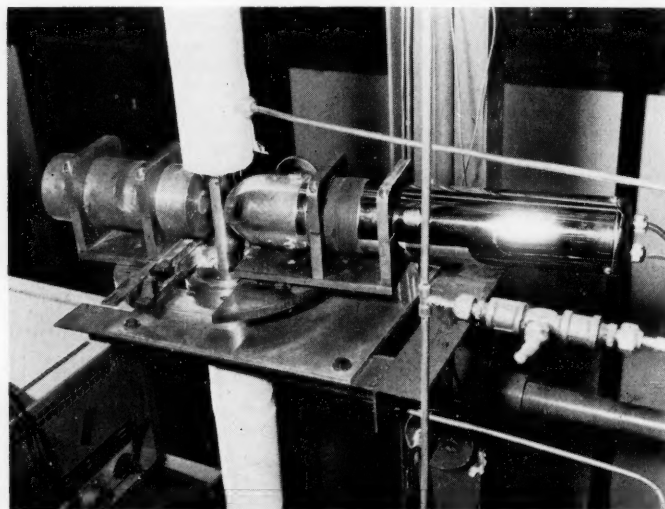


Fig. 3. Detailed view of carriage.

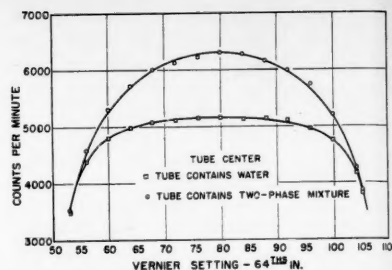


Fig. 4. Counting rates for typical run (run 28).

vey; an example of an application to gas-fluidized-solid systems may be found in a study by Grohse (8).

RADIATION-ABSORPTION METHOD

The attenuation of monoergic parallel gamma rays passing through a thin homogeneous absorbing medium of uniform thickness is given by the equation

$$\frac{I}{I^*} = e^{-\beta x} \quad (3)$$

where I/I^* is the fraction of the incident radiation penetrating a distance x in the absorber. The linear absorption coefficient β is dependent upon the nature of the absorbing material, absorber density, and radiation energy. The coefficient was determined experimentally so as to take into account deviations from Equation (3) arising from scattering and the gamma energy spectrum.

Application of Equation (3) is made for the flow of fluids in a pipe or tube. For a beam of gamma rays of finite dimensions passing through a tube diameter or chord, for example, the measured values of the radiation are I_m for a beam through a tube diameter D with the tube empty and I_w for a

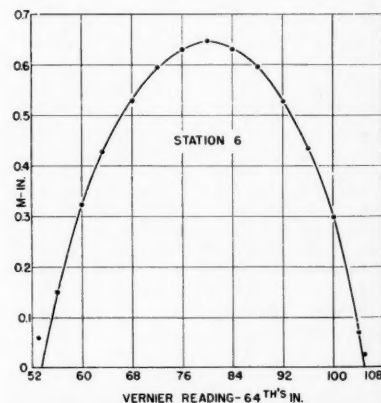


Fig. 5. Steam chordal lengths vs. vernier setting for graphical integration (run 28).

beam through a tube diameter with the tube full of water. The approximate relation between I_m and I_w is

$$I_w = I_m e^{-\beta_w D} \quad (4)$$

If I_{TP} represents the measured value of the radiation passing through a chordal length c in a steam-water mixture, then

$$I_{TP} = I_w e^{m(\beta_w - \beta_s)} \quad (5)$$

The effective chordal length of steam is m , the chordal length of water is l , and $m + l = c$. At low pressures the absorption coefficient for the steam β_s is very much smaller than the liquid-water value β_w and can be neglected.

The chordal length of steam m can be determined at any position in the tube by radiation measurements with the tube containing the two-phase mixture, preceded or followed by a measurement with the tube full of water at the same temperature (source decay neglected). A procedure of this type minimizes errors due to variations in the tube-wall thickness and the effect of scattering at the different measuring positions. The experimental value of β_w is calculated from Equation (4) and the water measurement is made at the appropriate temperature. This method neglects the temperature effect upon the density of the tube material. The gamma beam has a finite diameter, and thus the measured m corresponds to a mean position. All calculations were made on the assumption that the value for m actually corresponds to the chordal length of steam existing at the center of the gamma beam. Some of the consequences of this assumption are discussed in reference 16.

The values for m are plotted vs. the position (center of the beam) at which each measurement is made, and a graphical integration of such a plot yields the fraction of the cross-sectional tube area occupied by the steam. This quantity may also be taken as the volumetric fraction occupied by the steam R_s at the given cross section. The value R_s is termed the *void fraction*, and $1 - R_s$, or R_l , is called the *liquid holdup*.

For symmetrical flow with the water in an annular ring, an accurate measurement of the position at which m becomes zero indicates the thickness of the water ring. Some insight into the actual liquid distribution might be gained if a radial distribution could be found which accurately accounts for the remaining water in the core. A correlative attempt of this type was not successful. Further discussions may be found in reference 16.

EXPERIMENTAL

Natural-circulation Loop

The two-phase-flow test section used in these studies was an 0.872-in. I.D. vertical tube which was the hot leg of a natural-circulation loop. The loop has been de-

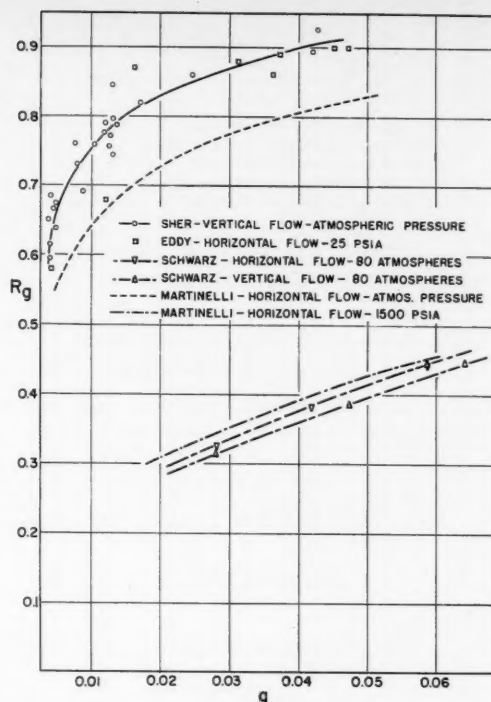


Fig. 6. Comparison of void measurements.

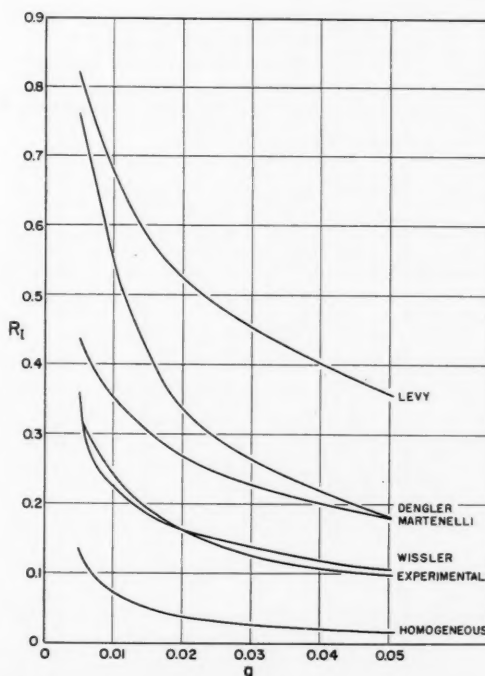


Fig. 7. Experimental liquid hold-up curve compared with predictions at atmospheric pressure.

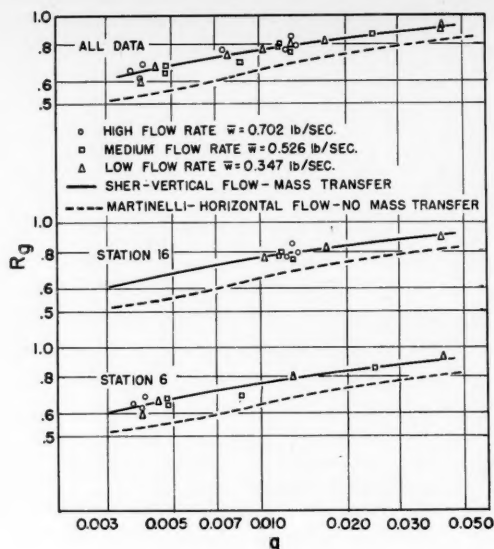


Fig. 8. Void data.

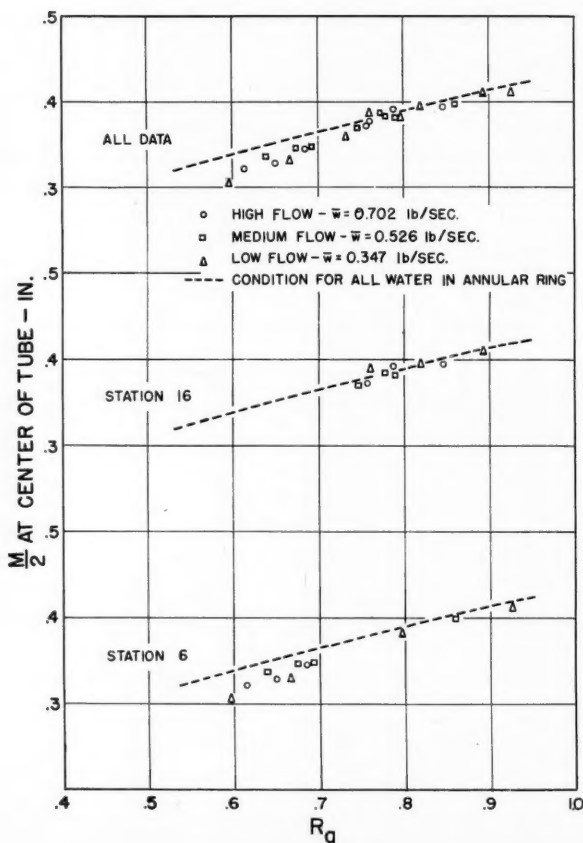


Fig. 9. Comparison of experimental chordal steam length at tube center with annular-flow-pattern calculation.

scribed in detail in references 1 and 18. Figure 1 illustrates the main components of the loop.

The electromagnetic flow meter was calibrated each day that a series of runs was to be made. The best flow control during two-phase operation was achieved by restricting the natural circulation. Small flow fluctuations were observed, and these (± 0.008 lb./sec. *max.*) increased with flow rate. Single-phase temperature measurements were uniform, but two-phase temperature measurements fluctuated $\pm 0.16^\circ\text{F}$. The power input to the loop was measured by two recording watt meters, and the heat removal in the cooler was controlled by the coolant temperature and flow rate.

The surge tank at the top of the loop was open to atmospheric pressure, and the static pressures at the measuring stations varied from atmospheric to slightly higher values. Three flow rates were selected to cover the range of operation of the natural-circulation loop, the average values being 0.702, 0.526, and 0.347 lb./sec.

The maximum quality was just over 4%. The experimental errors in the calculated qualities ranged from about $\pm 15\%$ at a quality of 0.0025 to less than 1.0% at the maximum qualities. Thermodynamic equilibrium was assumed for these calculations; however, if superheated water were present, an additional error would be introduced. Plots of the raw pressure-drop data vs. quality revealed that the curves for similar flow rates had the same shape but were displaced from each other by as much as 0.1% quality. The average displacement was less than 0.05% quality, and this displacement corresponded to a water-temperature error of 0.5°F . The experimental errors did not account for this discrepancy, and therefore the conclusion was reached that the water was flashing from a superheated state. The calculated qualities (based upon thermodynamic equilibrium) were corrected so that the quality would be zero at the position where the pressure drop per unit length started to decrease. These corrections are given in reference 18. The qualities reported in this paper and used in the pressure-drop calculations were the corrected values.

Method for Void Measurements

Selenium 75, with a half-life of 127 days, was used as the gamma source. About 10 mcurie. of selenium was contained in a 4-in.-diam. lead cylinder fitted with a 1/16-in.-diam. aperture. The source and a scintillation counter (model DS-1, Nuclear Instrument and Chemical Corporation) were mounted on a carriage which could be rotated around the tube wall and could be moved from one side of the tube to the other, thus traversing all chord positions. The carriage, carriage support, and tube mounting, source, scintillation tube, and scaler (model SC-7, Tracerlab 100) are shown in Figures 2 and 3.

The relationship between the readings of the vernier on the carriage and the actual position of the gamma beam in the tube was established for each tube mounting by determining the vernier readings for minimum gamma counting. These readings corresponded to the location of the inner tube wall. Traverses were made across the tube cross section by moving the carriage from

one side of the tube to the other and back. Measuring positions for the return traverse were the same as for the forward traverse, and the counting rates for each position were averaged. The maximum possible error in locating the center of the tube was ± 0.0039 in. Counting rates were about 4,000 counts/min. and greater, and at least 30,000 counts were obtained for each reading. (At 30,000 counts the probable statistical error is 1%.) The experimental value of β_w for each series of runs could be reproduced accurately to three figures, and a typical value was 0.310 in.^{-1} . The cross-sectional area of the tube, when full of water, could be determined within an error of less than 2%.

A typical two-phase run is illustrated in Figure 4, and a plot of the chordal steam lengths vs. the vernier readings is given in Figure 5. In general, the liquid distribution was found to be symmetrical about the axis of the vertical tube, and therefore it was not necessary to rotate the carriage about the tube to check the chordal measurements. The degree of reproducibility attainable is illustrated by runs 29 and 32: flow rate in lb./sec., 0.523 and 0.527; $(\Delta P/\Delta L)$, in lb./sq. ft. (ft.), 32.7 and 33.0; quality, 0.00475 and 0.00475; and void fraction R_v , 0.674 and 0.638. The station number refers to the vertical position of the gamma equipment and has the same value as the number of the pressure tap just below the carriage.

Inasmuch as the gamma beam was approximately $1/16$ in. in diameter, counting rates taken for two-phase flow at positions closer than $1/16$ in. from the inner edge of the tube could not be used. A quantitative correction for thickness of the gamma beam would involve the description of the annular flow pattern. (A more complete discussion is given in reference 16.)

Although the steady state operation of the loop was carefully controlled during each run, extremely small variations were practically unavoidable. Since the values of R_v are quite sensitive to quality over a considerable range, the gamma-absorption data were examined for any deviations due to the rather long time-averaged measurements involved. The procedure resulted in readings during the first half of a forward traverse being repeated after from 1 to 2 hr. had elapsed. The differences between such repeated measurements were no greater than the differences expected from an error analysis, nor were they greater than the differences between measurements which were repeated immediately. Even though the liquid-holdup determinations represent data taken over rather long periods of time, small, brief variations in the steady state operations appeared to have no significant effect.

VOID-FRACTION MEASUREMENTS

Measurements of the void fraction as a function of quality are given in Figure 6. Eddy's measurements (6) were made with horizontal flow at a pressure of 25 lb./sq. in. abs. The Martinelli correlation, established for horizontal flow at atmospheric pressure with no mass transfer, is low by about 10%. The data of Schwarz for horizontal and vertical flow at 80

atm. (1,180 lb./sq. in. abs.) as well as the Martinelli curve for 1,500 lb./sq. in. abs. are also included.

Figure 7 offers a comparison of the correlations and predictions for R_v vs. q and illustrates the wide discrepancies existing in the current literature on two-phase flow. The homogeneous model predicts values for R_v which owing to the assumption that the average linear velocities in each phase are equal, are about 80% lower than the experimental

curve. Levy, who considered horizontal two-phase flow with no mass transfer (10), predicted R_v values considerably higher than Martinelli's curve. Dengler experimentally determined R_v for vertical steam-water flow with heat transfer to the mixture from the tube wall (5). Although his values are also higher than Martinelli's, the curves actually cross, and better agreement with the experimental curve might be expected at higher qualities. Wissler (18) independently

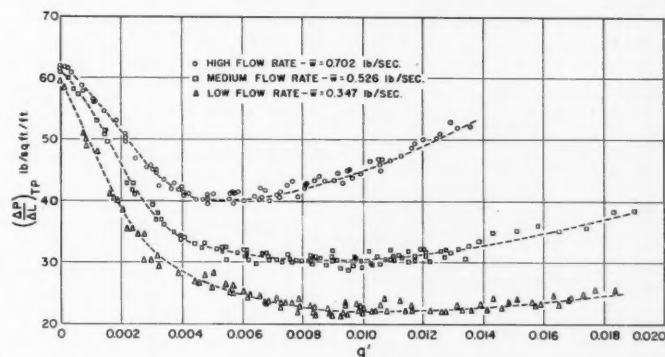


Fig. 10. Static-pressure-drop data for all measuring stations.

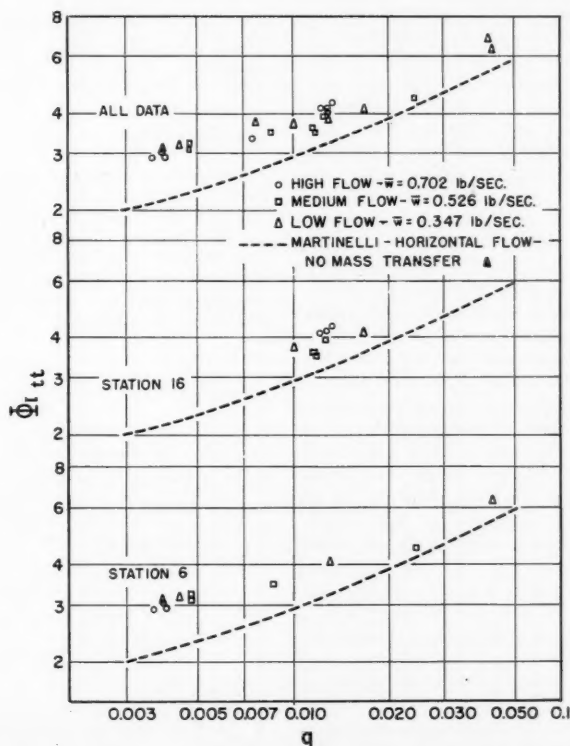


Fig. 11. Comparison of experimental ϕ_{tt} vs. q with Martinelli prediction.

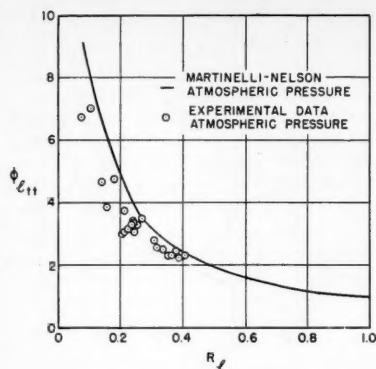


Fig. 12. Plot of ϕ_{11} vs. R_1 .

utilized a series of two-phase runs in the natural-circulation loop described in this article to evaluate a system of constants for three empirical relationships, one of which essentially defines R_1 as a function of the pressure and specific enthalpy of the mixture. His correlation fits the average experimental values quite well (usually within 10% or better) over the range of quality studied.

Detailed examinations of the Martinelli values for R_1 reveal that at high pressures and low qualities the Martinelli curves yield values greater than those calculated by the homogeneous method. Use of these Martinelli values leads to predicted momentum pressure drops which exceed the values calculated by the homogeneous method. One would expect that the homogeneous method would set an upper limit for R_1 .

Even though the scatter of the data for R_1 vs. q is within predicted error limits, further analyses were made in an attempt to discover regular patterns for the scatter. Figure 8 shows the data characterized by flow rate and station number. Neither the flow rate nor the position appear to have significant effects on the relationship between R_1 and q .

The attempts to interpret the gamma-absorption data in terms of detailed liquid distribution were not successful (16); however, other less exact relationships are of interest. Figure 9 shows the chordal lengths of steam found at the center of the tube plotted against the corresponding values for R_1 . The broken line represents the condition for all the water in an annular ring. The relative amount of water existing in the steam core is indicated by the horizontal distance between a point and the line. At station 16 (near top of riser) there is no apparent flow effect, and the assumption that all water is in an annular ring is valid. Further, no flow rate effect was apparent at station 6 (near bottom of riser), but a significant amount of water appears to be in the steam core at the lower values of R_1 .

TWO-PHASE PRESSURE DROPS

Table 1 lists the pressure drop per unit length evaluated for the head term $(\Delta P/\Delta L)_H$, the momentum change $(\Delta P/\Delta L)_M$, the frictional two-phase pressure drop $(\Delta P/\Delta L)_{TPF}$, and the static pressure differences $(\Delta P/\Delta L)_{TP}$. Comparisons are made by use of the homogeneous and Martinelli models. The homogeneous model leads to two-phase frictional and momentum pressure drops which are generally higher than those obtained from the Martinelli correlation, whereas the head terms are substantially lower. The homogeneous model yielded values for the total pressure drop per foot which were as much as 60% higher to 45% lower than the experimental values. Experimental values of R_1 were used to calculate the head and momentum terms in the Martinelli model. The data given in Table 1 represent conditions at stations corresponding to void-measuring positions. Static-pressure-drop data for all stations are given in Figure 10. The frictional two-phase pressure-drop relations are compared in Figure 11, which is a plot of ϕ_{11} vs. q . The experimental values of ϕ_{11} differ by as much as 30% from the Martinelli curve. The effects of flow rate and position are not apparent. Use of Martinelli's values for R_1 in computing the head and momentum terms would have resulted in a better fit of the ϕ_{11} values with the Martinelli curve. Another comparison of the experimental values of ϕ_{11} with the Martinelli values is given in Figure 12, which is a plot of ϕ_{11} vs. R_1 . An approximation of the Martinelli curves (independent of pressure) is $\phi_{11} R_1 \cong 1$.

ACKNOWLEDGMENT

The authors gratefully acknowledge the interest of Paul Lottes of the Argonne National Laboratory and Stanley Green of the Westinghouse Atomic Power Division. The research was made possible by an Atomic Energy Commission contract with the Department of Chemical Engineering, University of Minnesota.

NOTATION

c = distance between inner tube walls
 D = inside diameter of tube
 f = Fanning friction factor
 g = acceleration due to gravity
 g_c = proportionality factor
 G = mass velocity
 I = radiation intensity
 l = chordal length of water in tube
 m = chordal length of steam in tube
 P = static pressure
 q = calculated quality, lb. steam/lb. mixture
 q' = corrected quality
 R = fractional area or volume occupied by one phase
 v = specific volume

x = distance which gamma beam passes through absorber
 z = distance from a horizontal base plane
 $\Delta P/\Delta L$ = pressure drop per unit length

Greek Letters

β = linear gamma-absorption coefficient
 μ = dynamic viscosity

$$\phi_{11} = \left[\left(\frac{\Delta P}{\Delta z} \right)_{TPF} / \left(\frac{\Delta P}{\Delta z} \right)_{1F} \right]^{1/2}$$

for short increments in z

Subscripts

F = frictional quantity
 g = property of vapor
 H = a head quantity
 l = property of liquid
 m = result of attenuation in metal
 M = a momentum change quantity
 n = pressure tap number
 s = property of vapor
 TP = properties of two-phase mixture
 w = property of liquid

LITERATURE CITED

1. Alstad, C. D., H. S. Isbin, N. R. Amundson, and J. P. Silvers, *A.I.Ch.E. Journal*, **1**, 417 (1955); see also *A.N.L.-5409* (March, 1956).
2. Alves, G. E., *Chem. Eng. Progr.*, **50**, 449 (1954).
3. Anson, D., R. E. Belin, and M. L. Horlor, *Dept. Sci. Ind. Research, Dominion Physical Lab. Rept. R. 239*, Lower Hutt, New Zealand (Feb., 1955).
4. Bergelin, O. P., *Chem. Eng.*, **56**, No. 4, 104 (May, 1949).
5. Dengler, C. E., Ph.D. thesis, Mass. Inst. Technol., Cambridge (1952).
6. Eddy, K. C., M.S. thesis, Univ. Minn., Minneapolis (1954).
7. Gazley, C., Jr., *Rept. TPF-1*, Univ. Delaware, Newark (1947).
8. Grohse, E. W., *Genl. Elec. Research Lab. Rept. R.L.-1218* (Dec. 1954).
9. Isbin, H. S., R. H. Moen, and D. R. Mosher, *A.E.C.U.-2994* (Nov. 1954).
10. Levy, S., *Proc. Second Midwestern Conference on Fluid Mechanics*, 337 (1952).
11. Lockhart, R. W., and R. C. Martinelli, *Chem. Eng. Progr.*, **45**, 39 (1949).
12. McAdams, W. H., W. K. Woods, and L. C. Heroman, Jr., *Trans. Am. Soc. Mech. Engrs.*, **64**, 193 (1942).
13. Marchaterre, J. F., *A.N.L.-5522* (Feb. 1956).
14. Martinelli, R. C., and D. B. Nelson, *Trans. Am. Soc. Mech. Engrs.*, **70**, 695 (1948).
15. Schwarz, Karl, *V.D.I.-Forschungsheft*, **B20**, No. 445, 1 (1954).
16. Sher, N. C., M. S. thesis, Univ. Minn., Minneapolis (Sept. 1955).
17. Tomlinson, J. D., unpublished studies, Univ. Minn., Minneapolis (1952).
18. Wissler, E. H., Ph.D. thesis, Univ. Minn., Minneapolis (June, 1955).
19. Zmola, P. C., and R. V. Bailey, paper presented at Dec., 1954, meeting of Am. Soc. Mech. Engrs.

Presented at A.I.Ch.E. Pittsburgh meeting

Heat-conduction Losses in Reactor Waste Basins

STANLEY H. JURY

University of Tennessee, Knoxville, Tennessee

In connection with one method of waste disposal investigated at Oak Ridge National Laboratories, it has been proposed that radioactive wastes be fed into large out-of-door basins. The basins would be formed in the surface of the earth, the excavation being about 30 ft. in depth and several hundred in breadth. The bottom and sides of the basin would be sealed with an appropriate asphalt base material which may or may not be provided with cooling ducts. A thermal insulating layer of earth or equivalent may or may not be poured over the asphalt seal, and then the rest of the basin would be filled with coarse rock or equivalent for deentrainment purposes.

During start-up of a basin the radioactivity would build up and gradually heat the basin and waste to the boiling point of the waste contained therein. Subsequently a steady state would be attained, when the water fed to the basin would equal the steam loss from the basin. Also, the rate of heat generation by decay would equal the rate of heat loss through steam generation and feed preheating plus the rate of heat conduction into the earth beneath the basin if it is assumed that there are no cooling ducts in the asphalt seal.

From an engineering viewpoint it is easy to estimate for design purposes the various heat-flow rates if the loss into the earth is known. This loss is difficult to determine and is really the subject of this paper for the case wherein cooling ducts are not involved.

ANALYSIS OF STEADY STATE HEAT CONDUCTION IN EARTH

The actual plan of the basin was to be rectangular in shape with sloping sides which changed in pitch as they approached the bottom of the basin. Such a geometry complicates boundary conditions, and therefore it was considered necessary for mathematical convenience only, to adopt an idealized geometry which closely approximated the original. The basin is so shallow, with its length and breadth being approximately the same, that for purposes of heat conduction into the earth the heat losses should be essentially the same as for basin of zero depth and an area in contact with the earth which is circular and equal to the area in contact with the earth for the original pool, i.e., approximately 189,500 sq. ft. Thus the circular model basin has a radius R equal to 245.5 ft.

The mathematical problem involves a disk of radius R maintained at a temperature $\tau_b = 230^\circ\text{F}$, the disk being laid flat on the surface of the earth, which is assumed to be flat and of infinite extent behind this surface. If r is an arbitrary distance from the center of this basin to any point in the surface and Z is the normal distance from the surface of the earth of a point in the earth, then the differential conduction equation in cylindrical coordinates is

$$\frac{\partial^2 \tau}{\partial r^2} + \frac{1}{r} \frac{\partial \tau}{\partial r} + \frac{\partial^2 \tau}{\partial Z^2} = 0 \quad (1)$$

The limiting conditions are

$$\tau(r, 0) = \tau_b \quad 0 \leq r \leq R \quad (2)$$

$$k \left(\frac{\partial \tau}{\partial Z} \right)_{Z=0} - h(\tau - \tau_1) = 0 \quad r > R \quad (3)$$

where τ_1 is the temperature of the air over the earth's surface and h is the radiation-convection film coefficient for the cooling winds which naturally circulate over the surface of the earth; k is the thermal conductivity of the earth.

If one defines

$$T = \frac{\tau - \tau_1}{\tau_b - \tau_1} \quad (4)$$

then Equation (1) becomes

$$\frac{\partial^2 T}{\partial r^2} + \frac{1}{r} \frac{\partial T}{\partial r} + \frac{\partial^2 T}{\partial Z^2} = 0 \quad (5)$$

$$\begin{aligned} \frac{q}{\tau_b - \tau_1} &= k\pi \left(\frac{R}{2.5} \right)^2 \left[T(r=0, Z=0) - T\left(r=0, Z=\frac{R}{5}\right) \right] \frac{5}{R} \\ &+ k\pi \left[\left(\frac{3R}{2.5} \right)^2 - \left(\frac{R}{2.5} \right)^2 \right] \left[T\left(r=\frac{R}{5}, Z=0\right) - T\left(r=\frac{R}{5}, Z=\frac{R}{5}\right) \right] \frac{5}{R} \\ &+ k\pi \left[\left(\frac{5R}{2.5} \right)^2 - \left(\frac{3R}{2.5} \right)^2 \right] \left[T\left(r=\frac{2R}{5}, Z=0\right) - T\left(r=\frac{2R}{5}, Z=\frac{R}{5}\right) \right] \frac{5}{R} \\ &+ \dots \\ &+ k\pi \left[\left(\frac{10R}{2.5} \right)^2 - \left(\frac{9R}{2.5} \right)^2 \right] \left[T(r=R, Z=0) - T\left(r=R, Z=\frac{R}{5}\right) \right] \frac{5}{R} \end{aligned}$$

and Equation (2) may be written

$$T(r, 0) = 1 \quad 0 \leq r \leq R \quad (6)$$

While for Equation (3) one has

$$k \left(\frac{\partial T}{\partial Z} \right)_{Z=0} - hT = 0 \quad r > R \quad (7)$$

This problem was run off on the Oracle, a digital computer, to avoid

insuperable mathematical difficulty. To do so, the symmetry about $r = 0$ was recognized and a plane was envisioned as connecting the $r = 0$ axis with an arbitrarily chosen radial line in the surface of the earth which was $5R$ in length. The axis was also drawn to extend $5R$ from $Z = 0$. This axis and the radial line were each divided into twenty-five equal segments, each segment being $R/5$ long. The points of division were used then to establish a symmetrical 25×25 -point grid.

The differential problem was translated into the equivalent finite-difference problem with the finite increment chosen as equal to $R/5$. The Oracle thus computed the value of T for each of the 625 points of the grid. The result, of course, is approximate because, among other things, it is assumed that all earth beyond $5R$ along r or Z does not materially alter the heat conduction in the earth at the basin; i.e., the temperature distribution beyond $5R$ is essentially uniform. The results substantially satisfied this criterion.

Two cases of the foregoing problem were run off on the Oracle. The first case involved $h/k = 92.2$ reciprocal ft. The second case involved $h/k = 9.22$ reciprocal ft.

RESULTS

The heat conduction from the basin into the earth can be estimated with the formula

where

q = B.t.u./hr. heat loss from basin into earth

$\tau_b = 230^\circ\text{F}$.

$\tau_1 = 60^\circ\text{F}$. average year-around out-of-door temperature

For case 1

$q = 8,000$ B.t.u./hr.

(Continued on page 9M)

Relative Importance of Mass Transfer and Chemical Reaction in Fixed-bed Converters

H. E. HOELSCHER

The Johns Hopkins University, Baltimore, Maryland

One of the important considerations in the study or operation of a fixed-bed catalytic converter is the relative contribution of mass transfer and chemical reaction at the particle surface to the determination of the over-all reaction rate. It is obvious that, if mass transfer controls, the investigation is not a reaction study but is, in essence, a diffusion study. In industry, under such conditions, an increase in productivity can be obtained through an increase in flow rate. Conversely, if the process is controlled by the reaction occurring at or on the particle surface, then flow rate through the bed is not a significant parameter except insofar as it determines the contact time. Thus it is important in any research study utilizing a fixed-bed catalytic reactor to determine whether the rate of mass transfer between fluid phase and particle surface is approximately the same as the rate of reaction at or on the particle surface.

The word *control* as used in the previous paragraph designates a situation wherein one step is exceedingly slow in comparison with another and, hence, the over-all observed result depends upon the rate of that controlling step.

At the present time there are generally two methods used by those engaged in fixed-bed catalytic-reaction studies to determine the importance of mass transfer to the process under investigation. The first technique is to calculate the partial pressure drop through the "film" by use of the method of Wilke and Hougen (1) and/or that of Yang and Hougen (2) and to compare this with the partial pressure of the significant or limiting reactant in the gas phase. Others have varied the flow rate to observe its effect on conversion.

It is apparent that at constant contact time the rate-Reynolds-number relationship would appear as shown schematically in the figure. However, if one operates at a fixed-bed length and varies the Reynolds number and if, simultaneously, one finds oneself in the range designated by A in Figure 1, wherein the rate is varying almost linearly with Reynolds number, it is obvious that the effect of Reynolds number on mass transfer is confounded with the effect of contact time on reaction rate. Doubling the Reynolds number would increase the rate of mass transfer but would decrease the contact time—possibly in about the same proportion. Thus only quite sensitive analytical techniques would be expected to pick up the effect of a change

(Continued on page 8M)

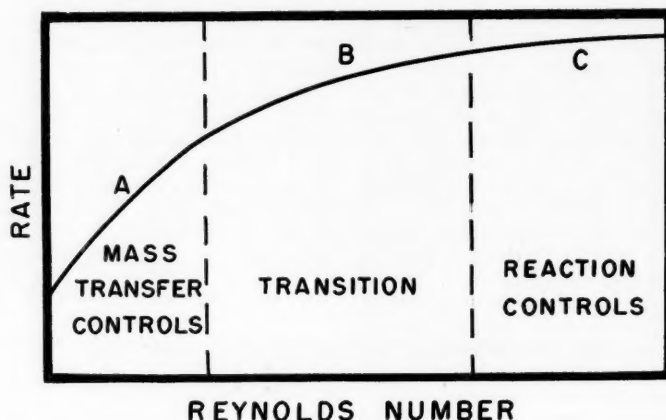


Fig. 1.

Dispersed-phase Holdup

H. R. C. PRATT

Atomic Energy Research Establishment, Harwell, Berkshire, England

In the paper "Dispersed-phase Holdup in Packed, Countercurrent Liquid-liquid Extraction Columns," by C. E. Wicks and R. B. Beckmann, which appeared in the December, 1955, issue of the *Journal* (page 426), reference is made to a paper on the same subject by Gayler and myself. Thus, on page 427 the following statement is made:

"Gayler and Pratt also present the following equation for normal holdup at flooding:

$$X_{flood} = 0.62 \frac{V_D^2 a_p}{g F^3}$$

which must be in error, for a substitution of the proper values for the variables into the equation resulted in values of X_{flood} greater than one, which is an impossibility."

The above expression is quoted incorrectly and should read* as follows:

$$X_{flood} = 0.62 \left[\frac{V_D^2 a_p \rho_d}{g F^3 \Delta \rho} \right]^{0.11}$$

*The symbols of Wicks and Beckmann are used here.

Further, substitution of data from the authors' paper, as well as our original data (2), indicates that neither of the above expressions gives values for X_{flood} greater than unity; the incorrect expression in fact gives impossibly low values of X_{flood} , owing to omission of the exponent.

The second of the above expressions represented an early attempt of ours to correlate holdup at the flood point for packed columns, and the authors may perhaps be interested in our later work. Thus, Thornton (7) has shown that for mechanically agitated columns, where the droplet size is determined entirely by the power input, the following expression for the holdup, derived originally by Gayler, Roberts, and Pratt (3) for packed columns, is applicable up to the flood point:

$$V_D + \frac{X}{1-X} V_c = F \bar{v}_0 X (1-X)$$

where \bar{v}_0 is the "characteristic droplet velocity."

By differentiating with respect to X , treating V_C and V_D as dependent variables, setting the differentials equal to zero, and eliminating V_C , V_D , and \bar{v}_0 , the following equation is obtained for the holdup at the floodpoint:

$$X_{flood} = \frac{(L_R^2 + 8L_R)^{0.5} - 3L_R}{4(1 - L_R)}$$

where $L_R = V_D/V_C$

This expression indicates that the holdup at the flooding point is dependent only upon the flow ratio and is independent of the actual flow rates and the physical properties of the phases, and it has been shown to be applicable to spray (5), rotary annular (7), rotary disk (6), and pulsed columns (6). (See also reference 4.) In the case of the packed column, however, hydrodynamical conditions are somewhat different since a transition occurs at the point where flooding would normally be expected to take place and a region of constant holdup sets in, in which the holdup remains constant as the dispersed-phase flow is increased up to the flood point. Consequently in the case of packed columns the above equation applies to the holdup at the upper transition point and not at the flood point. Presumably, however, the holdup at the flood point could in principle be obtained in this case by trial-and-error calculation from the expressions for the throughput and holdup at the upper transition point together with the correlation of flood-point data (1).

The authors' concept of three, rather than two, types of holdup is not without interest. It must be remembered, however, that the "permanent" holdup (2, 3) is much higher for solvents such as benzene and toluene, where the interfacial tension is high and the density difference small, than for the majority of other systems (reference 3, Table V). Consequently the difference between the author's "free" and the "operating" holdups would in most cases be small for packings sizes above the critical.

LITERATURE CITED

1. Dell, F. R., and H. R. C. Pratt, *Trans. Inst. Chem. Engrs. (London)*, 29, 89, 270 (1951).
2. Gayler, R., and H. R. C. Pratt, *ibid.*, 110.
3. Gayler, R., N. W. Roberts, and H. R. C. Pratt, A.E.R.E. CE/R 903 (6.3.53); *Trans. Inst. Chem. Engrs. (London)*, 31, 57 (1953) [excludes Table V].
4. Pratt, H. R. C., *Ind. Chemist*, 31, 505, 552 (1955).
5. Thornton, J. D., *Chem. Eng. Sci.* (to be published).
6. ———, D. H. Logsdail, and H. R. C. Pratt (to be published).
7. Thornton, J. D., and H. R. C. Pratt, *Trans. Inst. Chem. Engrs. (London)*, 31, 289 (1953).

HEVI DUTY

Tube Furnaces

Designed for Precision Testing

The Hevi Duty Combustion Tube Furnace is a complete unit ready for use. All the temperature control and indicating devices are located in the furnace base. A tap-changing transformer equipped with two selector switches offers you 48 steps of temperature control. This design allows close temperature regulation and means savings in power and maintenance. An indicating pyrometer and ammeter are mounted for easy observation.

Easily replaceable Silicon Carbide heating elements above and below the ceramic tube provide a uniform heat throughout the 12" chamber. Tubes of 1" to 2" O.D. may be used by substituting end plugs.

TEMPERATURE
TO 2600° F

Send for details in
Bulletin 254.



ZONE TEMPERATURE CONTROL

Extra versatility is offered by Tube Furnaces with two or more zones of control. These furnaces are built in the sizes to fit your needs.

HEVI DUTY ELECTRIC COMPANY

LABORATORY FURNACES

MULTIPLE UNIT

ELECTRIC EXCLUSIVELY

MILWAUKEE 1, WISCONSIN

Analog Computing for One and All

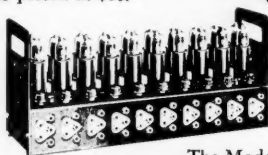
with GAP/R modular components



The Model K2-X Operational Amplifier is an octal-based plug-in unit which nobly serves as nucleus for accurate feed-back computing.

With an output of $\pm 100V$ the K2-X is priced at \$28. The K2-W at \$24. puts out an ample $\pm 50V$ with less power needed.

Model K2-P is a Stabilizing Amplifier used in tandem with the K2-W or K2-X. It provides long term DC Stability measured in microvolts. All plug directly into the HK (shown below) or other environments. The K2-P having inherent stability below 0.1 MV is priced at \$60.



The Model HK Operational Amplifier in the standard version offers 10 K2-W Amplifiers for analog calculations of infinite variety. A stabilized HK using K2-X and K2-P "paired" plug-ins provides greater output plus stability. The standard HK with 10 K2-Ws is \$425. The stabilized HK with 5 of above "pairs" is \$625.

Supplied also in a self-powered version as the compact Model HKR Operational Tenfold, all manifolds can be purchased in either standard or stabilized forms or in other combinations.

For rapid utilization of the HK or HKR, Model K- Modular Assembly units are offered either in kit form or assembled as Adder, Coefficient, Differentiator, Integrator or Unit-lag Passive Operational Plug-ins. Prices furnished on request.



One of the many "power packages" from GAP/R is the Model R-100 Regulated Power Supply, conservatively rated at 100 ma, $\pm 300VDC$, and modestly priced at \$165.

Indicated below are two possible arrangements whereby your laboratory or engineering office can obtain a basic computing facility at minimum cost.

20 OPERATIONAL AMPLIFIERS Plus Regulated Power	10 STABILIZED AMPLIFIERS Plus Regulated Power
2 HKs (with 20 K2-Ws) \$850. 1 R-100 Power Supply 165. \$1015	2 HKs (10X's + 10 P's) \$1250. 2 R-100 Power Supplies 330. \$1580.

For more details and other information please write to:

George A. Philbrick Researches, Inc.
230 Congress Street, Boston 10, Massachusetts

GAP/R

(Continued from page 144)

in Reynolds number on reaction rate if the process is operating in region A.

Calculation of the partial pressure drop of one component through the film by use of the previously mentioned methods is another standard way to ascertain whether or not mass transfer is of importance in the process; however, this technique is subject to some question and it may not yield answers which can lead to valid conclusions.

The equations developed by Wilke and Hougen (1) and summarized nicely by Yang and Hougen (2) may be shown to lead to the following:

$$\ln(P + \delta_A \phi_A) - \ln[P + \delta_A(\phi_A - \Delta \phi)] = \frac{r_A N^n M_m \delta_A}{m \left(\frac{\mu}{\rho D}\right)^{-2/3} G S_i} \quad (1)$$

where

- P = total pressure, atm.
- ϕ_A = partial pressure of component A, the component of interest to the problem, atm.
- $\Delta \phi$ = partial pressure drop of component A through the gas film surrounding the catalyst particle, atm.
- r_A = reaction rate, moles reacted/(sec.)(g.) of catalyst.
- N_B = modified Reynolds number = $D_p G / \mu$
- D_p = particle diameter
- n = a constant, usually taken equal to 0.51
- m = a constant, usually taken equal to 1.82
- M_m = mean molecular weight of gases in the reacting system
- $\mu / \rho D$ = Schmidt number
- G = mass velocity based on the empty cross-sectional area, g/(sq. cm.)(sec.)
- S_i = active surface area per unit of catalyst mass, sq. cm./g.

For a large number of reacting systems reported in the literature (the list of those referred to is presented as Appendix A) the following order-of-magnitude values apply:

$$\begin{aligned} 30 < M_m < 100 \\ 0.1 \text{ cm.} < D_p < 0.2 \text{ cm.} \\ 1 < (\mu / \rho D)^{-2/3} < 10 \\ \mu &\sim 10^{-4} \text{ g./cm.}(\text{sec.}) \\ r_A &\sim 10^{-6} \text{ moles/}(\text{sec.})(\text{g. of catalyst}) \end{aligned}$$

The constant δ_A in Equation (1) is given by

$$\delta_A = \frac{c + d - a - b}{a}$$

where a, b, c , and d are the stoichiometric coefficients in the reaction under study, viz:



Thus, by means of indicated approximate values and a total pressure of 1 atm.

$$\ln \frac{1 + \delta_A \phi_A}{1 + \delta_A \phi_A - \delta_A \Delta \phi} \sim \frac{10^{-3} \delta_A}{S_i \sqrt{N_B}} \quad (2)$$

wherein the group on the left is indicated to be of the order of magnitude of the group on the right. For a specific case, $\delta_A = -1$,

$$\ln \left[1 + \frac{\Delta \phi}{1 - \phi_A} \right] \sim \frac{10^{-3}}{S_i \sqrt{N_B}} \quad (3)$$

Values of S_i obtained from adsorption measurements are usually quite high, often as high as 10^4 sq. cm./g. Even with values much less than this it is apparent that for any reasonable value of N_B , $\Delta \phi \rightarrow 0$. Thus it is apparent that with the order-of-magnitude values stated, Equation (1) predicts that mass transfer can be of no importance regardless of the Reynolds number used. Again, this conclusion remains valid if the measured rate were different (for example as a result as temperature changes) by as much as three orders of magnitude.

It is obviously important in studies of the chemical-reaction rate in fixed-bed catalytic reactors to know where (on the figure) the process under study is operating. The conclusion to be drawn from the foregoing is that there is only one satisfactory technique for determining the relative importance of mass transfer and chemical reaction in such studies at the present time. The effect of Reynolds number on conversion or on the over-all reaction rate must be determined at constant contact time. When this is done, it will become evident as to whether or not flow rate is influencing the over-all reaction rate, and it is possible to determine therefrom the relative orders of magnitude of these two rates in the process.

LITERATURE CITED

1. Wilke, C. R., and O. A. Hougen, *Trans. Am. Inst. Chem. Engrs.*, **41**, 445 (1945).
2. Yang, K. H., and O. A. Hougen, *Chem. Engr. Progr.*, **46**, 146 (1950).

APPENDIX A

List of References Providing Data Leading to Equation (3)

1. Akers, W. W., and R. R. White, *Chem. Engr. Progr.*, **44**, 553 (1948).
2. Binder, G. G., and R. R. White, *ibid.*, **46**, 563 (1950).
3. Buckley, R. R., and R. J. Altpeter, *ibid.*, **47**, 243 (1951).
4. Hoelscher, H. E., and D. F. Chamberlain, *Ind. Eng. Chem.*, **42**, 1558 (1950).
5. Kayser, R. F., and H. E. Hoelscher, *Chem. Engr. Progr.*, **50**, 109 (1954).
6. Olson, R. W., R. W. Schuler, and J. M. Smith, *ibid.*, **46**, 614 (1950).
7. Potter, Charles, and Seymour Baron, *ibid.*, **47**, 473 (1951).
8. Swabb, L. E., Jr., and H. E. Hoelscher, *ibid.*, **48**, 564 (1952).

(Continued from page 143)

For case 2

$$q = 78,000 \text{ B.t.u./hr.}$$

Another quantity of interest is the thermal gradient in the earth at the center of the basin and $Z = 0$. This quantity may be estimated from the formula

$$\text{Gradient} = [T(r = 0, Z = 0) -$$

$$T(r = 0, Z = R/5)][\tau_0 - \tau_1]5/R$$

For case 1

$$\text{Gradient} = 0.485^\circ\text{F./ft.}$$

For case 2

$$\text{Gradient} = 0.473^\circ\text{F./ft.}$$

The gradient values are significant in that if one had, for example, an asphalt that would not stand more than 220°F. , one would need 21.2 ft. of earth in case 2 to insulate the boiling solution from the asphalt seal, and this figure is obviously prohibitive. The answer is not significantly different for case 1. In this regard, it should be stated that case 2 is the more realistic of the two because of the k value involved.

The values of T for the 625 grid points were considered too voluminous to be included in this paper.

CONCLUSIONS

The conclusions reached were that the steady state heat losses from the bottom of the basin would be negligible compared with the rate of radio heat generation. However, the temperature gradient at the bottom center of the pool is such that the pool would have practically to be filled with insulating material in order to ensure a low enough temperature in the bottom seal so as not to soften it and cause leakage.

The basin project was discontinued before data could be obtained. No comparable work seems to have been reported to date.

BOOKS

Unit Operations of Chemical Engineering. Warren L. McCabe and Julian C. Smith. McGraw-Hill Book Company, Inc., New York (1956). 945 pages. \$10.50.

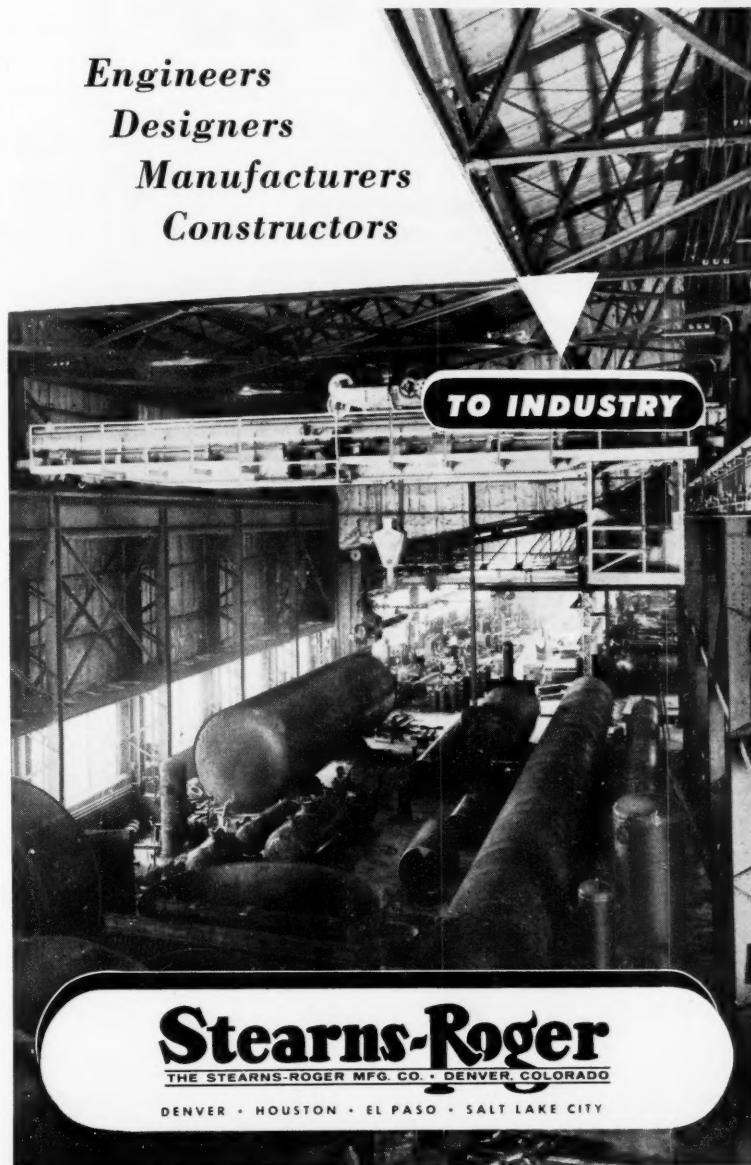
This book covers the same topics as the well-known earlier work "Elements of Chemical Engineering" by W. L. Badger and W. L. McCabe, the most recent edition of which was published in 1936. Newer unit operations, such as adsorption, ion exchange, and dialysis, are not included. However, the text of all sections has been completely rewritten to incorporate the added understanding of unit operations developed in the past twenty years. Old subject matter has been eliminated or rearranged to be consistent with new material.

The level of treatment is designed for undergraduate students, but the discussion has been carried to the point where students will find an easy transition to more advanced chemical engineering texts. In addition, new approaches have been incorporated; for example, the boundary-layer concept is introduced early in the fluid mechanics study, the theory of diffusion is based on the relative-velocity method, and the discussion of the separate mass transfer operations is preceded by a study of principles common to all.

In order to provide material for a three-semester sequence for unit operations and include the developments of recent years, while at the same time maintaining an adequate treatment of theory and equipment, the authors increased the length of the book from 660 to 945 pages. This increase was due primarily to the substantial expansion of the sections on fluid mechanics and flow of heat and the general approach to mass transfer, but was also due to the enlarged coverage of the distillation, mixing, and extraction sections.

To students, teachers, and practicing engineers alike, this book should be a welcome text, especially for those accustomed to the 1936 book. Although some of the solved problems and diagrams from the previous text have been included in modified form, most are replaced by new illustrations. All the unsolved problems are new. Mass transfer coefficients have been standardized to the Drew-Colburn coefficient. As before, a discussion of pertinent equipment aug-

Engineers Designers Manufacturers Constructors



TO INDUSTRY

Stearns-Roger
THE STEARNS-ROGER MFG. CO. • DENVER, COLORADO
DENVER • HOUSTON • EL PASO • SALT LAKE CITY



Applied Research

to give you better

SPRAY NOZZLES

• Shown above is a portion of Spraying Systems' own research facilities. Here the variables of nozzle design, fluid properties and operating conditions are studied and measured . . . to provide original data for better design and improved performance wherever spraying is involved.



WRITE FOR Catalog 24 . . . contains forty-eight pages of complete information on thousands of nozzle types and capacities.

SPRAYING SYSTEMS CO.
3210 RANDOLPH STREET • BELLWOOD, ILL.

ADVANCED SPRAY NOZZLE DESIGN FOR NEW DIMENSIONS IN CONTROL AND PERFORMANCE



INDEX OF ADVERTISERS

Beckman Instruments, Inc. Inside Back Cover	Philbrick Researches, Inc., George A. 8M
Bowen Engineering, Inc. 4M	Spraying Systems Co. 10M
Eimco Corp., The 6M	Stearns-Roger Mfg. Co. 9M
Hevi Duty Electric Co. 7M	Titanium Alloy Mfg. Div. 2
Librascope, Inc. 5M	York Process Equipment Corp. Inside Front Cover
Mixing Equipment Co. Outside Back Cover	

Advertising Offices

New York 36—Lansing T. Dupree, Adv. Mgr.; John M. Gaede, Asst. Adv. Mgr.; Paul A. Jolcuvar, Dist. Mgr.; Donald J. Stroop, Dist. Mgr.; Hale H. Carey, Dist. Mgr.; 25 W. 45th St., Columbus 5-7330.

Chicago 11—Richard R. Quinn, Dist. Mgr., 612 North Michigan Ave., Room 507, Superior 7-0385.

Cleveland 15—Eugene B. Pritchard, Dist. Mgr., 1836 Euclid Ave., Superior 1-3315.

Pasadena 1—Richard P. McKey, Dist. Mgr., 465 East Union St., Ryan 1-8779.

Dallas 28—Richard E. Hoierman, Dist. Mgr., 2831 El Capitan Drive, Davis 7-3630.

Birmingham 8, Ala.—Fred W. Smith, Dist. Mgr., 1212 41st St., B. H., 57-6806.

ments each topic covered. However, in keeping with the trend of approaching chemical engineering as a science, this book generally places more emphasis on the theoretical aspect than did its predecessor.

JOHN A. TALLMADGE

High Pressure Technology. E. W. Comings. McGraw-Hill Book Company, Inc., New York (1956). 572 pages. \$11.50.

An excellent collection of the reliable information available on high pressure, this volume is a comprehensive reference on the field, as it contains both theoretical aspects and practical know-how. Mr. Comings is quick to point out that much of the present-day information concerning high pressure has been the result of experience, that is, art or craft in contrast with science. A good reference list is available for the reader who is looking for background material and more complete current information on the variety of individual subjects treated.

Chapter two, "Chemical Processes," by N. R. Shreve, and Chapter three, "Metals," by H. C. Van Ness, deal with some of the practical applications as well as the limitations that exist in the use of high pressure. Shreve, of course, points out many of the present commercial processes that employ high pressure, and Van Ness notes some of the limitations of high-pressure application due to the deleterious effects on metals. Chapters entitled "Safety," "Equipment," and "Experimental Techniques" also deal with the purely practical aspects and are useful to the researcher in the field.

The remainder of the book deals primarily with the mathematical and theoretical treatment. Excellent chapters covering such topics as pressure cylinders, thermodynamics of liquids and gases, chemical equilibria, unit operations, and reactor design as specifically related to high pressure are presented. Realizing the inherent limitations on the theoretical treatment, not only of complex systems but also of systems under the extreme conditions imposed by high pressures, the author includes much information on empirical and generalized relations.

What at first may appear to the reader as broad, unrelated subject matter is tied together in the final chapter by a thorough study of ammonia synthesis, which serves as the classic example of the successful application of high pressure in modern industry. This chapter not only relates the subject matter from the previous chapters, but it also serves to reemphasize Mr. Comings's original premise, that high-pressure application is a combination of art and science.

The book also contains several appendices, including such items as pVT data, constants for various equations, glossary of terms used in high pressure, and a section on units and dimensions.

Because of the broad scope of the subject matter, many important points are not given complete, detailed treatment. The reader is therefore expected to have a fair understanding of chemical engineering principles.

RICHARD J. SCHOOPS

in
ning
book
the
ssor.
EDGE

Mc-
York

able
this
on
tical
Mr.
much
ning
peri-
with
able
ound
nfor-
jects

' by
als,"
the
nita-
sure.
the
ploy
ne of
ation
tals.
ent,"
deal
are

arily
etical
such
ody-
nical
actor
pres-
erent
, not
tems
d by
much
lized

er as
tied
ough
erves
essful
modern
s the
oters,
Mr.
high-
on of

open-
data,
ssary
ection

subject
e not
The
a fair
eering

HOOPS